


Proceeding


ISEH 2021





Proceedings of the 9th International Symposium on Environmental Hydraulics

July 19(Mon) - 21(Wed), 2021
Seoul National University, SEOUL, KOREA

Edited by

Il Won Seo
Jin Hwan Hwang
Yong Sung Park
Siyeon Kwon



Organizer

- Seoul National University
- Korea Water Resources Association (KWRA)



SEOUL
NATIONAL
UNIVERSITY



KOREA WATER
RESOURCES ASSOCIATION

Under the Auspices of

- International Association for Hydro-Environment Engineering and Research (IAHR)



Sponsoring and Supporting Organizations



BK21 Education & Research
Program for **InfraSPHERE**
Dept. of Civil & Environmental Engineering Seoul National University



ISAN CORPORATION



Institute of Construction and Environmental Engineering
Seoul National University



KICT
KOREA INSTITUTE of CIVIL ENGINEERING
and BUILDING TECHNOLOGY

o Table of Contents

Keynote Keynote Speech

Keynote 1	Longitudinal dispersion in the natural environment exploring contributing components 24 Ian Guymer (University of Sheffield, UK)
Keynote 2	Initiatives for water resources management considering Korea's natural restoration of rivers 25 Jae-Hyeon Park (K-water, South Korea)
Keynote 3	Vegetation hydrodynamics for climate mitigation and adaptation 27 Heidi Nepf (Massachusetts Institute of Technology, USA)
Keynote 4	Experimental and numerical study of wave attenuation by live <i>Phragmites australis</i> 29 Pengzhi Lin (Sichuan University, China)

Session A1 Dispersion

A1-1	Simulation of the near-field mass transport processes through a fishing net panel using OpenFOAM 34 Yang Xinyue, Carlo Gualtieri, Dongdong Shao
A1-2	Mixing characteristics of river confluence using water quality indicator in slow flow conditions 36 Geunsoo Son, Dongsu Kim, Siwan Lyu, Young Do Kim
A1-3	Improving an observation method on pollutant dispersion for analysis of two-dimensional river mixing 37 Donghae Baek, Il Won Seo
A1-4	Investigation of pollutant transport at upstream of notch installed weir 39 Sung Hyun Jung, Il Won Seo
A1-5	Non-Fickian transport induced by horizontal flow recirculation in in meandering open channels 41 Jun Song Kim, Il Won Seo, Donghae Baek
A1-6	Experimental investigation on longitudinal dispersion in a reach with willow patches 43 Kaisa Västilä, Un Ji, Juha Järvelä, Fred Sonnenwald, Hyung Suk Kim, Ian Guymer, Jungsun Oh



A1-7

- An autoregressive model for sewage flow prediction for chlorine dosage control** 45
Yuqing Liu, King Wah Choi, Joseph H. W. Lee

Session A2 Particle Laden Flows

A2-1

- Effect of turbulent motions on the sediment entrainment based on the three-dimensional PIV and PTV technique** 48
Hyounghul Park, Jin Hwan Hwang

A2-2

- Modeling of scour process under two-dimensional wall jet: insights in the scour development stage** 49
Geng Li, Binbin Wang

A2-3

- Reservoir sedimentation and flushing for the management of the Patrind hydro-power dam** 50
Joonwoo Noh, Yeonsoo Kim, Jisoo Yu

A2-4

- Using image conversion for suspended solid transport for 2D particle dispersion modeling** 51
Jaehyun Shin, Hoje Seong, Inhwan Park, Dong Sop Rhee

A2-5

- Identifying total sediment loads–suspended sediment load relationship using a two-level unsupervised clustering method** 53
Hyoseob Noh, Yong Sung Park

Session A3 Environmental Flows

A3-1

- The effect of turbulent flow motion on the sea urchin fertilization** 56
Hyounghul Park, Hojung You, Jin Hwan Hwang

A3-2

- The effect of obstacle configuration on the transport of neutrally buoyant particles** 57
Hojung You, Rafael O. Tinoco

A3-3

- A turbulence-based, two-layer model to predict sediment resuspension in vegetated flows** 58
Chien-Yung Tseng, Rafael Tinoco

A3-4

- Disparity of nutrient loading estimates associated with extreme-event observation** 60
Dong-Kyun Kim, Kwangsoon Choi, Youngsung Kim, Hye-Suk Yi, Suna Chong, Nam-Il Won, Hojoon Kim, Seung-Yoon Lee, Seungbin Yang, Hyung-Seok Park

A3-5

- Analysis of residence time distribution in retention zone of natural rivers** 61
Byunguk Kim, Il Won Seo

A3-6	Hyporheic exchange driven by rocks 63 Anzy Lee, Antoine Aubeneau, M. Bayani Cardenas, Xiaofeng Liu
A3-7	Electrochemical model for galvanic corrosion in drinking water supply systems 65 Lu Chang, Joseph H. W. Lee

Session B Jets

B-1	Self-preserving characteristics in 2D submerged offset jets 70 Subhasish Dey, Galla Ravi Kishore, Sk Zeeshan Ali
B-2	Mathematical model of Reynolds shear stress in a turbulent plane jet with Coandă effect 71 Sk Zeeshan Ali, Galla Ravi Kishore, Subhasish Dey
B-3	Effect of ambient turbulence on the entrainment into a turbulent jet - mean properties and processes at the turbulent/turbulent interface 72 Rana Sahebjam, Khashayar F. Kohan, Susan J. Gaskin
B-4	Estimate of attraction flow propagation as turbulent rectangular surface jet 75 Veronica Wiering
B-6	Prediction of transport and dissolution of oil & gas released from diverse oil blowout scenarios in the offshore Canada 77 Inok Jun, Rebekah Jeter, Scott A. Socolofsky, Ruixue Liu, Michel C. Boufadel, Youyu Lu, J. Samuel Arey
B-7	Chemically reacting chlorine jet mixing with CEPT sewage effluent 80 Q. S. Qiao, Joseph H. W. Lee

Session C1 Density Current

C1-1	The hydraulics of the salt tip in the estuarine contraction 84 Nguyen Ngoc Minh, Jin Hwan Hwang
C1-2	Numerical study of confluence channel flow with gravity currents 85 Minjae Lee, Yong Sung Park
C1-3	LES of colliding gravity currents 86 Angelos Kokkinos, Panagiotis Prinos
C1-4	Effects of rotation on stratified exchange flows over a submerged sill 87 Alan Cuthbertson, Jarle Berntsen, Janek Laanearu, Magdeli Asplin



C1-5

- Experimental turbidity current dynamics responding to a simultaneous loss of confinement and break of slope** 90
Jonathan Wilkin, Alan Cuthbertson, Sue Dawson, Dorrik Stow, Karl Stephen, Uisdean Nicholson

Session C2 Stratified Flows

C2-1

- Turbulent mixing across a sharp density interface** 94
Arefe Ghazi Nezami, Blair A. Johnson

C2-2

- Numerical simulation of aeration column in stratified environments** 96
Seongeun Choi, Jin Hwan Hwang

C2-3

- Examining the bio-physical processes of dam reservoir by spatio-temporal vertical profiling** 98
Jin Hwan Hwang, Dong-Hyun Kim, Hyung-Cheol Park, Seongeun Choi, Dong-Kyun Kim, Ho Joon Kim, Nam-Il Won

C2-4

- Buoyancy-driven exchange flows in inclined ducts** 99
Adrien Lefauve, Paul Linden

C2-5

- The anisotropy of symmetric Holmboe instabilities in stratified flows** 100
Adam J.K. Yang, E.W. Tedford, J. Olsthoorn, A. Lefauve, G.A. Lawrence

C2-6

- Assessment of the water circulation plan for water quality improvement of the Seonakdong River** 102
Sanguk Lee, Young Teck Hur, Youngsung Kim, Eul Rae Lee

Session D1 Morphodynamics

D1-1

- Investigation the impact of river interventions on fluvial morphodynamics** 104
Gergely T. Török, Gary Parker

D1-2

- Optimal shape of alternative gravel mounts in terms of flood control and aquatic habitat** 106
Pietro Beretta Piccol, Youichi Yasuda

D1-3

- Artificial formation of gravel mount with stacked boulders** 107
Youichi Yasuda, Pietro Beretta Piccoli Marco

D1-4

- A comparative study on sequent depth ratio and energy losses in hydraulic jumps on rough rectangular channels with adverse slopes** 108
Maisnam Bipinchandra Singh, Mukesh Kumar Yadav, Victoria Ningthoujam Ngangbam Romeji Singh

D1-5	Sequent depth ratio and energy losses in hydraulic jumps on rough near-prismatic channels with sediment flows 109
	Maisnam Bipinchandra Singh, Ngangbam Romeji, Mukesh Kumar Yadav Susilchandra Khuraijam
D1-6	Impacts of riparian vegetation features on the shear layer in partly vegetated channels 110
	Gerardo Caroppi, Kaisa Västilä, Paola Gualtieri, Juha Järvelä, Maurizio Giugni, Paweł M. Rowiński

Session D2 Vegetation

D2-1	Numerical study on the effects of vegetation on the intradelta lobe avulsion 114
	Dongxue Li, Weilun Gao, Dongdong Shao, Baoshan Cui
D2-2	Experimental and numerical modelling of Reynolds shear stress in open channel flows with double-layer vegetation 116
	Hamidreza Rahimi, Xiaonan Tang, Toktam Hatamisengeli, Prateek Kumar Singh
D2-3	Velocity reduction and drag in submerged canopies under oscillatory flow conditions 117
	Dominic van der A, Otto Neshamar, Niels G. Jacobsen, Tom O’ Donoghue
D2-4	Experimental reach scale methodology for analyzing integrated flow resistance due to woody vegetation patches 119
	Inhyeok Bae, Un Ji, Juha Järvelä, Kaisa Västilä
D2-5	Study on the physical habitat of river channel vegetation designated as an endangered species 121
	Takayuki Tanaka, Syunya Hazama, Ryuki Harata
D2-6	The impact of vegetation existence on flow structure in compound channels 124
	Yutong Guan, Xiaonan Tang

Session D3 Fish

D3-1	Surface roughness in billfishes: a guide to improving the design of engineered surfaces? 128
	M.T. Stewart, D.K. Wainwright, V.I. Nikora, S.M. Cameron, M. Thunert, T. Stoesser
D3-2	Fish swimming behaviour and kinematics in the wake of a vertical axis turbine 130
	Stephanie Müller, Valentine Muhawenimana, Pablo Ouro, Catherine Wilson, Jo Cable
D3-3	Exploration of the active sensory space of fish through CFD 132
	Ali Hassan Khan, Stefan Hoerner, Jeffrey A. Tuhtan



D3-4	Transient physical habitat modelling - simulation of stream macrozoobenthos habitat suitability using fuzzy logic approach 134 Sengdavanh Thepphachanh, Jürgen Stamm
D3-5	Attracting juvenile silver perch into the tube fishway with different diameters 136 Maryam Farzadkhoo, Stefan Felder, Iain M Suthers, William L Peirson, Richard T Kingsford, John H Harris
D3-6	An investigation of the hydrodynamic and fish behavior characteristics in brush-type fish passage: A pilot study in Iyidere, Turkey 138 Serhat Kucukali, Reinhard Hassinger

Session E1

Coast

E1-1	OpenFOAM modeling of wave pressures on a caisson armored with double-layer tetrapods on the rubble stones 142 Deok Ah Lee, Gun Hyeong Kim, Sung Bum Yoon, Sang-Ho Oh
E1-2	A novel approach to estimate the coastal protection provided by different saltmarshes species 144 Maria Maza, Javier L. Lara, Iñigo J. Losada
E1-3	Siphon well for protection of coastal aquifer from saltwater intrusion 147 Byunghee Nam, Roshina Babu, Namsik Park
E1-4	Simulation-optimization for sustainable groundwater management in small islands under drought conditions 148 Roshina Babu, Byunghee Nam, Namsik Park
E1-5	Calibration and assessment of numerical modelling in an embayed beach in case of presence or absence of submerged breakwaters 149 Minsang Cho, Kideok Do, In-Ho Kim, Hyun-Doug Yoon

Session E2

Ocean

E2-1	Evaluation of effects of river discharge on development of salinity stratification and hypoxia due to climate change in the Ariake Sea, Japan 152 Hao Lin, Shinichiro Yano
------	--

E2-2	Development of ecological model for dynamics of partial pressure of CO₂ in seawater considering the effects of stratification in the Yatsushiro Sea 154	154
Bing Xiong, Naoki Saito, Hiroto Komori, Shinichiro Yano, Keisuke Nakayama, Katsuaki Komai		
E2-3	Improvement of long term integration results of one-way nested regional ocean model by applying a new boundary small eddy additions technique 156	156
Van Sy Pham, Jin Hwan Hwang		
E2-4	Transport of Microplastics Contained in the Wastewater Discharged from the King Sejong Station in the West-Antarctica 157	157
Bo-Kyung Kim, Jin Hwan Hwang		
E2-5	Assessing the interplay of Sea Level Rises and Mangrove Species Richness: A Meta-analysis Approach 159	159
Giuseppe Francesco Cesare Lama		
E2-6	UAV-Based Remote Sensing for Coastal Environment 160	160
Hieu Trung Kieu, Cuc Duong, Hui Ying Pak, Dawn Pang, Adrian Wing-Keung Law		

Session E3

Estuary

E3-1	2-D numerical modelling of meandering estuaries 162	162
S. Haddout, K.L. Priya, Joan Cecilia C. Casila, A.M. Hogueane		
E3-2	Study on the relationship of salinity front characteristics and runoff in the north branch of the Yangtze River Estuary 163	163
Cuiping Kuang, Kuo Chen, Yunlong Wu, Jie Wang		
E3-3	Seasonal variation of sediment transport - a case study of Hyeongsan River Estuary, South Korea 165	165
Donghyeon Kim, Jin Hwan Hwang		
E3-4	An experimental study on the effects of physical factors in transport of microplastics in coastal area 167	167
Dongwook Hwang, Yong Sung Park		
E3-5	Investigation of bathymetry data and groin structures effect on the numerical results of the flow and salinity intrusion in the estuarine part of Yoshii river reach, Japan 169	169
Mohammed Al-Baghdadi, Ryosuke Akoh, Takahiro Hiratsuka, Shiro Maeno		
E3-6	Hydrodynamic velocities and forces beneath a tidal bubble bore 171	171
Muhammad Zain Bin Riaz, Shu-Qing Yang, Muttucumaru Sivakumar		



Session F1 Experiment-1

F1-1	Interfacial compound section transverse flow variation in symmetric and asymmetric compound open channel flow 174 P. Singh, X. Tang
F1-3	Lateral diffusion of stabilized air bubbles in a counterflow water tunnel 176 Soobum Bae, Scott A. Socolofsky, Binbin Wang
F1-4	Flow patterns and sediment transport at the Initial phase of the local scouring at the downstream of bed protection 178 Jungkyu Ahn, Jaelyong Lee, Jeongmin Lee, Jin Hwan Hwang, Sung Won Park
F1-5	Experimental study on throughflow and water purification characteristics of rockfill porous media 180 Ilyeong Han, Jaejong Lee, Gyoo Bum Kim
F1-6	Direct measurement of critical tractive force for revetment material 182 Dong Gyu Jung, Gwang Soo Kim, Young Do Kim, Yong Sung Park
F1-7	The effects of air cavity propagation on transient full pipe flows during emptying process ... 184 Rolando Perez, Arman Rokhzadi, Musandji Fuamba

Session F2 Experiment-2

F2-1	Near body flow field measurements on a fish robot 188 Dennis Powalla, Shokoofeh Abbaszadeh, Karla Ruiz, Stefan Hoerner, Dominique Thévenin
F2-3	Analysis of natural gas bubbles in the NETL high pressure water tunnel (HPWT) experiment and its application to natural seeps 190 Byungjin Kim, Scott A. Socolofsky, Binbin Wang
F2-4	Using GPS electronic floater in lab-scale study on the method of collecting river information 192 Chang Hyun Lee, Jeong Min Lee, Young Do Kim
F2-5	Effect of non-axial velocity component on the mean axial velocity measurements in thermal plumes using an air velocity transducer 194 Maria K. Stefanidou, Aristeidis A. Bloutsos, Panayotis C. Yannopoulos
F2-6	Estimation of carbon: chlorophyll ratio for phytoplankton using in-situ imaging FlowCytobot ... 196 Yaoyao Ma, Joseph H. W. Lee

Session F3 Remote Sensing-1

F3-1	Development of an image based method to track the fate of floating litter in rivers 200 Péter Grivalszki, Gábor Fleit, Alexander Anatol Ermilov, Sándor Baranya
F3-2	Assessing performance of a novel UAV-borne green LiDAR on vegetated rivers characterization: comparison with traditional airborne LiDAR bathymetry 201 Md. Touhidul Islam, Keisuke Yoshida, Satoshi Nishiyama, Koichi Sakai
F3-3	Riparian land-cover classification methodology of airborne laser bathymetry assisted deep learning of aerial photographs 203 Shijun Pan, Keisuke Yoshida, Junichi Taniguchi, Akihide Watanabe
F3-4	Water level monitoring for Hwang-Gang dam in North Korea using satellite remote sensing and inflow estimation for Gun-Nam flood control reservoir in South Korea 204 Jin-Gyeom Kim, Boosik Kang, Wansik Yu, Euiho Hwang
F3-5	Rapid extraction of water area using SAR remote sensing data 205 Ki-mook Kang, Eui Ho Hwang, Sunghwa Choi, Wansik Yu, Jingyeom Kim
F3-6	Study on optimum UAV photogrammetry operation using river information from local residents at small and medium-sized rivers in Japan 206 Ken Ichikawa, Masakazu Hashimoto, Shosuke Sato, Fumihiko Imamura, Arata Nasuno, Kaori Amaya, Susumu Naradate

Session F4 Remote Sensing-2

F4-1	The implementation of a surface image velocimetry to a small-sized river using a images taken with drone-mounted camera 210 Kwonkyu Yu, Binghao Liu, Namjoo Lee
F4-2	Estimating dispersive behavior using UAV-based spatio-temporal hyperspectral image 211 Yeonghwa Gwon, Eun Jin Han, Hojun You, Dongsu Kim, Young Do Kim
F4-3	Remote sensing for suspended sediment concentration using hyperspectral images in rivers 212 Siyoon Kwon, Il Won Seo
F4-4	A study on the establishment of algae mapping based on hyperspectral images 214 Gwang Soo Kim, Dong Gyu Jung, Jong Min Kim, Young Do Kim
F4-5	Analysis of flow characteristics using GPS floater in estuary 215 Jeong Min Lee, Chang-Hyun Lee, Young Do Kim



F4-6	Application of hyperspectral image for algae distribution in Andong dam 216
	Jong Min Kim, Yeong Hwa Gwon, Ye Lim Park, Dong Soo Kim, Young Do Kim

Session F5

Hydro-engineering

F5-1	Effects of the absence/presence of river bathymetric data in DEMs used for hydraulic modelling and flood prediction 220
	Nancy Joy Lim
F5-2	Evaluation of reservoir capacity of Singda reservoir using bathymetric data and geospatial techniques 222
	Victoria Ningthoujam, Maisnam Bipinchandra Singh, Ngangbam Romeji Singh
F5-3	Climatic impact and water balance analysis of Singda reservoir using hydrologic models and geo-hydrographic techniques 223
	Victoria Ningthoujam, Ngangbam Romeji, Gunadas Singh Keisam, Sylvia Nongthombam
F5-4	Using hydrological distributed model to evaluate the CHRS rainfall in generating discharge of Cileungsi River, Indonesia 224
	M. Pramono Hadi
F5-5	Development of the GeoCRP for the smart river management in the smart city 225
	Bonhyun Koo, Kyucheoul Shim, Eunjeong Lee
F5-6	Nature-based solutions as an overarching concept and river corridor management 227
	Hyoseop Woo
F5-7	Daily algal bloom risk forecast system for Lo Tik Wan, Hong Kong 229
	Jiuhao Guo, Joseph H. W. Lee

Session G1

Computational Fluid Dynamics

G1-1	Numerical Study on the Hydrodynamics of a Vegetated Lateral Cavity 234
	Luiz Oliveira, Taís Yamasaki, Johannes Janzen, Carlo Gualtieri
G1-2	SPH simulation of vortex flow in open channel expansion 236
	Chunli Wang, S. Samuel Li
G1-3	LES prediction of bistable flow in open-channel expansion 237
	Rui Zeng, S. Samuel Li

G1-4	Numerical Investigation of air entrainment in a hydraulic jump 239 Byung Joo Kim, Joongcheol Paik
G1-5	Implicit primal discontinuous Galerkin formulation for turbulent stresses in shallow water equations 240 Haegyun Lee, Namjoo Lee
G1-6	A numerical study on pressure fluctuations in free jump and submerged jump 242 Seongwook Choi, Sung-Uk Choi

Session G2 Shallow Water Flows

G2-1	High order method for shallow water flows over irregular topography with vegetation 244 Jaeyoung Jung, Jin Hwan Hwang
G2-2	Optimal layout of a tidal fence in a rectangular channel flow 245 Jisu Han, Jaeyoung Jung, Jin Hwan Hwang
G2-3	Development of 1-dimensional river hydraulic model (K-River) 246 Yeonsu Kim, Youngteck Hur, Junwoo Noh, Hyunuk An
G2-4	Simulations of pollutant storage effects within emergent vegetation using particle dispersion model 247 Inhwan Park, Sunmi Lee, Sanha Kim, Taewon Yoon
G2-5	Development of GPU-accelerated 2DH hydrodynamic and transport model 249 Sooncheol Hwang, Sangyoung Son
G2-6	Application of an unsteady-flow water quality model to determine required deicing fluid reduction at Memphis International Airport 250 Charles S. Melching, Chuck Pace

Session G3 Open Channel Hydraulics

G3-1	Numerical investigation on turbulence structure over backward-facing step for various step angles and Reynolds numbers 254 Jeonghu Lee, Van Thinh Nguyen
G3-2	Development of two-dimensional river flow analysis model using Godunov's scheme and TVD limiter 256 Eun-Taek Shin, Chang Geun Song



G3-3	Flow-3D CFD model of bifurcated open channel flow: 1. Setup and Validation 258 Nur Adani Adnan, Izihan Ibrahim, Saerahany Legori Ibrahim
G3-4	Study of the jet flow into a plunge pool using OPENFOAM 261 Rita Carvalho
G3-5	Numerical study of flow structure and pollutant mixing at river confluences 264 Se Hun Yun, Il Won Seo

Session H Machine Learning

H-1	The prediction of turbulent features of drainage channels covered by reed beds by using a Machine Learning approach 266 Giuseppe Francesco Cesare Lama
H-2	The development of real time prediction system for urban flooding in Incheon, South Korea 267 Dongmin Jang, Sung Won Park, Chang Hoo Jeong, Won Su Kim
H-3	Machine learning based spatio-temporal characterization of marine water quality evolution in Hong Kong 268 Tianan Deng, Huan-Feng Duan
H-4	Improvement of algal bloom identification by a big-data analysis using satellite images 269 Hye-Suk Yi, Dong-Kyun Kim, Kwangsoon Choi, Youngsung Kim, Suna Chong, Nam-Il Won, Hojoon Kim, Sunghwa Choi, Eui-ho Hwang, Yongbae Jung
H-5	Three types of machine learning technique for three different problems in water resource engineering · 270 Donghwi Jung, Soon Ho Kwon, Joong Hoon Kim
H-6	Watershed management in Nakdong river using big data analysis 271 Bu Geon Jo, Woo Suk Jung, Young Do Kim

Session S1 Rainwater Harvesting and Utilization

S1-1	Multi-purpose decentralized rainwater management: Philosophy, theory and a case study 274 Mooyoung Han
S1-2	Effects of multi-purpose rainwater management for responding to the climate crisis 276 Dong Geun Kwak, Mooyoung Han

S1-3	Rainwater use efficiency and optimization of Seoul Botanic Park in South Korea 278 Zion Kang, Kyungho Kwon
S1-4	Innovative technology to maintain clean rainwater in rainwater harvesting systems 280 Janith Dissanayake, Mooyoung Han
S1-5	Sustainable RFD (Rainwater for Drinking) system for rural health care facilities (HCF): A case study at Ly Nhan HCF in Vietnam 282 Hakyung Lee, Mooyoung Han

Session S2

Hydro-environment in Cities-Water Cycle, Metabolism and Management

S2-1	Feasibility of waste heat recovery from sewage in metropolitan cities 286 Jinsung An
S2-2	A pilot scale study for semiconductor wastewater reuse and ultrapure water production 288 Chong Min Chung
S2-3	Stochastic approaches for risk and resilience of groundwater systems under uncertainty 290 Jinwoo Im
S2-4	Development and application of a polar organic chemical integrative sampler (POCIS) for monitoring micropollutants in a drinking water treatment plant 292 Hyun-ah Kwon, Yongju Choi
S2-5	Oxidation of aldehydes found in finished recycled wastewater with heterogeneous transition metal catalysts and dissolved oxygen 294 Euna Kim, Georgia Cardoso, Daniel L. McCurry
S2-6	Development of sensor technologies for smart water quality management in future cities ... 296 Jong Kwon Choe, Junyoung Park

Session S3

Development of River Management Technology Using River Survey and Monitoring Drones

S3-1	The development of the drone operation platform for river survey and monitoring 300 Jaehyun Shin, Hoje Seong, Dong Sop Rhee
S3-2	Creation of a digital twin using LiDAR point cloud and high-resolution imagery acquired in river basins 302 Yun-Jae Choung



S3-3	Bathymetric Observation with UAV-based hyperspectral Image in Shallow Rivers 304 Hojun You, Dongsu Kim, Yeonghwa Gwon
S3-4	Development and application of HDM-2DF for analyzing river inundation and inland flooding 305 Chang Geun Song
S3-5	Discharge calculation using surface velocity measured by surface image velocity meter 307 Youngsin Roh, Seo Jun Kim
S3-6	Prediction of long-term bed elevation change based on gate operations: For Geum River 309 Chang Sung Kim, Seong Jun Kim
S3-7	Prediction of bed elevation change according to weir open operations: For Nakdong River 311 Seong Jun Kim, Chang Sung Kim

Session S4

Smart Safety Management of River Facilities

S4-1	Utilization of ROV for safety inspection of underwater structures 314 Eun Sang Im
S4-2	River levee surface erosion mitigation using eco-friendly biopolymer-ased soil treatment (BPST) 316 Yeong-Man Kwon, Sojeong Lee, Ilhan Chang
S4-3	Development of an algorithm for outlier detection processing of water level data measured by ultrasonic sensor 318 Inhyeok Bae, Un Ji
S4-4	Study on advanced early warning system for dam safety measurements 320 Seong-Bae Jo, Eun-Sang Im, Kichun Kang, Sukmin Yoon
S4-5	Drone application for water infrastructure reality modeling 322 Dong Soon Park, Taemin Kim

Session S6

Technical Strategy for Quality Control of Hydrological Data and Advanced Toolkits for IWRM

S6-1	Study on driftwood generation and deposition patterns by tsunami flow using numerical simulation 326 Tae Un Kang, Chang-Lae Jang
S6-2	Probabilistic flood risk assessment in the downstream area of dam 328 Beomjin Kim, Byunghyun Kim, Kun-Yeun Han

S6-3	Analysis of riverbank erosion risks using an advanced DSS toolkit for Sesan and Srepok river basin in Vietnam 330
	Jeongkon Kim, Le Van Thin
S6-4	Cast study: smart water management technology for the development of new capital city of the Indonesia 332
	Sang Young Park, Jin Hyeog Park
S6-5	A practical application of hybrid flood modeling in river 334
	Wanshik Yu, Yonsu Kim, Sunghoon Kim, Jiyoung Jung, Joonwoo Noh

Session S8

Green Energy & ICT of Clean Water

S8-1	Heat source and sink trends for internet data center cooling system 338
	Kwesi Mensah, Selorm Kwaku Anka, Tae In Ohm, Jong Woong Choi, Yong Cho, Sung Hoon Chu, Han-Young Kim, Jong Min Choi
S8-2	Eco-friendly floating photovoltaic power plant of K-water 340
	Hyunsik Jo, Hyunjun Kim
S8-3	Development of AI-driven composite sensor to expand energy management system in water treatment plant 342
	Sang Byeong An, Sung Taek Hong, Kuk Il Kim, Jin Hoon Kim
S8-4	Seismic behavior analysis of an RTU panel with friction pendulum system by tri-axial shaking table tests 344
	Bub Gyu Jeon, Sung Wan Kim, Da Woon Yun, Woo-Yong Jung

Session S9

Multi-dimensional River Operation and Management Techniques

S9-1	Levee monitoring using mobile mapping system 348
	Jisang Lee, Hong-Gyoo Sohn
S9-2	Probabilistic mapping of flood risk using multivariate statistical model 350
	Min-Kyu Jung, Hyun-Han Kwon
S9-3	A study on life cycle management through the performance evaluation model of river facilities .. 352
	Sooyoung Kim, Hyung-Jun Kim, Boram Kim, Kwang Seok Yoon



S9-4	Geospatial analysis and model development for specific degradation of ungauged watersheds in South Korea using multiple regression analysis and data mining	354
	Woochul Kang, Eun-kyung Jang, Pierre Y. Julien	
S9-5	Vulnerability assessment of watershed water quality for flow conditions	356
	Woo Suk Jung, Sung Eun Kim, Jae Hyun Kwon, Young Do Kim	

Session S10 Research Overview of Environmental Hydraulics Laboratory in Seoul National University

S10-1	Dispersion coefficients for analysis of intermediate mixing in rivers	360
	Kyong Oh Baek, Dong Yoel Lee, Il Won Seo	
S10-2	Modeling of non-Fickian transport incorporating transient storage zones in natural rivers	362
	Byunguk Kim, Il Won Seo	
S10-3	Development and application of two-dimensional hydrodynamic model (HDM-2D) for river flow analysis	364
	Chang Geun Song, Il Won Seo	
S10-4	Development and application of two-dimensional contaminant transport model (CTM-2D) for water quality analysis in rivers	366
	Jun Song Kim, Il Won Seo	
S10-5	Prediction of river water quality using machine learning models	368
	Siyeon Kwon, Il Won Seo	

o Foreword

The 9th International Symposium on Environmental Hydraulics is held in Seoul, Korea from July 19 to 21, 2021. The main theme of the symposium is “Advances in Hydro-Environments for an Era of Big Change.” The symposium is part of the International Association for Hydro-Environment Engineering and Research (IAHR). The ISEH series started in 1991. Previous symposia have convened in Hong Kong, Singapore, Tempe, Arizona, and Notre Dame, Indiana. It is the premier research conference that focuses on all aspects of applied hydraulic flows, including atmosphere and oceans, in engineering and science. The 9th ISEH is held in a format of the hybrid conference, allowing for the attendees to join the symposium in person at the venue or online everywhere.

The symposium spans classical, advanced experimental and numerical approaches to recent applications of remote sensing and artificial intelligence. Experts and young talented researchers are able to actively share research ideas in the wonderful surroundings of the campus of the Seoul National University and also in the online platform. A total of 177 papers are presented in 21 general sessions and in 10 special sessions each of which highlights specific topics related to the recent advances in environmental hydraulics. Featured keynote speakers are: Professor Ian Guymer from the University of Sheffield, UK; Professor Jae-Hyeon Park from the K-water, South Korea; Professor Heidi Nepf from the Massachusetts Institute of Technology, USA; and Professor Pengzhi Lin from the Sichuan University, China.

This proceeding is a collection of the accepted abstracts that were submitted to the ISEH 2021. The proceeding present papers in 10 parts: 1) Keynote lectures; 2) Mixing and transport of sediment and pollutant; 3) Jets and plumes; 4) Stratified flows and gravity currents; 5) Interface of eco- & environmental hydraulics and river morphology; 6) Coastal and estuarine processes; 7) Experiments, field measurements and remote sensing; 8) Computational and numerical methods; 9) Big data and machine learning in environmental hydraulics; and 10) Special topics. Some selected papers are published as the technical articles in the international journals such as Journal of Hydro-environment Research.

Il Won Seo | Chairman of LOC

Jin Hwan Hwang | Scientific Committee of LOC

Yong Sung Park | Secretary General of LOC

Siyoon Kwon | Secretary of LOC



o Local Organizing Committee

Il Won Seo, Seoul National University (Chairman)
Sung-Uk Choi, Yonsei University (Vice-chairman)
Won Kim, Korea Institute of Civil Engineering and Building Technology (Vice-chairman)
Yong Sung Park, Seoul National University (Secretary General)
Jun Song Kim, Seoul National University (Secretary)
Byunguk Kim, Seoul National University (Secretary)
Jungkyu Ahn, Incheon National University
Kyung Oh Baek, Hankyong National University
Eun-Sung Chung, Seoul National University of Science and Technology
Kun-Yeun Han, Kyungpook National University
Jin Hwan Hwang, Seoul National University
Un Ji, Korea Institute of Civil Engineering and Building Technology
Chang-Si Kim, ISAN Corporation
Dongsu Kim, Dankook University
Sung Eun Kim, Seoul Institute
Young Do Kim, Myongji University
Kil Seong Lee, Seoul National University
Myung Eun Lee, Hyundai Engineering & Construction
Woo Seok Lee, K-water
Siwan Lyu, Changwon National University
Jungsun Oh, Korea Institute of Civil Engineering and Building Technology
Sang-Ho Oh, Changwon National University
Inhwan Park, Seoul National University of Science and Technology
Mun Hyun Park, Dongbu Engineering
Dong-Sop Rhee, Korea Institute of Civil Engineering and Building Technology
Sangyoung Son, Korea University
Chang Geun Song, Incheon National University
Kyung Duk Suh, Seoul National University
Hyoseop Woo, Gwangju Institute of Science and Technology
Woon Kwang Yeo, Myongji University

o International Scientific Committee

Fabian Bombardelli, University of California, Davis, USA

Peter Davies, University of Dundee, UK

Ian Guymer, University of Sheffield, UK

Blair Johnson, University of Texas, Austin, USA

Andrew Kennedy, University of Notre Dame, USA

Joong Hoon Kim, Korea University, Korea

A.W.K. Law, Nanyang Technological University, Singapore

Qihua Liang, Loughborough University, UK

Xiaofeng Liu, Penn State University, USA

Jonathan Nelson, US Geological Survey, USA

Van Thinh Nguyen, Seoul National University, Korea

Nimish Pujara, University of Wisconsin, USA

Michael Piasecki, The City University of New York, USA

Jose Rodriguez, University of Newcastle, Australia

Pawel Rowinski, Polish Academy of Science, Poland

Dragan Savic, University of Exeter, UK

John Z. Shi, Shanghai Jiao Tong University, China

Yasuyuki Shimizu, Hokkaido University, Japan

Scott Socolofsky, Texas A&M University, USA

Thorsten Stoesser, University College London, UK

Rafael Tinoco, University of Illinois, Urbana-Champaign, USA

Yusuke Uchiyama, Kobe University, Japan

Dominic Van der A, University of Aberdeen, UK

Zhan Wang, Chinese Academy of Sciences, China

Hyoseop Woo, Gwangju Institute of Science and Technology, Korea

**The 9th International
Symposium on
Environmental Hydraulics**

Keynote Speech



Ian Guymer - Keynote

Title:

Longitudinal Dispersion in the Natural Environment Exploring Contributing Components

Brief description:

The description and management of water quality in rivers, estuaries and the coastal environment, is essential for ecological and human well-being. Predicting the effects of management strategies requires a knowledge of the hydrodynamic processes covering spatial scales of a few millimetres (turbulence) to several hundred kilometres (catchments), with a similarly large range of timescales from milliseconds to months.

Predicting underlying water quality processes and their human and ecological impact is complicated as they are often dependent on contaminant concentrations. Current water quality modelling methods range from complex three-dimensional computational fluid dynamics models, for short time and small spatial scales, to one-dimensional (1D) time dependent models, critical for economic, fast, easy-to-use applications within highly complex situations in catchments.

Most 1D models employ the concepts of Taylor, originally derived for pipe flow, where the mixing effects in a uniform geometry can be represented with some confidence in highly turbulent, steady flows. These are used within the 1D advection-dispersion equation but estimating the longitudinal mixing coefficient in all, but the most straight forward case is a challenge.

This presentation will outline the basic processes and describe the physical mechanisms that contribute to the magnitude of an overall 1D longitudinal dispersion coefficient. It will explore and quantify some of the mechanisms associated with river and estuarine flows. An overview of results from field and laboratory studies will be presented: from estimating longitudinal dispersion based on catchment characteristics; the effects of channel curvature and compound channel cross-sections; through patchy vegetation and hyporheic effects, to tidal and density effects in estuarine flows.

Ian Guymer
23rd June 2021

Initiatives for Water Resources Management considering Korea's Natural Restoration of Rivers

Park, Jae-Hyeon

CEO, K-water

*Corresponding: jhparkkwater@kwater.or.kr

Abstract

In today's climate uncertainty, natural restoration of rivers is an important task that all mankind must pursue in order to preserve sustainable rivers for the future generations. It is not simply a return or restoration to some point, but it is an enabler for river ecosystem to adjust or adapt itself, and find their natural states through their own resilience. In this regard, integrated water resources management considering entire water cycle from upstream to estuary is essential. Korea has been implementing integrated water management such as natural restorations of rivers and estuary brackish water zones. Based on the experiences of the past, visions for water resources management in the future will be shared.

Keywords: Rivers; Natural Restoration; Connectivity; Estuary; Water Resources Management

Natural Restoration of Rivers and Water Resources Management

Rivers are not simply a space where water flows but a passageway that connects all ecosystems from the upstream mountains to the downstream estuaries. The recent river management paradigms lead active discussions on river management policy based on sustainability of rivers such as climate change adaptation on water management, integrated water resources management and the natural restoration of rivers.

Rapid industrialization and development threaten the sustainability of rivers by altering their natural states. Therefore, natural restoration of rivers is necessary in order to preserve sustainable rivers and convey their value and prosperity to the future generations. Restoration of rivers is an enabler for river ecosystem to adjust or adapt itself, and find their natural states by enhancing their own resilience. The natural states of rivers are dynamic from every direction--clean water flows in the rivers without drying out, and they are also a home to various living organisms. Moreover, rivers are a living ground for both mankind and nature as with harmonious use of humans.

Considering the natural restoration of rivers, the Framework Act on Water Management of Korea stipulates that the impact on the water environment should be minimized when implementing national water resources management policies. In May 2020, the Korean Government devised a blueprint (Basic Concept) for the natural restoration of rivers with its vision of "Our Rivers where People and Nature Live in Harmony".

There are 12 strategies in the Basic Concept to achieve Rivers which Come to Life; Rivers which Clean Water Flows; Rivers in which Life Breathes; and Rivers in which (We) Live Together. With this Basic Concept, detailed plans for each watershed unit will be developed this year, and the plans would be included in the national/watershed water resources management plans so that its implementation can be ensured.

Restoration of Estuary Brackish Water Zone and Water Resources Management

Brackish water zones (Estuaries) complete water cycle by connecting rivers and oceans, and they have the highest productivity in the world. However, the water zones are an extreme environment that experiences complicated environmental stresses such as abnormal droughts and floods, sea level rise and changes in marine environment by climate variability; increase in coastal disasters; impacts of water management and human activities. Korea as well as other countries faces these problems, and active discussions are ongoing for estuary management based on land/ocean continuity in the recent ten years. The Netherlands is attempting to restore brackish waters through opening estuaries, and New Orleans (US) built a new estuary system with a big budget to respond to hurricane damage and sea level rise.

Rivers are not simply a space where water flows but a passageway that connects all ecosystems from the upstream mountains to the downstream estuaries. River management paradigms are shifting to water resources management based on sustainability and connectivity. In Korea, Numerous efforts have been made for integrated water resources management and the natural restoration of land/ocean continuity.

The natural restoration of Sihwa Lake is a phenomenal success story of estuary restoration and renewable energy development. Moreover, Gyeongin Ara Waterway represents waterway management techniques in estuaries. Currently, opening the gates on Nakdong River Estuary Barrage is at the implementation stage--allowing seawater inflow and estuary brackish water restoration. This could be another success story of estuary management and brackish water restoration, which is unprecedented in the world.

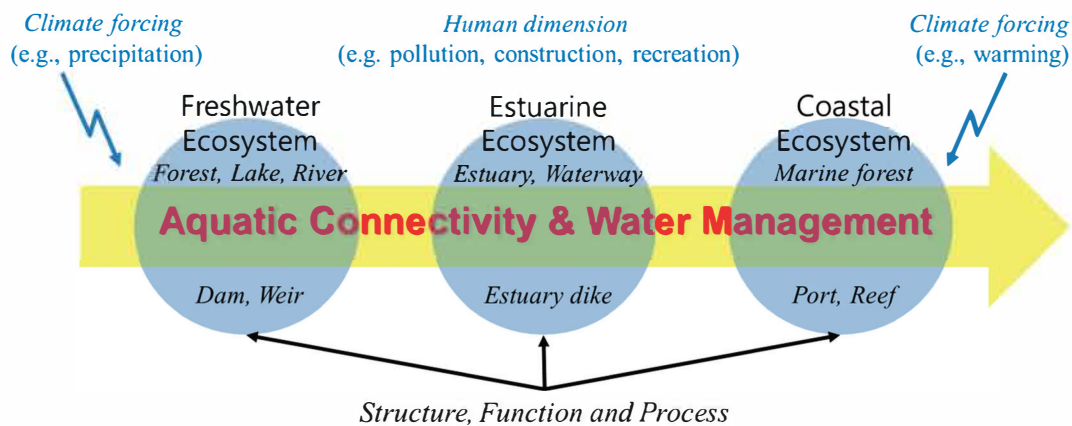


Fig. 1. River Connectivity from upstream to estuary for water resources management

Conclusions

The time has come to change the perception of rivers--it is not just an object of use, but a natural object where water flows. From now on, for the coexistence of people and nature, we should respect natural orders and pursue the functional harmony between water use and flood control, and rivers should be passed down to the future generations.

Integrated water resources management from upstream to estuary is a natural water resources management considering water cycle. It is also the most basic and leading water resources management for sustainable life with harmonizing people and estuary environment. Korea and K-water will continue our efforts to achieve this.

Vegetation Hydrodynamics for Climate Mitigation and Adaptation

Heidi Nepf¹

¹Department of Civil & Environmental Engineering,
Massachusetts Institute of Technology, Cambridge, MA USA

*Corresponding: hmnepf@mit.edu

Abstract

Coastal ecosystems, such as seagrass, provide many ecosystem services, including coastal protection and carbon sequestration. Because of this, coastal vegetation is considered an integral part of climate mitigation and adaptation. Predicting the value of these ecosystems with regard to coastal protection and/or carbon credit requires models for the interaction of fluid motion with flexible vegetation. This talk describes scaling laws that predict the drag on individual plants, and the extension of these laws to predict wave decay over a meadow of plants. For flexible plants, reconfiguration and drag are functions of the Cauchy number (ratio of hydrodynamic drag and the restoring force due to plant rigidity) and the ratio of wave excursion to plant height. Combining with other models, the prediction of wave dissipation can be used to estimate the minimum meadow length-scale needed to eliminate wave-driven sediment resuspension, a metric for restoration success and carbon retention.

Keywords: Wave dissipation; Coastal Vegetation Hydrodynamics;

Introduction

Seagrasses are coastal plants found throughout the world. They improve water quality and provide habitat that maintains biodiversity and, in particular, nursery habitat for economically important fish (Orth et al., 2006). They also reduce erosion associated with storms and waves (Arkema 2003). In addition, seagrass meadows sequester twice as much organic carbon per hectare as terrestrial soils (Fourqurean et al., 2012). Each of these ecosystem services is enhanced by the dissipation of wave energy provided by a meadow of seagrass, which creates low energy niches that reduce wave-driven resuspension and provide quiescent nursery habitat. By improving the prediction of wave dissipation by seagrass meadows, the valuation and restoration of these habitats can be improved.

Theory

Assuming linear waves and that only vegetation drag contributes to wave energy dissipation, the decay of waves across a meadow of vegetation can be represented as

$$\frac{a_w(x)}{a_{w,0}} = \frac{1}{1 + K_D a_{w,0} x} \quad \#(1)$$

in which $a_{w,0}$ is the wave amplitude at the leading edge of the meadow, and the wave damping coefficient K_D is

$$K_D = \frac{2}{9\pi} C_D n_b w_b k \frac{9 \sinh(kl) + \sinh(3kl)}{\sinh(kH) (\sinh(2kH) + 2kH)} \quad \#(2)$$

in which k is the wave number, H is the water depth, n_b is the number of blades per bed area, each of width w_b , and l is the height of the meadow, assumed to be rigid and stationary (Dalrymple et al. 1984). In fact, since seagrass blades are flexible, they bend and

move with the waves (called reconfiguration). To account for this, Eqn. 2 can be modified by replacing l with an effective meadow height, $l_{e,m,w}$, defined as the height of rigid meadow that produces the same drag as a flexible meadow of height l . Specifically, from scaling rules inferred from the balance of drag and blade rigidity (Lei and Nepf 2019)

$$l_{e,m,w} = \underbrace{1.1(Ca_w L)_b^{-1/4} l_b}_{\text{effective blade length.}} + \underbrace{l_r}_{\text{rigid sheath}} \quad \#(3)$$

Here, l_r is the sheath, the rigid portion of a real seagrass shoot that connects the blades to the below ground rhizome. The degree of reconfiguration and drag reduction in the flexible part of the shoot (blades) is described by the Cauchy number, which represents the ratio of hydrodynamic drag to restoring force due to stiffness,

$$Ca_w = \frac{1}{2} \frac{\rho C_{D,w} w_b U_w^2 l_b^3}{EI} \quad \#(4)$$

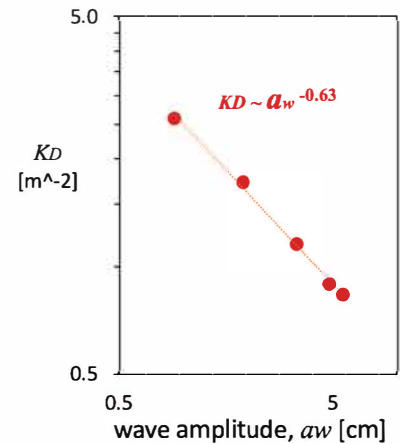
and the length ratio L , which compares the blade length l_b to wave excursion $A_w = U_w/\sigma$, in which $\sigma = 2\pi/T$ is the wave angular frequency.

$$L = \frac{2\pi l_b}{U_w T} \quad \#(5)$$

t_b is blade thickness, T is wave period, g is acceleration due to gravity, ρ is density of water, E is Young's modulus of elasticity, and $I = w_b t_b^3/12$ is the bending moment.

Results

The reconfiguration of the flexible seagrass blades increases as the wave forcing increases. As a result, the wave dissipation coefficient, K_D decreases as wave amplitude increases. The theory predicts a power dependence consistent with the observed trend (symbols). Once validated, the wave dissipation model can be used to estimate the minimum meadow length-scale needed to eliminate wave-driven sediment resuspension, a metric for restoration success and carbon retention.



Acknowledgement

This study received support from the US National Science Foundation, Grant 1659923. Any conclusions or recommendations expressed in this material do not necessarily reflect the views of the National Science Foundation.

References

- Arkema, K.K., et al., (2013) "Coastal habitats shield people and property from sea-level rise and storms," *Nature Climate Change*, 3, 913-920.
- Dalrymple, R. A., Kirby, J. T., & Hwang, P. A. (1984). Wave diffraction due to areas of energy-dissipation. *Journal of Waterway, Port, Coastal, and Ocean Engineering*, 110(1), 67-79.
- Fourqurean, J. et al. (2012). Seagrass ecosystems as a globally significant carbon stock. *Nature Geoscience*, 5(7), 505-509. <https://doi.org/10.1038/ngeo1477>.
- Orth, R. et al. (2006). A Global Crisis for Seagrass Ecosystems. *BioScience*, 56(12), 987. [https://doi.org/10.1641/0006-3568\(2006\)56\[987:agcfse\]2.0.co2](https://doi.org/10.1641/0006-3568(2006)56[987:agcfse]2.0.co2)

Experimental and numerical study of wave attenuation by live *Phragmites australis*

Zhengyu Hu¹, Huiran Liu², He Liu², Fang He¹ and Pengzhi Lin^{2*}

¹Ocean College, Zhejiang University

²State Key Laboratory of Hydraulics and Mountain River Development and Protection, Sichuan University

*Corresponding: cvelinpz@scu.edu.cn

Abstract

Various types of wetland vegetation are widely distributed in coastal region and they can serve as a natural barrier to wave action and wave induced erosion. In this study we conducted laboratory experiments in a large wave flume by using live *Phragmites australis*. The wave height variation, plant movement, and flow turbulence in the vegetation domain were measured and analyzed. A 3D fluid-structure interaction model, CgLes-Y code, was employed to simulate the individual stem movement under wave action and the simulation results were compared to the measurements. The 3D flow and vorticity structure around the stem is further investigated to understand the coupled motion of the flexible vegetation in a wave field. A 2D RANS model NEWFLUME was employed to study the wave damping by the vegetation. Specifically, the profiles of mean velocity and turbulence kinetic energy were simulated and compared to the measured data. The focus of the study was at the effect of plant reconfiguration during wave passages on the wave energy dissipation and wave height damping.

Keywords: Wave damping; Live vegetation; Turbulence; Stem reconfiguration

Introduction

Wetland vegetation plays a vital role in coastal ecosystem. The dynamics of flexible vegetation induced by waves can affect the local flow field, drag force, and wave energy dissipation. The nutrient and carbon cycling and sediment transport were strongly linked to flow structures within the vegetation domain. As most of the previous studied were either in field without detailed flow measurement or in laboratory using small-scale model vegetation, the flow dynamics around real vegetation, especially the flexible type such as live *Phragmites australis*, was poorly understood. Moreover, although the wave attenuation and turbulence mixing within the vegetation were investigated extensively, few models have been validated against measured turbulence kinetic energy in flexible vegetation domain.

Methods

As shown in Fig. 1, the experiments were carried out in a 75.0 m long, 1.8 m wide, and 2.0 m deep large-scale wave flume at Zhejiang University, China. The live *Phragmites australis* was transplanted from the west coast of Zhoushan, China to the flume.

To simulate FSI problem, the in-house CFD code called CgLes-Y code was adopted, where Y code is a solid solver for deformable structures (Munjiza,

2004). The immersion boundary method (IBM) is applied to calculating structural force on fluid.

To study the wave attenuation and turbulent mixing in vegetation, the RANS model NEWFLUME (Lin, 2008) that was based on the double-averaged Navier-Stokes equations, was employed:

- (1)
(2)

The double-averaged Reynolds shear stress was closed by a modified k-ε model.

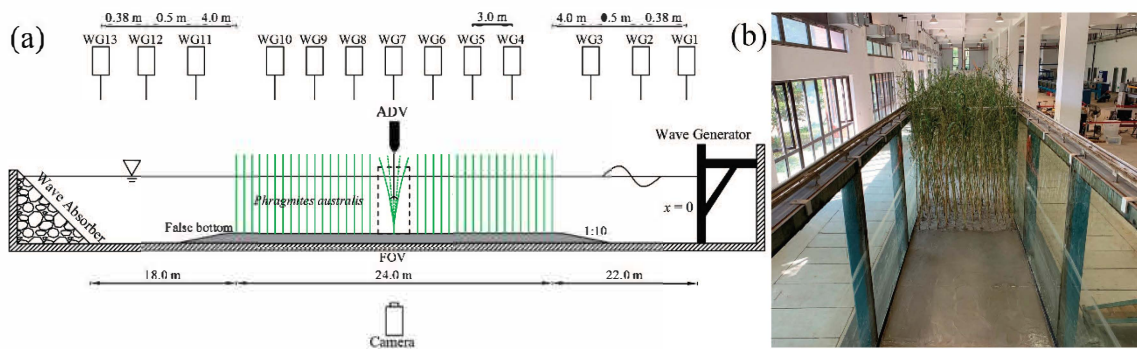


Fig. 1. (a) Sketch of the experimental setup (not drawn in scale) and (b) planted vegetation in the flume.

Results

In Fig. 2(a), It is clear that the waves can be attenuated by the vegetation. From Fig. 2(b) and Fig. 2(c), the root-mean-square (RMS) wave velocity and turbulence kinetic energy gradually increase from the bottom to the water surface. The numerical results agreed well with the experimental results. Fig. 2(d) shows the vorticity field and deformation of a vegetation stem, as simulated by CgLes-Y code.

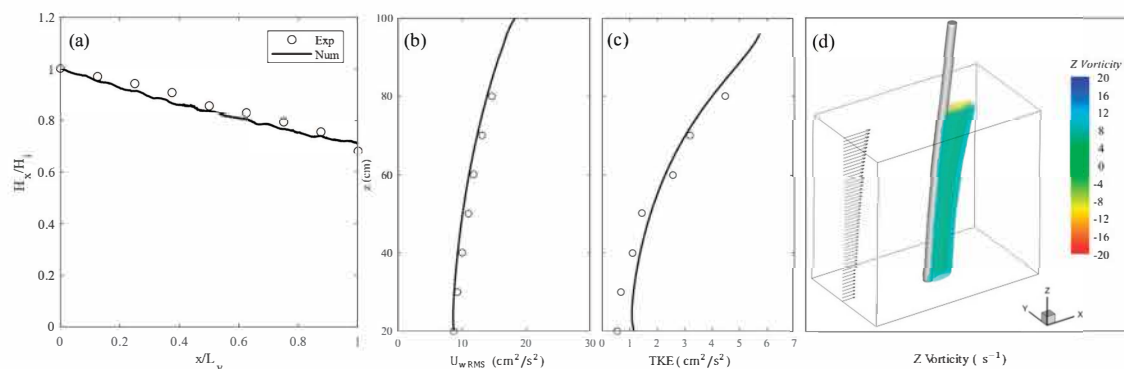


Fig. 2. (a) Wave height variation along vegetation, (b) profile of RMS wave orbital velocity, (c) profile of turbulence kinetic energy, and (d) simulated vorticity field and deformation of a flexible stem.

Conclusions

In this study, the wave energy dissipation, flow and turbulence, and plant dynamics within live *Phragmites australis* subjected to waves were investigated.

The numerical results of plant reconfiguration, wave damping, mean velocity, and turbulence agreed well with the measured data. It was found that the wave-induced stem motion is significant when the wave height and period are large, which resulted in drag reduction. However, the stem flexibility effect on wave height decay is only essential when the stem movement exceeds certain threshold.

Acknowledgement (If necessary)

This work is supported by the Key Program of Natural Science Foundation of China (52031002) and the Natural Science Foundation of China for Outstanding Young Scholars (52022092).

References

- Lin, P. (2008). Numerical Modeling of Water Waves. Taylor & Francis, Co.
- Munjiza, A. (2004). The Combined Finite-Discrete Element Method: Munjiza/Discrete Element Method. John Wiley & Sons, Ltd, Chichester, UK.

**The 9th International
Symposium on
Environmental Hydraulics**

A1 Session

Dispersion [A1-M2]



Simulation of the Near-field Mass Transport Processes through a Fishing Net Panel using OpenFOAM

Xinyue Yang¹, Carlo Gualtieri² and Dongdong Shao^{1,3*}

¹State Key Laboratory of Water Environment Simulation & School of Environment,
Beijing Normal University, China

²Department of Civil, Architectural and Environmental Engineering, University of Naples Federico II,
Napoli 80125, Italy

³Tang Scholar, Beijing Normal University, China

* Corresponding: Dongdong Shao (ddshao@bnu.edu.cn)

Abstract

A numerical model was established using OpenFOAM to investigate the wake characteristics and near field mass transport processes through a fishing net panel with different net solidities and incoming velocities. In this model, the net was treated as porous media, and the finite volume method was applied to solve the governing equations together with the standard κ - ε model for turbulence closure. Previous experimental data obtained using PIV-PLF was further used to calibrate and validate the model. The numerical results demonstrated that the porous media schematization could reproduce the blocking effect of the net on the mean flow field and the associated scalar transport with reasonable accuracy.

Keywords: Fishing net panel; Near field; Mass transport processes; Standard κ - ε model; OpenFOAM

Introduction

The associated near-field mass transport in the presence of fishing cages is rather complex (Suzuki et al., 2003). As a key component of fish cages, a net panel is a kind of porous and highly flexible structure. The flow field around the fishing net panel is dependent on a variety of factors including the net inclination angles, incoming velocities, net solidities, etc. Shao et al. (2020) found that the magnitude of the incoming velocity tends to affect the flow-velocity reduction factor U/U_0 more significantly than the net solidity in the near-field in their flume experiments. As far as we are aware, numerical studies on the near-field mass transport process through a fishing net panel are still lacking.

Methods

The numerical domain was 6 m long, 0.8 m wide and 0.3 m high. Uniform hexahedron cells were generated using mesh generator blockMesh, resulting in 4×10^6 cells (500×200×40). A user-defined solver passiveScalarPisoFoam was developed to simulate the velocity field and concentration field, which was established by adding the passive scalar transport equation in scalarTransportantFoam solver to pisoFoam solver. Turbulence was modelled with the standard k - ε model. All simulation scenarios are documented in Table 1. The numerical model was calibrated and validated against the experimental cases N2 and N1, respectively, reported in Shao et al. (2020).

Table 1. Parameters of OpenFOAM simulation cases

No.	Incoming velocity U_0 (m/s)	Turbulent kinetic energy	Turbulence dissipation rate ε	Net solidity S (%)	Porous resistance coefficient C_n	Time step Δt	Simulation time T (s)
-----	----------------------------------	--------------------------	---	-------------------------	-------------------------------------	-------------------------	----------------------------

		k (m^2/s^2)	(m^2/s^3)		(m^{-1})		
X1(N1)	0.142	5.39E-05	3.09E-06	19.0	9.8	0.02	50
X2(N2)	0.29	1.88E-04	2.01E-05	19.0	9.8	0.02	40
X3	0.5	4.88E-04	8.41E-05	19.0	9.8	0.01	30
X4	0.142	5.39E-05	3.09E-06	36.0	27.4	0.02	50
X5	0.5	4.88E-04	8.41E-05	9.8	3.4	0.01	30

Results

Among the cases with constant incoming velocity but varying net solidity, i.e. X1 versus X4 and X3 versus X5, the flow velocity reduction factor tends to increase with decreasing net solidity, whereas scalar concentration decay tends to increase with increasing net solidity. Among the cases with constant net solidity but varying incoming velocity, i.e., X1, X2 and X3, the flow velocity reduction factor tends to increase with increasing incoming velocity, whereas scalar concentration decay tends to decrease with increasing incoming velocity.

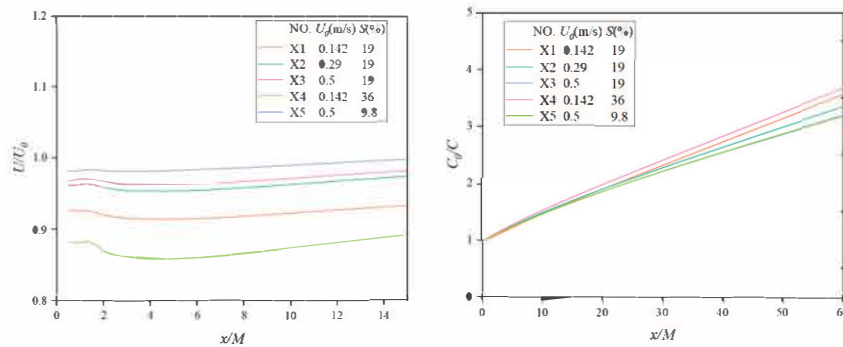


Fig. 1. (a) The flow-velocity reduction factor U/U_0 and (b) the scalar concentration decay C_0/C at different downstream locations.

Conclusions

The numerical results demonstrated that the porous media schematization could reflect the blocking effect of the net on the mean flow field. The flow velocity reduction factor showed a negative correlation with the net solidity and a positive correlation with the incoming velocity. At the same time, complete recovery of incoming velocity was observed to occur within the downstream extent of numerical measurements. The lateral profile of the scalar concentration still exhibited self-similarity and followed Gaussian. The incoming velocity had a more significant effect on the plume width than the net solidity, and the spreading of plume width was reduced with increasing incoming velocity.

Acknowledgement (If necessary)

This work was supported by the National Natural Science Foundation of China (Grant No. 51779012), National Key Research and Development Program of China (Grant No. 2018YFC1406404) and Interdisciplinary Research Funds of Beijing Normal University.

References

- Suzuki K, Takagi T, Shimizu T, Hiraishi T, Yamamoto K, Nashimoto K. (2010). Validity and visualization of a numerical model used to determine dynamic configurations of fishing nets. *Fisheries Science*, 69(4): 695-705.
- Shao, D. D., Huang L., Wang, R.Q., Gualtieri C, Cuthbertson A. (2021). Flow Turbulence Characteristics and Mass Transport in the near-Wake Region of an Aquaculture Cage Net Panel. *Water* 13, no. 3.

Mixing Characteristics of River Confluence using Water Quality Indicator in slow flow conditions

Geunsoo Son¹, Dongsu Kim^{1*}, Siwan Lyu², Young Do Kim³

¹ Dankook University, Yongin-si, Gyeonggi-do, South Korea

² Changwon National University, Changwon, Gyeongsangnam-do, South Korea

³ Myongji University, Yongin-si, Gyeonggi-do, South Korea

* Corresponding: dongsu-kim@dankook.ac.kr

Keywords: Confluence; Mixing; Electronic Conductivity; ADCP; Shear layer; Secondary flow

Abstract

The confluences of rivers are critical areas where tributaries meet with the main stream and the hydraulic and water quality characteristics are changed. Recently, many studies have analyzed the hydrodynamic mixing behaviors of confluences in real rivers using measurement equipment such as acoustic Doppler current profiler (ADCP). However, existing studies mostly focused on confluences of small and medium-sized rivers where there is a flow velocity. Furthermore, existing studies mostly considered the topographical characteristics of confluences using hydrodynamics and very few studies have been analyzed the water quality mixing behaviors of the confluences. Therefore, this study analyzed the mixing behaviors of tributaries that flow in the main stream of a large river that has a very large flow rate and a low flow velocity compared to those of tributaries using hydrodynamics and water quality characteristics. For hydrodynamics, the depth-averaged flow velocity distribution and secondary flow were analyzed using an ADCP. For water quality characteristics, the mixing behavior of confluence was analyzed using the electronic conductivity (EC) of the YSI as water quality indicator. The analysis results showed that the hydrodynamics using the exiting ADCP had limitations in analyzing the mixing behaviors in slow large rivers as in this study. When the mixing behaviors were analyzed in connection with a water quality indicator (EC), the results indicated that it was possible to analyze the mixing behaviors of slow large rivers like the river investigated in this study. Therefore, this study verified the possibility of analyzing the mixing behavior of confluence in slow large rivers by linking the hydrodynamics such as flow velocity distribution with a water quality indicator (EC).

Improving an Observation Method on Pollutant Dispersion for Analysis of Two-dimensional River Mixing

Donghae Baek^{1*} and Il Won Seo²

¹Korea Institute of Civil Engineering and Building Technology

²Department of Civil & Environmental Engineering, Seoul National University

* Corresponding: wes1204@snu.ac.kr

Keywords: depth-averaged transport modeling; shear dispersion; routing procedure; 2D tracer test

Abstract

The depth-averaged two-dimensional (2D) advection-dispersion equation (ADE) has been widely used to analyze the mixing phenomenon of the various dissolved and suspended matters in river systems. The 2D stream-tube routing procedure (2D STRP) has been the only method to calculate both longitudinal and transverse dispersion coefficients of 2D ADE simultaneously for the transient concentration conditions. In this study, the limitations of 2D STRP were quantitatively analyzed using the hypothetically generated data. Besides, the new routing-based observation method (2D STRP-i) and the remote sensing-based experimental framework for tracer tests were developed to overcome the limitations of existing determination methods for dispersion coefficients. The results showed that the longitudinal dispersion coefficients were similarly determined by both 2D STRP and STRP-i, while the existing 2D STRP generally underestimated the values of transverse dispersion coefficients compared to the results of 2D STRP-i.

Introduction

The depth-averaged two-dimensional (2D) advection-dispersion equation (ADE) has been widely used to analyze the mixing phenomenon of the various dissolved and suspended matters in river systems. In depth-averaged 2D ADE, dispersion coefficients are essential parameters to explain the spreading of pollutant clouds, caused by complexities of flow structures and river environments. The dispersion coefficients in 2D ADE can be calculated by the routing based-observation methods using the tracer test data. The 2D stream-tube routing procedure (2D STRP) has been the only method to calculate both longitudinal and transverse dispersion coefficients of 2D ADE simultaneously for the transient concentration conditions. In this study, the limitations of 2D STRP were quantitatively analyzed using the hypothetically generated data. Besides, the new routing-based observation method (2D STRP-i) and the remote sensing-based experimental framework for tracer tests were developed to overcome the limitations of existing determination methods for dispersion coefficients.

Methods

The performance of existing 2D STRP was evaluated in terms of the variation of Peclet number, and the spatially varied velocity distributions. The results of the evaluations showed that the existing 2D STRP well provided the temporal distribution of tracer concentration in the high Peclet number, but it could not reproduce the reliable results when the tracer clouds reached wall boundaries and the Peclet number decreased. Thus, the new routing-based observation method (2D STRP-i), as shown in Eq. (1), was developed to improve the drawback of the existing method. The 2D STRP-i derived from the 2D ADE in the orthogonal curvilinear

coordinate system, assuming the steady-state flow condition.

$$C(X_2, q, t) = \int_{\omega=0}^Q \int_{\tau=-\infty}^{\infty} \frac{C(X_1, \omega, \tau) U_{ST}}{4\pi(\bar{t}_2 - \bar{t}_1) \sqrt{S_L S_T}} \exp\left(\frac{[X_2 - X_1 - U_{ST}(t - \tau)]^2}{4D_L(\bar{t}_2 - \bar{t}_1)}\right) \cdot \sum_{m=-\infty}^{\infty} \left[\exp\left(\frac{-(q - 2mQ - \omega)^2}{4S_T(\bar{t}_2 - \bar{t}_1)}\right) + \exp\left(\frac{-(q - 2mQ + \omega)^2}{4S_T(\bar{t}_2 - \bar{t}_1)}\right) \right] d\tau d\omega \quad (1)$$

Results

2D STRP-i could adequately reproduce the reliable temporal distribution even if the effect of wall boundary was significant. The 2D STRP-i was applied to the remotely measured tracer data to calculate the dispersion coefficients. The Latin Hypercube Simulation was adopted to determine the optimum values of dispersion coefficients. The results of simulations showed that the RMSE distributions were non-convex with many local minima. In addition, the optimal dispersion coefficients were differently found according to the evaluation functions.

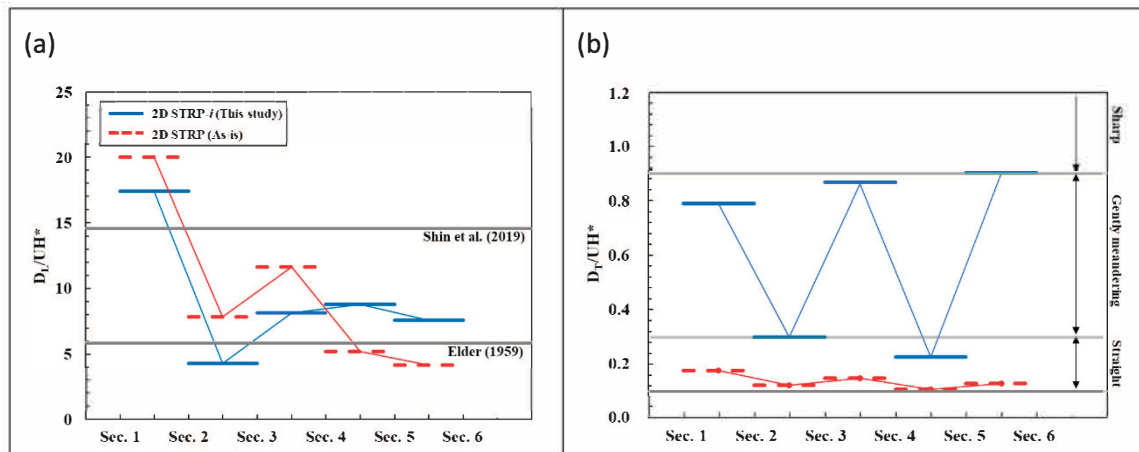


Fig. 1. The results of 2D STRP and 2D STRP-i for both (a) longitudinal and (b) transverse dispersion coefficients

Conclusions

In this study, multiple evaluation indices were selected to determine the dispersion coefficients more robustly. The results showed that the longitudinal dispersion coefficients were similarly determined by both 2D STRP and STRP-i, while the existing 2D STRP generally underestimated the values of transverse dispersion coefficients compared to the results of 2D STRP-i.

Acknowledgment

This work is supported by the Korea Agency for Infrastructure Technology Advancement(KAIA) grant funded by the Ministry of Land, Infrastructure and Transport (Grant 20DPIW-C153746-02).

Investigation of Pollutant Transport at Upstream of Notch Installed Weir

Sung Hyun Jung¹ and Il Won Seo^{1*}

¹ Department of Civil & Environmental Engineering, Seoul National University

* Corresponding: seoilwon@snu.ac.kr

Abstract

Notch installed weir causes flow deflection at the upstream of the weir and generates stagnation zones at both sides of the banks and between the notches. To analyze the storage mechanism according to the change of notch geometries, hydraulic experiments and numerical simulations are conducted in this study. The flow structure and concentration field in a wide area were measured using LSPIV (Large Scale Particle-Image-Velocimetry) and PCA (Planar-Concentration-Analysis) method. From the results, it is found that the storage zone area is increased as the distance between the notches increased, and the residence time of the pollutant in the storage zone also increased.

Keywords: Pollutant mixing, Notched weir, Storage zone model

Introduction

Understanding of pollutant mixing in rivers is important for water resource management and safe water supply. Factors influencing the mixing behavior of pollutants introduced into rivers are diverse, but studies of pollutant stagnation phenomenon due to storage zone caused by hydraulic structures are still insufficient. Especially, over 33,000 water intake weirs are installed in Korea, and most of the weirs are constructed for agricultural water intake purpose. At these weirs for irrigation purposes, most structures contain more than one notch at the weir crest. This notch shape causes flow deflection at the upstream of the weir and generates stagnation zones at both sides of the banks and between the notches.

Methods

When pollutant stagnation occurs due to the storage zone, the pollutant cloud is trapped in the storage zone, and therefore concentration distributions show the skewed distribution. To interpret these non-Fickian mixing problems, the storage zone model is suggested by many researchers.

$$\frac{\partial \bar{C}_f}{\partial t} + U_f \frac{\partial \bar{C}_f}{\partial x} - K_f \frac{\partial^2 \bar{C}_f}{\partial x^2} = \varepsilon_s T^{-1} (\bar{C}_s - \bar{C}_f) \quad (1)$$

$$\frac{\partial \bar{C}_s}{\partial t} = T^{-1} (\bar{C}_f - \bar{C}_s) \quad (2)$$

where \bar{C}_f is the spatial averaged concentration of the main flow zone; U_f is the spatial averaged velocity of the flow zone; K_f is the one-dimensional longitudinal dispersion coefficient of the main flow zone; ε_s is the ratio of storage zone area to the main flow zone area; \bar{C}_s is the spatial averaged concentration of the storage zone; T is the residence time of the cross-sectional area of the storage zone.

The main parameters of the storage zone model are the area of the storage zone and the mass exchange coefficient. To analyze the influence of weir notch geometries and flow characteristics on the storage mechanism, a hydraulic experiment and numerical simulation are

conducted.

The laboratory experiments were conducted using the surface LSPIV system to measure the horizontal mean flow characteristics in large areas, and Planar-Concentration-Analysis system was applied to measure the concentration change in the storage zone. The storage zone area was delineated from the flow velocity magnitude, and the mass exchange coefficient was calculated from the measured spatial-averaged concentration data in the storage zone. For numerical simulation, the three-dimensional (3D) Reynolds-averaged Navier-Stokes (RANS) model was applied to extend the geometric and hydraulic conditions change in a wider range.

Results

The velocity fields showed separation of the main flow in different transverse directions at the front of the notched weir. Low-flow regions were generated between the notches, and peak velocity was observed at the center of the notches. The concentration field in the storage zone showed that the tracer cloud moved to the notches of the weir and showed different retention time at the storage zone depending on the notch geometric and hydraulic conditions. The retention time of the tracer increased as the distance between notches and the height of the notch increased, and flow discharge decreased, resulting in smaller values of the mass exchange coefficient k_e . Both Fr and Re showed positive correlations with the exchange coefficient, while both parameters were insensitive to the size of the storage zone area.

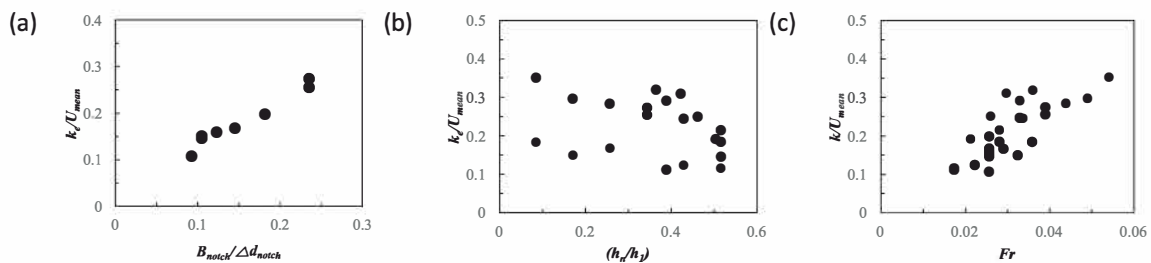


Fig. 1. Relationship between mass exchange coefficient and (a) distance between notches (b) weir height (c) Froude number

Conclusions

The influence of notched weir geometries and hydraulic parameters on the storage mechanism was revealed through experiments and numerical simulations. The size of the storage zone area increased as the distance between notches increased, while the storage zone area was insensitive to notch height for all cases. The retention time becomes longer as the distance between notches and notch height increased and as flow discharge decreased, which caused smaller values of the mass exchange coefficient. Both Fr and Re were positively correlated with the exchange coefficient but insensitive to the storage zone area.

Acknowledgement (If necessary)

This work is supported by the Korea Agency for Infrastructure Technology Advancement(KAIA) grant funded by the Ministry of Land, Infrastructure and Transport (Grant 20DPIW-C153746-02).

References

Bencala, K. E. and Walters, R. A. (1983). "Simulation of solute transport in a mountain pool-and-riffle stream: a transient storage model." *Water Resources Research*, Vol. 19, No. 3, pp. 718-724.

Non-Fickian transport induced by horizontal flow recirculation in in meandering open channels

Jun Song Kim¹, Il Won Seo^{1*}, and Donghae Baek¹

¹Department of Civil & Environmental Engineering, Seoul National University

*Corresponding: seoilwon@snu.ac.kr

Abstract

River meander induces complex three-dimensional (3D) flow behaviors including secondary flows and horizontal recirculating flows. This study conducts 3D numerical simulations in meandering open channels by controlling channel sinuosity to explore its impact on flow and solute transport. The sinuosity above 1.5 results in the emergence of horizontal recirculation zones near the outer banks, and the recirculation zones expand with increasing channel sinuosity. We quantify recirculating flow-induced Non-Fickian transport by measuring the tail power-law slope and truncated time of BTCs both changing remarkably with the onset of the recirculation zones. These results demonstrate that the recirculating flow works as a key driver of Non-Fickian transport in meandering rivers.

Keywords: Non-Fickian transport; River; Meander; Flow recirculation; Secondary flow

Introduction

A meander is one of the important features of rivers, generating complex flow behaviors such as secondary flows and recirculating flows (Shiono and Muto, 1998). The secondary flows promote transverse solute mixing, and the horizontal flow recirculation delay transport via trapping effect. The intricate interplay between the secondary flow and recirculating flow induces Non-Fickian transport manifested by anomalously long tails of breakthrough curves (BTCs). The late-time BTC tailing caused by the channel meander is often observed in field tracer tests in a sharply curved river (Seo et al., 2016). Despite the notable impact of the flow recirculation on contaminant transport in rivers, the detailed effects of the meander-driven recirculation zones on transport remain largely unknown.

Methods

In this study, we first generate six meandering channels that have a wide range of channel sinuosity from 1.03 to 2.42, as shown in Table 1.

Table 1. Geometric parameters of meandering channels for study cases.

Case	Depth (m)	Aspect ratio	Radius to width ratio	Sinuosity
SN103			8.00	1.03
SN111			4.00	1.11
SN136	0.115	20.3	2.40	1.36
SN157			2.00	1.57
SN190			1.71	1.90
SN242			1.50	2.42

We then resolve flow properties of the generated meandering channels using a 3D RANS solver integrated with the SST $k-\omega$ turbulence model available in OpenFOAM library, an open-source CFD code that solves Navier-Stokes equations via a finite volume method. The governing equations are 3D continuity and momentum equations in tensor notation, described as:

$$\frac{\partial U_i}{\partial x_i} = 0 \quad (1)$$

$$\frac{\partial U_i}{\partial t} + U_j \frac{\partial U_i}{\partial x_j} = -\frac{1}{\rho} \frac{\partial P}{\partial x_i} + \frac{\partial}{\partial x_j} \left[\nu \left(\frac{\partial U_i}{\partial x_j} + \frac{\partial U_j}{\partial x_i} \right) \right] - \frac{\partial}{\partial x_j} \overline{u_i u_j} \quad (2)$$

where the Reynolds decomposition term is solved by a SST $k-\omega$ turbulence model. With the simulated velocity and turbulence fields, we simulate solute transport using a 3D stochastic Lagrangian particle-tracking method.

Results

The flow simulation results show that the sinuosity larger than 1.5 exhibits the onset of horizontal recirculation zones near the apex of outer banks, and the area of recirculation zones increases with an increase in channel sinuosity. As shown in Fig. 1, the transport simulations reveal that the tail power-law slopes and truncated times change significantly with the emergence of the recirculating flow. Both BTC parameters present two regimes and increase remarkably when recirculation zones emerge.

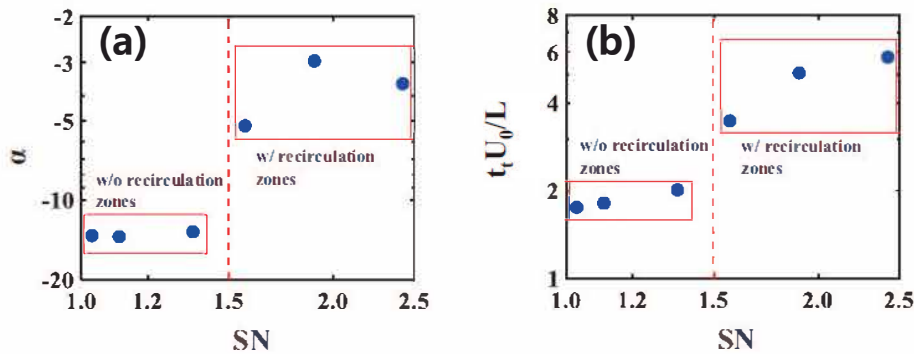


Fig. 1. Relationship between channel sinuosity and (a) power-law slope and (b) truncation time of BTCs.

Conclusions

The results of this study show that the sinuosity-driven recirculating flow is a driving factor of Non-Fickian transport in the meandering channels. The combined effects of the secondary flows and recirculating flows trigger Non-Fickian transport behaviors with late-time tailing of solute plume. The helical secondary flows transfer tracers into the recirculation zones actively by enhanced transverse dispersion, and the flow recirculation retards tracer transport by trapping the tracers to the slow flow regions.

Acknowledgement (If necessary)

This work is supported by the Korea Agency for Infrastructure Technology Advancement(KAIA) grant funded by the Ministry of Land, Infrastructure and Transport (Grant 20DPIW-C153746-02).

References

- Seo, I. W., Kim, J. S., & Jung, S. H. (2016). Numerical simulation of two-dimensional pollutant mixing in rivers using RAMS. *Procedia engineering*, 154, 544-549.
- Shiono, K., & Muto, Y. (1998). Complex flow mechanisms in compound meandering channels with overbank flow. *Journal of fluid mechanics*, 376, 221-261.

Experimental investigation on longitudinal dispersion in a reach with willow patches

Kaisa Västilä^{1*}, Un Ji², Juha Järvelä¹, Fred Sonnenwald³, Hyung Suk Kim⁴, Ian Guymer³, Jungsun Oh²

¹ Aalto University School of Engineering, Espoo, Finland

² Korea Institute of Civil Engineering and Building Technology, Goyang-Si, Korea

³ Department of Civil and Structural Engineering, University of Sheffield, UK

⁴ Department of Civil Engineering, Kunsan National University, South Korea

*Corresponding: kaisa.vastila@aalto.fi

Abstract

While most work on solute transport has focused on fully vegetated or non-vegetated flows, this work aims to investigate longitudinal dispersion in a reach with real-scale flexible willow patches.

Keywords: Longitudinal dispersion; Vegetation patches; Aggregated Dead Zone Model; Mixing

Introduction

Vegetation significantly controls the transport of soluble compounds in the hydro-environment, influencing many processes, such as the fate of nutrients (e.g. Kalinowska et al. 2019). Understanding of how vegetation affects mixing derived from small-scale simplified experiments has not been fully scaled up to the reach scale where vegetation typically consists of patches. Our ongoing work aims to investigate the influence of the patch properties and spatial distribution on the reach-scale longitudinal dispersion under real-scale flexible willow patches.

Methods

An experimental setup, reproducing the patch geometries and densities of natural floodplain shrubs, was established in an experimental trapezoidal channel with 3-4 m long patches of artificial foliated, branched plants. The water depths were approximately 0.7-0.9 m, wetted surface widths approximately 6 m and mean velocities 0.3-0.6 m/s. Salt was used as a conservative tracer and the concentrations were measured at two to six representative locations in the approximately 50 m long study reach. Data from four runs (Table 1) have already been analyzed. We optimized the parameters of the 1-dimensional Advection-Diffusion Equation (ADE) and Aggregated Dead Zone Model (ADZM). As there is a lack of readily applicable models for predicting the longitudinal dispersion coefficient (D_x) in reaches with vegetation patches, we compared the data against analytical models developed for uniformly vegetated (Lightbody & Nepf 2006; Sonnenwald et al. 2019b) and non-vegetated flows (Fischer 1975; Wang & Huai 2016).

Table 1. Hydraulic properties of the already analyzed vegetated test runs; analyses of further runs ongoing.

Test run	Patch layout	Discharge (m ³ /s)	Mean velocity (m/s)	Centerline flow depth (m)	Surface width (m)	Reach-scale patch volume fraction (-)
1	1	3.07	0.66	0.94	6.44	0.070
2	1	1.62	0.48	0.75	5.82	0.075
5	1	2.19	0.56	0.83	6.08	0.073
6	2	1.66	0.50	0.73	5.76	0.037

Results

For the four analyzed runs, both ADE and ADZM resulted in similar optimized mean velocities, proportional to discharge, and were suitable for predicting the downstream concentration distributions. The ADE longitudinal dispersion coefficient (D_x) ranged between 0.24-0.41 m²/s and the ADZM dispersive fraction (D_f) between 0.21-0.27, both slightly increasing with the increasing flow rate and cross-sectional mean velocity. The optimised D_x was approximately an order of magnitude higher than predictions for uniformly vegetated flows and an order of magnitude lower than predictions for non-vegetated flows (Figure 1), indicating that the tested models could serve as rough upper and lower limits of D_x for such reaches with patches covering less than 7% of the water volume. The ratio of volume contributing to dispersion to total reach volume (D_f) was approximately 3-7 times larger than the reach-scale ratio of the patch volume to total water volume.

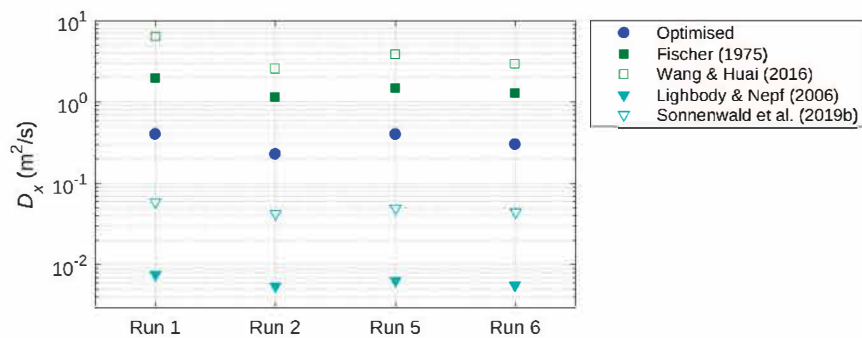


Figure 1. Optimised longitudinal dispersion coefficient (circle) compared to predictions for clear channels (squares) and uniformly vegetated channels (triangles).

Conclusions

The patches covering 4-7% of the water volume had a more substantial influence on D_x than could be expected from the simple aerial weighing of the vegetated and non-vegetated regions. In the future, data from four additional runs including non-vegetated reference condition will be included into the analyses. Such rare full-scale analyses will improve the predictions of the transport and retention of pollutants in real vegetated flows.

Acknowledgements

K.V. was supported by Maa- ja vesitekniikan tuki ry (Grant No. 33271) and Academy of Finland (330217). I.G. and F.S. Sonnenwald were supported by EPSRC Fellowship award EP/P012027/1. The authors are grateful to the many colleagues of KICT and KICT-River Experiment Center who participated in the experiments.

References

- Fischer, H.B. (1975). Discussion of 'simple method for predicting dispersion in streams' by R.S. McQuivey and T.N. Keefer. *J. Environ. Eng.* 101(3): 453-455.
- Kalinowska, M., Västilä, K., Rowinski, P. (2019.) Preface to Special Issue: Solute transport in complex natural flows. *Acta Geophysica* 67: 939–942. doi: 10.1007/s11600-019-00308-z
- Lightbody, A.F. & Nepf, H.M. (2006). Prediction of velocity profiles and longitudinal dispersion in salt marsh vegetation. *Limnology and Oceanography*, 51(1), 218-228.
- Sonnenwald, F., Stovin, V. & Guymer, I. (2019). A stem spacing-based non-dimensional model for predicting longitudinal dispersion in low-density emergent vegetation. *Acta Geophys.* 67(3): 943-949.
- Wang, Y. and Huai, W. (2016). Estimating the longitudinal dispersion coefficient in straight natural rivers. *Journal of Hydraulic Engineering*, 142(11): 04016048

An Autoregressive Model for Sewage Flow Prediction for Chlorine Dosage Control

Yuging Liu¹, King Wah Choi^{1*}, and Joseph Hun-wei Lee²

¹Department of Civil & Environmental Engineering, the Hong Kong University of Science and Technology

²Macau Environmental Research Institute, Macau University of Science and Technology,

*dkwchoi@ust.hk

Abstract

Real-time sewage flow prediction is essential for chlorine dosage control to achieve adaptive dosing rate and enhanced disinfection efficiency. In this study, an autoregressive (AR) model is employed to provide real-time prediction of the sewage flow in Stonecutters Island Sewage Treatment Works (SCISTW) of the Hong Kong Harbour Area Treatment Scheme (HATS). The results show that hourly changes in the sewage flow can be predicted using an autoregressive AR(4) model, with an accuracy of around 1.4 m³/s (relative error 4-5%).

Keywords: Sewage flow; real-time prediction; chlorine dosage control; autoregressive model

Introduction

Sewage flow rate is an essential operation parameter for wastewater treatment plants. A reliable sewage flow prediction is essential for advanced control strategy of chemical dosing systems (Li *et al.* 2019) and chlorination process. The Stonecutters Island Sewage Treatment Works (SCISTW) serves about 5 million residents living in the main urban areas of Hong Kong surrounding Victoria Harbour. Chemically enhanced primary treatment (CEPT) and chlorine disinfection are applied to protect the coastal water and nearby bathing beaches. At SCISTW, a flow-paced dosing control strategy is employed. Accurate sewage flow prediction is essential for disinfection dosage control.

Methods

The analysis is based on the historical sewage influent flow data (at 30-min time intervals) from January 1, 2019, to December 31, 2020. Considering the different characteristics of sewage flow variation in wet and dry season as well as different days of the week, the sewage flow data are partitioned to four time periods (summer-weekdays, summer-weekends, winter-weekdays, and winter-weekends). As the diurnal sewage flow variation reflects a deterministic usage pattern (reflective of consumption characteristics) perturbed by local and random factors, an auto-regressive model is employed to make maximum use of the real time data. The autocorrelation function (ACF) and partial autocorrelation function (PACF) are calculated to determine the order of the AR model required (Little 2014). 80% of the data is used for training, while the remaining 20% is the test set. The correlation coefficient (R), root mean square error (RMSE) and mean absolute percentage error (MAPE) are used to examine the model performance.

Results

The diurnal variation of the sewage flow rate exhibits similar patterns among the summer and winter season (Fig. 1), the minimum flow occurs at around 5:30am, the flow then increases to the first peak at around 11:30am. The maximum flow occurs at 22:30 pm reflecting the evening water demand. In the summer, the sewage flow rate is slightly higher than winter season which might be attributed to the expected higher consumption and rainfall events. Compared to the

weekdays, the first peak flow in the morning is delayed by about an hour and the second peak flow during the evening is slightly lower on weekends in both winter and summer.

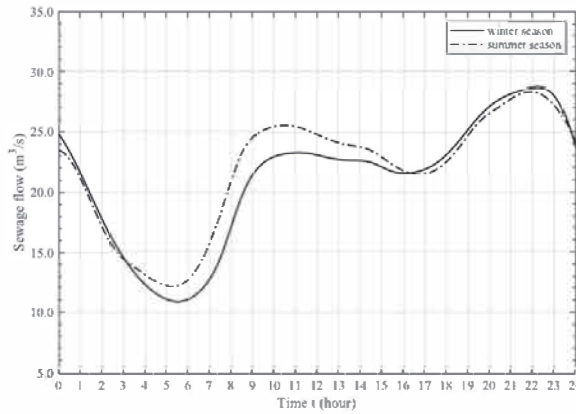


Fig. 1. Typical diurnal patterns of sewage flow at SCISTW in winter and summer season

The following AR (4) model is employed:

$$Q_t = \bar{Q}_t + \alpha_1(Q_{t-1}^m - \bar{Q}_{t-1}) + \alpha_2(Q_{t-2}^m - \bar{Q}_{t-2}) + \alpha_3(Q_{t-3}^m - \bar{Q}_{t-3}) + \alpha_4(Q_{t-4}^m - \bar{Q}_{t-4}) + \varepsilon \quad (1)$$

where Q_t and Q^m are the predicted and measured flows at time t , Q_{t-1}^m , Q_{t-2}^m , Q_{t-3}^m and Q_{t-4}^m are the measured flow at half hour, one hour, one-and-a-half hours and two hours prior to time t respectively, and \bar{Q}_t is the long term average flow at time t . Fig.1 shows that the model can well capture the sewage flow variation at 30 minute lead time.

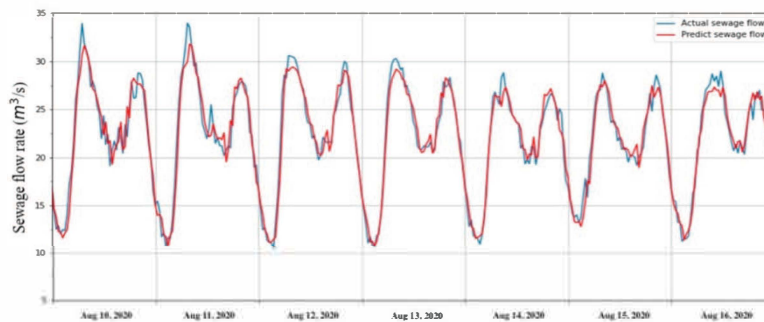


Fig. 2. Measured and predicted sewage flow for a week in summer season (Aug 10-16, 2020).

Concluding Remarks

The results indicate that the AR model is capable to give accurate predictions of the flow rate of sewage influent at SCISTW, with a correlation coefficient of around 0.98, and a root mean square (RMS) error of around $1.1 \text{ m}^3/\text{s}$ (relative error 4.5%).

Acknowledgement

This work is supported by a R&D project commissioned by the Drainage Services Department of the Hong Kong SAR Government.

References

- Li, J., Sharma, K., Liu, Y., Jiang, G. and Yuan, Z., (2019). Real-time prediction of rain-impacted sewage flow for on-line control of chemical dosing in sewers. *Water research*, 149, 311-321.
- Little, T.D., (2014). *The Oxford handbook of quantitative methods*. Oxford University Press, USA.

The 9th International
Symposium on
Environmental Hydraulics

A2 Session

Particle Laden Flows [A2-M1]



Effect of turbulent motions on the sediment entrainment based on the three-dimensional PIV and PTV technique

Hyoungchul Park^{1*} and Jin Hwan Hwang¹

¹Department of Civil & Environmental Engineering, Seoul National University, Korea

* Corresponding: hyungchul1288@snu.ac.kr

Keywords: Sediment entrainment; particle image velocimetry; boundary layer; turbulent coherent structure

Abstract

Sediment entrainment indicating the process where the sediment starts to float in the flow is the most fundamental morphodynamics phenomenon. Therefore, many researchers in fluvial geomorphology have performed theoretical and experimental studies to investigate how the sediment particle interacts with the flow motions and how it starts to move. Most of these studies have defined the initial motion of the particle as incipient motion and revealed that the particle starts to move by receiving momentum from the flow within the boundary layer. In particular, they have focused on the turbulent motions within the boundary layer since various turbulent coherent structures are generated near the bottom and in charge of producing the significant momentum inducing the sediment entrainment. In order to represent the effect of turbulent motions on sediment quantitatively, the Reynolds stress has been estimated from the measured velocity near the bed. The Reynolds stress is classified into four events based on the quadrant analysis to represent the continuous turbulent motion into the discrete event. Among them, the most frequent event is considered as the primary contributor of sediment entrainment. Even though many studies have researched the cause of sediment transport based on the quadrant analysis, the dominant event is still controversial depending on the studies.

Accordingly, the corresponding work investigates the effect of turbulent motions within the boundary layer on the sediment entrainment based on the image-based measurement technique. We performed laboratory experiment under the various flow and bed roughness conditions and acquired high-resolution flow field around the sediment by applying particle image velocimetry and sediment movement simultaneously when the particle starts to move. Based on the measured velocity data, the dominant turbulent event generating sediment entrainment is found by applying quadrant analysis and compared with the result of previous studies.

Acknowledgement

-

Reference

-

Modeling of scour process under two-dimensional wall jet: insights in the scour development stage

Geng Li¹, Binbin Wang^{1*}

¹ Department of Civil and Environmental Engineering, University of Missouri, Columbia, MO, U.S.

* Corresponding: wangbinb@missouri.edu

Keywords: Scour; 2-dimensional jet; turbulence; self-similarity; sluice gate.

Abstract

A simple 2-dimensional simulation was conducted to study the flow field in the development stage of a scour process caused by wall jets under a sluice gate. We particularly tested the skills of computational fluid dynamics (CFD) in quantifying the self-similarities of the overlying jets above the evolving scour bed. The simulation results show a self-preserved flow pattern throughout the entire scour development and the equilibrium stages. The main jet is bended toward the scour bed, and diverges to a returning jet and tail jet, which forms several well-defined eddies in the scour hole. To understand the self-similarity of the flow field, various global flow parameters (e.g., initial jet velocity, slot opening, etc.) and local jet parameters (e.g., local jet velocity, jet width, etc.) were applied for scaling the stream-wise, jet-wise, and cross-sectional distributions of the mean flow velocities. The self-similarity of the scour bed profiles was also investigated using various length scales in the scour. We evaluated three empirical equations (i.e., power-law, exponential-growth, and saturation-growth) in describing the temporal evolution of the scour depth. Lastly, we proposed a modified jet Froude number to model the normalized equilibrium maximal scour depth. The modified jet Froude number incorporates jet velocity attenuations along the downstream apron of the sluice gate, by taking into consideration of the wall jet theory in the scaling, rather than using simple dimensional analysis.

Acknowledgement

We would like to thank Flow Science, Inc. for providing the research license to carry out this study.

Reservoir sedimentation and flushing for the management of the Patrind hydro-power dam

Joonwoo Noh^{1*}, Yeonsoo Kim¹, Jisoo Yu¹

¹K-water Research Institute, Daejeon, Republic of Korea

* Corresponding: jnoh@kwater.or.kr

Keywords: Sedimentation; Flushing; Reservoir; Hydro-power; Bypass tunnel

Abstract

Pakistan Patrind hydropower project is proposed to harvest the power of water of the Kunhar River near Patrind village in Pakistan. It is located close to the Muzaffarabad city, apart from 120km Islamabad towards north east. This project is to construct ROR (Run of River) typed dam in the Kunhar River (EL. 765m) and divert the flow to main stream, the Jhelum River (EL.651.2m) to generate hydropower using 107.3m net water head. The storage volume of the reservoir is about 6Mt and is always exposed to the sedimentation. Due to geological characteristics, high concentrated sediment reduces the storage volume rapidly and an efficient sediment management is necessary to provide stable hydro power generation in the aspect of water resources and turbine system management.

Since January 1st of 2017 when the project initiated, the storage volume of the reservoir decreases up to 56% for two and half years due to sedimentation surveyed in the beginning of July 2019. Following the reservoir operation, sediment flushing is required immediately when storage volume reaches 50%. The bypass tunnel connecting the upstream and downstream of dam contributed to release high concentrated sediment during sediment flushing conducted for 10 days from July 22nd to 31st in 2019. This paper introduces and evaluates sediment bypass tunnel by comparing the surveyed results before and after the flushing. The results has also been compared with the computed ones using long term sediment transport model.

Using image conversion for suspended solid transport for 2D particle dispersion modeling

Jaehyun Shin¹, Hoje Seong¹, Inhwan Park², Dong Sop Rhee^{1*}

¹Korea Institute of Civil Engineering and Building Technology, Goyang-Si, Gyeonggi-Do, South Korea

²Seoul National University of Science and Technology, Seoul, South Korea

* Corresponding: dsrhee@kict.re.kr

Abstract

The importance of modeling to predict the changes to the river are becoming vital to river management. Localized seasonal heavy rain would cause the suspended solids to transport, which interfere with the river conveyance. This research will attempt to execute a suspended solid transport experiment in a real-scale field experiment to analyze the transportation of materials and use 2D particle dispersion modeling with image conversion to model and monitor the experiment results. Drones were used to capture images of the suspended solid transport, and then the remote sensing method of image conversion was applied to the image data to estimate the range of the suspended solid. The results showed the applicability of using image conversion and particle modeling to process data for suspended solid materials transported in water.

Keywords: Suspended solid; images; remote sensing; particle dispersion model; concentration;

Introduction

The recent climate changes have caused great instability in riverine environments, increasing the necessity of river monitoring. In addition, the importance of modeling to predict the changes to the river are becoming vital to river management. Especially in the summer, localized heavy rain would cause the suspended solids to transport, which interfere with the river conveyance. This research will attempt to execute a suspended solid transport experiment in a real-scale field experiment to analyze the transportation of materials and use 2D particle dispersion modeling with image conversion to model and monitor the experiment results.

Methods

The experiment was conducted in the River Experiment Center in Andong, which has a length of 50 meters with a width of 5 meters while the bottom length is 3 meters. The slope of the experiment was originally designed as a mild slope of 1/800. The discharge rate conditions for the experiment were 2 m³/s, as the water was pumped from the Nakdong River to a water tank for stabilization. The suspended solid was made with a mixture of water and silica. Then the mixture was injected into the water and transport occurred throughout the channel. At the downstream of the experimental flume, the laser sediment measuring equipment LISST (Laser In-Situ Scattering and Transmissometry) was used to find the concentration of the suspended solid. In addition, drones were used to capture images of the suspended solid transport. The images then became the base of the spatial and temporal analysis of the input mixture. This remote sensing method of image conversion was applied to the image data to estimate the range of the suspended solid. The pixels for the images would be converged to real scale size, and the measured results of the laser sediment equipment LISST was used for calibration and verification.

The conversion results would be used as an input for the 2D particle dispersion model. The model used for suspended solid transport was PDM-2D, which is a particle model developed to simulate pollutant mixing in rivers without the input of dispersion coefficients by adopting the step by step calculation method (Park and Seo, 2018). The step by step method is conducted by first calculating the horizontal translation, and then the vertical mixing based on the shear dispersion theory.

Results

The applied results to the 2D particle dispersion model proved its capability to reproduce the experiment well. This showed the applicability of using image conversion to acquire data for suspended solid materials transported in water. Therefore, the current study with real-scale experiment provided an interesting method on modeling the suspended solid transport.

a) Original image



b) Converted image

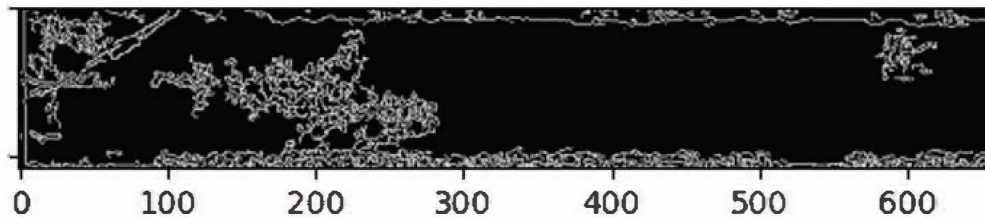


Fig. 1. Comparison between the original image and edge detected image.

Conclusions

This research executed a suspended solid transport experiment in a real-scale field experiment to analyze the transportation of materials and use 2D particle dispersion modeling with image conversion to model and monitor the experiment results. This showed the applicability of using image conversion and particle modeling to reproduce the movement of suspended solid materials in water. Therefore, the current study with real-scale experiment showed the applicability of using image conversion and particle modeling for suspended solid materials transported in water.

Acknowledgement

This work is supported by the Korea Agency for Infrastructure Technology Advancement(KAIA) grant funded by the Ministry of Land, Infrastructure and Transport (Grant 21DPIW-C153746-03).

References

Park, I.; Seo, I.W. (2018). Modeling non-Fickian pollutant mixing in open channel flows using two-dimensional particle dispersion model. *Adv. Water Resour.*, 111, pp. 105-120.

Identifying Total Sediment Loads—Suspended Sediment Load Relationship Using a Two-level Unsupervised Clustering Method

Hyoseob Noh¹, and Yong Sung Park^{1*}

¹Department of Civil & Environmental Engineering, Seoul National University

*Corresponding: dryspark@snu.ac.kr

Abstract

In this work, we aim to assess sediment rating curves and develop an alternative method applying a two-level clustering approach to measured bed- and suspended-load data. The hydraulic features to be considered include cross-sectional mean velocity, mean depth, bed slope, as well as sediment diameter distribution. The two-level unsupervised clustering method includes a Self-organizing map (SOM) at the first level in order to project the data space onto a comparatively low dimensional map. Then, a trained SOM network is clustered by using a Gaussian mixture model (GMM). Several distinguished patterns that will appear as a result of the clustering will be matched to the hydraulic regimes, thereby establishing each regime's physical meaning. It is expected that multiple sediment fraction models for each cluster will enhance total sediment load predictability.

Keywords: Suspended load; Bedload; Total sediment load; Sediment transport; Self-organizing map; Gaussian mixture model

Introduction

Measurement of total sediment load, which consists of bedload and suspended load, is essential in hydraulic engineering and geomorphology. However, it is challenging to measure bedload directly, which is often estimated from the measured suspended-load, e.g. using sediment rating curves such as Maddock's Table and the modified Einstein method. Although there have been efforts to partition total sediment load into bedload and suspended load fractions, results showed large scatter. Especially, the modified Einstein method requires sediment diameter distribution and detailed measurement point information, whose uncertainties add to the large scatter in the estimated value of total sediment load. In this sense, parsimonious linking suspended-load and bed-load will contribute to the academic and practical estimation of the total sediment load.

Methods

To figure out the total sediment load regime, a two-level unsupervised clustering approach, which iteratively performs Kohonen's self-organizing map (SOM) (Kohonen, 1990) and Gaussian mixture model (GMM), was exploited. The method repeats clustering varying the number of clusters. The best clustering result can be determined by finding a model that minimizes Akaike's Information Criterion (AIC) and Bayesian Information Criterion (BIC) which described as:

$$AIC = 2k - 2LL \quad (1)$$

$$BIC = k \ln(n) - 2LL \quad (2)$$

in which, k is the number of parameters in the model; LL is the log-likelihood of the model; n is the number of data point.

Results

The total sediment load in natural streams data from Williams and Rosgen (1989) was analyzed to figure out the underlying physics relating to total sediment load and suspended sediment concentration. We selected the model minimizing the AIC as the best model varying the number of clusters from 1 to 10 with 500 iterations, and the 4 was the optimal number of clusters. The SOM heat map (Fig. 1) of the four dimensionless variables showed good agreements with the clustering boundaries with the different colored cluster indices. Especially, the blue-colored cluster shows a small fraction of suspended sediment, and the orange-colored cluster is suspended sediment dominated. Bed material Reynolds number (Re_{d50}) and depth Reynolds number (Re_H) corresponded with the suspended load fraction, F_{sus} .

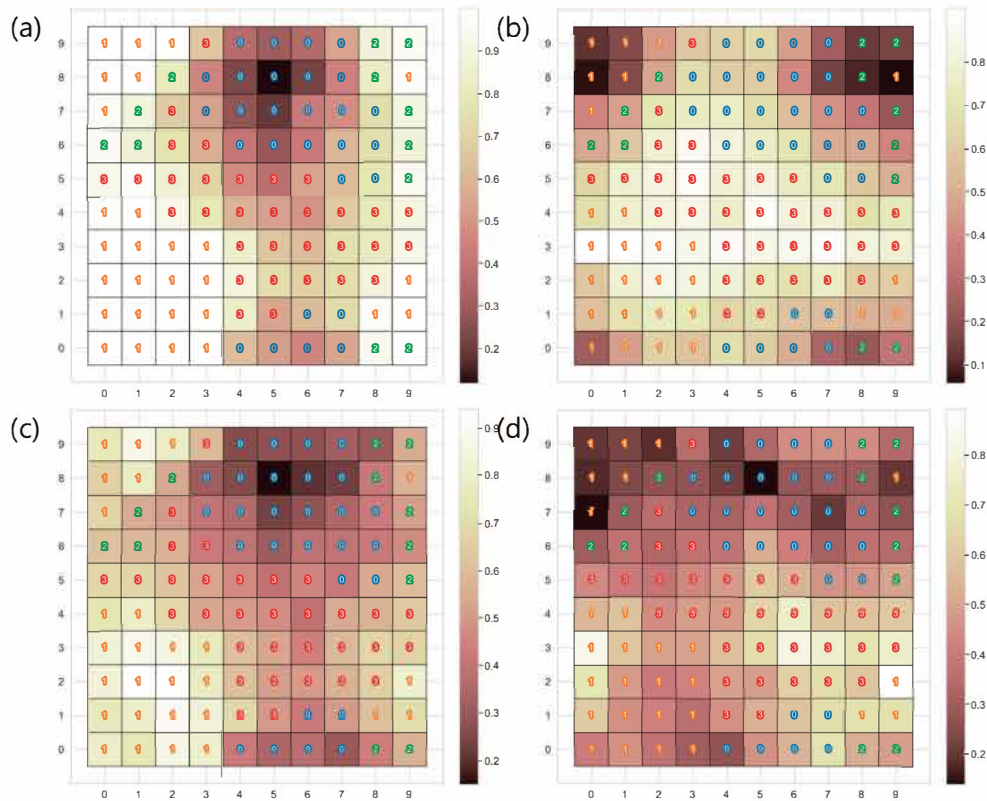


Fig. 1. Clustered heat maps of the SOM: (a) log-scaled suspended load fraction to total load (F_{sus}) (b) log-scaled bed material Reynolds number (Re_{d50}) (c) log-scaled depth Reynolds number (Re_H) (d) Froude number.

Conclusions

This study suggests the new regime divisions of the suspended load fraction to total load (F_{sus}) using an unsupervised pattern recognition method. Two Reynolds numbers with different characteristic lengths showed significant relation to F_{sus} . The algebraic relationship of each regime can be derived using this result.

Acknowledgement (If necessary)

This work is supported by the Korea Agency for Infrastructure Technology Advancement(KAIA) grant funded by the Ministry of Land, Infrastructure and Transport (Grant 21DPIW-C153746-03).

References

- Kohonen, T. (1990). The self-organizing map. *Proceedings of the IEEE*, 78(9), 1464-1480.
 Williams, G. P., & Rosgen, D. L. (1989). *Measured total sediment loads (suspended loads and bedloads) for 93 United States streams* (p. 128). Washington, DC: US Geological Survey.

**The 9th International
Symposium on
Environmental Hydraulics**

A3 Session

Environmental Flows [A3-T3]



The effect of turbulent flow motion on the sea urchin fertilization

Hyoungchul Park^{1*}, Hojung You² and Jin Hwan Hwang¹

¹Department of Civil & Environmental Engineering, Seoul National University, Korea

²Department of Civil & Environmental Engineering, University of Illinois at Urbana-Champaign, USA

* Corresponding: hyoungchul1288@snu.ac.kr

Keywords: Sea urchin fertilization; Lagrangian particle tracking algorithm; Standardized Morisita index

Abstract

The external fertilization of sea urchin is achieved through a process of complex interaction with the surrounding flow. Once eggs and sperms are released directly into the water, they follow complex flow motion until they collide into each other. Pair of egg and sperm are fertilized when the compatibility of gametes is satisfied. Since the success of fertilization can be easily observed, many studies have performed laboratory experiments and field observations to investigate the effects of surrounding flow on fertilization rate. They mainly estimated fertilization rate by extracting specimens from target locations and counting the number of fertilized eggs among the entire eggs, under the assumption that gametes are dispersed evenly in the entire domain. However, due to the complex flow structure within the boundary layer, gametes are dispersed erratically, causing unreliable results.

In order to overcome the limitation of previous studies, the corresponding study performed computational modeling based on the lagrangian particle tracking algorithm, which enables us to compute the fertilization rate accurately. Based on the results of modelling, we investigate the effect of flow characteristics behind the sea urchin body on the fertilization process under the various flow conditions. Specifically, first, we analyzed the flow structure behind the sea urchin and obtained the spatial distribution of gametes depending on the flow conditions. Second, the spatial distribution of gametes is quantified numerically based on the standardized Morisita index suggested by Smith-gill (1975) to describe the degree of aggregation of gametes. Finally, we computed the fertilization rate and hydrodynamic characteristics such as turbulent intensity and integral length scale and figured out how changing flow characteristic influences on the fertilization process of sea urchin by associating the standardized Morisita index with the fertilization rate.

Our results show that the fertilization rate increases with the increase of standardized Morisita index and decreases with the integral length scale. Specifically, the fertilization takes place when the gametes are more clustered and the vortex motion created by sea urchin is more strong.

Acknowledgement

-

Reference

Smith-Gill, S. J. (1975). Cytophysiological basis of disruptive pigmentary patterns in the leopard frog *Rana pipiens*. II. Wild type and mutant cell-specific patterns. *Journal of Morphology*, 146(1), 35-54.

The effect of obstacle configuration on the transport of neutrally buoyant particles

Hojung You^{1*}, Rafael O. Tinoco¹

¹ University of Illinois at Urbana-Champaign, Urbana, Illinois, USA

* Corresponding: hojungy2@illinois.edu

Keywords: 2D PIV; 2D PTV; neutrally buoyant particles

Abstract

The recent increase in use of surgical facial masks and PPE has magnified microplastic pollution in natural waters. When plastics are degraded into smaller particles, they are easily absorbed and transported onto various ecosystems. Since freshwaters transport a majority of plastics from the land to the sea, with accumulated plastics causing detrimental effect on aquatic biota along the way, we seek to develop an efficient microplastic management strategy by thoroughly understanding the transport mechanism of such particulate matter in water. Common obstacles in freshwater such as branches, logs and hydraulic structures are identified as local hotspots of microplastics. Hydrodynamic analysis of these locations provides a more efficient approach to capture and redirect plastics in freshwater ecosystems by predicting particle behaviors at different flow conditions. As an effort to identify flow characteristics creating hotspots of particles, we analyze the transport of neutrally buoyant particles when obstacles are installed in various configurations in a laboratory setting. The transport mechanisms of particles are analyzed depending on obstacles' dimensions and the spacing between neighboring obstacles when flow obstructions are located: (a) on the bed, and (b) at the free surface.

We conducted experiments on a closed-loop racetrack flume, using Particle Tracking Velocimetry (PTV) to track the transport of neutrally buoyant particles and Particle Image Velocimetry (PIV) to identify specific mean and turbulent conditions that determine particle retention or redirection. The spatial and temporal analysis of two-dimensional velocity fields yields valuable information on flow-structure-particle interactions and their response to changing hydrodynamic conditions due to different obstacle configuration. We expect current study to provide an efficient microplastic management strategy in freshwater ecosystem based on the : 1) prediction of plastic accumulation zones for monitoring or their removal in streams, and 2) effective design of artificial traps to target specific plastic materials without affecting transport of stream organisms.

A turbulence-based, two-layer model to predict sediment resuspension in vegetated flows

Chien-Yung Tseng^{1*} and Rafael Tinoco¹

¹ Department of Civil and Environmental Engineering, University of Illinois at Urbana-Champaign, Urbana, Illinois, USA

* Corresponding: cytseng2@illinois.edu

Abstract

Aquatic vegetation plays an important role in maintaining ecosystem services in natural water environments, such as wetlands, estuaries, riverine and coastal areas. To improve restoration efforts and protect vegetation habitats, it is paramount to understand how vegetation interacts with their surroundings to predict sediment transport and suspended sediment concentration (SSC) accurately, which will lead us to more accurate models of landscape evolution and water quality management. We conducted a series of laboratory experiments in a recirculating racetrack flume with rigid cylinder arrays to mimic vegetation. Light-weight sediment (walnut shells) was chosen as substrate according to scaling considerations. We used 2D planar Particle Image Velocimetry on horizontal and vertical planes to investigate the flow structures under different canopy densities. Profiles of SSC were measured via quantitative imaging, using the recorded sediment particles to obtain probability values for the concentration. We propose a two-layer, turbulence-based model to predict SSC in vegetated flows, considering turbulence generated from vegetation, from the bed, and from coherent structures caused by stem-bed-flow interaction into the near-bed turbulent kinetic energy.

Keywords: Turbulence; Vegetated flow; Sediment resuspension; Coherent structure

Introduction

Sediment transport has long been an essential issue for hydraulic and environmental engineers, which has been widely studied in open-channel flows. In the past, sediment transport and resuspension models relied on measurements of bed shear stress. However, studies have shown that bed shear stress models do not work in regions with vegetation due to ignoring the effect of turbulence generated by vegetation, which has been recognized as a prominent feature in natural flow environments that drives sediment resuspension. More studies are needed to better understand how water, sediment, and vegetation interact in regions with vegetation to predict sediment transport accurately in natural vegetated environments.

Methods

The experiment was conducted in a unidirectional, recirculating flume. The straight test section of the flume is 2 m long, 0.15 m wide, and 0.6 m deep. An array of rigid acrylic cylinders with diameter $d = 0.64$ cm and height $h = 10$ cm is used to simulate a high-stiffness aquatic vegetation canopy. Two densities were selected to cover from sparse to dense conditions, $ah = \{0.1 - 0.5\}$. Crushed walnut shells are chosen as sediment substrate, with a 10 cm thick sediment bed as the initial setup in the straight test region. The sediment density, $\rho_s = 1.2$ g/cm³ (water density, $\rho = 1.0$ g/cm³) with the median grain size, $D_s \approx 1$ mm. The walnut shell settling velocity, $w_s \approx 1$ cm/s. Five experimental runs with emergent vegetation arrays and three test runs with a bare-bed setup were conducted. Hydrodynamics measurements were conducted by Particle Image Velocimetry (PIV). Suspended sediment concentration (SSC) was estimated by counting the time-averaged particle pixels from the monochromatic images.

Results

We developed a two-layer, turbulence-based model to predict SSC in flows with emergent aquatic vegetation. Turbulence generated from vegetation, bed, and coherent structures caused by stem-bed-flow interaction are considered into the near-bed turbulent kinetic energy (TKE), which is the critical parameter that describes the impacts of vegetation-bed-flow interactions at the sediment-water interface. The model consists of two crucial variables, the effective bottom boundary layer, H_b , and the effective bed shear velocity, u_{beff}^* , that will change with mean velocity and array density:

$$H_b = \alpha \frac{1}{C_D^{1/2}} \left(\frac{2\nu k_s}{a^2 U} \right)^{1/4} \quad (1)$$

$$u_{beff}^* = \sqrt{0.19 \left(k_{tb} + k_{tv} + \frac{c}{0.19} \frac{\nu}{k_s} \sqrt{k_{tb} + k_{tv}} \right)} \quad (2)$$

where α is the experimental coefficient, C_D is the vegetative drag coefficient, ν is the kinematic viscosity, k_s is the bottom roughness, U is the mean flow velocity, k_{tb} is the bed shear TKE, k_{tv} is the vegetation generated TKE, c is an empirical coefficient that depends on the shape, orientation, array density, and stem Reynolds number of the vegetation.

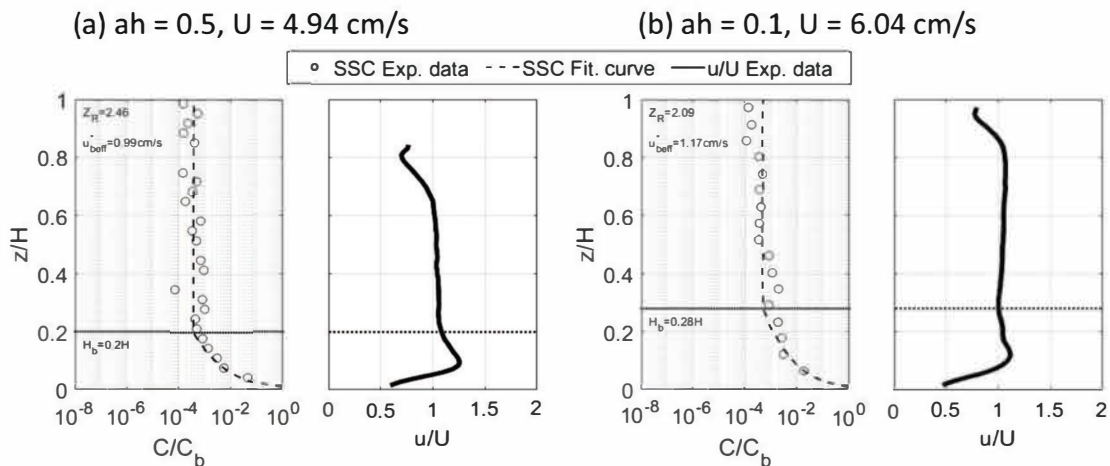


Fig. 1. Measured SSC profiles and the corresponding mean velocity profile in flows with emergent vegetation under (a) $ah = 0.5, U = 4.94 \text{ cm/s}$, (b) $ah = 0.1, U = 6.04 \text{ cm/s}$. Circles represent experimental data. Dashed lines represent the fitted curve for the SSC profile. Solid lines represent the velocity profile. Black dotted lines indicate the thickness height of the bottom boundary layer.

Conclusions

The proposed two-layer, turbulence-based model successfully predicts SSC in flows with emergent vegetation. The experimental data validated the model and is expected to provide critical information to future studies on sediment transport, landscape evolution, and water quality management in vegetated streams, wetlands, and estuaries.

Acknowledgment

CT acknowledges funding support from Taiwan-UIUC Fellowship. This study was supported by NSF through CAREER EAR 1753200.

Disparity of nutrient loading estimates associated with extreme-event observation

Dong-Kyun Kim^{1*}, Kwangsoon Choi¹, Youngsung Kim¹, Hye-Suk Yi¹, Suna Chong¹, Nam-Il Won¹,
Hojoon Kim¹, Seung-Yoon Lee¹, Seungbin Yang¹, Hyung-Seok Park¹

¹K-water Institute, 125 Yusungdaero1689, Daejeon, Republic of Korea

* Corresponding: dkkim@kwater.or.kr

Keywords: climate changes; nutrient loading, extreme rain events; harmful algal blooms

Abstract

Climate change is a critical factor to determine hydrological dynamics and ambient water quality in freshwater ecosystems. Particularly for nutrient loading, nitrogen and phosphorus dynamics vary largely according to intensity and frequency of rainfall events. Korea's Ministry of Environment operates water quality monitoring networks on a weekly basis. Despite their consistent observation routine, the sampling misses a certain amount of nutrient loading emerged from irregular rain events. In this respect, we hypothesize that these episodic rain events may exert a large influence on annual nutrient loading estimation, provided that approximately 60% of annual rainfall is biased to the summer monsoon period in Korea. To this end, the present study focuses on comparative nutrient loading estimates between two different sampling strategies. It highlights that data missing and observation failure for extreme events could downplay exogenous nutrient loads to induce summer harmful algal blooms in freshwaters.

Analysis of residence time distribution in retention zone of natural rivers

Byunguk Kim¹, Il Won Seo^{1*}

¹Department of Civil & Environmental Engineering, Seoul National University

*Corresponding: seoilwon@snu.ac.kr

Abstract

Solute transport modeling is the fundamental work for improved understanding of particles behavior in riverine system. In this study, considering the time-scale dependent behavior, we presented convolutional modelling decomposing the residence time in surface zone affected by Fickian behavior and storage effects. As a results, the proposed model yielded more accurate simulation in late time of breakthrough curves compared to other models.

Keywords: non-Fickian transport; residence time distribution; breakthrough curves; tracer test convolution

Introduction

Transient Storage Model (TSM) has been widely used due to its simple conceptualization that the storage mechanism can be described as equivalent to a first-order mass transfer (Bencala and Walters, 1983). However, recent studies have argued that the breakthrough curve lagged by natural storage zone does not behave exponentially as the TSM assumed. In this study, adopting the framework of Marion et al. (2008), we proposed the convolutional equation for non-Fickian transport applying the Routing Model and Advective Pumping Model (Elliott and Brooks, 1997). Further it was validated with the tracer test data and simulation results from other transport models.

Methods

The temporal concentration distribution can be expressed by residence time distribution (RTD), and mechanisms governing the RTD can be divided into two: thee Fickian behavior and storage effect. Those two decomposed system were modeled with Routing Model (RT model) and the Advective Pumping Model (APM) (Elliott and Brooks, 1997). This convolutional decomposition equation with the APM (CDE_{APM}) was formulated as follows:

$$C(t; x) = \int_0^t \left[\underbrace{\int_0^{\tau_2} \left[\frac{C(\tau_1; 0)U}{\sqrt{4\pi D_L \bar{T}}} \exp\left\{ \frac{\{x - (\tau_2 - \tau_1)U\}^2}{4D_L \bar{T}} \right\}} \right] d\tau_1}_{\text{Fickian behavior}} \right. \\ \left. \cdot \underbrace{\sum_{n=0}^{\infty} \left\{ \frac{(\alpha \bar{T})^n e^{-\alpha \bar{T}}}{n!} \right\} \left\{ \frac{\pi/T_h}{10.66 \frac{T_h}{t} + \left(\frac{t}{T_h} + 2 \right)^2} \right\}^n}_{\substack{\text{uptake process} \\ \text{Advective pumping model}}} \right] d\tau_2 \quad (1)$$

where C is solute concentration in surface flow, U is reach-averaged mean flow velocity, D_L is longitudinal dispersion coefficient, \bar{T} is mean time to travel distance x , α is trapping probability per unit time, T_h is residence time scale parameter, n is number of trapping, τ_1 and τ_2 are dummy time variable.

To validate the proposed model with measured data in a natural river, the tracer test was carried out at Gam Creek, consisting primarily of sand substrate, South Korea in 2019. At

the section 4.85 km away from injection point, mean travel time was 2.058 hr and maximum measured concentration was 5.18 mg/m³ with 12.8 cms of discharge.

Results

The simulation results of CDE_{APM} were compared to other popular modes: the ADE and TSM. Fig. 1 show that the accuracy comparison in the falling limb of breakthrough curves simulated from above three models at each sections. To quantitatively evaluate the accuracy differences, the power-law slope of breakthrough curve tails was subject for the comparison as summarized in Table 1. From the CDE_{APM} the average error rate of those at all sections was 0.195, which is far lower than 14.03 and 1.866 from the ADE and TSM, respectively. Therefore, the RTD tails formed from the CDE_{APM} attenuated more closely to the measured value on all sections than those of other two models.

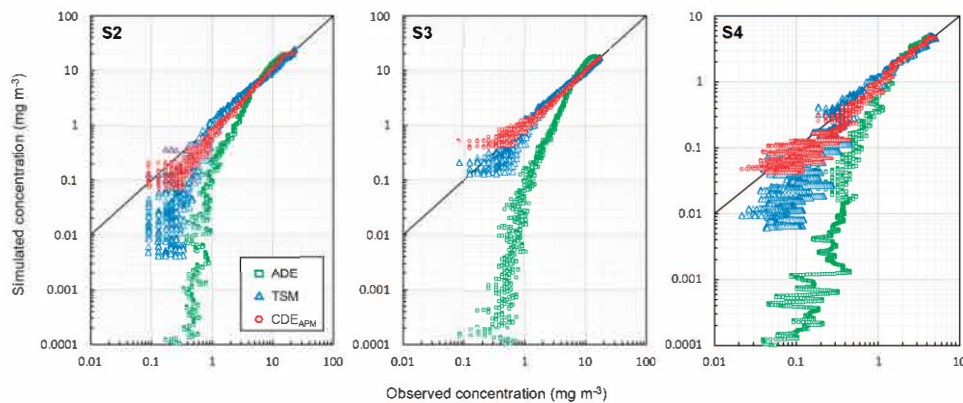


Fig. 1. Accuracy comparison of simulated concentrations compared to the observed concentrations by models

Table 1. Comparison of the power-law slope of the tail of BTCs at each section by models

	S2	S3	S4	Averaged error rate
Tracer test	3.789	6.298	3.811	-
ADE	92.39	103.4	16.35	14.03
TSM	16.11	17.46	6.001	1.866
APM	3.332	5.140	4.885	0.195

Conclusions

The storage mechanisms, which has been unidentified problem so far, can be represented with the residence time distribution in storage zone. In the GC2019 case, which was characterized by sandy and dune-shaped bed form with less other retention factors such as vegetations, the advective pumping model yielded accurate simulation results than other models.

Acknowledgement

This work is supported by the Korea Agency for Infrastructure Technology Advancement(KAIA) grant funded by the Ministry of Land, Infrastructure and Transport (Grant 20DPIW-C153746-02).

References

- Bencala K. E. and Walters R. A. (1983) Simulation of solute transport in a mountain pool-and-riffle stream: A transient storage model. *Water Resources Research*, 19, 718-724.
- Elliott, A. H. and Brooks, N. H. (1997). Transfer of nonsorbing solutes to a streambed with bed forms: Theory. *Water Resources Research*, 33(1), 123–136.
- Marion, A., Zaramella, M., and Bottacin-Busolin, A. (2008). Solute transport in rivers with multiple storage zones: The STIR model. *Water Resources Research*, 44(10), 1–10.

Hyporheic exchange driven by rocks

Anzy Lee¹, Antoine Aubeneau², M. Bayani Cardenas³, Xiaofeng Liu⁴

1 Dept. Civil and Environmental Engineering, Utah State University, 4110 Old Main Hill, Logan, UT, USA

2 Lyles School of Civil Engineering, Purdue University, West Lafayette, IN, USA

3 Department of Civil and Environmental Engineering, Institute of Computational and Data Sciences,
Pennsylvania State University, University Park, PA, USA

4 Department of Geological Sciences, The University of Texas at Austin, Austin, TX, USA

Corresponding author: Anzy Lee (anzy.lee@usu.edu)

Abstract

We investigated how rock clusters embedded in a finer grain matrix alter the near-bed flow and the exchange of surface and subsurface water. We found that the hyporheic flux is decreased with embeddedness but increased with spacing. We also observed in the smallest spacing case, the effect of the dead zone becomes significant preventing the flow recovery as the boulder less embedded.

Keywords: Hyporheic exchange; Ecstones; Surface-subsurface interactions

Introduction

As rocks are placed closer, the wake they generate can extend to their neighbors and interfere with the wakes of the adjacent elements. Fang et al. (2017) investigated the effects of boulder concentration on hydrodynamics and turbulent flow properties. When boulders were near each other, wake interference and skimming flow were observed, greatly reducing bed shear. Since spacing changes the near bed hydrodynamics, we expect it will also affect hyporheic exchange. In this study, we demonstrate how boulder spacing and embeddedness influence hyporheic exchange processes, especially the hyporheic flux.

Methods

We first generated an artificial fluvial channel with an array of four boulders placed upon the sediment bed in a staggered manner as shown in Figure 1.

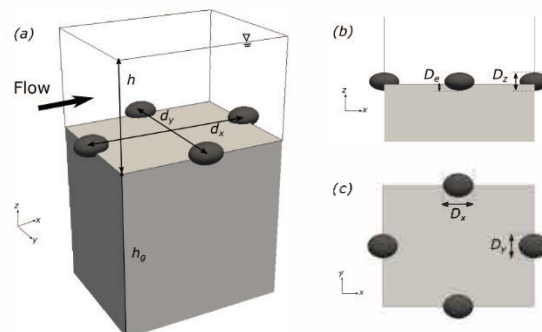


Fig. 1. (a) A geometry of a roughness element modelled by an ellipsoid (b) Side view (c) Plan view

We set the diameters of fluvial boulders as $D_x : D_y : D_z = 10 \text{ cm} : 8 \text{ cm} : 6 \text{ cm}$. The distance between the center of two adjacent boulders is d_x (x-axis) and d_y (y-axis), respectively. We define the parameter boulder spacing as $S = d_x/D_x = d_y/D_y$. We adopted BSK-orig computational method to quantify embeddedness which is $100 \cdot D_e/D_z$ where D_z is the total height of boulder and D_e is the embedded height, respectively. Since we used six different settings for spacing (2, 3, ..., 7) and seven for embeddedness (5, 20, 35, ..., 95%), $6 \times 7 = 42$ simulations were conducted

in total.

The three-dimensional channel flow is modelled by the Reynolds Averaged Navier-Stokes equations (RANS) with the $k - \epsilon$ closure scheme. The continuity and momentum equations are

$$\frac{\partial U_i}{\partial x_i} = 0 \quad (1)$$

$$\frac{\partial U_i}{\partial t} + U_j \frac{\partial U_i}{\partial x_j} = -\frac{1}{\rho} \frac{\partial P}{\partial x_i} + \frac{\partial}{\partial x_j} \left[\nu \left(\frac{\partial U_i}{\partial x_j} + \frac{\partial U_j}{\partial x_i} \right) \right] - \frac{\partial}{\partial x_j} \overline{u_i u_j} \quad (2)$$

With a fully-coupled surface-subsurface flow model, *hyporheicFoam*, developed by Li et al. (2020), the surface and subsurface flow fields are solved.

Results

Fig 2. shows the effect of boulder array setting on the hyporheic exchange rate. The interfacial flux increases as the embeddedness decreases (Fig. 2a) and as the spacing increases (Fig. 2b) except for the case with the smallest spacing. Generally, as boulders are less embedded, pressure variations increase, generating larger gradients across the riverbed, thus driving more hyporheic flux. For the smallest spacing setting, the inverse relationship between the embeddedness and flux no longer holds. When boulders are densely packed, the flow trapped in the dead zone between boulders does not accelerate or decelerate as much as it does in the loosely-packed case. In other words, in the smallest spacing case, the effect of the dead zone becomes significant preventing the flow recovery as the boulder less embedded.

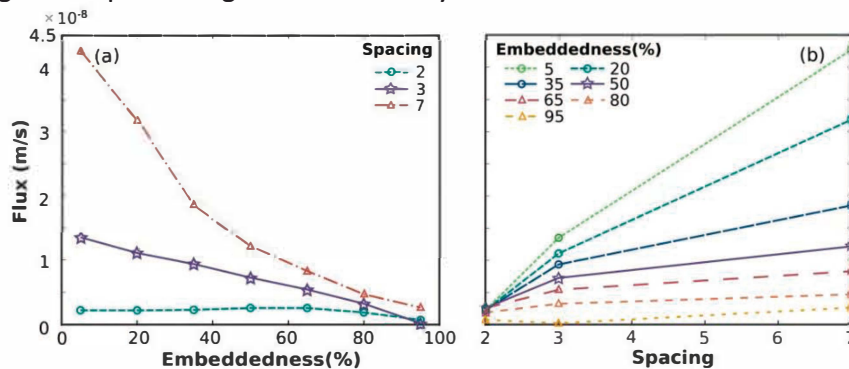


Fig. 2. The dependence of hyporheic flux on (a) Embeddedness (E) and (b) Spacing (S).

Conclusions

We investigated how boulder spacing and embeddedness affect the near-bed hydrodynamics and the surface-subsurface water exchange. We show that the hyporheic flux is decreased with embeddedness but increased with spacing.

References

- Fang, H. W., Liu, Y., and Stoesser, T. (2017) Influence of boulder concentration on turbulence and sediment transport in open-channel flow over submerged boulders. *Journal of Geophysical Research: Earth Surface*, 122, 2392–2410. <https://doi.org/10.1002/2017JF004221>
- Li, B., Liu, X., Kaufman, M. H., Turetaica, A., Chen, X., and Cardenas, M. B. (2020). Flexible and Modular Simultaneous Modeling of Flow and Reactive Transport in Rivers and Hyporheic Zones. *Water Resources Research*, 56(2), e2019WR026528.

Electrochemical model for galvanic corrosion in drinking water supply systems

Lu Chang¹, Joseph Hun-wei Lee^{2*}

¹Department of Civil & Environmental Engineering, Hong Kong University of Science and Technology, Hong Kong, China

²Macau Environmental Research Institute, Macau University of Science and Technology, Macao, China
*jhwlee@must.edu.mo

Abstract

Galvanic corrosion is a main reason for the pipe degradation and lead contamination in drinking water systems. The electrical potential distribution and species transport in the pipe are governed by the Laplace equation and the advection-diffusion equation respectively. The charge transfer rate at the electrode-electrolyte interface depends on the electric field across the interface and can be determined by electrochemical polarization experiments. In this study, a mathematical model is developed by coupling the electric potential field and the reactants transport. The predicted results of the model compare well with the measurement data.

Keywords: Drinking water supply system; Galvanic corrosion; Solder joint; electrochemical model; Mass transport

Introduction

Galvanic connection may occur in water supply systems and cause elevated Pb concentration (Ma et al., 2018). The tendency of losing electrons in galvanic pairs follows the electromotive force (EMF) series, and the potential difference between galvanic pairs is the driving force of the galvanic corrosion. The potential distribution in water can be described by the Laplace equation subjected to specific source and other boundary conditions (Munn & Devereux, 1991). However, previous studies mostly focus on steady-state and mainly sea water corrosion problems; an electrochemical theory for galvanic corrosion in drinking water supply systems – in particular the effect of water quality change during the corrosion propagation - has not been studied.

Methods

Consider a leaded solder joint (Fig.1), the galvanic cell consisting of a leaded solder (anode), a copper electrode (cathode), and water (electrolyte). According to the EMF series, lead and tin will preferentially corrode over copper. Chlorine will first serve as the oxidizer, followed by dissolved oxygen (DO) when chlorine is depleted.

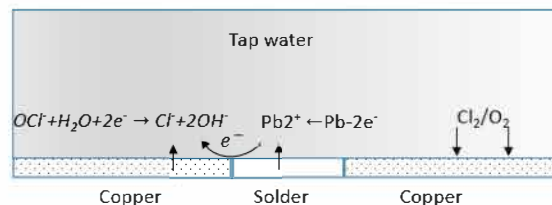


Fig. 1. Schematic illustration of the reactions occurring in a soldered pipe section

According to the continuity of the electrical charge and Ohm's law, the electric potential (φ) distribution can be shown to be governed by the Laplace equation:

$$\nabla^2 \varphi = 0 \quad (1)$$

The charge transfer rate at the electrode-electrolyte interface depends on the electric field across the interface and on the chemical potential gradient. Due to the galvanic corrosion,

reactants (Chlorine, DO, Pb) are consumed, and products (Cl^- , Pb^{2+} , Cu^{2+}) are released at metal surface with a rate proportional to the current density. The governing equation for mass transport of the k^{th} specie is:

$$\frac{\partial C_k}{\partial t} = \nabla^2 C_k + S_k \quad (2)$$

where C_k is the concentration of the k^{th} species in mg/L, t is time in second, and S_k (mg/L/s) is the source term for products and sink term for reactants. At the metal surface, the current density i is proportional to the normal gradient of potential. Owing to the polarization effect, i is a non-linear function of φ given by the Butler-Volmer equation.

$$i = -\sigma \frac{\partial \varphi}{\partial n} = i_0 \left[\exp \frac{2.303(\varphi - \varphi_{eq})}{\beta_a} - \exp \frac{2.303(\varphi - \varphi_{eq})}{\beta_c} \right] \quad (3)$$

where n is the normal direction, i_0 is the exchange current density at equilibrium potential (φ_{eq}), β_a and β_c are the Tafel constants, these four parameters can be measured by polarization method. At the symmetric and dead ends of the computation domain, the current density is zero. The reaction rate at the metal surface has a linear relationship with the current density, which is given by Faraday's law $R = \frac{i}{nF}$ (F =Faraday constant; n =valency).

Results

With the initial chlorine concentration of 0.5 mg/L, DO concentration of 8.5 mg/L, the predicted potential at $t=0$ and chlorine concentration at $t=1h$ and $2h$ are shown in Fig.2. A sharp potential gradient occurs at the junction point of copper and solder, resulting in a fast initial corrosion rate of Pb and consumption rate of chlorine. The predicted leaching curve of Pb and Cu agree well with the measurement data.

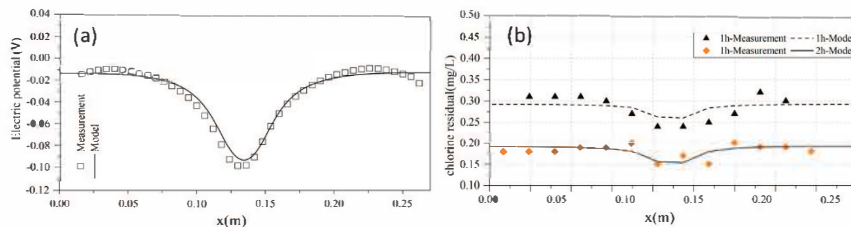


Fig. 2. (a) potential profile and (b) chlorine concentration along the soldered copper pipe.

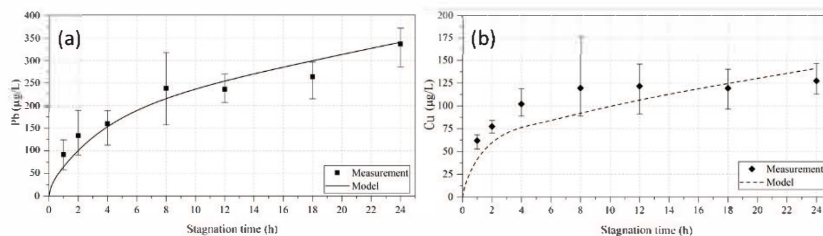


Fig. 3. The predicted leaching curve of (a) Pb, and (b) Cu, comparing with measurement data.

Conclusions

An electrochemical model to simulate the galvanic corrosion process in drinking water environment is formulated and validated against experimental data for the first time.

Acknowledgement

This research is supported by the Hong Kong Research Grants Council (Project 16216717).

References

- Ma, X., Armas, S. M., Soliman, M., Lytle, D. A., Chumbimuni-Torres, K., Tetard, L., & Lee, W. H. (2018). In situ monitoring of Pb²⁺ leaching from the galvanic joint surface in a prepared chlorinated drinking water. *Environmental Science & Technology*, 52(4), 2126-2133.
- Munn, R. S., & Devereux, O. F. (1991). Numerical modeling and solution of galvanic corrosion systems: part I. Governing differential equation and electrodic boundary conditions. *Corrosion*, 47(8), 612-618.

**The 9th International
Symposium on
Environmental Hydraulics**

B Session

Jets [B-T1]



Self-preserving characteristics in 2D submerged offset jets

Subhasish Dey^{1*}, Galla Ravi Kishore² and Sk Zeeshan Ali³

¹ Department of Civil Engineering, Indian Institute of Technology Kharagpur, West Bengal, India

² Department of Civil Engineering, Satya Institute of Technology and Management, Vizianagaram, Andhra Pradesh, India

³ Department of Civil Engineering, Indian Institute of Technology Hyderabad, Telangana, India

* Corresponding: sdey@iitkgp.ac.in

Keywords: Hydraulics; Jets; Turbulent flows

Abstract

Experiments were conducted to characterize the turbulent flow in two-dimensional (2D) submerged offset jets. The vertical profiles of time-averaged velocity and Reynolds stresses at different horizontal locations were detected to ascertain their self-preserving characteristics in the pre-attachment, impingement and wall jet regions.

The self-preserving characteristic in individual horizontal velocity profiles in different regions of submerged offset jets is observed by using the velocity scale as the jet velocity and the vertical length scale as the jet half-width from the point of occurrence of jet velocity in the pre-attachment region and from the boundary in the impingement and wall jet regions. In general, these scales are capable to bring down the data plots to a single band substituting self-preserving characteristic in individual horizontal velocity profiles. The thickening of jet layer in the pre-attachment and wall jet regions and the decreasing of jet layer in the impingement region are prevalent. However, the jet half-width in the wall jet region of submerged offset jet is greater than those of classical wall jet and submerged wall jet.

Furthermore, the self-preserving characteristic in the individual Reynolds shear stress profiles in different regions of submerged offset jets is examined by using the Reynolds shear stress scale as its peak value and the vertical length scale as the half-width of Reynolds shear stress above its null-point. Using these scales, the Reynolds shear stress profiles exhibit a self-preserving characteristic. The half-width of Reynolds shear stress thickens with the horizontal distance in the pre-attachment and wall jet regions, but the data plots do not follow any specific trend in the impingement region. On the other hand, the elevation of the null-point of Reynolds shear stress increases with an increase in horizontal distance in the pre-attachment and wall jet regions, but they decrease with horizontal distance in the impingement region. However, in the wall jet region, the half-width and the elevation of the null-point of Reynolds shear stress of submerged offset jets are greater than those of classical wall jet and submerged wall jet.

Finally, the self-preserving characteristics in the individual profiles of the Reynolds normal stresses are tested by using their scales as peak values of the horizontal Reynolds normal stress and the length scale as that of the Reynolds shear stress. They allow to collapse the data plots of the individual Reynolds normal stresses on a single band in different regions of submerged offset jets, substantiating that the self-preserving characteristic is prevailed.

Mathematical model of Reynolds shear stress in a turbulent plane jet with Coandă effect

Sk Zeeshan Ali^{1*}, Galla Ravi Kishore² and Subhasish Dey³

¹ Department of Civil Engineering, Indian Institute of Technology Hyderabad, Telangana, India

² Department of Civil Engineering, Satya Institute of Technology and Management, Vizianagaram, Andhra Pradesh, India

³ Department of Civil Engineering, Indian Institute of Technology Kharagpur, West Bengal, India

* Corresponding: zeeshan@ce.iith.ac.in

Keywords: Turbulent jets; Coandă effect; Reynolds shear stress

Abstract

When a turbulent plane jet is issued from a raised opening into the quiescent environments above a bottom-wall, the Coandă effect induces the jet to deflect towards the bottom-wall owing to the ambient fluid entrainment to produce a negative pressure zone. The flow zone upstream of the jet impingement point is called the pre-attachment zone. After the impingement of the jet, the flow develops on the bottom-wall over a certain downstream stretch, called the impingement zone. Beyond the impingement zone, a wall jet type flow is prevalent in the wall jet zone. In this study, we develop a mathematical model for the Reynolds shear stress profiles in various zones of a turbulent jet with Coandă effect. To this end, the two-dimensional Reynolds averaged Navier–Stokes equations together with the continuity equation are solved for the estimation of Reynolds shear stress. The mathematical derivations are based on the boundary layer approximation. In the pre-attachment zone, the velocity profile follows an exponential function. In addition, in the impingement- and wall jet-zone, it follows a combination of a power function within the inner layer and an exponential function within the outer layer of the jet. The exponent of the power function is obtained using the experimental data and coefficients of the exponential function are determined from the boundary conditions. The computed Reynolds stress profiles have a satisfactory agreement with the experimental observations.

The present mathematical model provides a detailed understanding of the Reynolds shear stress within the jet layer and may have implications related to hydraulic engineering, chemical engineering and industrial applications. The model outcomes are obtained for a given set of salient parameters related to the jet and therefore, the model may be useful to make sophisticated engineering software.

Effect of ambient turbulence on the entrainment into a turbulent jet – mean properties

Rana Sahebjam¹, Khashayar F. Kohan¹, and Susan Gaskin^{1*}

¹Department of Civil Engineering, McGill University, Montreal, Quebec, Canada

*Corresponding: susan.gaskin@mcgill.ca

Abstract

Studies of jets have mainly been in quiescent flows; however, as effluents are released into turbulent surroundings in engineering practice, the effect of the ambient turbulence on the jet entrainment and mixing is of interest. Hunt (1994) argued that if a jet or plume flow is subjected to external forcing, causing the jet structure to break down, entrainment would be reduced. Recent experimental research is extended to study of the passive scalar field of a turbulent jet ($Re = 5800$ and 10600) in a turbulent ambient flow using planar laser induced fluorescence. The large scales of the ambient turbulence advect the jet, while the entrained small scales modify and shorten the self-similar region of the jet flow, reducing jet-driven entrainment.

Keywords: jets, background turbulence, passive scalar

Introduction

Effluents are disposed of into the atmosphere or hydrosphere in the form of turbulent jets to reduce the local or acute impact of pollutant emissions. Until recently, research on jets in quiescent or unquantified turbulent flows (e.g. channel flows) was assumed to be conservative due to the assumed superposition of the jet induced turbulent entrainment and mixing, and turbulent diffusion. However, following Hunt's (1994) suggestion that external forcing of a jet or plume, by disrupting the jet structure, will reduce entrainment, experiments have confirmed decreased entrainment in a jet in a co-flow (Gaskin et al. 2004), an axisymmetric jet (Khorsandi et al. 2013, Perez-Alvarado 2016). The current study aims to investigate the jet dynamics that result in the reduced time-averaged (Reynolds averaged) entrainment through a study of the passive scalar field of a turbulent jet in a homogeneous isotropic ambient turbulence.

Methods

A turbulent axisymmetric jet was released into a quiescent and an approximately homogeneous isotropic turbulence with zero mean flow. The ambient turbulence was produced in a glass tank using a random jet array (RJA) (Variano & Cowen 2008). The jet flow ($Re = 5800$ and 10600) issued parallel to the RJA plane to maintain a constant level of ambient turbulence ($TKE = 4.4 \text{ cm}^2/\text{s}^2$) along the jet axis. Planar laser induced fluorescence measurements of a passive scalar allowed statistics to be obtained from cross-sections at axial distances of $x/D = 20, 30, 40, 50$ and 60 . The data was analyzed to obtain averages conditioned on the jet centroid, which allowed for the separation of the effect of the large scales and the small scales of the ambient turbulence on the jet, through removing the effect of jet meandering.

Results

Ambient turbulence vortices larger than the integral length scale of the flow advect the jet, while the smaller scales are entrained. This results in a meandering path of the jet and a larger jet boundary region (in which the intermittency of the jet increases from zero to one) due to

modulation of the jet boundary by the smaller eddies of the ambient. The downstream evolution of the jet in the turbulent ambient is compared to the jet in a quiescent ambient in terms of its centerline mean concentration and concentration rms, and its half-width obtained from averages conditioned on the centroid of the instantaneous images, shown in Figure 1.

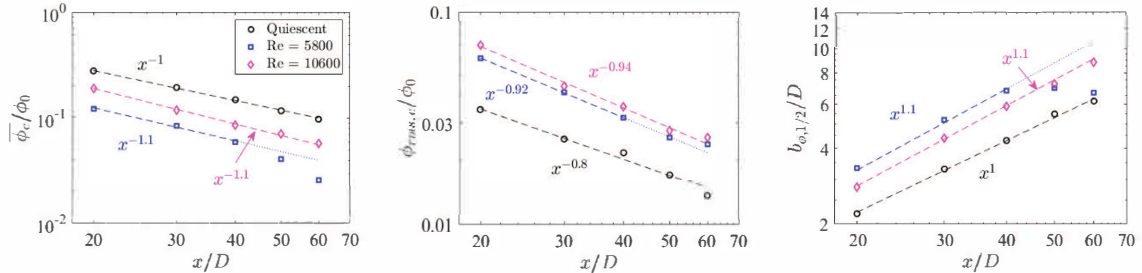


Fig. 1. Scalar statistics of a jet in an ambient turbulence: (a) Mean concentration (b) rms concentration and (c) concentration half-width

The mean centerline concentration decays more rapidly than that in a quiescent ambient, exhibiting self-similar behavior until jet break-up (i.e $x/D > 40$ in the $Re = 5800$ jet) due to the disruption due to the entrained ambient turbulence. The latter results in a greater rms concentration of the jet in the ambient turbulence, which decays with axial distance. The growth of the jet half-width is greater than that of a jet in a quiescent ambient, until the point of jet break-up in the $Re = 5800$ jet, when width growth stops. The lack of width growth indicates that there is no longer any jet-driven entrainment (the mean velocity has decayed to zero) and only molecular and turbulent diffusion occur beyond this point. The effect of the ambient turbulence is more noticeable on the $Re = 5800$ jet, due to its weaker mean momentum.

Conclusions

The dynamics of a jet released into a turbulent ambient has three regions of behavior, which depend on the relative turbulence intensity (ξ) and relative length scales (\mathcal{L}) between the ambient and the jet. Initially the jet is relatively undisturbed by the ambient turbulence. This is followed by a self-similar region with jet-driven entrainment in which the mean properties decay more rapidly than that in a quiescent flow due to advection by the larger scales of the ambient turbulence and entrainment of the smaller scales. Finally, once the ambient turbulence has broken-up the jet flow (no mean velocity, no width growth), only molecular and turbulent diffusion act on the passive scalar.

Acknowledgement

Funded by the National Science and Engineering Research Council of Canada (RGPIN 2016-04473).

References

- Gaskin, S., McKernan, M. & Xue, F. (2004) The effect of background turbulence on jet entrainment: an experimental study of a plane jet in a shallow co-flow, *Journal of Hydraulic Research*, 42(5), 533-542.
- Hunt, J.C.R. (1994) Atmospheric jets and plumes, In *Recent Research Advances in the Fluid Mechanics of Jets and Plumes*, 255, 309-334. Springer.
- Khorsandi, B., Gaskin, S. & Mydlarski, L.M. (2013) Effect of background turbulence on an axisymmetric turbulent jet, *Journal of Fluid Mechanics*, 736, 250-286.

- Perez-Alvarado, A. (2016) Effect of background turbulence on the scalar field of a turbulent jet. Ph.D. Thesis, McGill University.
- Variano, E.A. & Cowen, E.A. (2008) A random-jet-stirred turbulence tank, *Journal of Fluid Mechanics*, 604, 1-32.

Estimation of attraction flow propagation as turbulent rectangular surface jet

Veronica Wiering^{1*}

¹Federal Waterways Engineering and Research Institute, Germany

*Corresponding: veronica.wiering@baw.de

Abstract

Attraction flow propagation is a key factor for the detection of fishway entrances. Hydraulically, attraction flow can be considered as a turbulent rectangular surface jet. Defining surface jets as half-free jets, existing analytical approaches for jet propagation aspect ratios $W/H > 1$ are adapted for $W/H < 1$, which are typical for fishway entrances. Derived equations address jet propagation as a centerline velocity decay function dependent on W/H and the inner diffusion angle $\alpha_i = 5^\circ$. The results were validated for numerical runs using OpenFOAM. A well-funded, easily applicable engineering tool for estimating attraction flow propagation is presented.

Keywords: three-dimensional jet; attraction flow; aspect ratio; fishway; centerline velocity decay

Introduction

Fishway attraction flow is needed to guide the fish into the entrance pool of the fishway (e.g. Larinier, 1992). However, there is no common method to evaluate the interaction of fishway entrance aspect ratios W/H (where W is entrance width and H is water depth), attraction discharge and flow velocities as crucial parameters in order to reliably estimate attraction flow propagation in the planning process. Attraction flow behaves like a three-dimensional surface jet which can be defined as half-free jets with the water surface as symmetry plane. Studies of three-dimensional free (i.e. with no water surface present) jets show, that the aspect ratio of the orifice W/H is a determining factor for velocity decay along the centerline and thus the jet propagation (e.g. Rajaratnam, 1976). The focus of previous studies is on free jets and $W/H > 1$. The present study aims at deriving a simple tool for attraction flow estimation. In this, results obtained from CFD investigations of fish entrance specific surface jets and aspect ratios $1/8 \leq W/H \leq 1$ are compared with an established analytical approach (Kraatz, 1975) and available jet studies (Rajaratnam and Humphries, 1984; Madnia and Bernal, 1994; Gholamreza-Kashi et al., 2007).

Methods

In the present study, we chose the jet half-length L_x as relevant parameter to characterize attraction flow propagation. L_x equals the distance from the orifice to the point where the centerline velocity is half the outlet velocity u_0 and thus describes the longitudinal jet propagation.

Kraatz (1975) formulated equations to assess centerline velocity decay for plane and round free jets dependent on W/H and the inner diffusion angle α_i , which is affected by the initial turbulence at the orifice. Based on this, the following equations, called the Inner Diffusion Angle Concept (IDAC), are derived for rectangular surface jets to determine L_x :

$$\frac{L_x}{W} = \frac{2}{\tan(\alpha_i)} \quad 0 \leq W/H \leq 1/4 \quad (1)$$

$$\frac{L_x}{W} = \frac{1}{\sqrt{W/H} \tan(\alpha_i)} \quad 1/4 < W/H \leq 1 \quad (2)$$

The inner diffusion angle was set to $\alpha_i = 5^\circ$ for best accordance and thus lies within the range of 4.5° and 5.5° (Kraatz, 1975). To verify whether the above equations can be adopted to predict the propagation of rectangular surface jets with $W/H < 1$, eight hydro-numerical simulations with four different aspect ratios $1/8 \leq W/H \leq 1$ are used for comparison. Using a 3D RANS solver integrated with the SST $k-\omega$ turbulence model available in OpenFOAM a cubic waterbody with $40 \text{ m} \times 40 \text{ m} \times 20 \text{ m}$ ($x y z$) and a rectangular inlet with different sizes is modelled. The outlet velocity is set to a uniform profile of $u_0 = 1,5 \text{ m/s}$ which is a typical design velocity for fishways on German waterways.

Results

The CFD results of the jet half-length show that L_x decreases with increasing W/H for $W/H \leq 1$. Results show good agreement with equations derived from Kraatz (1975) and other studies, especially for $1/4 \leq W/H \leq 1$ (Fig. 1). Since IDAC assumes a constant L_x/W independent of W/H for $W/H \leq 1/4$, the deviation for $W/H = 1/8$ is about 14.5 %. The velocity decay along the centerline occurs faster than in the numerical data and results in a decreased L_x at $W/H = 1/8$.

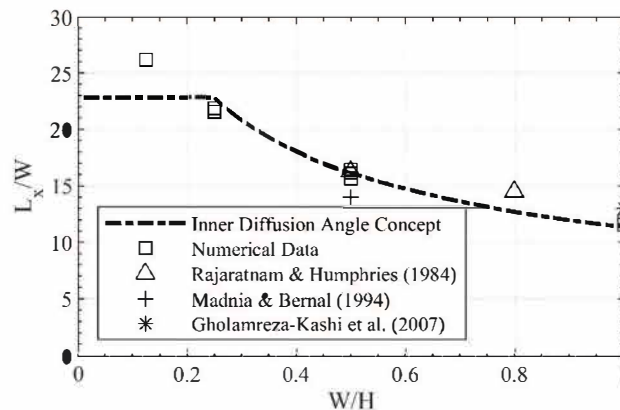


Fig. 1. Comparison of the predicted jet half-length of IDAC, previous studies and numerical simulations.

Conclusions

The analytical approach for round and plane jets with $W/H > 1$ was confirmed for rectangular surface jets with $W/H \leq 1$. The findings can be used to assess fishway attraction flow propagation by means an established approach.

References

- Gholamreza-Kashi, S.; Martinuzzi, R. J.; Baddour, R. E. (2007): Mean Flow Field of a Nonbuoyant Rectangular Surface Jet. In *Journal of Hydraulic Engineering* 133 (2), pp. 234–239. DOI: 10.1061/(ASCE)0733-9429(2007)133:2(234).
- Kraatz, W. (1975): *Ausbreitungs- und Mischungsvorgänge in Strömungen*. Dissertation. Technische Universität Dresden, Dresden, Germany.
- Larinier, M. (1992): Implantation des passes à poissons. In *Bull. Fr. Pêche Piscic* 326-327, pp. 30-40. DOI: 10.1051/kmae:1992004.
- Madnia, K.; Bernal, L. P. (1994): Interaction of a Turbulent Round Jet with the Free Surface. In *Journal of Fluid Mechanics* 261, pp. 305–332. DOI: 10.1017/S0022112094000352.
- Rajaratnam, N. (1976): *Turbulent jets*. Amsterdam, Oxford, New York: Elsevier Scientific Pub. Co (Developments in water science, 5).
- Rajaratnam, N.; Humphries, J. A. (1984): Turbulent non-buoyant surface jets. In *Journal of Hydraulic Research* 22 (2), pp. 103–115. DOI: 10.1080/00221688409499387.

Prediction of Transport and Dissolution of Oil & Gas Released from Diverse Oil Blowout Scenarios in the Offshore Canada

Inok Jun^{1*}, Rebekah Jeter¹, Scott A. Socolofsky¹, Ruixue Liu², Michel C. Boufadel², Youyu Lu³, and J. Samuel Arey⁴

¹Department of Civil and Environmental Engineering, Texas A&M University, College Station, TX, USA

²Civil and Environmental Engineering Department, New Jersey Institute of Technology, Newark, NJ, USA

³Department of Oceanography, Dalhousie University, Halifax, NS, Canada

⁴ExxonMobil Biomedical Sciences, Inc., Annandale, NJ, 08801, USA

*Corresponding: jjoda85@tamu.edu

Abstract

We simulate the behavior of subsea accidental oil blowouts under a variety of realistic ambient conditions, using two numerical models in tandem. The Viscous Breakup Model in Jets (VDROP-J) calculates evolving particle size distributions of gas bubbles and oil droplets from the source, and the Texas A&M Oilspill Calculator (TAMOC) simulates the fate and transport of the released petroleum fluids through the near-field water column. The simulation scenarios span a wide range of possible oil spill conditions: release depth, oil flow rates, orifice diameter, petroleum gas-to-oil ratio (GOR), subsurface chemical dispersant injection, oil compositions, and oceanographic conditions. The model results provide mass fluxes of oil surfacing and dissolution through the water column in different subsea oil spills. This study provides information to help assess the VOC inhalation hazards in the response zone, design response strategies, and develop risk management plans for future offshore oil well blowout and pipeline leaks.

Keywords: Numerical Model, Oil Spill Scenario, Oil Fate and Transport, Response Model

Introduction

Accidental subsea oil & gas releases can pose significant safety risks at the surface in the response zone, including potential explosion hazards and the health risk by inhalation of Volatile Organic Compounds (VOCs). Thus, it is important to know if released oil & gas may reach the surface, and if so, where, when, and how much the volume fluxes will be. We run the TAMOC and VDROP-J models to investigate a broad range of potential accidental offshore oil well blowouts under diverse ambient conditions.

Method

We use TAMOC to study the fate of petroleum released to the marine environment from a diverse range of subsea oil spill scenarios. TAMOC has been validated to an extensive suite of measurements from the near field of an oil spill accident up to 10 km radius of the spill source (Gros et al. 2017, Dissanayake et al. 2018) and to numerous laboratory studies of multiphase plume dynamics (Dissanayake et al. 2018, Socolofsky et al. 2008). TAMOC takes a Lagrangian, integral-model approach to simulate the formation of a plume of oil & gas, predict their transport dynamics through the water column, and track the dissolution and biodegradation of a full suite of pseudo-components of the petroleum mixture. We initialize TAMOC with results from VDROP-J, which has been validated to numerous laboratory studies of oil breakup (e.g., Zhao et al. 2016). VDROP-J simulates the evolving population of bubbles and droplets from a subsea release, considering particle-scale force balances and including break-up, coalescence, viscous stabilization of droplet size, and the changing oceanographic condition, including the turbulent dissipation rate along the plume trajectory. TAMOC calculates the required chemical

properties for the pseudo-components from the data available in the ADIOS oil library, developed by NOAA.

Simulation

This study focuses on the Newfoundland basin located offshore Canada in the North Atlantic Ocean. We used the model output from North Atlantic Model and the World Ocean Database as ambient ocean properties and currents. To estimate dissolved gas profiles, we compute the aqueous solubility of the air at the surface and correct that for temperature and pressure at depth. We obtain the composition of different oil types, including Saturates, Aromatics, Resins, and Asphaltenes (SARA) fractions, from the ADIOS database. Oil and gas composition data are input into the Peng-Robinson Equation of State, which simulates the physical properties of oil and gas in TAMOC, following Gros et al. (2018). The numerical simulation scenarios span a range of possible oil spill conditions: release depth, oil flow rates, orifice diameter, and gas-to-oil ratio. Table 1 shows the list of scenarios of oil and gas spills.

Table 1. Scenarios of Subsea Accidental Release of Oil & Gas in the offshore Newfoundland, Canada.

Variables	Range of Variations
Release Depth (Z)	[200, 400, 600, 800, 1,000] m
Flow Rate (Q)	[1,000, 3,000, 5,000] bpd
Orifice Diameter (D)	[0.01, 0.03, 0.05] m
Gas-to-Oil Ratio (GOR)	[500, 1000, 1500, 2000]

Results

Figure 1 shows an example model output in the oil budget graph comparing results for one spill scenario with two different GORs. The donut chart shows the total mass flux rate, and each color represents the portion of mass flux for each case, such as surfacing gas and oil and petroleum compounds dissolving into the water column and intrusion layer. As GOR increases, the more gas is released from the source and reaches the surface (yellow). The higher gas flux also generates smaller oil droplets, which dissolve more rapidly into the water (blue). Since the smaller droplets take a longer time to rise and move farther downstream, they have more chance to stay inside the plume (gray). We also analyze the fraction of surfacing mass for each component as a function of GOR, and Figure 2 shows the example graph for Benzene as a function of GOR for this release scenario. The higher GOR decreases the mass fraction of surfacing oil. This work will inform the development of an Offshore Response Guidance Table to support response efforts.

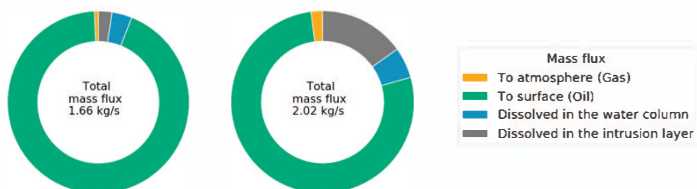


Figure 1. Oil Budget Graph for GOR = 500 & 2000
(Z = 400 m, Q = 1000 bpd, D = 0.03 m)

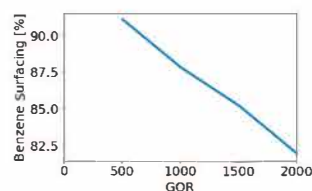


Figure 2. Fraction of Surfacing Benzene as a function of GOR

Acknowledgement

This work was funded by Department of Fisheries and Oceans Canada through their Multi-partner Oil Spill Research Initiative (MPRI), Project 1.04.

References

- Dissanayake et al. (2018). Integral models for bubble, droplet, and multiphase plume dynamics in stratification and crossflow. *Environ Fluid Mech.* 18, 1167-1202.
- Gros et al. (2017). Petroleum dynamics in the sea and influence of subsea dispersant injection during Deepwater Horizon. *PNAS*, 114(38), 10065-10070.
- Gros et al. (2018). Oil spill modeling in deep waters: Estimation of pseudo-component properties for cubic equations of state from distillation data, *Mar Pollut Bull*, 137, 627-637.

- Socolofsky et al. (2008) Double-Plume Integral Models for Near-Field Mixing in Multiphase Plumes. *J Hydraul Eng*, 134(6), 772-783.
- Zhao et al. (2016). A-DROP: A predictive model for the formation of oil particle aggregates (OPAs). *Mar Pollut Bull*, 106(1), 245-259.

Chemically reacting chlorine jet mixing with CEPT sewage effluent

Qiao, Q.S.¹ and Lee, J.H.W.^{2*}

¹Department of Civil & Environmental Engineering, the Hong Kong University of Science and Technology

²Macau Environmental Research Institute, Macau University of Science and Technology

* jhwlee@must.edu.mo

Abstract

Chlorine is widely used as chemical disinfectant in water and wastewater treatment plant. Yet the chlorination kinetics especially at high chlorine concentrations remains largely unknown. A set of experiments are carried out to examine the exertion of the chlorine demand when 10% NaOCl solution in form of turbulent buoyant jet is discharged into sewage that has received Chemically Enhanced Primary Treatment (CEPT). The total residual chlorine (TRC) and ammonia nitrogen concentration distributions in the chlorine jet are measured in field condition. The experimental results show that about 50 percent of the added chlorine mass flux is rapidly consumed within one second (in a very short distance) from the jet source. Jet model computations coupled with chlorination kinetics modeling reveal the organic reaction accounts for most of chlorine demand in the initial jet mixing process.

Keywords: Chlorination; jet mixing; chlorine demand; disinfection; primary treated sewage

Introduction

At the Stonecutters Island Sewage Treatment Works (SCISTW) of the Hong Kong Harbor Area Treatment Scheme (HATS), sodium hypochlorite NaOCl solution at a high concentration (10%) is discharged into CEPT treated sewage effluent in the flow distribution chamber (FDC) in the form of multiple turbulent dense jets to achieve intended rapid mixing effect. Field observations have revealed significant variations in chlorine consumption in the treatment system (Lee et al. 2017). Disinfection in SCISTW is essential to meet effluent standards. It is vital to optimize the chlorine dosage operation to minimize operation cost and reduce the environmental impact of HATS discharge on the receiving coastal waters.

There have been scant studies of chlorination kinetics at high concentrations (say 100,000 mg/L) used in wastewater disinfection. In addition, the injection of a concentrated chlorine solution into flowing sewage is quite different from the mixing of chlorine with sewage in a beaker test. When a chlorine jet is discharged into an ambient flow of treated effluent, the chlorine concentration in the jet decreases rapidly with distance from the source due to (i) turbulent entrainment with the surrounding fluid; and (ii) chemical reaction with the chlorine-demanding substances in the effluent. It is of great interest to develop a model that can predict the total residual chlorine (TRC) concentration distribution in chlorine jets.

Full Scale Experiments of Chlorine Jet in Flowing CEPT Effluent

Figure 1 shows the experimental setup of the chlorine jet mixing with ambient CEPT sewage flow. The fresh sewage from the sedimentation tank at the SCISTW was directly pumped into a test flume of 0.22 m width, 6.0 m length and 1.45 m height (Lee et al. 2017). Further, a broad-crest weir was installed in the flume to form a uniform sewage flow of 1.2 m/s. The 10% NaOCl solution was injected at nominal flow rate of 20 mL/s via a nozzle of 0.01 m diameter into the critical sewage flow above the weir. The vertical TRC and NH₃-N concentration distributions are measured by sampling with aid of a 2D traverse followed by standard chemical measurement.

The TRC mass flux at certain cross section of the chlorine jet is evaluated with $M = \int_0^r C_m u dA$

where C_m is the measured TRC concentration distribution, u is the jet velocity, and r is the jet width. Table 1 shows that for the coflowing jet with jet densimetric Froude number of about 2.0, the mass flux is 80% of the source mass flux at $x=0.1$ m from the source, and is 65% at $x=0.2$ m. The corresponding exertion of the chlorine demand is 20% and 35% over a time interval of about 0.1 s and 0.2 s. Moreover, the crossflow jet mixing case also demonstrates the extremely rapid chlorine demand near the jet source.

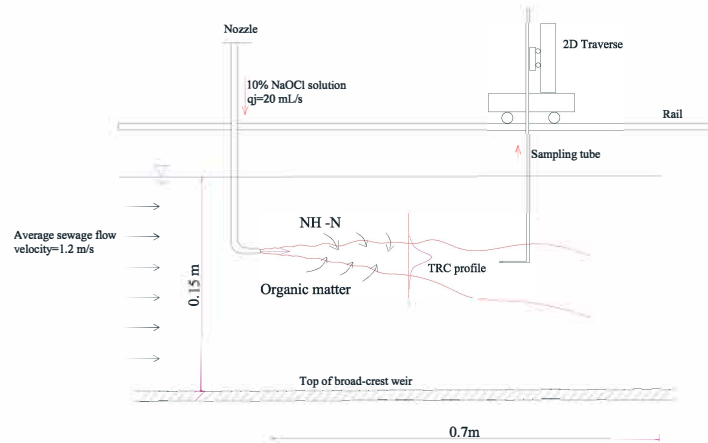


Figure 1 Experimental setup for chlorine jet mixing with CEPT sewage effluent flow.

Table 1 Summary of measured exertion of chlorine demand in mixing process

Jet mixing case	Sewage flow			Jet flow				Measured residual mass flux M/M_0	
	Temp. (°C)	U_a (m/s)	NH_3-N (mg/L)	C_0 (mg/L)	Angle (deg.)	q_j (mL/s)	M_0 (g/s)	at $x=0.1$ m (%)	at $x=0.2$ m (%)
Coflowing	22.0	1.2	35	112,000	0	20	2.24	80	65
Crossflow	20.5	1.2	35	125,000	-90	20	2.50	94	45

Results

The changes in TRC concentration due to physical mixing and chlorination kinetics along the jet can be well-predicted by coupling a validated Lagrangian buoyant jet model (Lee and Chu 2003) with a chlorination kinetics model that accounts for the reaction between free chlorine, ammonia, monochloramine, and organic compounds. The numerical computations (not shown) indicate that the organic reactions account for most of the chlorine demand in the jet mixing zone close to the source.

Acknowledgement

This work is supported by a grant from the Hong Kong Research Grants Council (GRF 16215618). The support and assistance of DSD staff at SCISTW are well-appreciated.

References

1. Lee, J.H.W., Qiao, Q.S., Chan, S.N., Choi, D.K.W. and Huang, J.C. (2017). "Field Experiments of Chlorine Demand in Disinfection of Treated Primary Effluent." *J. Environ. Eng. ASCE*, 143(11).
2. Lee, J.H.W. and Chu, V.H. (2003). *Turbulent Jets and Plumes - a Lagrangian Approach*, Springer, New York.

The 9th International
Symposium on
Environmental Hydraulics

C1 Session

Density Current [C1-T3]



The hydraulics of the salt tip in the estuarine contraction

Nguyen, Ngoc Minh¹ and Hwang, Jin Hwan²

^{1,2}Department of Civil & Environmental Engineering, Seoul National University

Keyword: the contraction, the baroclinic flow, the salt tip.

Abstract

Since the tidal flow interacts with the river flow, the water of the estuary is frequently stratified. Tide in the stratified flow makes the flows to be in baroclinic and barotropic modes. In which, the tide in the baroclinic mode induces more shear than the barotropic mode and influences more complicatedly on the estuary dynamics. The baroclinic flows are frequently found at the downstream of the constrictions of Hudson river where the widths are landward contracted. Although the baroclinic flows are proved to be very important to the convergences of the along estuary currents and the development of the density fronts such as the density fronts in Hudson River estuary (Geyer and Ralston, 2015), some parts in their dynamics have not been clearly understood, especially in the influence of the gradual contraction associated with the interaction of the ebb flow. Therefore, in order to clarify more about the role of the contraction associated with the existence of the baroclinic flow, we try to investigate the development of the density front at the end of the salt wedge that is salt tip. A result shows that a small internal bore along with an overturn appears during the slack before flood in the contraction when the baroclinicity appears.

Acknowledgement (If necessary)

This work was supported.....

Reference (If necessary)

Geyer, W.R. and Ralston, D.K., 2015. Estuarine frontogenesis. *Journal of Physical Oceanography*, 45(2), pp.546-561.

.

Numerical Study of Confluence Channel Flow with Gravity Currents

Minjae Lee¹, Yong Sung Park^{1*}

¹Department of Civil and Environmental Engineering, Seoul National University, Seoul, Korea
Corresponding: dryspark@snu.ac.kr

Keywords: Confluence Flow, Gravity Currents, Bed Discordance, Bed Concordance, Numerical Simulation

Abstract

Density difference due to temperature induces gravity currents which affect hydrodynamics. From field data set, temperature difference between main flow and tributary flow has been observed in confluence channel of Nakdong River and Hwang River in South Korea in summer and its difference is enough to induce gravity currents. When the temperature difference has been observed, mixing trend in confluence channel is somewhat different. It can be expected that tributary flow flows underneath main flow, in other words, gravity currents is occurred because density of tributary flow is higher than its for main flow. From this observation result, gravity currents can be considered that one of factors affects confluence flow. Primarily, confluence channel flow has complex behaviors such as flow deflection, separation, shear layer, and vortex. Its behaviors change depending on such factors which are density difference, bed elevation difference, momentum ratio, and confluence angle. In this study, gravity currents effects will be mainly investigated on flow structure in confluence channel with bed concordance and bed discordance through numerical simulations. Conditions of momentum ratio and confluence angle are maintained and different densities between main flow and tributary flow are applied in order to occur gravity currents and its results will compare to confluence flow with same density between the flows. Bed morphology which is bed elevation difference at confluence affects flow structures and its effects are expected more significant when gravity currents is occurred. Therefore, two geometries with and without bed elevation difference at confluence will be constructed and how flow structures change will be examined under the conditions having density difference between main flow and tributary flow.

LES of Colliding Gravity Currents

Angelos Kokkinos¹, Panagiotis Prinos¹

¹ Aristotle University of Thessaloniki, Department of Civil Engineering, Greece

* Corresponding: angeloks@civil.auth.gr

Keywords: *collision, gravity currents, turbulence, LES, OpenFOAM*

Abstract

In this work the flow occurring from the collision of two gravity currents is investigated numerically using Large Eddy Simulation (LES). A lock-release numerical experiment is used to simulate the collision of gravity currents. The focus is on the examination of the dynamical features of symmetric collision, i.e. currents with same densities and same heights. The resulting maximum height and vertical velocity after the collision as well as the turbulence characteristics are investigated. The simulations are performed using LES code, through the open-source OpenFOAM toolkit. Specifically, the model solves the Navier-Stokes equations along with a concentration transport equation, assuming the Boussinesq approximation for the density. A dynamic Smagorinsky SGS model is used for the evaluation of eddy viscosity for the description of turbulence. The model is validated using available laboratory measurements of Zhong et al. (Zhong et al., 2018). It is found that 3D LES can capture most of the physics observed in experiments from the early pre-collision stage, the collision, and the post-collision flow. Numerical simulations of colliding gravity currents are performed for a wide range of Grashof numbers (10^8 - 10^{12}) which extend the range achieved in laboratory experiments. The reasonable agreement of the model results with experimental measurements indicates the usefulness of LES in the study of gravity currents collision.

References

Zhong, Q., Hussain, F., & Fernando, H. J. S. (2018). Quantification of turbulent mixing in colliding gravity currents. *Journal of Fluid Mechanics*, 851, 125–147. <https://doi.org/10.1017/jfm.2018.488>

Effects of rotation on stratified exchange flows over a submerged sill

Alan Cuthbertson^{1*}, Jarle Berntsen², Janek Laanearu³ and Magdeli Asplin²

¹School of Science and Engineering (Civil Engineering), University of Dundee, UK

²Department of Mathematics, University of Bergen, Norway

³School of Engineering, Tallinn University of Technology, Estonia

*Corresponding: a.j.s.cuthbertson@dundee.ac.uk

Abstract

Stratified exchange flows occur in natural aquatic environments when horizontal density (i.e. baroclinic) and/or pressure (i.e. barotropic) gradients are initiated between adjacent connected water masses with different densities. This study presents 3D numerical simulations, utilizing the Bergen Ocean Model (BOM), of bi-directional exchange flows across an idealized trapezoidal sill obstruction for a range of parametric conditions in which Earth rotation is expected to affect exchange flow dynamics across the sill. The model results demonstrate that Coriolis forces increase the overall blockage of the saline water intrusion across the sill compared to equivalent non-rotating exchange flows, especially when the Rossby number associated with the saline intrusion is much less than unity. This effect is attributed to Ekman boundary layer dynamics and associated secondary flow circulations generated within the rotating exchange flows. The geostrophic adjustment also imposes strong control on the lateral distribution and extent of the saline intrusion across the sill and, hence, the parametric conditions under which full saline intrusion blockage is achieved for rotating sill exchange flows.

Keywords: Stratified exchange flow; sill dynamics; rotation; secondary flow, Ekman dynamics

Introduction

Stratified exchange flows are generated between adjacent water masses with different densities at coastal margins, for example, where natural topographic features such as submerged channels, sill obstructions or sediment bars control the intrusion of saline water into fjordic basins, tidal inlets, or estuaries. For submerged channels or sills that are relatively wide in comparison to the internal Rossby radius of deformation, Earth rotation effects are expected to introduce geostrophic adjustment of these internal fluid motions and thus alter the lateral distribution of the counter-flowing water masses, and the associated internal mixing processes and secondary flow circulations. The main aim of the study is to delineate the relative importance of Coriolis accelerations, net-barotropic forcing in the counterflowing water masses, and the relative sill submergence depth, in defining the range of parametric conditions under which partial or complete blockage of saline intrusions will occur across an idealized sill.

Methods

The channel-sill geometry under investigation in the BOM simulations is the same configuration as considered in the experimental study of Cuthbertson et al. (2018) (see Fig. 1 below).

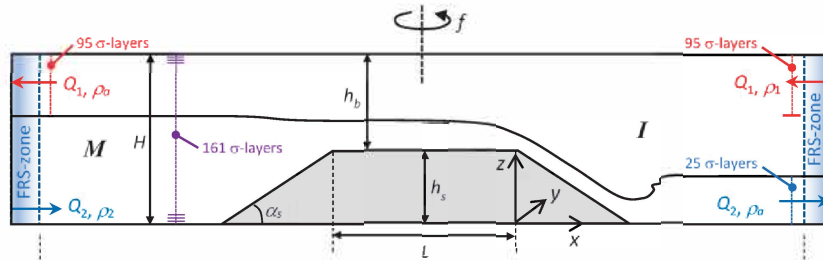


Fig. 1. Schematic representation of the BOM channel-sill model domain

BOM is a terrain-following σ -coordinate numerical simulation tool, designed for ocean modelling (Berntsen, 2000). The current study utilizes the fully non-hydrostatic version of the model at a laboratory scale equivalent to the experimental configuration, as outlined above. Full details of the BOM domain set-up and simulations are given in Cuthbertson et al. (2021). Net barotropic forcing was modelled by varying the volume flux ratio $Q^* = Q_1/Q_2$ ($= 0 - 9$) across the sill, while the relative sill submergence depth h_b/H ($= 0.075 - 0.634$) and Coriolis parameter $f = 2\Omega$ ($= 0 - 0.2136 \text{ rad s}^{-1}$) were also varied in the BOM simulations. The Rossby number based on the lower saline intrusion flow across the sill was estimated by $Ro = \bar{u}_{2,sill}/fB$, where $\bar{u}_{2,sill}$ is the average saline intrusion velocity, ranging between $Ro = 0.125 - 1.0$ for rotating exchange flows.

Results

Rotating exchange flows across the sill demonstrated geostrophic adjustment in the density and velocity fields (Fig. 2), with the dense water overflow steered to the right ($y \rightarrow 0$) and secondary circulations generated both in the lower saline intrusion and upper fresh water layers. A well-defined Ekman boundary layer was also shown to develop immediately above the sill crest. Under increasing rotation rates [i.e. $f = 0.0267 \rightarrow 0.1068 \text{ rad s}^{-1}$, Figs. 2(a), (b)], as well as for higher Q^* or lower h_b/H values (for otherwise identical parametric conditions), the lower saline intrusion layer was found to be increasingly blocked across the sill.

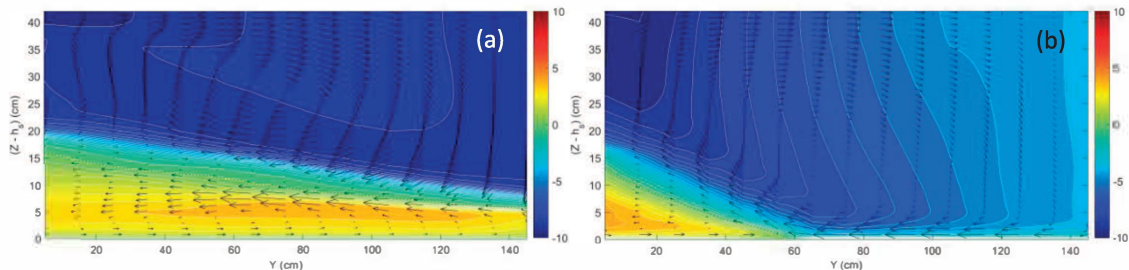


Fig. 2. Cross-sill plots of along-channel velocity field (i.e. contours at $\Delta U = 0.1 \text{ cm.s}^{-1}$, positive saline intrusion flow out-of-page) and secondary flow circulations (i.e. vector field) for simulations with Q^* : h_b/H : Ro values of (a) 6.0: 0.46: ~ 1 and (b) 6.0: 0.46: ~ 0.25 .

Conclusions

Numerical BOM simulations of rotating exchange flows across a submerged sill were used to define the parametric conditions under which partial and full saline intrusion blockage occurred. The effects of rotation, in particular, were increasingly important for simulations with $Ro \ll 1$, while parametric conditions with $Ro > 1$ had very limited influence on the exchange flow dynamics when compared to equivalent non-rotating sill exchange flows.

Acknowledgement

This work is supported by a Scottish Research Partnership in Engineering (SRPe) international grant for two research visits to the University of Bergen (<https://www.srpe.ac.uk/peer-awards>).

References

- Berntsen, J. (2000). USERS GUIDE for a modesplit σ -coordinate numerical ocean model. Technical Report 135, University of Bergen, Johs. Bruns gt.12, N-5008 Bergen, Norway. 48p.
- Cuthbertson, A., Laanearu, J., Carr, M., Sommeria, J. and Viboud, S. (2018). Blockage of saline intrusions in restricted, two-layer exchange flows across a submerged sill obstruction. *Environ. Fluid Mech.*, 18:27–57.
- Cuthbertson, A., Berntsen, J., Laanearu, J. and Asplin, M. (2021). Rotational effects on exchange flows across a submerged sill. *Environ. Fluid Mech.*, doi.org/10.1007/s10652-021-09779-5.

Experimental turbidity current dynamics responding to a simultaneous loss of confinement and break of slope

Jonathan Wilkin^{1*}, Alan Cuthbertson¹, Sue Dawson², Dorrik Stow³, Karl Stephen³, and Uisdean Nicholson³

¹School of Science and Engineering (Civil Engineering), University of Dundee, Scotland

²School of Social Science (Geography), University of Dundee, Scotland

³Institute of GeoEnergy, Heriot-Watt University, Scotland

*Corresponding: jzwilkin@dundee.ac.uk

Abstract

Turbidity currents, which travel downslope through river like channels along the seafloor, are the dominant process for delivering sediment stored upon continental shelves to deep water basins via the continental slope. This study presents a parametric series of experiments investigating the response of turbidity currents as they encounter a zone with simultaneous loss of lateral channel confinement and a break in channel slope angle. The results from the study demonstrate that the turbidity currents scour the bed area directly downstream of such transition zones, with the current flow properties and system topology directly affecting the geometry of the resulting bed deposit in the mini-basin.

Keywords: Turbidity currents; loss of confinement; slope break; deposition; mini-basins.

Introduction

Turbidity currents are one of the main transportation mechanisms on Earth, delivering terrestrial sediments to the deep ocean basins via the continental slope. These occur as relatively dense sediment-laden flows that are often confined within seafloor channels or canyon systems, propagating as highly turbulent and often supercritical slope flows that can reach velocities >10 m/s. These seafloor systems can terminate abruptly in response to relatively severe ($>2^\circ$) localised changes in gradient, or at the base of the continental slope, causing flows to often undergo a near-simultaneous loss of lateral confinement (LOC) and break of slope (BOS). This initiates a rapid change in turbidity current behavior and structure as the sediment-laden flow spreads radially and begins to deposit the sediment load. Within these settings, turbidity currents flows can produce large elongate scour features, termed *plunge pools* or *mega-flutes*, and mini-basin lobe deposits. However, the transitional flow processes producing these seafloor features remain relatively unknown. The main aim of this study is therefore to provide new insight into the turbidity current flow structure at LOC-BOS transitions, determining how these flow processes control the physical characteristics of the downstream mini-basin deposits.

Methods

A schematic of the experimental facility is shown in Fig. 1. The turbidity currents are initially fully confined within a 3.20 m-long, 0.30 m-high and 0.10 m-wide channel on an adjustable bed slope. At the end of the channel, there is a simultaneous LOC-BOS transition into a horizontal 2 m-long by 2 m-wide basin, where the unconfined turbidity current spreads radially and deposits its sediment load. A series of parametric runs are conducted varying both the initial bulk sediment concentration (12 – 18% by volume) and bed slope angle ($6 - 10^\circ$ at the turbidity current inlet). Ultrasonic Velocimeter Profiler (UVP) probes are positioned 0.15 m above the channel-basin bed, along the channel-basin centreline axis at distances 2.95 m, 3.25

m, 3.55m and 3.85 m from the inlet condition (see Fig. 1) to record the turbidity current flow field evolution throughout each experimental run. Three-dimensional representations of the resulting sediment deposits produced in the mini-basin downstream of the BOS-LOC are reconstructed into DEMs using a high-resolution photogrammetry technique (Penna et al., 2019). Each turbidity current flow was repeated to collect corresponding sediment concentration data 0.40 m downstream of the LOC-BOS transition in order not to affect the resulting deposit structure.

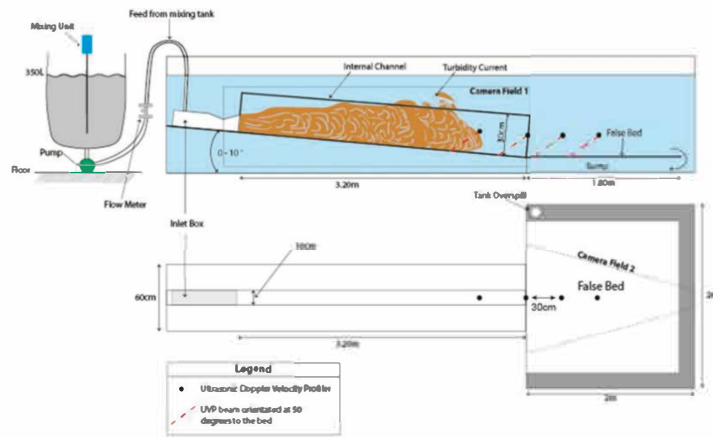


Fig. 1. Schematic representation of experimental facility

Results

Experimental runs show that sediment concentration is not the dominant control on the formation of elongate scour features downstream of LOC and BOS, with a relatively consistent levee-scour-lobe deposit arrangement generated (Fig. 2) within the mini-basin. Instead the dominant controls on the formation of such features appear to be the flow velocity transition in response to the LOC, as well as the severity of the BOS between the channel and basin.

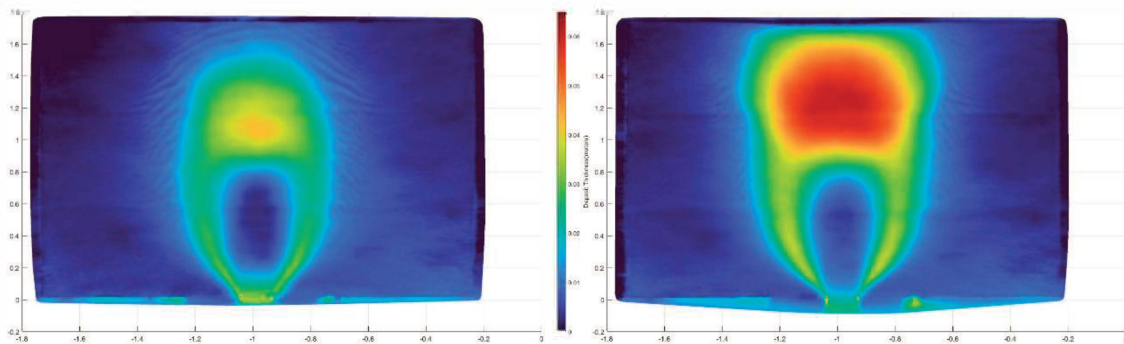


Fig. 2. Colourmaps showing the levee-scour-lobe deposit structure and thickness generated in the mini-basin for turbidity currents with volumetric concentrations of (a) 12% and (b) 18%.

Conclusions

Scaled experiments of turbidity currents encountering a simultaneous break of slope and loss of lateral confinement have been conducted to better understand the parametric conditions under which *plunge pool* or *mega-flute* scours and deposition lobes are formed. It is clear that the length of these scour features is determined by the severity of slope break, whilst the size of lobe deposit produced is related to the initial sediment concentration of the turbidity current.

Acknowledgement

The work presented is part of JW's PhD project funded by the Natural Environment Research Council (NERC) Centre for Doctoral Training (CDT) Programme in Oil and Gas [NEM00578X/1].

References

Penna, N., D'Alessandro, F., Gaudio, R., & Tomasicchio, G. R. (2019). Three-dimensional analysis of local scouring induced by a rotating ship propeller. *Ocean Eng.*, doi.org/10.1016/j.oceaneng.2019.106294

**The 9th International
Symposium on
Environmental Hydraulics**

C2 Session

Stratified Flows [C2-W3]



Turbulent mixing across a sharp density interface

Areife Ghazi Nezami¹, Blair A. Johnson^{1*}

¹Department of Civil, Architectural & Environmental Engineering, University of Texas at Austin, TX, USA

*Corresponding: blairjohnson@utexas.edu

Abstract

When gravity currents travel at sufficient velocity to generate strong shear between the current and ambient, significant mixing can occur at the head of the current and along the interface with the ambient fluid. However, if the current slows, turbulence in the head and shear at the interface may not be sufficient to sustain entrainment, instead relying upon ambient turbulence to enhance mixing between the different density layers. We perform an experimental study to characterize the role of ambient homogeneous isotropic turbulence in either mixing or sharpening an interface between two liquids of different densities. We use non-invasive optical techniques to measure the turbulent velocity and concentration fields to directly quantify turbulent diffusivity.

Keywords: Stratification; Turbulence; Experimental methods

Introduction

Industrial desalination generates brines that are often released back into the environment. Desalination brines discharged into coastal regions with weak currents or mild bathymetry do not necessarily mix with surrounding waters and can remain stably stratified (Hodges *et al.* 2011). There are several hydrodynamic forces at play in the mixing processes associated with brine discharges, including shear imposed by the velocity gradient of the discharge and turbulence at the bore front, among others. We are interested specifically in the role turbulence plays in a low mean shear environment, where ambient turbulence alone (i.e. absent mean flow or mean interfacial shear) encourages mixing across the density interface. To accomplish this, we are conducting a laboratory based experimental study to investigate the effect of homogeneous isotropic turbulence on a sharp density interface and identify the mechanisms that promote and/or inhibit interfacial erosion.

Methods

An experimental study is conducted in which high Reynolds number ($Re_\lambda \sim 300$) horizontally homogeneous isotropic turbulence with negligible secondary mean flows is generated in fresh water above a dense layer, consisting of either saltwater or a sugar-water solution. We use randomly actuated synthetic jet arrays (RASJA – Variano & Cowen 2008) to generate turbulence with the RASJA suspended at the top of a water tank, as in Johnson & Cowen (2018), to study mixing near the bottom of the tank. A schematic diagram of the experimental facility is shown in Fig. 1. Index matching is performed between the two fluids to ensure measurement accuracy.

Stereo particle image velocimetry (PIV) measurements are collected for turbulence analysis in the forced upper layer. Statistical metrics include turbulent kinetic energy, dissipation, spectra, and integral scales. Simultaneous laser induced fluorescence (LIF) measurements are used to visualize the dense layer and quantify the concentration as the two layers interact. Mixing is quantified using formulations described in Zhou *et al.* (2017), in which turbulent diffusivity is measured directly from LIF data.

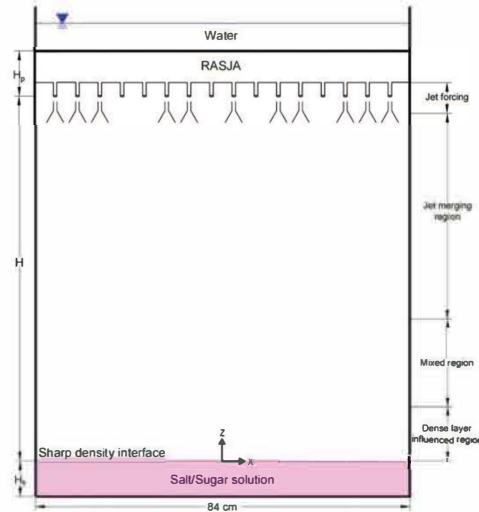


Fig. 1. Schematic of experimental facility; reproduced from Lagade (2019).

We apply the method of Zhou et al. (2017)

$$\kappa_e = \kappa \left(\frac{\partial z_*}{\partial t} \right)^2 \langle |\nabla b|^2 \rangle_{z_*} \quad (1)$$

where κ refers to molecular diffusivity, κ_e is effective diffusivity due to turbulence, b refers to buoyancy, and z_* describes the isoscalar surfaces. Using this method gives a refined metric of buoyancy gradients across the spatio-temporally varying two-dimensional concentration record and allows for a full exploration into how relative density and turbulence encourage mixing.

Results

The experimental results show that for large (order 1%) density differences between the layers, we see erosion of the dense layer such that upper layers are entrained into the ambient, but a sharp interface is maintained throughout. Turbulent diffusivity is enhanced most notably near the density interface, showing increases above molecular diffusivity to order 100, for the cases considered thus far. This study shows that the methods of Zhou et al. (2017) can be applied to measure turbulent diffusivity using LIF and PIV data in a facility designed to generate homogeneous isotropic turbulence at a sharp density interface.

References

- Hodges, B. R., Furnans, J. E., and Kulis, P. S. (2011). Thin-layer gravity current with implications. *Journal of Hydraulic Engineering*, 137(3):356-371.
- Johnson, B. A. and Cowen, E. A. (2018). Turbulent boundary layers absent mean shear. *Journal of Fluid Mechanics*, 835: 217-251.
- Lagade, J. A. (2019) Erosion of a sharp density interface by homogeneous isotropic turbulence. Master's Thesis. University of Texas at Austin.
- Variano, E. A. and Cowen, E. A. (2008). A random-jet-stirred turbulence tank. *Journal of Fluid Mechanics*, 604: 1-32.
- Zhou, Q., Taylor, J. R., Caulfield, C. P., and Linden, P. F. (2017). Diapycnal mixing in a layered stratified plane Couette flow quantified in a tracer-based coordinate. *Journal of Fluid Mechanics*, 823, 198-229.

Numerical simulation of aeration column in stratified environments

Seongeun Choi¹, Jin Hwan Hwang^{1, 2, *}

¹ Department of Civil and Environmental Engineering, Seoul National University, Seoul, South Korea

² Institute of Construction and Environment Engineering, Seoul National University, Seoul, South Korea

* Corresponding Author, jinhwang@snu.ac.kr

Abstract

Aeration is widely used to destroy the temperature stratification, but the previous studies use only linear or two-phase temperature profile. Therefore, this study creates a temperature profile based on the observed data and examines the mixing process by aeration. A numerical experiment is performed, and the site observation results are used to verify the numerical results are practical. The goals of this study are as follows: (1) The mixing behavior of the water body is examined. (2) The seasonal mixing process are studied based on the model which is verified the site observation data. (3) In addition, seasonal mixing efficiency is obtained.

Keywords: Numerical simulation; Aeration column; Stratification

Introduction

Temperature stratification is developed in many lake and reservoir, especially summer months, and it effectively controls vertical diffusion. The stable stratification conditions exist when lakes or reservoirs exhibit large thermal gradients, which the surface temperature is relatively high and the bottom temperature is relatively low. As a result, it has been long known that the water quality of the lower layers may be poor significantly (Kortmann et al., 1994). So, the aeration is used to reduce stratification and mainly installed in reservoirs to enhance water quality. This study gets the seasonal temperature profiles by site-observation and de-stratifies the water by the aeration numerically. Also, this work investigates the transport mechanism of oscillating bubbly plumes the mixing process and the seasonal mixing efficiency of the aeration.

Methods

In this study, numerical simulation is used to entirely represent the mixing behavior of water, which is hard only by site observation. In order to numerically reproduce the Yeongju dam by a numerical model, the model implements two phases, the gas and liquid phases and these phases are considered as incompressible and immiscible.

α represents the volume fractions of each cell and the range is 0 to 1 which implies full of gas and liquid, respectively. The equation for α is:

$$\frac{\partial \alpha}{\partial t} + \frac{\partial (\alpha u_i)}{\partial x_i} = 0 \quad (1)$$

and the transport properties are defined as follows (Menon, 2016):

$$\rho = \alpha \rho_l + (1 - \alpha) \rho_g \quad (2)$$

$$\mu = \alpha \mu_l + (1 - \alpha) \mu_g \quad (3)$$

where ρ , t , u_i , x_i and μ the density, time, velocity, coordinate and dynamic viscosity, subscript l and g means the liquid and gas, and the suffixes i, j can be 1, 2, 3 and represent x-, y- and z- directions, respectively. This model also considers the temperature and the density, especially of liquid, is changed with temperature linearly.

$$\rho_k = \rho - \beta \rho (T - T_{ref}) \quad (4)$$

where β is the coefficient of thermal expansion, constant of $3 \times 10^{-3}(\text{1/K})$, and T_{ref} is the reference temperature, constant of **273 K**.

Results

The comparison of site observation and simulation results at two locations is illustrated in Figure 1. The simulation results are obtained at 40 marks from -0.5 m to -20 m at 0.5 intervals. It can be seen that both results do not match near the area where two phases adjoin ($z = 0 \sim -2 \text{ m}$) due to the character of VOF method. Although the computational simulation results do not detect a slight change in temperature as like the site observation, the computational simulation results are generally corresponding with the site observation results.

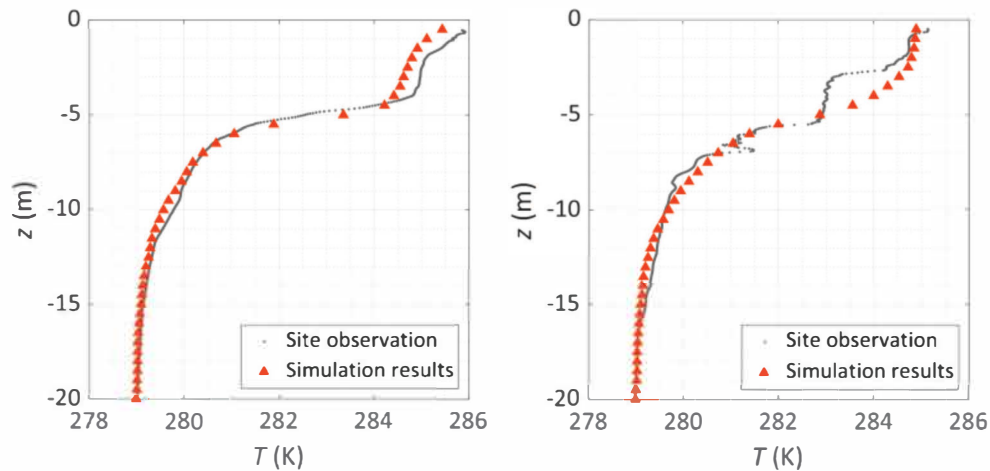


Fig. 1. The temperature of site observation and simulation results at two locations

Conclusions

The temperature stratifications are closely related to the water quality in lakes or reservoirs, so lots of reservoirs try to alleviate the stratification. In this study, the initial water temperature distributions are observed seasonally, and then the numerical simulations are studied to entirely represent the mixing behavior of water. It is confirmed that the observation result and the simulation result are mostly matched. Furthermore, it is expected that the numerical simulations will be able to obtain the seasonal mixing process and efficiency, which is difficult to obtain by only field observations.

Acknowledgement

This research was supported by Korea Environment Industry & Technology Institute(KEITE) through “Chemical Accident Response R&D Program”, funded by Korea Ministry of Environment(MOE) (ARQ201901179003)

References

- Kortmann, R. W., Knoecklein, G. W., & Bonnell, C. H. (1994). Aeration of stratified lakes: Theory and practice. *Lake and Reservoir Management*, 8(2), 99-120.
- Menon, S., Nagawkar, J., & Nilsson, H. (2016). Coupled Level-Set with VOF interFoam.

Examining the bio-physical processes of dam reservoir by spatio-temporal vertical profiling

Jin Hwan Hwang¹, Dong-Hyun Kim¹, Hyung-Cheol Park¹, Seung-Eun Choi¹, Dong-Kyun Kim²,
Ho Joon Kim², Nam-Il Won^{2*}

¹ Department of Civil & Environmental Engineering, Seoul National University, Seoul 08826, South Korea

² K-water Institute, 125 Yusungdaero1689, Daejeon, South Korea

*Corresponding: namilwon1248@gmail.com

Keywords: dam reservoir; vertical profile; bio-physical process; water quality; monitoring

Abstract

Water management in dam reservoirs has been studied as an overarching theme in water management. External factors, such as non-point pollutants flowing from the upper watershed, are the primary and most important targets for water management in dam reservoirs. However, the generation of organic matter by internal processes in dam reservoirs has also been recognized as a significant environmental parameter. Biological phenomena, such as the occurrence of cyanobacterial harmful algal blooming (CyanoHAB), occur in combination with environmental and physical factors, and are also closely related to seasonal environmental and ecological variables of dam water bodies. Although several phenomena have been identified through stationary environmental monitoring, there have been limitations in understanding biophysical phenomena without in-situ continuous vertical measurement of multiple environmental factors. In this study, the continuous environmental profiling of the dam reservoir was carried out during multiple ecologically distinct seasons using the Yoing Ocean Data Acquisition profiler (YODA, JFE-Advantech). The continuous in-situ vertical operation of YODA successfully showed the characteristics of seasonal algae generation and stratification phenomenon. The characteristics of benthic diatom blooming in spring and of CyanoHAB in summer were well observed in terms of vertical distribution. The destruction of vertical stratification by bubble plume of underwater circulation system were also well measured, showing the applicability of YODA to evaluate the environmental engineering effort to manage water quality. As of natural phenomena, the fate of turbid water caused by heavy rainwater inflow were clearly shown in terms of stratification, propagation, and mixing. These results suggest that the biophysical processes of the dam reservoir could be detailed through the vertical profiling of the entire dam reservoir with the combination of biological and ecological data, presenting the scientific foundation for the eco-friendly dam operation based on watershed management.

Buoyancy-driven exchange flows in inclined ducts

Adrien Lefauve¹, Paul Linden

¹Department of Applied Mathematics and Theoretical Physics, University of Cambridge, UK

* Corresponding: lefauve@damtp.cam.ac.uk

Keywords: *Stratified flows, exchange flows, stratified turbulence, stratified mixing, estuaries*

Abstract

Buoyancy-driven exchange flows arise in the natural and built environment wherever bodies of fluids at different densities are connected by a narrow constriction, such as estuaries or seas on either sides of a strait. In this paper we study these flows in the laboratory using the canonical stratified inclined duct experiment, which sustains an exchange flow in an inclined duct of rectangular cross-section over long time periods [1].

We study the behaviour of these sustained stratified shear flows by focusing on three dependent variables: the qualitative flow regime (laminar, wavy, intermittently turbulent or fully turbulent), the mass flux (net transport of buoyancy between reservoirs) and the interfacial thickness (thickness of the layer of intermediate density between the two counter-flowing layers). These variables are all relevant in practical applications to predict the exchange rate and mixing of active or passive scalars (e.g. salt, heat, pollutants, nutrients...).

Dimensional analysis reveals five non-dimensional independent input parameters: the duct aspect ratios in the longitudinal direction A and spanwise direction B , the tilt angle θ , the Reynolds number Re (based on the initial buoyancy difference driving the flow) and the Prandtl number Pr (we consider both salt and temperature stratifications). After reviewing the literature and open questions on the scaling of regimes, mass flux and interfacial thickness with A , B , θ , Re , Pr , we present the first extensive, unified set of experimental data where we varied systematically all five input parameters and measured all three output variables with the same methodology.

Our results in the (θ, Re) plane for five sets of (A, B, Pr) reveal a variety of scaling laws, and a non-trivial dependence of all three variables on all five parameters, in addition to a sixth elusive parameter. We further develop three classes of candidate models to explain the observed scaling laws: (i) the recent volume-averaged energetics of [2]; (ii) two-layer frictional hydraulics; (iii) turbulent mixing models. While these models provide significant qualitative and quantitative descriptions of the experimental results, they also highlight the need for further progress on shear-driven turbulent flows and their interfacial waves, layering, intermittency and mixing properties.

References

- [1] Meyer & Linden, J. Fluid Mech., vol. 753, 2014, pp. 242–253
- [2] Lefauve, Partridge & Linden. J. Fluid Mech., vol. 848, 2019, pp. 508–544

The anisotropy of symmetric Holmboe instabilities in stratified flows

Adam J.K. Yang^{1*}, E.W. Tedford¹, J. Olsthoorn¹, A. Lefauve², and G.A. Lawrence¹

¹Department of Civil Engineering, University of British Columbia

²Department of Applied Mathematics and Theoretical Physics, University of Cambridge

*Corresponding: jyangay@mail.ubc.ca

Abstract

The anisotropy of Holmboe instabilities is investigated using single wavelength simulations (SWS), multiple wavelength simulations (MWS), and a laboratory experiment. The rightward and leftward propagating instabilities are separated with a Fourier transform enabling a direct comparison of the fluctuation fields between the simulations and linear stability analysis. The decomposition and superposition of the fluctuation fields provide a new insight into the origin of Reynolds stresses. Conventionally, only the statistics of horizontal and vertical velocity fluctuation pairs, (u',w') , are presented to show the degree of anisotropy in turbulent fields. Here, we present these (u',w') -pairs using both theory-based and statistical approaches.

Keywords: *Stratified flow, Holmboe instability, anisotropy of fluctuation field, Reynolds stress*

Introduction

We are interested in the shear-induced instability of a statically stable fluid. Such background flows occur in many geophysically relevant situations in straits, estuaries, and oceans (Smyth and Winters, 2003; Yang et al., 2019; Caulfield, 2021). As these instabilities grow at the interface, they contribute to the interfacial shear stress and mixing between the layers. The best known shear instability is the Kelvin-Helmholtz instability, which quickly grows into stationary billows and then breaks down into three-dimensional turbulence. When a density profile is sharper than the velocity profile, the Holmboe instability arises. In recent years increasing attention has been paid to this instability and the mixing associated with it (Tedford et al. 2009; Caulfield, 2021).

Methods

In this study, we first use linear stability theory to reveal the anisotropy via particle orbits of Holmboe waves. We then use single wavelength direct numerical simulations (SWS) and multiple wavelength direct numerical simulations (MWS). The initial setup of MWS is the same as SWS except for the length of the domain, allowing for wave spectrum evolution. The simulations are compared with a laboratory experiment.

Results

With the mean flow profiles (Fig. 1a), the comparison of (u',w') -pairs between the linear stability analysis and MWS is shown in Fig. 1(b)&(c). The (u',w') -pairs in MWS are presented based on joint probability density functions, where the darker shading denotes higher probability and the lighter shading denotes lower probability. When we average the (u',w') -pairs, the vertical structure of the Reynolds stress is obtained (Fig. 1d).

Conclusions

For the rightward propagating wave, both the MWS and linear theory show that (u',w') -pairs orientated are towards the 2nd and 4th quadrants ($u'w' < 0$) within the shear layer above the density interface, illustrating anisotropic fluctuation field. The (u',w') -pairs for the leftward propagating waves mirror those of the rightward propagating waves. On average, a negative

Reynolds stress is produced. The (u', w') -pairs from SWS and laboratory experiments, and the corresponding linear stability prediction, show a similar orientation; see Yang et al. (2021) for a detailed description. The vertical structure of the Reynolds stresses in the simulations and laboratory experiment agrees with the linear stability prediction.

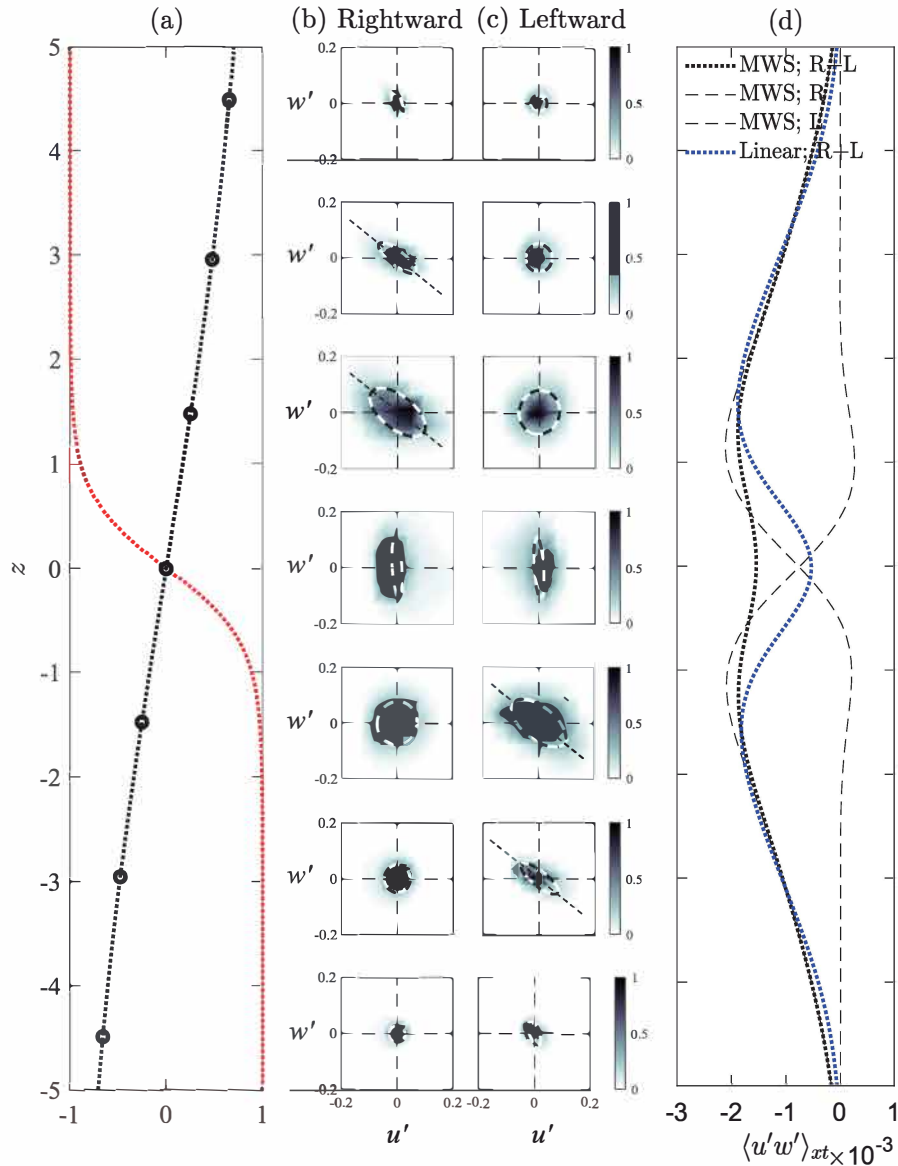


Fig. 1. Flow fields of MWS for the period $t = 250-330$ and linear stability analysis: (a) mean density (red) and velocity (black) profiles from the MWS, (u', w') -pairs for the (b) rightward and (c) leftward propagating waves, and (d) the Reynolds stresses

References

- Caulfield, C. P. (2021). Layering, instabilities, and mixing in turbulent stratified flows. *Annual Review of Fluid Mechanics*, 53.
- Smyth, W. D., & Winters, K. B. (2003). Turbulence and mixing in Holmboe waves. *Journal of Physical Oceanography*, 33(4), 694-711.
- Yang, A. J., Tedford, E. W., & Lawrence, G. A. (2019). The spatial evolution of velocity and density profiles in an arrested salt wedge. *Theoretical and Applied Mechanics Letters*, 9(6), 403-408.
- Yang, A. J., Tedford, E. W., Olsthoorn, J., Lefauve, A., & Lawrence, G. A. (2021). Reynolds stresses in Holmboe instabilities: from linear growth to saturation. arXiv preprint arXiv:2103.12220.

Assessment of the Water Circulation Plan for Water Quality Improvement of the Seonakdong River

Sanguk Lee^{1*}, Young Teck Hur¹, Youngsung Kim¹, Eul Rae Lee¹

¹ K-water Institute, Daejeon, Korea

* Corresponding: lsu@kwater.or.kr

Keywords: 2D hydrodynamic and water quality model; CE-QUAL-W2; Eco-Delta City; water circulation;

Abstract

The Seonakdong River was originally the main stream of the Nakdong River, but it has been maintained in its current state since the construction of the Daejeo Water Gate and Noksan Water Gate, which were constructed to supply agricultural water to the Gimhae Plain in 1934. In the Seonakdong River, inflow through the Daejeo Water Gate and discharge through the Noksan Water Gate and Noksan Drainage Pumping Station are being carried out, and these operations are intermittently operated according to the tidal conditions of the open sea, and these operational conditions cause water quality deterioration due to long term stay of pollutants. The need for water quality improvement in the Seonakdong River basin is increasing in accordance with development plans such as Eco-Delta City construction and various social demands

Water quality improvement through water circulation can be limitedly applied according to various factors such as water level difference between Nakdong and Seonakdong Rivers and tide levels of the open sea. In order to analyze the current water circulation plan, the water circulation flow rate was simulated using a two-dimensional hydrodynamic and water quality model (CE-QUAL-W2). Result of the analysis result shows that introducing river water from the main stream of the Nakdong River through facilities is more effective than the current water circulation plan, and the target water quality can be achieved during the environmental impact assessment.

**The 9th International
Symposium on
Environmental Hydraulics**

D1 Session

Morphodynamics [D1-M1]



Investigation of the impact of river interventions on fluvial morphodynamics

Gergely T. Török^{1,2,3,*} and Gary Parker^{3,4}

¹Budapest University of Technology and Economics, Department of Hydraulic and Water Resources Engineering

²TKI - Water Management Research Group

³Department of Civil and Environmental Engineering, University of Illinois at Urbana-Champaign

⁴Department of Geology, University of Illinois at Urbana-Champaign

* Corresponding: torok.gergely@epito.bme.hu

Abstract

Our study is based on 3D CFD model examinations of the impact of wing dams. We look for characteristics that are expected to play an important role (e.g., bed material, geometry) in the morphodynamic changes caused by such interventions. Based on these characteristics our 3D model tests can be performed. Using schematic 3D models with real morphodynamic parameters, the morphodynamic, geometric and water level changes resulting from a given intervention can be quantified². However, our goal is to develop an analytical procedure that allows the results to be generalized. Based on our 3D model result analysis, we are looking for relationships between sensitive parameters, e.g., wing dam width, longitudinal wing dam density, characteristic bed material, etc.

Keywords: Wing dams; 3D CFD; high water level

Introduction

Several studies (e.g., Pinter et al., 2008) have investigated the impact of interventions such as wing dams on high water levels. The findings of these mainly statistical analysis-based examinations are based on trend analysis of measured data. To complement these, we attended to develop a methodology that allows conclusions to be generalized using physical-based considerations.

Methods

3D CFD modeling of bed changes plays a crucial role in our study (Török et al., 2017). Using schematic channel models with real river morphodynamic parameters, we investigate what new equilibrium bed geometries are formed due to different wing dam placement and width. Our study's ultimate goal is to determine the additional resistance to flow in the altered bed geometry caused by the wing dams. For this, we apply the so-called Einstein Partition (Garcia, 2008). The method says that the effective resistant coefficient (C_f) can be split into two parts: the one represents the resistance caused by the skin friction (C_{fs}) and the other characterizes the resistance resulting by the bed forms (C_{ff}). Respectively, the total depth (H) can be separated for H_s and H_f (Eq. 1 and Eq. 2). Furthermore, Eq. 3 and 4 create relationships between the different roughnesses (C_f , C_{fs} and C_{ff}) and the depths (H , H_s and H_f) associated with them.

$$C_f = C_{fs} + C_{ff} \quad (1)$$

$$H = H_s + H_f \quad (2)$$

$$\rho C U^2 = \rho g H S \quad (3)$$

$$C = \left[\frac{1}{k} \ln \left(11 \frac{H}{k_s} \right) \right]^{-2} \quad (4)$$

where ρ is water density, U is depth-averaged velocity, g is gravity acceleration, κ is von Karman's constant and k_s is effective roughness height.

Finally, based on the appropriate form of the equations, the resistance caused by the wing dams (C_{ff}) can be derived as a function of the H , S , and S values that can be determined from the 3D model results.

Results

Our investigations were carried out with the Hungarian Danube parameters: with a bed material of a sand-gravel mixture, assuming a 200m wide riverbed. The herein presented results belong to a wing dam length one-eighth of the channel width. We examined the resistance caused by the wing dams at different longitudinal densities. The longitudinal wing dam density is characterized by the number of wing dams per 1000 meters of the channel.

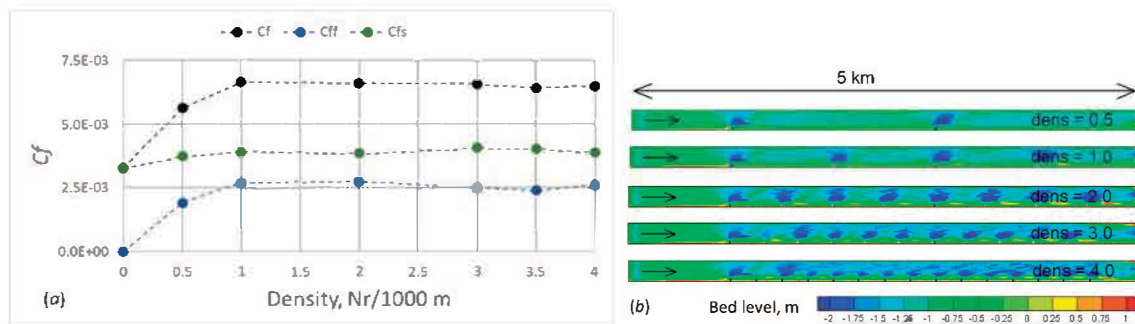


Fig. 1. (a) Relationship between intervention longitudinal wing dam density and additional resistance and (b) the equilibrium bed geometry formed by the wing dams.

Conclusions

The estimated case results show that there may be a limit in the intervention density above which the value of the resistance resulting by the bed forms (C_{ff}) does not increase further. In this quasi-constant range, the effective resistance coefficient (C_f) roughly doubles the value without the wing dams (Density = 0).

As a result of the narrowed bed, the bed material becomes rougher, due to which the surface roughness increases slightly.

Knowing the altered channel width, bed material and partitioned resistance coefficient, 1D model investigations become possible⁴, which allow the calculation of the changes in the bed slope and water level on a large scale.

Acknowledgment

The OTKA PD 135037 grant supported this work. The first author's funding is also acknowledged from the János Bolyai fellowship of the Hungarian Academy of Sciences.

References

- [1] N. Pinter, A. A.; Jemberie; J. W. F. Remo; R. A. Heine; B. S. Ickes: "Cumulative impacts of river engineering, Mississippi and Lower Missouri rivers", River Research and Applications 26(5):546 – 571, 2008
- [2] G. T. Török; S. Baranya; N. Rüther: "3D CFD modeling of local scouring, bed armoring and sediment deposition", WATER, 9:(1) Paper 56. 23 p. 2017
- [3] M. Garcia: "Sedimentation Engineering: Processes, Measurements, Modeling and Practice", American Society of Civil Engineers, ISBN: 978-0-7844-0814-8, 2008
- [4] G. Parker: "1D Sediment Transport Morphodynamics with applications To Rivers and Turbidity Currents", e-book. http://hydrolab.illinois.edu/people/parkerg/morphodynamics_e-book.htm, 2004

Optimal shape of alternative gravel mounts in terms of flood control and aquatic habitat

Mr. Pietro Beretta Piccoli^{1*} and Prof. Dr. Youichi Yasuda^{1*}

¹ Department of Civil Engineering, College of Science and Technology, Nihon University, Japan

* Corresponding: pietro.beretta@nihon-u.ac.jp, youichi.yasuda@nihon-u.ac.jp

Keywords: *Gravel mounts, Meandering flow, Habitat suitability modelling, Flood control*

Abstract

The installation of alternative gravel mounts inside channelized rivers could represent a simpler and more economically profitable alternative to classic river restoration projects. A previous study [Beretta et al. (2020)] has highlighted the potential improvements to flow heterogeneity and aquatic habitat during flood stages thanks to this new strategy, although disturbances to existing flood protection structures have also been highlighted. This research aims to find the optimal gravel mount shape that could meet the different objectives' demands. The experiments are conducted in a 0.8m wide rectangular channel, where 7 arrowhead-shaped gravel mounts are inserted on alternated shores. Different heights and widths of gravel mount are tested and further data are collected above flat gravel bed (mount's height equal 0cm). The discharge $Q_{\text{channel}}=58.8$ l/s is kept constant, while two different slopes are studied (1/500 and 1/100). The habitat improvements and the disturbances to flood protection engineering are assessed by scaling the model 1:15, representing a theoretical 12m wide channelized river section (slope is scale independent). The requirements of Ayu sweet fishes are modelled using the habitat suitability method. The flow velocity and water surface are measured using electrical-magnetic current meter and point gauge respectively. Above flat gravel bed with 1/500 slope, subcritical flow with flat water surface is formed. The flow condition is a typical open channel flow on a gravel bed (quasi-normal flow). By increasing the height of the alternative gravel mounts, undular waves are formed in the center of the channel, while the water surface profile near the sidewall remains flat. A reduction flow area is generated behind each gravel mount. There, the flow is characterized by low turbulence intensity (in this case standard deviation), sensible velocity reduction and considerable improvement of the habitat suitability (refuge region). During flood stages, both flow speed and water surface differences between the center of the channel (main flow) and the side walls becomes larger with increasing gravel mount height. By modifying the slope to 1/100, the main flow's velocity and wavy surface become stronger, while the reduction flow areas behind each gravel mount shrink. The experimental results suggests that the refuge region above gravel bed during flood stages might be less effective when compared to what observed by 1/500 slope. In prototype scale, considerable habitat improvements are expected from the introduction of gravel mounts, in particularly near the bed where the reduction flow areas are observed. From the relationships between habitat improvement, water surface rise and mount's shape, is possible to construct reference diagrams, although they remains related to the single discharge and fish species studied here. Further research should focus on expanding the known applicability range of the gravel mounts.

Reference

P. Beretta Piccoli, Prof. Dr. Y. Yasuda and Prof. Dr. R. Boes, *Installation of alternative gravel banks in channelized river*, 22nd IAHR-APD Congress 2020, Sapporo (Japan).

Artificial formation of gravel mount with stacked boulders

Youichi Yasuda^{1*} and Pietro Beretta Piccoli Marco²

¹Professor, Department of Civil Engineering, College of Science and Technology, Nihon University

²Research assistant, Department of Civil Engineering, College of Science and Technology, Nihon University

* Corresponding: yasuda.youichi@nihon-u.ac.jp

Keywords: Gravel mount; Stacked boulders; Surface jet flow; Seepage flow; Flood stages

D. Environmental hydraulics and river morphology

Abstract

The river construction for flood measures might produce a big damage as degradation of riverbed, local scouring in construction area, the formation of naked rock, and a disappearance of gravel bed. This might be caused by poor information on the relation between a local flow and a stability of gravel bed during floods. The formation of a surface jet flow in which the main flow lifts to the water surface is effective for the preservation of gravel bed during flood stages, and this proof has been confirmed from both physical models and applied fields [Yasuda (2020)].

The artificial formation of spawning area was applied by supplying gravels in river bed, but the most of spawning area was lost after flood stages. The stability of gravel bed for spawning of aquatic animals should be recommended as a sediment of gravel with the stacked boulders under the formation of surface jet flows. Also, the formation of seepage flow in the sediment of gravel is important for aquatic habitat. The flow passing over stacked boulders must be formed as a surface jet flow for both normal and flood stages.

This paper presents the artificial formation of gravel mount with stacked boulders.

As a field work, the stacked boulders with 40 cm size are installed for the formation of an artificial gravel mount (streamwise direction 5m, transverse width 3 m) in a small river with 15 m wide. The stacked boulders are settled in order to form a shallow flow passing over the boulders. Also, gravels with various sizes of 1 cm to 15 cm are filled around the stacked boulders in order to form seepage flow in the filled gravels. The configuration of filled gravels is formed as a gravel mount with 1/10 slope. The relationship between velocity and water depth was measured. Also, the formation of seepage flows in the mount was confirmed by using a dye.

In a physical model, 1/10 scale model based on Froude similarity was applied for the installation of gravel mount with stacked boulders. The stability of the gravel mount during flood stages has been investigated. The flow condition passing over the gravel mount was characterized for the formation of a surface jet flow during flood stages.

Acknowledgement

This work was supported as a preservation project of eels on food culture and resources by general incorporated foundation.

Reference

Youichi Yasuda, 2020, Improvement of flow condition in channelized river due to stacked boulders, 2nd ACEER Conference, invited lecture (to be published).

A COMPARATIVE STUDY ON SEQUENT DEPTH RATIO AND ENERGY LOSSES IN HYDRAULIC JUMPS ON ROUGH RECTANGULAR CHANNELS WITH ADVERSE SLOPES

Maisnam Bipinchandra Singh^{1*}, Mukesh Kumar Yadav², Victoria Ningthoujam¹, Ngangbam Romeji Singh³

¹Research Scholar, Department of Civil Engineering, National Institute of Technology, Manipur, India

²M.Tech. Student, Department of Civil Engineering, National Institute of Technology, Manipur, India

³Assistant Professor Department of Civil Engineering, National Institute of Technology, Manipur, India

* Corresponding: bpinmaisnam@gmail.com

Keywords: Rough channels, Adverse slopes, Hydraulic jump; Momentum equation; Frictional force

Abstract

Super Critical flows through sluice gate or spillways possess high energy which should be reduced to avoid damage to structures and downstream erosion of the river reach. This study aims at finding the variation of sequent depth ratio in adverse slope hydraulic jumps. In comparison to classical jump on prismatic channels minor sequent depth ratio is observed in adverse slope hydraulic jump in rough bed channels. The analysis of experiment is theoretically based on the momentum equation. Weight of water in the control volume and friction force is introduced in momentum equation for rough channel beds having roughness height, 0.002m and 0.003m. An attempt has been made to develop a relationship between upstream Froude number and the sequent depth ratio for rough channels with adverse slopes. Energy losses in the different adverse slopes were significant compared to horizontal bed. Three negative slopes of the channel flume, 0.11°, 0.23° and 0.34° were considered in this study.

SEQUENT DEPTH RATIO AND ENERGY LOSSES IN HYDRAULIC JUMPS ON ROUGH NEAR-PRISMATIC CHANNELS WITH SEDIMENT FLOWS

Maisnam Bipinchandra Singh^{1*}, Ngangbam Romeji², Mukesh Kumar Yadav³, Susilchandra Khuraijam⁴

¹ PhD Research Student, Department of Civil Engineering, National Institute of Technology, Manipur, India

² IAHR Member (B-65814), Assistant Professor, Department of Civil Engineering, National Institute of Technology, Manipur, India

³ Junior Research Fellow (DST-CCP-HICAB), Department of Civil Engineering, National Institute of Technology, Manipur, India

⁴ Project Field Assistant (DST-CCP-HICAB), Department of Civil Engineering, National Institute of Technology, Manipur, India

* Corresponding: bpinmaisnam@gmail.com

Keywords: Prismatic channels, Sequent Depths, Densimetric Froude number,

Abstract

Super Critical flows through sluice gate or spillways possess high energy and suspended sediments. The energy is dissipated by hydraulic jumps to reduce damage to structures and downstream erosion of the river reach. This study aims at finding out the effect of sediments on sequent depth ratio and energy losses in hydraulic jumps in prismatic horizontal rectangular channels. The experimental observations for hydraulic jumps in clear water and sediment laden water were conducted in a rectangular channel flume of dimensions 0.6m wide, 0.8m high and 16m long. For sediment laden experiment, sand particle of size 75 μ m were added upstream of the jump. In every single test run 1kg of sand were added and the amount of transported sand was collected at the end of the flume with the help of sediment trap. The densimetric Froude number and Froude number, sequent depths and energy loss for the clear water flow and the sediment laden flow were compared.

Sample data were collected from a natural channel 'Maklang stream', Imphal West, Manipur, India, where hydraulic jump takes place in the downstream of an uncontrolled weir located at Latitude 24°46'6.32N and Longitude 93°49'44.01"E. The channel carries sediment discharge in the range of 0.25–14.64 gm/day as measured using suspended sediment samplers and velocities using a flow probe having accuracy 0.01 fps were taken. The measurements were taken in an interval of ten days. Sediment concentration were taken 10 metres upstream and 10 metres downstream to compute the effect of sediment transport that takes place in the jump. The hydraulic jump parameters from field data has been compared with the lab measurements and are found to have a good correlation.

Impacts of riparian vegetation features on the shear layer in partly vegetated channels

Gerardo Caroppi^{1,2*}, Kaisa Västilä¹, Paola Gualtieri², Juha Järvelä¹,
Maurizio Giugni², and Paweł M. Rowiński³

¹Department of Built Environment, Aalto University School of Engineering

²Department of Civil, Architectural and Environmental Engineering, University of Naples Federico II

³Institute of Geophysics, Polish Academy of Sciences

*Corresponding: gerardo.caroppi@aalto.fi

Abstract

In partly vegetated channels the different drag conditions between the vegetated area and the main channel alter the flow structure, impacting the transport of sediments and pollutants. Hydrodynamic processes in such systems have been conventionally analyzed using rigid cylinders. Such representation neglects the key role played by vegetation morphology, presence of foliage, and flexibility, on the flow-vegetation interaction. In this study the differences associated with two alternative vegetation representations, foliated shrubs with understory grasses, and rigid cylinders, are investigated. Dynamically similar shear layers had analogous distributions of flow properties. Plants morphology, spacing, and dynamic motion resulted to markedly affect the shear penetration into the vegetation. For foliated vegetation, results showed the momentum exchange to be more efficient and to take place over wider portions of the vegetated area.

Keywords: Partly Vegetated Channels; Shear Layer; Vegetation; Reconfiguration

Introduction

Vegetation along river margins laterally interacts with the flow, altering the mean and turbulent flow structure and governing the transport processes in partly vegetated channels (e.g. Xu et al., 2019). Owing to the additional resistance exerted by vegetation, the velocity within the vegetated area (U_1) is lower than that in the main channel (U_2 , with $\Delta U = U_2 - U_1 > 0$). In analogy to canonical mixing layers, a shear layer (SL) develops in between. The presence of large-scale vortices govern the lateral momentum exchange between the two areas of the channel. The bulk vegetative drag, described by $C_D a$, plays a key role on the SL dynamics by controlling U_1 and, in turn, the total strength of the shear λ (Caroppi et al., 2021). Despite the key control of vegetation morphology, foliage, and flexibility on the vegetative drag (Västilä and Järvelä, 2014), hydrodynamic processes in such systems have been conventionally investigated by simulating vegetation with cylinders. For submerged vegetation, flexibility and spatial arrangement have been found to govern the shear penetration within the vegetation (e.g. Monti et al., 2020), determining the extent w_p of the exchange zone, i.e. the region within the vegetation actively exchanging momentum with the open water. In this study, the SLs induced by flexible foliated model vegetation were compared with dynamically similar SLs induced by rigid cylinders, focusing on the exchange processes at the vegetative interface.

Methods

Experiments were carried out at the Environmental Hydraulics Lab of Aalto University, in a flume partly covered by flexible foliated plants and grasses (F tests) and at the Laboratory of Hydraulics of University of Naples Federico II, where vegetation was simulated by using rigid cylinders (R tests) (Caroppi et al., 2021). Since a direct comparison between foliated flexible plants and an array of cylinders is not possible, the similarity was established in terms of

resulting SLs features. Three pairings of SLs, λ_1 , λ_2 and λ_3 , presenting similar normalized scaling velocity (λ), length (as described by the SL width to momentum thickness ratio δ/θ), and bulk vegetative drag $C_D a$ were established (Table 1). All the SLs presented large-scale vortices with Strouhal number of ~ 0.032 . From λ_1 to λ_3 , $C_D a$ and λ progressively decreased due to increasing vegetation reconfiguration in F tests and due to cylinder density reduction for R tests.

Table 1. Key shear layer quantities for F and R tests.

Pairing	Run	U_1 (m/s)	ΔU (m/s)	λ (-)	$C_D a$ (m ⁻¹)	δ (mm)	δ/θ (-)	w_p/θ (-)
λ_1	F1	0.04	0.32	0.8	10.9	201	5.5	3.5
	R1	0.09	0.75					0.6
λ_2	F2	0.21	0.57	0.6	1.6	176	4.8	3.1
	R2	0.23	0.74					0.3
λ_3	F3	0.53	0.74	0.4	0.6	144	4.3	1.1
	R3	0.38	0.54					0.1

Results

Results for λ_2 pairing are shown in Figure 1. Similar SLs had analogous distributions of normalized velocity (Figure 1, a) and Reynolds stress (b). w_p/θ , i.e. the exchange zone normalized width, was up to ten times larger for F relative to R tests (Table 1). The efficiency of the lateral momentum transport, as described by the turbulent correlation coefficient r_{uv} , was up to 40% higher for F tests (Figure 1, c). The λ_1 and λ_3 pairings showed similar results.

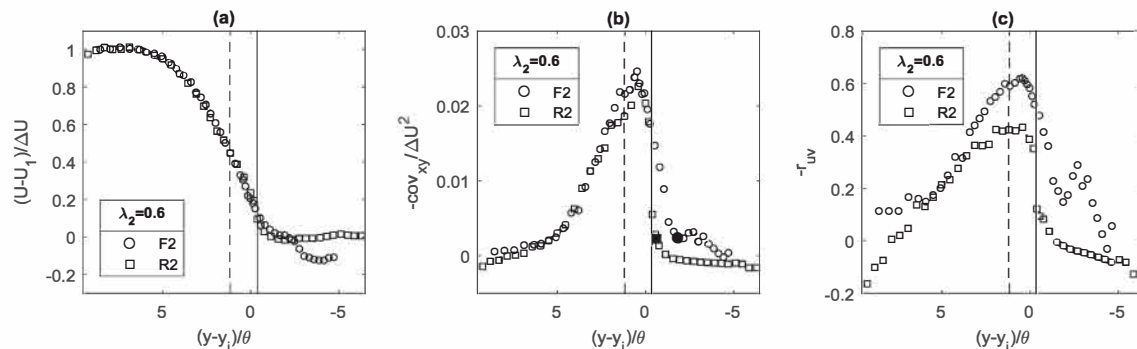


Fig. 1. Lateral distributions of normalized longitudinal velocity (a), Reynolds stress (b) and r_{uv} (c) for λ_2 pairing. Dashed and solid lines indicate the interface position for F and R tests, respectively. y_i is the position of the inflection point of the velocity profile.

Conclusions

Including riparian vegetation features into the simulation of flow in partly vegetated channels led to improved description of lateral momentum exchange, with effects on shear penetration w_p and efficiency of lateral momentum transport. Results highlighted the importance of properly addressing vegetation features in the simulation of vegetated flows.

References

- Caroppi, G., Västilä, K., Gualtieri, P., Järvelä, J., Giugni, M., Rowiński, P.M. (2021). Comparison of Flexible and Rigid Vegetation Induced Shear Layers in Partly Vegetated Channels. *Water Resour. Res.* 57, 1-17
- Monti, A., Omidyeganeh, M., Eckhardt, B., Pinelli, A. (2020). On the genesis of different regimes in canopy flows: A numerical investigation. *J. Fluid Mech.* 891, A9
- Västilä, K., Järvelä, J. (2014). Modeling the flow resistance of woody vegetation using physically based properties of the foliage and stem. *Water Resour. Res.* 50, 229–245.

Xu, Z.X., Ye, C., Zhang, Y.Y., Wang, X.K., Yan, X.F. (2019). 2D numerical analysis of the influence of near-bank vegetation patches on the bed morphological adjustment, *Environmental Fluid Mechanics*

**The 9th International
Symposium on
Environmental Hydraulics**

D2 Session

Vegetation [D2-M2]



Numerical Study on Vegetation Effects on Intradelta Lobe Avulsion

Dongxue Li^{1,2}, Weilun Gao^{1,2,3}, Dongdong Shao^{1,2,4*}, Baoshan Cui^{1,2}

¹ State Key Laboratory of Water Environment Simulation & School of Environment, Beijing Normal University, Beijing, China

² Yellow River Estuary Wetland Ecosystem Observation and Research Station, Ministry of Education, Shandong, China

³ Research and Development Center for Watershed Environmental Eco-Engineering, Beijing Normal University, Zhuhai, China

⁴ Tang Scholar, Beijing Normal University, Beijing, China

* Corresponding: ddshao@bnu.edu.cn

Abstract

The intradelta lobe avulsion, which causes channel shift inside the delta lobe, can create new coastal wetlands and benefit wetland restoration. This study conducted numerical simulations of non-vegetated and vegetated scenarios with different combinations of river discharge, sediment concentration, Chezy coefficient, and vegetation height and density using Delft3D to quantify the effects of vegetation on the occurrence of intradelta lobe avulsion. The results of non-vegetated scenarios show that the frictional effects dictate the river mouth bar distance, and the avulsion location can be predicted by maximum cumulative bed shear stress. The existence of vegetation results in shorter river mouth bar distance and avulsion distance. Besides, the avulsion time tends to be longer for vegetated scenarios, which is presumably because the vegetation traps more suspended sediment on the natural levee and increases the bank strength. Our findings have important implications for predicting the future avulsion of the intradelta lobe and improving the management of deltas and estuaries.

Keywords: Vegetation; Intradelta lobe avulsion; Natural levee; Numerical modeling; Delft3D

Introduction

River deltas are among the most economically and ecologically valuable regions on the planet. The evolution of river deltas comprises the abandonment of old delta lobes and the creation of new (active) delta lobes due to river avulsions. As one type of river avulsions, the intradelta lobe avulsion causes channel shift inside the delta lobe. Previous studies suggest that intradelta lobe avulsion is controlled by the river mouth bar stagnation that results in back filling of the river channel, which further increases the overbank flow at the natural levees and eventually leads to the avulsion (Canestrelli et al., 2014; Edmonds et al., 2009). However, the natural levees are commonly colonized by vegetation, and their relevant effects on the avulsion at the natural levees are still elusive.

Methods

In this study, we adopted a rectangular domain with a river channel cutting through the shoreline and refined cell near the river mouth in Delft3D (Fig. 1a). The open boundaries include an upstream river boundary and three seaward boundaries. Constant bank-full discharge was prescribed at the upstream river boundary with a uniform grain size of 200 μm and a density of 2,650 kg/m^3 . The initial channel width and depth are 15 m and 3 m, respectively. The basin slope is 4×10^{-4} , and the morphological scale factor is 100. Besides, we adopted different combinations of river discharges (45 m^3/s , 90 m^3/s), sediment concentration (0.5 kg/m^3 , 1 kg/m^3), and Chezy coefficient (65 $\text{m}^{1/2}/\text{s}$, 75 $\text{m}^{1/2}/\text{s}$) and generated natural levees based on the unstable jet regime proposed in Canestrelli et al. (2014) (Fig. 1b). In addition, we

simulated vegetated scenarios with different vegetation height (0.01 m, 0.1 m, 1 m) and stem density (0.05 m⁻¹, 1 m⁻¹, 3 m⁻¹). The vegetated scenarios automatically updated the vegetation distribution every 60 minutes, and the vegetation was removed when the velocity was greater than 1 m/s or the water depth was greater than 1.4 m.

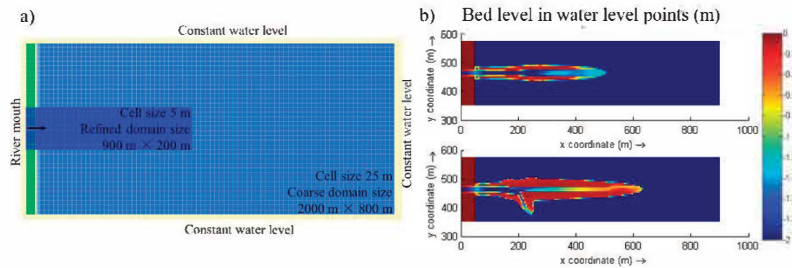


Fig. 1. a) The configurations of the computational domain and open boundaries and b) the simulated natural levees and intradelta lobe avulsion for a non-vegetated scenario.

Main Results

The numerical simulation results show that our natural levee and avulsion distance are consistent with those presented in Canestrelli et al. (2014) (Fig. 2a, R²=0.94) and Edmond et al. (2009) (Fig. 2b, R²=0.91) for vegetated scenarios. Additionally, the presence of vegetation significantly decreases the river mouth bar distance (Fig. 2c) and avulsion distance (Fig. 2d) but increases the avulsion time (Fig. 2e).

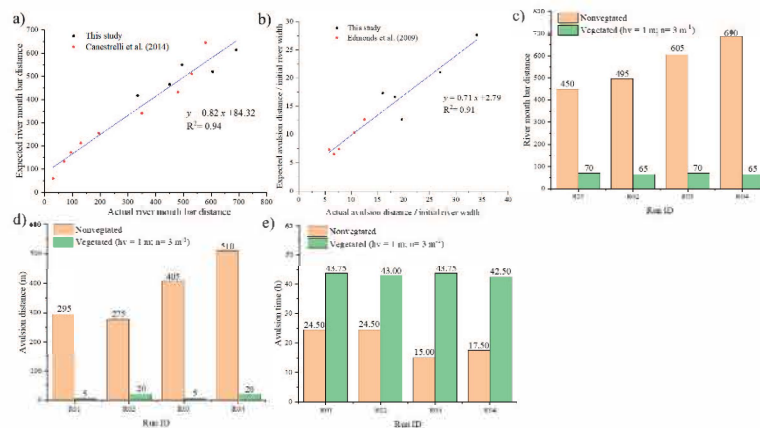


Fig. 2. Comparisons between this study and (a) Canestrelli et al. (2014) and (b) Edmonds et al. (2009), and the effects of vegetation on (c) the river mouth bar distance, (d) avulsion distance, and (e) the avulsion time.

Conclusions

The results of non-vegetated scenarios are consistent with previous studies, validating our simulations. The presence of vegetation significantly decreases the river mouth bar distance and the avulsion distance but increases the avulsion time, which is presumably due to the increased sediment deposition and bank strength on the natural levees. Our findings have important implications for predicting the future avulsion of the intradelta lobe and improving the management of deltas and estuaries.

References

- Canestrelli, A., Nardin, W., Edmonds, D.A., Fagherazzi, S., Slingerland, R.L., 2014. Importance of frictional effects and jet instability on the morphodynamics of river mouth bars and levees. *Journal of Geophysical Research Oceans*, 119(1): 509-522.
- Edmonds, D.A., Hoyal, D.C.J.D., Sheets, B.A., Slingerland, R.L., 2009. Predicting delta avulsions: Implications for coastal wetland restoration. *Geology*, 37(8): 759-762.

Experimental and numerical modelling of Reynolds shear stress in open channel flows with double-layer vegetation

Hamidreza Rahimi^{1*}, Xiaonan Tang¹, Toktam Hatamisengeli² and Prateek Kumar Singh¹

¹Department of Civil Engineering, Xi'an Jiaotong-Liverpool University

²Department of Mathematics, Shahrood University of Technology

* Corresponding: Reza.rahimi@xjtlu.edu.cn

Keywords: Open channel flow; Reynolds shear stress; Turbulence intensity, CFD modelling.

Abstract

Vegetation plays an important role in flow characteristics of natural open channels such as rivers. There are some studies which evaluated the impact of vegetation in open channel flows, but their modelling are not close to nature situation and usually only cover on single type of vegetation. Vegetation in natural channels is usually denser in lower layer and sparser in upper layer. In this study, a series of laboratory experiments have been undertaken to study the impact of double layer vegetation in both emergent and submerged conditions. The vegetation was modelled by an array of PVC dowels with two different heights of 10 cm and 20 cm. The experiments were carried out in a rectangular hydraulic flume in Xi'an Jiaotong-Liverpool University. Velocity measurements were taken by using 3-D Acoustic Doppler Velocimeter (ADV) and Propeller Velocimeter in order to obtain key parameters such as turbulence intensity, Reynolds stress and turbulence kinetic energy. Ansys Fluent was used to simulate the same sets of vegetation configurations using K- ϵ model with mesh sensitivity analysis to capture the inflection over the short vegetation region. The numerical study was explored for the double layer vegetation, and showed that the modelling results have good agreement with the experimental data for different vegetation configurations. It has been concluded that the flow in double layer vegetation is more complicated compare to flow through single layer vegetation.

Acknowledgement

The financial support awarded by Xi'an Jiaotong-Liverpool University for this research project (RDF-15-01-10) is gratefully acknowledged.

Velocity reduction and drag in submerged canopies under oscillatory flow conditions

Dominic van der A^{1*}, Otto Neshamar¹, Niels G. Jacobsen² and Tom O'Donoghue¹

¹ School of Engineering, University of Aberdeen, AB24 3UE, Aberdeen, United Kingdom

² Harbour Coastal and Offshore Engineering, Deltares, Boussinesqweg, 1, 2629 HV Delft, The Netherlands

* Corresponding: d.a.vandera@abdn.ac.uk

Abstract

An experimental and analytical study of in-canopy velocities under oscillatory flows is presented. The experiments, conducted in a large-scale oscillatory flow tunnel, cover a wide range of flow amplitudes, with in-canopy velocity reductions ranging between 0.2-0.8 of the free stream velocity. Results from an analytical model with nonlinear drag compare favourably to the experimental data. With application to theories for free surface waves over canopies in mind, the effects of linearisation of the drag are analysed by comparing the linearised and nonlinear model predictions. A unified empirical formula for in-canopy velocities will be presented, which depends on two non-dimensional parameters related to inertia and drag forces. The unified formula allows for easy assessment of the maximum in-canopy velocity for applications such as sediment transport predictions.

Keywords: oscillatory flow; drag force; canopies; velocity reduction

Introduction

Coastal vegetation such as seagrass, mangroves and salt marsh vegetation can contribute to coastal defence by attenuating wave energy and stabilising the seabed. While many previous studies have focused on wave attenuation caused by vegetation canopies, the in-canopy velocities have received less attention, despite their importance in determining canopy drag and sediment transport. The aim of the present work is to obtain, for the first time, velocity and drag force measurements for submerged canopies under full-scale wave conditions, and to use these measurements to develop analytical models for in-canopy velocity reduction which can be implemented in large-scale morphodynamic models.

Methods

Experiments were conducted in the Aberdeen Oscillatory Flow Tunnel (Fig. 1a). The submerged vegetation canopy was represented by a 7 m long array of rigid cylinders (130 mm tall and 8 mm in diameter), placed in a staggered arrangement with two different densities: 'sparse' with 579 stems/m² and 'dense' with 1736 stem/m² (Fig. 1b,c). Flow conditions involved five sinusoidal oscillatory flows with 6s flow period and velocity amplitudes ranging from 0.2-1.0m/s. In- and above-canopy velocity measurements were made with a Laser Doppler Anemometer (LDA), and forces were measured on one of the cylinders in the array using a 6-axis submersible load cell.

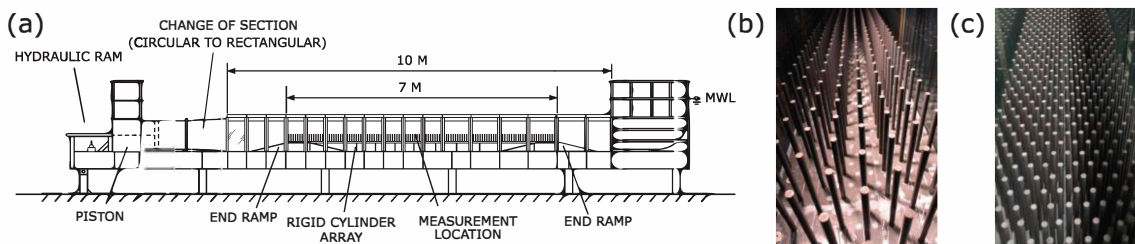


Fig. 1. Experimental set-up: (a) Aberdeen Oscillatory Flow Tunnel (b) sparse canopy (c) dense canopy. Adopting a two-layer approach similar to Lowe et al. (2005), the (non-dimensional) momentum equation for purely oscillatory flow over a canopy of rigid cylinders becomes:

$$\Gamma_I \frac{\partial \widehat{U}}{\partial \widehat{t}} = \frac{\partial \widehat{u}_0}{\partial \widehat{t}} + \Gamma_f |\Delta \widehat{U}| \Delta \widehat{U} - \Gamma_D |\widehat{U}| \widehat{U} \quad (1)$$

where \widehat{u}_0 is the free-stream velocity, \widehat{U} is the bulk in-canopy velocity (both non-dimensional), and $\Delta \widehat{U} = \widehat{u}_0 - \widehat{U}$. The non-dimensional parameters Γ_I , Γ_f , and Γ_D relate to the inertia force, canopy interface friction and drag force on the stems, and depend on the canopy and oscillatory flow characteristics. Two solutions to Eq. (1) are investigated: 1) a linear solution in which the friction and drag terms are linearised based on Lorentz's condition of identical work, and 2) a nonlinear solution which accounts for the nonlinearity of the friction and drag terms.

Results

The velocity profile shown in Figure 2a shows a boundary layer formation and overshoot in the shear layer above the canopy and a significantly reduced and nearly vertical velocity profile within the canopy. The in-canopy velocity magnitude is 26% of the free-stream velocity, which is well predicted by both models. Figure 2b shows that the velocity phase lead increases throughout the shear layer and reaches a maximum value of about 70 degrees within the canopy, which is also well predicted by the linear and nonlinear model solutions. However, Figure 2c shows that only the nonlinear model reproduces the temporal variation of the in-canopy velocity accurately, as it captures the higher harmonic generation by the canopy.

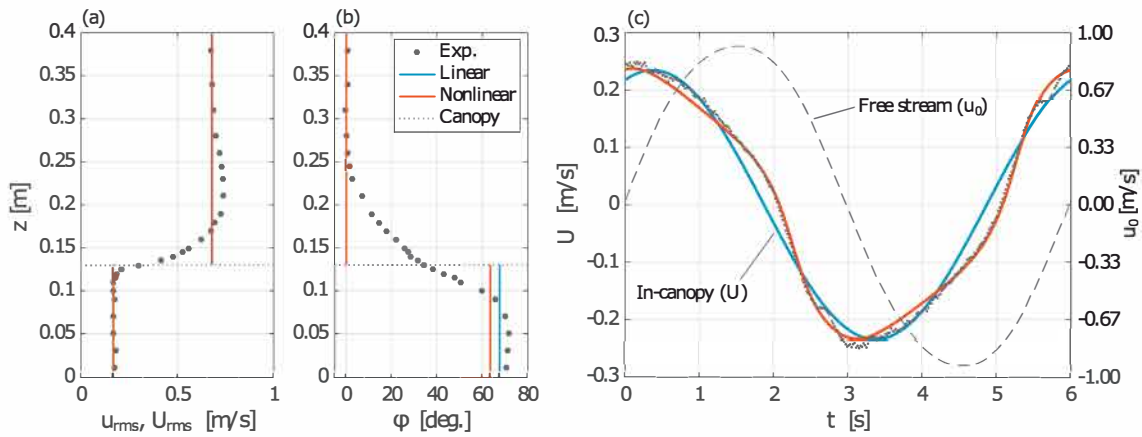


Fig. 2. Comparison between experiment and the two models for the dense canopy and largest free stream velocity: (a) root-mean-square velocity profile (b) velocity phase lead of the first harmonic compared to free-stream velocity (c) time variation of the in-canopy velocity.

Conclusions

New laboratory experiments and two models for the bulk in canopy velocity are presented, one in which the canopy drag depends non-linearly on the flow velocity and one in which the drag is linearized. Both models represent the measured velocity reduction and phase-lead, however only the non-linear model can represent the time-variation of the in-canopy velocity, which is important for in-canopy sediment transport rate predictions.

References

Lowe, R. J., Koseff, J. R., Monismith, S. G., 2005. Oscillatory flow through submerged canopies: 1. velocity structure. *Journal of Geophysical Research*, C10016.

Experimental reach scale methodology for analyzing integrated flow resistance due to woody vegetation patches

Inhyeok Bae^{1,2}, Un Ji^{1,2*}, Juha Järvelä³, Kaisa Västilä³

¹University of Science and Technology

²Korea Institute of Civil Engineering and Building Technology

³Aalto University School of Engineering, Espoo, Finland

*Corresponding: jjiun@kict.re.kr

Abstract

Since vegetation is a significant cause affecting the water level in streams by resisting the flow, a comparative evaluation of flow resistance due to vegetation patches is essential for environmentally preferable design and management of streams. This study aimed at improved experimentation for evaluating the reach-scale flow resistance due to vegetation patches by using artificial willow bushes while reproducing the physical characteristics and scale of natural woody vegetation. The reach-scale friction factor was estimated according to the density and shape condition of the vegetation patches by measuring the water surface slope using high-accuracy pressure sensors in several flow conditions. The experiment results were compared with the friction factors predicted by several theoretical models. This study provides a practical methodology for investigating the flow resistance due to woody vegetation patches with complex spatial distributions.

Keywords: Blockage factor; Flow resistance; Full-scale experiment; Vegetation patches; Vegetative roughness

Introduction

Vegetative flow resistance depends on its physical properties, spatial distribution, and hydraulic and topographical conditions (Nikora et al. 2008). Previous studies have evaluated flow resistance by substituting natural vegetation to cylinder form to simplify the complex shape of plants, and only few experimental studies have been considered the effects of physical properties of foliated plants and the reconfiguration caused by the flexibility of natural plants on the flow resistance (Västilä and Järvelä 2014). We aim to present a practical methodology of assessing river flow resistance by extending the study that has been conducted with theoretical and limited-scale experiments to natural-field conditions.

Methods

Reach-scale friction factor according to hydraulic conditions was evaluated for three layout vegetation patches with different density and spatial distribution conditions in a stream-scale experimental flume (Figure 1). The bulk friction factor f of the experimental section was calculated using the water surface slope measured through the high-accuracy pressure sensors A and B. The physical shape information of artificial vegetation patches was determined using point cloud data collected through Terrestrial Laser Scanning (TLS).

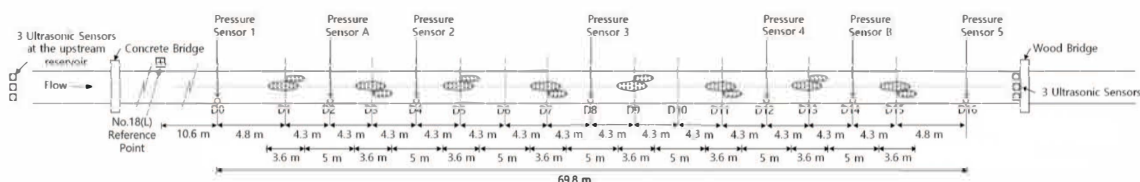


Fig. 1. Stream-scale experiment channel

The vegetation friction factor f'' is calculated by subtracting the bed friction factor f' from the bulk friction factor f as shown in the equation below, according to the linear superposition principle.

$$f = f' + f'' \quad (1)$$

The results of the experiment are compared with the prediction of several momentum-based models (Järvelä 2004; Baptist et al. 2007; Luhar and Nepf 2013; Västilä and Järvelä 2014), and practical methods are presented to quantify the physical properties of plants and terrain conditions to put them into variables in these models.

Results

The experiment results show that strong correlations between the flow resistance and the blockage factor B_x , which is the vegetation blockage rate for the flow cross-sectional area. In the case of dense vegetative patches with high B_x (=0.4), f was observed up to 4.9 times higher than non-vegetated cases. For the low density with low B_x (=0.2), f was up to 2.3 times larger than a non-vegetated condition. Additionally, precise measures of geometry and physical properties of vegetation and channel and parameterization of the adopted momentum-based models had made a reasonable prediction of reach-scale friction factors.

Conclusions

This study tested the vegetative flow resistance according to the density and spatial distribution of patchy vegetation with branched and foliated willow bushes based on a stream-scale experiment. Measurement of water surface slopes based on the high-accuracy pressure sensors in field conditions has been effective in the estimation of the flow resistance by detecting fine slope changes. Experimental results show that the blockage factors of willow bushes precisely observed by TLS could be noted as the key measure for evaluation of flow resistance due to vegetation. Parametrization of momentum-based models to consider the complex geometric properties of vegetation and channel in natural conditions has been performed, and it has been validated by comparison with the flow resistance measured in experiments.

Acknowledgement

This work was supported by the National Research Foundation of Korea (NRF) grant funded by the Korea government (MSIT)(No.2019R1C1C1009719).

References

- Baptist, M. J., Babovic, V., Rodríguez Uthurburu, J., Keijzer, M., Uittenbogaard, R. E., Mynett, A., and Verwey, A. (2007). On inducing equations for vegetation resistance. *Journal of Hydraulic Research*, 45(4), 435-450.
- Järvelä, J. (2004). Determination of flow resistance caused by non-submerged woody vegetation. *International Journal of River Basin Management*, 2(1), 61-70.
- Luhar, M., and Nepf, H. M. (2013). From the blade scale to the reach scale: A characterization of aquatic vegetative drag. *Advances in Water Resources*, 51, 305-316.
- Nikora, V., Larned, S., Nikora, N., Debnath, K., Cooper, G., and Reid, M. (2008). Hydraulic resistance due to aquatic vegetation in small streams: field study. *Journal of hydraulic engineering*, 134(9), 1326-1332.
- Västilä, K., and Järvelä, J. (2014). Modeling the flow resistance of woody vegetation using physically based properties of the foliage and stem. *Water Resources Research*, 50(1), 229-245.

Study on the physical habitat of river channel vegetation designated as an endangered species

Takayuki Tanaka^{1*}, Syunya Hazama¹, and Ryuki Harata¹

¹ National Institute of Technology, Toyota College, Dep. Civil Engineering, Japan

* Corresponding: tanaka-c@toyota-ct.ac.jp

Abstract

The phenomenon that the vegetation of the country's endemic species in the river channel decreases is occurring in various rivers. Possible reasons include changes in the waterside environment due to human activities such as river improvement and the use of herbicides, and the growth of highly fertile alien species such as those brought in for ornamental purposes. The Suemori City Sewage Canal, which is the observation site, is inhabited by various vegetation such as endangered species, exotic species, and species endemic to Japan. In this study, we will grasp the riverbed materials and flow conditions in rivers where endangered species and alien species that are endemic to Japan compete and inhabit. This will clarify the habitat of river vegetation designated as an endangered species.

Keywords: Endangered species, River flow conditions, Riverbed material, Vegetation

Introduction

Vegetation in the river channel creates a rich biological environment, so it plays an important role in considering the conservation of the river environment. Among them, the phenomenon that the vegetation of the country's endemic species in the river channel decreases is occurring in various rivers. Possible reasons include changes in the waterside environment due to human activities such as river improvement and the use of herbicides, and the growth of highly fertile alien species such as those brought in for ornamental purposes. Conserving endangered species and maintaining biodiversity are very important in considering the river environment. The Suemori City Sewage Canal, which is the observation site this time, is a canal that flows into the Hiranoi River, which is the Kiso River system, and flows through Godo Town, Gifu Prefecture, Japan. This waterway is inhabited by various vegetation such as endangered species such as *Potamogeton malaianus* and *Sparganium japonicum*, exotic species such as *Elodea nuttallii*, and Japanese endemic species such as *Potamogeton crispus* and *Myriophyllum sperratus*.

Methods

In this study, we investigated the vegetation overgrowth, measured the flow velocity, and investigated the riverbed material at the observation target site. This will clarify the habitat of river vegetation designated as an endangered species. This canal is a small canal with a channel length of about 1 km, and there are no inflowing rivers between them, and the distance between

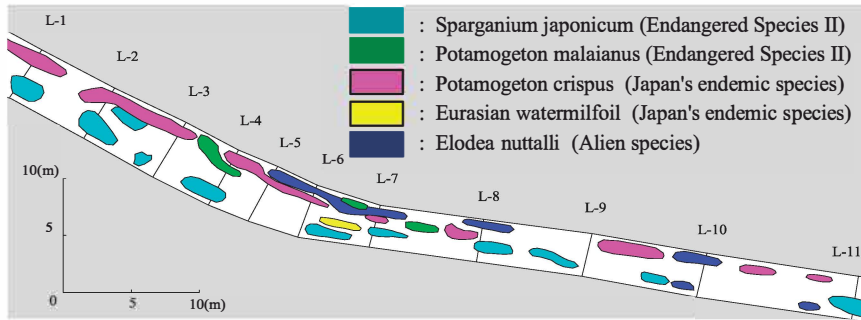


Fig. 1. Vegetation overgrowth at the observation point



Fig. 2. Sparganium japonicum

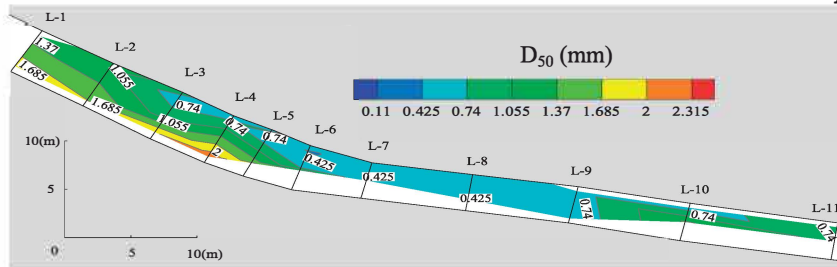


Fig. 3. Contour line of median grain size D_{50} of riverbed material

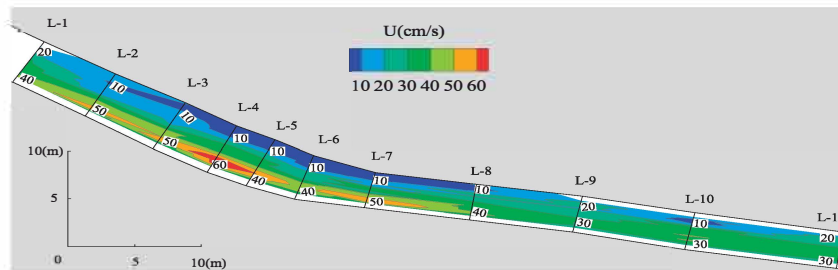


Fig. 4. Contour line of main flow velocity U averaged in water depth

observation points are short. Therefore, we consider that physical factors are larger than water quality factors as factors that affect vegetation growth.

Results

Fig.1. shows the vegetation overgrowth at the observation point. It can be confirmed that the Potamogeton crispus and Elodea nuttalli are mainly on the left bank side, and the Sparganium japonicum (Fig.2.) are flourishing on the right bank side. Since the river meanders at this point, there is a difference in flow velocity between the outer and inner banks, which is thought to affect the habitat of vegetation in the river channel.

Fig.3. shows the contour lines of the median grain size D_{50} of the riverbed material at the observation site. From this, it is considered that the riverbed material of this river is mainly sand. In addition, it was clarified that the riverbed material at the site where Sparganium japonicum inhabits has a larger grain size than the riverbed material at the site where Potamogeton crispus and Elodea nuttalli inhabit.

Fig.4. shows the contour lines of the main flow velocity U averaged at the water depth at the observation point. The flow velocity is higher on the right bank side than on the left bank side throughout the river channel. The riverbed material is deposited on the left bank side of L-2 to L-7, and many Potamogeton crispus and Elodea nuttalli are prosperous, so the flow velocity is considered to be small.

Conclusions

From the results of this study, it was clarified that the *Potamogeton crispus* and *Elodea nuttalli*, which propagate by cutting leaves, inhabit the fine left bank side of the riverbed material, which easily invades the roots. In addition, it was clarified that *Sparganium japonicum*, which breeds by running branches, has a high flow velocity and inhabits the spots where *Potamogeton crispus* and *Elodea nuttalli* do not inhabit.

References

Jan, R., Kamila, V. (2018). Interannual dynamics of a rare vegetation on emerged river gravels with special attention to the critically endangered species *Corrigiola litoralis* L. *A journal of plant ecology and systematics*, Vol. 53, 213-225.

The Impact of Double-layered Rigid Vegetation on Flow Structure

Yutong Guan¹, Xiaonan Tang^{2*}, and Yujia Zhang³

^{1,2,3}Department of Civil Engineering, Xi'an Jiaotong-Liverpool University

*Corresponding: Xiao.Tang@xjtlu.edu.cn

Abstract

Flow structure in vegetated channels is highly three-dimensional. This study focuses on the characteristics of flow through the mixing layered vegetation partially covered in an open channel. A series of experiments were conducted to investigate the velocity distributions in the vegetated zone under different flow conditions. Reynolds shear stress was calculated based on 3D measurements using ADV (Acoustic Doppler velocimeter). Observed results show that the flow has distinct features in three layers: the lower, mediate, and upper layer. A prominent shear stress layer is found at the upper edge of tall vegetation, indicating strong momentum exchange in this transition region.

Keywords: Reynolds stress; vegetated channel; double-layer vegetation; mixing layer

Introduction

Aquatic vegetation has a great impact on the flow structures of natural rivers. Additional resistance generated by the vegetation retards the velocity, which will result in reduced channel capacity and sediment deposition (Tang & Knight, 2001; Gunawan et al. 2010). Furthermore, the shear layer caused by vegetation affects the boundary shear stress distributions, which is of great importance in bank protection and bed stability.

Typically, in vegetated channels, a strong momentum exchange occurs at the vegetation top, resulting in significant Reynolds stress in this region (Tang and Knight, 2008; Tang et al., 2010, Tang 2019). Despite the dominant role of drag force of vegetation in the vegetated flow, shear stress distributions in double-layered, partially vegetated channels remain unclear. This paper gives a brief description and reasonable explanations of the shear layer flow structure.

Methods

Plastic dowels of 10cm and 20 cm height were used to simulate rigid vegetation in this study. The double-layered vegetation was arranged to cover half width of 40 cm wide channel. The details of the experimental setting and measurements was given by Tang et al (2021). Summary of the experiment parameters is listed in Table 1.

Table 1. Summary of experimental parameter

Case	vegetation density	tall vegetation height (cm)	short vegetation height (cm)	water depth (cm)	flow rate (L/s)
R1	0.0315	10	20	9	8.24
R2				12	11.38
R3				22	2.20
R4				25	24.80

Reynolds shear stress is calculated from Equation (1).

$$\tau_{yx} = -\rho \overline{u'v'} \quad \#(1)$$

Results

Take measurement points w4, w8, w12, w14 and w18 for example. The point of w4 is behind the short vegetation, while the location w8 is behind the tall vegetation. Measurement point w12 and w14 is at the interface between vegetated zone and free flow zone. The results in Figure 1 show the vertical variation of the Reynolds stress cross the channel. The flow field in the short vegetation zone has more obvious fluctuation than in the tall vegetation zone under submerged conditions (scheme R4). At the near-bottom layer and the upper edge of the short vegetation, the curve shows a sharp turning point, indicating a strong momentum exchange occurring at this location.

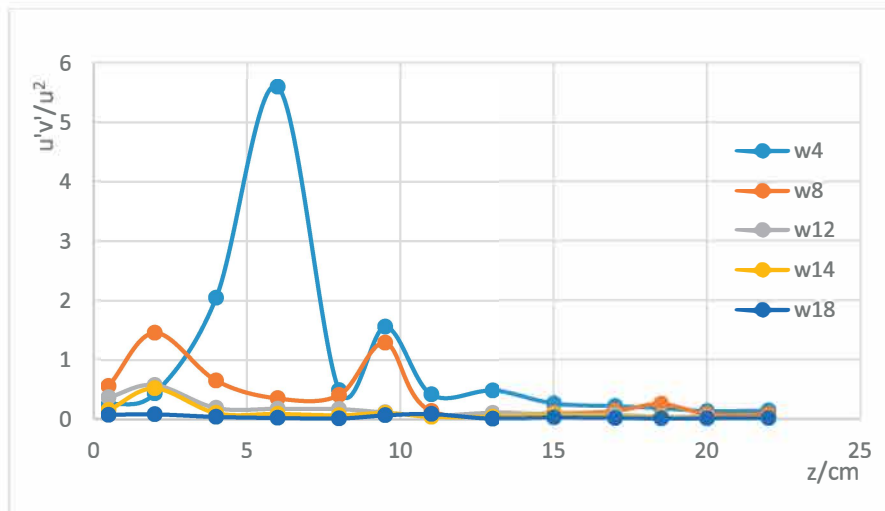


Fig.1 Relationship between dimensionless Reynolds stress and vertical locations

Conclusions

The existence of vegetation has a great impact on the channel flow field. The vegetation height is one dominant factor affecting the velocity profiles and stress field. Reynolds shear stress in the double-layered vegetation zones shows more obvious fluctuations than that in the free flow zones. Strong momentum exchange often occurs near the bed or at the upper edge of the vegetation.

References

- GUNAWAN, B., STERLING, M., TANG, X., KNIGHT, D.W. 2010. Measuring and modelling flow structures in a small river. In *River Flow 2010*, 179-186, Dittrich, A. Koll, K. et al. (Editors).
- TANG, X., KNIGHT, D.W. 2001. Experimental study of stage-discharge relationships and sediment transport rates in a compound channel. *Proceedings of the 29th IAHR World Congress*, 69-76, Sept. 16-21, Beijing, China.
- TANG, X., KNIGHT, D. W. 2008. Lateral depth-averaged velocity distributions and bed shear in rectangular compound channels. *Journal of Hydraulic Engineering*, 134, 1337-1342.
- TANG, X., STERLING, M. & KNIGHT, D.W. 2010. A general analytical model for lateral velocity distributions in vegetated channels. *River Flow 2010*, 469-476.
- Tang, X., Guan, Y., Zhang, Y., Zhang, W., Liu, T., Yi, X. 2021. Effect of vegetation on the Flow of a partially-vegetated channel. *IOP Conf. Series: Earth and Environmental Science*, 668, 012050, DOI:10.1088/1755-1315/668/1/012050
- Tang, X. (2019). A Mixing-Length-Scale-Based Analytical Model for Predicting Velocity Profiles of Open Channel Flows with Submerged Rigid Vegetation. *Water and Environment Journal*, 33, 610-619.

**The 9th International
Symposium on
Environmental Hydraulics**

D3 Session

Fish [D3-T1]



Surface roughness in billfishes: a guide to improving the design of engineered surfaces?

Stewart, M.T.¹, Wainwright, D.K.², Nikora, V.I.¹, Cameron, S.M.¹, Thunert, M.³ and Stoesser, T.^{4*}

¹ School of Engineering, University of Aberdeen

² Peabody Museum of Natural History, Yale University

³ Thorlabs, Lübeck

⁴ Civil, Environmental & Geomatic Engineering, University College London

* Corresponding: mstewart@abdn.ac.uk

Abstract

The function served by the distinctive skin roughness patterns found on the bodies of billfish remains poorly understood. This is due in part to a lack of detailed information on the three-dimensional morphology of the skin roughness. To address this issue, novel high-resolution measurements of striped marlin, sailfish and swordfish skin samples are reported here. The results highlight the distinct and varied morphology of skin roughness amongst different species within the billfish family. The roughness data acquired from these measurements provides a benchmark from which realistic roughness models based on billfish skin roughness can now be developed for testing in physical and numerical experiments. This is a crucial foundational step in the wider goal of establishing the potential engineering applications of billfish-inspired roughness patterns.

Keywords: Billfish; Surface roughness; Nature-Inspired

Introduction

The natural world can provide a wealth of inspiration for the creation of engineered surfaces with improved efficiencies for applications involving heat and mass transfer, the transport of fluids and the movement of bodies through fluid media. A classic example is the riblet structure of shark skin and in this respect, billfishes (e.g. sailfish, swordfish, spearfish, and marlin) may also provide a potentially fruitful source to draw inspiration from. Like sharks, billfishes are apex marine predators, and exhibit numerous forms of roughness across their bodies. However, their surface morphology is wholly unlike the denticles found on sharks. Despite numerous hypotheses having been promoted to explain their exceptional swimming capabilities, the role played by the surface roughness of their bodies remains poorly understood. Consequently, the potential practical hydro-environmental engineering applications that could follow also remain to be investigated. This is primarily due to a lack of detailed information on the three-dimensional morphology of their skin roughness. The aim of this study is to tackle this problem by providing high resolution measurements of billfish skin roughness. The expectation is that this data can then be developed into realistic roughness models for future testing to uncover the possible functional roles of the roughness.

Methods

In this study, samples of skin from the bodies of a striped marlin, sailfish and swordfish were measured, each using a different technique, to assess their respective roughness properties. Firstly, gel-based stereo-profilometry was performed on a fresh sample of striped marlin skin. Secondly, surface profilometry measurements were carried out on a silicon mould of a piece of skin from the mid-body region of a sailfish using a confocal displacement sensor. Thirdly, Optical Coherence Tomography (OCT) was used to make a volumetric measurement of a fresh sample of skin taken from the body of a swordfish. Data points were collected every 4 µm in

the x- and y-directions for the marlin and sailfish measurements, and every 20 μm for the swordfish. Vertical (z) resolution for the OCT measurement was 1.95 μm .

Results

Figure 1 shows a comparison of the three measured skin surface samples. The marlin skin exhibits two discernible features. The first are elongated and narrow scales, typically pointed at both ends and broadly aligned to form sinuous channels. Despite being fully embedded within the epidermal layer, the scales still have a visible footprint on the outer surface of the fish which would be felt by the surrounding flow. The second are small spiny scales, which tend to populate the surface randomly. The sailfish skin sample is characterized by the presence of v-shaped protrusions, similar to previous reports (e.g. Sagong *et al.*, 2008), which tend to form in a staggered arrangement. For the swordfish, the skin is populated with numerous small spiny scales. The distribution of these scales appears to be more orderly than for the spiny scales seen on the marlin skin. In addition, they tend to be aligned in the direction of the flow and are grouped in varying numbers. This picture is in good agreement with previous illustrations (Potthoff & Kelley, 1982; Nakamura, 1983).

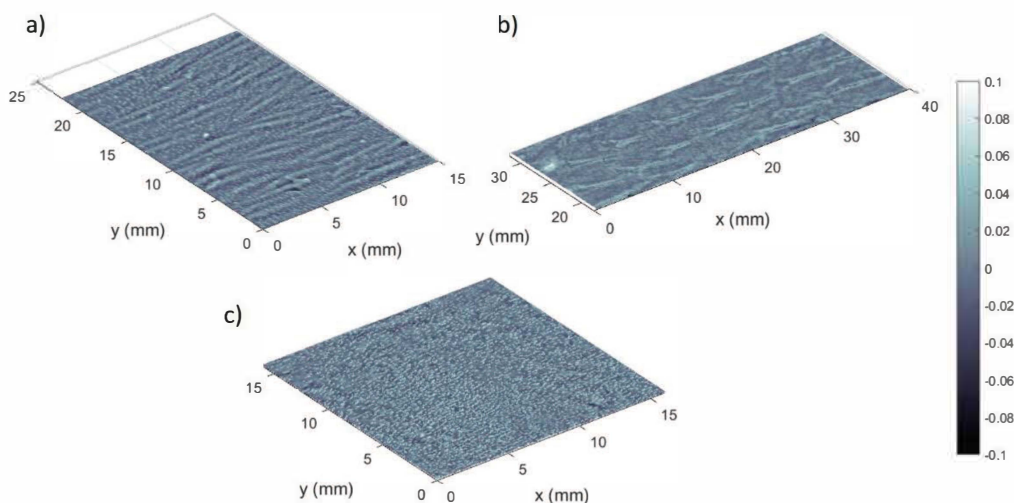


Fig. 1. Digital elevation maps of a) marlin, b) sailfish and c) swordfish skin (heights in mm).

Conclusions

These preliminary results highlight the diverse scale morphology across the species of billfish. The measurements also provide, for the first time, a benchmark for the development of realistic roughness models based on the skin surface of billfishes which can be taken forward for hydrodynamic testing. Such models would be ideally suited for physical deployment in laboratory flumes or digitally, in numerical simulations.

References

- Nakamura, I. (1983). Systematics of the billfishes (Xiphiidae and Istiophoridae). Publications of the Seto Marine Biological Laboratory, 28(5-6), 255-396.
- Potthoff, T., & Kelley, S. (1982). Development of the vertebral column, fins and fin supports, branchiostegal rays, and squamation in the swordfish, *Xiphias gladius*. Fish. Bull, 80(2), 161-186.
- Sagong, W., Kim, C., Choi, S., Jeon, W. P., & Choi, H. (2008). Does the sailfish skin reduce the skin friction like the shark skin? Physics of Fluids, 20(10), 101510.

Fish swimming behaviour and kinematics in the wake of a vertical axis turbine

Stephanie Müller^{1*}, Valentine Muhawenimana¹, Pablo Ouro^{1,3}, Catherine Wilson¹ and Jo Cable²

¹ Hydro-Environmental Research Centre, School of Engineering, Cardiff University, Cardiff, CF24 3AA, UK

² School of Biosciences, Cardiff University, Cardiff, CF10 3AX, UK

³ School of Mechanical, Aerospace and Civil Engineering, University of Manchester, Manchester, M13 9PL, UK

* Corresponding: MullerS1@Cardiff.ac.uk

Abstract

Deemed as environmentally friendly, hydrokinetic vertical axis turbines (VAT) present a promising alternative with low environmental implications compared to traditional hydropower projects; however, little is known about their impact on fish. Here, we investigate juvenile rainbow trout (*Oncorhynchus mykiss*) response to a single VAT under confined laboratory conditions for two discharges and turbine operation conditions using motion tracking. Velocity measurements reveal a region of low momentum in the turbine wake and regions of flow acceleration on either side of the turbine. Fish spatial usage and the number of upstream passing fish did not differ among flow conditions and turbine states examined. Our novel study underpins that VAT are a renewable energy technology with low environmental impact.

Keywords: vertical axis turbine; Particle Image Velocimetry; fish behaviour; motion tracking

Introduction

The globally rising energy demand urges a need for sustainable, environmentally friendly energy technologies. The tremendous environmental impacts of traditional, large-scale hydropower plants resulted in a greater focus on small-scale alternatives (Anderson et al., 2014) such as hydrokinetic vertical axis turbines (VAT). These devices operate in low-to-medium velocity ranges and shallow free-flowing waters, such as rivers and estuaries, allowing versatile deployment. Despite their potential as a renewable energy scheme, a vital research gap remains in their impact on fish behaviour. The limited literature on this reports changes in spatial usage, passage, and schooling behaviour (Castro-Santos and Haro, 2013; Molloy et al., 2017) and a reduced collision and injury risk when colliding with turbine blades (Castro-Santos and Haro, 2013). Our laboratory study examines the relation between upstream and downstream hydrodynamics of a single VAT and the swimming behaviour of juvenile rainbow trout (*Oncorhynchus mykiss*) in a confined test section for two flow conditions and turbine operation states.

Methods

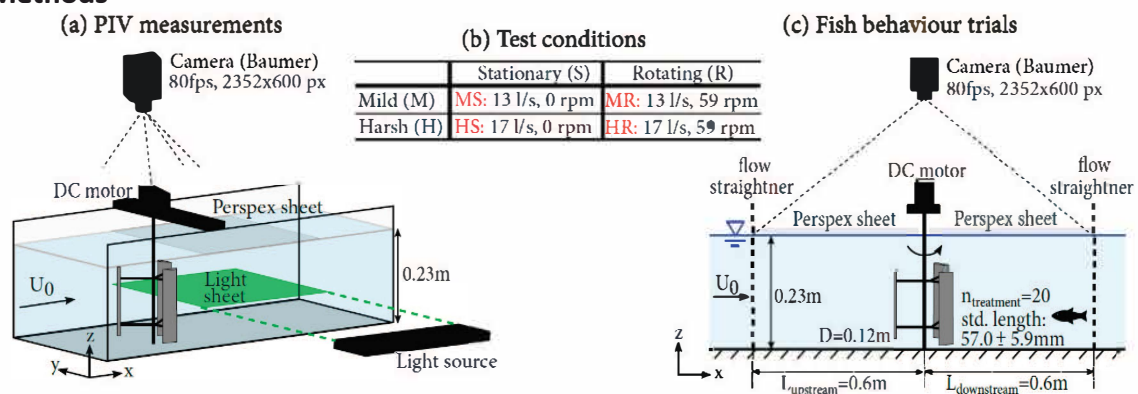


Fig. 1. Experimental setup for (a) PIV measurements and (c) fish behaviour experiments, with experimental test conditions (flow discharge (l/s) and turbine rotational speed (rpm)) indicated in (b).

Experiments were undertaken in an open channel recirculating flume (10x0.3x0.3m, LxWxH) in the hydraulic laboratory at Cardiff University, UK. The flume was equipped with a confined test section (1.2x0.3x0.23m, LxWxH) with a three-bladed VAT in its centre. Upstream and downstream hydrodynamics were quantified using particle image velocimetry (PIV) (Fig. 1 a), with data analysed using PIVlab. Thereafter, juvenile rainbow trout swimming behaviour (Fig. 1c) was recorded for 10min using a top-mounted camera for two flow conditions (mild, M and harsh, H) and two turbine operation states (stationary, S and rotating, R) (details in Fig. 1b), with fish released at the downstream end of the test section. Fish spatial preference, location, and kinematics were examined using JWatcher and an adapted open-source motion tracking algorithm. Statistical analysis was conducted using R, with p-value significance taken at 0.05.

Results

Immediately downstream of the rotor, a low momentum wake region, asymmetric to the centerline and shifted towards the upstroke side, was generated. The streamwise mean velocity on either side of the turbine increased due to the blockage generated by the turbine's rotor. During the tests, fish predominately swam and held station downstream of the VAT and

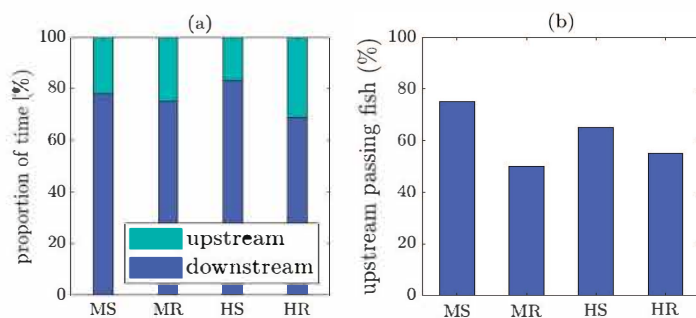


Fig. 2. Fish behaviour results, showing (a) percentage time spent upstream and downstream of the VAT and (b) percentage of fish passing from the downstream region into the upstream region for all test conditions (Fig. 1b).

passed into the upstream region despite the increase in momentum on either side of the turbine. Neither turbine state nor flow condition significantly influenced time spent upstream and downstream (Fig. 2a) nor percentage of upstream passing fish (Fig. 2b) (GLM, $p > 0.001$). Particularly during the “mild” treatment, fish swam near the turbine and exhibited no avoidance behaviour.

Conclusions

These experimental observations provide new insights into fish behavioural adaptations to flow from VATs and will help to refine turbine array designs to harness the full potential of river and estuary energy. Future research will investigate changes in swimming kinematic and associated impacts on energy expenditure depending on swimming location, and the impact of channel confinement on fish swimming behaviour.

Acknowledgement

This work was supported using seed funding from Cardiff University's GCRF QR Funding from the Higher Education Funding Council for Wales (SP111) and the EPSRC WISE CDT (EP/L016214/1.1).

References

- Anderson, D., Moggridge, H., Warren, P. and Shucksmith, J. (2014). The impact of 'run-of-river' hydropower on the physical and ecological condition of rivers, *Water and Environment Journal*, 29, pp. 268-276. doi: 10.1111/wej.12101.
- Castro-Santos T. and Haro A. (2013). Survival and Behavioral Effects of Exposure to a Hydrokinetic Turbine on Juvenile Atlantic Salmon and Adult American Shad. *Estuaries and Coasts* 38(1), 203-214. doi: 10.1007/s12237-013-9680-6.
- Molloy S., Batt J., Eddington J., Mahon-hodgins L., MacNeil A. M., Kregting L., Bibeau E. (2017). Tidal Turbine Marine Life Interaction study: Fish. pp. 24.

Exploration of the active sensory space of fish through CFD

Ali Hassan Khan^{1*}, Stefan Hoerner², and Jeffrey A. Tuhtan¹

¹Centre for Biorobotics, Department of Computer Systems, Tallinn University of Technology, Estonia

²Institut für Strömungstechnik und Thermodynamik, Otto-von-Guericke Universität, Magdeburg, Germany

*Corresponding Author: ali.khan@taltech.ee

Abstract

Fish use their lateral line flow sensing system for vital activities including locating food, avoiding predators and navigation in dark and turbid waters. Recent scientific studies on the lateral line clearly show that they are capable of sensing pressure, velocity and accelerations of the near-body flow fields, as well as their gradients. However, due to the complexity of turbulent flows, the wide range of fish body geometries and possible orientations in flow fields, there remain large knowledge gaps in the intensity and extent (“active sensory space”) of these near-body fields. The main objective of this work is to show that computational fluid dynamics models can be used to estimate the active sensory space around fish-like bodies. Therefore, a CFD model of flume with fish-like body inside is developed to investigate near body flow at Froude number, $F_r = 0.14, 0.29, 0.43, 0.57$ and 0.71 respectively. The characteristic length of the fish-like body under consideration is $L = 30$ cm. The proposed CFD model is validated and verified using LDA (Laser Doppler Anemometry) measurements. Results from this study will help us in examining how fish successfully sense through near body flow fields with pressure, velocity, acceleration and their gradients and determining those parameters which effect the active sensory space of fish bodies.

Keywords: Lateral line; sensory space; computational fluid dynamics; turbulent flows

Introduction

Many aquatic animals are possessed with hydrodynamic receptors to detect their surroundings especially in those situations where visibility is limited e.g. low lighting or high turbidity in water. Fish have an array of hydrodynamic receptors along the body called lateral line system which they use for navigation, schooling and for predator-prey interactions. The lateral line system is comprised of mechanoreceptors called neuromasts, which are further classified as either superficial neuromast or canal neuromasts (Fig. 1, top left). Superficial neuromasts are very small in size (10-50 μm in diameter), and are distributed over the surface of the fish body and are sensitive to local particle motion (velocity) [1]. Canal neuromasts are located beneath the scales, and detect pressure gradients in the flow. Both types of neuromasts are equipped with special cells integrated into epithelium. These cells are connected with gelatinous which forms the cupula (Fig. 1, bottom left). Cupula are directly connected to the central nervous system of fish to transmit the flow information to brain. Any minute changes in the flow are immediately detected by the fish whether it is an obstacle or prey. The lateral line system's anatomy varies considerably between and within species. The extent to which different fish body shapes (morphology) represent adaptations to the hydrodynamic conditions to which fish are exposed, remains as a major knowledge gap. There is a wide diversity of lateral line size for the detection of hydrodynamic signals in distinct behavioral contexts and environments, and limited knowledge on how the body shape influences the hydrodynamic sensing around a fish-shaped body. To understand the relation between body morphology and sensing ability (distance, stimulus intensity and frequency) we must explore the sensory space of fish. There are several methods to investigate the sensing extent; [2] investigated the potential flow field around moving fish. Current advancements in field of computational fluid dynamics can now allow for the simulation, assessment and visualization of turbulent, 3-dimensional (3D) flows field around it to explore and uncover how the active sensory space is affected by the body shape.

Methods

In this study, we have used computational fluid dynamics (CFD) to investigate the sensory space of fish. The sensory space is evaluated as the iso-surfaces of field variables including the dynamic pressure, velocity, acceleration and their gradients, around the fish body. Any disruption in the near body field, alters the shape and distribution of the field variables, and this distortion can be used in the detection of sensory space around the body. The fish body considered in this study is modelled in SolidWorks with the body measurements taken from real fish. To simulate the flow field variables around fish body in the open channel flow, the volume of fluid method is applied to model the multiphase setup. The open source software toolkit OpenFOAM using RANS comparing k- ϵ and k- ω -SST turbulence

models is used to investigate the effect of turbulence model and Froude numbers on the spatial distribution of the pressure and velocity fields. The 3D domain with fish body inside and boundary conditions is shown in Fig. 1 (right).

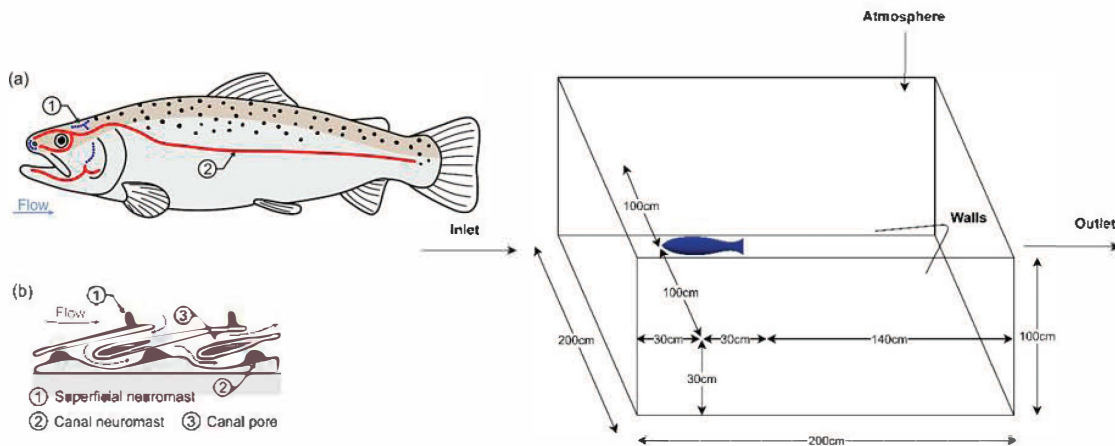


Fig. 1. Left: Lateral line sensing system of living fish. Right: simulated 3D domain with specified boundary conditions.

In the OpenFOAM environment, the general meshing utility *blockMesh* is used to generate the domain with the inlet, outlet, side walls and atmospheric boundary conditions. Fish geometry is imported in stereolithography (.stl) format into OpenFOAM and snapped into the domain using *snappyHexMesh* utility. To resolve the boundary layer, mesh regions and layers were added around the fish body limiting the y^+ value to 0.40. The total number of iterations in this simulation were 20k with a time step of $\Delta t = 0.001$. Whereas for sampling the data, the last 10k iterations are considered. The reason for choosing the smaller Δt is to fulfil the CFL condition and stabilize the numerical model. Mesh statistics of the domain after snapping the imported geometry are as follows:

Table1: Mesh Statistics

Mesh resolution	Domain	No of elements	Type of elements	Max. aspect ratio	Mesh non-orthogonality	Max. skewness
Coarse	3D	2.5M	Hybrid (Hexahedral, Polyhedral, Prism)	12.4230	4.5483	1.4765

Alternatively, an 2D-LDA (Laser Doppler Anemometry) experimental setup was established to measure the flow field at inlet cross section, wake point matrix and cross section in XY- plane with a total 740 measuring probe points within the laboratory flume.

Results

The results obtained from numerical analysis of the fish are validated with the experimental data obtained using LDA (Laser Doppler Anemometry) measurements. The Pressure iso-surfaces predicts, that the shape of the pressure field around the fish shaped body is far more complex then the commonly assumed ovoid which is useful in determining the active sensory space around different fish species.

Acknowledgement

This project has received funding from the European Union Horizon 2020 Research and Innovation Programme under the Marie Skłodowska-Curie Actions, Grant Agreement No. 860800 as well as the Estonian Research Council Grant PRG1243. We are thankful to our team from Otto-von-Guericke University Magdeburg-Germany for providing us the 2D-LDA measurement data for validation.

References

- [1] J. A. Tuhtan and J. F. Fuentes-Pérez, "How do fish sense flow?," *2th Int. Symp. Ecohydraulics (ISE 2018)*, p. 4, 2018.
- [2] E.-S. Hassan, "Mathematical description of the stimuli to the lateral line system of fish derived from a three-dimensional flow field analysis," *Biol. Cybern.*, 1992, doi: 10.1007/bf00197726.

Transient physical habitat modelling - simulation of stream macrozoobenthos habitat suitability using fuzzy logic approach

Sengdavanh Thepphachanh^{1*}, Jürgen Stamm¹

¹Technische Universität Dresden, Institute for Hydraulic Engineering and Technical Hydromechanics,
Faculty of Civil Engineering, Germany

*Corresponding: sengdavanh.thepphachanh@tu-dresden.de

Abstract

Physical habitat modelling has been widely used to quantify ecological responses to spatiotemporal environmental heterogeneity in running waters. Employing the concept of physical habitat modelling, this study simulates suitability for the macrozoobenthos using crisp logic (species' tolerance threshold) and fuzzy logic. Three abiotic parameters namely water depth, velocity, and substrate are used to evaluate benthic invertebrate habitats. The results from two approaches shows a consensus of habitat availability provided from hydraulic conditions. However, the application of fuzzy logic produces continuous habitat suitability maps, which give significantly more information than the binary approach and allows the assessment of habitat quality distribution in the study area.

Keywords: Habitat suitability, Physical Habitat Modelling, Macrozoobenthos, Fuzzy logic

Introduction

In 2000, European Union Water Framework Directive (EU-WFD) was adopted with an aim to achieve "good ecological status" for all water bodies in the European region. Therefore, many attempts have been made to improve hydromorphological conditions of the rivers with the expectation of improved ecological conditions. This results in a high number of cost-intensive restoration projects throughout Europe in the last two decades. Evidences from unsatisfied results of river restorations show a need for ecological functionality analysis tool that focuses on the hydromorphological changes together with biological recovery and river characteristics. In other words, it requires a tool which can estimate the effect of planned restoration activities as well as hydrological relevant measures (e.g. extraction of discharge for hydropower, damming, flood retention measures, separation canals, etc.) onto the river ecology. Habitat modelling, therefore, is established to comply with these requirements.

Methods

In this study, two approaches are used to evaluate the distribution of habitat suitability along the hydromorphological gradients of the river reach. Both approaches need information from 2d-HN model (depth and velocity) and substrate map for habitat suitability simulation. First, water depth and velocities computed using Hydro_AS-2D were adjusted using Bezzola method (Bezzola, 2002) so that bottom shear stress based on substrate and depth-averaged velocity at each point is known. Then, habitat model runs in two scenarios using two approaches. The first approach overlays this information with hydraulic tolerance of selected species (table 1). In this approach, the point is defined as habitable if all the following conditions are met: 1) depth > 0.01 m, 2) Bezzola-adjusted bottom shear stress < 2 N/m², and 3) any preferred substrate type is present; otherwise, the point is non-habitable. The second approach applies fuzzy logic rules, formulated from these preferences. Depth, velocity, and substrate are classified into fuzzy sets, and the fuzzy rules defining habitat suitability are created. Instead of binary result, habitat suitability value ranges from 0 to 1 (from non-preferable to most preferable for species).

Table 1. Preferred shear stress and substrate of species used in habitat modelling.

Taxon	Shear stress preference [N/m ²]	Substrate preference
Ancylus fluviatilis	1.64	Mesolithal, Mikrolithal, Makro-Megalithal, subM, LPTP, CPOM, FPOM
Athripsodes albifrons	0.44	Akal, Mesolithal, Mikrolithal
Baetis lutheri	1.35	Akal, Mesolithal, Mikrolithal, Makro-Megalithal, subM, LPTP
Psychomyia pusilla	0.64	Mesolithal, Mikrolithal, Makro-Megalithal

Abbreviations of substrate types: subM = submerged macrophytes, LPTP = living parts of terrestrial plants, CPOM = coarse particulate organic matter, FPOM = fine particulate organic matter.

Results

The model is simulated for one year (365 days) period and the results of the model using two methods show a similarity in habitat suitability map shapes. The habitable area simulated from the first approach are basically the area with high suitability simulated from the fuzzy logic approach. Likewise, non-habitable area from the first method are the area with low suitability from the fuzzy method.

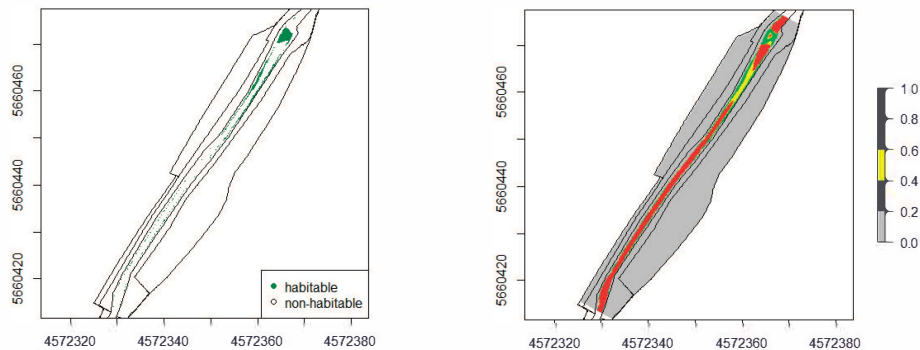


Fig. 1. Habitat suitability map using (left) crisp and (right) fuzzy logic.

Conclusions

The habitat model presented in this study allows the assessment of habitat suitability based on crisp logic and fuzzy logic. The results of this study show an agreement in both approaches. A distribution of habitat suitability has an inverse relationship (negative correlation) with discharge. The results show that during the peak days, habitat with high suitability is limited; and when flows decrease, the highly suitable habitats for species are found.

References

- Bezzola, G. (2002). Fließwiderstand und Sohlenstabilität natürlicher Gerinne unter besonderer Berücksichtigung des Einflusses der relativen Ueberdeckung. Dissertation, Eidgenössische Technische Hochschule Zuerich.
- Tatis-Muvdi, R., & Stamm, J. (2019). Transient modelling of physical habitat for stream macrozoobenthos at intermediate spatial and temporal scales—Moving towards more dynamic descriptions of hydromorphology.
- Wolter, C., et al. (2013). Review on ecological response to hydromorphological degradation and restoration. Deliverable D1.3, Project REFORM, REstoring rivers FOR effective catchment Management. European Commission, 7th Framework Programme, Grant Agreement 282656.

Attracting juvenile silver perch into the Tube Fishway of different scales

Maryam Farzadkhoo^{1*}, Stefan Felder¹, Richard T Kingsford², Iain M Suthers², John H Harris²,
William L Peirson¹

¹ Water Research Laboratory, School of Civil and Environmental Engineering, UNSW Sydney,
NSW 2052, Australia

*e-mail: maryam.farzadkhoo@unsw.edu.au

² Centre for Ecosystem Science, School of Biological, Earth and Environmental Sciences, UNSW
Sydney, NSW 2052, Australia

Abstract

River infrastructure is recognized as a threat for migratory fish species worldwide and fishways of different types have thus been installed to restore river connectivity. A novel fishway design, the UNSW tube fishway, has been developed recently. A key component for successful operation of the Tube Fishway is to use flow to attract fish into a transfer chamber prior to fish lifting. Herein, we investigated the attraction success into the transfer chamber of the Tube Fishway, comparing the attraction for different chamber diameters (0.1 m to 0.4 m) and attraction velocities (0 m/s to 0.5 m/s), for a threatened native fish species in Australia. Groups of five silver perch (*Bidyanus bidyanus*) were reliably attracted into the transfer chamber independent of the transfer chamber diameter. The highest fish entry was achieved for attraction velocities at the slotted entrance of 0.15 m/s and 0.3 m/s for all chamber sizes.

Keywords: fish attraction; laboratory experiments; slotted entrance; transfer chamber

Introduction

Many anthropogenic in-stream barriers, such as dams and weirs, contribute to decline in migratory freshwater fish populations. Although, fishways are one of the viable solutions to facilitate fish migration (Katopodis et al., 2001), major reductions have shown in some freshwater fish population (Mallen-Cooper et al., 2007). Yet, the effectiveness of fishways is uncertain for multiple fish species and many operate as selective filters (Baumgartner et al., 2018). To address this limitation, the UNSW Tube Fishway was developed to lift fish past barriers with heights between 2 m and 100 m (Harris et al., 2019). A key component in the successful operation of the Tube Fishway is fish attraction into the transfer chamber. Herein, the effectiveness of attraction was tested for 1) variation in diameters of the transfer chamber and 2) attraction velocity at the slotted entrance, to identify preferable attraction conditions.

Methods

Experiments were carried out in a recirculating open channel flume of 6 m length, 0.6 m width and 0.6 m height at the UNSW Water Research Laboratory. The transfer chamber of the Tube Fishway was in the upstream section of the channel followed by a test section in which the fish were released and monitored. Entrance to the Tube Fishway was tested for different transfer chamber sizes with interior diameters of $D = 0.1$ m, 0.225 m, and 0.4 m. Attraction flow was introduced at the upstream end of the transfer chamber and fish were attracted by flow through a vertical slot with 0.03 m width across the full height of the entrance chamber. Different attraction flow velocities at the slotted entrance to the transfer chamber of $V = 0$, 0.15, 0.3, and 0.5 m/s were tested. An overflow weir was used at the end of the test section to keep the water level constant and maintain an air space 20% inside the transfer chamber for all flow conditions. Fish were classed into two fish sizes of small and large with an average total body length of 60 ± 1.22 SE mm and 90 ± 1.26 SE mm, respectively. Four repetitions per each combination were conducted with groups of five naive juvenile silver perch. Suitable fish

acclimation condition was defined based on pilot experiments. Fish were released into the test section and acclimated for an hour without any attraction flow. Once attraction flow was established, fish entry into the chamber was continuously monitored for one hour with video cameras from top and side views. Manual video processing provided details on the maximum number of fish inside the chamber at any given time, the time that fish stayed in the chamber, and number of entries.

Results

Figure 1 shows the recorded number of silver perch that entered the transfer chamber of different diameters (D) and attraction flow velocities (V). The results indicate that silver perch were attracted into the transfer chamber irrespective of velocities, chamber diameters, and fish size. The highest number of attracted fish was observed for $V = 0.15$ m/s and 0.3 m/s for large silver perch and 0.15 m/s for small silver perch. Irrespective of their size, fish remained longer in the transfer chamber (up to 92% of the experimental duration) for velocity of 0.15 m/s and the cumulative number of entry attempts was significantly higher (up to 200).

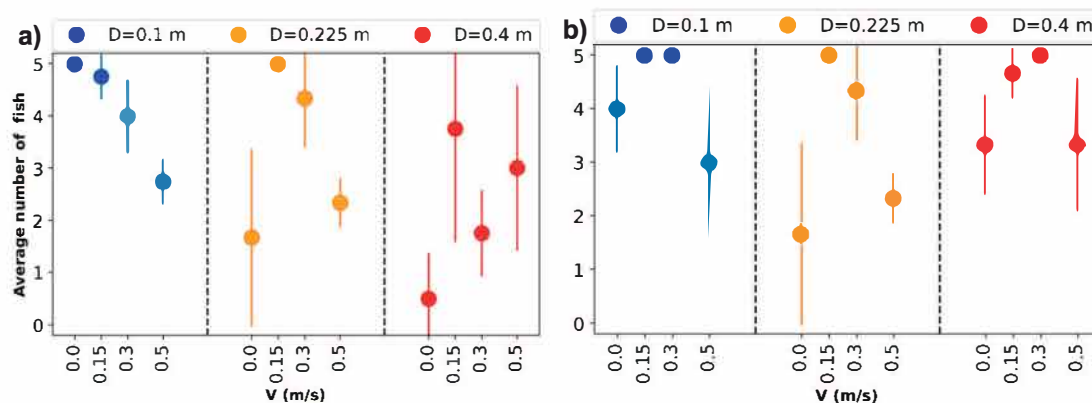


Figure 1 – Mean (\pm SD) number of silver perch that entered the transfer chamber of different diameters and attraction flow velocities: a) Small silver perch, b) large silver perch

Conclusions

The present findings provide evidence that silver perch of different sizes can be attracted into different transfer chamber scales. This is an important milestone for the Tube Fishway operation since it suggests that the transfer chamber can be scaled to suit local fish populations. The experiments identified the most favorable attraction velocity for silver perch (i.e., $V = 0.15$ m/s). This research is ongoing involving repeated experiments with further Australian native fish species to further optimize the attraction into the transfer chamber of the Tube Fishway.

References

- Baumgartner, L.J., Boys, C.A., Marsden, T., McPherson, J., Ning, N., Phonekhampheng, O., Robinson, W.A., Singhanouvong, D., Stuart, I.G. and Thorncraft, G., 2018. Comparing fishway designs for application in a large tropical river system. *Ecological Engineering*, 120: 36-43.
- Harris, J.H., Peirson, W.L., Mefford, B., Kingsford, R.T. and Felder, S., 2019. Laboratory testing of an innovative tube fishway concept. *Journal of Ecohydraulics*, 5(1): 84-93.
- Katopodis, C., Kells, J. and Acharya, M., 2001. Nature-like and conventional fishways: alternative concepts? *Canadian Water Resources Journal*, 26(2): 211-232.
- Mallen-Cooper, M., Brand, D. and Ecology, 2007. Non-salmonids in a salmonid fishway: what do 50 years of data tell us about past and future fish passage? *Fisheries Management* 14(5): 319-332.

An investigation of the hydrodynamic and fish behavior characteristics in brush-type fish passage: A pilot study in İyidere, Turkey

Serhat Kucukali^{1*} and Reinhard Hassinger²

¹Department of Civil Engineering, Hacettepe University

*Corresponding: kucukali78@gmail.com

²Department of Civil Engineering, Kassel University

Abstract

The fish passage performance and flow structure of the brush fish pass were investigated at the İncirli Small Hydropower (SHP) Plant on İyidere River which is located in the East Black Sea region of Turkey. The spatial distributions of velocity vectors, power velocity, and turbulent kinetic energy (TKE) were presented. The flow-bristle interaction creates a reduced velocity and low turbulence resting zones. The data revealed that brush fish passage provides passage for small-bodied fish ($L_f < 15$ cm) in a high gradient channel with a slope of 10%. The monitoring data revealed that bristles as flexible hydraulic elements are beneficial for migrating fish in practice.

Keywords: Brush fish passage; Energy dissipation; Turbulence kinetic energy; Passage efficiency

Introduction

The technique of using brush elements as hydraulic-energy absorber in fish way had been firstly applied in year 2002 in Germany and currently around 60 brush fish ways have been in operation in Europe. In brush fish pass, the energy dissipation is rather effective because the large number of flow-induced vibrating bristles initiate strong energy dissipation. Rahn (2011) conducted systemic experiments in a diagonal brush fish pass and Rahn (2011) found that a significant amount of energy dissipation (>50%) takes place in the brush blocks. The literature lacks a study that examines flow structure and fish passage efficiency of a brush fish pass simultaneously at prototype scale. Although, physical models widely used under controlled conditions; in physical models scale effects might exist (Kucukali and Hassinger, 2018) and actual operational conditions of fish pass structures (i.e. variable headwater and tailwater water levels) cannot be well-simulated accordingly. In this study, we focused on the flow structure of brush fish pass considering the passage performance of fish species endemic to Turkey.

Methods

Under the scope of the project, we completely removed the existing orifice pool-type fishway and we built a new diagonal brush fish pass at İncirli Weir located on the İyidere River, Eastern Black Sea River Basin in Turkey, has a catchment area of 1053 km² and length of 53 km. The reason for the diagonal arrangement is that in this kind of configuration the flow is cross-exchanged constantly. By grouping of brush blocks, pools can be formed between the groups of brush bars. For normal operating conditions, the total level difference between the upstream and downstream of fish pass structure is 5 m. The bed slope of the fish passage is 10% and it has a total length of 46 m. The areal density of the brushes is selected according to the result of a designing process which is based on an equilibrium of forces. The brush density is a function of slope, discharge, water depth, bristle diameter, bristle length and grouping pattern

of the brush modules. An acoustic Doppler velocimeter (Sontek 50-MHz ADV) was used to measure the three-dimensional instantaneous velocity fields. The turbulence quantities were collected at 50 Hz frequency during a sampling time of 30 seconds. Moreover, a local power velocity V_{pm} , which is thought to be an useful parameter to understand fish migration patterns, is defined as

$$V_{pm} = \sqrt[3]{\frac{\sum V_i^3}{n}} \quad (1)$$

where V is the resultant velocity and n is the number of velocity samples. The spatial distribution of the turbulent kinetic energy (TKE) in the flow field is important, because the energy dissipation is resulted from the turbulence generation. Hence, the turbulent kinetic energy per unit mass k is calculated using Eq. (2)

$$k = \frac{1}{2}(\overline{u'^2} + \overline{v'^2} + \overline{w'^2}) \quad (2)$$

Results

The spatial distribution of the V_{pm} through the fish pass is shown in Fig. 1a. Behind of brush blocks are characterized by reduced velocity zone which can be used by fish as potential resting areas and refuges. The spatially-averaged turbulent kinetic seems to be considerably lower in brush fish than in technical fish passes for a same dissipated power. With compared to technical pool-type fish pass, spatially-averaged TKE in the basin reduced by 35% (Fig. 1b). Also, maximum velocity is reduced by about 30%.

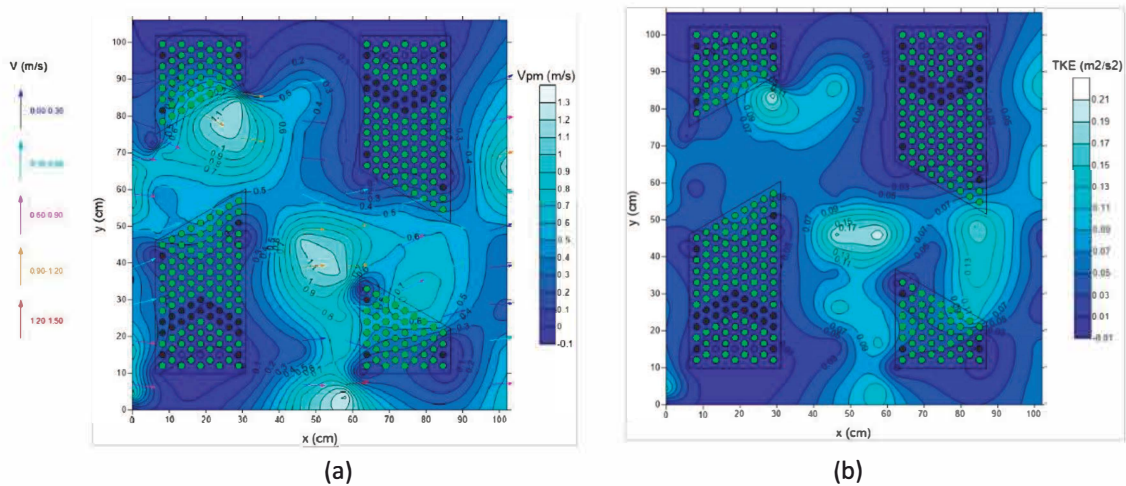


Fig. 1. (a) Velocity vectors and power velocity distribution around brush blocks and (b) turbulent kinetic energy distribution in horizontal plane at the mid-depth.

Conclusions

The bristles as energy absorbers represent a cost-effective option, which can be retrofitted at any time existing structures, to improve the hydraulic conditions in fish passages. We obtained satisfactory passage efficiencies for fish species endemic to Turkey. The passage efficiency of target fish species *Salmo coruhensis* was calculated as 82.4%.

References

- Rahn, S. (2011). *Hydraulische Untersuchung der Strömungsverhältnisse in Borstenfischpässen mit Dreifachriegeln*. Master Thesis in Faculty of Civil and Environmental Engineering, University of Kassel (in German).
- Kucukali, S., Hassinger, R. (2018). Flow and turbulence structure in a baffle–brush fish pass. *PI Civil Eng-Water Management*, 171(1), 6-17.
- Shiono, K., & Muto, Y. (1998). Complex flow mechanisms in compound meandering channels with overbank flow. *Journal of fluid mechanics*, 376, 221-261.

**The 9th International
Symposium on
Environmental Hydraulics**

E1 Session

Coast [E1-W1]



OpenFOAM modeling of wave pressures on a caisson armored with double-layer tetrapods on the rubble stones

Deok Ah Lee¹, Gun Hyeong Kim^{1*}, Sung Bum Yoon¹ and Sang-Ho Oh^{2*}

¹Research Institute, HYCERG Inc.

²School of Civil, Environmental and Chemical Engineering, Changwon National University

*Corresponding: coast.oh@gmail.com

Abstract

This study reports numerical investigation on the horizontal wave pressure acting on a solid caisson that is armored with double-layer tetrapods on the core-layer of rubble stones. OpenFOAM modeling was conducted to numerically simulate the wave pressure on the upright wall of the caisson. The simulation result was compared with the experimental data, which showed fairly good agreement between the simulation and the measurement. Hence, the coefficients of porous media for the armor-layer, middle-layer, and the core-layer in front of the caisson can be successfully applied in modeling the wave pressure on this type of structure.

Keywords: OpenFOAM; Caisson; Wave pressure; tetrapod; core layer

Introduction

The front wall of a caisson is occasionally protected by concrete armor units to reduce wave loading on the caisson. This type of structure is called as horizontally composite breakwater. Sometimes, similar as rubble mound breakwater, rubble stones are placed in front of the caisson and covered with concrete armor units. Little research has been conducted on the wave pressure acting on this special type of horizontally composite breakwater. Very recently, an experimental study was carried out for this type of structure to suggest a design guideline considering different coverage rates and the shoulder width of the armor layer (Oh and Lee, 2020), as shown in the left panel of Fig. 1. By making use of the laboratory data produced in the previous study, OpenFOAM modeling was performed in this study to reproduce the measured wave pressures along the front wall of the caisson.

Methods

Numerical simulations were performed using the waves2Foam model where waves are generated by the relaxation method. The waves2Foam library provides three solvers according to the conditions of the computational domain when simulating the wave values. In order to simulate the porous media of armor and core layers, the porousWaveFoam solver was used (Jensen et al., 2014).

The length of the wave generation section was approximately 2 times of the wave length, and the rest sections were configured the same as the experiment. The grid size ranged from 0.02 to 0.035 m for horizontal (x) and vertical (y) directions. In order to accurately reproduce the geometry of waves and the structure, the numerical grids were more densely constructed near the water surface and the peripheries of the structure. In the lateral (z) direction, only one grid was set. The right panel of Fig. 1 shows general view of the grid around the structure.

Concerning the parameters related to the porous media, the values used by Lee et al. (2019) were applied. For the core layer, the porosity was set as $n = 0.44$, whereas the median diameter $D_{50} = 0.01$ m. For the middle layer, $n = 0.3$ and $D_{50} = 0.016$ m, $\alpha = 500$, and $\beta = 2.0$. The values of the last two parameters were determined following Jensen et al. (2014). For the double layer tetrapods, $n = 0.33$, $D_{50} = 0.075$ m, $\alpha = 200$, $\beta = 0.7$ were applied, respectively.

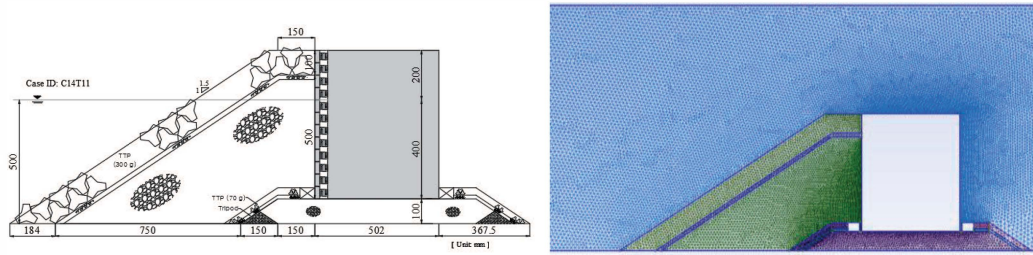


Fig. 1. Side view of the experimental model and grid of the numerical model

Results

Fig. 2 shows a comparison of the time series of the measured and simulated wave pressure at different elevations on the caisson. Overall, the numerical model reproduces the experimental results well. Although the degree of agreement between the experiment and simulation varied depending on the wave conditions and the elevations at the front wall of the caisson, generally good agreement was obtained with the present setup of the OpenFOAM model. As the observation time elapsed, the degree of inconsistency increased due to the influence of reflected waves at the wave board and the structure as well.

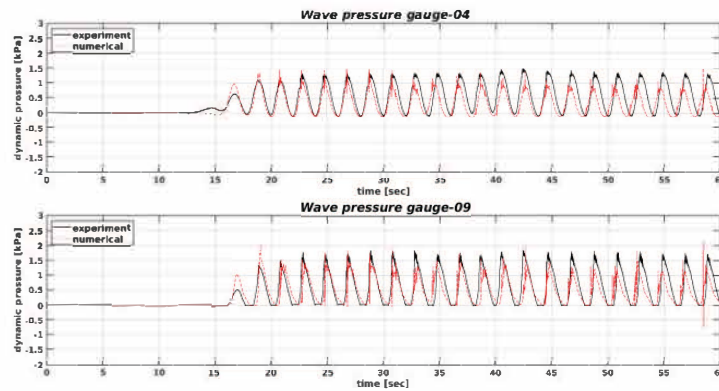


Fig. 2. Comparison of the time series of the measured and simulated wave pressure on the caisson.

Conclusions

The numerically simulated wave pressure coincided fairly well with the measured value. This demonstrates the adequacy of porous media coefficients in the present model for simulating the wave pressure on the caisson that is compositely armored with tetrapods and rubble stones.

Acknowledgement

This study is part of a research project titled “Development of Design Technology for Safe Harbor from Disasters”, which is funded by Ministry of Oceans and Fisheries of Korea (Project No. 20180323).

References

- Jensen, B., Jacobsen, N.G., & Christensen, E. D. (2014). Investigations on the porous media equations and resistance coefficients for coastal structures. *Coastal Engineering*, 84, 56-72.
- Lee, G. S., Oh, S.-H., & Yoon, S. B. (2019). Evaluation of empirical porous-media parameters for numerical simulation of wave pressure on caisson breakwater armored with tetrapods. *Journal of Korean Society of Coastal and Ocean Engineers*, 31(6), 344-350 (in Korean).
- Oh, S. H., & Lee, J. S. (2020). Experimental investigation of horizontal wave pressure on the caisson protected by armor blocks on the rubble-mounted core. *Journal of Marine Science and Engineering*, 8(9), 691.

A novel approach to estimate the coastal protection provided by different saltmarshes species

Maria Maza^{1*}, Javier L. Lara¹ and Iñigo J. Losada¹

¹IHCantabria - Instituto de Hidráulica Ambiental de la Universidad de Cantabria

* Corresponding: mazame@unican.es

With the aim of analyzing the relationship between the standing biomass of a coastal vegetation field and its flow energy attenuation capacity, a new set of experiments considering different saltmarshes meadows and flow conditions are carried out. A new relationship between the standing biomass and the obtained wave attenuation is found. This relationship will help to quantify the expected coastal protection service provided by different saltmarshes according to their biomass and the incident flow conditions, avoiding the use of any parameter that needs to be calibrated. This may represent a paradigm shift in modelling the energy attenuation produced by different species of saltmarshes.

Keywords: coastal protection, wave attenuation, standing biomass, saltmarshes

Introduction

Estimation of the flow energy dissipation induced by an ecosystem that accounts for its characteristics and the incident hydrodynamic conditions is crucial if ecosystem-based coastal protection measurements want to be implemented. Characterization of a vegetated ecosystem by measuring leaf traits, biomechanical properties of plants and the number of individuals per unit area involves a lot of effort. Previous studies have shown that flow energy attenuation positively correlates with standing biomass (Maza et al., 2015). Standing biomass can be a unique variable defining the flow energy attenuation capacity of the ecosystem. In addition, this variable has been already characterized for many ecosystems and it can be estimated by aerial images. Then, to further explore its relation to the induced energy attenuation on the flow, a new set of experiments using real vegetation with contrasting morphology and biomechanical properties, and subjected to different incident flow conditions, is proposed. The obtained standing biomass-attenuation relationships will help to quantify the expected coastal protection provided by different vegetated ecosystems based on their standing biomass and the flow conditions.

Experimental set-up

Experiments are run in the small flume at University of Cantabria. Four vegetation species with contrasting biomechanical properties and morphology are selected: *Spartina maritima*, *Salicornia* sp., *Halimione* sp. and *Juncus* sp. Plants are taken from different Cantabria estuaries. After collecting a total of 105 boxes of vegetation they are directly brought to the laboratory to introduce them between two false bottom pieces already constructed leading to a 9.05 m long meadow (Figure 1). Once located into the flume, the meadow is tested under different waves and current conditions considering three water depths. Wave height is measured using 15 capacitive free surface gauges. Three meadow conditions are considered: 100% standing biomass, 50% standing biomass and 0 standing biomass.

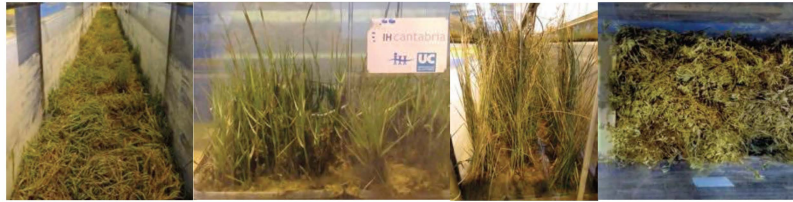


Fig. 1. View of *Salicornia* sp., *Spartina* sp., *Juncus* sp. and *Halimione* sp. fields.

Results

The wave attenuation analysis is performed by obtaining the wave damping coefficient, β , for each test following Dalrymple et al. (1984), Mendez et al. (2004) and Losada et al. (2016). A direct relationship between the species standing biomass and β is observed. Additionally, it is found that there is a strong influence of the submergence ratio (SR) in the resulting wave attenuation due to the extremely different geometrical properties of the different species. Then, a relationship between the obtained β and a new parameter considering both, the standing biomass and the SR is obtained. Figure 2 displays β as a function of the standing biomass times the SR for four regular wave conditions.

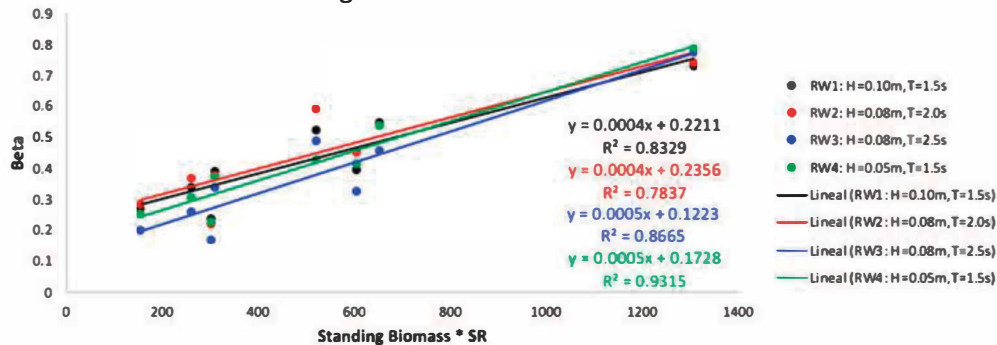


Fig. 2. β as a function of standing biomass times the SR for the four vegetation species and the two densities considered for each one of them, and four regular wave conditions.

As can be observed in Figure 2, a linear relationship is obtained between β and $StandingBiomass * SR$ for all tested wave conditions, leading to high correlation coefficients, $\rho^2 > 0.78$. It is important to note that species with highlight different biomechanical properties and morphological traits are all fitting to the same line. This highlights the importance of this new parameter in the resultant wave attenuation.

Conclusions

The obtained relationships provide the basis for the inclusion of standing biomass as a key parameter for estimating the coastal protection provided by different saltmarsh species.

Acknowledgement

The work leading to this paper has been funded under the Retos Investigación 2018 (grant RTI2018-097014-B-I00) program of the Spanish Ministry of Science, Innovation and Universities. M. Maza is sincerely grateful to the Spanish Ministry of Science, Innovation and Universities for the funding provided in the grant Juan de la Cierva Incorporación (BOE de 27/10/2017).

References

- Dalrymple, R.A., Kirby, J.T., Hwang, P.A. (1984): Wave diffraction due to areas of energy dissipation, *J. Waterw. Port Coast. Ocean Eng.* 110, 67–79.
- Losada, I.J., Maza, M., Lara, J.L. (2016): A new formulation for vegetation-induced damping

- under combined waves and currents, *Coastal Engineering*, 107, 1-13.
- Maza. M., Lara, J.L., Losada, I.J., Ondiviela, B., Trinogga, J., Bouma, T.J. (2015): Large-scale 3-D experiments of wave and current interaction with real vegetation. Part 2: Experimental analysis, *Coastal Engineering*, ELSEVIER, vol. 106, pp. 73-86.
- Mendez, F.J., Losada, I.J. (2004): An empirical model to estimate the propagation of random breaking and non-breaking waves over vegetation fields. *Coast. Eng.* 52, 103–118.

Siphon Well for Protection of Coastal Aquifer from Saltwater Intrusion.

Byunghee Nam¹, Roshina Babu², and Namsik Park^{1*}

¹ Department of Civil Engineering, Dong-A University, South Korea

² Department of Civil and Environmental Engineering, The University of Utah Asia Campus

*Corresponding: nspark@dau.ac.kr

Keywords: Saltwater intrusion, Laboratory experiments, siphon well, Float-laser device

Abstract

In coastal aquifers, freshwater from inland meets the seawater and forms an interface. However, due to climate change, sea-level rise, drought, and increase in groundwater use, the interface can move inland. Seawater intrusion decreases groundwater resources and pollutes the existing groundwater wells with seawater. There are different methods for mitigating seawater intrusion; however, most of them suffer from costs and power requirements. This study focuses on developing the concept of a cost-effective saltwater pumping system, named siphon well.

Siphon well works on the principle of gravity to remove the salt water from the coastal aquifer, thereby reducing saltwater intrusion. The hydraulic head difference between the groundwater table of the coastal aquifer and the sea level powers the siphon well. Since siphon well relies entirely on tides as a power source, it could be applied more efficiently in the coastal areas having large tidal ranges.

A sharp interface numerical model was developed to simulate the effect of siphon well in coastal aquifers. Siphon well is introduced in a hypothetical aquifer subjected to excessive pumping. The effectiveness of siphon well in controlling seawater intrusion is measured in terms of volume change in freshwater and saltwater. Under excessive pumping conditions, the volume of saltwater increases and that of freshwater decreases in an aquifer. It was found that an aquifer with a siphon well can recover freshwater depletion due to pumping faster than one without a siphon well. The study indicated that this new cost-effective saltwater pumping method can control saltwater intrusion in coastal aquifers.

Acknowledgement

This work was supported by a NRF (National Research Foundation of Korea) Grant funded by the Korean Government (NRF-2019H1A2A1076177), and the Dong-A University Research Fund.

Simulation-optimization for sustainable groundwater management in small islands under drought conditions

Roshina Babu¹, Byunghee Nam², and Namsik Park^{2*}

¹ Department of Civil and Environmental Engineering, The University of Utah Asia Campus

² Department of Civil & Environmental Engineering, Dong-A University

*Corresponding: nspark@dau.ac.kr

Keywords: Small islands; Simulation-optimization; Saltwater intrusion; Sustainability index; Groundwater pumping; Droughts

Abstract

Groundwater in small islands occurs in the form of freshwater lenses that maintain equilibrium between the natural groundwater recharge from rainfall and the surrounding seawater. Due to various climatic, hydrogeological, physiographic, and management factors, these freshwater lenses are under the constant threat of saltwater intrusion. Among the above factors, droughts are one of the major climatic causes that magnify the threat of saltwater intrusion as drastic changes in freshwater lens volume can occur following droughts. Hence management of groundwater pumping rates during droughts is essential to prevent saltwater intrusion and ensure the sustainability of the freshwater lens under future climate conditions. This paper develops a simulation-optimization model to determine the sustainable optimal pumping rates from individual wells under drought conditions in small islands. Three indicators based on reliability, resilience, and vulnerability definitions are used to describe the sustainability of groundwater pumping. The objective of the model is to maximize the volume and duration of freshwater pumping while minimizing saltwater intrusion. The linked simulation-optimization model consists of a calibrated sharp interface numerical model and a genetic algorithm-based optimization. The model is applied to test a representative drought on the Pacific island of Tongatapu. Two groundwater management scenarios - unplanned pumping and rainfall responsive optimized pumping are explored. The current study suggests that temporal pumping management in response to variation in rainfall during droughts can increase the sustainability index of groundwater pumping wells. The methodology given in this study can be used as an approach to the management of groundwater resources and to ensure the sustainability of small islands' freshwater lenses in the future.

Acknowledgment

This research was supported by the Dong-A University Research Fund.

Calibration and assessment of numerical modelling in an embayed beach in case of presence or absence of submerged breakwaters

Minsang Cho¹, Kideok Do², In-Ho Kim³, and Hyun-Doug Yoon^{1*}

¹Department of Civil & Environmental Engineering, Myongji University

²Department of Ocean Engineering, Korea Maritime and Ocean University

³Department of Earth and Environmental Engineering, Kangwon National University

*Corresponding: hdyoon@mju.ac.kr

Abstract

A submerged breakwater is a coastal structure that can protect from coastal erosion by dissipating high-wave energy and preventing sand loss. It is important to understand the impacts of a submerged breakwater on hydrodynamics and morphological changes for coastal erosion management and countermeasure. XBeach, a process-based model, is used to simulate nearshore hydrodynamics and morphological response to storm. A variety of parameters are included in XBeach, and several parameters related to the wave breaking and effects of wave non-linearity are important to accurately predict morphological changes for storm conditions. In this study, calibration and assessment of XBeach modelling are performed to compare the parameter differences between with and without submerged breakwaters in an embayed beach.

The results of this study show that changes in the coastal environment by submerged breakwaters affect parameter calibration.

Keywords: Embayed beach; Submerged breakwaters; Hydrodynamics; Morphodynamics; XBeach

Introduction

It is necessary to control the high-wave energy invading from offshore to prevent coastal erosion and protect the backbeach structures. A submerged breakwater is a coastal structure that can effectively control wave energy as well as prevent sand loss (Lee, 1999). It is important to understand the impacts of a submerged breakwater on hydrodynamics and morphological changes for coastal erosion management and countermeasure. XBeach, process-based model, was developed to simulate nearshore hydrodynamics and morphological response to storm. XBeach includes a variety of parameters, and calibration of these is required. Parameter calibrations of XBeach were mostly carried out to beach without coastal structures (Do and Yoo, 2020; Kalligeris et al., 2020). In this study, calibration and assessment of XBeach modelling are performed to compare the parameter differences between with and without submerged breakwaters in an embayed beach.

Methods

Bongpo beach, an embayed beach located on east coast of Korea, is the target area in this study. To setup the XBeach modelling for condition with and without submerged breakwaters, field observation data were collected before and after submerged breakwaters were installed (see Table 1). The collected data were input as initial and offshore boundary conditions. The parameters used for calibration and assessment are *gamma*, *facua* and *bedfriccoef*. parameters related to the wave breaking (*gamma*) and effects of wave non-linearity (*facua*) are important to accurately predict morphological changes for storm conditions. The bed friction coefficient, *bedfriccoef*, is used to consider the effect of bed friction on the sea around submerged breakwaters, which is normally installed in shallow water zone (Lee, 1999). By

combining the three parameters mentioned, 260 numerical simulations were performed under condition with and without submerged breakwaters.

	Before installation	After installation
Storm-induced wave	2013 winter swell (Hs,max = 6.30 m, Tp = 12.16 s)	2020 typhoon MAYSAK (Hs,max = 5.43 m, Tp = 10.01 s)
Storm surge	0.385 m	0.950 m
Bathymetry data	Depth of pre- and post-storm (Oct 29, 2013 ~ Feb 24, 2014)	Depth of pre- and post-storm (Aug 25, 2020 ~ Sep 6, 2020)

Results

Numerical simulation results show that submerged breakwaters affected the change in *facua* value in the center of Bongpo beach. As shown in Fig. 1, in the case of no submerged breakwaters, it was seemed to predict more accurately when the *facua* was small (< 0.3). On the other hand, in the case of submerged breakwaters installed, it was predicted more accurately when the *facua* was large (> 0.3). the *facua* parameter is related to cross-shore sediment transport. As coastal retreat decreases due to submerged breakwaters, a change value of *facua* occurred. The relationship between submerged breakwater and parameters is to be analyze clearly through additional numerical simulations.

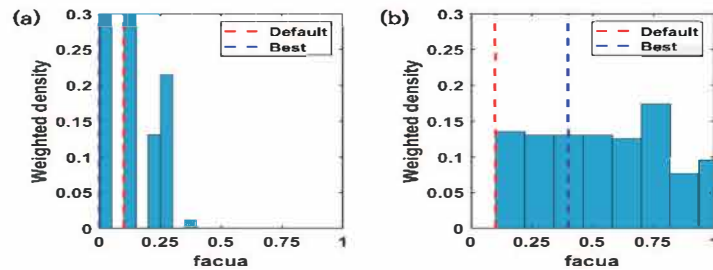


Fig. 1. Histogram on weighted density of *facua* for two conditions: (a) without and (b) with submerged breakwaters.

Conclusions

The results of this study show that changes in the coastal environment caused by installing submerged breakwaters affect parameter calibration. A change in the value of *facua* occurs as the coastal retreat changes by submerged breakwaters. It is necessary to investigate the effect of the presence of submerged breakwaters on the parameter change through additional numerical simulations.

Acknowledgement

This research was a part of the project titled 'Practical Technologies for Coastal Erosion Control and Countermeasure', funded by the Ministry of Oceans and Fisheries, Korea(20180404).

References

- Do, K. & Yoo, J. (2020). Morphological response to storms in an embayed beach having limited sediment thickness. *Estuarine, coastal and shelf science*, 234, 106636.
- Kalligeris, N., Smit, P.B., Ludka, B.C., Guza, R.T. & Gallien, T.W. (2020). Calibration and assessment of process-based numerical models for beach profile evolution in southern California. *Coastal engineering*, 158, 103650.
- Lee, C. E. (1999). Analysis of wave fields over submerged breakwaters. *Journal of Korean society of coastal and ocean engineering*, 11(2), 95-106.

**The 9th International
Symposium on
Environmental Hydraulics**

E2 Session

Ocean [E2-W2]



Evaluation of effects of river discharge on the development of salinity stratification and hypoxia due to climate change in the Ariake Sea, Japan

Hao Lin¹, Yuya Sato¹, Shinichiro Yano^{2*}

¹Department of Civil Engineering, Kyushu University

* Corresponding: yano@civil.kyushu-u.ac.jp

Abstract

The consequences of climate change on the coastal environment, such as the occurrence of salinity stratification and the frequency of hypoxia, are becoming even more serious. The Ariake Sea, as one of the most important shallow coastal area, plays a significant role on fishery economy in Japan. This study conducts different scenarios of flood patterns and uses the numerical models by Delft3D to evaluate the effects on salinity stratification and the hypoxia due to climate change in the bay. The results show that salinity stratification is prone to occur in the flood period and it is difficult to dissipate in a large-scale flood. Moreover, as the increase of peak discharge and duration, the development of hypoxia at the bottom layer lasted longer.

Keywords: hypoxia; salinity stratification; flood patterns; climate change; Ariake Sea

Introduction

According to the AR5 Synthesis Report of IPCC, the world's air temperature is getting higher, with an expected global temperature increase of 1 to 5 °C by the end of this century (IPCC, 2014). Changes in precipitation patterns caused by climate change are expected to affect the marine environment. Problems such as sea level rise, sea temperature rise and ocean acidification are accelerating, it is significant to look for climate change adaptation for sustainable development. In recent years, extreme precipitation events due to climate change occurred frequently, which may cause a large amount of freshwater flow into the Ariake Sea. As a result of freshwater inflowing, threats like salinity stratification and the development of hypoxia will lead to coastal environmental deterioration. Thus, this study attempts to investigate the effects of different flood patterns on the salinity stratification and the hypoxia in the Ariake Sea, to give supports for the adaptive measurements.

Methods

This study uses the hydrodynamic model and lower-trophic ecosystem model by Delft3D, which are the same as Tadokoro and Yano (2019). Calculation domain is a combination of the Ariake Sea and the Yatsushiro Sea (Fig. 1). The horizontal grid is a rectangular grid with a Cartesian frame of reference and the vertical grid uses σ coordinate system, where the number of σ -layers is defined as 10 layers with 5% \times 3, 10% \times 4, 15% \times 3 from surface to bottom. Open boundaries are located outside the inlet to the Ariake Sea and on the line connecting Kabashima and Akune. Heat flux model uses the Murakami model, which prescribes the relative humidity, air temperature and the net solar radiation. SGS-turbulence model and k- ϵ turbulence model are used to describe turbulence processes. Freshwater inflows are considered from eight A-class rivers, nine large B-class rivers and the north and south drainage gates of the Isahaya Bay Sea-Dike. The lower-trophic ecosystem model is based on the results of hydrodynamic model. Fig. 3 shows the conceptual diagram of the ecosystem model. The main processes are photosynthesis, production and consumption of oxygen, decomposition of organic matter, settlement of particulate organic matter, nitrification, mineralization and reaeration on the sea surface. Dissolved oxygen (DO) is also included as one of components in the model. Model parameters are same as the setting in Tadokoro et al. (2018).

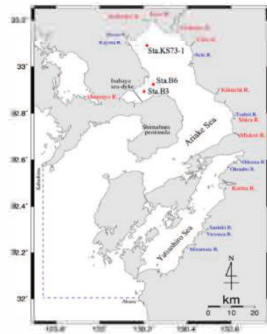


Fig. 1 Calculation domain

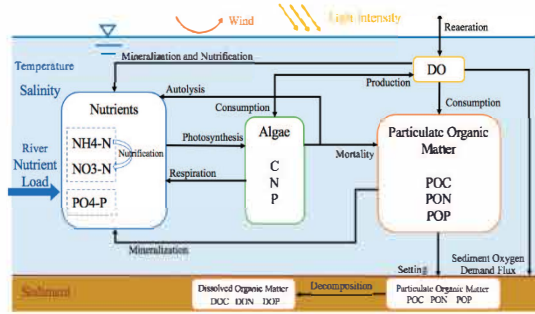


Fig. 2 Conceptual diagram of lower-trophic ecosystem model

Results

It can be observed that the influx of a large amount of freshwater may diminish the vertical mixing and lead to the salinity stratification (figure omitted). As shown in Fig. 3 and Fig. 4, it indicates that the duration of hypoxia at the bottom layer increased with the increase of the magnitude of floods. Particularly, the duration of hypoxia lasted for three weeks in 2018 (Fig. 3b). Furthermore, not only the magnitude of floods but the duration is also one of the inducements affecting the development of hypoxia.

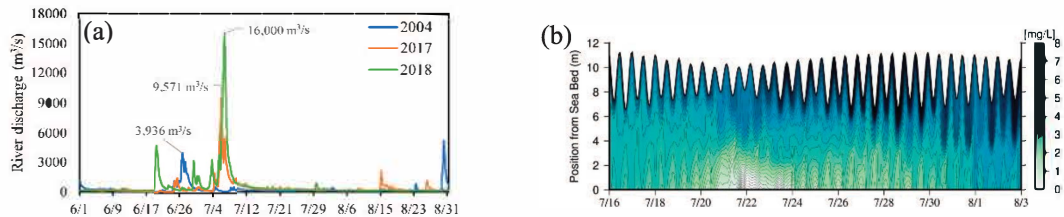


Fig. 3 (a) Total discharge of A-class rivers in 2004, 2017 and 2018, (b) isopleth of DO at Sta.B3 in 2018.

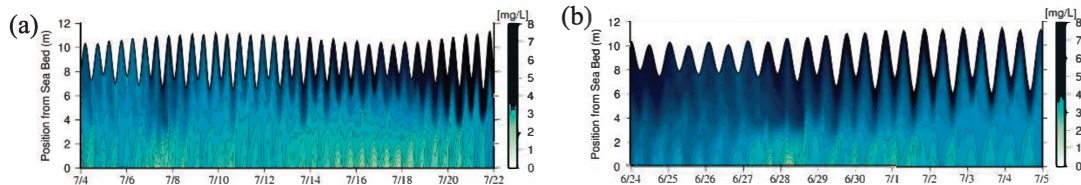


Fig. 4 (a) Isoleth of DO at Sta.B3 in 2017, (b) isopleth of DO at Sta.B3 in 2004.

Conclusions

It is clarified that changes in flood patterns affected the development of hypoxia in the Ariake Sea. Long duration and large-scale floods are easily to cause the salinity stratification and continuous hypoxia, which will have an adverse effect on the ecological system. In this way, we can clearly understand the impact of changes in flood patterns on the development of hypoxia and provide a basis for adaptation.

References

- IPCC (2014): Climate Change 2014 Synthesis Report
- Tadokoro, M., & Yano, S. (2019). Evaluation of effects of temperature and river discharge changes due to climate change on hypoxia in the Ariake Sea. *Journal of Japan Society of Civil Engineers, Ser. B2 (Coastal Engineering)*, 75(2), I_1231-I_1236.
- Tadokoro, M., Nakamura, Y., Qin, P. & Yano, S. (2018). Evaluation of effects of temperature change of air, river water, and sea water on development of stratification and anoxic water due to climate change in the Ariake Sea. *Journal of Japan Society of Civil Engineers, Ser. B2 (Coastal Engineering)*, 74(2), I_1147-I_1152.

Development of ecological model for dynamics of partial pressure of CO₂ in seawater considering the effects of stratification in the Yatsushiro Sea

Bing Xiong¹, Naoki Saito¹, Hiroto Komori¹, Shinichiro Yano^{1*}, Keisuke Nakayama²,
Katsuaki Komai³

¹Department of Civil Engineering, Kyushu University

²Department of Civil Engineering, Kobe University

³School of Earth, Energy and Environmental Engineering, Kitami Institute of Technology

* Corresponding: yano@civil.kyushu-u.ac.jp

Abstract

The partial pressure of carbon dioxide in seawater ($p\text{CO}_2$) fluctuates with the development of stratification, which makes it complicated to estimate the contribution of shallow coastal waters to the fixation of atmospheric carbon dioxide (C_{atm}). In this study, we conducted field measurements for $p\text{CO}_2$ dynamics under three different seawater mixing conditions in the Yatsushiro Sea, Japan. Base on the measurement results, we developed a three-dimensional ecological model that can simulate the $p\text{CO}_2$ dynamics affected by stratification. As a result, the $p\text{CO}_2$ dynamics strongly associated with stratification development were revealed from the field measurements. And the developed model shows good reproducibility of measurement results.

Keywords: blue carbon; $p\text{CO}_2$; 3D ecological model; Yatsushiro Sea; climate change

Introduction

Shallow coastal waters with vegetations such as seagrass, mangroves, salt marshes, have recently attracted extensive scientific attention, due to their high efficiency in the storage and sequestration of C_{atm} . And the carbon stored and sequestered by marine organisms is called “blue carbon” (Nellemann et al., 2009). However, due to the complexity of the tempo-spatial distribution of $p\text{CO}_2$ in the shallow coastal waters, it is difficult for us to accurately assess the amount of C_{atm} absorption of them. In addition, some studies reported that $p\text{CO}_2$ would probably fluctuate with the development of density stratification due to riverine freshwater effluents (Kone et al., 2009). But the effect of stratification on $p\text{CO}_2$ distribution in shallow coastal waters has been unclear due to the scarcely related researches.

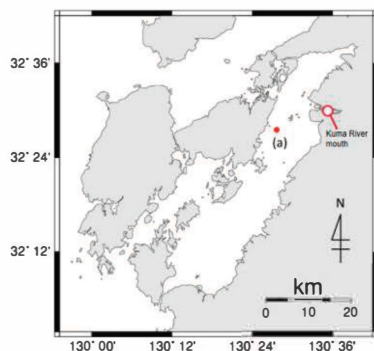


Fig. 1 Location of field measurement.

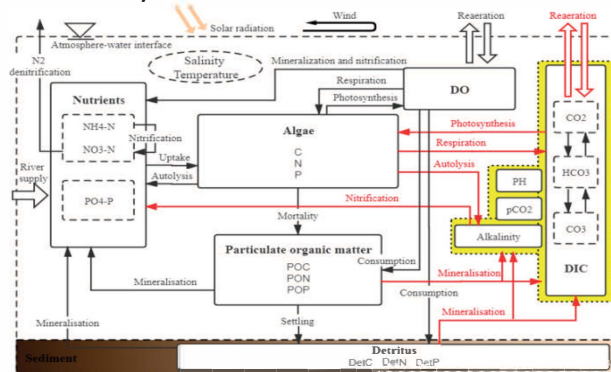


Fig. 2 Conceptual diagram of ecological model.

Methods

The field measurement point was set near the mouth of Kuma River in the northern Yatsushiro

Sea as shown in Fig. 1. Other details of the field measurements are omitted here.

The numerical model of pCO₂ dynamics was developed using the generalized coastal numerical model Delft3D. The model consists of a hydrodynamic model and a lower-trophic levels ecological model. The calculation of the ecological model was conducted by coupling the results of the hydrodynamic model. The main processes included in the ecological model are photosynthesis, respiration, and death of phytoplankton, sedimentation, and mineralization of organic matter, nitrification, and reaeration, etc., shown in Fig. 2.

Results

As shown in Fig. 3, as long as seawater under a strong density stratification condition, the pCO₂ in seawater also strongly stratified. Moreover, under the conditions of weak stratification and well-mixing, the vertical distributions of pCO₂ are also basically consistent with the distribution of sigma-t (σ_t), the figures are omitted here. And by comparing the measurement results and the simulation results, we find that this model shows good reproducibility to the measurement results, both in hydrodynamics and ecology. The results of statistical validation between the simulated and observed values are shown in Table 1.

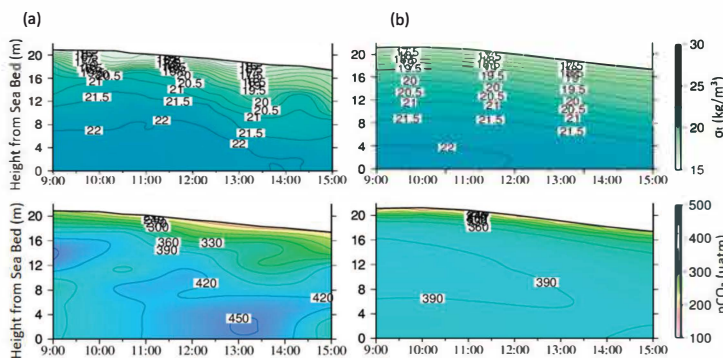


Fig.3 Field measurement results (a), and simulation results (b) of σ_t distribution (top) and pCO₂ distribution (bottom), during the strong stratification period (August 2, 2019).

Table 1. The statistical model validation.

	RMSE ^a	RMSPE ^b	NSE ^c	N ^d
Salinity	0.93	2.99%	0.68	423
Temperature	1.29	6.25%	0.91	423
σ_t	0.97	4.61%	0.79	423
DIC	33.89	1.90%	0.85	89
TA	41.14	2.02%	0.78	89
pCO ₂	40.73	14.48%	0.67	89

^a RMSE: root mean square error.

^b RMSPE: root mean squared percentage error.

^c NSE: Nash-Sutcliffe efficiency.

^d N: number of samples

Conclusions

As a result of this study, we found out from the field measurements that there is a strong association between the pCO₂ dynamics and stratification development in the Yatsushiro sea. And a lower-trophic levels ecological model that can basically reproduce the distribution of pCO₂ in the Yatsushiro sea has been developed, which supports us to further study the pCO₂ dynamic in shallow coastal waters.

Acknowledgement

This research was carried out by JSPS KAKENHI Grant-in-Aid for Scientific Research (B) (JP18H01545). Here, we express our gratitude.

References

- Nellemann, C., Corcoran, E., Duarte, C. M., Valdes, L., De Young, C., Fonseca, L., Grimsditch, G. (Eds) (2009): Blue carbon. A rapid response assessment., 80p, United Nations Environmental Programme, GRID-Arendal, Norway.
- Koné, Y. J. M., Abril, G., Kouadio, K. N., Delille, B., & Borges, A. V. (2009). Seasonal Variability of Carbon Dioxide in the Rivers and Lagoons of Ivory Coast (West Africa). *Estuaries and Coasts*, 32(2), 246–260.

Improvement of long term integration results of one-way nested regional ocean model by applying a new boundary small eddy additions technique

Van Sy Pham^{1*}, Jin Hwan Hwang²

¹Vietnam Institute of Meteorology, Hydrology and Climate change

²Department of Civil & Environmental Engineering, Seoul National University

* Corresponding: phamsytm@gmail.com

Keywords: small-scale generation; added small scales; ocean regional circulation model; Big-Brother Experiment; methodology; downscaling.

Abstract

In dynamical downscaling and nesting procedure using regional oceanographic models, generation of small-scale structure is really an important issue. In many previous studies, the good reproduction of small-scale features in one-way nested regional circulation model when driving by large-scale flows as well as information supplied from global-scale model output or observation at lateral boundaries and incorporates with local forcing have been shown. However, this research find that generation of small-scale motions are too weak even sustain the energy at larger scales. This leads to degradation of the nested regional ocean model's results. Besides, the research proposed an efficient technique, named "boundary small eddy additions" which helps improve the quality of results of the nested regional ocean models even though stimulating sources absent in the simulating domain. In this method, new adding artificial small-scales motions, that are generated from the information of large-scale, are added at the boundaries of nested model. This technique can significantly reproduce small scale features of the model and help to reduce the horizontal resolution jump different between driving data and nested model.

Transport of Microplastics Contained in the Wastewater Discharged from the King Sejong Station in the West-Antarctica

Bo-Kyung Kim¹ and Jin Hwan Hwang^{1*}

¹Department of Civil & Environmental Engineering, Seoul National University

*Corresponding: jinhwang@snu.ac.kr

Abstract

Microplastics found in the pristine Antarctic Ocean may have originated from wastewater discharged from the scientific research station residing in Antarctica. In this study, the numerical modeling is performed on the transport of microplastics found in the wastewater discharged from the King Sejong Station residing in Antarctica. The denser particles which have their falling velocity are accumulated near the release source, while the lighter particles which have no falling velocity are transported to the head of the cove. Also, the travel distances of PP and PET are increased by 1.8 and 1.3 times, respectively, due to the wave-induced force. We show that the wastewater discharged from the research stations in Antarctica can be a principal cause of microplastic contamination in the seawater around there.

Keywords: Microplastics; Waves; Wastewater; King Sejong Station; Antarctica

Introduction

Microplastics, which are less than 5 mm, become one of the major causes of marine environmental pollution. Recently, it has been found in the Antarctic Ocean, which is known as an unspoiled sea, so many studies have been conducted to understand the level of microplastics contamination in the Antarctic Ocean. Studies on the transport of microplastics originating from outside the Antarctic Ocean have been conducted through field surveys and numerical modeling. As investigated by Gröndahl et al. (2009), the effect of microplastics caused by human activities such as wastewater discharged from the scientific research station inside Antarctica is expected to be quite large, but research on this is insufficient.

Methods

This study reproduces the seawater flow around the King Sejong Station, located on the coast of Marian Cove, King George Island, West Antarctica, using a hydrodynamic model. In the flow model, Delft3D-FLOW, oceanographic variables such as tides, wind, and currents are set at the boundary as input data. The wave model, Delft3D-WAVE, is online-coupled with the flow model to consider the mass transport generated by waves. We then figure out the transport of microplastics contained in the wastewater discharged from the King Sejong Station. The two most common types of polymers found in the wastewater are simulated: Polypropylene (PE) and Polyethylene terephthalate (PET). Two methods are used to see the transport of fine particles in water: Eulerian (Kim et al., 2018) and Lagrangian method (Ku and Hwang, 2018). In this study, the Lagrangian Particle tracking method is used to determine the location and distance of the particles over time by calculating the advection, diffusion, and the falling velocity of particles as below.

$$\mathbf{X}(t + \Delta t) = \mathbf{X}(t) + \mathbf{U}(x, y, z, t)\Delta t + R\sqrt{2\mathbf{K}\Delta t} - \mathbf{w}_s(t)\Delta t$$

where \mathbf{X} is the particle location, \mathbf{U} is the Eulerian velocity field of flow, \mathbf{K} is the diffusion coefficient, and \mathbf{w}_s is the falling velocity of particle.

Results

The particle tracking results for each case indicate that PP with a density less than that of seawater is transported far from the particle release source and moves to the head of the cove, but PET with a density greater than that of seawater is relatively accumulated near the release source. When determining the location of the particle, the falling velocity of the particle is considered. In the case of PET, its falling velocity is faster than PP, so it sinks relatively quickly. It also shows that both particles are transported farther when the wave effect is considered than it is not. This is because the wave-induced force is added to the momentum equation in the hydrodynamic model as the wave model is combined. In order to quantitatively compare the transport of particles, the travel distance of the particles for 12 hours is averaged for each case. When the wave is applied, the travel distance of PP and PET increases by about 1.8 and 1.3 times, respectively, which means that PP, a light particle floating mainly around the surface layer, is more affected by waves. It seems to

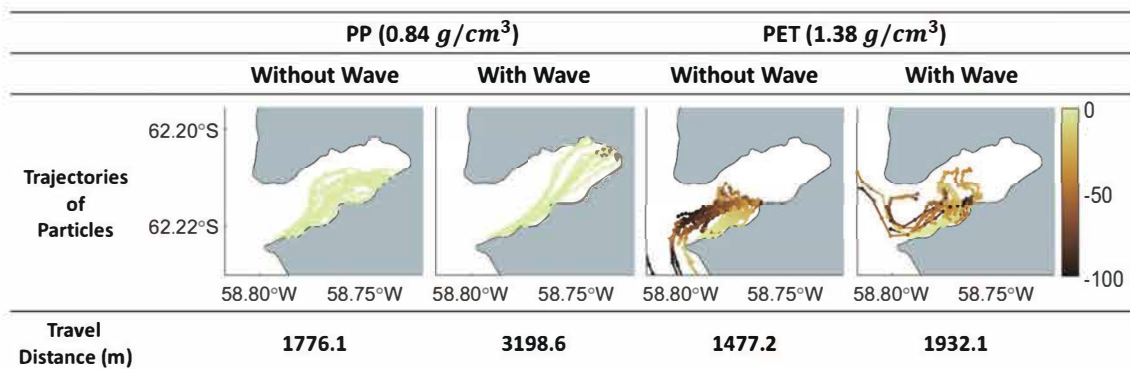


Fig. 1. Lagrangian particle tracking and travel distance of each microplastic according to the wave effect

Conclusions

This study indicates that the transport of microplastics depends on their characteristics. The denser particles tend to accumulate near the particle release location due to their falling velocity, while the lighter particles can be transported further along the surface layer, regardless their falling velocity. In addition, it is confirmed that the wave is the crucial factor in simulate the transport of microplastics. In particular, the lighter particles have a longer travel distance due to the influence of waves, and can be accumulated to the innermost part of Marian Cove. Therefore, it is concluded that the research station located on the coast of the cove can contribute to the accumulation of microplastics within the cove.

Acknowledgement

This research was supported by Korea Environment Industry & Technology Institute(KEITE) through “Chemical Accident Response R&D Program”, funded by Korea Ministry of Environment(MOE) (ARQ201901179003).

References

- Gröndahl, F., Sidenmark, J., & Thomsen¹, A. (2009). Survey of waste water disposal practices at Antarctic research stations. *Polar Research*, 28(2), 298-306.
- Kim, N. H., Pham, V. S., Hwang, J. H., Won, N. I., Ha, H. K., Im, J., & Kim, Y. (2018). Effects of seasonal variations on sediment-plume streaks from dredging operations. *Marine pollution bulletin*, 129(1), 26-34.
- Ku, H., & Hwang, J. H. (2018). The Lagrangian Coherent Structure and the sediment particle behavior in the lock exchange stratified flows. *Journal of Coastal Research*, (85), 976-980.

Assessing the interplay of Sea Level Rises and Mangrove Species Richness: A Meta-analysis Approach

Giuseppe Francesco Cesare Lama^{1*}

¹Department of Agricultural Sciences, University of Naples Federico II, Italy

* Corresponding: giuseppefrancescocesare.lama@unina.it

Keywords: Mangrove plants; Sea Level Rise; Meta-analysis; Environment.

Abstract

The objective of this study is the analysis of the interplay between the species richness of Mangroves and peculiar traits of coastal ecosystems. The main focus was the analysis of sea level rises by means of a proper meta-analysis approach. It was possible observing that the species richness was also related in different ways to other components of coastal and marine ecosystems in general, as salinity among others. The analysis was carried out with the support of dedicated open-source tools and platforms Geographic Information Systems (GIS) aiming at retrieving the most suitable and complete database for research purposes. The preliminary results of this work embody a database to be employed in other researches on different species and ecosystems.

UAV-Based Remote Sensing for Coastal Environment

Hieu Trung Kieu¹, Cuc Duong^{1,2}, Hui Ying Pak^{1,2}, Dawn Pang¹, and Adrian Wing-Keung Law^{1,3*}

¹ Environmental Process Modelling Centre, Nanyang Environment and Water Research Institute, Nanyang Technological University, 50 Nanyang Avenue, Singapore 639798, Singapore

² Interdisciplinary Graduate School, Nanyang Technological University, 50 Nanyang Avenue, Singapore 639798, Singapore

³ School of Civil and Environmental Engineering, Nanyang Technological University, 50 Nanyang Avenue, Singapore 639798, Singapore

*Corresponding: cwklaw@ntu.edu.sg

Keywords: UAV; remote sensing; coastal monitoring; hyperspectral imaging

Abstract

Remote sensing based on a small and portable hyperspectral camera mounted onto an Unmanned Aerial Vehicle (UAV) is becoming increasingly popular for observations, surveys and compliance inspections. The approach is cost-effective and widely practicable in field applications, especially for monitoring in areas which are difficult to access. In particular, the approach carries several advantages over traditional satellite-based imaging, including high spatial resolution, minimal atmospheric interference, and flexible monitoring. At the same time, the deployment remains challenging particularly for industrial applications, as various issues need to be addressed to ensure operating safety and achieve high-quality data collection, including regulations, technical parameters, and environmental conditions.

In this study, we perform UAV-based hyperspectral and multispectral imaging of high level of turbidity in the coastal water of Singapore during land reclamation exercises. The objective is to monitor the movement of the sediment plumes and to assess the maximum sediment concentrations. The study shall be ongoing for the next two years. For the planning of the flight exercise, both the operator permits (i.e. pilot licenses) and activity permits (i.e. permission to fly) are required by the team members for authorization. The industrial UAVs carrying hyperspectral and multispectral cameras are automated to operate from the shoreline to the survey field for data acquisition, and then return to the launching location upon completion. The hyperspectral camera is capable of collecting images with a total of 61 spectral bands while the multispectral camera has 10 bands, both covering the VIS and NIR spectrum. During the survey flight, the coordinates of the UAV and the solar intensity variation are recorded for later georeferencing and field calibration. In-situ water sampling is conducted simultaneously at different locations of the survey area to measure the total suspended solids (TSS) concentration. The field measurement data is further enriched via an autonomous turbidity sensor. Both the UAV flight and the field sampling are performed until normal safety guidelines as well as additional requirements stipulated for the COVID situation. The entire data set, comprising the hyperspectral images, multispectral images, and field measurements, are then fed to a Convolutional Neural Network (CNN) to train a deep learning model to predict TSS concentration and generate turbidity contour maps of the survey area. Preliminary results will be presented in the conference to share our experience of the hyperspectral imaging exercise and the challenges in deploying for measurements in coastal environment.

Acknowledgment: This work was supported by the Singapore Maritime Institute through Grant Number SMI-2020-MA-02.

**The 9th International
Symposium on
Environmental Hydraulics**

E3 Session

Estuary [E3-W3]



2-D Numerical Modelling of Meandering Estuaries

S. Haddout^(a), K.L. Priya^(b), Joan Cecilia C. Casila^(c), and A.M. Hogueane^(d)

^(a)Department of Physics, Faculty of Science, Ibn Tofail University, B.P. 133 Kenitra, Morocco.

^(b)Department of Civil Engineering, TKM College of Engineering, Kollam 691005, India.

^(c)Land and Water Resources Division, IAE, CEAT, University of the Philippines Los Baños, College, Laguna
4031, Philippine.

^(d)Centre for Marine Research and Technology, Eduardo Mondlane University, PO Box 128, Quelimane,
Mozambique.

Corresponding Author email: soufian.haddout@gmail.com

Keywords: Sebou River (Morocco); meander; 2-D numerical analysis; Erosion.

Abstract

Meandering estuaries require some level of hydrodynamic and morphologic analysis. The details of the hydraulic and morphologic features through meander evolution in estuary can be simulated through a numerical model. A CCHE2D (iRIC) model (i.e., Center for Computational Hydro-science and Engineering, two-dimensional model) was adopted to investigate the hydraulic and morphologic changes through meander's evolution. A meandering Sebou estuary in Morocco was studied and considered for morphological modeling by 2-D numerical analysis. The Sebou estuary is an area with high agricultural potential, and is becoming one of the most important industrial zones in Morocco, and contains many meandering channels. The K- ϵ turbulent model and secondary current were considered for modeling complex flow pattern. The model takes into account both high and low tide conditions with different simulation scenarios under different river discharges. From the results, it was found that velocity is higher in the deeper part of the estuary, especially in the middle estuary section. Also, most of time, flow is sub-critical along the estuary. This study is significant for monitoring siltation process to keep the estuary navigable.

References

- Xiao, Y., G. Zhou, and F. S. Yang. "2D numerical modelling of meandering channel formation." *Journal of Earth System Science* 125.2 (2016): 251-267. <https://doi.org/10.1007/s12040-016-0662-5>.
- Haddout, S., Igouzal, M., & Maslouhi, A. (2016). Analytical and numerical study of the salinity intrusion in the Sebou river estuary (Morocco)—effect of the “Super Blood Moon”(total lunar eclipse) of 2015. *Hydrology and Earth System Sciences*, 20(9), 3923. <https://doi.org/10.5194/hess-20-3923-2016>, 2016.

Study on the relationship of salinity front characteristics and runoff in the North Branch of the Yangtze River Estuary

Cuiping Kuang¹, Kuo Chen¹, Yunlong Wu^{1*}, Jie Wang¹

¹ College of Civil Engineering, Tongji University, Shanghai, China.

*Corresponding: mrwdd@tongji.edu.cn

Abstract

In the salinity front zone where the salinity gradient reaches the maximum, the mass transport and circulation structure are different. In this study, the responses of the horizontal salinity front in the North Branch (NB) of the Yangtze River Estuary (YRE) to the runoff are studied by a 2D numerical model established on MIKE21. The results show that: (1) there is an obvious double front phenomenon in the NB, which are located in the upstream and downstream respectively. (2) With the increase of runoff, two salinity fronts move toward the open sea, the intensity of the first front decreases, while the intensity of the second front increases first and then decreases. (3) The relationships of the intensity and position of the salinity front with the runoff are quadratic and linear respectively, however, the quadratic term coefficients of the first and second front are positive and negative respectively.

Keywords: Salinity front; the Yangtze River Estuary; North Branch; Runoff; Numerical model.

Introduction

Due to the complexity and variability of the river regime in the YRE, the mechanism of river-sea interaction has been a research hotspot in recent years. As an important physical phenomenon of the YRE, the salinity front has a significant influence on the tidal current, material migration and deposition process. The position of the front is usually determined by the maximum salinity gradient (Mao et al., 1963). The density difference near the salinity front forms a barrier effect, which affects the mass transport and exchange. The observations show that the migration of the underwater delta is consistent with the variations of the salinity front in the YRE, which indicates that the salinity front has a certain influence on the sediment transport and the underwater delta evolution. (Mao et al., 1963). The observations show that the spatial distribution of higher chlorophyll-a concentration corresponds well with the distribution of the salinity front. At present, the relevant studies have revealed the basic variation characteristics of the salinity front in the YRE (Wu et al., 2014), however the study on mechanism of the salinity front to the runoff are still insufficient. This study mainly focuses on the responses of the salinity front of the NB to the runoff.

Methods and Model setup

The maximum horizontal salinity gradient (H_{sg}) is taken as the criterion to define salinity front, which is calculated by $H_{sg} = \Delta \bar{s} / \Delta x$, where $\Delta \bar{s}$ is the variation of vertical-averaged salinity in the distance Δx . We select a representative longitudinal profile to analyze the variation of H_{sg} , this profile is located along the talweg in the NB, which is shown in Fig. 1. The open sea boundary of the numerical model is set as M₂ tide, the discharge boundary is set to eight different runoffs in the range of 10000~80000 m³/s with an interval of 10000 m³/s. The other parameters are shown in Table 1.

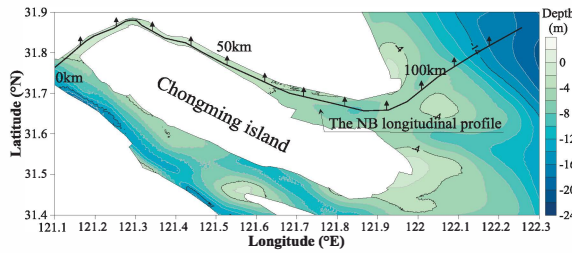


Fig. 1. The topography and the selected longitudinal profile in the NB

Table 1. Model parameters.

Parameter	Value
Manning number ($m^{1/3}/s$)	60-98
CFL number	0.8
h_{dry} (m)	0.005
h_{flood} (m)	0.05
h_{wet} (m)	0.1
Time step (s)	0.01-30

Results

As shown in Fig. 2, the salinity front of the NB presents a double-front pattern. With the increase of runoff, the salinity front moves toward the open sea, the intensity of the first front decreases, while the intensity of the second front increases first and then decreases. Fig. 3 shows the relationship between the salinity front eigenvalues (position and intensity) and runoff. It can be found that R^2 is above 0.85, indicating that there is a functional relationship between the salinity front eigenvalues and runoff. i.e., The relationships of the intensity and position of the salinity front with the runoff are quadratic and linear respectively, however, the quadratic term coefficients of the first and second front are positive and negative respectively.

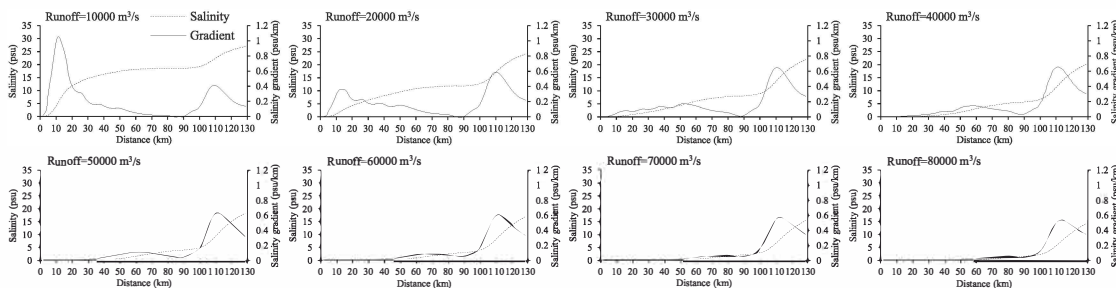


Fig. 2. The response characteristics of salinity and salinity gradient to runoff in the NB.

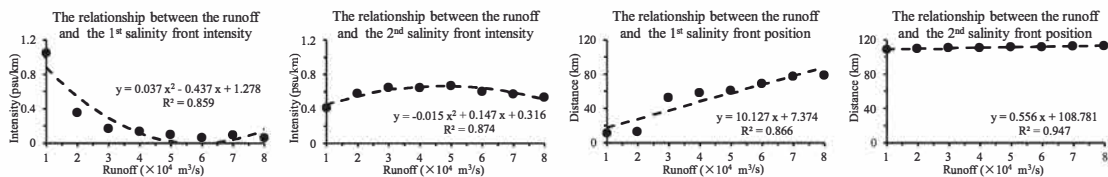


Fig. 3. The functional relationship between salinity frontal eigenvalue and runoff in the NB.

Conclusions

There is an obvious double-front phenomenon in the NB of the YRE, and with the increase of runoff, the main salinity front (the front intensity is the largest) moves and merges from the first front to the second front. The relationships of the intensity and position of the salinity front with the runoff are quadratic and linear respectively, however, the quadratic term coefficients of the first and second front are positive and negative respectively.

References

- Wu, H., Shen, J., Zhou, J. R., Zhang, J., & Li, L. (2014). Characteristics of the Changjiang plume and its extension along the Jiangsu Coast. *Continental Shelf Research*, 2014, 76(2):108-123.
- Mao, H. L., Kan, T. C., & Lan, S. F. (1963). A preliminary study of the Yangtze diluted water and its mixing processes. *Oceanologia et Limnologia Sinica*, (03), 3-26.

Seasonal variation of sediment transport - a case study of Hyeongsan River Estuary, South Korea

Dong Hyeon Kim¹ and Jin Hwan Hwang^{1*}

¹Department of Civil & Environmental Engineering, Seoul National University

*Corresponding: jinhwang@snu.ac.kr

Abstract

A 3d hydrodynamic model and sediment transport model was set up for the Hyeongsan River Estuary located in Yeongil Bay, South Korea. The hydrodynamic model was coupled with the wave model to consider wind and wave effects for sediment transport in the estuary. The coupled model was verified using the in-situ observation and the observation station data in the study area, which has very complex hydrodynamic and transport processes, and it was applied to investigate the seasonal patterns of sediment transport. In addition, the particle tracking method was employed to evaluate the distribution and possible accumulation of particles by seasonal variation in the estuary. According to the upstream river discharge, sediment transport occurred during the flood season and was mainly deposited at the confluence region with the small stream and near the groins in the right bank of the river mouth. Besides, the topography changed upstream from the confluence and near the river mouth in the flood season.

Keywords: Sediment transport; Estuary; Hydrodynamic model; In-situ observation

Introduction

Investigating the physical and transport processes in the river estuaries is essential for managing the estuary (Kim and Hwang, 2020). However, the physical processes, such as the hydrodynamic, transport, and mixing processes, are great complex in the estuary. In order to understand these physical characteristics, numerous numerical models were developed for decades. The Hyeongsan river estuary located in Yeongil Bay, South Korea, has complex physical processes. In particular, the study for sediment transport processes is crucially important due to the potential risk of transport for particles with absorbed heavy metal discharged from the industrial complex. Sediment transport in the river estuary depends not only on upstream discharge and topography of the river but also propagation of tide and wave from the ocean, the mixture of fresh water and saline water, and wind-driven flow. In this study, the hydrodynamic model coupled with wave model, Delft3D-Flow and SWAN (Simulating Waves Nearshore) respectively was used to consider the physical characteristics of the river estuary.

Methods

In order to simulate the flow motion in the river estuary, Delft3D-Flow, which solves continuity, three-dimensional hydrostatic shallow water equation, and the $k-\epsilon$ turbulence model via a finite-difference method, was used. The model domain is shown in Fig. 1. It covers not only downstream of the Heongsan river but also the Yeongil Bay.

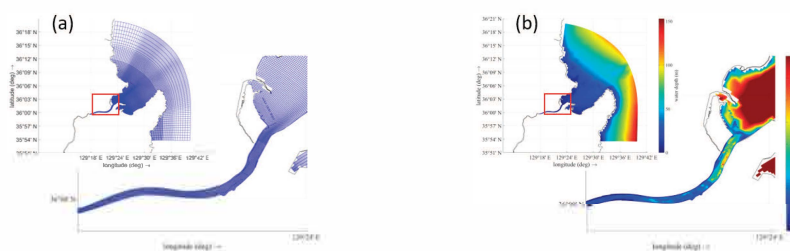


Fig. 1. Curvilinear grids for the model domain (a) and its bathymetry (b)

In addition, the open boundary conditions of the models were composed using the GCMs (Global Circulation Models) results which are HYCOM (Hybrid Coordinate Ocean Model), WW3 (Wave Watch 3), CFSv2 (Climate Forecasting System version 2), and the gauging station data. The field campaign was performed to verify the coupled model. The surface ocean current in Yeongil Bay was estimated by tracking the GPS surface drift, and the spatial distribution of physical variables such as velocity, water temperature, and salinity is obtained using moving-vessel measurements (Rennie et al., 2010). Mainly, water temperature, salinity, and density were measured using YODA Profiler (Yoing Ocean Data Acquisition Profiler, JFE-Advantech) to obtain high spatial resolution data (Kim et al., 2018)

Results

The sediment transport simulation results show that bedload was transported upstream of the confluence and near the river mouth (Fig 2(a)). A relatively small amount of bedload was transported downstream of the confluence because the flow velocity above the river bed was slow by deeper water depth and groins. As shown in Fig. 2(b), the morphological change occurred prominently upstream of the confluence and sill of the river mouth.

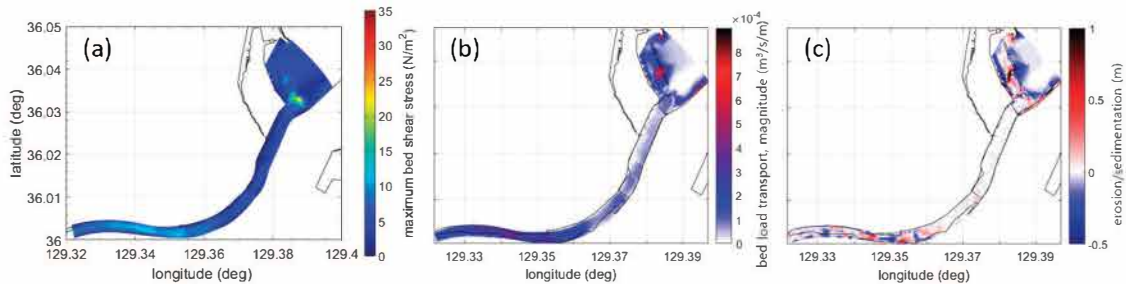


Fig. 2. (a) bed shear stress, (b) bedload transport, and (c) morphological change in flood season (2019.09.23)

Conclusions

This study shows that the sediment transport in the river estuary occurred dominantly in the river discharged. The Hyeongsan River has a significant difference in discharge during flood and drought seasons. Besides, the tidal amplitude is small as around 0.15 m. Therefore, bedload was rarely transported except for flood season and the downstream of the confluence by the groins.

Acknowledgement

This research was a part of the project titled “Improvements of ocean prediction accuracy using numerical modeling and artificial intelligence technology” funded by the Ministry of Ocean and Fisheries, Korea.

References

- Kim, N. H., & Hwang, J. H. (2020). Optimal Design of Water Quality Monitoring Networks in Semi-Enclosed Estuaries. *Sensors*, 20(5), 1498.
- Kim, N. H., Hwang, J. H., & Dong Hyeon, K. (2018). Evaluation of Mixing and Stratification in an Estuary of Korea. *Journal of Coastal Research*, (85), 96-100.
- Rennie, C. D., & Church, M. (2010). Mapping spatial distributions and uncertainty of water and sediment flux in a large gravel bed river reach using an acoustic Doppler current profiler. *Journal of Geophysical Research: Earth Surface*, 115(F3).

An Experimental Study on the Effects of Physical Factors in Transport of Microplastics in Coastal Area

Dongwook Hwang¹, and Yong Sung Park^{1,2*}

¹Department of Civil & Environmental Engineering, Seoul National University
Integrated Research Institute of Construction and Environment, Seoul National University

*Corresponding: dryspark@snu.ac.kr

Abstract

We investigate transport of microplastics in coastal area. In recent years, the microplastics have been found so considerably from the equatorial seas to the polar ocean that much concern has been raised about the pollution. However, there is a lack of the research on the microplastics in coastal area considering some physical factors. The present research focuses on factors affecting the transport of the microplastics in coastal sediment. A set of the experiments are conducted with an oscillating water tunnel with a detachable sediment basin that generates sufficiently large Reynolds numbers flow. By reproducing near-bed hydrodynamics and sediment transport with plastic particles, we are intended to observe the correlation with each factor such as the wave-forcing, properties of sediment and plastics, and to yield an analytical expression for the transport rate of the microplastics.

Keywords: Hydrodynamics; Microplastics; Oscillating water tunnel; Coastal sediment; Boundary layer

Introduction

Recently, concerns have been rising over pollution of the coastal and marine environments for microplastics. It entered the ocean experiences physical changes in coastal; such as arrival, departure, deposition and fragmentation of particles (Brennan et al., 2018). So, as they need to interact with the dynamics of coastline, this research focuses on transport of them in near-bed and coastal sediment. To study that in lab-scale experiment, it uses an oscillating water tunnel (OWT, or U-tube) that makes it possible to consider in larger Reynolds number flow than two-dimensional wave basin. The Reynolds number based on the maximum free-stream velocity and the maximum displacement of water particles is on the order of $O(10^5)$. Moreover, it can make to consider the horizontal velocity only, in order to investigate intensively the movement of the particles on the near-bed. Using the equipment, therefore, the main goal of this experimental study is to figure out the effects of physical factors, that is for the effects of boundary layer to the transport of the microplastics, and for interactions between the wave forcing and that.

Methods

In this study, we built an oscillating water tunnel that has square-shape with water depth of 0.30 m and equipped a sediment basin, and spherical particles having the sizes of 3 mm and 6 mm are used as the microplastics. A set of the experiment are conducted according to the experiment cases as indicated in Table 1. Changing the input velocity for the actuator, the particle size and the status of the sediment basin are intended to observe how their properties affects to the plastics. So, we first estimate the maximum free-stream velocity and the thickness of the boundary layer by utilizing a particle image velocimetry (PIV) system to get the precise information for the generated flow and to explore the relation between the wave and the seabed. To compare the results, the system is conducted on the bed without the sediment basin first. In addition, the PIV particles are used with the mixture of two different sizes of $\phi 10$

μm and $\phi 20 \mu\text{m}$, their specific gravities of 1.03 and 1.4, respectively.

Table 1. Input parameter for the experimental study cases.

Input Velocity (mm/s)	Particle size (mm)	Depth of Sediment Basin (mm)	Input Velocity (mm/s)	Particle size (mm)	Depth of Sediment Basin (mm)
200	No Particles	No Sediment 0.15	500	No Particles	No Sediment 0.15
	3	No Sediment 0.15		3	No Sediment 0.15
	6	No Sediment 0.15		6	No Sediment 0.15

We then compare flow velocity field and the properties obtained from the PIV system in each case, and compute the bed shear stress, τ_b as function of inviscid free-stream velocity, U with neglecting viscous effect outside the boundary layer, described as:

$$U = U_0 \operatorname{sech}^2 \left[\sqrt{\frac{3H}{4h^3}} (x - Ct) \right] \quad (1)$$

$$\tau_b = \frac{1}{2} C_f \rho_w |U|U \quad (2)$$

where C is phase velocity, C_f is friction coefficient and ρ_w is water density.

Results

As a results of the first experiment case, the horizontal velocity field is obtained as shown in Fig. 1. The thickness of boundary layer and the maximum free-stream velocity are computed at about 2.758 mm and 0.028 m/s, respectively.

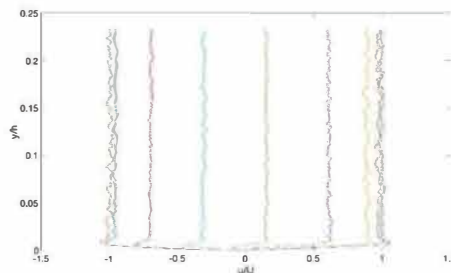


Fig. 1. Estimated horizontal velocity field

Conclusions

The results of this study show that the friction in the boundary layer has an effect on the transport of the microplastics, as the boundary layer shows plainly. Also, it indicates that there seems to be changes in the flow according to the wave velocity and the size of the plastic particles. The comparison result will be presented on our meeting.

Acknowledgement (If necessary)

This work was supported by the National Research Foundation of Korea(NRF) grant funded by the Korea government(MSIT) (No. NRF-2020R1F1A1070390).

※ MSIT: Ministry of Science and ICT

References

Brennan, E., Wilcox, C., & Hardesty, B. D. (2018). Connecting flux, deposition and resuspension in coastal debris surveys. *Science of the Total environment*, 644, 1019-1026.

Investigation of bathymetry data and groin structures effect on the numerical results of the flow and salinity intrusion in the estuarine part of Yoshii river reach, Japan

Mohammed Al-Baghdadi^{1*}, Ryosuke Akoh¹, Takahiro Hiratsuka¹, and Shiro Maeno¹

¹ Graduate School of Environmental and Life Science, Okayama University, Japan

*Corresponding: al-baghdadi@s.okayama-u.ac.jp

Abstract

The estuarine part of Yoshii river (Okayama prefecture, Japan) embraces an important ecosystem with different animal and plant lifeforms. Conservation plans have paid particular attention to a tidal flat 2.6 km away from river mouth. Correct assessment of salinity intrusion effect on this tidal flat is the aim of our research. In this article, we use a quasi-3D numerical model to simulate flow and salinity intrusion into the river. Systematic field observations of salinity have been performed at upstream and downstream sections to verify model performance. Bathymetry data from different sources, along with field surveying data at some points, were examined to decide the correct representation of riverbed elevation. Groin structures effect was also considered with respect to the already constructed groins or the suggested ones. We concluded with some recommendations on the improvement of flow conditions in the target area.

Keywords: Tidal river; Bathymetry; Groin; Field observation; Shallow-water equations

Introduction

The estuarine part of Yoshii river starts from the river mouth up to 7.37 km upstream where “Kamogoshi” weir structure is constructed. Our focus area is a tidal mudflat, so called “Otogo area”, located at about 2 to 2.6 km from river mouth where salinity intrusion is affecting the natural habitat of reed fields and crabs. This location has suffered from previous improvement works in Yoshii river where the channel was straightened leading to reduction in the mudflat area. In recent years, some groin structures have been constructed as protection measure, but more effort is necessary to ensure the endurance of the ecosystem in this area. Therefore, the Japanese River Bureau is considering more comprehensive plan of maintenance and conservation in this area, and possibly, of replicating this environment in another section of Yoshii river.

Methods

Field observations included setting measurement points upstream and downstream of the river reach from Sep. 2020 to Feb. 2021. Each point consisted of a vertical configuration of (5 or 6) electrical conductivity loggers attached to a rope and spaced at 1 m interval.

A quasi-3D shallow-water numerical model discretized by finite volume method on an unstructured triangular mesh written by (Akoh and Ishikawa, 2011) has been implemented in this study. The model assumes linear vertical distribution of salinity as shown in Fig. 1(a) in which σ is the relative salinity ($\sigma = S/S_0$ where S is the salinity at any depth, and S_0 is maximum salinity in the river). On the other hand, the salinity deviation $\Delta\sigma$ is approximated by a parabola depending on the average relative salinity $\bar{\sigma}$ and an experimentally determined constant α_0 which we call the deviation coefficient as described in Fig 1(b) and Eq. 1.

$$\Delta\sigma = 4\alpha_0\bar{\sigma}(1-\bar{\sigma}) \quad (1)$$

Different bathymetry data sources, namely: cross-sectional, Geospatial Information authority

(GSI) and Airborne Lidar Bathymetry (ALB) were considered. Furthermore, in situ survey for the elevation of certain points and groin structures in the study area has been conducted.

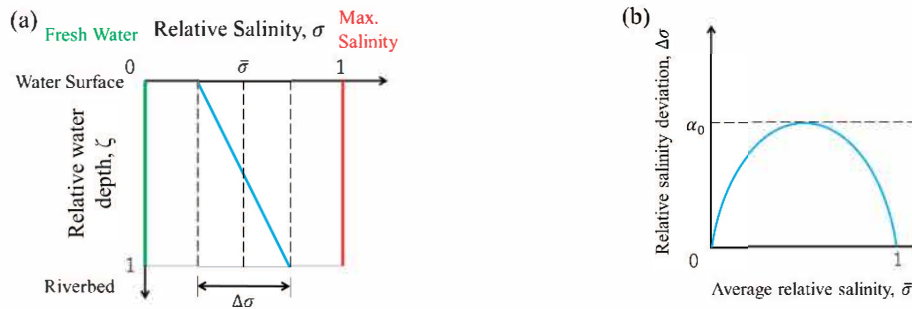


Fig. 1. Sketch of vertical salinity distribution: (a) Vertical distribution of relative salinity and (b) Approximation curve of relation between relative salinity deviation and average relative salinity (Akoh et al., 2014)

Results and conclusion

Field observation salinity data were taken at different depths while the model solves for a depth-averaged behavior. For example, Fig. 2 shows salinity at river downstream during a period when high discharge event has occurred and flushed out the salinity. Model behavior reflects the flushing and the recovery effect as well as the tidal variations. The observations loggers on the other hand has suffered from the growth of barnacles except loggers 5 and 6 near the bottom, so it can be realized that no flushing has occurred at the river mouth lower layer but some effect has happened at the upper layer.

Effect of corrected riverbed elevation data and suggested cases of groin structures were studied. This study concluded with recommendations to improve the flow and salinity behavior in Yoshii river with focus on the tidal flat "Otogo area".

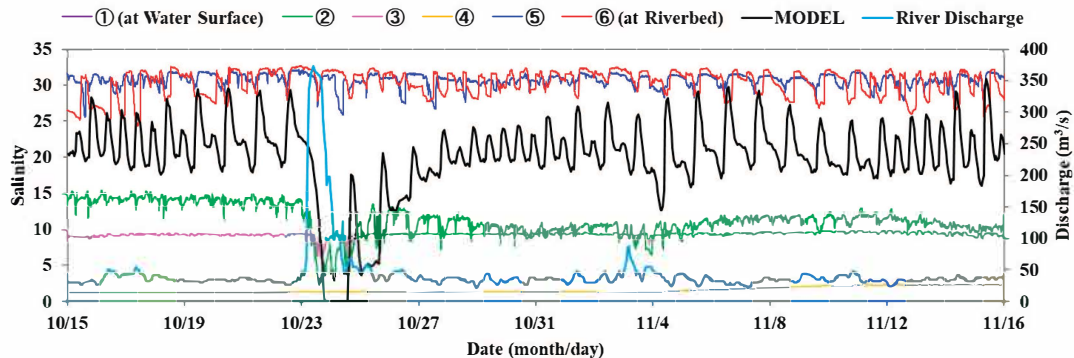


Fig. 2. Salinity at the downstream observation point (1.1 km from river mouth): Lines from 1 to 6 are the vertically placed loggers, while the black line is the depth-averaged model result. Note: Loggers 1 to 4 are neglected due to growth of barnacles.

References

- Akoh, R., Ishikawa, T., (2011). DEVELOPMENT OF NUMERICAL FORMULATION FOR QUASI-3D FLOW MODEL BY USING CIP-FVM ON TRIANGULAR MESH (in Japanese). Journal of Japan Society of Civil Engineers, Ser. B1 (Hydraulic Engineering) 67, I_1207-I_1212.
- Akoh, R., Ishikawa, T., Yasukouchi, M., Tsuruta, Y., (2014). DEVELOPMENT OF A TWO-DIMENSIONAL DISPERSION MODEL FOR THE SEAWATER INTRUSION IN TAKASE RIVER (in Japanese). Journal of Japan Society of Civil Engineers, Ser. B1 (Hydraulic Engineering) 70, I_877-I_882.

HYDRODYNAMIC VELOCITIES AND FORCES BENEATH A TIDAL BUBBLE BORE

MUHAMMAD ZAIN BIN RIAZ⁽¹⁾, SHU-QING YANG⁽²⁾ & MUTTUCUMARU SIVAKUMAR⁽³⁾

^(1,2,3) School of Civil, Mining and Environmental Engineering, University of Wollongong, Wollongong, Australia
mzbr518@uowmail.edu.au, shuqing@uow.edu.au, siva@uow.edu.au

ABSTRACT

The development of a bore in an open channel is a sudden change in water surface elevation propagating upstream. In terms of depth and velocity, a sharp discontinuity occurs and this leads to hydrodynamic shock at the bore front. The impact of different types of forces under bores on sediment transport is not clear, hence specially designed experiments were conducted to clarify the mechanism of sediment initiation, although some physical experiments were performed during last two decades. In this study, a laser Doppler anemometer, a highly sensitive force transducer and ultrasonic displacement meters accompanied by video recordings were used to investigate simultaneously the incipient motion of sediment under tidal bubbles bores. No sediment motion was observed during the initial steady flow, but sliding, rolling and short hops were observed during the breaking bore. The initiation of sediment motion was closely related to the passage of the breaking roller. According to the experimental results, upward vertical force due to swelling in free water surface before the roller toe was the main force in destabilizing the particles. Later, a large upstream longitudinal force was found to be the dominant cause promoting upstream particle motion during the breaking roller passage.

Keywords: Incipient motion, Physical modelling, Force transducer, Tidal bore

**The 9th International
Symposium on
Environmental Hydraulics**

F1 Session

Experiment-1 [F1-W1]



Interfacial compound section transverse flow variation in symmetric and asymmetric compound open channel flow

P. Singh^[1], X. Tang^{[1]*}

¹Department of Civil Engineering, Xi'an Jiaotong-Liverpool University (XJTLU)

*Corresponding: Xiao.Tang@xjtlu.edu.cn

Abstract

An experimental analysis of symmetrical and asymmetrical channels is considered over three depth ratios varying from small to large. In this study, shear stress contributes to Reynolds stress and spanwise advection due to transverse current are experimentally explored.

Keywords: Reynold shear stress; secondary currents, compound open channels

Introduction

Apparent shear is a measure of the net effect of viscous shear, turbulence together with the action of vortices induced between main-channel and floodplain(s) (Singh and Tang, 2020a, b). Two components of large-scale motions, namely advective dispersion ($\rho(\overline{u_x u_y})$) and the transverse current ($\overline{\tau_{yx}}$), where ρ is the density of fluid and $\overline{u_x u_y}$ is the time-averaged product of streamwise and lateral velocities, are key characteristics to measure momentum exchange in any compound channel (Proust and Nikora, 2020). This paper presents a study of uniform flow, which is explored experimentally over two sets of compound channels.

Methods

Six test runs were undertaken (see Table 1), and three-dimensional velocities were measured using side and down-looking Acoustic Doppler velocimeter (ADV). Figure 1 shows the normalized depth-averaged velocity distribution for two cases with an accuracy of ± 1 to 3% of the measured mean velocities

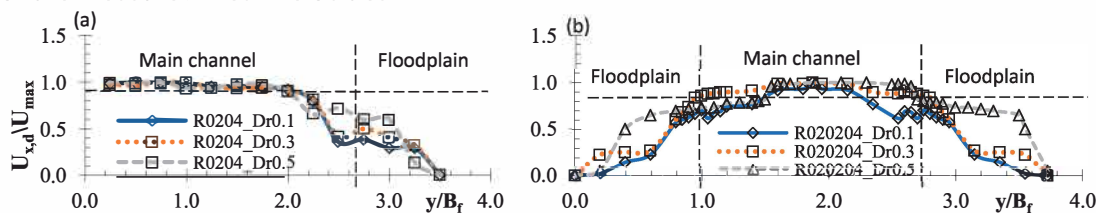


Figure 1. Distribution of normalized depth average velocity using maximum velocity over the cross-section for configurations (a) R0204; (b) R020204.

Table 1. Summary of the flow conditions, where R denotes rectangular, the next numeral signifies floodplain width (20cm), and the last numeral is bankfull height (4cm).

	Case	D_r (H-h/H)	Aspect ratio	Width ratio	Q_t (l/s)	U_{mc} (m/s)	U_{fp} (m/s)	λ
Asymmetric	R204	0.1			16.83	0.4146	0.0978	0.6183
	R204	0.3	13.625	1.4	21.14	0.4564	0.1390	0.5331
	R204	0.5			35.23	0.5208	0.2509	0.3497
Symmetric	R20204	0.1			5.03	0.2846	0.1133	0.4307
	R20204	0.3	8.625	2.2	10.16	0.4449	0.1779	0.4288
	R20204	0.5			20.42	0.5945	0.3046	0.3223

Each point measurement in the cross-sections was taken at an interval of 2.5-5 mm in the vertical direction and an interval of 10 to 50 mm in the lateral direction.

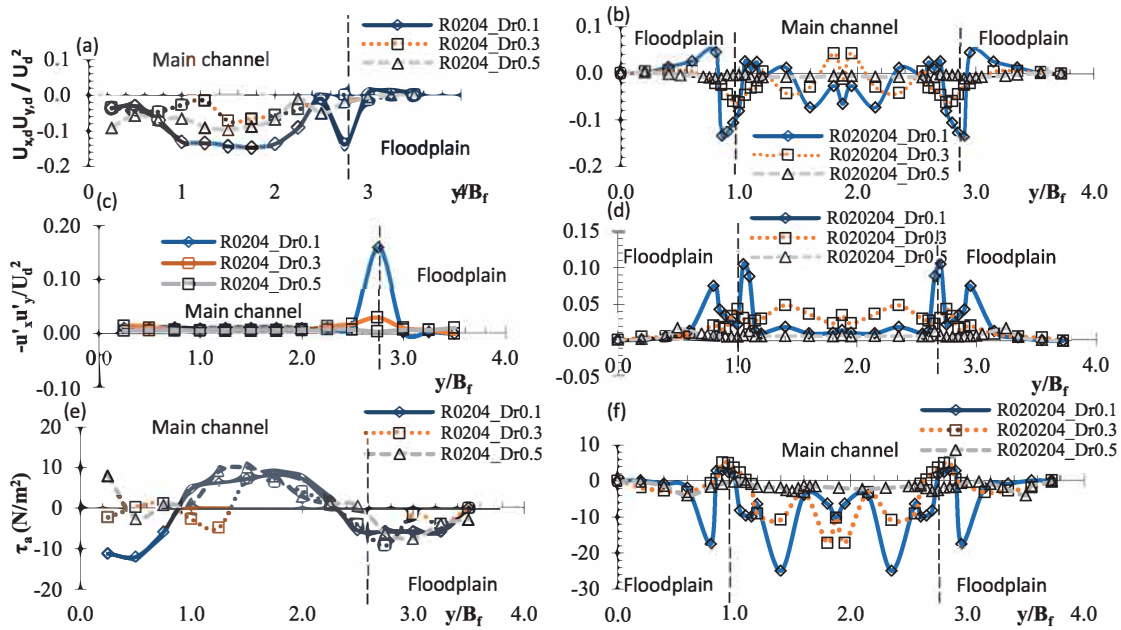


Figure 2. Cross sectional distribution of (a-b) transverse currents (c-d) Reynolds stress ($-u'_x u'_y$) & (e-f) apparent shear stress (τ_a).

Results

The strong anisotropy of the turbulence near the junction is commonly noticed. However, the effect of Reynold shear stress (Fig. 2 a-b) and transverse current (Fig. 2 c-d) in the asymmetric channel with the same floodplain width is higher than that in symmetric channels (see Fig. 2). The apparent shear effect (Fig. 2 e-f) thus catapults in the asymmetric channels with maximum advect momentum transfer near the interface. In addition, dimensionless shear $\lambda = (u_{mc} - u_{fp}) / (u_{mc} + u_{fp})$ is higher in the asymmetric channel (R204) than the symmetric channel (R20204) (Table 1). This increase in λ is due to an increase in maximum velocity in the main channel of asymmetric channels where geometric difference and proximity of wall resistance exist, which is higher in symmetric channels.

Conclusions

The study of turbulence statistics and normalized mean flow velocity difference shows that the channels having the same floodplain width and bankfull height (h) but having different main channel width (b), behaves differently on Reynold shear stress and transverse current near the interface. The effect of these parameters increases for asymmetric channels than symmetric channels.

Acknowledgement (If necessary)

The authors would like to acknowledge the financial support by the National Natural Science Foundation of China (No. 11772270) and the Key Special Fund (KSF-E-17).

References

- Proust, S., & Nikora, V. I. (2020). Compound open-channel flows: effects of transverse currents on the flow structure. *Journal of Fluid Mechanics*, 885.
- Singh, P. K., & Tang, X. (2020a). Estimation of apparent shear stress of asymmetric compound channels using neuro-fuzzy inference system. *Journal of Hydro-Environment Research*, 29, 96-108.
- Singh, P., & Tang, X. (2020b). Zonal and Overall Discharge Prediction Using Momentum Exchange in Smooth and Rough Asymmetric Compound Channel Flows. *Journal of Irrigation and Drainage Engineering*, 146(9), 05020003.

Lateral Diffusion of Stabilized Air Bubbles in a Counter-flow Water Tunnel

Soobum Bae¹, Scott A. Socolofsky^{1*}, Binbin Wang²

¹ Department of Civil and Environmental Engineering, Texas A&M University, College Station, TX 77843

² Department of Civil and Environmental Engineering, University of Missouri, Columbia, Missouri 65211

* Corresponding: ssocolofsky@civil.tamu.edu

Abstract

Submarine seeps of hydrocarbons are important to the oceanic carbon cycle. The dynamics of turbulence within the wakes of rising methane bubbles controls their fate during their ascent through the water column. For ellipsoidal bubbles, the vortex shedding in the wake region creates alternating low-pressure zones, and thus facilitates the wobbling motion of rising bubbles, which directly affects the lateral spreading of the bubbles. We conducted a series of laboratory experiments with an air bubble suspended freely in a small-scale water tunnel with a downward flow to collect high temporal resolution data with the Particle Image Velocimetry (PIV) technique using a high-speed camera. Bubble wobbling frequency and displacement from its trajectories under the controlled velocity profile were analyzed to quantify the diffusion of the wobbling bubbles. The experimental lateral diffusion coefficient showed a good match with the effective diffusion coefficient computed based on the observed lateral spreading of bubbly flow from natural seeps in Mississippi Canyon (MC 118) in the Gulf of Mexico. This result links the lateral wobbling motion of a single rising bubble with the diffusion of a large group of bubbles (i.e., bubble plumes) from the deep ocean.

Keywords: Lateral diffusion; Bubble wobbling; PIV measurements; Counter-flow water tunnel

Introduction

Seep bubble flares transport natural gas from the seabed vertically upward in the ocean water column. Small bubbles are advected by their buoyancy, and the lateral spreading of gas bubbles results from turbulent diffusion caused by their wobbling motion and by background turbulence in the ocean. Acoustic images and measurements with remotely operated vehicles (ROV) have demonstrated that the lateral growth of such bubble flares mainly stems from the turbulent diffusion of the bubbles (Wang et al. 2020). However, the connection between this lateral diffusion of a large group of bubbles and single bubbles remains unclear when the ambient turbulence is negligible.

Methods

A newly developed small-scale water tunnel was used to arrest an air bubble with counter-current flow. Seven sets (2,005 images each) of stabilized single bubble images with PIV seeding particles in the test region were collected at 200 FPS using a thin laser light sheet and high-speed camera. Image processing with manual edge detection of the air bubble was performed to improve the probability of vector detection and to calculate the centroid and the equivalent spherical diameter (*ESD*) of the bubble in each image. An open-source PIV tool, PIVLab, was utilized for the PIV analysis using three successive moving interrogation areas with 50 % overlap, followed by outlier detection with local median filter and interpolation replacement. The mean wobbling distance (λ) of the air bubble is defined as half of the wobbling orbit and was calculated from the time-series trajectories of the bubble centroids from the collected images. Autocorrelation of the fluctuating velocity of the bubble and its spectrum were then computed to obtain the mean wobbling frequency (f) and period (τ) of the bubble. With these spatial and temporal characteristics of the bubble wobbling motion,

lateral diffusivity (K_a) of the wobbling bubble was determined using the mean square displacement equation for 1-D Brownian motion:

$$\langle \lambda^2 \rangle = 2K_a t = 2K_a \left(\frac{1}{2} \tau \right) = K_a \tau \quad (1)$$

Results

The stabilized bubble in the water tunnel showed the wobbling distance (= **0.9 ESD**) similar to its equivalent spherical diameter with a mean frequency of **4.6 Hz**. These characteristics of the wobbling motion yielded the lateral diffusivity of the single bubble to be $2.4 \times 10^{-4} \text{ m}^2/\text{s}$. The reported lateral diffusivity of $3.0 \times 10^{-4} \text{ m}^2/\text{s}$ for field observations of bubbly flows using a random-walk diffusion seep model, in which the bubble dissolution and the crossflow were included, agreed well with the experimental single bubble diffusivity.

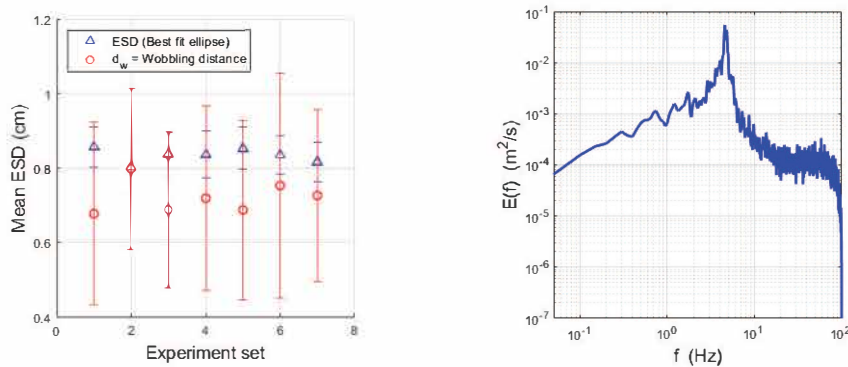


Fig. 1. The ratio between the mean equivalent spherical diameter and the wobbling distance (left panel) and frequency-domain spectral density peaked at 4.6 Hz (right panel).

Conclusions

The lateral diffusion of a stabilized wobbling bubble under a counter-flowing current in a water tunnel was quantified to cross-validate the random walk model for lateral diffusivity and the observed lateral spreading of seep bubbles. The image analysis for the bubble wobbling motion showed the similarity in diffusivity measured for a single bubble in the laboratory and for a large group of bubbles in the field. This experimental result confirms that the wobbling motion of a rising bubble is the dominant factor determining the lateral diffusion coefficient for weak bubbly flows from deep ocean natural seeps.

Acknowledgment

This work was supported in part by grants from the Gulf of Mexico Research Initiative (GoMRI, GISR Consortium, and Syn-bubbles project), the Texas A&M Energy Institute, and the U.S. Department of Energy, National Energy Technology Laboratory (NETL, grant number DE-FE0028895).

Reference

- Haljasmaa, I. V. (2006), On the drag of fluid and solid particles freely moving in a continuous medium, Ph.D. thesis, 185pp, University of Pittsburgh, Pittsburgh, Pennsylvania.
- Thielicke, W. and Stamhuis, E. J. (2014) PIVlab – Towards User-friendly, Affordable and Accurate Digital Digital Particle Image Velocimetry in MATLAB. Journal of Open Research Software, 2: e30, DOI: <http://dx.doi.org/10.5334/jors.bl>
- Wang, B., Jun, I., Socolofsky, S. A., DiMarco, S. F., & Kessler, J. D. (2020). Dynamics of gas bubbles from a submarine hydrocarbon seep within the hydrate stability zone. Geophysical Research Letters, 47, e2020GL089256. <https://doi.org/10.1029/2020GL089256>

Flow Patterns and Sediment Transport at the Initial Phase of the Local Scouring at the Downstream of Bed Protection

Jungkyu Ahn¹, Jaelyong Lee¹, Jeongmin Lee¹, Jin Hwan Hwang^{2*}, and Sung Won Park³

¹Incheon National University, Incheon, South Korea

²Seoul National University, Seoul, South Korea

³Korea Institute of Science and Technology Information, Daejeon, South Korea

*Corresponding: swpark@kisti.re.kr

Abstract

Local scouring is one of the most challenging topics in the fluvial hydraulics. Especially, Local scouring at the downstream of the fixed bed has also been analyzed with various approaches for the decades. Hoffmans (1997) classified the temporal changes of the maximum scour depth which is the deepest point in the scoured hole along the center-line. In the initial phase, the flow in the scour hole is nearly uniform. The erosion capacity of the bed materials in this phase is also most severe in the scour processes. In this study, flow pattern in the scoured hole was measured and analyzed based on the Froude number at the longitudinal transition. And temporal change of the scoured hole was analyzed with respect to the flow condition. Cyclic motion of the sediment particle was analyzed at the end of the scour hole.

Keywords: Local scouring; Fluvial hydraulics; Maximum scour depth; Froude number; Cyclic motion

Introduction

Previously, Hoffmans (1997) analyzed the time dependent mechanisms of the scouring and four phases of the local scour hole. In the initial phase, the flow in the scour hole is nearly uniform. The erosion capacity of the bed materials is most severe in the scour process. Experiments with fine bed materials by Breusers (1967) showed that at the beginning of the scour hole evolution some bed material near the upstream scour slope goes into suspension. Otherwise, some of the particles will settle down and be re-suspended owing to the large bursts of the turbulent flow near the channel bed, while some particles with a jump height smaller than a defined saltation or characteristic length, such as water depth or turbulent shear layer thickness at the transition, are transported as bed load to the downstream of the channel. In recent years, various researches about the local scouring have been analyzed with experimental and numerical approaches.

Methods

In this study, local scouring at the initial phase of scour process was analyzed with experimental approaches. 15 m long experimental flume with re-circulating water supply system was setup and filled with sand grain (median size of particle= 1.6 mm). And the Vectrino was applied for the flow velocity and bed elevation change with respect to the time and longitudinal distance. Flow patterns and turbulences in the scoured hole at the initial temporal phase were measured and analyzed with the sediment transport at the same time. Two cases of the flow condition were established in this experimental research. In the initial phase of the local scouring downstream of the fixed bed, which was introduced by Hoffmans (1997), we tried to analyze mechanism of the flow and sediment transport and their mutual interaction. Temporal change of the deepest point of the local scoured hole was analyzed for the future time phase and the flow characteristics at the longitudinal transition of the bed was also analyzed.

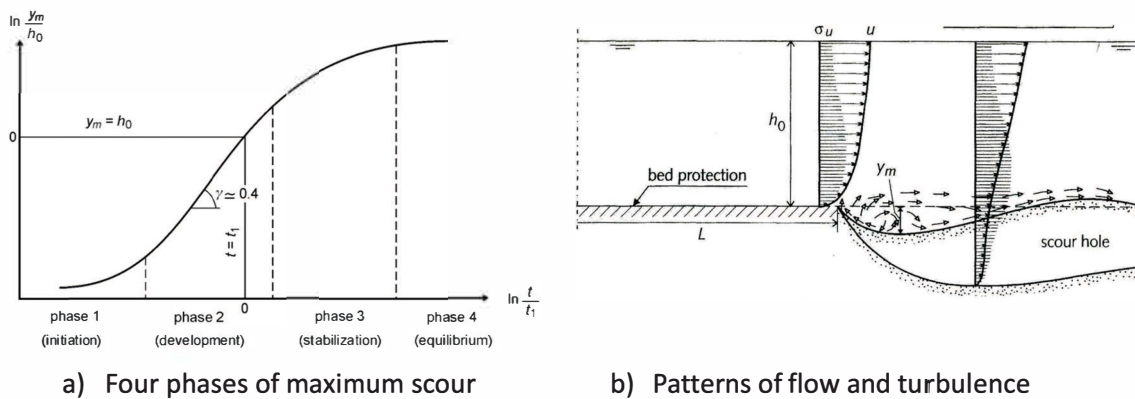


Figure 1. Schematic diagrams of the local scour time phases (left) and flow patterns in the coured hole (right) by Hoffmans (1997)

Results

The flow pattern at the longitudinal transition was analyzed with uniform flow. And right behind the transition, backward flow and circulation was made. Therefore, vertical averaged value of the flow velocity in the upper layer of the water was quite larger than those in the lower later of the water near the channel bottom. Also, turbulent shear layer is drastically developing toward downstream of the channel. Development of the turbulent shear layer is from the difference of the flow velocity and roughness of bed materials. Therefore, this shear force caused the sediment transport from the bottom such as particle jumping and rolling downstream.

Conclusions

In this study, we analyzed the flow and sediment transport in the initial phase of the local scouring at the downstream of the fixed bed. Mutual interaction of the turbulent flow and particle movement at the longitudinal transition was revealed with experimental approach. Form the results, three kinds of the time phase of local scouring at the downstream of the fixed bed will also be analyzed. And total development of maximum scour depth will be classified with advanced experimental analysis. Design of the hydraulic structures in the rivers and streams will be improved reasonably.

Acknowledgement

This work is supported by the National Research Foundation of Korea (NRF) grant funded by the Korea government (Grant No. 2019R1F1A1062727).

References

- Hoffmans, G. J. C. M. (1997), Scour Manual, CRC press. A. A. Balkema, Rotterdam.
- Breusers, H. N. C. (1967), "Time Scale of Two-dimensional Local Scour", Proceedings of 12th IAHR Congress, Fort Collins, Colorado, pp. 275-282.
- Park, S. W., Hwang, J. H., and Ahn, J. (2019), "Physical Modeling of Spatial and Temporal Development of Local Scouring at the Downstream of Bed Protection with Low Froude Number", Water, 11(5), pp. 1041.

Experimental study on through-flow and pollutant dispersion characteristics of rockfill porous media

Ilyeong Han^{1*}, Jaejong Lee¹, Gyoobum Kim²

¹Biryong Corporation, Seongnam-si, Gyeonggi-do, Korea

²Daejeon University, Daejeon-si, Korea

* Corresponding: iyhan101@naver.com

Abstract

It is evident that the hydrodynamic dispersion dominates solute transport in porous media. The physical properties that affect the hydraulic conditions of rockfill could be described by hydraulic mean radius of voids within the rockfill. This study conducts to explore the relationship between the hydraulic mean radius of rockfill porous media and the hydro-dispersive parameters. Slug injection test results reveal that the hydraulic mean radius of rockfill has a power type functional relationship with the hydro-dispersive parameters. The c-t curves estimated by the power type proposed formula were fairly well matched with the observations.

Keywords: Hydrodynamic dispersion; Rockfill; Hydraulic mean radius; Hydro-dispersive parameters; Slug injection test

Introduction

The hydrodynamic dispersion in porous media depends on variables such as the hydraulic conditions, the physical properties of the medium which can be represented by the dispersivity, and transport length scale. And The physical properties that affect the through-flow and mixing conditions of rockfill include the shape, size and roughness of particle, void ratio and tortuosity of voids within the rockfill. Those variables are included in a hydraulic mean radius calculation formula except tortuosity. Therefore, a correlation between the hydraulic mean radius and the dispersivity is expected to exist.

Methods

Dimensional analysis

The relation between dispersivity and hydraulic mean radius was able to be confirmed by the dimensional analysis in that only the medium properties were taken into consideration.

Materials and hydraulic mean radius determination

River gravel was graded into four sieve classes of rock particles : RGXL, RGL, RGM, RGS. A random sample of rock particle was selected and categorized, according to Zingg diagram, into four basic shapes. Average values of shape factor of the 371 samples were calculated. Then, hydraulic mean radius was determined by formula (Sabin and Hansen, 1994) with the known values of the size and shape of the particles and void ratio of the rockfill (Table 1).

Table 1. Particle size, shape factor and void ratio for hydraulic mean radius determination

Materials	Particle								Rockfill		
	Average size (cm)			Shape frequency				Shape factor	Void ratio	Hydraulic mean radius (cm)	
	a	b	c	Disk	Rod	Blade	Sphere				
River gravel (371 samples)	RGXL	5.07	3.51	2.47	26%	26%	9%	36%	1.82	0.64	0.206
	RGL	3.99	2.79	1.73	44%	21%	15%	20%	1.91	0.41	0.101
	RGM	2.07	1.43	0.88	35%	12%	27%	26%	1.96	0.39	0.048
	RGS	0.93	0.75	0.40	41%	24%	10%	25%	1.87	0.45	0.003

*a=*major axis, *b=*intermediate axis, *c=*minor axis

Slug injection test and hydro-dispersive parameters determination

The river gravels were filled into an acrylic-walled flume, which had a dimension of 150 cm long, 50 cm wide and 20 cm deep, in layer of 10 cm high. A slug of NaCl was instantaneously injected into the upstream of the flume. The solute concentrations were obtained by four EC sensors installed at the distances of 20 cm, 40 cm, 60 cm and 80 cm from the point source. The values of hydro-dispersive parameters were obtained by **dimensionless $C_R - t_R$** type curve (Sauty, 1980) matching method.

Results

The Reynolds number and hydro-dispersive parameters increases, indicating power type relationship, with an increase in hydraulic mean radius. The power type formulas relating the longitudinal dispersivity α_x to the hydraulic mean radius *m* were produced (Fig. 1). The *c-t* curves estimated by the proposed formula were fairly well matched with the observations in RMSE from 13.8 to 19.7 (Fig.2).

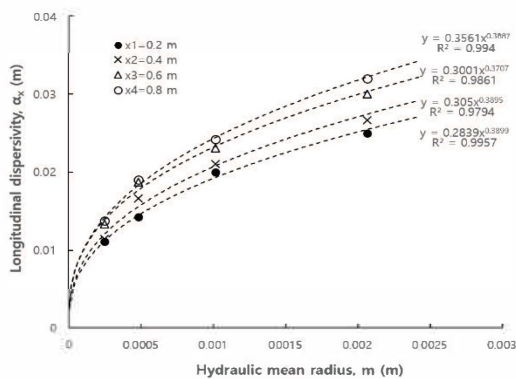


Fig. 1. Relation curves and proposed formulas

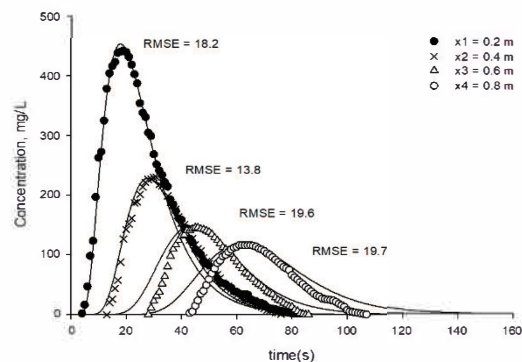


Fig. 2. Estimated *c-t* curves and observations

Conclusions

The results of this study show that the hydraulic mean radius of rockfill porous media has a power type relationship with the hydro-dispersive parameters. Once the hydraulic mean radius is determined using the information of the mean size and shape of particle, void ratio of rockfill that are design elements obtained in the past, one can make useful use of the proposed power type formulas for pre-estimating the hydro-dispersive parameters for the design of rockfill hydraulic structures such as a contact oxidation waterway.

Acknowledgement

This work was supported by Korea Environment Industry & Technology Institute (KEITI) through Demand-response Water Supply Program, funded by Korea Ministry of Environment (MOE) (2018002650002).

References

- Sabin, G. C. W., & Hansen D. (1994). The effects of particle shape and surface roughness on the hydraulic mean radius of a porous medium consisting of quarried rock. *Geotechnical testing journal*, 17, 43-49.
- Sauty, J. P. (1980). An analysis of hydrodispersive transfer in aquifers. *Water Resources Research*, 16(1), 145-158.

Direct Measurement of Critical Tractive Force for Revetment Material

Dong Gyu JUNG¹, Gwang soo KIM², Young Do KIM², Young Sung PARK³

¹Department of Civil & Environmental Engineering, Inje University

²Department of Civil & Environmental Engineering, Myongji University

³Department of Civil & Environmental Engineering, Seoul National University

*Corresponding: ydkim@mju.ac.kr

Abstract

To evaluate the strength enhancement effect due to the addition of coagulant enhancer on scouring, an experimental study was conducted in a high-speed flume using two types of sediments and biopolymer additives as strength enhancement agents. Considering the added water and the characteristics of the coagulant enhancer, we described a method to identify the optimum water content and decided the optimum amount of water and a procedure to eliminate the desiccation cracks caused by the added water in preparation of the coagulant-enhanced sediment material. When scouring occurred, we measured the sediment scouring and soil loss rate. Then, the changes in the resistance of the sediment materials with respect to scouring, while varying the amount of the coagulant enhancer, was evaluated and a guideline for practical application was proposed from the measurement data including high-speed flow conditions.

Keywords: Shear Stress, Tractive Force, Reynolds Stress, PIV, Shear Plate

Introduction

Overflowing of a river could lead to erosion in the embankment and its eventual failure. In some places, the risk of overflowing increases in the changing climate with increased frequency of floods exceeding the planned flood capacity. Since erosion occurs when the bottom shear stress exerted by flow exceeds a threshold value, a variety of methods have been applied to increase the strength of the embankment surface using, e.g., revetment blocks, vegetation mats, rubbles, sack gabions, and on-site vegetation. For the safe design of riverbanks, it is important to determine hydraulic characteristics of the embankment surface material, including the roughness coefficient, critical flow velocity, and critical bottom shear stress.

Methods

In this study, Experiments were performed for three conditions, and the results are listed in Table 2: absence of desiccation cracks in SC (Sand + Clay), presence of desiccation cracks in SCB (Sand + Clay + Biopolymer), and absence of desiccation cracks in SCB.

Table 1. Generation of desiccation cracks

	Flowrate Q (m ³ /s)	Velocity V (m/s)	Calculated Shear Stress τ_c (kg/m ²)	Soil Loss SL (%)	Desiccation crack
SC01	0.074	2.34	19.53	2	X
SC02	0.100	2.68	24.86	38	X
SCB01-1	0.052	1.47	13.68	3	O
SCB02-1	0.074	2.44	22.01	45	O
SCB01-2	0.074	2.44	21.41	3	X

SCB02-2 0.100 3.33 40.01 3 X

When desiccation cracks were generated, the material became vulnerable to scouring, even with additives or coagulation enhancement. Therefore, the experimental conditions for the generation of desiccation cracks were excluded, and the cracks were fully removed before starting the experiments.

$$SL = \frac{SV_t}{SV_0} \quad (1)$$

In this study, scouring evaluation was performed to verify the strength enhancement effect of the biopolymer additives. The loss rate for evaluating the degree of scouring was calculated by measuring the scouring depth of the material in the water channel using ultrasound water level gauges as follows (SL is Soil Loss, SV_t is Soil Loss volume for time, SV₀ is Initial Soil volume):

Results

The protection ability of the bed materials against scouring was evaluated using the shear stress and soil loss rate measured experimentally in this study. A 15% loss rate was observed as the threshold of the material in this study. The marginal shear stress of the specimen composed of a clay bed material mixed with biopolymer was increased by at least 2.3 times compared to that of a specimen composed of only clay bed material. The sand mixed with biopolymer showed increased strength of approximately 4 times compared to that of the pure sand specimen.

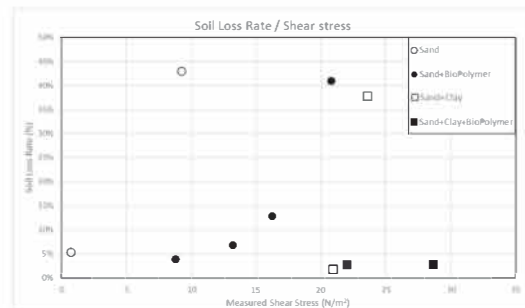


Fig. 1. Soil loss rates of the material mixtures.

Conclusions

In this study, the strength improvement effects were assessed by adding bio-polymer to the materials that make up the stream. The evaluation quantified and evaluated the Soil loss from experiments within the fluid and calculated the allowable shear stress of the materials configured. Tests have shown that bio-polymer significantly increases the allowable shear stress. The results of this study indicate that the strength of various materials and strength enhancement agents can be assessed at the time of recent increase in eco-friendly river environment construction projects.

Acknowledgement

This work is supported by the Korea Agency for Infrastructure Technology Advancement(KAIA) grant funded by the Ministry of Land, Infrastructure and Transport (Grant 21AWMP-B114108-06).

References

ASTM D7277-08. 2016. Standard Test Method for Performance Testing of Articulating Concrete Block (ACB) Revetment Systems for Hydraulic Stability in Open Channel Flow, ASTM International.

The effects of air cavity propagation on transient full pipe flows during emptying process

Rolando Perez^{1*}, Arman Rokhzadi², and Musandji Fuamba³

¹Master student, Department of Civil, Geological and Mining Engineering, Polytechnique Montréal

² Postdoctoral intern, Department of Civil, Geological and Mining Engineering, Polytechnique Montréal

³Professor, Department of Civil, Geological and Mining Engineering, Polytechnique Montréal

*Corresponding: rolando-yezid.perez-pulido@polymtl.ca

Abstract

The Sewer Network Systems (SWSs) are designed mainly to collect, transport, and evacuate the surface runoff. The interest of the engineer is to design hydraulic networks mainly flowing at a free surface regime. However, the system can be pressurized by events such as intense storms, which exceed the pipe capacity, or increase the urban surfaces that decrease the percolated water and increase the surface runoff. After such events, the pipe starts a process in which the flow decreases, then the water level inside the conduit decreases, and the pipe is emptying.

The emptying process creates a transient condition from pressurized to a partially pressurized flow inside the pipe so that an air cavity is formed that propagates upstream of the pipeline.

Some authors such as Pozos et al. (2010) or Coronado-Hernández et al. (2017) indicated that the air cavities could cause problems such as deterioration of pipe fittings and joints, oscillations, structural damage, increase in head losses, overflows, water hammer pressures, or sub-atmospheric pressures, which increase the risk of collapse or buckling of the pipe.

Some experimental and theoretical investigations have been carried out to understand the emptying process and the dynamic of the air cavity. Researchers such as Benjamin (1968) or Montes (1997) have studied the behavior of air cavity and the effects of different parameters, including viscosity, flow velocity, air propagation speed, cavity shape, and flow depth.

Previous researchers have studied some parameters of the air cavity under stagnant or steady-state flow conditions. However, the air cavity propagation in a horizontal pipe, where the flow rate continuously decreases, needs more clarity to complete the previous experimental studies.

This study performs two types of experiments in a laboratory setup consisting of upstream and downstream reservoirs connected by a horizontal transparent PVC pipe with a diameter (D) of 10 cm and the length (L) of 5.12 m. The parameters measured in the tests were the flow rate in the pressurized section, the water depth in the free surface section, and the pressure along the pipe. In the first experiment, called NIF, there is no initial flow inside the pipe. Thus, both reservoirs initially start with the same water level, and the pipe downstream end is closed. Subsequently, the pipe downstream end is opened, and the air cavity forms propagating upstream. The second experiment, named WIF, starts under initial steady flow conditions. Thus, the downstream reservoir is empty, and the pipe downstream end is open. As the flow rate decreases, the air cavity begins to propagate upstream.

It was found that when the small cavity appears, the pressure in NIF decreases from upstream to downstream due to the friction loss. However, in WIF, a negative pressure has to form inside the pipe to balance the momentum between inside and outside the pipe, as Montes (1997) indicated. The effect of negative pressure is more dominant than the effect of friction loss. Thus, the pressure along the pipe is almost constant

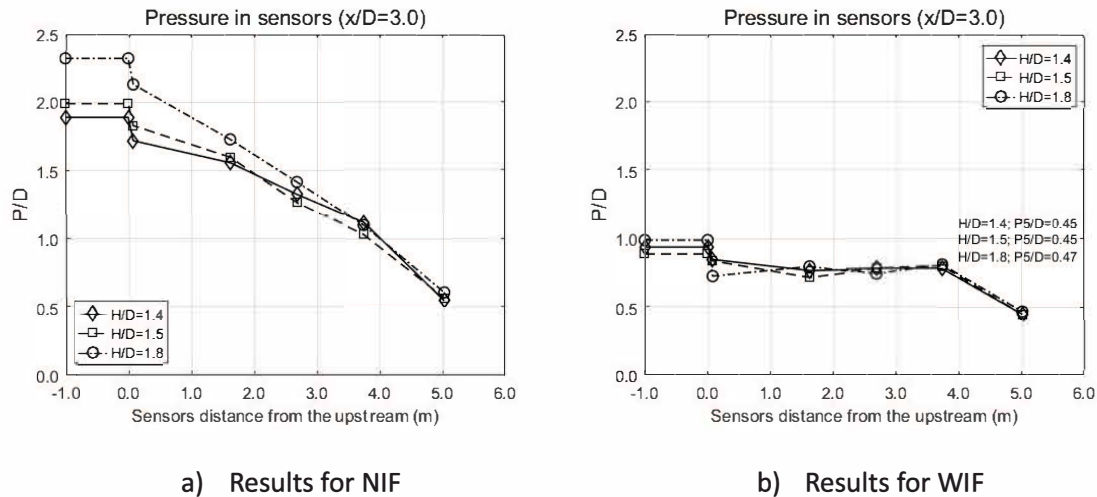


Fig. 1. Pressure in sensors when cavity is at $x/D \approx 3.0$.

As shown in Figure 1, when the cavity advance to $x/D \approx 3.0$, in which x represents the distance of the cavity leading edge from the pipe downstream end, the pressure within the cavity is atmospheric for NIF. For the case of WIF, the pressure measured by the sensor for the cavity (= 0.45D) is lower than the water level measured in the pipe (=0.608 D). This difference could be due to negative pressure inside the cavity equal to $-0.158D$. Note that the negative pressure at $x/D \approx 3.0$ ($-0.158D$) is higher than the negative pressure when the cavity is at $x/D \approx 1.0$ ($-0.28D$), indicating that the negative pressure is less intense as the cavity advance.

In addition, it was found that the flow number, defined as $F=V(gD)^{-0.5}$, in which V is the velocity far upstream of the cavity, for the cavity inception is $F \approx 0.859$, while the value calculated by Montes (1997) is $F \approx 1.0$. Furthermore, when the cavity is formed ($x/D \approx 3.0$), the flow number in the tests is $F \approx 0.859$, while Montes (1997) calculated it as $F \approx 0.581$. These discrepancies could be affected by the friction loss that was not considered by Montes (1997).

Keywords: Partially transient flow; Air cavity; Depressurization wavefront; Emptying process; Negative pressure.

References

- Benjamin, T. B. (1968). Gravity currents and related phenomena. *Journal of Fluid Mechanics*, 31(2), 209-248. doi:org/10.1017/S0022112068000133
- Coronado-Hernández, O., Fuertes-Miquel, V., & Angulo-Hernández, F. (2017). Emptying Operation of Water Supply Networks. *Water*, 10(1). doi:10.3390/w10010022
- Montes, J. S. (1997). Transition to a Free-surface flow at end of a horizontal conduit. *Journal of Hydraulic Research*, 35(2), 225-241. doi:10.1080/00221689709498428
- Pozos, O., Gonzalez, C. A., Giesecke, J., Marx, W., & Rodal, E. A. (2010). Air entrapped in gravity pipeline systems. *Journal of Hydraulic Research*, 48(3), 338-347. doi:10.1080/00221686.2010.481839

**The 9th International
Symposium on
Environmental Hydraulics**

F2 Session

Experiment-2 [F2-W2]



Near body flow field measurements on a fish robot

Dennis Powalla^{1*}, Shokoofeh Abbaszadeh², Karla Ruiz¹, Stefan Hoerner¹ and Dominique Thévenin¹

¹Institute for Fluid Dynamics and Thermodynamics, University Otto von Guericke, Magdeburg, Germany

²Institute of Electric Power Systems, University Otto von Guericke, Magdeburg, Germany

* Corresponding: dennis.powalla@ovgu.de

Abstract

The velocity field around a fish shaped sensor device was investigated in terms of the development of its biomimicking propulsion system with unconventional actuators. 2D-LDA (Laser Doppler Anemometry) measurements were carried out in an open surface laboratory flume. The gained data about the flow field supports the ongoing design process and yields information about the flow structure in the test set up. It will allow for the determination of suitable boundary conditions and provide validation data for parallel numerical investigations.

Keywords: 2D-LDA-Measurement; fish robotic; environmental hydraulics

Introduction

Fish compatibility assessment for hydropower facilities according to the state of the art is based on tests with live fish and leads to considerable stress and in many cases to serious injury and death of the animals deployed in these studies (Silva et al. 2018). A robotic fish acting as a propelled sensor for hydraulic conditions, is currently under development in terms of the RETERO-project (www.retero.org). This project aims for a reduction of live fish testing for hydropower facility assessments. The active sensor will be deployed in combination with computational fluid mechanics and additional data gained by passive sensors (Tuthan et al. 2018), which will lead to a predictive model, that should act as a substitute for current live fish approaches.

Methods

The design of the robotic device is based on the shape of a brown trout, which is target species in the research domain investigated. With aim to investigate the near body flow conditions and necessary propulsion forces for the robotic propulsion system, measurements were carried out in a laboratory flume with a cross section of 1200 X 600 mm² (WxH)(see Fig. 1 (right)).

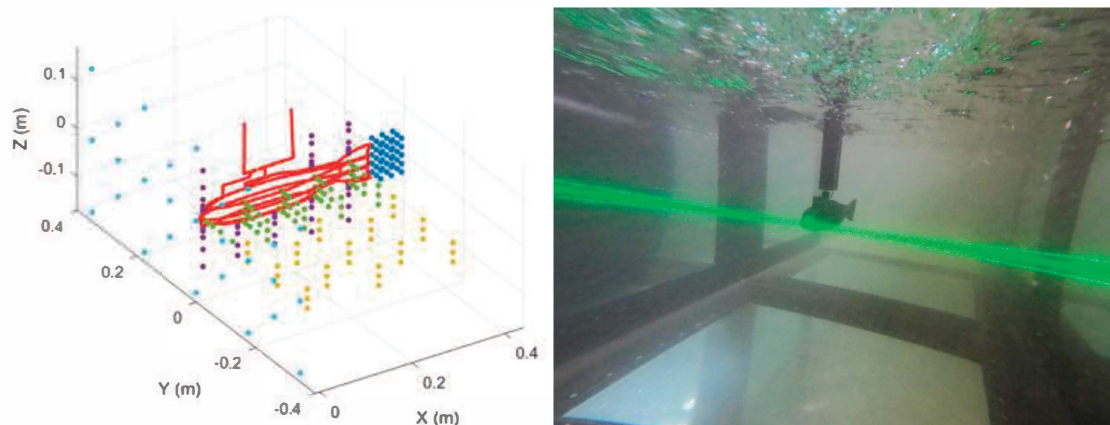


Fig. 1. Point cloud for 2D-LDA (left) experimental set up in laboratory flume (right)

The experimental setup covers flow measurements in a volume of 500×600×300 mm³ (L×W×H), where different areas of interest were observed such as inlet cross section, wake point matrix, cross section in XY-plane near and far body as well as near body measurements in XZ-plane (the different areas are displayed by different colours in Fig. 1 (left)). A 2D-LDA system is

deployed allowing for accurate measurements in the vicinity of the robot.

Results

In total, 740 probe points were measured by the 2D-LDA system to investigate the flow field in the laboratory flume around a static body - representing a fish like robotic device. The measurements provide a 3D velocity profile and turbulence distribution over the cross section perpendicular to the flow direction of the flume. The cross-section data will be used as a boundary condition at the inlet for numerical studies. Figure 2 displays the velocity vectors around the body (right) and the velocity field based on the interpolation of the data points in the XY-plane at z equals zero (left). The velocity field plot illustrates regions with detached boundary layer and wake generation. It allows for the determination of the separation point in the boundary layer.

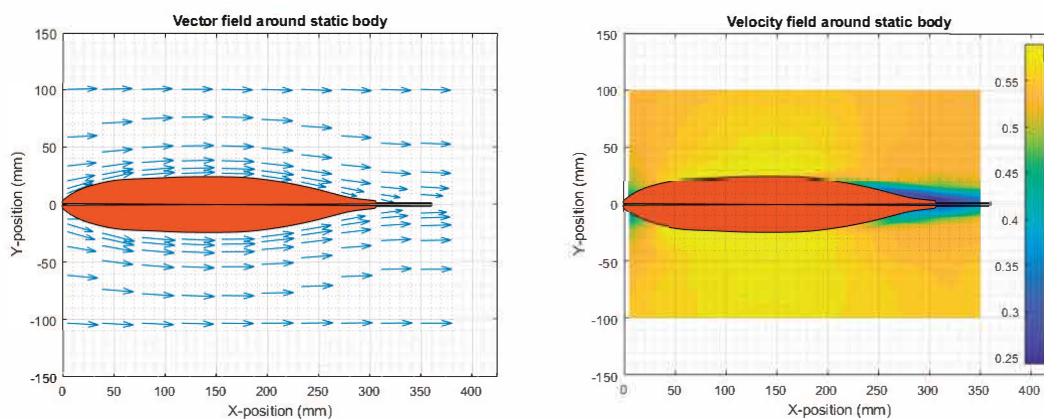


Fig. 2. Vector field around static body (left) and velocity field around static body (right)- fish surrogate is displayed as filled polygon shape (orange)

Conclusions

The variety of the data obtained in this setup will provide a detailed knowledge of the flow conditions close to the body and facilitate the ongoing design process. In addition, these investigations build a basis for the validation of numerical investigations by means of computational fluid dynamics, such as the fluid-structure interaction on fish shaped bodies or a determination of an active sensory space of fish.

Acknowledgement

We would like to thank our team from Tallinn University of Technology Estonia for collaborating in this work and providing us with the sensory devices. The CAD and 3D Printing work of Yanneck Kiiski is highly acknowledged.

References

- Silva, A. T.; Lucas, M. C.; Castro-Santos, T.; Katopodis, C.; Baumgartner, L. J.; Thiem, J. D.; Aarestrup, K.; Pompeu, P. S.; O'Brien, G. C.; Braun, D. C.; Burnett, N. J.; Zhu, D. Z.; Fjeldstad, H.-P.; Forseth, T.; Rajaratnam, N.; Williams, J. G. & Cooke, S. J. The Future of Fish Passage Science, Engineering, and Practice *Fish and Fisheries*, **2018**, *19*, 340-362
- Tuhtan, J.; Fuentes, J.; Angerer, T.; Schletterer, M. Monitoring upstream passage through a bypass pipe and drop at the fish lift Runserau: Comparing dynamic pressure measurements on live fish with passive electronic fish surrogates. 12th International Symposium on Ecohydraulics Aug19 Aug24, 2018, Tokyo, JAPAN, 2018.

Analysis of natural gas bubbles in the NETL High Pressure Water Tunnel (HPWT) experiment and its application to natural seeps

Byungjin Kim¹, Scott A. Socolofsky² and Binbin Wang³

¹Department of Ocean Engineering, Texas A&M University, College Station, Texas, U.S.

²Department of Civil & Environmental Engineering, Texas A&M University, College Station, Texas, U.S.

³Department of Civil & Environmental Engineering, University of Missouri, Columbia, Missouri, U.S.

Abstract

In order to understand the fundamental behavior of the kinematics and dissolution process of natural gas bubbles in the ocean environment, the National Energy Technology Laboratory (NETL) of the U.S. Department of Energy conducted experiments for methane and mixtures hydrocarbon bubbles (methane/ethane/propane) in their high-pressure water tunnel (HPWT) under different simulated oceanic conditions (pressure, temperature, salinity, and dissolved gas concentration). For each experiment, images of individual bubbles were recorded with a high speed and high definition camera to observe the behavior of the hydrate armoring process on the bubble and the impact of gas hydrate on the mass transfer from hydrocarbon bubbles to the surrounding water. A numerical model, the Texas A&M Oil spill Calculator (TAMOC) was adjusted to simulate the experiments in the NETL HPWT, and the results were compared with those in the NETL report by Levine et al (2015). Using the experimental data, we validated our numerical model for estimating the mass transfer between the bubbles and water. Particularly, this study helped understand the effect of hydrate skins on the mass transfer rates during and after hydrate formation and dissociation. These simulation results provide insights of 1) which mass transfer rate coefficients are appropriate before and after the hydrate transition time, and 2) whether the solubility of hydrocarbon gas or gas hydrate should present the concentration at the bubble/water interface.

Keywords: Gas hydrate; Mass transfer rate; Gas hydrate film thickness

Introduction

Mass transfer between bubbles and the surrounding ambient water is an important process in subsea blowouts and seepages from natural sources at the seabed. However, the mechanism of mass transfer is not fully understood due to current constrains in in-situ observations and modeling. One important uncertainty is the effect of hydrate coatings on hydrocarbon bubbles, which complicate the dynamics of the subsea mass transfer process from natural gas bubbles. Most laboratory investigations of hydrate on hydrocarbon bubbles have been limited to quiescent systems or where natural bubble motions are mechanically restricted. However, the NETL HPWT allows for an analysis of the kinetics of hydrate formation on methane and natural gas (methane/ethane/propane mixture) bubbles under different pressure, temperature and background dissolved gas conditions in a counter-current simulating the ocean water column. The high-pressure water tunnel (HPWT) data include video observations of the shrinkage of individual bubble before, during, and after hydrate skin growth on a single bubble. This dataset should provide answers to the dynamics of the hydrate skin formation and the dissolution rate of hydrate-coated bubbles under different ambient gas concentrations. The ultimate goal of our work is to utilize these observations to deliver a comprehensive analytical model of mass transfer at the bubble/water interface.

Methods

The mass transfer rate dm/dt in the HPWT is related to the observed bubble diameter d_e by

$$\frac{dm}{d t_{NETL}} = \frac{\rho A dd_e}{2 dt} \quad (1)$$

Where ρ is the gas density and A is the surface area of the bubble, taken as $\pi d_e^2/4$. The raw camera images were analyzed to compute bubble diameter (d_e), and linear regression was used to compute the best-fit slope for the shrinkage rate during the experiment time, yielding a value for dd_e/dt . From a mechanistical point of view, a dissolution model can be developed for the mass transfer equation (Clift et al., 1978).

$$\frac{dm_i}{d t_{TAMOC}} = -A\beta_{emp,i}(C_{s,i} - C_{a,i}) \quad (2)$$

where β_{emp} is the empirical mass transfer coefficient and C_s and C_a are the solubility and the concentration of component i in the ambient fluid, respectively. These two equations allow us to estimate the mass transfer coefficient β_{emp} by comparing dm/dt from the bubble shrinkage measurements (Eq.1) and from the dissolution model (Eq.2). In this comparison, we use the Peng-Robinson equation of state in TAMOC to compute ρ , C_s , and C_a .

Results

Using the dissolution model under the quiescent conditions calibrated to the HPWT data, we simulate the evolution of bubble sizes under changing ambient conditions. Fig. 1 shows an example of simulation results of a hydrate bubble compared to the measurement data. The mass transfer rates used in the model are those for dirty bubbles of free gas multiplied by an amplification factor of 1.9 based on the regression calibration described above. This factor accounts for the turbulent enhancement of mass transfer due to the turbulent pipe flow in the HPWT. The model-data comparison shows a good agreement, and we conclude that the presence of hydrate shells during free rise of a bubble does not change the dissolution significantly compared to dirty, free-gas bubbles.

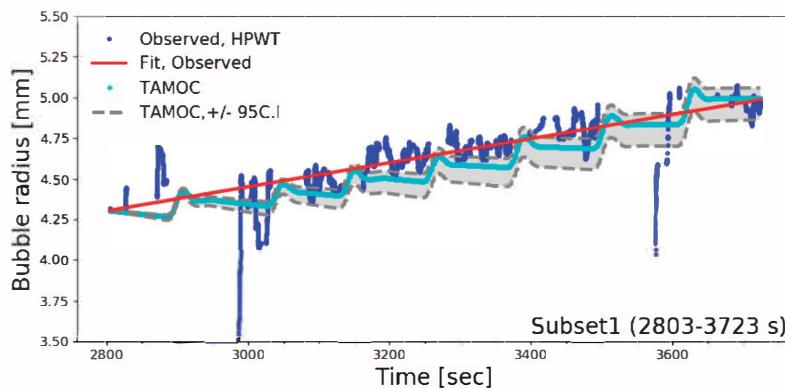


Fig. 1. TAMOC simulation for a C1C2C3 bubble with hydrate skin in seawater at decreasing pressure

Conclusions

Mass transfer rates are faster than dirty bubble ($1.9 \times \beta_{emp}$) in the HPWT and dominant dissolving phase during bubble rise in water column is free gas regardless of bubble state (pure, or covered with hydrate skin).

Reference

Warzinski, R. P., Lynn, R., Haljasmaa, I., Leifer, I., Shaffer, F., Anderson, B. J., and Levine, J. S. (2014). Dynamic morphology of gas hydrate on a methane bubble in water: Observations and new insights for hydrate film models. *Geophysical Research Letters*, 41(19), 6841-6847, DOI:10.1002/2014GL061665

Using GPS electronic Floater in Lab-Scale Study on the method of collecting river information

Chang Hyun Lee, Jeong Min Lee, Young Do Kim¹

¹Department of Civil & Environmental Engineering, Myongji- University

²Department of Environmental Engineering, Inje- University

³Department of Civil & Environmental Engineering, Myongji- University

*Corresponding: lch5435@naver.com

Abstract

There are many excesses of the allowable river flow due to abnormal weather at home and abroad. At this time, it is difficult for people to directly enter and obtain information about river information, so obtaining information in an indirect way should be important. As a result, there is a surface image velocity measurement method or a method using GPS electronic Floater. Since it is important to acquire river information, flow rate, water quality, river information, etc., we want to verify the usefulness of GPS electronic Floater in obtaining river information through intuitive and new IOT-based measurement rather than measurement. As a preliminary study, the part of the Lab-Scale channel was captured using the GPS electronic Floater own particles. After analysis using LS-PIV technique, data from verified electromagnetic speedometers (Flow Tracker) were compared and analyzed with real values. Research was conducted through the LS-PIV technique in Lab-Scale for GPS electronics Floater. Furthermore, it showed the utility of the wealthy in acquiring river information such as flow rate and velocity as well as acquiring water quality information using GPS electronic Floater. GPS electronic Floater is not only used in floods, but can also be applied to small and medium-sized rivers with low depth and low flow rates that cannot be measured with ADCP or ADV. In addition, continuous research is expected to be of great help to river measurement systems in the future.

Keywords: Stream Information Collection, Lab-Scale, GPS Electronic Floater , Measurement

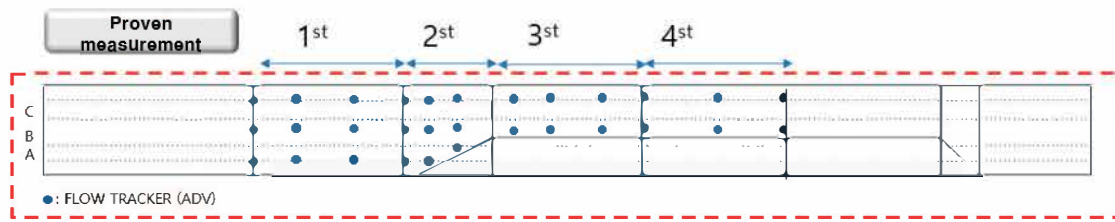
Introduction

Recently, cases due to bad weather are increasing. There are many collection methods, such as a method of directly entering and measuring a river to collect measurement data, observing a measurement time error, and a measurement method that requires a lot of manpower and time in the process of acquiring existing river information. Methods for obtaining simple and accurate river information are being improved and demanded.

In the case of ADCP, two-dimensional analysis is mainly performed, including measuring the flow rate and depth of the river and measuring the measuring surface of the river. However, in the case of measuring equipment such as adcp, adv, etc., a blind spot occurs, so measurement can be performed using an electronic Floater.

Methods

Segment the channel section in the experimental channel and measure the points using a flow tracker validated for the segmented section. After that, the flow rate in the waterway is measured by flowing the GPS electronic Floater. At this time, a GO-PRO camera is installed on the top of the measurement channel to take an image using the PIV technique in the experimental channel and measure the flow rate value.



Results

In the experiment, Flow Tracker's measurements were not smooth due to the secondary flow in the first to third sections. As a result, the accuracy fell a lot, and accordingly, the PIV technique was applied as a fourth section for measuring the flow rate of the electronic Floater. And when the flow rate was measured using the PIV method, the Flow tracker result Case 1 had a profile equal to 0.1 m/s. Case 2 results also obtained a profile similar to the verified results.

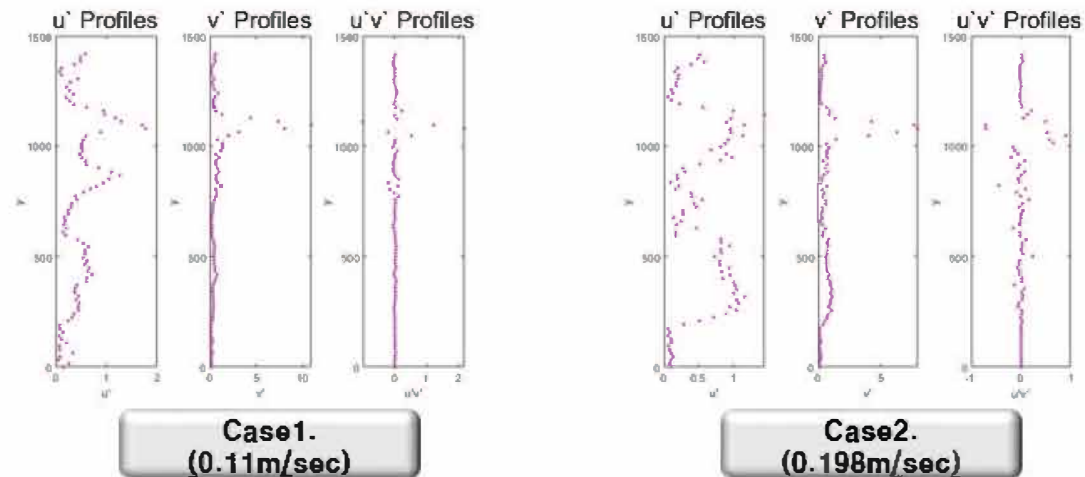


Fig. 1.. Flow rate calculation profile using the piv method of cases 1 and 2

Conclusions

Recently, limitations have been raised in obtaining river information. Accordingly, a field measurement method using advanced equipment was proposed. A method of obtaining river information using a GPS electronic unit and a drone is presented. At this time, the verified result value, the flow tracker value, and the measurement method using electronic Floater were compared, and the flow calculation result using the PIV technique was compared and analyzed. Using the PIV method in field experiments can be used as a new measurement method for obtaining river information. In the future, it will be reviewed through the results of application to actual rivers using electronic Floater.

Acknowledgement (If necessary)

This research was conducted with the support of the Ministry of Environment's Chemical Accident Response Environmental Technology Development Project (201800196001), and we are grateful for this support.

References

Jang, j, y, & Jong, J. H. (2015).Experiments of Water Surface Velocity and GPS-equipped floater speed in the Artificial Channel. National Institutes of Environmental Research, p.163.

Effect of non-axial velocity component on the mean axial velocity measurements in thermal plumes using an air velocity transducer

Maria K. Stefanidou¹, Aristeidis A. Bloutsos^{1,2}, and Panayotis C. Yannopoulos^{1*}

¹Environmental Engineering Laboratory, Department of Civil Engineering, University of Patras, Greece

²Hydraulics & Geotechnical Engineering Division, Department of Civil Engineering, University of West Attica, 122 43, Athens, Greece

*Corresponding: yannopp@upatras.gr

Abstract

The measurement of air velocities in thermal plumes is not an easy task, because of the rather small velocity magnitudes and local temperature change. Therefore, techniques other than hot wire should be used, like the particle image velocimetry (PIV). PIV is an expensive technique, that we couldn't afford. Thus, we decided to use the air velocity transducer, which is affordable, and it can measure satisfactorily the velocity if the direction is known. However, in regions with vortices and/or entrainment, this technique measures greater velocity magnitudes than real ones. Therefore, the present study proposes a modification, which reduces such effects and makes the technique convenient for such measurements.

Keywords: measurement technique; mean velocity; thermal plume

Introduction

The measurement of the mean flow velocities of thermal plumes in air environments, using the cost-effective air velocity transducer, is a challenge. Even if the main flow direction is known, as it happens in vertical plumes, the above method is considerably affected by the horizontal velocity components due to vortices and/or entrainment. This effect is expected to be insignificant at the plume centreline regions, where turbulent and entrainment velocities become minimal (Lee and Chu, 2003). In contrary, at locations off centreline with intense horizontal velocity components, the transducer effect is considerable, and it cannot be neglected. This is the main reason that the use of air velocity transducers is very limited in such flow measurements. The present study proposes a convenient modification that reduces the effect due to non axial velocity components and improves considerably the measurement accuracy.

Methods

The air velocity transducer, model 8465 TSI, is used for velocity measurements in the main flow direction (axial) of an air thermal plume. The transducer characteristics are given in Table 1.

Table 1. Technical characteristics of the air velocity transducer, model 8465 TSI.

Characteristic	Measurement conditions	Performance
Measurement error	reading at 18-28 °C	±2%
	full scale reading	±2%+0.005×selected velocity range
	readings at 28-60 °C	+6.4%
Temperature compensation	at 28-60 °C	It is provided
Temperature range	0–93 °C	
Transducer repeatability	for measurements 0.5–5 m/s	less than ±1%
Response to flow	tested at 7.5 m/s	0.2 s for 63% of final value
Velocity direction	In parallel to transducer needle	satisfactory

If the transducer is used as suggested by the firm, it is observed that, in regions of intense non

axial velocity components, it measures significantly greater values (up to about double) than they are. This effect can be reduced, if the transducer probe is mounted within a hollow cylinder made from cardboard, as shown in Fig. 1. The cylinder cuts off undesired velocity components.



Fig. 1. Transducer probe mounted in a hollow cardboard cylinder of 1-cm radius and 2-cm height.

The case studied concerns the transducer use for axial velocity measurements in a thermal plume originated vertically upwards from a horizontal ring source in the room atmosphere. The mean diameter and the width of the ring is 12 cm and 1 cm, correspondingly. The air velocity and temperature at the exit was 527 mm/s and 68.5 °C, correspondingly. The room air was calm with 20-°C temperature. The experimental measurements carried out using the transducer within the cylinder and, then, the measurements were repeated at the same transverse locations at 5 cm above the plume exit using the transducer without the cylinder.

Results

The values of measurements using the transducer without the cylinder at each transverse location are compared in Fig. 2 with the corresponding values using the transducer within the cylinder. The latter was calibrated at centreline regions by recording paths of small cotton tufts. It was found that the values measured must be multiplied by 1.1. It is evident that the measurements using the transducer within the cylinder are smaller than those without the cylinder, exempting values close to the plume centreline. The latter remain practically unaffected by either use or not the cylinder, because the velocities in the region near centreline are vertical.

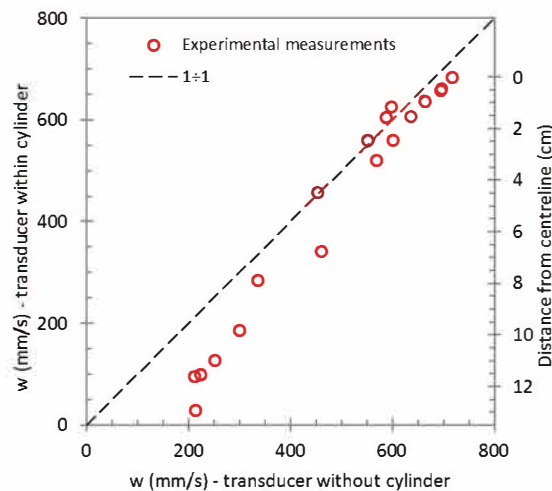


Fig. 2. Comparison of velocities measured using the transducer without cylinder with the corresponding ones measured using the transducer within the cylinder.

Conclusions

The results of this study show that the use of the air velocity transducer mounted within the hollow cylinder is a convenient tool for the measurement of axial velocities in thermal plumes.

References

Lee, J. H. W., & Chu, V. (2003). *Turbulent Jets and Plumes – A Lagrangian Approach*. Kluwer, USA.

Estimation of carbon: chlorophyll ratio for phytoplankton using in-situ Imaging FlowCytobot

Yaoyao MA¹, Joseph H. W. LEE^{2,3*}

¹Department of Civil & Environmental Engineering, The Hong Kong University of Science and Technology

²Macau Environmental Research Institute, Macau University of Science and Technology

³Institute for Advanced Study, The Hong Kong University of Science and Technology

*jhwlee@must.edu.mo

Abstract

Carbon: chlorophyll ratio (CCHL) is an important parameter in water quality models and is usually calibrated against field data. The use of a constant CCHL value cannot explain the observed significant diurnal dissolved oxygen variations in coastal waters. This study reports continuous imaging of algal concentrations at a marine fish farm with the use of an *in-situ* Imaging FlowCytobot (IFCB). Based on estimation of organic carbon from the bio-volumes on the algal images and direct measurements of chlorophyll-*a*, the carbon to chlorophyll ratio can be measured continuously for the first time. In accordance with theory, it is shown that the CCHL can vary significantly over an algal bloom cycle - in the range of 10 to several hundred.

Keywords: Phytoplankton; carbon: chlorophyll ratio; Imaging FlowCytobot; dissolved oxygen; diurnal variation.

Introduction

The carbon to chlorophyll *a* ratio (CCHL) is an important parameter in water quality models of phytoplankton and dissolved oxygen (DO) dynamics. The relationship between phytoplankton carbon biomass and chlorophyll *a* (chl-*a*) concentration is non-linear because of the complex influences by algal species, light, nutrient and temperature. CCHL value is usually calibrated by matching model predictions of algal and DO concentrations to field data; reported values are typically in the order of magnitude ~10 (e.g. Thomann & Fitzpatrick, 1982). In previous water quality models concerned with weekly or seasonal average behavior, the CCHL ratio is often assumed to be constant. However, the assumption of a constant CCHL often fails to reproduce short term D.O. trends (Lee et al. 1991). The use of a constant CCHL value in the order of 10 cannot account for the significant diurnal DO variation during an algal bloom (when > 4 mg/L increase of DO over a day has been observed in subtropical waters).

Phytoplankton carbon biomass can be estimated from the cell biovolume through microscopic measurement and flow cytometry. The Imaging FlowCytobot (IFCB) is an automated, submersible device that can acquire *in situ* high-frequency microalgae data of up to 40,000 high-resolution images (3.4 pixels/μm) per hour (Olson & Sosik, 2007). Cellular carbon content can be estimated from the cell bio-volume calculated from a captured image. We report herein the use of IFCB to obtain continuous measurements of carbon-to-chlorophyll ratios.

Methods

An IFCB has been successfully deployed at the Yim Tin Tsai Fish Culture Zone, Tolo Harbour, Hong Kong for about 2 years since March 2019. In the IFCB algal cell images are captured at high frequency on a 5 mL sample every 20 minutes. Because of some chain-forming algae, several cells may form a long chain and are also captured in a single image. Algal concentration

can be represented by the number of algal images per unit volume. Typically, the IFCB processes three 5 mL samples per hour (around 60 samples over 24 h). During March 2019 to April 2021, the algal concentrations (image counts/mL) are obtained for each sample collected on days when the instrument was operating normally. The hourly average is calculated to examine the diurnal and long-term variations.

Cell biovolumes are determined from the two-dimensional outlines in each image, using a distance map method (Moberg & Sosik, 2012). The Matlab-based routine for bio-volume extraction available online (<https://github.com/hsosik/ifcbanalysis/wiki>) is employed. The unit of biovolume directly obtained from IFCB images is pixels³, 3.4 pixels/micron is used to convert biovolumes into μm^3 . Carbon biomass (pgC cell^{-1}) are then estimated from biovolume (μm^3) using well-accepted conversion equations (Menden-Deuer & Lessard, 2000).

$$\text{pgC cell}^{-1} = 0.216 * \text{biovolume}^{0.939} (\mu\text{m}^3) \quad (1)$$

$$\text{pgC cell}^{-1} = 0.288 * \text{biovolume}^{0.811} (\mu\text{m}^3) \quad (2)$$

Equation (1) is for all species except for large diatoms ($>3000 \mu\text{m}^3$) in which case equation (2) is used to account for the lower carbon content in large diatoms due to the decrease of carbon density with increase of biovolume. Direct measurements of Chl-*a* are also made (using standard methods in the laboratory) on samples collected at YTT during field surveys. In this way a set of corresponding pairs of carbon and Chl-*a* concentration measurements for samples taken over a wide range of conditions can be obtained. In previous study, a dynamic determination of CCHL in terms of the time-varying saturating light intensity (I_s), phytoplankton grow rate (μ_{max}), temperature limiting factor is proposed (Lee *et al.* 1991).

$$\text{CCHL} = \frac{\alpha * I_s}{\mu_{\text{max}} * g(T) * e} \quad (3)$$

A constant α of 6 mg C/mg Chl-*a* ly is adopted in the model. Comparison between the CCHL obtained based on IFCB measurements and the model computed value is conducted.

Results

The IFCB successfully monitored the algae dynamics over the past two years. The continuous hourly and monthly averaged image count variations are shown in Figure 1. It is seen that there are more images in the spring and summer than in winter; the mean algal concentration is 1,459 images/mL. A typical diurnal variation is observed, increasing during the daytime and decreasing at night. The image count is highest at 4pm, and lowest at 5am.

The CCHL values are shown in Figure 2. Based on IFCB estimated carbon biomass data, the CCHL ratio are in the range of 9 to 415 $\mu\text{g C} / \mu\text{g Chl-}a$. The model computed CCHL ratio are in the range of 37 to 266 $\mu\text{g C} / \mu\text{g Chl-}a$. The data show that the CCHL ratios obtained by the two methods are similar, confirming the reliability of the data based on IFCB images. In addition, CCHL values of over 100 are often measured - which are much greater than the typical values of CCHL used in previous water quality model studies.

Concluding Remarks

The IFCB has been proved to be a useful tool for continuous algal dynamics monitoring. The carbon-chlorophyll ratio has been derived from IFCB data for the first time; the estimated CCHL values are in reasonable agreement with theory.

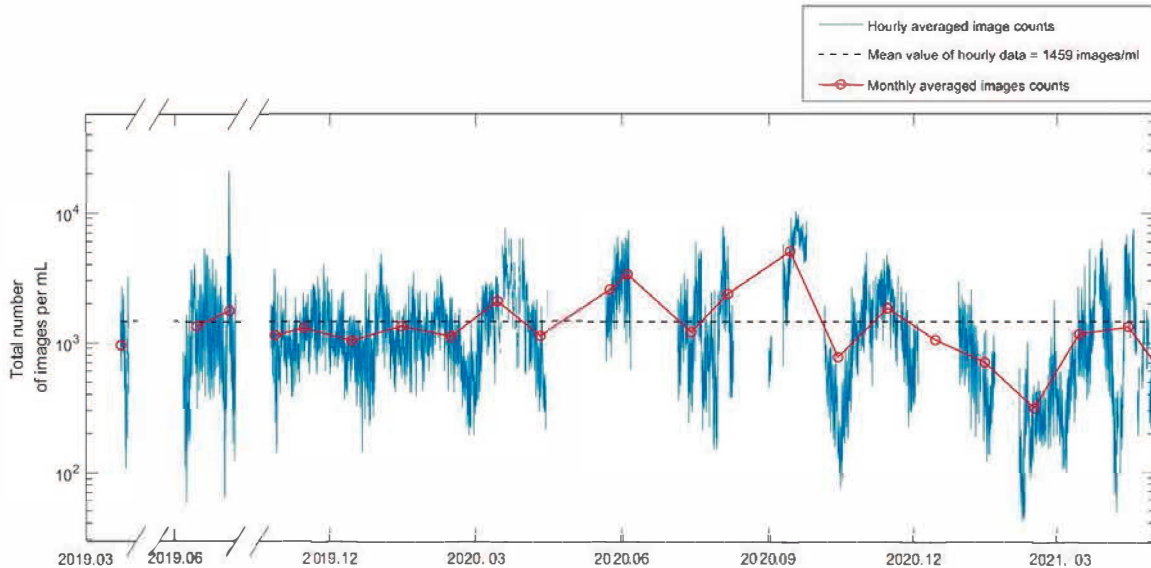


Figure 1. Observed time history of algal (image) concentration by the IFCB at Yim Tin Tsai, Hong Kong

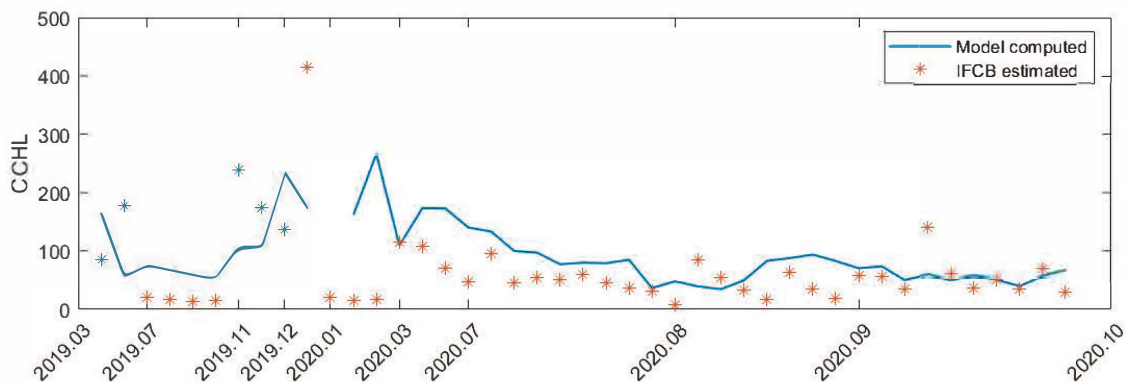


Figure 2. Comparison of CCHL estimates from IFCB data with theoretical prediction (Eq.3)

Acknowledgement

This work was supported by a R&D project commissioned by the Agriculture, Fisheries and Conservation Department of the Hong Kong SAR Government.

References

1. Lee, J. H. W., Wu, R. S. S., & Cheung, Y. K. (1991). Forecasting of dissolved oxygen in marine fish culture zone. *Journal of Environmental Engineering, ASCE*, 117(6), 816-833.
2. Menden-Deuer, S., & Lessard, E. J. (2000). Carbon to volume relationships for dinoflagellates, diatoms, and other protist plankton. *Limnology and Oceanography*, 45(3), 569-579.
3. Moberg, E. A., & Sosik, H. M. (2012). Distance maps to estimate cell volume from two-dimensional plankton images. *Limnology and Oceanography: Methods*, 10(4), 278-288.
4. Olson, R. J., & Sosik, H. M. (2007). A submersible imaging-in-flow instrument to analyze nano- and microplankton: Imaging FlowCytobot. *Limnology and Oceanography: Methods*, 5(6), 195-203.
5. Thomann, R. V., & Fitzpatrick J. J. (1982). "Calibration and verification of a mathematical model of the eutrophication of the Potomac Estuary", HydroQual Inc., USA.

**The 9th International
Symposium on
Environmental Hydraulics**

F3 Session

Remote Sensing-1 [F3-T2]



Development of an image based method to track the fate of floating litter in rivers

Péter Grivalszki^{1*}, Gábor Fleit¹, Alexander Anatol Ermilov¹, Sándor Baranya¹

¹Department of Hydraulic and Water Resources Engineering, Budapest University of Technology and Economics, Hungary

* Corresponding: grivalszki.peter@epito.bme.hu

Keywords: image based method, plastic litter, rivers

Abstract

Besides water and natural sediments, rivers transport different kind of floating debris as well, such as wood and plastic. Since rivers function as corridors for solid pollutants, it is of great importance to understand their behavior in the river and to design potential mitigation measures to reduce the waste load of seas and oceans. The Danube River in Hungary also faces with the issue of floating plastic waste, especially in the rising limb of flood waves, when the near bank zones of the river are greatly exposed to the debris. In a research project related to this study, an innovative plastic waste collector instrument is developed, called LitterTrap. The automatic, innovative equipment made of 100% recycled plastic has already been successfully applied in smaller rivers, however, the Danube River is characterized with very different hydrological features, which calls for a preliminary research. In order to optimize the waste collector, a video-based algorithm is developed, based on video footages recorded at the nearbank zone of the river, which is able to analyze the transported debris in terms of quantity, temporal behavior as well as composition. In this study, we introduce the developed image processing methodology and through field tests, the applicability is assessed and recommendations are made for further improvements.

Acknowledgement

This work was supported by the Blue Planet Climate Protection Foundation through their Research Work Scholarship Program, 2020/21.

Assessing performance of a novel UAV-borne Green LiDAR on vegetated rivers characterization: comparison with traditional Airborne LiDAR Bathymetry

Md. Touhidul Islam^{1*}, Keisuke Yoshida¹, Satoshi Nishiyama¹, Koichi Sakai²

¹Graduate School of Environmental and Life Science, Okayama University, Japan; ²Pasco Corporation, Japan; *Corresponding: touhidul-islam@s.okayama-u.ac.jp

Abstract

LiDAR-based remote sensing technologies have been utilized to survey stream channel and floodplain topography along with vegetation distributions for decades. However, traditional platforms, such as airborne LiDAR bathymetry (ALB), have drawbacks, including flight altitude, point density, and scanning angle, which prevent the sensor from conducting a practical survey of the vegetated rivers. More recently, UAV-borne LiDAR offers a way to characterize vegetated river environments with several inherent benefits over ALB. In this study, a new advanced UAV-borne green LiDAR system (GLS) was compared to the existing ALB for surveying the vegetated and gravel-bedded lower Asahi River in Japan. Findings revealed that the cost-effective GLS performed relatively well, although a few missing bathymetric data points in deeper areas were evident during the UAV campaign. To conclude, the novel technique could be regarded as practical since the GLS-derived information could feasibly serve as input and validation data in hydrodynamic-numerical models and riparian vegetation elucidation.

Keywords: ALB; Hydrodynamic modeling; UAV-borne LiDAR; Vegetation

Introduction

Riverine environment data primarily consists of topo-bathymetric and riparian vegetation attributes, which are difficult and costly to quantify but are crucial for river engineering planning and management tasks. However, to overcome several challenges in field surveys, more recently, a novel UAV-borne green LiDAR system (GLS) (TDOT GREEN, 2020) has been promising to attract river and coastal engineers. The overarching advantage of the cost-effective GLS over other LiDAR-based techniques (*i.e.*, ALB) is to simultaneously obtain both homogeneous laser point clouds of around 100 points/m² and high spatial resolution aerial images. As a case study in this research, the riverine environment of 1.6 km reach of the vegetated lower Asahi River, Japan, was assessed using both the ALB and GLS techniques. Finally, this study would be valuable to prepare a balanced scenario for vegetated river management measures by advancing our understanding of the recently designed technique.

Methods

With a normal water level, ALB (February 2019) and digital drone-mounted GLS (March 2020) were used to conduct river topo-bathymetry and vegetation attribute measurements. Herein, for performing a depth-averaged numerical simulation, the missing data found in the UAV campaign were updated using the existing ALB data. Also, to verify the LiDAR-based data and to validate simulated values, ground-truth measurements were carried out.

Results

Findings retrieved using LiDAR-based digital terrain data (Fig.1a) revealed no flood with substantial bed deformation during the measurement time of 2019–2020. The maximum water depth (Fig.1b) was approximately 4.96 m (1.79 FTU, turbidity) and 2.08 m (0.80 FTU, turbidity), respectively, for the underwater measurements using the ALB and GLS (before updating

missing data). It was saliently featured that the GLS point clouds over the present ALB illustrated the submerged artificial infrastructure (Fig.1c) of the river in detail, including its shape, patterns, and eroded parts, which could be helpful in maintenance and construction tasks, if necessary.

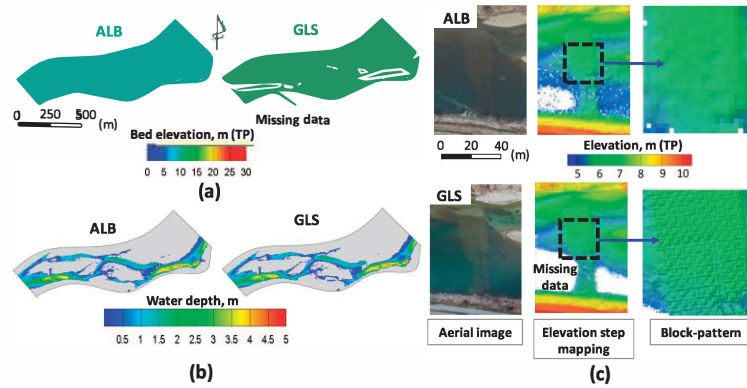


Fig. 1. (a) Bed elevation, (b) numerically simulated water depth mapping, and (c) reproducibility of submerged infrastructure; herein, Tokyo Peil (TP) denotes the average sea level in Tokyo Bay, Japan.

Results of vegetation attribute illustration (Fig.2) revealed that GLS performed reasonably well, almost identically to the ground-truth observations and the respective high spatial resolution aerial image with a ground sampling distance of 3 cm/pixel.

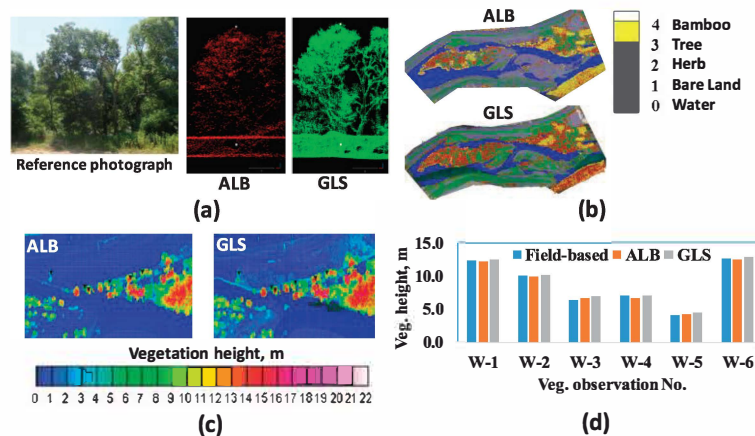


Fig. 2. (a) Vertical structure, (b) land cover mapping, (c) vegetation height contour map, and (d) a comparison of ground-surveyed woody vegetation heights with estimates based on ALB and GLS data.

Conclusions

Based on GLS's applicability in light of its shortcomings, the new advanced technology could be considered convenient and practical for shallow and shorter reach assessment. However, to get a better insight, assessing seasonal variation performance is highly recommended.

Acknowledgement

This work was funded in part by JSPS KAKENHI Grant No. 18K04370.

References

TDOT GREEN. (2020). Product website and spec sheet of TDOT GREEN. Retrieved from <https://amuse-oneself.com/en/service/tdotgreen>.

RIPARIAN LAND-COVER CLASSIFICATION METHODOLOGY OF AIRBORNE LASER BATHYMETRY -ASSISTED DEEP LEARNING OF AERIAL PHOTOGRAPHS

Shijun PAN^{1*}, Keisuke YOSHIDA¹, Junichi TANIGUCHI², and Akihide WATANABE²

¹Okayama University, Okayama, Japan

* Corresponding: p4b36znn@okayama-u.ac.jp

²TOKEN C.E.E. Consultants Co., Ltd, Tokyo, Japan

Keywords: Riparian land-cover classification, ALB, deep learning, semantic segmentation

Abstract

Land cover classification (LCC) has been acting as a fundamental character in hydraulic research works and practical tasks in terms of both flood control and riverside environment conservation. In recent years, massive flooding under the global climate change has drove hydraulic researchers to re-evaluate the river flow capacity accurately with the aid of refined LCC map. Such a map commonly contains the data of vegetation attributes (i.e., height and density) distributed in rivers. More recently, the detailed data for the river cross-section and those attributes have been measured and estimated using effective remote sensing methods like airborne laser bathymetry (ALB). For this work, we developed a new methodology for mapping the LCC (water area, bare ground, herbaceous species, arborous species, and bamboo grove) in rivers. The image processing technique of Deeplabv3+ (Chen *et al.*, 2018) for semantic segmentation was used for aerial photographs taken during the ALB measurement period. Additionally, we upgraded the technique for incorporating the ALB dataset: the laser point cloud (n) and vegetation height (l) (digital surface model data minus digital terrain model data). Appending an auxiliary module to the original technique, we concatenated these two types of data (aerial photographs and ALB dataset). Herein, we set the spatial resolution of 320pixel*320pixel (0.2m/pixel) for aerial photographs and 32pixel*32pixel (2m/pixel) for ALB dataset. We applied our method to ALB dataset measured in November 2017 for the approximately 4.5 km-long lower reach of the Asahi River, Japan. As the analysis condition, the combined datasets (aerial photographs and ALB dataset) were separated spatially into two parts: one part (15.0 KP to 17.4 KP) for training, and another part (13.2 KP to 15.0 KP) for validating. Herein, the kilometer post (KP) value signifies the longitudinal distance in kilometer from the river mouth. Results revealed that our method predicts the LCC map more precisely in case of use of combined dataset, especially for the detection of herbaceous species, comparing with predictions using aerial photographs only. Furthermore, comparing with existing analysis results based on the ALB dataset only (the same data as our method) for the LCC mapping, all the precision values of our methodology for the vegetation classification have been improved over 20% (herbaceous species for 22.7%, arborous species for 20.5%, and bamboo grove for 25.2%).

Water level monitoring for Hwang-Gang dam in North Korea using satellite remote sensing and inflow estimation for Gun-Nam flood control reservoir in South Korea

Jingyeom Kim^{1*}, Boosik Kang², Wansik Yu¹, Euiho Hwang¹

¹ K-water Research Institute, Daejeon, Rep. of Korea

² Dankook University, Yongin, Gyeonggi-do, Rep. of Korea

* Corresponding: jg_kim@kwater.or.kr

Keywords: Remote sensing, Satellite, North Korea, Imjin river, Transboundary river

Abstract

The Imjin River originates from North Korea and flows to South Korea. About 67% of the total watershed area of 8,117.5 km² is located in the North Korean region. For this reason, the North Korean water resource development plan has a direct impact on South Korea, which is located downstream. Also, due to the operation of the Hwanggang Dam, there is a risk of water resource reduction and flood damage in downstream of the Imjin River. The Hwanggang Dam is located about 42 km away from the military demarcation line, and the reservoir capacity is estimated to be about 300 to 400 million tons. South Korea is preparing for the discharge of the Hwanggang Dam by constructing a Gunnam Flood Control reservoir of about 70 million tons to protect against floods from the upper reaches of the Imjin River.

On September 6, 2009, a large discharge from the Hwanggang Dam caused a flood in Yeoncheon-gun in South Korea, which resulted in damage to life and property. Recently, on August 5, 2020, the water level at the 'Pil-Seung' Bridge increased sharply along with heavy rain, and the highest water level ever since observation occurred, and a flood warning was issued and nearby residents were evacuated.

In this study, rainfall-runoff analysis and satellite data were used to estimate the operating method and discharge of the Hwanggang Dam in North Korea, and finally to analyze the effect of the Gunnam Flood Control Area. In order to quantitatively estimate the discharge of North Korea's Hwanggang Dam, the reservoir inflow was estimated using a lumped rainfall-runoff model, the water level of the reservoir was monitored using satellite image analysis, and dam release was estimated using a reservoir operation algorithm.

In the case of the inflow between August 5-7, 2020, the additional release from the Hwanggang Dam in North Korea is about 67%, and it is estimated about 2/3 of the total inflow in the Gunnam Flood Control reservoir. Estimates of the inflow between August 10-12 are underestimated compared to the observed values, which is expected to have additional release to secure flood control capacity at the Hwanggang Dam in North Korea in preparation for additional rainfall.

Acknowledgement

This work was supported by Korea Environment Industry & Technology Institute (KEITI) through Advanced Water Management Research Program (AWMP), funded by Korea Ministry of Environment(MOE)(79622)

Rapid extraction of water area using SAR remote sensing data

Ki-mook Kang¹, EuiHo Hwang^{1*}, Sunghwa Choi¹, Wansik Yu¹, Jingyeom Kim¹

¹Water resources satellite research center, K-water Research Institute, Korea

* Corresponding: ehhwang@kwater.or.kr

Keywords: Water area, Flood mapping, SAR, Remote sensing, Gamma-distribution fitting

Abstract

Due to the unprecedented long rainy season and typhoon that occurred on the Korean Peninsula in this year, flood damage has appeared throughout the basin and urban areas. To monitor water-related disasters, it is more important than anything else to have a preemptive response system rather than follow-up measures, and to establish a national system based on rapid acquisition of remote sensing data that can reduce disaster damage. In this study, the flood damage on the Korean Peninsula was analyzed using SAR (Synthetic Aperture Radar) that capable of observing water body in surface through clouds during a flood disaster.

The SAR remote sensing data used in this study are Sentinel-1, Cosmo-SkyMED, TerraSAR-X, ICEYE, KOMPSAT-5, and etc. We applied both radiometric and geometric calibration for calculating the georeferenced backscattering coefficient in SAR data. And it applied the speckle filter and the Gamma-distribution fitting technique are used to extract the water body for mapping flooded area. The gamma distribution of the water body and the land part was extracted from the histogram of the image and the optimum threshold was set based on this, and the accuracy of the water body was improved by about 90% or more. In addition, the detection accuracy of the flooded area was improved by correcting the terrain distortion of SAR image in consideration of the slope and curvature of the DEM. For rapid flood area detection, we applied the automatic process during the heavy rain and the typhoon (Aug 7th 2020~Sep 9th 2020).

Despite our effective process and results, there were limitations in analyzing and utilizing rapid acquisition of satellite data as it was difficult to observe and secure satellites at the time of the most severe flood damage. In the future, it is believed that it is possible to establish a flood monitoring and response system across the watershed through the use of various commercial satellites and the development of C-band SAR satellite (CAS500-5; Compact Advanced Satellite 500-5) for water resources and water-related disasters to shorten the observation period and improve precision.

Acknowledgement: This study is supported by the Korea Ministry of Environment, South Korea, under the Demand Responsive Water Supply Service Program (Grant number 2019002650004).

Study on optimum UAV photogrammetry operation using river information from local residents at small and medium-sized rivers in Japan

Ken Ichikawa^{1, 3*}, Masakazu Hashimoto², Shosuke Sato², Fumihiko Imamura²,
Andre Araujo Fortes¹, Arata Nasuno³, Kaori Amaya³ and Susumu Naradate³

¹ Graduate School of Engineering, Tohoku University

² International Research Institute of Disaster Science, Tohoku University

³ Fukken Gijyutsu Consultants Co.

*Corresponding: ichikawa@sendai.fgc.co.jp

Abstract

This study examined ways to enhance the efficiency of UAV photogrammetry technology, which is used as one of the maintenance methods for small and medium-sized rivers managed by local governments in Japan. River managers are facing many problems in terms of human resources and costs. They are required to solve these problems in order to continue river maintenance and management to reduce flood risks. In this study, the altitude was lowered for the areas where trees were overgrown and the embankment was subsided, which were informed by the residents involved in the river, such as the river protection association, while the altitude was increased for the other areas to improve efficiency. Efficiency was evaluated in terms of the time taken to photograph and analyze the data. As a result, we proposed an accurate and cost effective observation method using the river information provided by local residents.

Keywords: Small and medium-sized rivers; UAV photogrammetry; optimization; Information from local residents

Introduction

The use of UAV photogrammetry to understand river channel geometry and evaluate the characteristics of the hydrological environment, as well as the challenges of this technology in river research and management, have been identified (Tamminga et al., 2016). In Japan, the use of UAV photogrammetry is being considered as a maintenance and management method for small and medium-sized rivers with long river length, where the local government is the river administrator, due to the low cost and ease of use of the technology. The financial situation of local governments makes it desirable to develop the best method to further reduce the cost. In Japan, there is a possibility of obtaining useful information for river maintenance and management through river protection activities conducted by residents in some areas, but it has not yet been utilized. In Japan, it is possible to obtain useful information for river maintenance and management through community-based river protection activities in some areas, but this information has not yet been utilized. Therefore, the purpose of this study is to examine whether UAV photogrammetry, which is one of the river maintenance and management tools, can be optimized and costs can be reduced by using river information obtained from residents for small and medium-sized river maintenance and management, and to examine future issues.

Methods

The river to be surveyed is the Miarai River, a river managed by Miyagi Prefecture that flows through Taiwa Town, Miyagi Prefecture. The data obtained from the residents who are engaged in river protection activities was that "there are areas of bank subsidence, vegetation

overgrowth, and sediment accumulation". Therefore, we set the shooting altitude in three cases: 50 m altitude for all the sections, 90 m altitude for all the sections, and 50 m altitude only for the section where we obtained information from the residents. The 50-meter altitude point cloud is characterized by a measurement accuracy of about 5 cm for the embankment height, which is higher than the accuracy of 10 cm for the 90-meter altitude. In addition, there are more point clouds that capture the ground surface under thick vegetation compared to the 90m altitude. The shooting width was set to 50m and the shooting length to 1,000m.

Table 1. Altitude setting for UAV photogrammetry in this study.

Case	altitude 50m	altitude 90m	River width	Extended shooting
1	1,000m	-	50m	1,000m
2	-	1,000	50m	1,000m
3	500m	500m	50m	1,000m

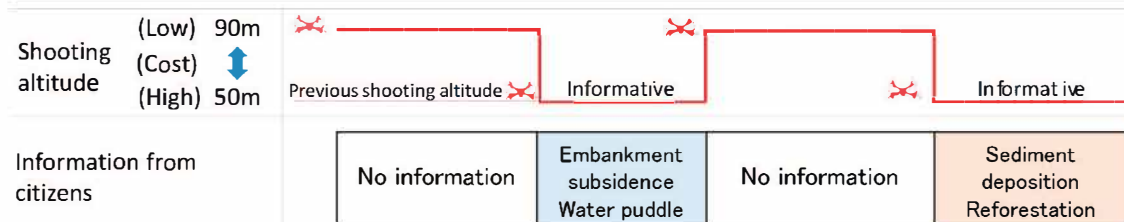


Fig. 1. Case3 : Information obtained from residents and altitude settings for UAV photogrammetry.

Results

UAV photogrammetry and point cloud generation were carried out at three different shooting altitude combinations. The results of the survey are shown in Table-2: Case 1, where the entire length of the river was photographed at an altitude of 50m, took the longest time to photograph and generate point clouds, followed by Case 3 and Case 2. We were able to reduce the cost by 19% (Case 1: Case 3) without compromising the accuracy of the operation without information by including river information from the residents in advance.

Table 2. Changes in the availability and cost (time) of using resident information.

Case	altitude		UAV shooting time : a (min)	Point group generation time : b (min)	a+b (min)	Ratio	Number of photos (piece)	Use of resident information
	50m	90m						
1	1,000m	-	35	48	83	1.00	714	No
2	-	1,000	23	13	36	0.44	382	No
3	500m	500m	28	39	67	0.81	650	Yes

Conclusions

By partially lowering the flight altitude based on river information from residents, we were able to ensure sufficient accuracy in areas with thick trees and sediment accumulation, where accuracy tends to be poor.

The following issues need to be addressed in the future. In UAV photogrammetry, more accurate location information (from place to place) is necessary to determine the range where the altitude should be lowered. In order to make more advanced use of information from residents in the future, it will be necessary to improve the information collection format.

References

Tamminga, A., Hugenholtz, C., Eaton, B. & Lapointe, M. (2015). Hyperspatial remote sensing of channel reach morphology and hydraulic fish habitat using an unmanned aerial vehicle (UAV): A first assessment in the context of river research and management. *River research and applications*, 31(3), 379-391.

**The 9th International
Symposium on
Environmental Hydraulics**

F4 Session

Remote Sensing-2 [F4-T3]



The implementation of a Surface Image Velocimetry to a Small-Sized River using a Images taken with Drone-mounted Camera

Kwonkyu Yu^{1*}, Binghao Liu^{2,3}, and Namjoo Lee³

¹ Dong-eui University, Busan, Korea

* Corresponding: pururumi@deu.ac.kr

² Dong-eui University, Busan, Korea

³ Kyungsung University, Busan, Korea

Keywords: drone; surface image velocimetry; orthogonal projection; Fourier transform

Abstract

SIV (surface image velocimetry) is a promising technique in measuring water surface velocity fields. It is a safe method since it does not require physical contact with water bodies. It is also very economical in labor and in time. However, since most SIV systems are in a fixed position, mounted a tripod or a pole, their angle of view is limited vertically. Using a drone-mounted camera, we were able to get a good vertical angle of view. Nonetheless, to put it in practical use, we do have to resolve the problem of stabilizing shaky images obtained by the drone. In image processing for surface image velocimetry, a slight sway of the drone could cause large errors, which were not acceptable in practical terms.

The present study aims to develop a system measuring surface velocities of river surfaces using images captured by a drone-mounted camera. To use a drone-captured video image for surface image velocimetry, we had to stabilize or make orthogonal projected images that took into account the swaying of the drone. The first step was to calibrate the camera and estimate its internal parameters. As the second step, the GPS coordinates and flight attitude information from the drone's flight log file were incorporated. Using the information above and a couple of ground control points, the images from the video were transformed into orthogonal images. Theoretically, if we had applied these orthogonized images to a SIV system, we should have been able to calculate the water surface velocity. However, since there were so many sources of error, for example, the orthogonizing process, the flight information of the drone, etc., it was hard to extract appropriate results. Therefore, we used the Fast Fourier Transform technique to properly render the spatio-temporal images to a series of orthogonized images. This technique has two strong points. Since internal and external camera parameters are utilized, ground control points are no longer necessary. This means that this system can be applied to larger rivers where ground control points are hard to find. Also, proper analysis of shaken images is achievable with the Fast Fourier Transform.

Acknowledgement: This work was supported by Korea Environmental Industry & Technology Institute(KEITI) through Aquatic Ecosystem Conservation Research Program, funded by Korea Ministry of Environment(MOE)(2020003050002)

Estimating dispersive behavior using UAV-based spatio-temporal hyperspectral image

Younghwa Kwon¹, Eun Jin Han², Hojun You³, Dongsu Kim^{1*}, Young Do Kim⁴

¹ Dankook University, Yongin, Gyeonggi-do, South Korea

² National Institute of Environmental Research, Seogu, Incheon, South Korea

³ The University of Iowa, Iowa City, Iowa, USA

⁴ Myongji University, Yongin-si, Gyeonggi-do, South Korea

* Corresponding: dongsu-kim@dankook.ac.kr

Keywords: Hyperspectral; Dispersion Coefficient; UAV; Spatio-temporal image; Remote Sensing

Abstract

The dispersive behavior in the riverine environments has been scrutinized and documented in the mathematical form of dispersion coefficient used for physical modeling of mixing process. Considering the presence of difficulty for direct measurement of dispersion coefficient, noticeable indirect procedures relying mainly on tracer test or flow velocity measurement have been successfully developed, whereas, in parallel, direct measurements of tracer such as Rhodamine using several dedicated water quality sensors still requires cumbersome and laborious field works. Sometimes it is impossible or hard to conduct in-situ tracer test due to limited access for the difficult site and flow conditions. In such perspectives, remote sensing-based approaches with recent popular platforms like unmanned aerial vehicle (UAV) alternatively demonstrated the feasible potential ways to identify and track the spatial movement of tracer in non-intrusive way. Conventional RGB images taken from UAVs, however, could limit their applicability within the visible range, such as colored tracer like Rhodamine can be tool quickly deteriorated and diluted for RGB image captured in UAV altitude to be hardly identified as mixing process has progressed toward downstream. This study attempted to apply hyperspectral image mounted on UAV replacing RGB camera, where we anticipated the hyperspectral camera can be much more sensible to capture nearly invisible tracer throughout ongoing dilution process. In the study, we applied Corning microHSI camera mounted on DJI Matrice 600 and collected the spatio-temporal hyperspectral images at various transects via hovering the UAV and continuous monitoring over time. The Rhodamine was released in upstream of Gam stream located in South Korea and has been monitored in the downstream 10 km nearly equally spaced with 5 transects. Concurrently, three Rhodamine sensors were installed for each transect to gather the concentration of the tracer, and the results were compared with the intensity of hyperspectral reflectance to build relationship with actual Rhodamine concentration. The preliminary results demonstrated that hyperspectral approaches substantiated the acceptable degree of Rhodamine distribution compared with in-situ sensors and longitudinal dispersion coefficient.

Remote Sensing for Suspended Sediment Concentration using Hyperspectral Images in Rivers

Siyoon Kwon¹, Il Won Seo^{1*}

¹Department of Civil & Environmental Engineering, Seoul National University

*Corresponding: seoilwon@snu.ac.kr

Abstract

Suspended sediment, one of the crucial physical factors occurring in natural rivers, changes the river morphology and has an enormous influence on water quality management. However, the obtainable data of suspended sediment is insufficient since the Suspended Sediment Concentration (SSC) measurement mainly depends on the direct measurement method using a conventional sampler, which requires a lot of cost and manpower. Thus, in this study, a hyperspectral image-based SSC measurement technique was developed through a UAV-mounted hyperspectral measurement system to perform a remote SSC measurement. For a universal application that takes into account the optical variability of suspended sediment, an intrinsic hyperspectral dataset of SSC for each sediment characteristic was constructed through a laboratory experiment and a field-scale experiment. The developed SSC measurement technique was assessed according to sediment properties at the Nakdong River in South Korea. The results showed that considering optical variability of suspended sediment from hyperspectral imagery would show better performance than previous models with more accurate SSC measurement in rivers.

Keywords: Suspended sediment, Hyperspectral image, Remote sensing, Optical variability

Introduction

The demand for remote sensing in the water environment increases as the variation in the water quality of rivers increases due to recent industrialization and climate change. Existing river monitoring methods have relied on direct measurement, making it difficult to collect vast amounts of data for monitoring and predicting continuous changes in the river environment. However, measurement of suspended sediment by remote sensing technique is challenging due to a complicated physical mechanism and heterogeneous optical properties due to various particle sizes and mineralogy (Dethier et., 2020). From these reasons, the variability of apparent and inherent optical properties induce the low performance of SSC remote sensing in terms of both empirical and analytical method. This optical variability of suspended sediment is essentially investigated for universal SSC measurement using remote sensing techniques.

Methods

In this study, Recursive Feature Elimination (RFE) was employed to extract the relevant spectral bands to suspended sediment from the experiment dataset. From the RFE-selected spectral bands, Support Vector Regression (SVR) was developed to estimate SSC.

In the SVR, the relationship between SSC and reflectance value, which is defined as Eq. (1) is derived by solving the optimization problem with Eq. (2) as the objective function and Eq. (3) as the constraint to solve the $f(x_{ij})$ that distributes within the deviation (ε). Thus, Eq. (1) is derived as the flattest regression function and less than a deviation ε from actual SSC values (y_i) for all reflectance values of each band (x_{ij}).

$$f(x_{ij}) = \sum_{i=1}^n w_i g(x_{ij}) + b_i \quad (1)$$

$$\min \frac{1}{2} |w|^2 + C \sum_{i=1}^n (\xi + \xi_i^*) \quad (2)$$

$$\begin{cases} y_i - f(x_{ij}) - b_i \leq \varepsilon + \xi_i^* \\ f(x_{ij}) + b_i - y_i \leq \varepsilon + \xi_i \\ \xi_i, \xi_i^* \geq 0 \end{cases} \quad (3)$$

Where w_i are weight coefficients; b_i is the bias; $g(x_{ij})$ is kernel functions for nonlinear transformation; C is penalty factor; ξ_i and ξ_i^* are slack variables to determine the degree of penalty that the error exceeds ε .

Results and conclusions

In this study, the optical variability of suspended sediment was measured according to sediment properties in the experiment (Fig. 1 (a)). From this heterogeneous dataset, the Recursive Feature Elimination (RFE)-based Support Vector Regression (SVR) model accurately reproduced the spatio-temporal SSC distributions (Fig. 1 (b)). Despite low visibility and optical variability, the developed SVR model successfully resolved the optical variability of SSC with the widely distributed spectral importance.

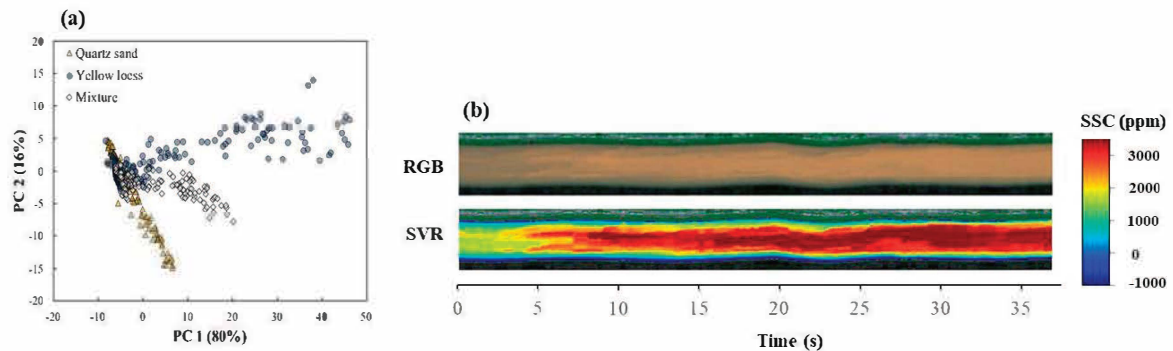


Fig. 1. (a) Hyperspectral spectrum according to sediment types in the space of Principal Components (PC); (b) Spatio-temporal distribution of SSC retrieved by the RFE-SVR model

Acknowledgment

This work is supported by the Korea Agency for Infrastructure Technology Advancement(KAIA) grant funded by the Ministry of Land, Infrastructure and Transport (Grant 20DPIW-C153746-02).

References

- Dethier, E.N., Renshaw, C.E., Magilligan, F.J. (2020). Toward Improved Accuracy of Remote Sensing Approaches for Quantifying Suspended Sediment: Implications for Suspended-Sediment Monitoring. *J. Geophys. Res. Earth Surf.* 125.

A study on the establishment of algae mapping based on hyperspectral images

Gwang Soo Kim¹, Dong Gyu Jung², Jong Min Kim and Young Do Kim^{1*}

¹ Department of Civil & Environmental Engineering, Myongji University

² Department of Environmental Engineering, Inje University

* Corresponding: ydkim@mju.ac.kr

Keywords: hyperspectral image; Blue-green algae; green algae; mapping

Abstract

Recently, changes in the water environment have occurred due to abnormal climate change. As a result, overgrowth of algae is frequently occurring in Korea. Toxic substances and tasteless substances produced by algae such as harmful blue-green algae are deteriorating water quality and have a great impact on the ecosystem. Algae occur in a wide distribution in rivers and reservoirs, and the current algae survey method requires a lot of manpower and time as intermittent surveys are conducted on a point or line basis. In Korea, many studies on bird monitoring using satellite images and RGB images have recently been conducted to reduce manpower and time. In this study, algae mapping was performed by taking RGB images and hyperspectral images in the upper stream Yeongju Dam. DJI's RGB drone and M-600 Pro were used as drones, and CORNING's microHSITM 410 SHARK was used as the hyperspectral sensor, and the NIR (visNIR) wavelength can be analyzed at 400-1000 nm, and the hyperspectral sensor is orthogonal. Images were collected using a gimbal in order to take an image with the camera. In order to perform radiation correction before taking the image, radiation correction was performed by photographing a reflective cloth for radiation correction on the same line as the drone.

In this study, spectral information data of algae culture solution samples that were previously conducted in the previous study were used to study algae mapping in the upper stream of Andong Lake and Yeongju Dam. Blue-green algae showed spectral characteristics at 670 nm, and green algae showed spectral characteristics at 477-510 nm. Mapping for algae is established through hyperspectral images, and through this study, a wide survey method for algae in rivers, reservoirs, and dams is proposed and applied to rivers.

Acknowledgement

This work is supported by the Korea Agency for Infrastructure Technology Advancement(KAIA) grant funded by the Ministry of Land, Infrastructure and Transport (Grant 21DPIW-C153746-03).

Analysis of Flow Characteristics Using GPS Floater in Estuary

Jeong Min Lee¹, Chang-Hyun Lee², Young Do Kim³

¹ Department of Civil & Environmental Engineering, Inje University

² Department of Environmental Engineering, Myongji University

³ Department of Environmental Engineering, Myongji University

Keywords: Estuary, Flow characteristics, GPS Floater, Lagrangian, Surface Drifter

Abstract

In this study, by comparing and analyzing the measurement data using the GPS Floater and the salinity measurement data in the Estuary, it was confirmed whether the behavioral characteristics of the GPS electronic rich man appeared consistently. It also tried to prove the utility of GPS Floater. In the Estuary water area, it is a section where freshwater and seawater meet, and continuous monitoring is required due to water quality problems in the section where freshwater is trapped. A lot of manpower and equipment are required to check the distribution of freshwater and seawater in brackish water. Typically, there are repair and water quality measurement equipment, but these equipment have limitations. Therefore, in order to check how the flow characteristics of each section in the brackish water area appear, we tried to use GPS electronic wealth. And the data of the GPS Floater and the salinity data measured in the vertical direction were compared. GPS Floater was injected at 1km upstream of Jwasuyeonggyo Bridge located in Suyeong River, and data of GPS Floater was secured by falling at low tide and high tide. And the salinity measured from the left, middle, and right sides of the left, middle, and right sides of the left Suyeong Bridge and Suyeong Bridge were averaged and compared with the GPS Floater data. Since the GPS Floater floats on the surface as a Surface Drifter, it can be seen that it extends further downstream at high tide. This was consistent with the salinity data measured at each bridge. Therefore, water quality monitoring in the section where the freshwater layer is confined should be conducted near the Jwa- Suyeong Bridge during high tide and near the Suyeong Bridge during low tide. As a result of this, it does not consume a lot of manpower and equipment, and if you use GPS Floater, we can quickly grasp the flow characteristics.

Acknowledgement

This research was supported by Korea Environment Industry & Technology Institute (KEITI) through The Chemical Accident Prevention Technology Development Project, funded by Korea Ministry of Environment (2018001960003). We would like to express our gratitude for the support we have received.

Application of Hyperspectral Image for Algae Distribution in Andong Dam

Jong Min Kim¹, Yeong Hwa Gwon², Ye Lim Park³, Dong Soo Kim² and Young Do Kim^{1*}

¹Department of Civil & Environmental Engineering, Myongji University

²Department of Civil & Environmental Engineering, Dankook University

²Department of Environmental Engineering, Inje University

*Corresponding: ydkim@mju.ac.kr

Abstract

In order to cope with the green algae phenomenon, it is necessary to quickly monitor the occurrence status and distribution of blue-green algae, but the current algae survey method is to directly identify through water collection and measure the overall algae concentration through a speculum or sensor. There is a limit to understanding the overall distribution of blue-green algae in rivers. In order to solve this problem, many studies on the occurrence and distribution of algae using remote sensing techniques to measure the spatial distribution of the plane unit are in progress. In this study, the algae warning system was classified based on blue-green algae, and the Andong dam was collected and compared with spectral information through spectroscopic and identification to calculate the optimal band ratio, and the blue-green algae concentration was expressed as a spatial distribution.

Keywords: Algal bloom; Blue-green algae; UAV; Hyperspectral images

Introduction

Algae are causing various social issues for reasons such as climate change. The timing of appearance and change of algae is different from the past according to seasonal weather conditions, water quality conditions. In order to cope with the many damages caused by the green algae phenomenon, it is necessary to understand and understand the current status of algae in the river about the occurrence and behavior of algae, and to promptly monitor them. However, as a current survey method for algae, the survey is being conducted through a speculum using direct water collection or intermittent measurement in point/line units using a sensor. Therefore, it requires a lot of support in terms of time, manpower, and cost. Therefore, a method of surveying algae with spatial distribution in plane units is required. In this paper, we present and show a technology that can calculate the algae distribution of the spatial distribution of the plane unit by collecting and analyzing the current spectral information in the river through remote monitoring through the advanced equipment hyperspectral sensor and unmanned aerial vehicle (UAV).

Methods

The luminance of liquid collected by hyperspectral images includes bottom reflection, absorption by water column, water surface reflection, and absorption into the atmosphere.

$$L_T(\lambda) = L_b(\lambda) + L_c(\lambda) + L_s(\lambda) + L_p(\lambda) \approx L_b(\lambda) \quad (1)$$

Here, $L_T(\lambda)$ is the wavelength, $L_b(\lambda)$ is the total luminance, $L_c(\lambda)$ is the bottom reflection of the river, $L_s(\lambda)$ is the absorption by the water column, $L_{bp}(\lambda)$ is the water surface reflection, and $L_b(\lambda)$ is the absorption by the atmosphere.

$$R(\lambda) = R_{object}(\lambda) - R_{base}(\lambda) \quad (2)$$

R_{object} is the reflectivity of the river water in which the tide is floating, and R_{base} is the reflectivity of the river water that has been filtered.

$$X = \ln\left[\frac{R(\lambda_1)}{R(\lambda_2)}\right] \quad (3)$$

Here, X is the band ratio, and $R(\lambda)$ is the reflectivity to the wavelength.

Results

The result of calculating the optimal band ratio in Fig. 1 is $C = -117239.4204X + 68248.4327$.

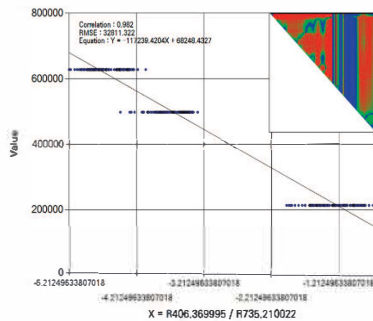


Figure 1. Calculation of optimal band ratio

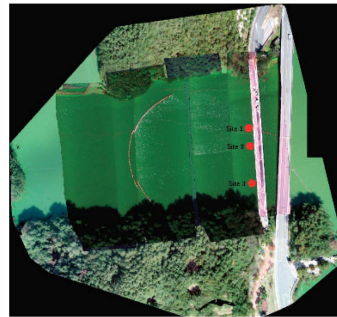


Figure 2. Algae distribution mapping result

In Fig. 2, the inspection results of Site 1 are 622,678 Cells/ml, Site 2 is 213,467 Cells/ml, and Site 3 are 497,833 Cells/ml, and the mapping results are 637,692 Cells/ml, 286,854 Cells/ml, and 576,970 Cells/ml. The error rate ranged from 2% to 26%.

Conclusions

As a result of this study, the results according to the concentration of blue-green algae are shown so that the spatial distribution can be confirmed. It showed high accuracy at relatively low concentration, and low accuracy at high concentration. This appears to be a limitation in comparison with respect to the lack of existing data and the exact point, and it is considered that it can be improved through further research

Acknowledgement (If necessary)

This work is supported by the Korea Agency for Infrastructure Technology Advancement(KAIA) grant funded by the Ministry of Land, Infrastructure and Transport (Grant 21DPIW-C153746-03).

References

Gwon, Y. H. (2020). Development of spectral library for hazardous chemicals using hyperspectral image. Master's Course. dissertation, University of Dankook.

You, H. J. (2018). Development of riverine bathymetry survey technique using drone-based hyperspectral image. Ph. D. dissertation, University of Dankook.

**The 9th International
Symposium on
Environmental Hydraulics**

F5 Session

Hydro-engineering [F5-T2]



Effects of the absence/presence of river bathymetric data in DEMs used for hydraulic modelling and flood prediction

Nancy Joy Lim

Department of Computer and Geospatial Sciences, University of Gävle, Sweden

* Corresponding: naylim@hig.se

Abstract

This study examines the effects of both bathymetric data and Digital Elevation Model (DEM) resolution on flood modelling and prediction results. Two-dimensional hydraulic simulations were conducted using DEMs produced from LiDAR data, with and without the river bathymetry, at different resolutions. Results showed that model performance increased using high resolution DEM with bathymetric data. Furthermore, it showed that areas dominated by flatter terrains were most sensitive to the effects of using LiDAR only data and lower resolution, producing larger extents and water volumes. The inclusion of bathymetric data and usage of higher resolution DEM in hydraulic modelling are thus needed to obtain more accurate flood model results.

Keywords: bathymetry, DEM, flood, hydraulic model, resolution

Introduction

An important input to any hydraulic model is the Digital Elevation Model (DEM) that represents the area's topography, through elevation values. It is used together with other hydraulic parameters to compute flow, water depth, and estimate flood extents, which are important outputs needed for flood prediction and hazard mapping. Nevertheless, DEMs derived from remote sensing provide poor coverage of underwater elevation. River bathymetric data, therefore, has to be derived separately (e.g. from hydrographic surveying), and combined with the topographic data. Since this data is not widely available (e.g. regional or national scales), there are cases that flood modelling is conducted without it. Hence, the objectives of this study are to determine: (1) how the bathymetric data affect the accuracy of hydraulic model results; and (2) how results from different resolution DEMs can further be influenced by the absence/presence of the bathymetric data.

Methods

Two rivers in Sweden (Testebo and Voxna) were used as test cases for the study. In producing the DEMs, two sets of Triangular Irregular Networks (TIN) models were initially created from LiDAR (Li), and the combination of LiDAR + bathymetric ($Li+B$) data. These were then rasterised to different resolution DEMs (3, 5, 10, 15, 20, 25 and 50 m), and used as the main elevation data input for the modelling. Hydraulic simulations were conducted with the two-dimensional model CAESAR-LISFLOOD. Flows equivalent to the reference data ($Q_{Testebo} = 160 \text{ m}^3/\text{s}$; $Q_{Voxna} = 360 \text{ m}^3/\text{s}$) were simulated. Manning's roughness used ($n_{Testebo} = 0.07$; $n_{Voxna} = 0.05$) were based on earlier optimal calibration results from using different resolutions DEMs (cf. Lim & Brandt, 2019). In quantifying model performance, feature agreement statistics (Eq. 1) was used. The equation accounts for the total size of overlap (A), overestimated (B), and underpredicted (C) by the model, in relation to the reference data, to determine the model's goodness-of-fit. Maximum performance is 100%, while negative values indicate that size of overestimation exceeds overlap size.

$$F = \frac{A - B}{A + B + C} \times 100 \quad (1)$$

Results

Generally, DEMs without the bathymetric data generated larger flood extents (Fig. 1), and larger overestimation of the flooding, leading to lower performances (Table 1). Performance also decreased as the resolution became coarser. There were also differences between the two study areas. Testebo river produced negative performance results when using Li , from 10 to 50 m resolution, due to large model overestimation. The part where flat areas are inherent were the most sensitive to the lack of bathymetric data, and had the largest extent in the said study site. On the other hand, the presence of

steeper slopes in the floodplain that bounded the water, prevented the flood from expanding laterally. Rather, it produced an effect that increased the water surface elevation. Maximum channel water depth (D_{max}) was also underestimated to several metres when using Li only data because of the lack of channel elevation.

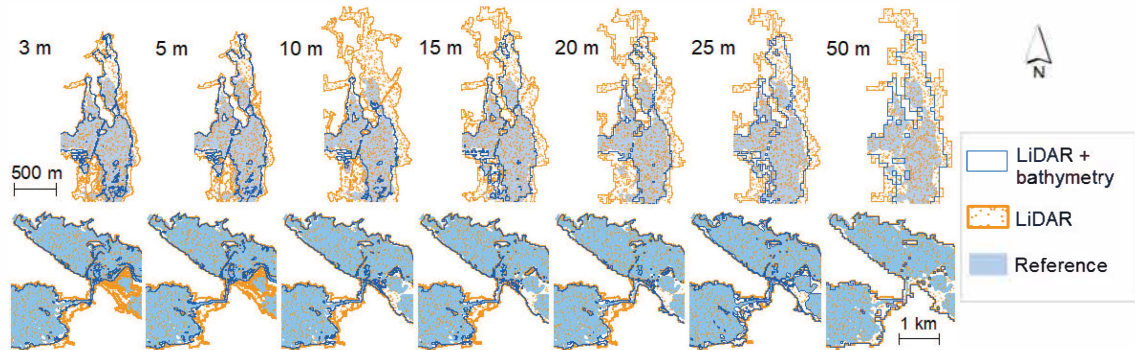


Fig. 1. Flood extent results for Testebo(top) and Voxna (bottom) rivers using different resolution DEMs, produced with and without the bathymetric data. Results are overlaid on the reference flood.

Table 1. Maximum water depths, sizes of inundation areas and model performances from the different data used.

Res. (m)	Testebo river						Voxna river					
	LiDAR + bathymetry			LiDAR			LiDAR + bathymetry			LiDAR		
	D_{max} (m)	Area (km ²)	F (%)	D_{max} (m)	Area (km ²)	F (%)	D_{max} (m)	Area (km ²)	F (%)	D_{max} (m)	Area (km ²)	F (%)
3	9.169	0.624	46.45	2.653	0.945	19.36	8.044	4.52	73.58	5.255	5.63	63.76
5	8.960	0.639	46.55	2.682	0.950	18.73	7.295	4.39	76.26	5.248	5.61	64.32
10	8.800	0.512	58.97	3.046	1.288	-11.43	7.563	5.40	71.05	5.158	5.92	59.96
15	7.949	0.738	41.79	3.050	1.258	-9.26	7.489	5.40	70.98	5.270	5.92	60.18
20	8.253	0.689	45.59	3.068	1.256	-9.20	7.636	5.46	69.26	5.115	5.93	59.41
25	8.461	0.790	37.84	3.103	1.227	-7.12	8.392	5.71	63.52	5.048	5.95	58.55
50	8.710	0.927	19.81	2.902	1.264	-10.51	8.233	5.78	61.84	4.878	5.92	58.63

Larger water volumes were produced from Li , but they were lowest for the 3 m and 5 m DEMs. Nevertheless, the 50 m resolution did not result to the largest volume. Volume differences between Li and $Li+B$ were also low for this resolution and the 25 m DEM (Fig. 2), especially for Voxna river. $Li+B$ data produced smaller volumes for higher resolution DEMs, but the 3 m data did not result to the smallest volumes in both rivers.

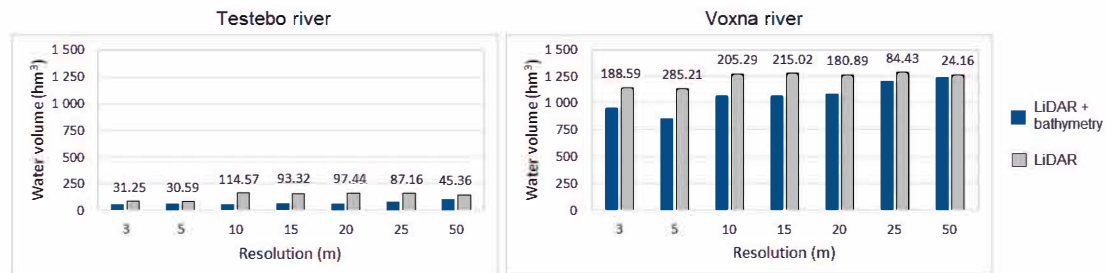


Fig. 2. Water volumes (hm³) generated from the simulations using the different datasets. Differences in volume (in hm³) between DEMs with and without the bathymetric information are shown as labels in the graphs.

Conclusions

The inclusion of bathymetric data in DEMs used for flood prediction is important to attain better model performance, while its exclusion leads to overestimated flood extents and water volume, and underestimated water depths in the channel. Resolution used also affects outputs from DEMs without the bathymetric information. Coarser DEMs, in particular, cause more detrimental effects to the results.

References

Lim, N. J., & Brandt, S. A. (2019). Flood map boundary sensitivity due to combined effects of DEM resolution and roughness in relation to model performance. *Geomatics, Natural Hazards and Risk*, 10(1), 1613–1647. <https://doi.org/10.1080/19475705.2019.1604573/>

EVALUATION OF RESERVOIR CAPACITY OF SINGDA RESERVOIR USING BATHYMETRIC DATA AND GEOSPATIAL TECHNIQUES

Victoria Ningthoujam^{1*}, Maisnam Bipinchandra Singh¹, Ngangbam Romeji Singh²

¹ Research Scholar, Department of Civil Engineering, National Institute of Technology, Manipur, India

² Assistant Professor Department of Civil Engineering, National Institute of Technology, Manipur, India

* Corresponding: victo.ning@gmail.com

Keywords: Sedimentation, Bathymetry, Remote Sensing, GIS, Reservoir capacity.

Abstract

Reservoirs are open storage area or lakes created by impounding streams carrying sediments. Sediments reduce both the water quality and quantity in the reservoir which in turn effects the management of the reservoir. The assessment of the sedimentation rate ensures sustainability of water from reservoir for various purposes. In this study, Singda reservoir catchment, Manipur, India is selected as it is the main source of potable water in Imphal, which is the capital city. Due to prevailing drinking water scarcity, this reservoir must be studied thoroughly and analyze the parameters which affects the water properties and as well as its capacity. The main objective of this study is to assess sedimentation in this reservoir using remote sensing and GIS techniques. DEM, Landuse map, Soil map and hydrometeorological data were used. In order to estimate the capacity or volume of the reservoir, bathymetry of the reservoir is studied. The bathymetry is carried out using 3D coordinates generated from the study area .A contour map and a 3D map of the reservoir was produced. A multi temporal approach analysis is taken up so that we can predict the life span of the reservoir for future management.

CLIMATIC IMPACT AND WATER BALANCE ANALYSIS OF SINGDA RESERVOIR USING HYDROLOGIC MODELS AND GEO-HYDROGRAPHIC TECHNIQUES

Victoria Ningthoujam^{1*}, Ngangbam Romeji², Gunadas Singh Keisam³, Sylvia Nongthombam⁴

¹ PhD Research Student, Department of Civil Engineering, National Institute of Technology, Manipur, India

² IAHR Member (B-65814), Assistant Professor Department of Civil Engineering, National Institute of Technology, Manipur, India

³ Project Assistant (DST-CCP-HICAB), Department of Civil Engineering, National Institute of Technology, Manipur, India

⁴ Project Associate Addl. (DST-CCP-HICAB), Department of Civil Engineering, National Institute of Technology, Manipur, India

* Corresponding: victo.ning@gmail.com

Keywords: Sedimentation, bathymetry, hydrometeorological, reservoir capacity, volumetric, hydrographic.

Abstract

Reservoirs are open storage area or lakes created by impounding streams carrying sediments. Sediments reduce the water quality and quantity in the reservoir which in turn effects the management of the reservoir. The assessment of the sedimentation rate ensures sustainability of water from reservoir for various purposes. In this study, Singda reservoir catchment, Manipur, India is selected as it is the main source of potable water in Imphal, which is the capital city and provide irrigation water to nearby agricultural areas. The Singda Reservoir is fed by two main streams/channels which are originated near the Kharam and Konsakhul villages. Due to prevailing scarcity of drinking water, it is a must to study the reservoir thoroughly and analyze the parameters which affects the water properties and as well as its capacity. The main objective of this study is to assess the climate change impacts on the water balance, reservoir capacity and accelerated sedimentation rate in the Singda reservoir. DEM, Landuse map, Soil map and hydrometeorological data were used. In order to estimate the capacity or volume of the reservoir, bathymetry of the reservoir is studied. Bathymetry analysis is carried out using 3D coordinates generated from the study area from ground survey database. A contour and 3D map of the reservoir was reproduced. A multi temporal approach analysis of spatial data was also taken up so that we can predict the life span of the reservoir for future management.

The hydrological models as SWAT and TOPMODEL are used to evaluate the runoff to the reservoir catchment. Sedimentation rate is worked and partially validated using in-situ field measurements of the two channels feeding the reservoir using depth integrated sediment sampler. Simultaneously the volumetric estimation of the Singda reservoir is evaluated using field hydrographic survey with a depth Echo Sounder (Dual Frequency).

Using Hydrological Distributed Model to evaluate the CHRS rainfall in Generating Discharge of Cileungsi River, Indonesia.

M. Pramono Hadi^{1,2}

- 1) Laboratory of Environmental Hydrology and Climatology, Faculty of Geography, Universitas Gadjah Mada
- 2) Center for Environmental Studies, Universitas Gadjah Mada

Corresponding: mphadi@ugm.ac.id

Keywords: Cileungsi watershed, distributed modelling, flow hydrograph, CHRS portal.

Abstract

The Cileungsi watershed with an area of 211 km² is a watershed with dynamic land use changes not far from Jakarta. This land use changes will affect the water yield of the watershed. In addition, economic activities, such as the development of this area into an industrial area, will increase the burden of water utilization. Discharge characteristics at the catchment outlet were assessed based on a distributed hydrological model. This hydrological model was built based on hydrograph recording with AWLR at Narogong Station. Slope area method is used to create stage-hydrograph rating curve. Rain as an input model is obtained from field recording data at several rain gauges which are then extrapolated based on the characteristics of the rain distribution obtained from the CHRS portal. Hydrologic routing with the Muskingum-Chunge method was used to produce flow hydrographs. The model parameters were determined based on the rain events on March 14, 15 and 16, 2020 which produced three flood hydrographs.

Based on the resulting modeling parameters and measurement hydrographs, it can produce a flow hydrograph for most of the year. The adjustment of the CHRS rainfall data was carried out by trial and error in order to obtain a hydrograph model with less errors. The comparison of the CHRS rainfall was then correlated with the adjusted rainfall to determine its accuracy. The adjusted rain is considered to have a better truth value. This hydrological modeling is seen as an inverted model, namely a model to find out the correctness of the input, namely rain. The degree of confidence chosen can be used to decide whether the use of the CHRS portal data can be used to provide discharge data for a watershed with mostly lack of rainfall data.

Development of the GeoCRP for the smart river management in the smart city

Bonhyun Koo^{1*}, Kyucheoul Shim¹, and Eunjeong Lee¹

¹Institute of Smart Disaster Management, JBT Co., Seoul, Korea

*Corresponding: kevinkoo@ejbt.co.kr

Abstract

In this study, in order to efficiently perform smart city river management, we developed a GeoCRP(Geo City River management Platform) that connects flood analysis models on the web and provides information by converting input and output data into a database. In the GeoCRP, a watershed analysis model, a river flow analysis model and an urban runoff analysis model were applied to perform flood analysis in smart city. This platform is able to obtain more reliable results by step-by-step approach to urban runoff that may occur in smart city through the applied model. In addition, since all analysis processes such as data collection, input data generation and result storage are performed on the web, anyone in an environment that can access the web without special equipment or tools can perform analysis and view results.

Keywords: Smart city, Flood management, Watershed runoff, River flow, Urban runoff

Introduction

As many cities are developed close to rivers, interest in urban flood analysis is increasing. Tate and Maidment (1999) derives the flooded area by combining the topographic data of the TIN model and the HEC-RAS model. Yoo et al. (2006) estimated the flooded area using the SWMM model to estimate the amount of urban flooding and analyzed the estimated flood damage in connection with the GIS database. However, most of the studies used a single model or did not consider the urban environment, so the accuracy of flood analysis was not high.

Methods

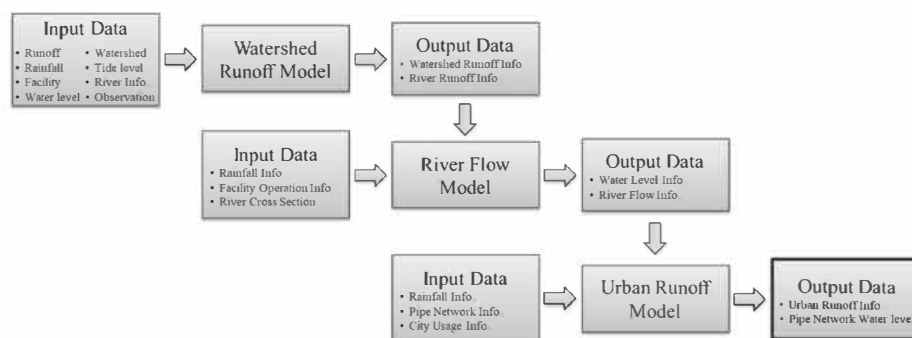


Fig. 1 Urban flood analysis process

To obtain high-accuracy urban flood analysis result, the results were sequentially derived by linked several models as shown in Fig. 1. A watershed runoff analysis in the Nakdong river is performed to derive the flooding area in the EDC area. After that, based on the runoff information derived through the watershed runoff analysis, river flow analysis of the rivers near the EDC area is performed. Through river flow analysis, water level and river flow information for each river section can be obtained, and the city runoff is finally analyzed based on the information. Through this analysis, it is possible to obtain information on the flooded area in the city when a flood occurs by

acquiring the amount of surface runoff in the delta area.

Results

Fig. 2 shows that the platform effectively provides the results of the three models through various functions. Fig. 2 (a) and (b) are the results of watershed runoff analysis and show the results of watershed runoff and channel runoff at each point. Based on the results, more accurate river flow analysis results could be obtained. The river flow analysis result shows the water level and flow rate information of river for each cross section of river according to the time flow, as shown Fig. 2(c). Finally, Fig. 2(d) shows the results of urban runoff analysis. It provides information on the water level of pipeline network and outflow from manholes over time.

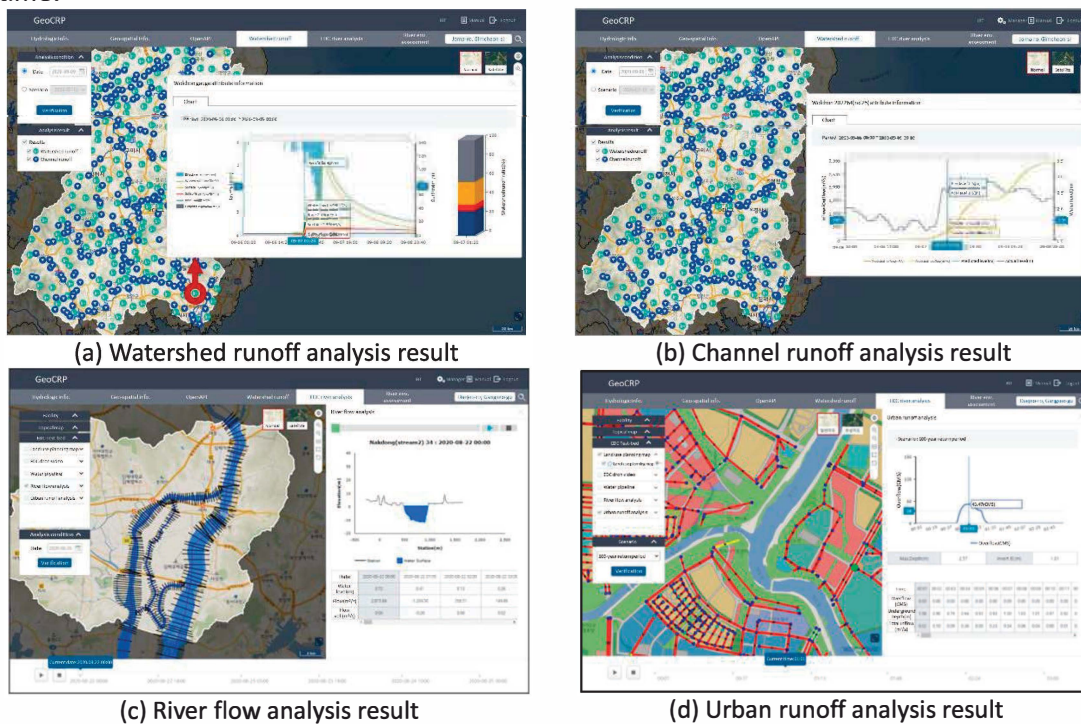


Fig. 2 Flood analysis results of GeoCRP

Conclusions

In this study, in order to perform urban runoff analysis for the delta area of EDC, the GeoCRP was developed by linking the watershed runoff analysis module in the west-nakdong river area, the river flow analysis module of rivers around EDC and the urban runoff analysis module in the corresponding area. The developed system analyzes three modules every day at midnight and stores the derived results in a database. The saved results can be inquired through the GeoCRP and the result that changes during the analysis period can be intuitively checked through the animation function. In the current version of the GeoCRP, flood analysis was performed according to changes in rainfall under actual environmental conditions. In future research, we plan to conduct research so that users can perform flood analysis by changing conditions.

Acknowledgement

This work is supported by the Korea Agency for Infrastructure Technology Advancement(KAIA) grant funded by the Ministry of Land, Infrastructure and Transport (Grant 21AWMP-B121100-06).

References

- Tate, E., and Maidment, D. (1999). Flood Plain Mapping Using HEC-RAS and ArcView GIS. Center for Research in Water Resources, The University of Texas, Austin, TX.
- Yoo, H.-H., Kim, W.-S., Kim, S.-S. (2006). "Inundating disaster assessment in coastal areas using urban flood model." *Journal of the Korean Society of Surveying, Geodesy, Photogrammetry and Cartography*, Vol. 24, No. 3, pp. 299-309.

Nature-based Solutions as an overarching concept and river corridor management

Hyoseop Woo¹

¹School of Earth Science and Environmental Engineering, Gwangju Institute of Science and Technology
*Corresponding: hswoo0603@gmail.com

Abstract

Nature-based solutions utilize ecosystem functions and services to tackle the societal challenges that humankind faces, such as climate change, food security, and natural disasters. It has come to the fore in Europe first in the late 2000s, while many similar or subset concepts have already been widely practiced. We can locate them, based on their concept and main targets, along a spectrum of the river management practices (including technologies) as Gray infra at a far end, Close-to-river technology (or practice) next, Nature-based management of river channel and floodplain or BGI next. The far-left side is the natural river corridors, which is also called Natural infra.

Keywords: NbS; Blue-green infra; Green infra; Gray infra; River corridor management

Introduction

Nature-based solutions, or simply NbS, are defined by IUCN (2016) as ‘the actions to protect, sustainably manage and restore natural or modified ecosystems that address societal challenges effectively and adaptively, simultaneously providing human well-being and biodiversity benefits. In a word, it utilizes the ecosystem functions and services to tackle the societal challenges that humankind faces, such as climate change, food security, and natural disasters. IUCN and World Bank jointly introduced the NbS in 2008 as an overarching concept of existing ecosystem-based approaches, including, among others, eco-disaster risk reduction and green infrastructures. In this paper, those similar approaches with different naming are categorized first, and then a hierarchy or a series of subsets of those differently named ones is identified. Finally, they are arranged in the management spectrum of the river corridor.

NbS as an overarching concept

Woo and Han (2020) summarized in a table the NbS and its similar approaches (or practices) according to their basic concept and primary targets as follows:

- NbS: Solving socio-environmental issues using ecosystem processes
- EE (Ecological engineering): Integrated design of human society and ecosystem, mainly for solving environmental issues
- Eco-DRR (Ecological disaster risk reduction): Reduction of disaster risk by protection and management of ecosystem, mainly for natural disaster risk management
- GI (Green infra): (narrow meaning) Urban stormwater management by mimicking nature and/or utilizing natural processes. (broad meaning) Solving socio-environmental issues by ecosystem management both in built and natural environments
- LID (Low impact development): Best management practices for maintaining the hydrological condition at pre-development, mainly for land development works
- CRT(Close-to-nature river works): Use of natural material and restoration of natural river morphology in the river works, mainly for river restoration

In the above explanations, EE is an applied ecology that has been academically developed since the 1960s for the utilization of ecological function as an engineering mechanism (Mitsch and Jorgensen, 1989). In that sense, EE may be different from the other practices listed above.

Fig. 1 shows the hierarchy of the NbS-related practices listed above. It is a conceptual diagram in which all the practices are arranged in a sequence based on each practice's inclusiveness. In

other words, it is the diagram showing which practice is a subset of which one under the umbrella of NbS. In this figure, Eco-DRR is omitted since it can be included in BGI. CRT is a nature-mimicking technology for river works, which is within the scope of BGI.

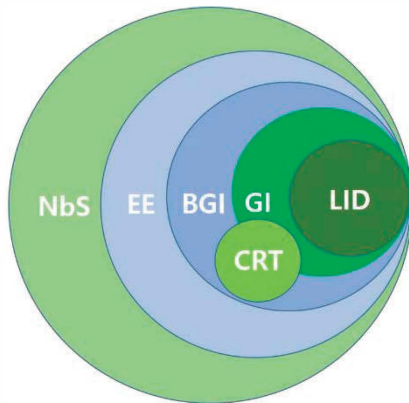


Fig. 1 A conceptual diagram showing the subsets of NbS (Woo and Han, 2020)

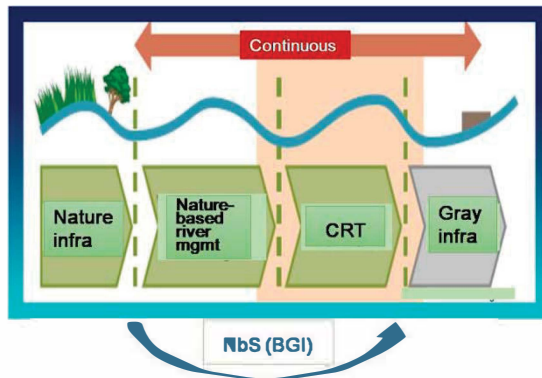


Fig. 1 Subsets of NbS applied to river corridor management (adopted by Woo, 2019 based on NERC, 2017)

NbS focused on the management of the river corridor

Now, we can apply NbS and the relevant practices to the river corridor management. Fig. 2 shows a spectrum of the river management practices and technologies starting from the traditional river technology or gray infra at far right. The next stage is the CRT based on the two principles: Using natural material and making the river corridor as close to nature as possible. The next is the nature-based management of river channel and floodplain such as the Dutch practice of "room-for-the-river," levee setback and removal, and restoration of floodplain including old channels and natural marsh. It is corresponding to BGI, or NbS in general. The far-left side is the natural river corridor, which is called "Natural infra."

Conclusions

Nature-based solutions overarch the relevant practices encompassing from LID through BGI. For the river corridor management, a broad spectrum of different practices is available between the traditional river practice, or gray infra, at a far end and natural infra at the other end. In between, we can locate the close-to-river technologies (or practice) and the blue-green infra. NbS is not new. Nevertheless, it is helpful as an overarching concept as shown in Fig. 1, especially for education and making the public understand.

Acknowledgment

This work is supported by the Korea Agency for Infrastructure Technology Advancement (KAIA) (Grant 21AWMP-B114119-06).

References

- IUCN (International Union for Conservation of Nature). 2016. Nature-based solutions to address global societal challenges. Cohen-Shacham, E., et al. edited.
- Mitsch, W.J. and Jørgensen, S.E. 1989. Ecological engineering: An introduction to ecotechnology. John Wiley & Sons, Inc., NY, 472 pp.
- NERC. 2017. Green approaches in river engineering - supporting implementation of green infrastructure. H.R. Wallingford, England.
- Woo, H. 2019. Close-to-river technology viewed from nature-based technology. Annual conference of KSEIE, Sangji Univ.. June. (in Korean)
- Woo, H. and Han, S. W. 2020. Topological system of nature-based solutions and its similar concepts on water management. Ecology and resilient infrastructure, 7(1): 15-25. (in Korean)

Daily Algal Bloom Risk Forecast System for Lo Tik Wan, Hong Kong

Jiuhao GUO¹, Joseph H. W. LEE^{2,3*}

¹Department of Civil & Environmental Engineering, The Hong Kong University of Science and Technology

²Macau Environmental Research Institute, Macau University of Science and Technology

³Institute for Advanced Study, The Hong Kong University of Science and Technology

*Corresponding: jhwlee@must.edu.mo

Abstract

In eutrophic coastal waters harmful algal blooms (HAB) often occur and present challenges to environmental and fisheries management. In this study, we present operational daily forecasts of algal bloom risk for a key fish culture zone located in the southern waters of Hong Kong at the mouth of the Pearl River Estuary. The bloom risk forecast is based on a validated vertical stability theory and a data-driven artificial neural network (ANN) model that assimilates high frequency data to predict sea surface temperature (SST), vertical temperature and salinity differential with an accuracy of 0.28°C, 0.15°C and 0.44 psu. The risk forecast is in good agreement with field observations and illustrated with an observed algal bloom in stratified waters in the wet season.

Keywords: Coastal algal bloom, Density Stratification, Daily forecast system, Fisheries management

Introduction

Harmful algal blooms (HAB) in eutrophic coastal waters can give rise to serious environmental and economic impacts and is a complex global issue. Under favorable environmental conditions, population of microscopic phytoplankton can grow rapidly to bloom levels (Chlorophyll-*a* > 10 mg/m³) and persist for weeks or even months. HAB causes harmful impacts including water discoloration, severe dissolved oxygen (DO) depletion, beach closure, massive fish kills or shellfish poisoning. Prognostic forecasts of algal bloom can be very useful for fisheries management – and yet this is a notoriously difficult problem.

Using high-frequency (10 min interval) water quality data, we have recently developed a daily algal bloom risk forecast model based on the integration of a well-validated vertical stability theory (Wong et al., 2009) with a data driven artificial neural network (ANN) model for prediction of daily vertical temperature and salinity (density) differential (Guo et al., 2020). The system has been successfully applied to Yim Tin Tsai fish culture zone (FCZ) located in a weakly-flushed tidal inlet in Tolo Harbour. In this study we extend the bloom risk forecast to Lo Tik Wan - a fish culture zone located in more open estuarine waters at the mouth of the Pearl River Estuary.

Prediction of Algal Bloom risk

Lo Tik Wan fish (LTW) is around 10 m deep, and located adjacent to the Lamma Island channel in the southern waters of Hong Kong. 3D hydrodynamic modeling has revealed that in the summer wet season (May to October) the FCZs in open waters are strongly affected by the freshwater (Lee et al., 2006). The water is typically strongly stratified in the wet season. According to the stability theory, a necessary condition for a bloom to occur is for the vertical turbulence to fall below a threshold value E_c . Fig. 1 shows a schematic diagram of the daily routine to predict the likelihood of algal blooms: (i) a general hybrid ANN model to forecast the daily-average value of sea surface temperature (SST) and vertical temperature and salinity differential, ΔT_z and ΔS_z respectively, on the next day (day t) as a function of real time data of various hydro-meteorological variables at different time lags. Two models are considered: one for the case when *in-situ* temperature/salinity data is available the day before - at day $t - 1$ (Model B); alternatively Model A makes predictions based only on readily available hydro-meteorological data (e.g. for days of equipment breakdown). (ii) Based on the ANN output, coupled with tidal predictions and meteorological data, a water column stability factor for the next day can be calculated (Wong et al. 2009). Let μ be the algal growth rate, l the euphotic layer depth derived from Secchi depth measurement, and E the estimated diffusivity derived from predicted SST, density gradient, wind speed and tidal range. The water column stability can be computed as:

$$\text{Hydrodynamic stability factor } (R) = \frac{\text{critical turbulence } (E_c)}{\text{estimated diffusivity } (E)} = \frac{4\mu l^2}{E\pi^2} \quad (1)$$

$R \ll 1$ indicates a strongly mixed water column and hence no algal bloom will occur, while $R \gg 1$ indicates a stable water column which favors the formation of algal bloom. A prognostic probability, $P(B)$, indicating the algal bloom risk on the next day, can then be predicted by considering the combined effect of

hydrodynamic stability risk and nutrient availability (N for total inorganic nitrogen and P for orthophosphate):

$$P(B) = P(B|R) \cdot P(B|N, P) = P(B|R) \cdot \min[P(B|N), P(B|P)]$$

$$P(B|R) = \frac{1}{1 + \mu_R \cdot R^{-a}}, \quad P(B|N) = \frac{1}{1 + \mu_N \cdot N^{-b}}, \quad (B|P) = \frac{1}{1 + \mu_P \cdot P^{-c}} \quad (2)$$

where $\mu_R = 5.86$, $\mu_N = 1.45$, $\mu_P = 1.26$, $a = 1.12$, $b = 1.61$, $c = 1.33$.

Results

The performance of the ANN models is evaluated using root mean squared error (RMSE) and Pearson correlation coefficient (CORR). Table 1 shows a summary of the ANN model performance for SST, ΔT_z and ΔS_z . Model A predicts the SST, ΔT_z and ΔS_z with a RMSE of **0.40°C**, **0.32°C** and **0.93 psu**; the availability and assimilation of real time data (Model B) reduces the corresponding errors to **0.28°C**, **0.15°C** and **0.44 psu**.

Fig. 2 shows an example of the variation of the estimated vertical diffusivity, algal bloom risk, DO and chlorophyll fluorescence in July-August 2018. During this period, nutrient is not limiting and hence the bloom risk is mainly controlled by the hydrodynamic stability. A stable water column ($E < E_c$) is observed starting from late July due to significant density stratification and the bloom risk ($P(B)$) ranges from 0.4 to 0.8 during this period. On the other hand, the observed chlorophyll fluorescence and a marked DO differential between surface and bottom (indicative of photosynthetic production in the surface layer) clearly indicates an algal bloom event from late July to early August – with a secondary bloom observed at late August. Generally, the bloom occurrence is well correlated with the predicted algal bloom risk.

Conclusions

Operational daily forecasts of algal bloom risk at a key fish culture zone in open estuarine waters have been presented. The results show that the predicted algal bloom risk correlates well with the bloom occurrence. The applicability of the bloom risk forecast system has been demonstrated for both weakly-flushed tidal inlets (Guo et al. 2020) and open estuarine waters (this study).

Acknowledgement

This study is supported by a R&D project on “Pilot Study of Red Tide Early Warning System using Real-time Phytoplankton Monitoring” from the Agriculture, Fisheries and Conservation Department (AFCD) of the Hong Kong SAR Government (AFCD/FIS/01/18).

References

1. Guo, J. H., Dong, J. H., Lee, & J. H. W. (2020). A real time data driven algal bloom risk forecast system for mariculture management, *Mar. Pollut. Bull.*, Volume 161, Part B, 111731.
2. Lee, J. H. W., Harrison, P. J., Kuang, C. P., & Yin, K. D. (2006) Eutrophication Dynamics in Hong Kong Coastal Waters: Physical and Biological Interactions. *The Environment in Asia Pacific Harbours*, (E. Wolanski, Ed.), Springer, 187-206.
3. Wong, K. T. M., Lee, J. H. W., & Harrison, P. J. (2009). Forecasting of environmental risk maps of coastal algal blooms. *Harmful Algae*, 8, 407–420.

Table 1 Performance of ANN models on prediction of SST (°C), ΔT_z (°C) and ΔS_z (psu) at day t in Lo Tik Wan FCZ

Target	Inputs	RMSE		CORR	
		Training	Testing	Training	Testing
Model A					
SST	[AirT] ₄ , [GSR] ₂ , [SST _{NP}] ₁ , [Rain] ₂ , [Wind] ₂ , [TR] ₀	0.40	0.71	1.00	0.99
ΔT_z	[AirT] ₄ , [GSR] ₂ , [SST _{NP}] ₁ , [Rain] ₂ , [Wind] ₂ , [TR] ₀	0.32	0.41	0.77	0.74
ΔS_z	[Rain] ₄ , [PRF] ₇ , [Wind] ₂ , [TR] ₀	0.93	1.34	0.77	0.77
Model B					
SST	[SST _{YTT}] ₁ , [AirT] ₄ , [SST _{NP}] ₁ , [Rain] ₂ , [Wind] ₂ , [GSR] ₂ , [TR] ₀	0.28	0.27	1.00	0.99
ΔT_z	[(ΔT_z) _{YTT}] ₁ , [AirT] ₄ , [SST _{NP}] ₁ , [Rain] ₂ , [Wind] ₂ , [GSR] ₂ , [TR] ₀	0.15	0.17	0.96	0.96
ΔS_z	[(ΔS_z) _{YTT}] ₁ , [Rain] ₄ , [PRF] ₇ , [Wind] ₂ , [TR] ₀	0.44	0.46	0.97	0.97

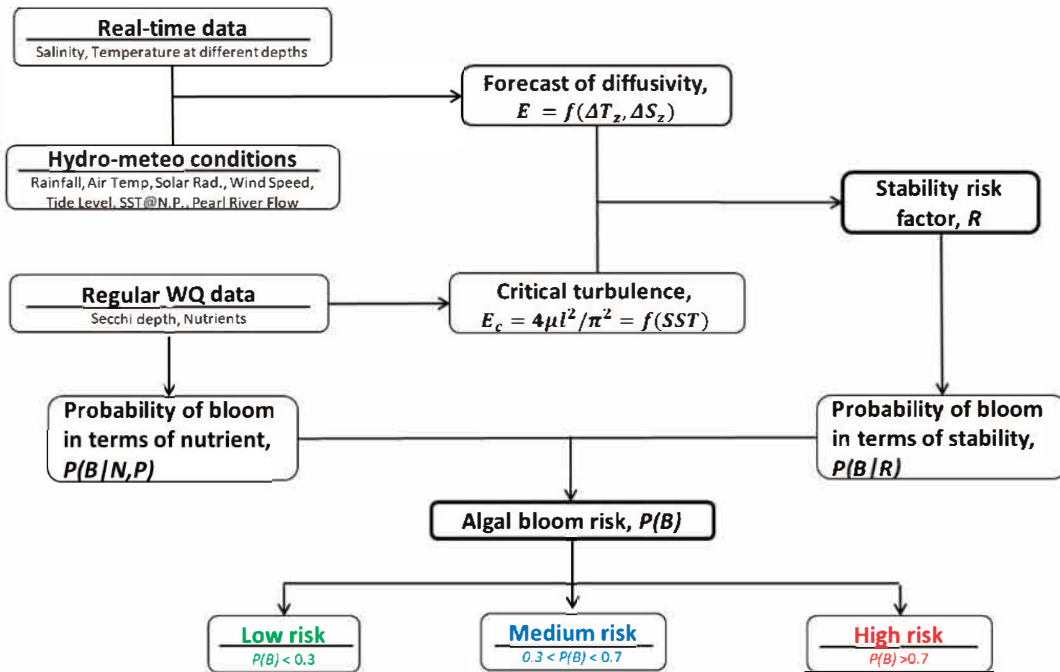


Fig. 1 Daily algal bloom risk forecast framework as a function of hydrodynamic stability risk factor and nutrient availability.

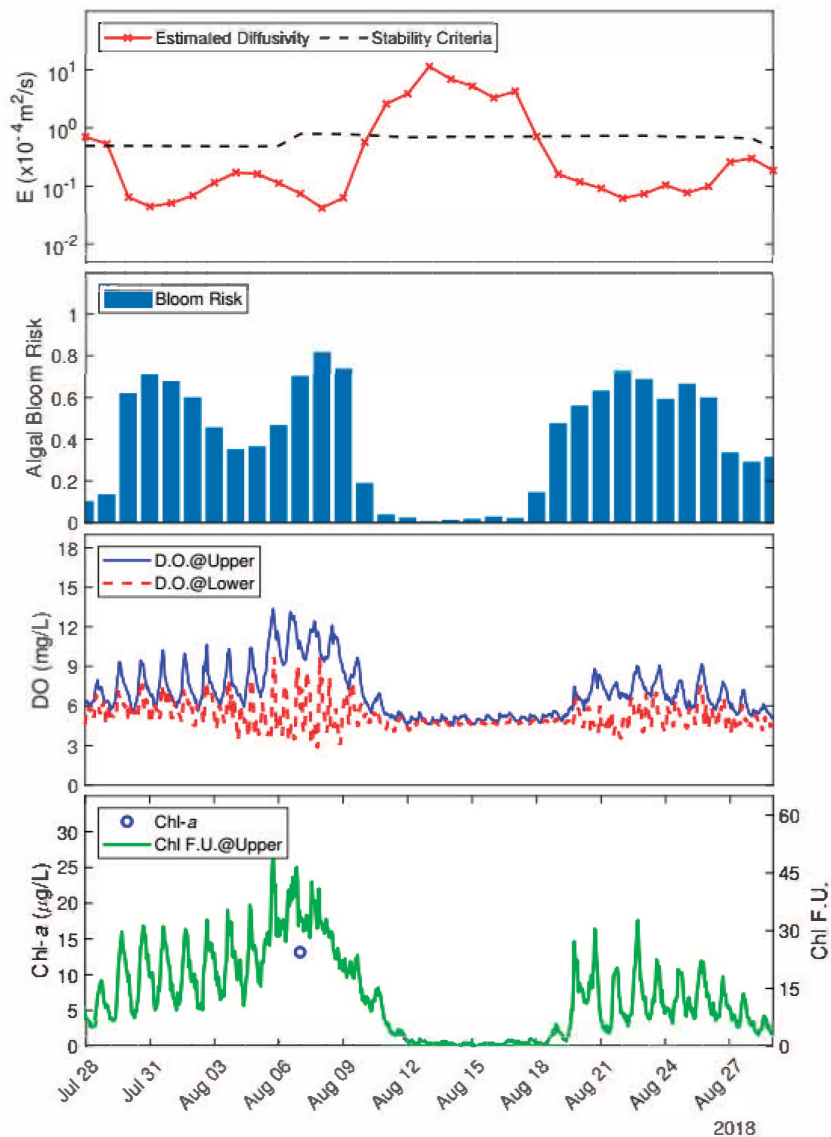


Fig. 2 Example of bloom risk forecast and field observation of a diatom bloom events at Lo Tik Wan FCZ (Causative species: *Chaetoceros salsubineum*; cell count on 7 Aug 2018: 5.96×10^6 cells/L)

**The 9th International
Symposium on
Environmental Hydraulics**

G1 Session

Computational Fluid Dynamics [G1-W1]



Numerical Study on the Hydrodynamics of a Vegetated Lateral Cavity

Luiz Oliveira¹, Taís Yamasaki¹, Johannes Janzen¹, Carlo Gualtieri^{2*}

¹ Engineering, Architecture and Urban Planning and Geography College, Federal University of Mato Grosso do Sul, Campo Grande, Brazil

² Department of Civil, Architectural and Environmental Engineering, University of Napoli Federico II, Naples, Italy

* Corresponding author: carlo.gualtieri@unina.it

Abstract

Lateral cavities are a type of transient storage zones that occur in riverine systems. They play an important role in mass transport processes, especially due to a higher residence time. In this study, a numerical simulation of flow past a lateral cavity with vegetation was performed to assess the impact of the vegetation on the cavity hydrodynamics. The vegetation drag was represented by an anisotropic Darcy-Forchheimer porous media model, as opposed to the traditional cylinder array method. The numerical model predicted well the flow behaviour in the vegetated cavity, showing that the porous media approach is suitable to represent vegetation in lateral cavities. In addition, these investigations build as a basis for further studies, such as the effect of vegetation on the mass exchange in lateral cavities or its effect on sedimentation rates.

Keywords: Lateral Cavity; Mass Exchange; Open Channel; Computational Fluid Dynamics (CFD).

Introduction

Lateral cavities are an important feature of rivers because they generate complex flow behaviours, such as recirculating flows, and thus create heterogeneity in the river section (Xiang et al., 2019). The cavities promote the transient storage of mass, the increase in biodiversity, enhanced sedimentation rates and vegetation growth (Jackson et al., 2013). The study of lateral cavities, especially in vegetated cases, is a new topic and its full characteristics are largely unknown. This abstract aims to present a tool to increase the knowledge in the area, reducing the embedded computational cost of Computational Fluid Dynamics (CFD) simulations of vegetated lateral cavities.

Methods

The studied geometry was based on the physical experiments of Xiang et al. (2019) (Case 2), which was used to validate our numerical model. The geometry consisted of a channel with an adjacent, rectangular cavity. The flow in the channel had a bulk flow velocity of $U = 0.101$ m/s, and it was completely turbulent ($Re = 9000$) and subcritical ($Fr = 0.102$). The lateral cavity aspect ratio was set as 0.6, which corresponds to a single circulation inside the cavity volume.

We solved the flow properties using a 3D LES solver (pimpleFOAM) coupled with the anisotropic Darcy-Forchheimer porous model available in OpenFOAM library, an open-source CFD code that solves Navier-Stokes equations via a finite volume method. The governing flow equations in the tensorial form are described as:

$$\frac{\partial \bar{u}_i}{\partial x_i} = 0 \quad \{ i = 1, 2, 3 \} \quad (1)$$

$$\frac{\partial \overline{u}_i}{\partial t} + \frac{\partial}{\partial x_j} (\overline{u}_i \overline{u}_j) = -\frac{1}{\rho} \frac{\partial \overline{p}}{\partial x_i} + \frac{\partial}{\partial x_j} [\mu(2\overline{S}_{ij}) - \tau_{ij}] + \overline{S}_{M,i} \quad (2)$$

$$\overline{S}_{M,i} = \left(-\mu d + \frac{\rho |u_{jj}|}{2} f \right) u_i \quad (3)$$

in which the overbar indicates resolved quantities. In Eq. (2), $\overline{S}_{M,i}$ is the sink term related to the vegetation drag (m/s^2), and it was calculated based on the Darcy-Forchheimer formulation of porous media, as shown in Eq. (3). The vegetation had density $\alpha = 0.1332 \%$. The flow was calculated using the WALE sub grid model.

Results

The flow simulation results show that a single circulation zone is present inside the volume and the flow velocity is at least 60% slower than the unaltered portion of the channel. As shown in Fig. 1, the centre of the vortex occurs at the middle of the cavity in the (y -axis) and has a peak in velocity at the shear layer between the main channel and the lateral cavity ($(y - y_0)/H = 0$). In the same picture the model followed closely the experimental data and wall-resolved LES from Xiang et al. (2019), with a maximum deviation, from the experimental values, of $0.0506 u/U$.

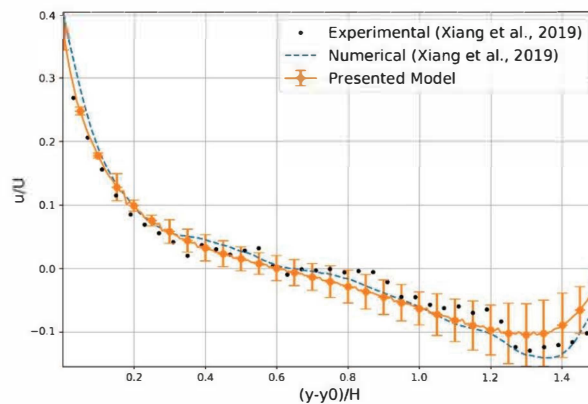


Fig. 1. Velocity distribution inside the lateral cavity volume, where $U = 0.101$ m/s is the bulk velocity, $y_0 = 0.30$ m is the beginning of the cavity and $H = 0.1$ m is the depth of the flow.

Conclusions

The results of this study show that the Darcy-Forchheimer model can represent vegetation drag in recirculation flows such as lateral cavities and groyne fields. The usage of this model represents an economical option for studying these flows as traditional approaches need for their solution larger computational resources.

Acknowledgement

This study was financed in part by the Coordenação de Aperfeiçoamento de Pessoal de Nível Superior - Brazil (CAPES) -Finance Code 001.

References

- Jackson, T. R., Haggerty, R., Apte, S. V. and O'Connor, B. L.: A mean residence time relationship for lateral cavities in gravel-bed rivers and streams: Incorporating streambed roughness and cavity shape, *Water Resour. Res.*, 49(6), 3642–3650, doi:10.1002/wrcr.20272, 2013.
- Xiang, K., Yang, Z., Huai, W. and Ding, R.: Large eddy simulation of turbulent flow structure in a rectangular embayment zone with different population densities of vegetation, *Environ. Sci. Pollut. Res.*, 26(14), 14583–14597, doi:10.1007/s11356-019-04709-x, 2019.

SPH simulation of vortex flow in open channel expansion

Chunli Wang¹, and S. Samuel Li^{1*}

¹ Department of Building, Civil & Environmental Engineering, Concordia University

*Corresponding: sam.li@concordia.ca

Keywords: Lagrangian simulation; Vortex dynamics; Flow separation; Channel expansion; Secondary flow

Abstract

Expansions commonly exist in natural river channels as well as in man-made open channels. Expansions connect a narrow channel section at upstream with a relatively wide channel section at downstream. In an expansion, the width of channel increases in the main flow direction. The flow emerges as a jet from the narrow channel and typically separates in the expansion from one or both of the sidewalls. Flow separation gives rise to vortices, violent turbulence, complex eddy motions, and vigorous fluid mixing. Persistent vortices and eddy motions can erode channel-boundary materials (sediments), leading to channel instability problems. This paper considers a horizontal, straight-wall expansion, and computes the vortex and eddy motions using the Smoothed Particle Hydrodynamics (SPH) approach. This approach has the advantage that no mesh is needed to calculate spatial derivatives in the governing momentum and mass conservation equations. These equations become sets of ordinary differential equations, and thus are simple to work with. The computational conditions match an available scaled laboratory model. The suitability of the laminar viscosity model and a sub-particle scale model for turbulence closure for the computations is assessed. The computational results include details about the temporal and spatial evolutions of turbulent eddies and vorticity distribution. The results are consistent with laboratory observations and capture the behaviours of subcritical flow in an expansion. This paper further investigates the effect of bottom geometric feature (humped bottom) on the reduction of flow separation. Proper values for the viscosity in SPH computations of expansion flow are discussed.

Acknowledgement

This work is supported by the Natural Sciences and Engineering Research Council of Canada (NSERC) through Discovery grant held by S. S. Li.

LES prediction of bistable flow in open-channel expansion

Rui Zeng¹ and S. Samuel Li^{1*}

¹Department of Building, Civil and Environmental Engineering, Concordia University
*Corresponding: sam.li@concordia.ca

Abstract

For a given set of hydraulic conditions, the flow in an open-channel expansion can exhibit either of two possible equilibrium stable states, depending on the flow history. The objective of this paper is to investigate the characteristics of bistable flow in the expansion using large eddy simulation (LES). This paper allowed for the influence of flow history by imposing three different initial conditions. The LES results agree well with experimental data. The spatial distributions of mean-flow velocity show two equilibrium states as a pseudo-mirror image of each other. The existence of bistable flow explains the presence of asymmetric flow patterns in a perfectly symmetric geometry. Fitting a hump at the channel bottom forces flow uniformity and symmetry about the channel centreline. The findings from this paper would help find strategies for flow energy conservation and channel-boundary erosion control. This paper contributes to an improved ability to predict bistable flow.

Keywords: Bistable flow; Large Eddy Simulation; Open-channel expansion; Flow separation

Introduction

Because of turbulent bistable flow (TBF), even if the geometry of an open-channel expansion is symmetrical about the centreline, the velocity profiles of either of the two stable equilibrium state are not. Previous studies of expansions have mostly focused on suppressing the flow separation near the sidewalls by improving their design, but none have addressed the question of flow bistability and asymmetry. The purpose of this paper is to present bistable flow characteristics using large eddy simulation (LES) and explore the usage of a hump to control bistability, and thus enhance the conveyance efficiency.

Methods

We simulated two-phase incompressible viscous three-dimensional (3-D) flow passing through two rectangular channel sections, connected by a straight-wall expansion. The simulations covered the case where the channel-bottom was flat as well as the case where the channel-bottom had a triangular hump. A summary of geometric, hydraulic, and numerical conditions of LES runs are shown in Table 1. In addition to the runs listed in table 1, sensitivity runs were carried out to test mesh and time independence.

Table 1 Hydraulic, numerical and geometric conditions of LES runs.

Run ID	Q (L/s)	h_o (cm)	h_e (cm)	U_o (cm/s)	Δt (s)	Node $\times 10^6$	Bottom	Initial condition
R2	10.23	18.57	18.81	32.2	0.006	2.56	Flat	(i)
R6	10.23	18.57	18.81	32.2	0.006	2.56	Flat	(ii)
R7	10.23	18.57	18.81	32.2	0.006	2.56	Flat	(iii)
R8	11.8	17.27	17.67	39.9	0.004	2.65	Hump	(i)

The governing equations are the Navier-Stokes momentum equation and continuity equation. The finite volume method implicitly yields filtered governing equations

$$\frac{\partial u_i}{\partial t} + \frac{\partial}{\partial x_j} (u_i u_j) = -\frac{1}{\rho} \frac{\partial p}{\partial x_j} + \frac{\partial}{\partial x_j} \left(\nu \frac{\partial u_i}{\partial x_j} + \tau_{ij} \right) + \rho g_i; \quad \frac{\partial u_j}{\partial x_j} = 0. \quad (1)$$

The subgrid stress τ_{ij} is treated using the Smagorinsky-Lilly model. The influence of flow history is investigated by imposing three different initial conditions (Table 1): (i) stagnant water column in the left expanding flank of the downstream channel, (ii) stagnant water column in the right flank, and (iii) stagnant water column in both the left and right flanks. Numerical model simulations matched the experiments of Najafi-Nejad-Nasser and Li (2015).

Results

The LES results of pressure and 3D velocity fields compare well with experimental data. R2 and R6 differ only in initial conditions (Table 1), and a comparison of the flow field between them reveals the influence of flow history on the equilibrium flow state (Figure 1). There exists flow separation with eddy motions of different sizes and strengths in the left and right sides of the channel. All the flow features of R6, such as flow separation and reversal, were just opposite of those of R2.

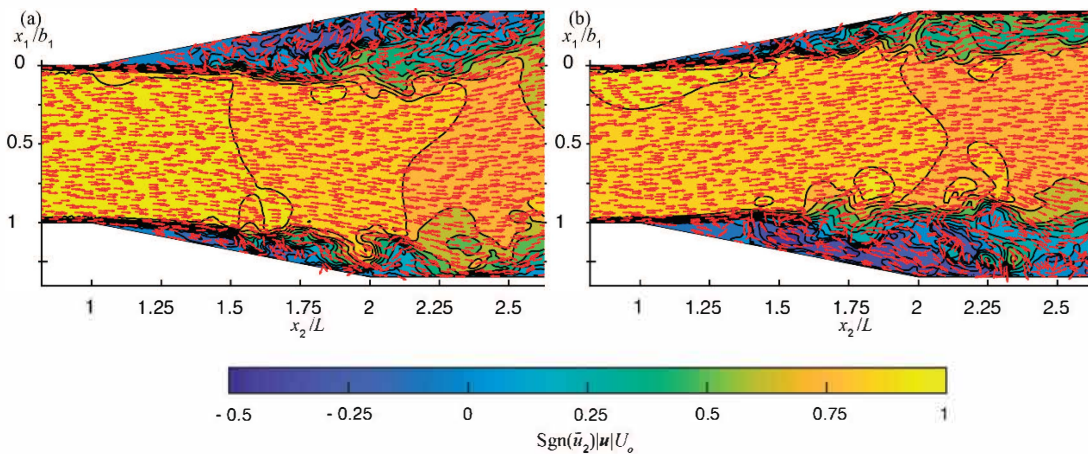


Fig. 1. Mean-flow velocity vectors at middle depth ($x_3 = 0.48h_0$) for Runs (a) R2 and (b) R6. Flow reversal occupied the areas of negative contour values

Conclusions

This paper presents LES predictions of TBF in a straight-wall expansion with or without a hump at the bottom. For a specified approach flow, two stable equilibrium flow states can possibly exist in the expansion depending on the flow history (initial condition). The two flow states are virtually mirror images of each other, in terms of velocity, pressure gradient and eddy patterns. This demonstrates flow bistability. Predictions of pressure and free-surface position compare well with laboratory experiments. Fitting a hump at the expansion's bottom reduces the area of flow reversal, separation and eddy motions, compared to the case of a flat-bottom expansion. It improves flow uniformity and channel stability.

References

Najafi-Nejad-Nasser, A., & Li, S. S. (2015). Reduction of Flow Separation and Energy Head Losses in Expansions Using a Hump. *Journal of Irrigation and Drainage Engineering* 141 (3): 1–9.

Numerical Investigation of air entrainment in a hydraulic jump

Byung Joo Kim¹ and Joongcheol Paik^{1*}

¹ Department of Civil Engineering, Gangneung-Wonju National University

*Corresponding: paik@gwnu.ac.kr

Keywords: Hydraulic jump, air entrainment, wall jet, numerical simulation

Abstract

The hydraulic jump at the inflow Froude number of 7.5 is typically classified as a steady jump which is stable, well-balanced, and insensitive to downstream conditions. Such hydraulic jumps are characterized by both intense eddy motions inside the jump roller and intense fluctuations of free surface, accompanied by high level of energy dissipation through the sudden transition from a supercritical flow to a subcritical flow. The interface between the jump roller and the shear layer near the bottom is also characterized by a trough void fraction due to the strong air entrainment at the jump toe. In this work, we numerically investigate the dynamical behaviors of turbulent flow in such hydraulic jump with the ratio of the downstream depth to the upstream inflow depth of 9.5 using a large-eddy simulation with a localized dynamic sub-grid scale model. A hybrid volume of fluid multiphase modeling approach is employed to simulate free surface fluctuations, air entrainment and bubble tracking, and the segregated and dispersed flow behaviors. The comparison of numerical results with available experimental observations obtained at the same flow configurations reveals that the present numerical simulation well reproduces the time-averaged vertical profiles of mean velocity, void fraction and turbulence intensity at the center of the jump roller as well as time-averaged free surface distribution with good agreement with the measurements. The present simulation elucidates the dynamic behaviors of coherent vortical structures consisting of local low pressure regions using flow visualization techniques. The intense unsteadiness of high and low pressure regions near the bottom is linked with the interactions of these vortical structures and the inverting vertical velocity fluctuations with the bottom wall.

Acknowledgement

This work was supported by the National Research Foundation of Korea (NRF) grant (2019R1A2C1090809) funded by the Korea government (MEST).

Implicit primal discontinuous Galerkin formulation for turbulent stresses in shallow water equations

Haegyun Lee^{1*} and Namjoo Lee²

¹Department of Civil & Environmental Engineering, Dankook University

²Department of Civil Engineering, Kyungsoong University

*Corresponding: haegyun@dankook.ac.kr

Abstract

Though the discontinuous Galerkin (DG) method has been widely applied as an effective numerical tool for hyperbolic conservation equations (such as shallow water equations (SWEs), compressible Navier-Stokes equations, etc.), one of the well-known drawbacks is its inconvenience in the treatment of second or higher derivative terms. So far, as a traditional approach, flux formulations have been applied in DG SWEs modeling. In this study, the BR2 (Bassi-Rebay 2) scheme, a well-known primal formulation in the DG community, was employed and combined with the implicit Euler backward difference scheme for SWEs. The developed model was applied to a few benchmark problems and good agreements were observed.

Keywords: Discontinuous Galerkin; Implicit scheme; Primal formulation; Shallow water equations; Turbulent stress

Introduction

The popularity of the discontinuous Galerkin (DG) methods is due to the high-order spatial accuracy on unstructured meshes and the characteristics of local conservation. These features are derived from the independent incorporation of basis functions and degrees of freedom (DOFs) in each cell. The DG methods can be said to be a natural choice for the solution of the hyperbolic equations, which encompass the compressible Euler equations, shallow water equations (e.g., Lee and Lee, 2016; Lee 2019), and so on. However, it might be challenging when extended to 2nd-order diffusion problems, such as turbulent stress terms in the above mentioned equations.

The issue on 2nd-order derivatives is related to the approximation of the numerical fluxes for the viscous terms and these have to be resolved as the discontinuities at the cell interface in a consistent manner. Among the several schemes, the second Bassi-Rebay (BR2, Bassi and Rebay, 2002) scheme was chosen in this study. In this paper, the primal DG formulation, BR2 is briefly described and a couple of case studies are provided with conclusions.

Implicit BR2 Formulations

Due to the discontinuities at the cell interface, the numerical fluxes should be employed for the SWEs. In this study, Roe numerical flux and BR2 (Bassi and Rebay, 2002) scheme are used for the convective fluxes and turbulent stresses, respectively. Additionally, for the efficient time marching, the backward implicit scheme is used in temporal discretization. Details can be found in Lee (2021).

Case Study

Two case studies are presented for the validation of the developed model. Both are known to have a practical importance and have been attempted in many studies. First one is the flow in the lateral contraction channel (Fig. 1). As a classical test, it was investigated experimentally by Ippen and Dawson (1951). As a second case, the partial dam-break flow is simulated (Fig. 2),

which was suggested by Fennema and Chaudhry (1990). In both cases, reasonable agreements are observed (Lee, 2021).

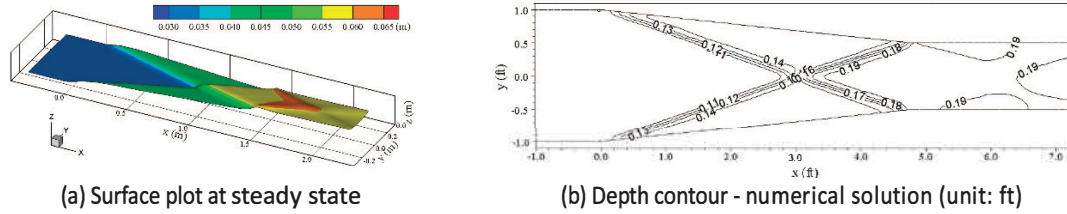


Fig. 1. Flow in a laterally contracting channel

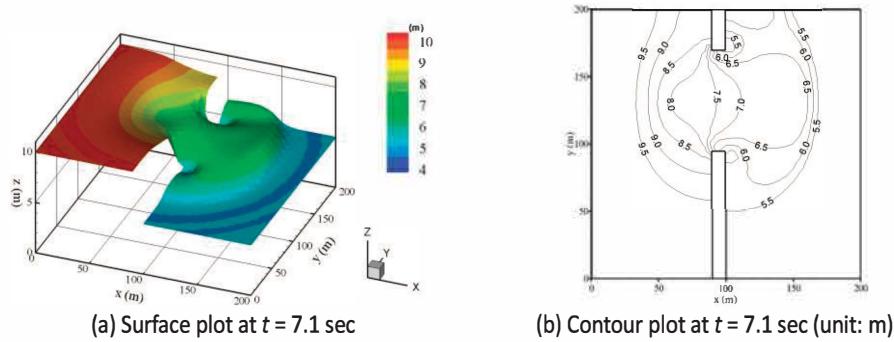


Fig. 2. Surface and contour plot at $t = 7.1$ sec.

Conclusions

As an implementation of the efficient BR2-based primal formulation, the Implicit Discontinuous Galerkin (IDG) method is proposed for the numerical modeling of the shallow water equations. The developed primal formulation was designed to overcome the drawbacks of the previous flux formulation (Lee and Lee, 2016; Lee 2019) and to serve as a good and improved alternative despite the additional burden by the increase in the coding effort. Much work remains to be done for future study.

Acknowledgement

This work was supported by Korea Environment Industry & Technology Institute (KEITI) through Aquatic Ecosystem Conservation Research Program, funded by Korea Ministry of Environment (MOE) (2020003050002).

References

- Bassi, F., & Rebay, S. (2002). Numerical evaluation of two discontinuous Galerkin methods for the compressible Navier-Stokes equations, *International Journal for Numerical Methods in Fluids*, 40, 197-207.
- Fennema, R.J. & Chaudhry, M.H. (1990). Explicit methods for 2-D transient free-surface flows, *Journal of Hydraulic Engineering*, 116, 1013-1034.
- Ippen, A.T., & Dawson, J.H. (1951). Design of channel contractions, high-velocity flow in open channels, *A Symposium Transactions, ASCE*, 116, 326-346.
- Lee, H. (2019). Implicit discontinuous Galerkin scheme for shallow water equations, *Journal of Mechanical Science and Technology*, 33, 3301-3310.
- Lee, H. (2021). Discontinuous Galerkin discretization of shallow water equations in implicit primal formulations for turbulent stresses, *Journal of Mechanical Science and Technology* (in press).
- Lee, H., & Lee, N. (2016). Wet-dry moving boundary treatment for Runge-Kutta discontinuous Galerkin shallow water equation model, *KSCE Journal of Civil Engineering*, 20, 978-989.

A numerical study on pressure fluctuations in free jump and submerged jump

Seongwook Choi¹, Sung-Uk Choi^{1*}

¹ Department of Civil & Environmental Engineering, Yonsei University

*Corresponding: schoi@yonsei.ac.kr

Keywords: pressure fluctuations, free jump, submerged jump, developed zone, k- ω SST model

Abstract

The flow over an embankment-type weir shows four different flow regimes depending on the tailwater level. They are swept-out jump, optimum jump, submerged jump, and washed-out hydraulic jump as the tailwater depth increases for a constant discharge. The optimum jump is the hydraulic jump in which the transition from the supercritical to subcritical flows occurs at the toe of the weir and is named like that because the efficiency of the energy dissipation is the best. The swept-out jump and the optimum jump are called the free jump. The domain of the hydraulic jump can be divided into developing zone, developed zone, transition zone, and open-channel flow zone, and the developed zone, in particular, shows an extremely complicated flow structure. The developed zone includes the wall-jet region and roller region above the wall-jet region. The flow, accelerated over the slope of the weir, ejects horizontally in the wall-jet region, and the strong re-circulation is generated and a significant amount of air is entrained through the water surface in the roller-region. The air entrainment and highly turbulent flow induces pressure fluctuations on the bed, and the pressure fluctuations are known to be responsible for severe damage of the bed. This study presents numerical simulations of both free jump and submerged jump of the flow over an embankment-type weir. The URANS equations are solved with the k- ω SST turbulence model. Special emphasis is placed on the computations of pressure fluctuations in the developed zone of the both jumps, and the mean value and RMS of pressure fluctuations are provided. The computed pattern of the pressure fluctuations is confirmed by comparisons with measured data. The impact of submergence of the hydraulic jump on the pressure fluctuations is given and discussed.

Acknowledgement

This work is supported by the National Research Foundation of Korea (NRF) grant funded by the Korea Government (NRF2017R1A2A2A05069836).

**The 9th International
Symposium on
Environmental Hydraulics**

G2 Session

Shallow Water Flows [G2-W2]



High order method for shallow water flows over irregular topography with vegetation

Jaeyoung Jung¹ and Jin Hwan Hwang^{1*}

¹Department of Civil & Environmental Engineering, Seoul National University

* Corresponding: jinhwang@snu.ac.kr

Keywords: Porous shallow water equations; Riemann problem; Finite volume methods

Abstract

The present study proposes a numerical method for solving shallow water equations with irregular topography and vegetated field. Introducing the concept of porosity into traditional shallow water equations, we revisited porous shallow water equations, and which lead to considerable computational saving by simplifying complexity of fluid-vegetation interactions into sub-grid model based on the concept of porosity. Since the governing system is non-strictly and nonlinear hyperbolic system, we faced two difficulties in implementing a stable numerical solver. Firstly, multiply solutions may be arisen, and which lead to the ill-posed problem. Secondly, discontinuity can be arisen even if the initial conditions are continuous. To overcome those problems, we investigate the structures of exact solutions to Riemann problems of porous shallow water equations. And we reflect those structures in the algorithm of the numerical scheme so that numerical model can properly approximate the exact solutions. Specifically, stationary wave reconstruction is applied, and which make it possible to treat the geometric discontinuities stably. Moreover, high order accuracy is obtained by using the 5th order weighted essentially non-oscillatory method for spatial reconstruction and the 3rd order Runge-Kutta scheme for temporal integration. Extensive numerical experiments were carried out to verify our numerical code and showed good agreements with analytical solutions.

Acknowledgement

This research was funded by National Research Foundation of Korea (NRF) grant funded by Korean Government Ministry of Science, ICT & Future Planning (No. 2020R1A2B5B01002249), and administratively supported by the Institute of Engineering Research at the Seoul National University

Optimal layout of a tidal fence in a rectangular channel flow

Jisu Han¹, Jaeyoung Jung², and Jin Hwan Hwang^{2*}

¹Department of Earth and Environmental Engineering, Columbia University in the city of New York

²Department of Civil & Environmental Engineering, Seoul National University

* Corresponding: jinhwang@snu.ac.kr

Keywords: PDE-constraint optimization; Quasi-global optimum; Shallow water equations;

Abstract

The present study investigates the features of an optimal tidal array using OpenTidalFarm, an open-source code for the gradient-based optimization problem with the partial differential equation constraint. A tidal strait is modeled as a shallow rectangular channel encompassing the farm site to an inner rectangular zone. Shallow water equations were solved to generate the flow field. The amount of energy harvested by the turbines was simulated as a bottom friction function. The complexity involved in identifying a global optima prompted us to introduce the concept of quasi-global optimum (QGO), which makes it possible to save considerable computational costs by utilizing a local optimum as a surrogate for the true global optimum. From intensive numerical experiments, we found that the shape of an optimal array is largely dependent on the initial layout of the farm. A non-dimensional parameter, E ; which is a function of optimization constraints (OC) such as the minimum turbine distance and farm site width, was proposed to elucidate the propensity of the QGO layout. The shape of the QGO was a linear barrage until E reached to 1 and evolved into a downstream-convex parabola and subsequently into a sharp “V” shape as E increases beyond 1. As more turbines were added to an array, the QGO was no longer a single barrage, and the turbines were separated from the barrage depending on the values of OC. We also showed that tuning the design constraints can significantly enhance the power output (up to 50%) for the same number of turbines deployed.

Acknowledgement

This research was funded by National Research Foundation of Korea (NRF) grant funded by Korean Government Ministry of Science, ICT & Future Planning (No. 2020R1A2B5B01002249), and administratively supported by the Institute of Engineering Research at the Seoul National University

Development of 1-dimensional river hydraulic model (K-River)

Yeonsu KIM¹, Youngteck Hur¹, Junwoo Noh¹, Hyunuk An^{2*}

¹K-water research institute, Daejeon, KOREA

²Local Environmental Engineering Department, Chungnam National University, Daejeon,
KOREA

* Corresponding: Hanlight20@hotmail.com

Keywords: 1D Hydraulic model; River; Discontinuous flow; Finite volume method

Abstract

There are a large number of weirs installed in rivers of Korea, and these characteristics are not common in other countries. When the flow passes through a structure such as a weir, discontinuous flow occurs. In terms of numerical simulation, it affects the numerical instability due to the balance between the flow term and the source term. In order to solve these problems, many researchers used empirical formulas or numerical scheme simplification. Recently, researches have been conducted to use more accurate numerical scheme. K-River was developed to reflect the characteristics of domestic rivers and calculate the discontinuous flow more accurately. For the verification of K-River, 1) numerical experiment simulations with a bump in the bed, 2) laboratory experiment of hydraulic jump simulation, 3) real river were performed. K-River verified its applicability by simulating results similar to the exact solution and observed value in all simulations.

Simulations of pollutant storage effects within emergent vegetation using particle dispersion model

Inhwan Park^{1*}, Sunmi Lee¹, Sanha Kim¹, and Taewon Yoon¹

¹Department of Civil Engineering, Seoul National University of Science and Technology

*Corresponding: ihpark@seoultech.ac.kr

Abstract

Particle tracking simulation was conducted using the PDM-2D to reproduce mixing behaviors under the partly vegetated flow. The model calculates two-dimensional solute mixing adopting vertical profiles of velocity instead of using the Fickian dispersion models following the Fick's law. In this model, vertical velocity profiles were generated using the power-law and the log-profile, respectively, for the emergent vegetation and the non-vegetated regions. The simulation results show that the bifurcation of the solute cloud due to solute trapping by the vegetation patch. The results indicate that the model adequately reproduced the storage effects caused by the velocity defects within vegetation patch.

Keywords: Pollutant mixing; Emergent vegetation; Storage zone; Particle dispersion model; Fickian dispersion model

Introduction

Predictions of solute mixing behaviors are important to protect aquatic environment from water pollution accidents. Damage mitigation plans for water pollution accidents could be more precisely established by obtaining the details of arrival, retention time, and concentration of those pollutants. However, in vegetated flow, accurate predictions of mixing behaviors using the Fickian dispersion models become difficult due to the deformation of vertical velocity structures. Thus, in this study, the solute mixing simulations in emergent vegetation conditions were conducted using the two-dimensional Particle Dispersion Model (PDM-2D), which calculate the shear dispersion from vertical profiles of velocity instead of using the Fickian dispersion models (Park et al., 2018). In this model, shear flow was reproduced using the power-law and the log-profile, respectively, for the emergent vegetation and the non-vegetated regions.

Methods

In this study, solute transport simulation was conducted under the partly vegetated flow referring to the study of Västilä et al. (2019) where the flow analysis was conducted near vegetation patch having 4 m length and 1.5 m width. Under the vegetated flow, particle tracking simulation was conducted using PDM-2D in which the governing equation is given as below.

$$x_i(z_1, t + \Delta t) = x(z_1, t) + u_i(z_1)\Delta t + R\sqrt{2\varepsilon_h\Delta t} \quad (1)$$

$$x_i(z_2, t + \Delta t) = x(z_1 + R\sqrt{2\varepsilon_z\Delta t}, t + \Delta t) \quad (2)$$

where x_i is the particle position; u_i is the flow velocity; z_1 and z_2 are vertical position of a particle at time t and $t + \Delta t$, respectively; $\varepsilon_h = \alpha_h hu^*$ and $\varepsilon_z = \alpha_z \sqrt{kd}$ are horizontal and vertical diffusion coefficient, respectively; k is the turbulent kinetic energy; d is the stem diameter; R is the random number following the Gaussian distribution. The detailed

simulation conditions were give as following table. The value of α_z has been suggested as 0.9 for the emergent vegetation condition (Nepf, 1999).

Table 1. Simulation conditions of solute transport in partly vegetated flow.

Flowrate, Q (m^3/s)	Depth, h (m)	Stem diameter, d (m)	α_h	α_z	No. of particles
1.0	0.93	0.04	0.15	0.9	10000

Results

The particle tracking simulation results were presented in Fig. 1. The solute clouds were shown with bottom elevation contours of a channel having trapezoidal cross-section. The simulation results show distinct features that the solute cloud was bifurcated by the solute trapping of vegetation patch. The resistance due to the vegetation patch leads to decrease of mean flow velocity and increase of vertical diffusivity. Thus, the shear dispersion decreases within the vegetation patch, and the difference of those mixing properties to the non-vegetated area induced non-Fickian mixing behaviors.

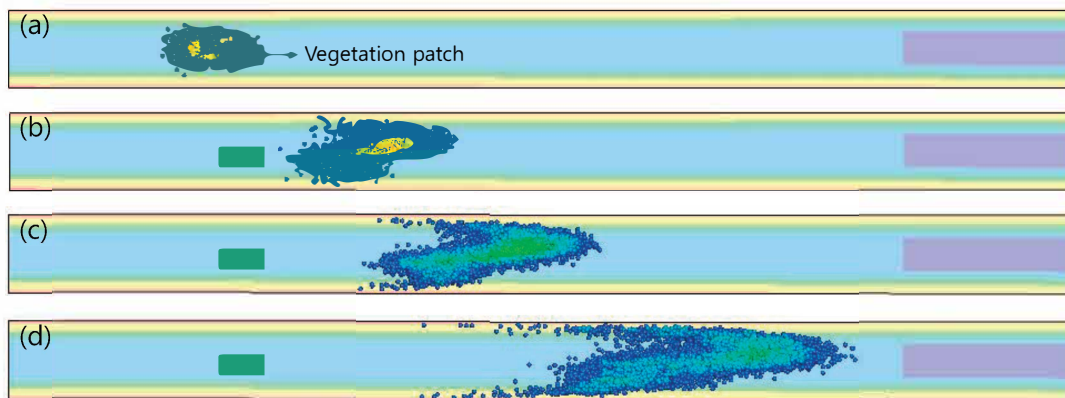


Fig. 1. Particle tracking simulation results in partly vegetated flow: (a) Time = 40 sec; (b) Time = 90 sec; (c) Time = 140 sec; (d) Time = 200 sec

Conclusions

The particle tracking simulation was conducted using the PDM-2D in the partly vegetated flow. For the simulation, in the emergent vegetation patch, shear flow was reproduced using the power law, and the vertical diffusion induced by turbulence was adopted. According to the theoretical interpretations, shear dispersion in vegetation reduces due to the decrease of mean velocity gradient by the increase of the vertical diffusivity. The simulation results were adequately reproduced the aforementioned physical analysis and the solute trapping due to the vegetation patch.

Acknowledgement

This study was supported by the Research Program funded by the SeouTech (Seoul National University of Science and Technology).

References

- Nepf, H. M. (1999). Drag, turbulence, and diffusion in flow through emergent vegetation. *Water Resources Research*, 35(2), 479-489.
- Park, I., & Seo, I. W. (2018). Modeling non-Fickian pollutant mixing in open channel flows using two-dimensional particle dispersion model. *Advances in Water Resources*, 111, 105-120.
- Västilä, K., Lee, C., Kim, D., Kim, S., Kim, J. & Järvelä, J. (2019). Measurement of lateral and wake flows associated with stream-scale willow patches. *Proceedings of the 38th IAHR World Congress*, Sep. 1-6, Panama City, Panama.

Development of GPU-Accelerated 2DH Hydrodynamic and Transport Model

Sooncheol Hwang¹ and Sangyoung Son^{1*}

¹ School of Civil, Environmental and Architectural Engineering, Korea University

*Corresponding: sson@korea.ac.kr

Keywords: GPU acceleration; Boussinesq-type model; Advection-diffusion equation; Scalar transport model

Abstract

This paper describes a two-dimensional depth-integrated hydrodynamic and a passive scalar transport model based on the GPU-accelerated Boussinesq model, called Celeris. Celeris is the first Boussinesq-type wave solver with an interactive simulation environment using a graphical user interface. The interactive environment enables a user to alter the water surface, the bottom topography and model parameters even as calculations are in progress. It also visualizes the simulation results simultaneously so the user can check the results without data post-processing. This study couples the extended Boussinesq equations with the depth-averaged advection-diffusion equation to simulate the scalar transport. The 2DH advection-diffusion equation was discretized numerically using a hybrid finite volume-finite difference method in the same manner as the governing equations in Celeris. The advective flux term is discretized using FVM while the diffusive term is discretized using FDM. Besides, an eddy viscosity model describing energy dissipation due to wave breaking was implemented in the model, and an eddy diffusivity associated with the eddy viscosity was considered in the diffusive term. Four benchmark tests were carried out to validate the developed model. Two analytical cases in one-dimensional and two-dimensional flow conditions were conducted, and the computed results showed very close agreements with negligible numerical diffusion. Next, a vortex shedding in a wake behind a submerged island and a dye transport caused by this was numerically reproduced, and reasonable agreement was observed from the comparison. Finally, dye transport due to a solitary wave propagating along irregular bathymetry was investigated. The computed results showed good agreement with the experimental data. Also, the eddy viscosity model was additionally validated since this experiment included the effects of wave breaking. The modeled results showed that the maximum surface water level decreased as the eddy viscosity model was implemented.

Acknowledgement

This work is supported by the National Research Foundation of Korea (NRF) grant (NRF-2019R1A2C1089109).

Application of an unsteady-flow water quality model to determine required deicing fluid reduction at Memphis International Airport

Charles S. Melching^{1*} and Chuck Pace²

¹Melching Water Solutions LLC, Greenfield, WI, U.S.

²EA Engineering, Science and Technology, Hunt Valley, MD, U.S.

*Corresponding: steve.melching17@gmail.com

Keywords: Deicing fluid, Dissolved Oxygen, Biochemical oxygen demand, Pollution control

Abstract

The application of deicing fluids and anti-icing fluids (hereafter deicing fluids) to aircraft and paved surfaces, respectively, at Memphis International Airport (MEM) places an additional biochemical oxygen demand (BOD) on the receiving streams. These fluids flow unhindered through the airport drainage system to two short streams—Hurricane Creek and Days Creek. Within a few hours the flow from these creeks reaches Nonconnah Creek and the deicing fluids must travel 13 km through Nonconnah Creek to McKellar Lake, which is an oxbow lake of the Mississippi River. During periods when the water level in the Mississippi River is low the deicing fluids pass through Nonconnah Creek in less than a day and then their concentrations are greatly dissipated by the massive flows of the Mississippi River. However, when the Mississippi River is at high levels the traveltime in Nonconnah Creek is greatly increased and the BOD load can affect the dissolved oxygen (DO) resources of Nonconnah Creek. The Mississippi River is prone to high levels in the winter and spring which also is the period when deicing fluids are applied at the airport. So, MEM was required by the State of Tennessee to study the effects of deicing fluids on Nonconnah Creek and to develop a management plan for deicing fluids. An intensive field survey of flow, BOD, and DO was done for the three creeks for 5 deicing events from November 2014 through January 2016. The deicing events of March 4, 2015 and January 22, 2016 resulted in measured DO concentrations less than the 5 mg/L standard. The DUFLOW model was calibrated for flow, BOD, and DO for the combined effects of deicing events on February 16 and 22 and March 4, 2015, and it was tested for the deicing event of January 22, 2016. The DUFLOW model then was applied to determine the allowable loads of BOD for the March 4, 2015 and January 22, 2016, events that would keep the DO concentration in Nonconnah Creek at or above the DO standard. Because these events also involved substantial backwater from the Mississippi River, a relation between the allowable BOD load and Mississippi River water level was developed. The ten largest applications of deicing fluids between 2006 and 2016 were compiled together with the highest water level on the Mississippi River for each of these events. It was found that if a 25% reduction of the BOD load was applied 9 of the 10 events would move into the safe region of the BOD load vs. water level relation. The once in 10 years frequency of BOD loads above the acceptable range was deemed acceptable by the

State of Tennessee and MEM is currently installing deicing pads to achieve the 25% reduction goal.

The 9th International
Symposium on
Environmental Hydraulics

G3 Session

Open Channel Hydraulics [G3-W3]



Numerical Investigation on Turbulence Structure over Backward-Facing Step for Various Step Angles and Reynolds numbers

Jeonghu Lee^{1*} and Van Thinh Nguyen²

^{1,2}Department of Civil & Environmental Engineering, Seoul National University

*Corresponding: tmflvl3@snu.ac.kr

Abstract

Backward Facing Step (BFS) flows have been widely investigated due to its significant roles in abundant natural and engineering flow systems. This study carries out several 2D RANS (Reynolds averaged Navier Stokes equation) numerical simulations for BFS geometry under various step angles and Reynolds numbers, in order to investigate the reattachment length and wall shear stress distribution behind the step. The gradually increasing step angles and Reynolds number result in the reattachment length located further from the step up to a certain threshold in each case. The skin friction distribution calculated in the vicinity of bottom behind the step indicates that the minimum wall shear stress occurs just in front of the reattachment point, and its minimum value becomes larger as the step angle increases.

Keywords: BFS; RANS; Reattachment length; Wall shear stress

Introduction

Flow over BFS has been considered as a representative case study for separation flows in abundant natural and engineering flow systems. Among a lot of significant factors over BFS, the location of the reattachment zone and its flow structure play an important role in design of flow systems. Although there were a number of numerical and laboratory experiments to investigate the flow over BFS (as reviewed by Chen et al., 2018); such as flow separation, reattachment length, etc.; most of the previous studies were focused on the right angle step only. For the reattachment length, it showed that the reattachment length increases gradually as Reynolds number and step angle become larger; and it tends to be constant from a certain Reynolds number and step angle. However, the turbulence characteristics depending on the various Reynolds numbers and step angles has barely been investigated. In this study, several numerical simulations of the flow over the BFS were conducted and validated against the observation data (Ruck and Makiola, 1993) to verify turbulence structure in terms of wall shear stress distribution in the vicinity of the bottom behind various step angles.

Methodology

This study is to numerically investigate the flow pattern and turbulence structure of the flow over BFS with various step angles and Reynolds numbers, as shown in Table 1.

Table 1. Parameters of experimental cases (Ruck and Makiola, 1993)

Step Angle(°)	Expansion Ratio	Reynolds Number
10, 15, 20, 25, 30, 45, 90	2	15000, 47000, 64000

The expansion ratio is the ratio of outlet thickness to the inlet thickness in the BFS geometry and the Reynolds number is based on the maximum velocity on the step edge and inlet thickness. The flow properties over the BFS are resolved using RANS with $k-\omega$ turbulence closure model by an open source CFD software, OpenFOAM. The reattachment length is found where the sign of the velocity near the bottom is switched from minus to plus behind the step and normalized by the step height h_s . The wall shear stress τ_b over the bottom is also

measured numerically and presented as the skin friction C_f which is calculated as $\frac{\tau_b}{0.5U_o^2}$ where U_o denotes the maximum streamwise velocity on the step edge.

Results

It shows that the reattachment length tends to be a constant when the step angles is larger than 30° and it is no longer dependent on the Reynolds number as shown in Fig. 1. Based on the well calibrated simulation configuration, the wall shear stress distributions presented by skin friction (C_f) can be calculated and compared at various step angles. The results of the skin friction on the the bottom reveal that the minimum skin friction occurs in the front of the reattachment point, where the skin friction value becomes zero, for all the step angles ($10^\circ \sim 90^\circ$) as shown in Fig. 1(b). In addition, it turned out the minimum value of the skin friction gradually decreases as the step angle increases.

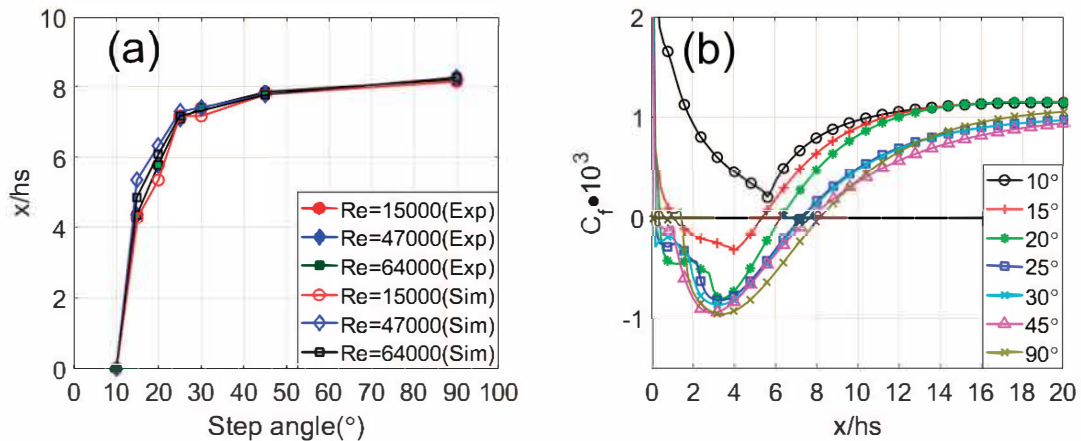


Fig. 1. Comparison of the reattachment lengths between the results by RANS and the observation data (Ruck and Makiola, 1993) as a function of step angle for $Re > 15,000$, $ER=2$ (a), Mean skin friction as a function of the normalized distance for $ER=2$, $Re=47000$ (b)

Conclusions

The results of this study reveal that the reattachment length behind the step in BFS flow increases as the step angle and Reynolds number increase, and it converges to a constant length from a certain threshold value. The wall shear stress distribution on the bottom behind the step, presented by the skin friction, is calculated differently based on the different step angles. The minimum value of the skin friction is found larger as the step angle increases.

Acknowledgement

This study is supported by the BK21(4th) grant funded by the National Research Foundation (NRF) and the National Research Foundation of Korea grand funded by the Korean Government (NRF-2020R1A6A3A13076720).

References

- Chen, L., Asai, K., Nonomura, T., Xi, G., & Liu, T. (2018). A review of Backward-Facing Step (BFS) flow mechanisms, heat transfer and control. *Thermal Science and Engineering Progress*, 6, 194-216.
- Ruck, B., & Makiola, B. (1993). Flow separation over the inclined step. In *Physics of Separated Flows—Numerical, Experimental, and Theoretical Aspects* (pp. 47-55). Vieweg+ Teubner Verlag, Wiesbaden.

Development of Two-Dimensional River Flow Analysis Model Using Godunov's Scheme and TVD Limiter

Eun Taek Shin¹, Chang Geun Song^{1,*}

¹Department of Safety Engineering, Incheon National University, Academy-ro 119, Incheon, ROK

* Corresponding: baybreeze119@inu.ac.kr

Abstract

Most natural disasters in Korea are water-related consequence. In particular, river flooding due to extreme rainfall occurs frequently, causing severe damages. In order to prevent and respond to such disasters in advance, it is very important to predict and interpret the flow of rivers. Current river flow analysis framework is mostly dependent on one-dimensional model because of its macroscopic capability to the long span including the main stream and tributaries. Although one-dimensional flow analysis model has an advantage in short calculation time, it cannot reflect the detailed topography in natural rivers accurately, and is also unable of predicting the varying flow phenomena along the transverse direction. Such being the case, two-dimensional flow analysis model is an alternative to analyze the detailed motion of water movement near the confluence or major rivers with wide width. In particular, wet and dry problems in natural rivers and rapid flows around structures are still challenging issues in two-dimensional flow analysis. To solve this problem, we developed a two-dimensional flow model using the Godunov scheme and the TVD limiter to obtain stable and accurate results. The flow rates were checked with the Riemann's solutions, and it provided reliable results in various discontinuous flow problems.

Keywords: wet/dry; natural river; Godunov method; Riemann's problem; river flow

Introduction

Since the existing flow analysis should reflect river information of wide terrain, the flow analysis was performed through the one-dimensional flow analysis model. However, in the case of severe curvature of the river, such as the meandering river, the accuracy of the flow analysis is poor. Therefore, in order to solve this problem, a two-dimensional flow analysis model that reflects the actual river shape is necessary. In natural streams, shock waves generated by the collapse of dams and embankments can occur, and transition flow and hydraulic jump can occur due to separation of flow zones. In addition, various flow characteristics such as wet/dry problems and discontinuous flows due to the flood volume are challenging problems. To solve these problems, we applied the Godunov method, one of the Riemann's solutions, and the TVD limiter to provide stable and accurate results in the two-dimensional river flow analysis modeling.

Methods

The shallow water equations, which can be obtained from the depth-averaged Reynolds equations, are known to be useful in interpreting shock waves in the river flow that can occur in natural phenomena. Consider the two-dimensional shallow water equations

$$\mathbf{U}_t + \mathbf{F}(\mathbf{U})_x + \mathbf{G}(\mathbf{U})_y = \mathbf{S}(\mathbf{U}) \quad (1)$$

where the vectors of conserved variables and fluxes are

$$U = \begin{bmatrix} h \\ hu \\ hv \end{bmatrix}, F = \begin{bmatrix} hu \\ hu^2 + \frac{1}{2}(gh^2) \\ huv \end{bmatrix}, G = \begin{bmatrix} hv \\ huv \\ hv^2 + \frac{1}{2}(gh^2) \end{bmatrix}, S = \begin{bmatrix} 0 \\ ghS_{ox} - ghS_{fx} \\ ghS_{oy} - ghS_{fy} \end{bmatrix} \quad (2)$$

We used the Godunov type finite volume method to solve the two-dimensional shallow water equation. Godunov's scheme is a conservative numerical scheme for solving Riemann problems at each inter-cell boundary (Toro, E. F., 1999). We applied the MUSCL scheme for second-order accuracy in terms of time and space, and used TVD methods to avoid the expected spurious oscillations (B. van Leer., 1985).

Results

We simulated the dam collapse experiment for verification of the flow analysis model (Fraccarollo and Toro, 1995). Through this, it is possible to evaluate the model performance of capturing shock waves property, which included the numerical instability observed in the dry bed. In addition, the results of other studies and the results of the developed model were compared, and as a result, it was confirmed that the shock waves generated at the time of the dam collapse were better captured.

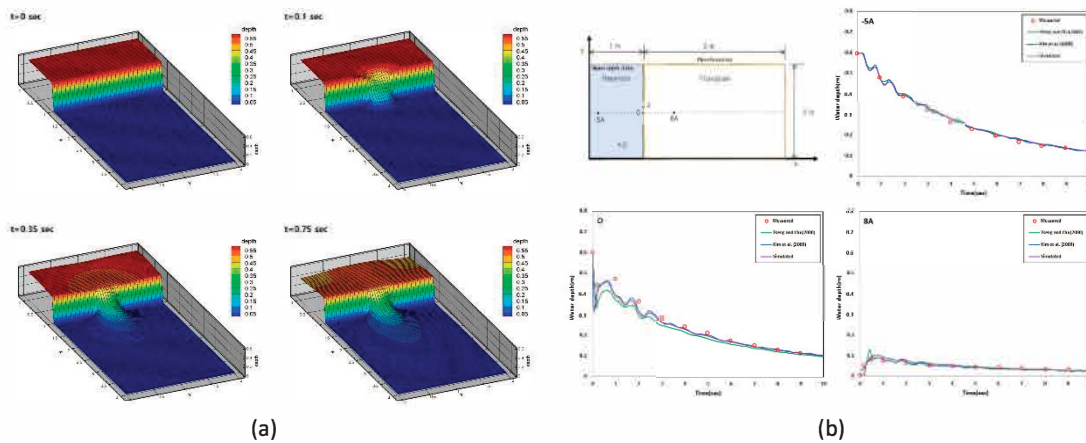


Fig. 1. Flow depths by dam collapse problem (a) and comparisons with measurements (b).

Conclusions

This result shows that among the basic performances that the flow analysis model should have, it is possible to analyze shock waves occurring near the discontinuous region. However, in physical sense, various conditions such as irregular bed and external environment changes frequently occur. Therefore, in the future, more verifications and validations will be conducted to have the model equipped with robustness and generality.

Acknowledgement

This work is supported by the Korea Agency for Infrastructure Technology Advancement(KAIA) grant funded by the Ministry of Land, Infrastructure and Transport (Grant 21DPIW-C153746-03).

References

- Toro, E. F. (1999). *Riemann Solvers and Numerical Methods for Fluid Dynamics*. Berlin: Springer-Verlag. ISBN 3-540-65966-8.
- B. van Leer. (1985). On the Relation between the Upwind-Difference Scheme of Godunov, Enguist-Osher and Roe. *SIAM J. Sci. Stat. Comput.*, 5(1):1-20
- Fraccarollo, L., and E. F. Toro (1995). Experimental and numerical assessment of the shallow water model for two-dimensional dam-break type problems, *J. Hydraul. Res.*, 33, 843–864

Flow-3D CFD Model of Bifurcated Open Channel Flow: Setup and Validation

Nur Adani Adnan^{1*}, Izihan Ibrahim¹ & Saerahany Legori Ibrahim¹

Department of Civil Engineering, International Islamic University Malaysia

*Corresponding: adaniadnan@gmail.com

Abstract

Bifurcation is a morphological feature present in most of fluvial systems; where a river splits into two channels, each bearing a portion of the flow and sediments. Extensive theoretical studies of river bifurcations were performed to understand the nature of flow patterns at such diversions. Nevertheless, the complexity of the flow structure in the bifurcated channel has resulted in various constraints on physical experimentation, so computational modelling is required to investigate the phenomenon. The advantages of computational modelling compared with experimental research (e.g. simple variable control, reduced cost, optimize design condition etc.) are widely known. The great advancement of computer technologies and the exponential increase in power, memory storage and affordability of high-speed machines in the early 20th century led to evolution and wide application of numerical fluid flow simulations, generally referred to as Computational Fluid Dynamics (CFD). In this study, the open-channel flume with a lateral channel established by Momplot et al (2017) is modelled in Flow-3D. The original investigation on divided flow of equal widths as simulated in ANSYS Fluent and validated with velocity measurements.

Keywords: Bifurcation, Open Channel Flow, CFD, Numerical modelling, Flow-3D, Ansys Fluent.

Introduction

Divided or bifurcated flow is very complex and highly three dimensional especially in the vicinity of the junction (Ramamurthy et al, 2007). The prediction of flow in open channel flow is extremely difficult because it is transient and turbulent, mostly occurring in irregular and curved geometry, and the elevation of the free surface varies with time (Kamel, Ilhem, Ali & Abdelbaki, 2014). As such, physical experimentation is a rigid and unwieldy method to investigate open channel flow, and CFD is now preferred to simulate the fundamental physical equations that characterize flow in the channel. The aim of the present paper is two folds is to compare simulated streamwise velocities in the lateral channel of bifurcated open channel flows in Flow-3D CFD model with measurements of Momplot et al. (2017)

Methods

The flume setup in Flow-3D CFD model replicates the work of Momplot et. al. (2017) as shown in Fig. 1. The inlet discharge was set at 0.004 m³s⁻¹. The baffles were placed at the downstream ends of main and lateral channels at 0.098-m high to represent the outflow weirs of equal heights (Fig. 1). The numerical simulations are highly dependent on the computational domain size as well as grid point density and distribution. If not properly considered, they may affect the accuracy of the numerical result (Bonakdari, Kouyi & Wang, 2011). In this paper, three sets of mesh sizes (820,443 cells; 946,665 cells at refinement area; 1,014,300 cells) have been established to assess model sensitivity. The numerical simulations are performed using the CFD software Flow-3D. Three types of turbulence model (RNG turbulence model; k-e turbulence model; k-w turbulence model) are tested in this study based on the work of Momplot et al. (2017).

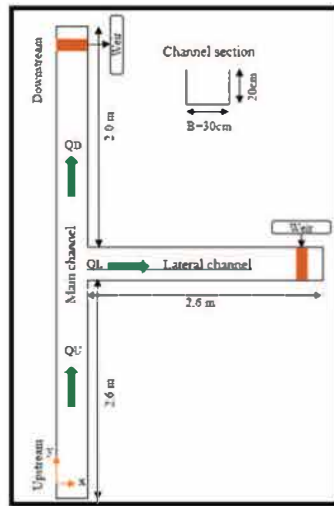


Fig. 1 Flume geometry setup in Flow-3D CFD model

Results

In this paper, the numerical modelling in Flow-3D is performed to investigate velocity distributions in the lateral channel at locations $x/B=2.5$ and the elevations at $z=0.09$ m. Fig. 2a shows the results of Flow-3D simulations (velocities in the lateral channel) utilizing the three available turbulence models, as compared with 2D PIV measurements by Momplot et al. (2017). For these model runs, the mesh size is fixed at 946,665 cells as refined within the bifurcation area. Fig. 2b portrays the comparison between measurements with Flow-3D results, using RNG turbulence model, for different mesh sizes.

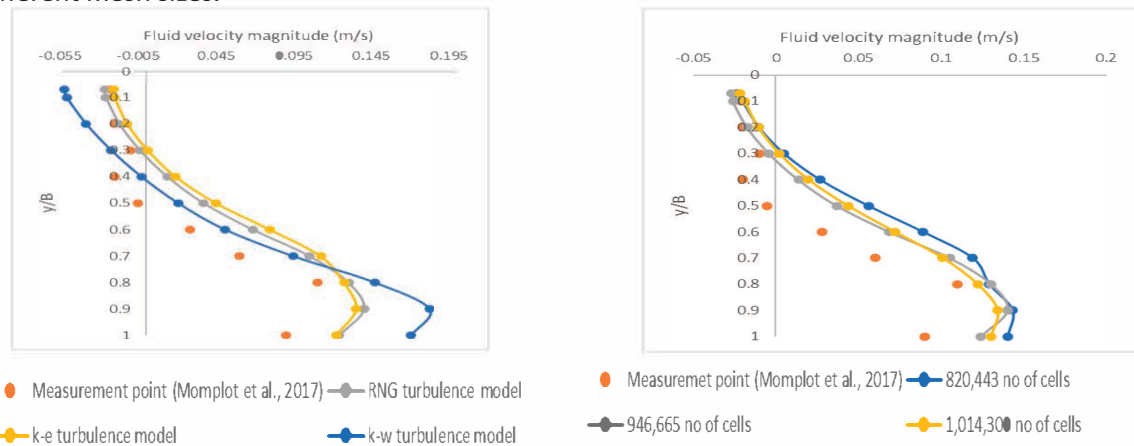


Fig. 2. Comparison between the horizontal velocity result from measurement point in physical experimentation (Momplot, 2017) with Flow-3D CFD model utilizing different turbulence model (a) and different numbers of cells size (b), at $x/B=2.5$ and elevation $z=0.09$ m.

Conclusions

This paper is aimed at comparing the measured and computed velocity distributions in the lateral channel of divided open channel flow based on the work of Momplot et al. (2017). The simulation results using Flow-3D agree quite well with experimental values observed previously. Therefore, the use of this CFD model is considered viable in the investigation of divided flows in open channels of equal widths.

References

- Bonakdari, H., Lipeme-Kouyi, G., & Wang, X. (2011). Experimental validation of CFD modeling of multiphase flow through open channel confluence. In *World Environmental and Water Resources Congress 2011: Bearing Knowledge for Sustainability* (pp. 2176-2183).
- Kamel, B., Ilhem, K., Ali, F., & Abdelbaki, D. (2014). 3D simulation of velocity profile of turbulent flow in open channel with complex geometry. *Physics Procedia*, 55, 119-128

Momplot, A., Lipeme Kouyi, G., Mignot, E., Rivière, N., & Bertrand-Krajewski, J. L. (2017). Typology of the flow structures in dividing open channel flows. *Journal of Hydraulic Research*, 55(1), 63-71.

Ramamurthy, A. S., Qu, J., & Vo, D. (2007). Numerical and experimental study of dividing open-channel flows. *Journal of Hydraulic Engineering*, 133(10), 1135-1144

Study of the flow falling into a plunge pool using OpenFOAM®

Rita F. Carvalho^{1*}

¹University of Coimbra, MARE-Marine and Environmental Research Center, Dep. of Civil Engineering

*Corresponding: ritalmfc@dec.uc.pt

Abstract

The description of the flow in a plunge pool is complex and the flow patterns has great interest to better access the behaviour of the flow and its understanding. The use of 3D numerical model becomes common in hydraulic engineering and new physics can be taken into account. In this work, the velocity, pressure field, air and sediment concentration of the flow from a turbulent water flow falling from a horizontal structure, passing through the atmosphere and impinging into the plunge pool is investigated with OpenFOAM®, using different solvers and different physics.

Keywords: Jet, Plunge pool flow; Turbulence, Air entrainment, sediment, OpenFOAM®

Introduction

A coherent stream over a structure can detach and fall freely into a pool. The entire process is accompanied by a great deal of spray and aeration (Ervin and Falvey, 1987). The mechanisms can be divided into the following: (1) spreading of the jet (2) air entrainment by the entering jet, (3) diffusion in the pool, (4) impact on the pool bottom, and (5) recirculation of flow in the plunge pool (Castillo and Carrillo, 2017). The influence and presence of air and sediment that can be transported within the nappe and moving into the pool is not well understood and has a great influence in the all process. A better knowledge of the air concentrations downstream of a nappe flow case would be important to designers (Wood, 1991). This work presents different solvers to describe the flow into a pool, and the detailed effects of the flow considering air and sediment that can be described by the different solvers.

Methods

The hydraulics of the jet was reproduced using OpenFOAM®v.18.12 within interFoam solver (Carvalho *et al.*, 2019), which considers a single set of Navier Stokes equations (1-2) for the fluids considered isothermal, incompressible and immiscible and an additional equation to describe the free-surface within Volume of Fluid (VOF) model (3). The turbulence was described within k- ω SST Reynold's averaged Navier Stokes equation, which is known to be the best RANS modelling choice for predicting water elevation and velocity profiles. AirInterFoam and SedInterFoam solvers were developed from interFoam solver and are now applied to a flow (see Table 1) in order to take into account the air entrainment generated in spread and impinging into the water as sub-grid model (4), the sediments contained in the water in one way coupling (5) or both in multiphaseEulerFoam, which considers a set of Navier Stokes equations (1-2) for each flow.

$$\nabla \cdot \rho \bar{v} = 0 \quad (1)$$

$$\frac{\partial \rho \bar{v}}{\partial t} + \nabla \cdot (\rho \bar{v} \bar{v}) = -\nabla p^* - \mathbf{g} \cdot \mathbf{x} \nabla \rho + \nabla \cdot \boldsymbol{\tau} + \mathbf{F} \quad (2)$$

$$\frac{\partial \alpha}{\partial t} + \nabla \cdot (\alpha \bar{v}) + \underbrace{\nabla \cdot [\mathbf{v}_c \alpha (1 - \alpha)]}_{\text{compressible term}} = 0 \quad (3)$$

$$\frac{\partial \alpha_g}{\partial t} + \nabla \cdot (\mathbf{v}_g \alpha_g) + \underbrace{\nabla \cdot [\Gamma_{\alpha_g} \nabla \alpha_g]}_{\text{compressible term}} = S_g \quad (4)$$

$$\frac{\partial c}{\partial t} + \nabla \cdot \left(\mathbf{v} - \mathbf{v}_s \frac{\mathbf{g}}{|\mathbf{g}|} \right) c = \nabla \cdot (\mathbf{v}_t \nabla c) \quad (5)$$

Table 1. Geometric parameters of the flow.

Parameters	h_{upstream} (m)	U_{upstream} (m/s)	Re	k	ϵ	ω
all cases	0.02	10	20000	0.375	26.95	71.87

Results

All simulations (Fig. 1) show the flow leaving upstream structure, the trajectory in the air and entering into the pool, generating strong turbulence and multiphase flow. The velocity decreases when it penetrates the waterbed, but the main flow remains strong, pushing the water away. Part of the kinetic energy of the water is converted into pressure energy, which extends to the bottom. Air concentration field requires airInterFoam or multiphaseEulerFoam solvers, being interFoam unable to describe air concentration correct distribution. Sediment suspension distribution require sedInterFoam or multiphaseEulerFoam. Only multiphaseEulerFoam can describe spray formation and movement along the jet, which is normally seen in wave breaking and is of particular interest for a correct description.

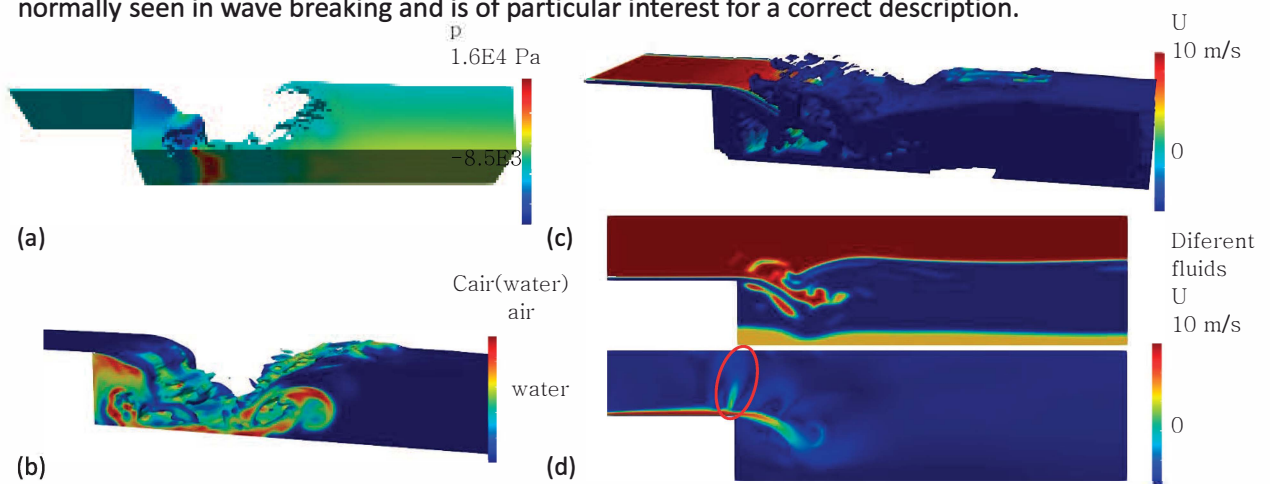


Fig. 1. Stream over a structure, detaching and falling into a pool (a) interFoam (b) airInterFoam, (c) sedInterFoam and (d) multiphaseEulerFoam.

Conclusions

Case study allows to conclude that all solvers based on RANS and VOF method are appropriate to evaluate flow, velocity and pressure field, mixing and energy dissipation in the plunge pool. Particular details require specific solvers. Comparisons of the different solver results show differences, in recirculating flow.

Acknowledgement

The authors acknowledge the Laboratory for Advanced Computing at University of Coimbra for providing HPC, computing. URL: <https://www.uc.pt/lca>.

References

- Castillo, L. G., and J. M. Carrillo. 2017. "Comparison of methods to estimate the scour downstream of a ski jump." *Int. J. Multiphase Flow* 92 (Jun): 171–180. <https://doi.org/10.1016/j.ijmultiphaseflow.2017.03.006>.
- Rita F. Carvalho, M. Nazmul A. Beg, Pedro M. Lopes (2019), Experimental and numerical characterisation of a jet impingement on a pool, E-proceedings of the 38th IAHR World Congress, Sept. 1-6, 2019, Panama City, Panama, <https://doi.org/10.3850/38WC092019-1764>.
- Ervine D.A., Falvey H.T. (1987). Behaviour of turbulent water jets in the atmosphere and in

plunge pools. Proc. of the Institution of Civil Engineers, Volume 83, Issue 1, March 1987, pp. 295-314.

Wood, I. R. 1991. Air entrainment in free-surface flows. Madrid, Spain: International Association for Hydro-environment Engineering and Research.

Numerical study of flow structure and pollutant mixing at river confluences

Se Hun Yun¹ and Il Won Seo^{1*}

¹ Department of Civil & Environmental Engineering, Seoul National University

*Corresponding: seoilwon@snu.ac.kr

Keywords: river confluence; pollutant mixing; river bed discordance; discharge ratio; secondary currents; CFD modeling

Abstract

When two streams merge at a confluence, the flow after the confluence changes dynamically. These complex three-dimensional (3D) flow and turbulent processes around the confluence make the particular characteristics such as secondary currents and flow deflection, shear layer, and recirculation zone. Among the various factors that affect the flow characteristics at the confluences, the river bed discordance between the two streams is often caused by the dredging in the main stream for various purposes such as securing water depth for flood prevention, aggregate collection for construction material, etc. This study carries out 3D numerical simulations of flow and scalar transport at 90-degree channel confluence by controlling the channel discordance and discharge ratio to explore its impact on hydrodynamics and pollutant transport. The river bed discordance ratio is defined as the ratio of the step height to the downstream water depth, and discharge ratio is ratio of branch channel flowrate to the main channel flowrate after the confluence. We resolve flow fields using 3D Reynolds-averaged Navier-Stoke equations coupled with a SST $k-\omega$ turbulence closure scheme. Typical cases of the velocity results are validated with laboratory experiment data, then the scalar transport for contaminant was simulated by combining the simulated velocity fields. With the fixed bed discordance ratio, as the discharge ratio increased, the influence of the tributary was getting bigger and the mixing of the contaminants introduced from the tributary was completed earlier in the shorter distance. In the case of a constant discharge ratio, the vertical flow in the falling direction became larger as the height of the step of the tributary increased. At the same time, since the velocity of the horizontal flow through the tributary also increased, mixing proceeded vigorously. When the bed discordance ratio was over 0.815, the pollutant coming from the tributary collided into the opposite bank of the mainstream, which accelerated transverse mixing.

Acknowledgement

This work was supported by the Korea Agency for Infrastructure Technology Advancement(KAIA) grant funded by the Ministry of Land, Infrastructure and Transport (Grant 20DPIW-C153746-02).

**The 9th International
Symposium on
Environmental Hydraulics**

H Session

Machine Learning [H-M1]



The prediction of turbulent features of drainage channels covered by reed beds by using a Machine Learning approach

Giuseppe Francesco Cesare Lama^{1*}

¹Department of Agricultural Sciences, University of Naples Federico II, Italy

* Corresponding: giuseppecesare.lama@unina.it

Keywords: vegetated channels; turbulence; machine learning

Abstract

The main purpose of this work is the evaluation and the validation of predicted turbulent features induced by hydrodynamic interaction between rigid emergent reed beds and water flow at real scale obtained by employing a machine learning approach. The paramount dataset processed in this study was collected during six field experiments carried out in a vegetated reclamation channel under different scenarios of riparian vegetation management. In detail, Reynolds shear stresses and Turbulent Kinetic Energy were obtained by processing the 3D components of water flow velocity acquired by an acoustic Doppler velocimeter (ADV) at 100 Hz, located at the vegetated channel's upstream cross section. The measuring grid was composed of 15 measuring points, distributed along 5 vertical lines. The experimental cross sectional distributions refers to three scenarios: (i) channel in a condition of total abandonment, with infesting reed beds in natural undisturbed conditions, (ii) a riparian vegetation management scenario of central riparian vegetation cleaning, with the presence of two side buffers of reed beds in undisturbed conditions and (iii) a condition of complete reed beds cleaning along the whole vegetated channel. The promising outcomes of this study represent an useful tool for the prediction of the effects of riparian vegetation in vegetated reclamation channels under colonized by such a widespread riparian specie as reed.

Acknowledgement

The Authors of the present study want to thank Prof. Federico Preti, Prof. Luca Solari, Dr. Alessandro Errico and Dr. Simona Francalanci for their support during the experimental analysis. Thanks also to Melanie Maxwald and Eng. Daniele Maffi for data acquirement during the hydraulic tests, and to Eng. Leonardo Gianecchini from "Consorzio di Bonifica 1 Toscana Nord" and his staff for their precious support during the field activities.

The development of real time prediction system for urban flooding in Incheon, South Korea

Dongmin Jang^{1*}, Sung Won Park¹, Chang Hoo Jeong¹, Won Su Kim¹

¹Korea Institute of Science and Technology Information, Daejeon, South Korea

* Corresponding: jmin@kisti.re.kr

Keywords: real-time prediction; urban flooding; artificial intelligence; coupled modeling

Abstract

Recently, the frequency and intensity of local heavy rain tend to be increased due to climate change, and the increase of surface runoff due to urbanization (Increase of impermeable area) and lack of rain detention storage due to the development of lowland are expected to accelerate the serious damage caused by flooding. In addition, in the case of urban areas where rivers are located, the rise in the river water level causes backflow in the urban basin, which increases flood damage. Accordingly, the developing a real time prediction system of urban flooding must be necessary for quick and accurate response to risk of flooding emergency in urban area. We are develop an integrated flood prediction solution that combines real data, artificial intelligence and supercomputing technologies. Our solution consists of a rainfall prediction, 1-d pipe network prediction and 2-d inundation prediction systems, and each system is closely coupled. The rainfall is predicted by using artificial intelligence technology (ConvLSTM) based on radar and observation data of KMA during 2010-2018. And, of the overflow in manhole and flowrate in the pipe is calculated by SWMM(Storm Water Management Model), that is developed by US EPA, and the 2-d flood prediction model used in our solution is 2DIS, which is finite difference inundation model based on 2-D shallow-water equations. Our solution operates 8 times a day every 3 hours for the response of flooding in Incheon, South Korea, and flooding risk information produced by solution is provided in a 3D GIS environment.

Machine learning based spatio-temporal characterization of marine water quality evolution in Hong Kong

Tianan Deng¹, Huan-Feng Duan^{1*}

¹The Hong Kong Polytechnic University, Kowloon, Hong Kong SAR

* Corresponding: hf.duan@polyu.edu.hk

Keywords: water quality; machine learning; spatio-temporal variation; coastal environment

Abstract

Water eutrophication has become a global crisis on marine water quality and coastal environment since last century. The Harmful algal blooms (HABs) as the disastrous events in eutrophic waters have been reported frequently worldwide and caused acute damages on both local hydro-environment and aquaculture economy. In particular, enclosed sea waters are more vulnerable to be eutrophicated in that trapped wastewater, limited tide influence, slow water circulation and long water retention time. In order to mitigate potential HABs incidents, it is meaningful to accurately characterize and understand the relationship between algal growth dynamics and water quality evolution.

However, to analyze the algal growth and evolution from a process-based perspective is extremely complicated due to the not well-understood theories, uncertainties of boundary conditions and high non-linearities in marine waters. In addition, spatial and temporal variations of hydrological conditions in enclosed sea are significant: the entrance portion is more affected by oceanic dynamics while the inner zone behaves more like an inland limnological system which makes the analysis of algal growth in enclosed sea areas more challenging. Recently, the machine learning (ML) method has been increasingly resorted to handle complex and uncertain problems such as water quality prediction. The advantages of robustness and no requirement of any prior knowledge regarding the dynamics and mechanism of HABs outbreak and evolution process demonstrate the great potential of ML for the HABs analysis. However, most of current ML-based studies focus on algal growth at single spot or several spots only, while few researches inspect the spatio-temporal variations of marine water quality for coastal environment management.

In this study, the Tolo harbor in Hong Kong is taken as example, where is an almost landlocked sea area suffered from more than 30% HAB events occurred in Hong Kong, to analyze critical factors contributing to algal growth from spatio-temporal perspective based on two different ML methods. Specifically, Tolo Harbour is subdivided into three subzones namely the Inner Harbour, Buffer Zone and Tolo Channel. Considering the spatial variations on hydrological conditions, three monitored datasets for the past 30 years (spanning from 2008 to 2018) of different subzones (monitoring station TM3, TM6, TM8) are used for training and testing these ML models. The differences of significant variables contributing to algal growth among three subzones are discussed based on the results of the ML applications. Finally, the results of this study will be applied to understand, explain and analyze the water quality evolution process in this marine water region in Hong Kong.

Improvement of algal bloom identification by a big-data analysis using satellite images

Hye-Suk Yi^{1*}, Dong-Kyun Kim¹, Kwangsoon Choi¹, Youngsung Kim¹, Suna Chong¹, Nam-Il Won¹,
Hojoon Kim¹, Sunghwa Choi¹, Eui-ho Hwang¹, Yongbae Jung¹

¹ K-water Institute, 125 Yusungdaero1689, Daejeon, Republic of Korea

* Corresponding: yihs@kwater.or.kr

Keywords: harmful algal blooms; satellite, sentinel-2; big data; spatial monitoring

Abstract

Quick detection of algal blooms (i.e., high chlorophyll-a concentration) in freshwaters is imperative for effective monitoring of spatial water quality distribution in the context of ecological health and assessment. With the recent advancement of technology, satellite images have been deemed as practically useful tools to identify the spatial distribution of algal blooms. Our study aimed to predict chlorophyll-a concentrations using 13-band satellite images derived from Sentinel-2 (spatial resolution: 10m x 10 m, time interval: 5 days). In order to validate the values from the satellite images, we compared them with simultaneously observed chlorophyll-a concentrations based on fluorescence measurement. The goal of this study is to improve the accuracy of predictions induced from satellite images. The analytical techniques (multiple linear regression, decision-tree classifier, and artificial neural network) were comparatively evaluated. The results showed that artificial neural network exhibited the best performance among them, improving more than 37% accuracy compared to that of multiple linear regression. In the end, it was successful to create algal bloom maps using a new algorithm to analyze spatial algae management.

Three Types of Machine Learning Technique for Three Different Problems in Water Resource Engineering

Donghwi Jung¹, Soon Ho Kwon², and Joong Hoon Kim^{1*}

¹School of Civil, Environmental and Architectural Engineering, Korea University, South Korea.

²Future and Fusion Lab of Architectural, Civil and Environmental Engineering, Korea University, South Korea.

*Corresponding: jaykim@korea.ac.kr

Keywords: Machine learning technique; Water resources engineering; Surrogate modeling; Dimensionality reduction; Real-time operation control; Supervised and unsupervised learnings; Reinforcement learning

Abstract

Machine learning (ML) techniques are transforming daily lives, industries, and various scientific/engineering disciplines in the recent decade. This review paper investigated three types of ML applied to three different water resources engineering problems: (1) real-time urban flood-inundation prediction (supervised learning); (2) drought impact factor analysis (unsupervised learning); and (3) real-time control of water distribution system pumps (reinforcement learning). In the first study, a surrogate modeling approach (meta-modelling) was presented for real-time prediction of urban flood-inundation. The surrogate modeling approximates the outputs of a system given the input data which are originally computed based on a set of system governing equations. In the second study, a framework based on principal component analysis (a dimensionality reduction method) was introduced to identify the critical drought impact factors among various hydrological and atmospheric variables. In the third study, water distribution system pump operation was optimized through deep reinforcement learning. Finally, this review paper summarizes potential research topics and directions with ML technique in water resources engineering.

Acknowledgement

This work was supported by the National Research Foundation of Korea(NRF) grant funded by the Korea government(MSIT) (No. 2020R1C1C1006481).

Watershed Management in Nakdong River Using Big Data Analysis

Bu Geon Jo¹, Woo Suk Jung², and Young Do Kim^{1*}

¹ Department of Civil & Environmental Engineering, Myongji University

² Department of Environmental Engineering, Inje University

*Corresponding: ydkim@mju.ac.kr

Abstract

Recently, interest in big data has been increasing both at home and abroad. The importance of using big data in the water resource field is being emphasized. Basic data related to water should be sufficient for water management. In recent years, for effective integrated water management in developed countries, a watershed management plan using big data is being attempted. In the case of Japan, watershed characteristics are identified using water environment data and social science data. A watershed management plan is prepared by analyzing the characteristics of the watershed in various ways. The water environment management plan in Korea is established based on the load, and there is a lack of variety of data. Each river has different characteristics. The Nakdong River basin consists of 22 mid-watershed, and each mid-watershed has various problems and characteristics. Therefore, it is judged that a watershed management plan according to the characteristics of the watershed is necessary. This study aims to diagnose a watershed through a comprehensive analysis of the watershed using big data analysis. Use water-related indicators to assess your watershed. In addition, a visualization analysis, the characteristics of the basin's basic data and analyzes the basin characteristics based on big data analysis through the results to find a customized basin management plan.

Keywords: Big Data; Visualization Analysis; Watershed characteristics; Watershed management;

Methods

In this study, Water environment big data was built for water quality analysis. For the purpose of collecting basic data, it is to lay the foundation for performing data mining analysis through the establishment of big data on the water environment. The list of data for the construction of big data can be classified into meteorological observations, watershed status, reservoirs, water/sluices, water quality, water ecosystem, pollution source status, sewerage, waterworks, and others (processing facility status and business status such as development projects). Finally, it is to explore customized water quality improvement measures such as visualization analysis, data model analysis, and numerical model analysis for integrated water management using big data information.

```

%matplotlib inline
import pandas as pd
import matplotlib.pyplot as plt
import seaborn as sns; sns.set()
sns.palplot(sns.color_palette())
data = pd.read_csv("NM.csv", encoding='CP949')
plt.figure(figsize=(15,10))
#styles = ["white", "dark", "whitegrid", "darkgrid", "ticks"]
sns.set(style="whitegrid", palette="muted")
# Draw a categorical scatterplot to show each observation
sns.swarmplot(x="Obs", y="BOD", data=data)
plt.show()

%matplotlib inline
import pandas as pd
import matplotlib.pyplot as plt
import seaborn as sns
data = pd.read_csv("nakdong.csv", encoding='CP949')
plt.figure(figsize=(15,15))
sns.set(font_scale=1.5)
sns.heatmap(data = data.corr(), annot=True, fmt = '.2f',
            linewidths=2.5, cmap='Blues')
plt.title('Observation Correlation analysis', size=20)
plt.show()
    
```

Fig. 1. Visualization analysis source code using Python

Results

As a result of analyzing the middle areas of the Nakdong River basin using visualization analysis and basic data analysis, the characteristics of each middle area were different. BOD and T-P, which are the main water quality items, differed in the water quality items that affect each mid-zone. It can be used as basic data to prepare a management plan that additionally reflects the characteristics of the watershed from the existing river management plan.

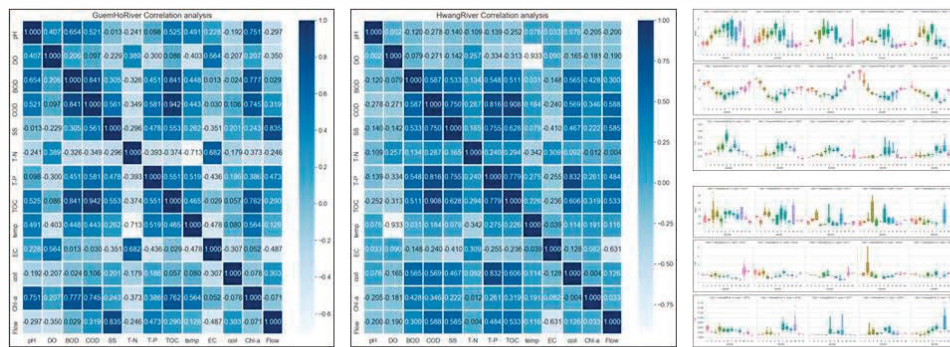


Fig. 1.

Conclusions

The results of this study show that the establishing Nakdong River Integrated Water Management Big Data and presenting the technology to use Nakdong River water management big data analysis, the direction to establish an advanced water management system for the improvement of water quality in the Nakdong River basin can be suggested. Existing water management has a wide range of practical difficulties due to the diversification of subjects, but based on this project, the importance of integrated water management in the Nakdong River basin and the direction of practical and practical watershed management measures can be presented.

Acknowledgement

This work was supported by the National Research Foundation of Korea(NRF) grant funded by the Korea government(MSIT)(NRF-2020R1F1A1076887).

References

Kim, J. T. (2014). Lowess and outlier analysis of biological oxygen demand on Nakdong main stream river. J. of The Korean Data and Information Science Society, 25(1), 119-130
Jung, W. S., Kim, Y. D. (2019). Effect of abrupt topographical characteristic change on water quality in a river. KSCE J. of Civil Engineering, 23(7), 3250-3263.

**The 9th International
Symposium on
Environmental Hydraulics**

S1 Session

Rainwater Harvesting and Utilization [S1-M1]



Multi-purpose decentralized rainwater management: Philosophy, theory and a case study

Mooyoung Han

Department of Civil & Environmental Engineering, Seoul National University
myhan@snu.ac.kr

Abstract

To overcome the climate crisis and to enhance the resilience of water infrastructure, a new water management paradigm is required. The new paradigm is based on the role and importance of rainwater which should be collected and used instead of draining. In this paper, the philosophy and theory of multipurpose rainwater management and a successful case study at Star City are presented.

Keywords: Decentralized; Philosophy; Rainwater management; Star City

Introduction

The new trends of water management to overcome the climate crisis are suggested in the names of LID, SUDS, Sponge City, etc. in many countries including Korea. It is important to consider why and how we should do rainwater management as a water management philosophy. The theory should be developed for a micro-catchment hydrological system to design and operate it. Star City Rainwater Management System is discussed as a successful model of multi-purpose decentralized rainwater management.

Philosophy

The new water management paradigm is suggested to answer why and how we should do water management, and it is compared with the old water management paradigm. As a philosophy, we should do rainwater management:

- 1) to consider rainwater as a resource instead of waste.
- 2) to collect and manage rainwater from the source before it is united and becomes strong.
- 3) to collect the upstream instead of downstream so that we can utilize the potential energy before it is polluted
- 4) to use it multiple benefits instead of just draining it.
- 5) to do rainwater management as a social responsibility so that any development should not alter the existing water status.

Theory

Because the existing hydrological theory is developed for an area of large scale with a single purpose of flood mitigation, the control and mitigation at the endpoint are not possible. A new hydrological theory is developed from the knowledge and experience of existing hydrology which is to collect from a micro catchment, utilize for a multipurpose, and control it. Figure 1 shows all different combinations for a micro-catchment hydrological system (Han and Nguyen, 2019).

The process at a small building rooftop can be described as an R-D model. By installing storage and utilization, it is possible to manage water for multiple purposes such as flood mitigation and water-saving which can be described as the R-S-U-D model. The way how to design and evaluate is published and software for easy application is available.

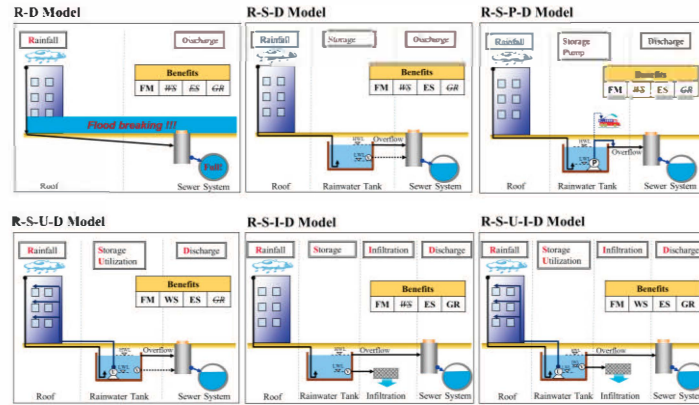


Fig. 1. Models of Micro-catchment Rainwater Management system

Case Study

The Star City RWHS in South Korea is a successful case that is designed to alleviate water-related disasters. Star City is a large commercial/residential complex with four buildings, each having between 35 and 57 stories. The catchment area comprises 6,200m² of four rooftop areas and 45,000m² of terraces and gardens throughout the complex. The Star City RWHS has been in use since 2007 and the results show its great potential as a preparation/adaptation strategy for floods and droughts. It is equipped with 3000 m³ rainwater tanks with three tanks 1000m³ each, with the function of flood mitigation, water conservation, and emergency (Han and Mun, 2011). Since then, the Rainwater system is still working successfully with the maintenance cost of less than 5 \$ per year for each household.

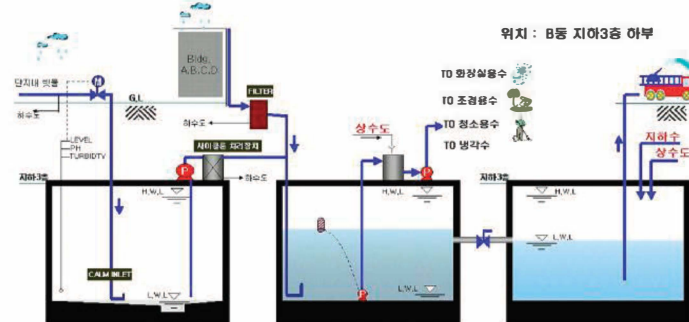


Fig. 2. Schematic Diagram of Star City Rainwater Management system

Conclusions

To enhance resilience water infrastructure against the climate crisis, a new water paradigm of rainwater management is proposed. The philosophy and why and how to do water management should be considered as a new water paradigm. The hydrological theory of the micro catchment system is developed. The software to design and evaluate the multiple benefits of the rainwater management system is available. The new paradigm of rainwater management should be included in the (re)development of the city as a climate mitigation/adaptation strategy.

References

- Hydrological design of micro-catchment multipurpose rainwater management system, by Han and Nguyen International Water Association (IWA), 2019.
- Han M.Y., Mun J.S. 2011. Operational data of the Star City rainwater harvesting system and its role as a climate change adaptation and a social influence. Water Science & Technology. 2011;63(12):2796-801.

Effects of Multi-Purpose Rainwater Management for Responding to the Climate Crisis

Dong Geun Kwak¹, and Moo Young Han^{1*}

¹Department of Civil & Environmental Engineering, Seoul National University

*Corresponding: myhan@snu.ac.kr

Abstract

Multipurpose rainwater management (RWM) is drawing attention as a solution to climate crisis. In this study, performance indicators, criteria, and quantitative evaluation methods for various expected effects of RWM are proposed, and the performance of a RWM case applying a new RWM technology was evaluated. The resilience of the water cycle aspect of the existing water system was evaluated through the water balance analysis according to the rainfall scenario, and further, the analysis results of eight multi-value effects (MVE) were expressed in a rose diagram. It was found that water cycle improvement (WCI) and MVE were excellent as the RWM goals were achieved by type in small-scale watershed and connected to the nature-based solution (NBS)-type RWM facility. Using the method and results proposed in this study, it is possible to plan, design, and evaluate a multipurpose RWM system with high response to climate crisis.

Keywords: Rainwater management (RWM), Climate crisis, Water cycle, Resilience

Introduction

Globally, climate crisis and urbanization have distorted the water circulation system (Singh et al., 2018). Increased discharge and rapid drainage increase the possibility of urban flooding, and the shortage of air and soil water due to reduction of infiltration and evapotranspiration has a great influence on urban heat islands and carbon generation (Hirabayashi et al., 2013). This distortion of the water cycle caused by climate crisis is a very complex water problem, leading to fire problems. Existing RWM methods still have limitations in solving various problems as the top priority is to control peak discharge. Therefore, a new concept of RWM technology is needed to overcome the limitations of existing RWM technology.

Methods

Positive Impact Development (PID) is a multi-purpose RWM technology that restores the water cycle before development, solves water problems or fire problems that have become difficult due to climate crisis, and improves the resilience of existing water management systems. The developed PID-RWMM (Rainwater Management Model) was used for water balance analysis and performance evaluation (Fig. 1).

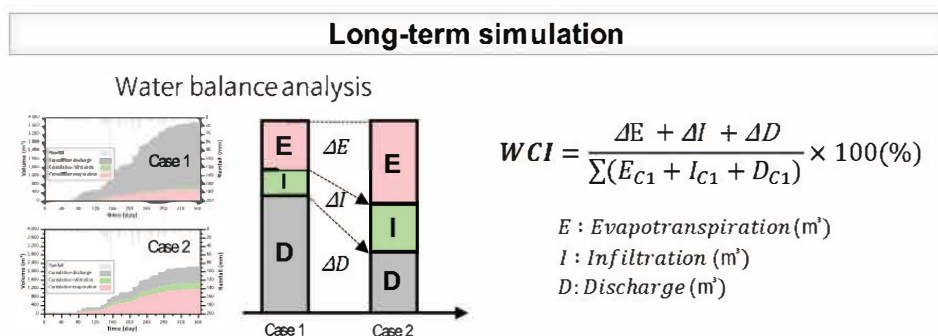


Fig. 1. Performance evaluation result of two types of RWM systems.

The water balance was analyzed by applying long-term real rainfall for an virtual area in Seoul. The resilience was evaluated through the analysis of the change in the improvement rate of water cycle according to the change in rainfall pattern. Furthermore, water saving, water independence, flood prevention, soil water recharge, air quality improvement, temperature reduction, energy saving, and carbon reduction (CR) were evaluated (Fig. 2).

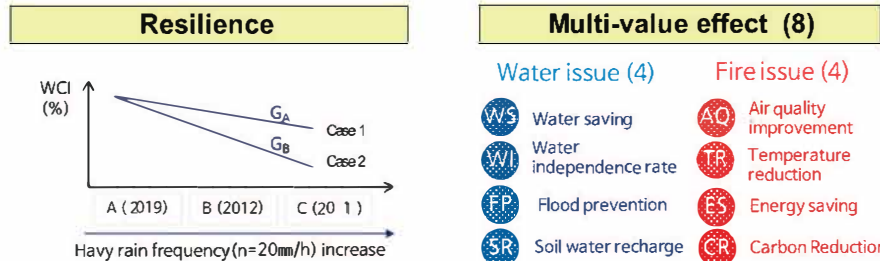


Fig. 2. Performance evaluation result of two types of RWM systems.

Results

As a result of water balance analysis by applying real rainfall in 2012, Case 1 (existing method) was 37.5% and Case 2 (PID) was 70%, showing an improvement of about 32.5%. In addition, when the rainfall pattern changes to adverse conditions, the amount of WCI change in Case 2 was smaller than that in Case 1, which means that resilience is good as a response to climate crisis. In addition, as a result of MVE analysis, Case 2 was excellent in all items, and FP, WI, and AQ were particularly effective. This is judged to be the effect of case 2's NBS-based differential connection type design. That is, the superiority of PID technology was verified by comparing and analyzing the performance indicators proposed for the existing RWM system and the PID type RWM system.

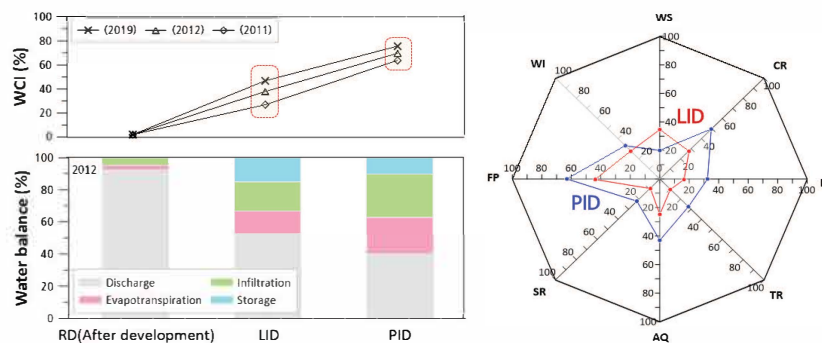


Fig. 3. Performance evaluation result of two types of RWM systems

Conclusions

Using the new concept of PID technology and performance evaluation method proposed in this study, it is possible to plan, design, and evaluate a more eco-friendly and resilient RWM system to respond to climate crisis and improve water circulation.

References

Singh U. K., Kumar B. (2018). Climate Change Impacts on Hydrology and Water Resources of Indian River Basins. *Current World Environment*, 13, 32-43
Hirabayashi Y., Mahendran R., Koirala S., Konoshima L., Yamazaki D., Watanabe S., Kim H., Kanae h. (2013). Global flood risk under climate change. *Nature Climate Change*, 3, 816-821

Rainwater use efficiency and optimization of Seoul Botanic Park in South Korea

Zion Kang and Kyungho Kwon

STORMWATER Co., Ltd.

*Corresponding: kwonkh@stwater.co.kr

Abstract

As a decentral RMF, rainwater is harvested and used as irrigation water for trees and green area in Botanic Park Seoul. The Rainwater harvesting system is composed of Catchment area 7,570 m², Storage Tank 620m³, Use Tank, Pre -treatment facility and Tap water supply. Based on the water level change and the bottom area of storage tank of 177.14 m² the used rainwater is about 10.72m³ per period. The storage volume of the Seoul Botanic Park seems to be smaller than needed for the suitable supply for the usage. Further research is underway for the optimization of facilities.

Keywords: Rainwater use; Botanic park; water cycle; Optimization; Storage volume

Introduction

The Seoul Metropolitan Government implements a policy to minimize the impact on natural water circulation and water environment caused by development and expand decentral rainwater management facilities(dRMF) to secure sustainable water resources due to climate change. As a decentral RMF, rainwater is harvested and used as irrigation water for trees and green area in Botanic Park Seoul. The Monitoring tasks are under way to look at the current status of rainwater use amount and to find improvements for better efficiency of the system

Methods

Botanic Park Seoul is located at Magok-dong 812, Gangseo-gu, Seoul. The Rainwater harvesting system is composed of Catchment area 7,570m², Storage Tank m³, Use Tank m³, Pre -treatment facility and Tap water supply(Fig.1). The water level is measured form 2020.07 to 2021.04.

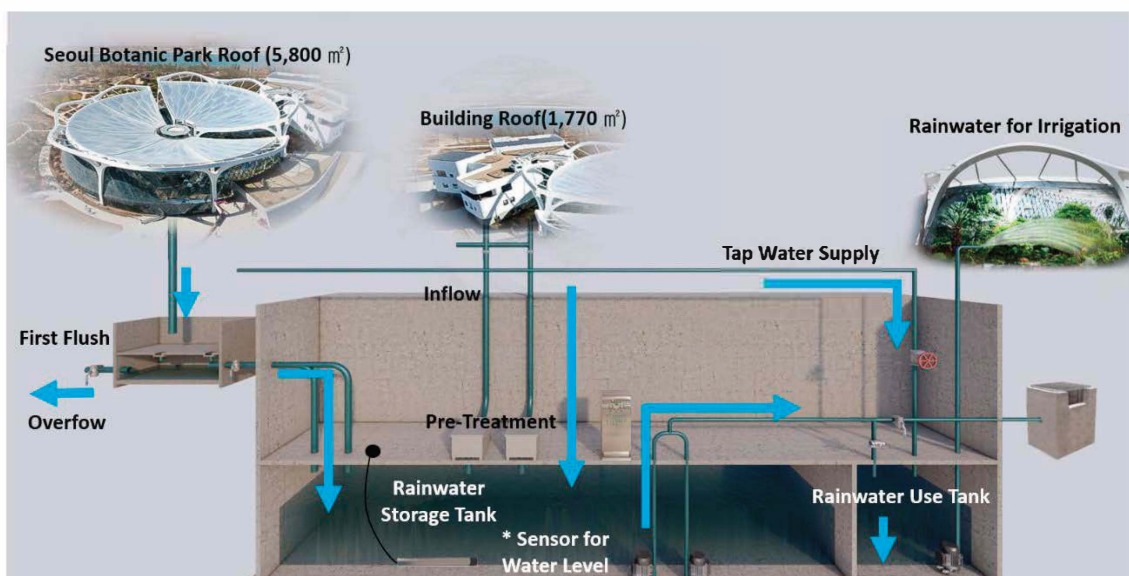


Fig. 1. The Rainwater harvesting system at the Botanic Park Seoul.

Results

The water level change of the storage tank was measured during the monitoring period. The Fig. 2 shows, that the water level has changed due to storage and use of rainwater on time. The storage tank was filled with rainwater at the early rainy season already and had not any more capacity to be filled. And it was emptied in 2~3 weeks.

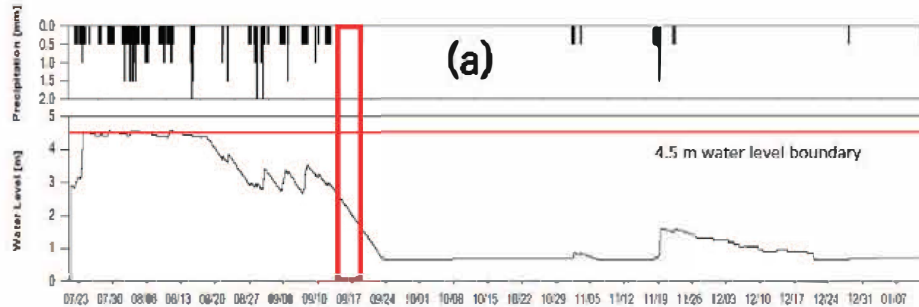


Fig. 2. The measured water level from 20.07 to 21.01

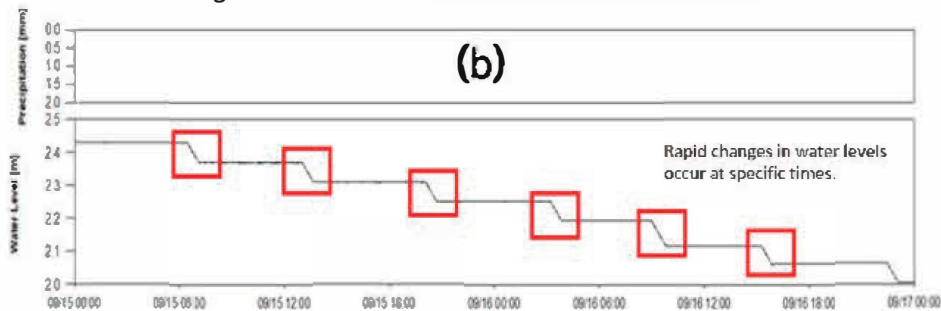


Fig. 3 The measured water level by use from 20.09.15-09.17

Table 1. Amount of used Rainwater

periods	Time (min)	water Level(m)	water level(m)	Depth(m)	Used RW (m ³)
9.15 06:30 ~ 9.15 07:08	38	2.429	2.371	0.058	10.27
9.15 13:03 - 9.15 13:40	37	2.371	2.312	0.058	10.27
9.15 20:06 - 9.15 20:44	38	2.312	2.253	0.057	10.10
9.16 03:13 - 9.16 03:50	37	2.253	2.195	0.058	10.27
9.16 08:59 - 9.16 09:48	49	2.195	2.119	0.076	13.46
9.16 15:15 - 9.16 15:54	39	2.118	2.062	0.056	9.92

The stored rainwater was pumped approximately every six to seven hours, with an average depth of 0.058 m during about 38 minutes. Based on the water level change and the bottom area of storage tank of 177.14 m² the used rainwater is about 10.72m³ per period.

Conclusions

Rainwater harvesting system in the Seoul Botanic Park is actively operating. The efficiency of rainwater use facilities is greatly influenced by the mass balance between the catchment area, storage volume and usage amount. The storage volume of the Seoul Botanic Park seems to be smaller than needed for the suitable supply for the usage. Further research is underway for the optimization of facilities.

References

SEOUL METROPOLITAN GOVERNMENT (2019). The Seoul Metropolitan Government Framework Ordinance on the Restoration of Water Circulation and Low Impact Development

Innovative technology to maintain clean rainwater in rainwater harvesting systems

Janith Dissanayake¹ and Mooyoung Han¹

¹Department of Civil & Environmental Engineering, Seoul National University

*Corresponding: myhan@snu.ac.kr

Abstract

Rainwater harvesting (RWH) can be used as a tool to avert urban water crises. However, due to issues pertaining to the inconsistent harvested rainwater quality, RWH has been received poorly by the public. This study investigated cost-effective methods to improve the harvested rainwater quality using a lab-scale RWH tank system. The lab-scale tanks were retrofitted with different inlet/outlet configurations to assess their effect on bottom sediment re-suspension. The result showed more than 50% reduction in sediment re-suspension when tank was fabricated with a J-type inlet. When the initial water level was high, sediment re-suspension was low due to the cushioning effect. These results may be used to suggest design or modification recommendations for existing RWH tanks.

Keywords: Rainwater Harvesting; sediment resuspension; particle separation; multiple tank systems

Introduction

Many researchers have reported poor harvested rainwater quality citing the high particulate matter concentrations in harvested rainwater quality (Simmons et al., 2001). Particulate matter can affect the subsequent treatment processes such as disinfection, thus they must be removed during treatment. As the storage time in RWH tanks are long, most of the particulate matter settles in the storage tank. As these settled particulate matter hold other contaminants such as heavy metals, resuspension of the sediment layer should be minimized. Magyar et al., 2011 studied various inlet/outlet arrangements with a tank fabricated with an I-type inlet. Recently, many research suggest the use of J-type inlets, therefore, a comprehensive investigation is needed to assess the effect of inlet/outlet configurations when the tank is fabricated with a J-type inlet. This study aims to fill this research gap.

Methods

In this study, we fabricated a downscaled cylindrical acrylic tank with a diameter of 15 cm and a height of 20 cm. The height of the tank at 3 L was calculated (H) and outlets were made at 0.33 H and 0.6 H. Three types of inlets (I, L, J-types) with a 5 mm internal diameter were fabricated. The flow through the pipe under the flow rates considered in this study was turbulent ($Re > 4000$), similar to what is observed in real-scale tanks. Then, one liter of 2 g/L of kaolin clay solution was introduced to the tank, after which the clay solution was left for 24 h to facilitate clay particle sedimentation. After 24 h, double-distilled water was introduced by a pump until the tank reached its full capacity of 3 L. The inlet/outlet configurations were varied, but the other parameters were kept constant, as described in Table 1. Turbidity was measured at 30 s intervals after the water was introduced to the system by collecting 25 mL water samples from the outlet at 0.33 H for 2 min. After the tank reached full capacity, suspended solids in the water column were measured.

Table 1. Specifications of the sediment resuspension experiments.

Investigation	Inlet type	Inlet height/H	Flow rate (L/min)	Initial water level/H	Amount of Kaolin settled for 24 h (g)
Inlet type	I, L, J	0.25	1.5	0.33	2
Inlet height	J	0.1, 0.25, 0.5	1.5	0.33	2
Flow rate	J	0.25	1.5, 2, 2.5	0.33	2
Initial water level	J	0.25	1.5	0.33, 0.5, 0.75	2
Amount of bottom sediment	J	0.25	1.5	0.33	0.5, 1, 2

Results

When the tank was fabricated with the J-type inlet, sediment resuspension was reduced by a factor greater than two (Figure 1). The initial rise in turbidity can be attributed to the resuspension of sediments due to the turbulence created by water influx. Under the I-type inlet, the sedimented particles get momentum as a result of collision with the incoming water mass that gives them sufficient energy to overcome gravitational forces. Under a J-type inlet such phenomena cannot be observed, because J-type inlets create upward flow conditions. Therefore, the resuspension in a tank retrofitted with a J-type inlet is less.

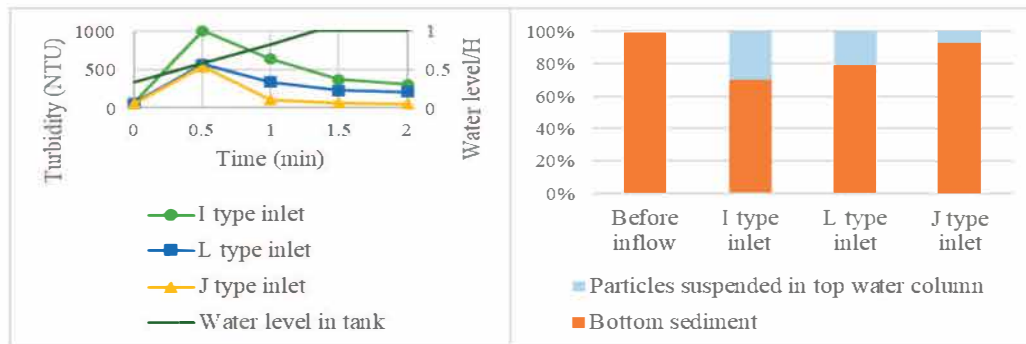


Fig. 1. Turbidity variations and distribution of kaolin mass according to inlet type.

Conclusions

The results of this study show that J-type inlets are much suited for reducing particle resuspension. Further, the study demonstrated that flow velocities need controlling by selecting a pipe diameter considering the self-cleaning velocity as well. We did not investigate the effect of the geometry of the tank on sediment resuspension, therefore, further studies in that direction is recommended.

Acknowledgement (If necessary)

This research was funded by Science and Technology Support Program through the National Research Foundation of Korea (NRF) funded by the Ministry of Science and ICT(MSIT) (grant number: NRF-2018K1A3A9A04000025).

References

1. Simmons, G.; Hope, V.; Lewis, G.; Whitmore, J.; Wanzhen, G. Contamination of potable roof collected rainwater in Auckland, New Zealand. *Water Res.* 2001, 35, 1518–1524
2. Magyar, M.; Ladson, T.; Mitchell, V.; Diaper, C. The effect of rainwater tank design on outlet water quality. *Aust. J. Water Res.* 2011, 15, 71–84

Sustainable RFD (Rainwater for Drinking) System for rural Health Care Facilities (HCF) : A Case Study at Ly Nhan HCF in Vietnam

Hakyung Lee¹, Mooyoung Han^{1*}

¹Department of Civil & Environmental Engineering, Seoul National University

*Corresponding: myhan@snu.ac.kr

Abstract

Drinking water supply issue is critical in rural areas in Vietnam. Rainwater for Drinking (RFD) system was installed at the rural health care center in Vietnam to deal with the drinking water issues. Local materials and labor were employed for the system installation and an educated local manager was employed. For a better and sustainable system, water quality and water quantity were periodically examined by the manager. By this careful monitoring, users can drink safe treated water which meets Vietnam and WHO drinking water quality standards. All monitoring datasets are shared on an online platform to achieve reliable system management. RFD system applicability for rural health care centers was convinced. The expansion of the RFD system will contribute to solving the drinking water issue for better public health and dedicate it to the achievement of the sustainable development goal 6.

Keywords: rainwater for drinking, safe drinking water, SDG 6, health care center, developing countries, Vietnam

Introduction

Rural areas in Vietnam struggles with water contamination and low water supply rate issues. Advanced drinking water supply system is hard to be extended to remote areas. The drinking water resource is normally bottled water purchased from the city which is expensive compared to the income of residents. With its higher annual precipitation rate in Vietnam than the global average, rainwater is a viable solution concerning its safety as a drinking water resource. Therefore, WASAT (Water and Sanitation Appropriate Technology) Center conducted a pilot project at a rural health care center in Vietnam. We herein aimed to install an RFD system and identify its stability and sustainability as an appropriate drinking water supply system.

Methods

The case study site is LyNhan HCF (Health Care Facility) in a rural area of Vietnam which was designed to supply water for more than 300 users in the HCF every day. To examine its sustainability, water quality and quantity were monitored periodically to discover maintenance issues and derive proper solutions. Also, a data-sharing platform was designed and system managers were educated.

Results

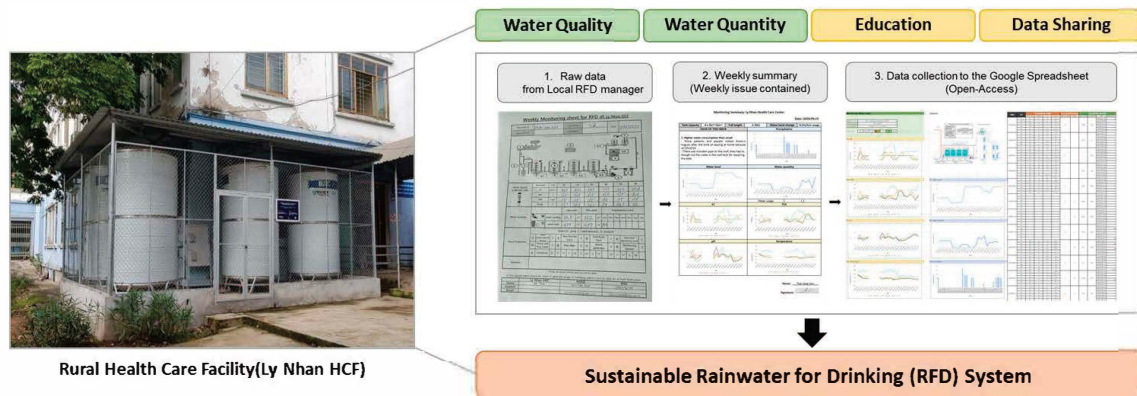
Water quantity test results show that maintenance failure, no water day, and water consumption fluctuation issues are revealed. Careful maintenance is required. By water usage tracking based on water level and water meter, rapid water usage can be controlled by alarming the excessive water usage and announce not to waste the water, and prevent the no-water day occurrence. Water quality test results show that some abnormal TDS, EC data were

examined and some parameters did not meet the microbial standard. By prompt tank cleaning and UV filter change, water quality can be convinced.

Local RFD manager conducted the monitoring and data was collected on the online platform. Responsibility inspiration was achieved by the education for managers and open-data access to the whole project team. Triple-checking was conducted by the local manager and Korean researcher that led to accurate data compilation. Base on that, a reliable archive is completed.

Conclusions

Rainwater for Drinking System was installed in rural HCF in Vietnam as a viable solution for drinking water issues. Water quality was stable and outbroken issues were directly solved. Stable water quantity will be secured by careful management by RFD managers and users. Also, a sense of ownership is inspired by open access to monitoring data and advanced education about the system. The RFD system in rural areas requires proper design and installation depending on the site. By careful maintenance, the sustainability of the RFD system will be achieved. Ultimately, safe drinking water can be supplied for the public health of HCF users.



Acknowledgment (If necessary)

This research was supported by Science and Technology Support Program through the National Research Foundation of Korea(NRF) funded by the Ministry of Science and ICT(MSIT) (grant number: NRF-2018K1A3A9A0400002)

**The 9th International
Symposium on
Environmental Hydraulics**

S2 Session

**Hydro-environment in Cities-Water Cycle,
Metabolism and Management [S2-M2]**



Feasibility of waste heat recovery from sewage in metropolitan cities

Jinsung An*

Department of Biological & Environmental Engineering, Semyung University

*Corresponding: jsan@semyung.ac.kr

Abstract

In order to reduce energy consumption and emission of greenhouse gases, the unused energies such as hydrothermal energy and recycled energy (e.g., sewage heat, incineration heat) have recently gaining interest to scientists and politicians. Among them, sewage heat is very close to the consumer and exists in a place with high energy density in the city, so its availability is higher than that of other unused energy sources. In this study, temperatures of sewage influent and effluent were measured in real time to evaluate its availability as a heat source in the metropolitan cities in Korea. Risk factors that can cause corrosion and scale in heat pump and heat exchanger operations were measured. Furthermore, a feasibility of waste heat recovery from sewage was discussed with consideration of economic and politic aspects.

Keywords: Sewage heat; Unused energy; Carbon neutral; Sewage characteristics; Benefit/cost analysis

Introduction

In order to cope with the emission of greenhouse gases caused by the excessive use of fossil fuels and the resulting climate change, various countries, including Korea, are implementing policies to convert fossil fuels into de-fossil fuels. In Korea, de-fossil fuels are being actively promoted in various fields ranging from electricity generation to transportation. However, no active changes have been observed in the heating and cooling sectors, which account for a significant portion of the final energy consumption compared to the electricity generation and transportation sectors. In this situation, interest in unused energy such as sewage heat, which was not used in the past due to lack of technology and lack of awareness, is increasing. In this study, the feasibility of waste heat recovery from sewage in cities was evaluated.

Methods

Using temperature sensors, the temperatures of the influent and effluent of the sewage treatment facility were measured in real time (10 min intervals). In addition, sewage samples were collected, and analyzed for pH, electrical conductivity, hardness, chloride, sulfate, and M-alkalinity.

Results

As a result of real-time measurement of sewage temperatures for 3 months, it was confirmed that the temperature fluctuation range was very low compared to air temperature, exhibiting a distribution of about 10 to 25 °C. In the meantime, the concentrations of ammonium ions, and M-alkalinity were relatively high in untreated sewage (influent), indicating that there is a possibility of causing a corrosion and/or scale in the evaporator of the heat pump when the sewage influent was directly used.

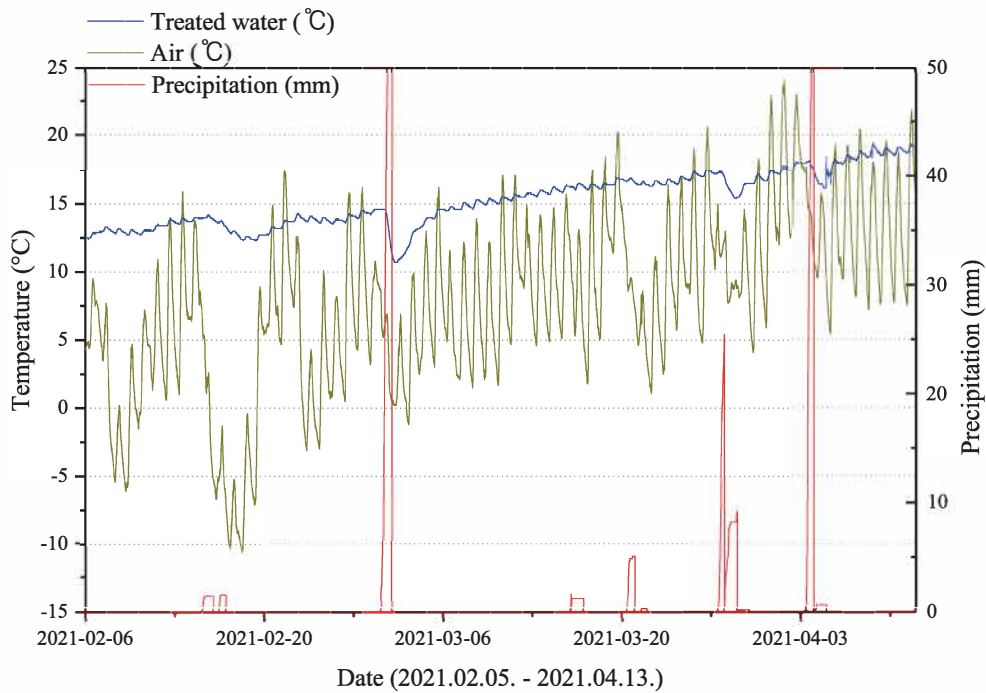


Fig. 1. Time series data (10 min intervals) of temperature for the effluent of sewage treatment plant.

Table 1. Sewage quality analysis results for evaluating the appropriate operability of heat pump and heat exchanger.

Classification	Influent	Effluent	Standard for cooling water management
pH	6.9	7.0	6.5-8.0
Electric conductivity ($\mu\text{S}/\text{cm}$)	965	799	≤ 800
Hardness ($\text{mg-CaCO}_3/\text{L}$)	139	130	≤ 150
Chloride (mg/L)	126	121	≤ 200
Sulfate (mg/L)	71.1	80.3	≤ 200
M-alkalinity ($\text{mg-CaCO}_3/\text{L}$)	182	75	≤ 200

Conclusions

It was demonstrated that the temperature characteristics of sewage were suitable for heat recovery and utilization in urban areas owing to their low variability compared to the ambient air temperature. When the sewage influent was directly used in the heat pump, the necessity of some water treatment was confirmed to avoid the corrosion and/or scale, based on cooling water quality standards. In the case of sewage effluent, it seems that additional treatment is not required.

Acknowledgement

This work was supported by the Korea Ministry of Environment (MOE) as Waste to Energy-Recycling Human Resource Development Project.

A Pilot Scale Study for Semiconductor Wastewater Reuse and Ultrapure Water Production:

Chong Min Chung^{1*}

¹Department of Environment Science & Biotechnology, Jeonju University, Jeonju 55069, Korea

*Corresponding: cmchung@jj.ac.kr

Abstract

In this work, the combined coagulation/flocculation (CF), membrane bioreactor (MBR), reverse osmosis (RO) and biological activated carbon (BAC) processes were sequentially applied in pilot scale, to reuse a semiconductor wastewater as the feed of ultrapure water (UPW) production facility. The combined CF and MBR were found to be appropriate pretreatment method to minimize the potential fouling in the following RO unit. Upon the pretreatment, the dominant foulants on the RO membrane surface were organic compounds which could be effectively removed by chemicals-in-place based on mixed sulfuric/citric acid. While almost complete rejection of ionic species was observed in the RO unit, liquid chromatography with organic carbon detector revealed that more than 21% of the remaining total organic carbon (TOC) could be removed by the BAC treatment. The TOC concentration in the final effluent was averaged to 49 ppb to satisfy the criteria to feed the UPW facility.

Keywords: Water reuse; coagulation; membrane bioreactor; reverse osmosis; biological activated carbon; ultrapure water

Introduction

Over the last decade, water reclamation and reuse are getting more popular in local communities and industries for an efficient utilization of limited, high-quality fresh water supplies (Hsu et al., 2009). Wastewater from semiconductor manufacturing facilities, one of the major industries with high water demands, could be a representative example to carry high loading contaminants both in quantity and concentrations. The semiconductor manufacturing facilities normally receive the industrial water from public or own potable water supply plants, for ultrapure water (UPW) production, cooling, and sanitary purposes. Nevertheless, recently increasing costs both for water supply and central wastewater treatment have forced internal wastewater reclamation and reuse as a sustainable maintenance strategy. The aim of this study was to investigate the technological feasibility of a pilot-scale four-stage wastewater treatment system for reclamation of the fluoride-rich inorganic wastewater, the primary semiconductor wastewater in generation rate. The four-stage system included coagulation/flocculation, membrane bioreactor (MBR) units as best available pretreatment practices to remove fluoride ions and organic compounds, respectively (Brik et al., 2006). After the pretreatment, scale formation and fouling on the RO membranes can be alleviated to prolong the operation(life) time of the RO membrane. The effluent from the MBR was introduced into the followed by RO units, while a biological activated carbon (BAC) unit was employed as the post-treatment.

Methods

Figure 1 illustrates the schematic diagram of the pilot-scale four-stage wastewater treatment system to generate feed water for UPW production. The treatment capacity of each stage was different to utilize the existing treatment processes.

Results

Our pilot-scale four-stage system was operated for more than 210 days (August 2016 to March 2017). Table 1 shows the maximum concentrations of major water quality of treated water after each treatment unit in the four-stage recycle system.

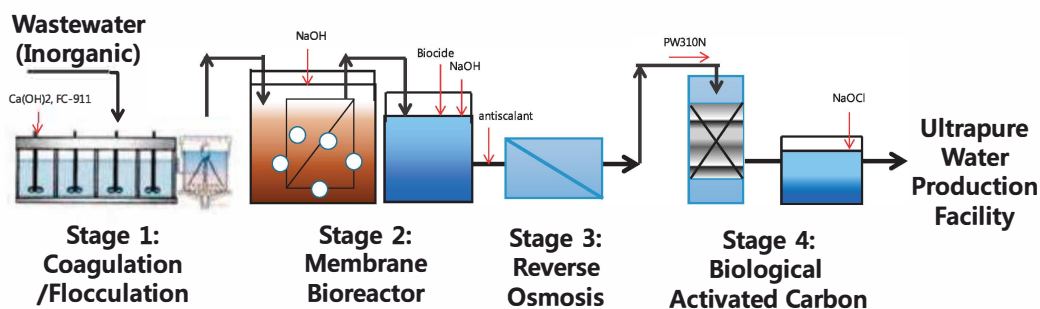


Fig. 1. Schematic diagrams of the four-stage wastewater reclamation system.

Table 1. Maximum concentrations of treated water after each treatment unit in the four-stage recycle system.

	Unit	Influent	Stage 1	Stage 2	Stage 3	Stage 4
pH		2.8	8.9	7.2	6.5	7.9
Conductivity	$\mu\text{s}/\text{cm}$	5,660.0	1,001.0	1,042.0	47.8	85.4
TOC	$\mu\text{g}/\text{L}$	5,248	5,140	1,309	62	49
Methanol	$\mu\text{g}/\text{L}$	-	748	33	6	5
Ethanol	$\mu\text{g}/\text{L}$	-	1,290	13	4	<1
TN	mg/L	17.8	16.7	15.4	2.8	4.3
T-P	mg/L	2.0	1.5	0.31	0.20	0.20
F ⁻	mg/L	608.0	18.9	12.3	4.9	4.9
Ca ²⁺	mg/L	0.5	176.0	178.0	0.3	0.3
Mg ²⁺	mg/L	0.1	8.3	8.4	0.02	0.02
T-Si	mg/L	17.9	19.7	20.0	0.4	0.4

Conclusions

In this study, a four-stage wastewater treatment system with coagulation/flocculation, MBR, RO, and BAC unit process was evaluated to reuse a fluoride-rich inorganic semiconductor wastewater for UPW production. Significant amounts of organic/inorganic compounds were removed through coagulation/flocculation and MBR units. The MBR effluent met the water quality requirement for RO feed. In addition, pretreatment by coagulation/flocculation and MBR could be appropriate method to minimize the RO membrane fouling. In particular, a pH control during the biological treatment (MBR) was found to significantly alleviate the RO membrane fouling. Upon the pretreatment, the dominant foulants on RO membrane surface were organic deposits which could be effectively removed by chemical cleaning of H₂SO₄. LC-OCD measurements revealed that more than 21% of the remaining TOC can be further removed by BAC post-treatment. The final effluent fully satisfied the criteria for UPW water quality. Our four-stage wastewater treatment system should be more competitive upon upcoming increases in public cost for water supply and wastewater treatment along with stricter environmental regulations.

References

- Brik, M., Schoeberl, P., Chamam, B., Braun, R. and Fuchs, W. (2006) Advanced treatment of textile wastewater towards reuse using a membrane bioreactor. *Process Biochemistry* 41(8), 1751-1757.
- Hsu, Y.-L., Wu, H.-Z., Ye, M.-H., Chen, J.-P., Huang, H.-L. and Lin, P.H.-P. (2009) An industrial-scale biodegradation system for volatile organics contaminated wastewater from semiconductor manufacturing process. *Journal of the Taiwan Institute of Chemical Engineers* 40(1), 70-76.

Stochastic approaches for risk and resilience of groundwater systems under uncertainty

Jinwoo Im*

Sonny Astani Department of Civil and Environmental Engineering, University of Southern California

*Corresponding: jinwooim@usc.edu

Abstract

Uncertainty is ubiquitous in risk analysis associated with groundwater contamination. Risk predictions are subject to uncertainty due to our inability to fully characterize the subsurface environment at all relevant scales and our lack of knowledge of all underlying physical-bio-chemical processes occurring (which lead to biases in predictions and error in model conceptualization). To tackle this challenge, computationally efficient stochastic methods are needed. In this talk, we will provide an overview of a series of stochastic based methods that are aimed to 1) compute the uncertainty associated in risk analysis and 2) improve our fundamental understanding of the underlying physics of a given physical attribute in the subsurface environment. This talk is divided into 3 parts. We start by illustrating the importance of coupling hydrological and public health models to improve the estimation of aquifer resilience and reliability in the presence of emerging contaminants. Second, we make use of recent developments in genetic programming to show how the combined use of data and prior knowledge of the physics involved can be used to identify the governing equations of a given system. We illustrate the performance of the genetic programming method in a series of problems relevant to the subsurface environment such as soil moisture dynamics and solute transport. Finally, we propose an innovative method that allows to incorporate block scale multi-mass transfer fluxes in random walk particle tracking. Each of the 3 objectives of this talk has its own research question in order: What are potential health risks from emerging contaminants in heterogenous aquifers? How could the measured data be incorporated into the process of establishing governing equations for hydrogeological systems? How could the solute transport in groundwater achieve an accurate but still computationally efficient multi-rate mass transfer between mobile and immobile phases? Addressing these fundamental questions is key to better support the decision-making process in the groundwater risk management.

Keywords: Health risk; Resilience; Uncertainty; Monte Carlo simulation; Genetic Programming; Random Walk Particle Tracking

Introduction

It is a challenging issue to assess the human health risks and the aquifer resilience under the contamination of groundwater systems. Under limited resources to characterize heterogeneous subsurface systems and complex contaminant toxicity, there is uncertainty in contaminant transport modeling in aquifers and health risk estimation at an environmentally sensitive location. In order to achieve reliable risk and resilience assessment, several stochastic approaches (i.e., Monte Carlo simulation (MC), Genetic Programming (GP), and Random Walk Particle Tracking (RWPT)) are utilized in this study.

Methods

- 1) MC simulation is used to investigate the impact of the interplay between two sources of uncertainty in risk and resilience predictions associated with Bisphenol A (BPA). These two sources of uncertainty are: (1) hydraulic conductivity heterogeneity and (2)

emerging contaminant toxicity.

- 2) GP is employed to identify the structure of the governing equation in subsurface system models from measured data. GP is a stochastic optimization approach that aims to optimize programs through evolutionary processes in consecutive generations for a specific task. Based on GP, the system identification method, named by GPfSI, is developed to discover governing differential equations from the data measured from multi-physics systems (e.g., hydrogeological systems).
- 3) On the basis of a previously developed GPU-based RWPT method (Rizzo et al., 2019), the new method, named by PAR2MT, is developed to incorporate multi-rate mass transfer of contaminants between mobile and immobile phases. PAR2MT performs the parallel computation of mass transfer rates based on the grid block, which allows to describe more accurate mass transfer phenomena than the computation based on the whole grid in the previous methods.

Results

- 1) Our results highlight that the magnitude and uncertainty of the aquifer resilience due to BPA vary in a non-trivial manner with the heterogeneity of the conductivity field (Im et al., 2020). We also show that the functional shape of the BPA dose-response model is critical in risk management.
- 2) GPfSI is successfully demonstrated by identifying the canonical reference system models from the given data (Im et al., 2021). In addition, it suggests simple models (i.e., single ordinary differential equations) for the data from the complex lumped-element model and finds accurate models for the column experiment data by capturing tailing effects.
- 3) PAR2MT results show that the contaminant transport from block-based mass transfer exhibits more non-Fickian behaviors than from grid-based mass transfer, delaying late arrival times of solute at the control plane. Furthermore, by performing PAR2MT with different levels of aquifer heterogeneity, it is found that the aquifer heterogeneity dictates contaminant transport behaviors over mass transfer properties as the level of the aquifer heterogeneity increases.

Conclusions

The investigations carried out in this presentation provide the numerical tools that could be employed to assess the risks and resilience of groundwater systems under uncertainty in a robust manner. The results of these approaches will be solid grounds for decision-making process in the site investigation and management.

Acknowledgement

All authors gratefully acknowledge the financial support by the National Science Foundation under Grant Number 1654009 and Jinwoo Im acknowledges the Kwanjeong Educational Foundation for financial support.

References

- Im, J., Rizzo, C. B., & de Barros, F. P. (2020). Resilience of groundwater systems in the presence of Bisphenol A under uncertainty. *Science of The Total Environment*, 727, 138363.
- Im, J., Rizzo, C. B., de Barros, F. P., & Masri, S. F. (2021). Application of genetic programming for model-free identification of nonlinear multi-physics systems. *Nonlinear Dynamics*, 104(2), 1781-1800.
- Rizzo, C. B., Nakano, A., & de Barros, F. P. (2019). PAR2: parallel random walk particle tracking method for solute transport in porous media. *Computer Physics Communications*, 239, 265-271.

Development and application of a polar organic chemical integrative sampler (POCIS) for monitoring micropollutants in a drinking water treatment plant

Hyun-ah Kwon¹, and Yongju Choi^{1*}

¹Department of Civil & Environmental Engineering, Seoul National University

*Corresponding: y.choi81@snu.ac.kr

Abstract

Passive sampling has been known as one of the monitoring methods because it overcomes low detection limits of micropollutants in the environment and presents a representative concentration value through long-term monitoring. In this study, a passive sampler, polar organic compound integrative sampler (POCIS), is applied to monitor micropollutants in a drinking water treatment plant with a cage to protect the sampler that is designed to prevent hydrological effects, thereby verifying reliability to minimize effects caused by a flow fluctuation. Three per- and polyfluoroalkyl substances (PFASs), which are currently being studied worldwide, is targeted. To derive a sampling rate and check the accuracy of the passing sampler, the concentration change scenarios are set. Applying it to the drinking water treatment plant to confirm and verify its applicability. It is expected to be capable of improved operation in drinking water treatment plants.

Keywords: Passive sampling; Micropollutants; Water quality monitoring; Time-weighted average concentration; Sampling rate

Introduction

A monitoring of micropollutants in water is a crucial issue to protect human health and environment. Among various micropollutants, PFASs have been often detected in drinking water and potentially have high risks to humans and environment at trace levels. A conventional monitoring method (grab sampling) only gives a one-time concentration. Moreover, this method is costly and required to go through a complex multi-step for pre-treatment. A passive sampling can provide a time-weighted average concentration (C_{TWA}) without maintenance, supervision and power supply. POCIS as a passive sampler is often employed for monitoring for a wide range of polar substances. However, a monitoring of PFAS using POCIS in drinking water treatment plant has rarely studied due to lack of adequate monitoring technique and lack of drinking water legislation related to PFASs. This study aims at developing a field applicable passive sampling method using POCIS for PFASs in drinking water treatment plant.

Methods

POCIS with Oasis HLB as a sorbent is employed as a diffusive passive sampler for three commonly detected PFASs (PFOS, PFOA, and PFHxS). Oasis HLB is inserted into two PES membrane like a sandwich, and they are fixed between stainless steel rings. A calibration experiment in a laboratory is designed for the improvement of accuracy of sampling rate (R_s) based on concentration change scenario shown in Table 1. After the experiment, the membrane and sorbent are separated and eluted with methanol. The extracts are analyzed using liquid chromatography-tandem mass spectrometry (LC-MS/MS).

Results and Conclusions

A calibration experiment in a laboratory is performed by analyzing a decreasing concentration of PFASs in water for 28 days. As a result, a sampling rate, a key factor in passive sampling, is obtained via equation (1). This ensures that C_{TWA} and POCIS acts as a kinetic sampler showing a linear uptake kinetic for an appropriate deployment period ($t_{1/2}$; the half of the equilibrium concentration), equation (2) and (3) respectively.

$$C_w(t) = \frac{C_w(0) \left\{ 1 + \frac{K_{sw}M_s}{V_w} \exp \left[- \left(1 + \frac{K_{sw}M_s}{V_w} \right) \frac{R_s t}{K_{sw}M_s} \right] \right\}}{1 + \frac{K_{sw}M_s}{V_w}} \quad (1)$$

$$C_{TWA} = \frac{M_a}{R_s \cdot t} \quad (2)$$

$$t_{1/2} = \frac{\ln 2}{\frac{R_s}{K_{sw}M_s}} \quad (3)$$

The concentration change scenarios will be done as three different concentration changes for 10 days to confirm whether it is calculating the exact C_{TWA} from the derived sampling rate, and the expected results are as follows.

Table 1. The expected results of concentration change scenario experiments

Scenario	1 st stage		2 nd stage		3 rd stage		C_{TWA}
	Conc.	Deployment period	Conc.	Deployment period	Conc.	Deployment period	
1	100 µg/L	5 day	500 µg/L	3 day	200 µg/L	2 day	240 µg/L
2	200 µg/L	2day	100 µg/L	5 day	500 µg/L	3 day	240 µg/L
3	500 µg/L	3day	200 µg/L	2 day	100 µg/L	5 day	240 µg/L

The corresponding results demonstrate that POCIS has accuracy and reliability in response to changes in concentrations of PFASs in drinking water treatment plants. Finally, we will validate an applicability and reliability in field by designing a sampler cage that can ignore the fluctuation of flow causing negative effects to sampler. It is anticipated that the passive sampling contributes to manage the risk of PFAS to human and the drinking water treatment plant economically.



Fig. 1 Scheme of overall study

Acknowledgement

This research has been performed as Project No D-T-001 and supported by Korea Water Resources Corporation (K-water).

Oxidation of aldehydes found in finished recycled wastewater with heterogeneous transition metal catalysts and dissolved oxygen

Euna Kim¹, Georgia Cardosa¹, and Daniel L. McCurry^{1*}

¹Department of Civil & Environmental Engineering, University of Southern California, Los Angeles, CA 90089

*Corresponding: dmccurry@usc.edu

Abstract

The shortage of California drinking water sources has recently drawn attention to the use of recycled wastewater. A recent study has documented the presence of carbonyl compounds in final recycled water effluent that went through multiple advanced treatment processes. We applied heterogeneous catalysts of Pt/C to perform kinetic and isotope label experiments for optimizing aldehydes oxidation conditions and identifying the reaction mechanism. The results show that formaldehyde was oxidized most efficiently, producing formic acid with nearly 100 % mass balance. Other single chain aldehydes were also oxidized in drinking water treatment conditions. An ¹⁸O-isotope experiment revealed that both dissolved oxygen and water incorporated into the products. This study highlights application of heterogeneous catalyst for oxidizing low weight molecules in finished recycled wastewater.

Keywords: Heterogeneous catalyst; Aldehyde oxidation; Potable water reuse;

Introduction

Treated wastewater is expanding as a source of potable water given that current resources are decreasing due to population growth and extended periods of drought. Advanced oxidation processes following reverse osmosis can remove most trace organic compounds present in the treated wastewater. However, low molecular weight compounds have been detected in finished recycled wastewater. A recent study identified carbonyl compounds, including single chain saturated and unsaturated aldehydes, as accounting for more than 30% of dissolved organic matter found, and it is concerning given that these aldehydes are classified as probable human carcinogens. Heterogeneous catalysts have been widely studied to oxidize aldehydes for synthetic purposes and in air. In this study, we aim to identify kinetics of aqueous aldehyde oxidation using molecular oxygen as the terminal electron acceptor, by applying heterogeneous catalysts under mild conditions, and determine the role of the oxygen by performing isotope-labeling experiments.

Methods

For kinetic experiments, six single-chain-saturated aldehydes and one single-chain-unsaturated aldehyde were chosen as oxidation targets: formaldehyde, acetaldehyde, propionaldehyde, butyraldehyde, pentanal, hexanal and crotonaldehyde. After suspending heterogeneous Pt/C catalysts in a buffer solution, each aldehyde was injected in the reactor to initiate the oxidation of aldehydes. Aliquots were extracted periodically and filtered with a syringe filter (0.2 μM, PTFE). Organic compounds in the sample were derivatized by either 2,4-Dinitrophenylhydrazine (2,4-DNPH) or 4-Bromo-N-methylbenzylamine (4-BNMA) coupled with 1-Ethyl-3-(3-dimethylaminopropyl)carbodiimide (EDC) to facilitate quantitative analysis of reactants and products via high resolution HPLC-MS/MS (Figure 1). Dissolved oxygen concentration was measured by modified Winkler method.



Figure 1. Derivatization of aldehydes with 2,4-DNPH and carboxylic acids with 4-BNMA coupled with EDC.

For isotope-label experiment, ^{18}O -labeled water (H_2^{18}O) was utilized to track the oxygen atoms during the reaction process. The mixture of Pt/C, water, and reactant in 2 mL HPLC vials were then stirred for 2 ½ hours and filtered through a 0.2 μm syringe filter, and all derivatizing procedures were kept the same.

Results

The kinetic experiments show that formaldehyde was oxidized the fastest, with a first-order observed rate constant of 5.86 h^{-1} ($\pm 0.20 \text{ h}^{-1}$, triplicate), corresponding to a half-life of 7.1 minutes. From acetaldehyde to butyraldehyde, the oxidation rate increased as the length of the chain increased: 1.70 h^{-1} for acetaldehyde, 1.95 h^{-1} for propionaldehyde and 2.74 h^{-1} for butyraldehyde. However, aldehydes with longer chains than butyraldehyde showed no difference in the reaction rate (ANOVA, $p > 0.05$): 2.39 h^{-1} for pentanal and 2.65 h^{-1} for hexanal. The reaction profile of acetaldehyde oxidation at a higher initial concentration shows that molecular oxygen is consumed during the aldehyde oxidation process and eventually depleted, stopping aldehyde oxidation. This proves that the molecular oxygen in aqueous solution plays an important role in aldehyde oxidation, consuming one oxygen molecule to oxidize 3.80 aldehyde molecules.

The isotope-label experiment indicated that oxygen atom in carbonyl group of butyraldehyde was exchanged with ^{18}O in water within 5 min, producing geminal diol. It was oxidized into its corresponding carboxylic acid inserting oxygen atom from either dissolved oxygen or water. From these results, it is expected that aldehyde oxidation reacts through two different pathways and is still under study.

Conclusions

This study suggests that single-chain aldehydes were oxidized to carboxylic acids with heterogeneous catalyst under drinking water treatment conditions. As understanding the reaction mechanism with heterogeneous catalysts is important for improving the transformation of aliphatic aldehydes, isotope experiment proved that oxygen atoms from molecular oxygen and water incorporate into carboxylic acids. For the overall reaction, dissolved oxygen plays an essential role for oxidizing those aldehydes when applying the heterogeneous catalyst. Significant research remains to be done optimizing catalyst composition for reducing the cost of producing the heterogeneous catalyst.

Acknowledgement

E.K. was partially supported by a USC Provost Fellowship. We acknowledge additional funding from the National Science Foundation (Award No. CBET-1944810).

References

- Marron, E. L., Prasse, C., Buren, J. V., & Sedlak, D. L. (2020). Formation and Fate of Carbonyls in Potable Water Reuse Systems. *Environmental Science & Technology*, 54(17), 10895-10903.
- Marquis, B. J., Louks, H. P., Bose, C., Wolfe, R. R., & Singh, S. P. (2017). A new derivatization reagent for HPLC–MS analysis of biological organic acids. *Chromatographia*, 80(12), 1723-1732.

Development of Sensor Technologies for Smart Water Quality Management in Future Cities

Jong Kwon Choe^{1*} and Junyoung Park¹

¹Department of Civil & Environmental Engineering, Seoul National University

*Corresponding: jkchoe@snu.ac.kr

Abstract

Providing access to clean water is one of grand challenges for engineering identified by the U.S. National Academy of Engineering as well as one of the UN's Sustainable development Goals (SDGs). In many developed countries, reclaiming and reusing water from a variety of sources including previously-used domestic and industrial water has been considered to be a potentially important alternative to existing water supplies that can enhance sustainability and resilience of water management, especially in urban areas. This presentation will cover examples of sensor technologies developed for detection of emerging contaminants in water and how sensor technologies can potentially contribute to data collection and management of water quality in cities.







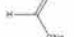
Keywords: Non-Fickian transport; River; Meander; Flow recirculation; Secondary flow

Introduction

Water quality sensor technologies can play an important role in smart water management in urban areas because of its ease of use and applicability for autonomous data collection. However, most water quality sensor technologies developed up to date focus on basic parameters such as pH and total dissolved solids. Only limited sensor technologies are available for detection of emerging contaminants (e.g., pharmaceutical and personal care products, disinfection byproducts, and perfluorinated compounds), which are detected in urban and natural water sources. There is a need to develop a sensor that can selectively and efficiently detect these emerging contaminants.

Methods

As the part of this presentation, a DNA-aptamer based sensor has been developed for detection of perfluorinated alkyl substances (PFAS). Briefly, the aptamer has been selected via in vitro selection (also known as SELEX). The selected aptamer has been modified to have a fluorophore and a quencher. When a target compound (i.e., PFAS) binds to the aptamer, the quencher is released and the fluorescence intensity increases.

Compound	Molecular structure	MW (g/mol)
Perfluorooctanoic acid (PFOA)		414.07
Perfluoroheptanoic acid (PFHpA)		364.06
Perfluorohexanesulfonic acid (PFHxS)		400.12
Perfluoropentanoic acid (PFPeA)		264.05
Perfluorononanoic acid (PFNA)		464.08
Perfluorooctanesulfonic acid (PFOS)		500.13
Sodium formate (HCOONa)		68.007

Binding affinity of the selected aptamer to various PFAS compounds listed in Table above were investigated and binding mechanisms were elucidated using a series of characterization techniques including nuclear magnetic resonance (NMR) and circular dichroism (CD).

Results

The aptamer showed high binding affinity to PFOA, PFHpA and PFHxS and poor binding affinity to sodium formate, PFPeA, PFNA, and PFOS. Results suggest that the aptamer is selective towards perfluoroalkyl carbons with carbon length of 6 to 7 and functional group (-COOH, -SO₂OH) at the tail does not significantly influence the aptamer binding to a target compound.

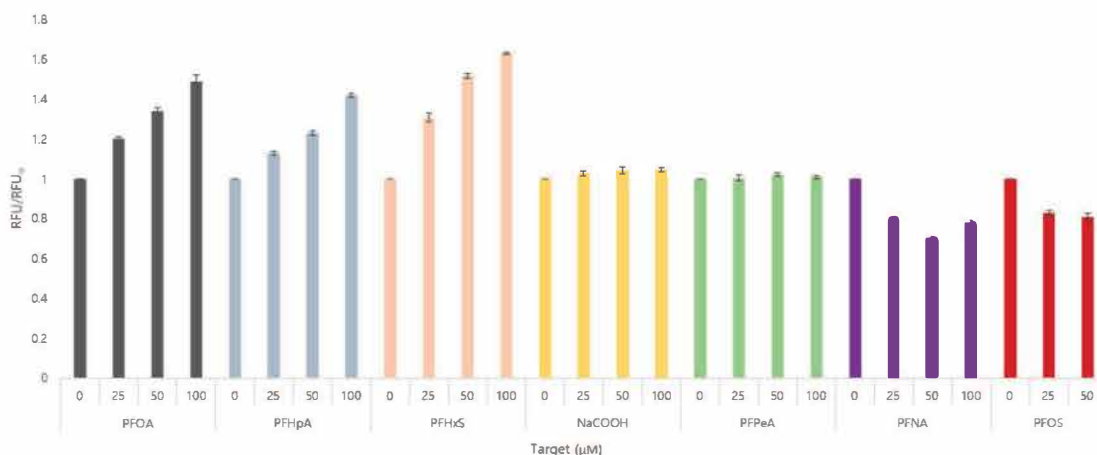


Fig. 1. Aptamer binding to PFAS compounds and Sodium formate.

Conclusions

The results of this study show that the selected aptamer can be utilized for detection of one of important emerging contaminants, PFAS. Furthermore, the study shows the importance of development of water quality sensor technologies for their application in water quality data collection, which is very important component for smart water management in future cities.

Acknowledgement (If necessary)

References

**The 9th International
Symposium on
Environmental Hydraulics**

S3 Session

**Development of River Management Technology
Using River Survey and Monitoring Drones [S3-T1]**



The development of the drone operation platform for river survey and monitoring

Jaehyun Shin¹, Hoje Seong¹, Dong Sop Rhee^{1*}

¹ Korea Institute of Civil Engineering and Building Technology, Goyang-Si, Gyeonggi-Do, South Korea

* Corresponding: dsrhee@kict.re.kr

Abstract

The demand for river monitoring and river topography survey is increasing recently in Korea, therefore the necessity for technology development using drone survey have escalated. To follow these changes, a drone operation platform is being developed for smart river management including river survey and monitoring, which is based on bathymetric LiDAR and hyperspectral image utilization. For the utilization of the drone operation platform, a graphic user interface will be implemented in the software for the platform managers and users. Also the measured data will be analyzed quasi real-time to be used as initial conditions for the flow and contaminant transport models. This will lead to the development of a system estimating river information for the river operation and management.

Keywords: drone operation platform, river monitoring, river survey, bathymetric LiDAR; hyperspectral image

Introduction

Climate change in the Korean peninsula have caused the river configuration and environment to change, but the current established river data have its limits in reflecting the latest up-to-date information leading to low accuracy in estimating environmental changes. Therefore, the demand for river monitoring and river topography survey is increasing recently in Korea, and the necessity for technology development using drone survey have escalated. The river management paradigm is currently changing due to development of state-of-the-art technology such as drones, so the transfer to smart river management using these technological improvements is progressing. To follow these changes, a drone operation platform is being developed for smart river management including river survey and monitoring, which is based on bathymetric LiDAR and hyperspectral image utilization.

Methods

The development of the drone operation platform will enable frequent and periodical river surveys, which will enhance the response to flood damage and repairs in flood seasons. Also, the regular surveys will facilitate data acquisition for continuous river changes for accurate measured data. Since the river environment is changing rapidly, prediction of river data using conventionally measured data will not be able to guarantee accuracy; frequent measurements in flood seasons will improve data usage for modeling and other river management related activities.

For the utilization of the drone operation platform, a graphic user interface will be implemented in the software for the platform managers and users. A system that displays the data processing results as well as the drone operating aerial map is needed, which will be

connected to the river database including the riverside facilities. Also the measured data will be analyzed quasi real-time to be used as initial conditions for the flow and contaminant transport models. This will lead to the development of a system estimating river information for the river operation and management. Further development and cost decrease of tech and equipment will later result in data modeling using the elaborate data acquired using the LiDAR and hyperspectral cameras.

Results

The continuous research will lead to the development of a system estimating river information for the river operation and management. The bathymetric LiDAR using red and green dual lasers are being developed for the accurate detection of the river bathymetry as well as the water depth. The RGB and hyperspectral images will be processed using optimized band ratio analysis and support vector machine tech to acquire data such as velocity, water depth, sediment concentration in the river. Then the acquired data using drones will be sent to the drone platform with the database and server, which can be processed into spatial riverine data. The spatial riverine data will undergo another data process sequence where the modeling for flow and water quality will be conducted for the estimation to river environment change.

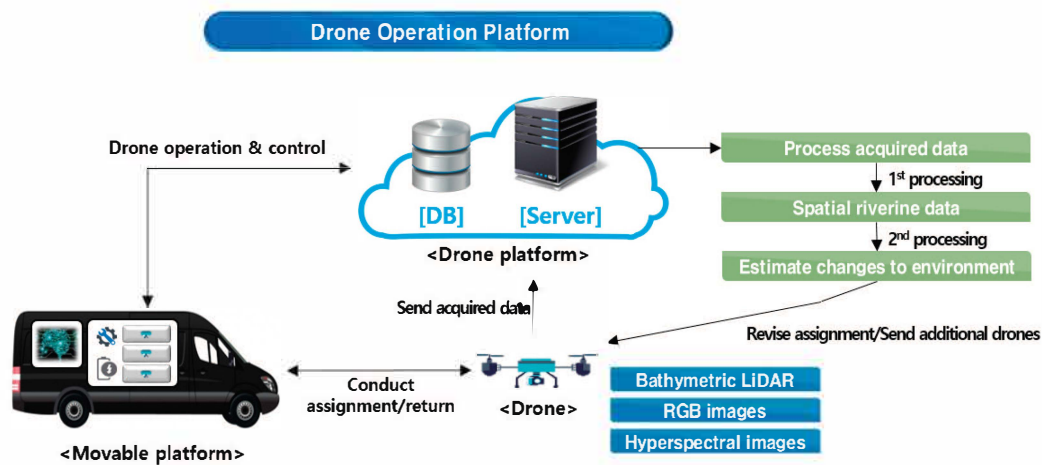


Fig. 1. Diagram of the drone operation platform.

Conclusions

The development of the drone operation platform will enable frequent and periodical river surveys, which will facilitate the acquisition of quasi real time data for modeling and estimation to the changes to the environment. The former riverine database based on point and lateral surveys will be expanded into full two-dimensional data across the river which can be used for high quality river flow and water quality modeling. Using the technology that is being developed in this research will increase the possibility for real-time customized data for the river management, researchers and public users.

Acknowledgement

This work is supported by the Korea Agency for Infrastructure Technology Advancement (KAIA) grant funded by the Ministry of Land, Infrastructure and Transport (Grant 21DPIW-C153746-03).

Creation of a digital twin using LiDAR point cloud and high-resolution imagery acquired in river basins

Yun-Jae Choung^{1*}

¹Geospatial Research Center, Geo C&I Co., Ltd.

*Corresponding: chyj@geocni.com

Abstract

A river-customized digital twin can be utilized for monitoring the object changes and predicting the object movements in river basins. This research proposes the process for designing a river-customized digital twin using the LiDAR point cloud and the high-resolution imagery acquired in the selected river basins through the following steps. In the first step, the LiDAR point cloud located under the water surface were manually removed. Then, the digital surface model (DSM) was generated from the given LiDAR point cloud by using the interpolation method. Next, the high-resolution imagery were integrated with the generated DSM to produce the initial river-customized digital twin. In future research, the additional datasets such as the real-time water quality data would be integrated to produce the advanced river-customized digital twin.

Keywords: Digital twin; LiDAR point cloud; High-resolution imagery; River basin

Introduction

A digital twin is defined as “a virtual representation of an object or system that spans its lifecycle, is updated from real-time data, and uses simulation, machine learning and reasoning to help decision-making” (IBM, 2021). Creation of a digital twin in river basins is important for virtually representing the objects in river basins with the real-time information. This research proposed an efficient methodology for creating the river-customized digital twin using the high-resolution imagery and LiDAR point cloud acquired in the river basins.

Methods

First of all, the water areas were extracted from the given high-resolution imagery by using the artificial intelligence technique (Fig. 1).

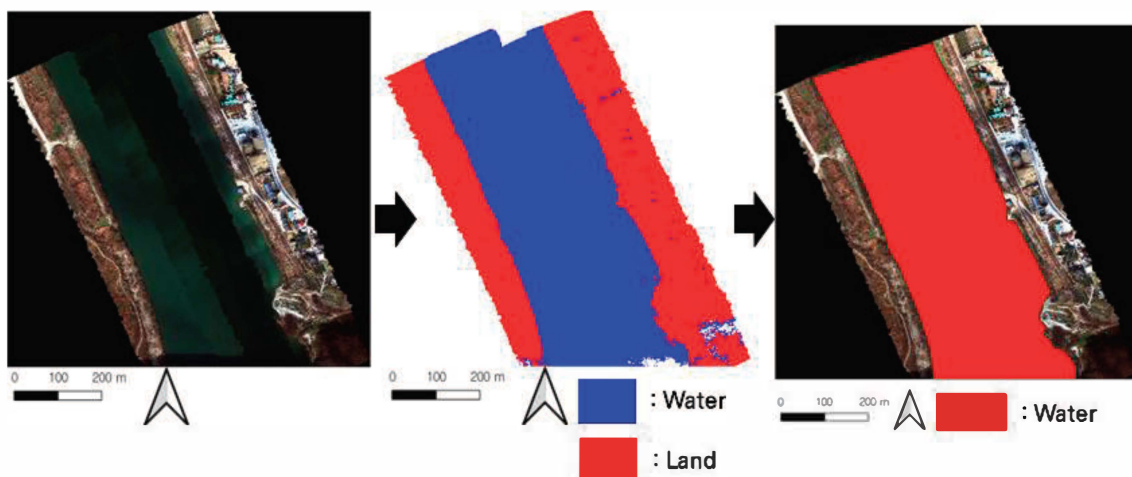


Fig. 1. Process showing the extraction of water areas from the given high-resolution imagery by using the artificial intelligence technique.

Then, the LiDAR points located under the water surface were manually removed the

given LiDAR point cloud. Next, the digital surface model (DSM) was generated from the given LiDAR point cloud by using the triangulated irregular network (TIN) interpolation (Fig. 2).

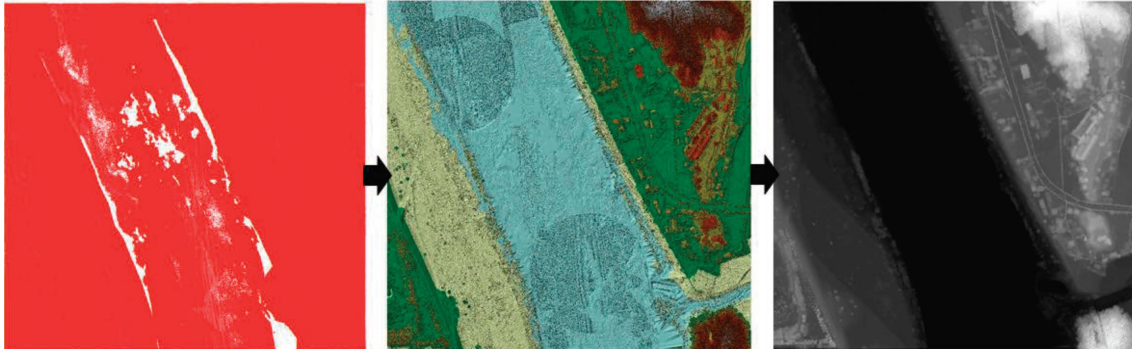


Fig. 2. Process showing the generation of the DSM from the given LiDAR point cloud by using the TIN interpolation.

Finally, the initial river-customized digital twin was generated by integrating between the high-resolution imagery and the generated DSM (Fig. 3).

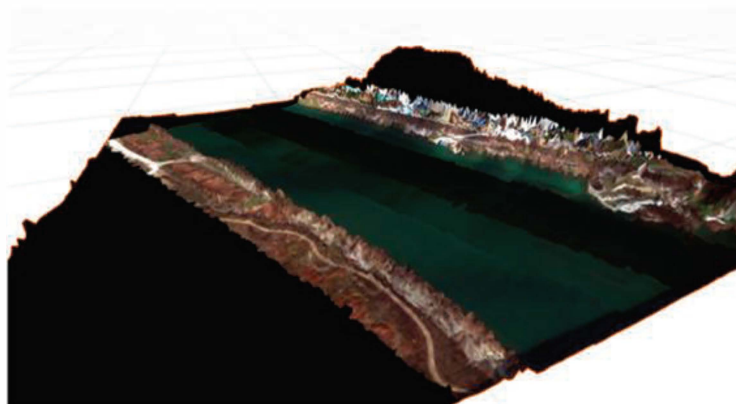


Fig. 3. Initial river-customized digital twin was generated by integrating between the high-resolution imagery and the generated DSM.

Conclusions

In this research, the initial river-customized digital twin was generated by integrating between the given high-resolution imagery and the DSM generated using the LiDAR point cloud acquired in the river basins. In future research, the additional datasets such as the real-time water quality data would be integrated to produce the advanced river-customized digital twin.

Acknowledgement

This work is supported by the Korea Agency for Infrastructure Technology Advancement(KAIA) grant funded by the Ministry of Land, Infrastructure and Transport(Grant 21DPIW-C153746-03).

References

IBM (2021). Cheat sheet: What is Digital Twin? <https://www.ibm.com/blogs/internet-of-things/iot-cheat-sheet-digital-twin/> (Accessed April 14, 2021).

Bathymetric Observation with UAV-based Hyperspectral Image in Shallow Rivers

Hojun You¹, Dongsu Kim^{2*}, Younghwa Kwon²

¹The University of Iowa, Iowa City, Iowa, USA

²Dankook University, Yongin-si, Gyeonggi-do, South Korea

* Corresponding: dongsu-kim@dankook.ac.kr

Keywords: Hyperspectral; Bathymetry; UAV; Optimal Band Ratio; River Morphology;

Abstract

Fluvial bathymetry is one of the most important measurable factors in research on river environments. Spatially distributed water-depth information is vital to studies in fluvial geomorphology and stream ecology and plays a central role in many river management applications, particularly those that involve in-stream habitat assessments, which are time-consuming and often limited in spatial scale for high-resolution surveys. Among the remote-sensing techniques, this study shed highlights on bathymetric survey driven by UAV-based hyperspectral image for very shallow small stream to identify ripples and dunes. The technique developed in this study produces basic data that are useful for periodic investigation of bed variations and research on rivers and overcomes the technical limitations of classical in-situ bathymetric measurement, which forms the basis of the conventional river topography measurement technology and reduces the time and monitoring cost. The developed technique took advantage of the correlation between the spectral characteristics and the water depth using hyperspectral images measured by a UAV, which provides the final 2D representation of the spatial distribution of depths based on the hyperspectral images. We also developed and implemented an algorithm for finding the optimal band ratio to derive the optimal correlation between the optimal band ratio and the depth using the reflectance of hyperspectral images collected by a hyperspectral sensor mounted in a UAV.

Acknowledgement

This work is supported by the Korea Agency for Infrastructure Technology Advancement(KAIA) grant funded by the Ministry of Land, Infrastructure and Transport (Grant 21DPIW-C153746-03).

Development and Application of HDM-2DF for Analyzing River Inundation and Inland Flooding

Chang-Geun Song^{1*}

¹ Department of Safety Engineering, Incheon National University

* Corresponding: baybreeze119@inu.ac.kr

Abstract

In recent years, there are more concerns for flood due to the increased localized downpour and surcharged rainwater discharged from sewage collection system. The fundamental causes of the increase of urban flooding are the climate change and intensive urbanization. Existing researches on the urban flood prediction have been conducted to analyze either the river inundation or inland flooding, or simply add up the individual inundation elements to elucidate comprehensive flood phenomena. This research conducted a series of analysis examining the results of individual flooding and simultaneous flooding. The result revealed that the simultaneous flooding can consider the weighted influence of the flood damages.

Keywords: HDM-2DF; river inundation; inland flooding; comprehensive flooding

Introduction

Among the various environmental disasters, flood is the most common hazard all around the world. The main reasons for this are the extensive and far-ranging geographical formation of river, low-lying residence in coastal and riparian zone and human settlement to secure the surface and groundwater resources. Prevalent studies on the urban flood modelling have been attempted to analyze either the river inundation or inland flooding, or simply add up the individual inundation elements to route comprehensive flood phenomena. However, this approach does not consider the physical flooding mechanism correctly and thereby overestimating the flood damage, which causes excessive design and waste of financial resources and human labors. Researches on the analysis of inundation in urban areas have been implemented through various ways, and the results were compared with actual inundation data. A series of modeling experiments revealed that multiple sources of flooding must be considered simultaneously and that comprehensive flooding simulations are necessary. This research developed a 2D numerical model for predicting hydrodynamic behavior of complex flooding, and implemented a quantitative analysis of flooded area and flow velocity compared with single type flooding simulation results.

Description of Model

In this study, HDM-2D, a general purpose two-dimensional surface water flow model that can simulate channel flows (Song et al., 2012; Seo and Song, 2012), was extended and entitled as HDM-2DF (Kim et al., 2018). The model is capable of flood simulation incorporating multiple sources of inundation such as river inundation and inland flooding. In modeling aspect, the river inundation is activated by assigning internal anomaly boundary condition and discontinuous initial conditions while the inland flooding can be successfully implemented by external mass reflector.

Results

The typhoon Maemi caused severe damages in September, 2003, and the Masan free trade zone located in southern part of South Korea is selected as target region. The area of the target region was bounded as 210,000 m² among the Masan free trade zone including the ocean in the south and Sanho River in the west. As presented in Fig. 1, the finite element mesh was generated with 36,669 nodes and 42,300 elements. Every building within the target area was included in mesh layout because buildings can disturb the runoff of flow. Due to the river inundation and inland flooding during the period of the typhoon Maemi, the riparian zone as well as the coastal area was seriously submerged as shown in Fig. 1(b) and (c). After detailed analysis, it was founded that the results by simultaneous flooding gave the inundation depth increased from 20.4% to 63.6% and the flow velocity from 10.5 % to 81.7 % compared to the single flood simulation.

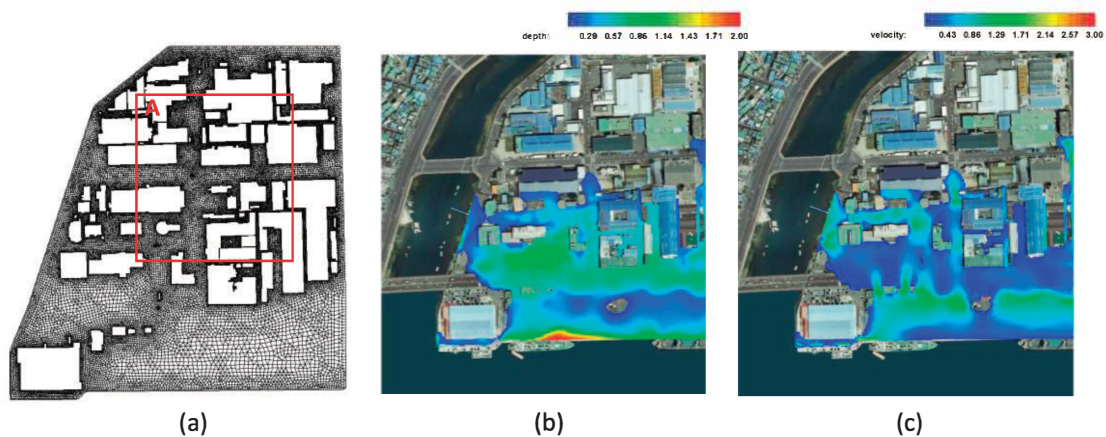


Fig. 1. Mesh layout and results: (a) mesh generation, (b) flood depth and (c) inundation velocity

Conclusions

This research conducted a series of analysis examining the results of individual flooding and simultaneous flooding. The result revealed that the simultaneous flooding can consider the weighted influence of the flood damages. A software suite for analysis of surface water flow and transport entitled RAMS+ (ver. 1.0) was released as of Feb. 5th, 2021 to interface the solvers including HDM-2DF and CTM-2D-TX with the pre- and post-processor. Anyone who has interest can visit <http://ramsplus.net> and download the experience version.

Acknowledgement

This work is supported by the Korea Agency for Infrastructure Technology Advancement(KAIA) grant funded by the Ministry of Land, Infrastructure and Transport (Grant 21DPIW-C153746-03).

References

- Seo, I. W., & Song, C. G. Numerical simulation of laminar flow past a circular cylinder with slip conditions. *International Journal for Numerical Methods in Fluids*, 68(12), 1538 - 1560.
- Song, C. G., Seo, I. W. & Kim, Y. D. Analysis of secondary current effect in the modeling of shallow flow in open channels. *Advances in Water Resources*, 41, 29-48.
- Kim, H. J., Rhee, D. S. & Song, C. G. Numerical computation of underground inundation in multiple layers by adaptive transfer method. *Water*, 10, 85.

Discharge Calculation using Surface Velocity Measured by Surface Image Velocity Meter

Youngsin Roh¹, and Seo Jun Kim²

¹Dept of Advanced Infra-structure, Korea Institute of Hydrological Survey

² Department of Civil Engineering, Myongji University

*Corresponding: rohys@kihs.re.kr

Abstract

The SIV(Surface Image Velocimetry) was developed to measure flow velocity field using image process technology, and a method of discharge calculation from the surface velocity is required to measure river discharge. In this study, discharge calculation for the surface velocity was analyzed for the purpose of examining the applicability of the SIV. 3 CCTV cameras for SIV were installed at the test bed to verify surface velocity and discharge calculated by IVM and VPM. In order to analyze applicability of discharge calculation using surface velocity measured by SIV, index velocity data at various range of flow were collected and we also conducted individual measurements. Based on the results, the relationship between index velocity(surface velocity) with mean velocity was developed and parameters for VPM were determined to calculate discharge. The discharge calculated by two methods were compared with result by H-ADCP measurement data and H-Q rating curve.

Keywords: Surface velocity; SIV; IVM; VPM

Introduction

Until now, as a method of using velocity measured from a fixedly installed velocity meter to estimate mean velocity, the index velocity method(IVM) and velocity profile method(VPM) are most widely used, and these are commonly used to calculate discharge for H-ADCP measurement. IVM calculates discharge by using the relationship between index velocity measured by H-ADCP and mean velocity from individual discharge measurements in various ranges. The VPM estimates discharge by theoretical velocity profile of open channel, index velocity is used to determine parameters of velocity profile. The Most important thing in these methods is that maximum velocity or velocity measured at core flow of the channel is the best index velocity. Because it is very difficult and expensive to install H-ADCP at the core flow area, if the maximum velocity could be measured using non-contact surface velocity meter such as SIV(Surface Image Velocimetry), it will be the most efficient method to measure discharge continuously, because they can measure surface velocity field. Therefore, in order to examine the applicability calculate discharge from surface velocity, 3 CCTV cameras for SIV were installed at test bed and 3 types discharge calculation methods including surface velocity factor(k=0.85) were applied to calculate discharge.

Methods

SIV calculates the surface velocity of the flow using the cross-correlation method from the analysis of the distribution of grey-level intensity in IA(interrogation area)(Raffel et al., 2000). The displacement is determined by matching the IA in first image with highest correlation with the IA within SA(searching area) in the next image. Correlation coefficient for grey scale intensity of IA can be calculated by Eq. (1) and the velocity is calculated by dividing the displacement by the image time interval.

$$R_{ab} = \frac{\sum_{i=1}^{MX} \sum_{j=1}^{NY} [(a_{ij} - \bar{a}_{ij})(b_{ij} - \bar{b}_{ij})]}{[\sum_{i=1}^{MX} \sum_{j=1}^{NY} (a_{ij} - \bar{a}_{ij})^2 \sum_{i=1}^{MX} \sum_{j=1}^{NY} (b_{ij} - \bar{b}_{ij})^2]^{1/2}} \quad (1)$$

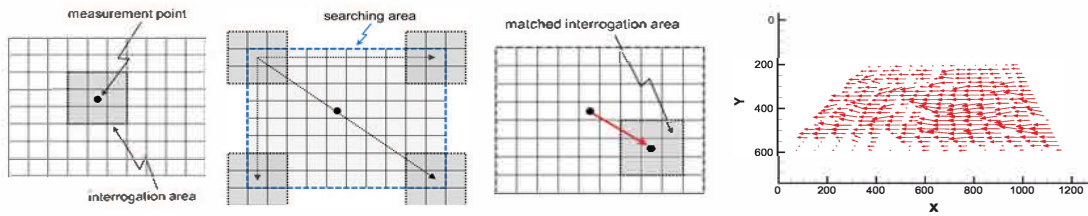


Figure 1. Surface velocity calculation by SIV(Kim et al., 2013)

Results

In this study, surface velocity field measured by SIV was used to calculate the discharge using k-factor, IVM and VPM. In k-factor method, the discharge was calculated by med-section area method using surface velocity and area of each section in flow section area and mean velocity was calculated by multiplying the surface velocity by $k=0.85$. In IVM, the relationship between the mean velocity and index velocity was developed using the surface velocity as the index and the discharge was calculated from this index rating. The VPM estimates discharge by Chiu(1988)'s non-dimensional 2-D velocity distribution based on the entropy, the surface velocity was used to determine parameters of the velocity distribution.

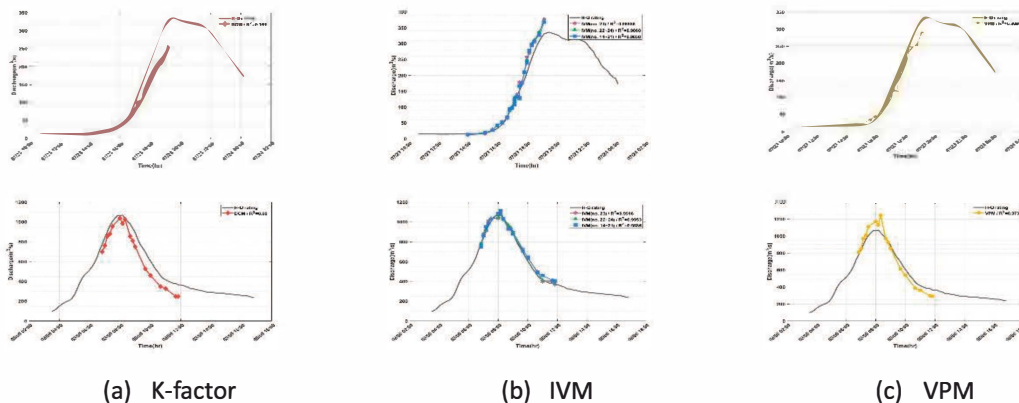


Figure 2. Results of discharge calculation

Conclusions

3 types of methods were applied to calculate the discharge using the surface velocity measure by SIV and relative error of k-factor, IVM and VPM with result by H-Q rating were 16.6.8%(min 2.3 and max 34.8%), 7.8%(min 0.04 and max 31.0%) and 11.63%(min 0.9 and max 42.9%) respectively. The maximum difference was found at low flow condition under 0.5m/s.

Acknowledgement

This study was supported by Korea Environment Industry & Technology Institute(KEITI) as "Service Program for Demand-Responsive Water Supply", funded by the Korea Ministry of Environment(MOE). [2020002650003]

References

- Chiu, C.-L. (1988). "Entropy and 2-D velocity distribution in open channels." *Journal of Hydraulic Engineering, ASCE*, Vol. 114, No. 7, pp. 738-756.
- Kim, S. J., Yu, K., and Yoon, B. (2013). "Error Analysis of Image Velocimetry According to the Variation of the Interrogation Area." *Journal of KWRA.*, Vol. 46, No. 8, pp 821-831.
- Raffel, M., C. Willert and J. Kompenhans (2000) "Particle Image Velocimetry, A Practical Guide." Springer-Verlag.

Prediction of long-term bed elevation change based on gate operations: For Geum River

Chang Sung Kim^{1*} and Seong Jun Kim¹

¹Department of R&D, Korea Institute of Hydrological Survey

*Corresponding: csckim@kihs.ac.kr

Abstract

In this study, the characteristics of long-term bed elevation changes according to the gate opening were analyzed using HEC-RAS of the Geum River. The study area is 130.47 km from the downstream of Daecheong Dam to the estuary bank of Geum River. In 2012, three weir were installed in Geum River due to Four-River project. Currently, Sejong weir is dismantled, Gongju weir is partially dismantled, and Baekje weir is open all the time. The HEC-RAS program, a one-dimension numerical analysis model, was used to predict long-term bed elevation change and model was constructed under the gate opening condition. Model verification was conducted from 2015 to 2019, and long-term bed elevation change was simulated for 10 years. If accurate data can be collected through continuous monitoring in the future, it is expected to produce more reliable results.

Keywords: Gate, Geum River, long-term bed elevation change, HEC-RAS, Sedimentation

Introduction

Bed elevation change in river is the rising and falling of the river bed due to the difference in sediment load. The factors causing bed elevation changes in streams are classified into natural and artificial factors. First, natural factors include floods or heavy rain, and artificial factors include in-stream installation such as dam, weir, and dredging. Specially, the artificial factors have a great influence on bed elevation changes. The in-stream installation blocks flow and sediment load and causes sediment deposition in the upstream of the in-stream installation. The sediment deposition in river results the problems such as rising flood level, lowering capacity of river, and reducing stability of the in-stream installation. This sediment deposition occurs over a long period of time. Therefore, prediction of long-term bed elevation change in river is essential for river planning and maintaining.

Methods

Long-term bed elevation change was simulated using HEC-RAS, a one-dimensional numerical analysis model. The HEC-RAS program can calculate the amount of similar transfer taking into account the particle size distribution, and calculate the composition ratio of bed soil through simulation of classification phenomenon (USACE, 2016). The flow is calculated using the quasi-rectification model, and the bed fluctuation is calculated using the Exners equation.

$$\frac{1}{1-\lambda} \frac{\partial Q_s}{\partial x} + B \frac{\partial z}{\partial t} = 0 \quad (1)$$

Results

The simulation was conducted under the condition of no gate for 130.47 km from Daecheong Dam to the estuary of the Geum River. The simulation was conducted with the water gate removed from the input data. It was confirmed that sedimentation proceeded in all sections, and erosion occurred at the confluence of Gam stream and Miho stream.

Conclusions

The model was constructed using the HEC-RAS program for the 130.47 km section from Daecheong Dam to estuary bank of the Geum River, and the bed elevation change analysis was performed as gate open condition. Prediction of bed elevation change requires comparison with verifiable survey results, but has a limitation of simple prediction due to the absence of data. However, the simulation was conducted under similar conditions (w/o gate) in which Sejong weir is dismantled, Gongju weir is partially dismantled, and Baekje weir is always open. In the future, if accurate data can be collected through continuous monitoring, it is expected that more reliable results can be derived.

Acknowledgement

This work is supported by the Korea Agency for Infrastructure Technology Advancement(KAIA) grant funded by the Ministry of Land, Infrastructure and Transport (Grant 21DPIW-C153746-03).

References

- MOLIT, River master plan report (modified) of Geum river basin, Ministry of Land, Infrastructure and Transport, 2009.
- USACE, 2016. HEC-RAS river analysis system user's manual, US Army Corps of Engineers.

Prediction of bed elevation change according to weir open operations: For Nakdong River

Seong Jun Kim¹ and Chang Sung Kim^{1*}

¹Department of R&D, Korea Institute of Hydrological Survey

*Corresponding: csckim@kihs.re.kr

Abstract

In this study, the characteristics of bed elevation changes according to the gate opening were analyzed using HEC-RAS of the Nakdong River. The study area is 292.37 km from the downstream of Gudam bridge to the Nakdong estuary of the Nakdong River. The HEC-RAS program, a 1D numerical analysis model, was used to simulate bed elevation change. The simulations were performed in two scenarios from 2017 to 2019. Scenario 1 was constructed under the condition of fully opened gate, and scenario 2 was constructed under the conditions of gate installation. As a result of the simulation, it was confirmed that under the conditions of scenario 1, deposition occurred in most sections of Hapcheon-Changnyeong weir ~ Changnyeong-Haman weir (about 40 km). In addition, it was predicted that the flow including the sediments in the main stream of the Nakdong River was not interrupted by the weir structure and continuously changed the river bed.

Keywords: Bed elevation change, Gate, HEC-RAS, Nakdong River, Sedimentation

Introduction

In Korea, a total of 16 new multi-functional weirs and large-scale dredging have been implemented through the Four Major Rivers Project, which was carried out with the aim of efficient water management centered on national rivers and improving river flooding capacity. Rapid anthropogenic changes in rivers due to dredging have a significant effect on the erosion and sedimentation of the riverbed. This greatly changes the flow characteristics of the original river due to the rapid change of the river topography. The eight multifunctional weirs installed in the Nakdong River are divided into fixed weirs and movable weirs, and the opening of the gate is expected to have a great influence on the fluctuations of the riverbed. However, in Korea, there have been studies on the change of riverbed due to the opening of gate, but few cases have reviewed the impact of the gate operation.

Methods

The input data of the HEC-RAS model include topography, flow, water level, particle size distribution, and sediment data. In this study, topographic data (BAI report, 2018) that was conducted for river surveys on the Nakdong River in 2017 was used, and in the weir gate opening scenario model, two sections from Banbyeon stream to the Gangjeong Goryeong weir and Gangjeong Goryeong weir to the estuary bank. In addition, the simulation was conducted with the sluice gate removed in accordance with the gate opening scenario.

Results

The results of the bed elevation changes according to Scenario 1 and Scenario 2 from January 1, 2017 to December 31, 2019. Scenario 1 result in the upstream section (Gudam bridge ~ Gangjeong Goryeong weir) showed that the maximum +2.55 m bed elevation was raised and the -3.35 m bed elevation was lowered. The simulation results of the upstream section of Scenario 2 were predicted as +2.54 m sedimentation and -4.37 m erosion. The result of scenario 1 in the downstream section (Gangjeong Goryeong weir ~ Estuary Bank) showed that

the maximum +7.08 m bed elevation was deposited and the -4.85 m bed elevation was eroded. As a result of scenario 2, a maximum +4.68 m bed elevation was deposited and a -3.88 m bed elevation was eroded.

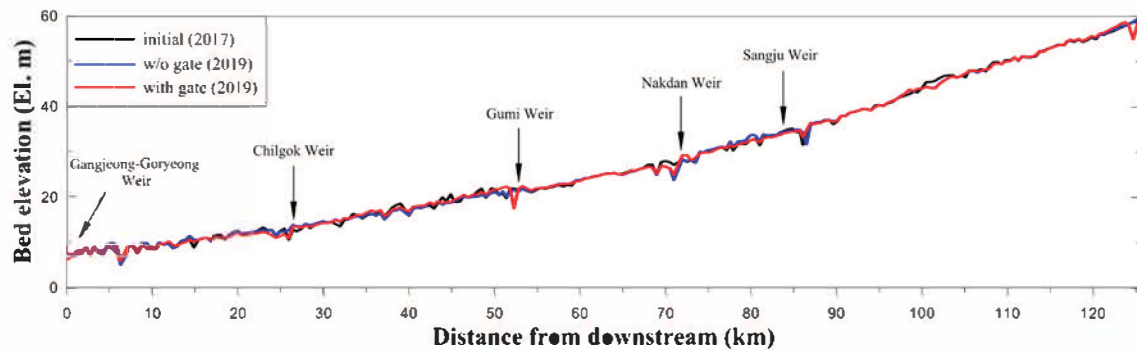


Fig. 1. Bed elevation change in upstream by scenario

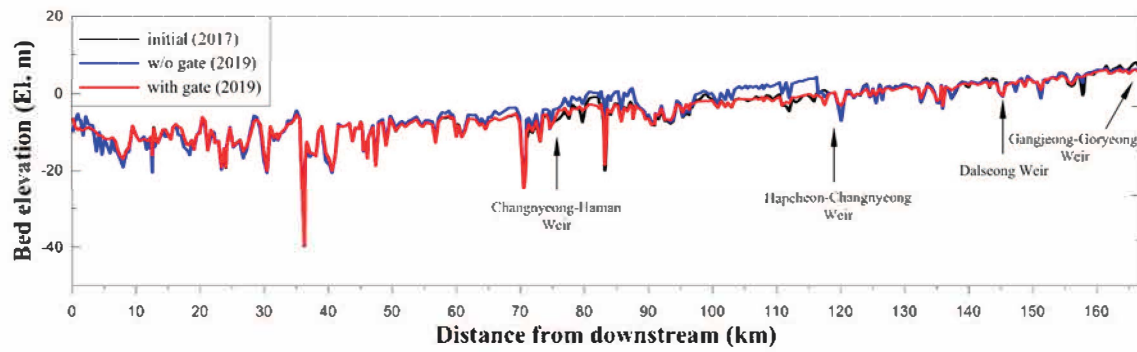


Fig. 2. Bed elevation change in downstream by scenario

Conclusions

The model was constructed using the HEC-RAS program for the 292.37 km section from Gudam Bridge to the estuary bank of the Nakdong River, and the bed elevation change analysis was performed for two scenarios. Scenario 1 is the condition of the full opening of the gate (w/o gate) and Scenario 2 is the condition of the gate installation (with gate). Prediction of bed elevation change requires comparison with verifiable survey results, but has an academic limitation of simple prediction due to the absence of data. However, it can be judged that it has undergone a certain degree of verification procedure because it is composed identically to the model boundary conditions of the existing research report. In the future, if accurate data can be collected through continuous monitoring, it is expected that more reliable results can be derived.

Acknowledgement

This work is supported by the Korea Agency for Infrastructure Technology Advancement(KAIA) grant funded by the Ministry of Land, Infrastructure and Transport (Grant 21DPIW-C153746-03).

References

- BAI, 2018. Report of audit on the status of the four major rivers restoration project and the performance analysis, The Board of Audit and Inspection of Korea, Seoul, Korea.
- MOLIT, River master plan report (modified) of Nakdong river basin, Ministry of Land, Infrastructure and Transport, 2013.

**The 9th International
Symposium on
Environmental Hydraulics**

S4 Session

**Smart Safety Management of River Facilities
[S4-T1]**



Utilization of ROV for safety inspection of underwater structures

Eun Sang Im¹

¹Water Infrastructure Research Center, K-water Research Institute, k-water

*Corresponding: esim89@kwater.or.kr

Abstract

Recently, with the implementation of the Special Act on Safety and Maintenance of Facilities and the Framework Act on Sustainable Infrastructure Management (Infrastructure Management Act), The system of facility safety management is being changed from the existing safety-oriented management system to performance-oriented and proactive maintenance system. In particular, the current government intends to establish a smart safety management system through the digitalization of aging national infrastructure by establishing the "Korean version of New Deal" policy. Accordingly, in the case of land structures, digitalization is actively carried out by utilizing the latest technologies such as drones and video matching technologies. On the other hand, underwater structures are still dependent on divers for underwater inspections. Therefore, this study developed ROV for dam inspection to acquire digital data of underwater structures and conducted research on underwater image matching technology to expand its usability. The research results are also actively used for underwater inspections of dams and other underwater structures.

Keywords: Underwater Structures, ROV, Underwater Inspection, Safety Maintenance

Introduction

Currently, Korea is seeing a rapid increase in SOCs, which have been more than 30 years since the completion of construction. In particular, water infrastructure facilities, such as dams, river facilities, and harbors that are adjacent to water, are relatively aging, and maintenance is urgently needed. It was necessary to strengthen the maintenance function of old facilities because it was highly likely that the aging of the SOC would be adversely affected not only in terms of safety problems but also in terms of maintenance of the facilities, resulting in huge budget waste. Thus, the government amended the Facility Safety Act in 2018 and enacted the Infrastructure Management Act in 2020 to realize efficient maintenance by introducing the asset management concept. However, the inspection of underwater structures has problems such as the risk of human accidents and the limitations of the scope of the survey, as the safety management of the water infrastructure relies on a diving survey. Therefore, in order to overcome these problems, the research team developed a K-water_ROV 01 in the first year. We further developed K-water_ROV 02 & 03 to improve its usage performance and validate it's the performance. It also presented a manual to operate the ROV. We also studied techniques to improve underwater images and to correct geometric distortions. Studies have also been conducted on convergence techniques using SLAM and SfM technologies.

Development and utilize of ROV

In this study, a small ROV weighing less than 20kg was developed as shown in Fig. 1 with various functions such as water depth maintenance, direction maintenance, posture maintenance, 4K-class video, and close-up of the survey surface. The ROVs are equipped with a multi-beam sonar for ROV operation and a USBL system for underwater location of ROV tracking. Currently, K-water is actively used to inspect conditions such as concrete damage,

rock erosion, etc. and water leaks by utilizing ROV for various underwater structures such as water circulation systems, water solar facilities, multi-function beams, and sediment sites.

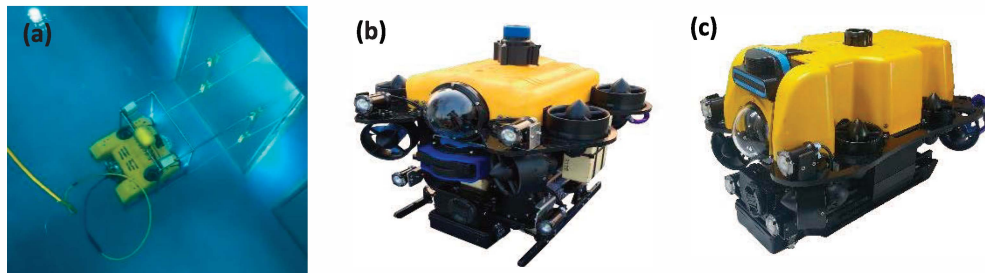


Fig. 1. Developed ROV and (a) K-water_ROV 01, (b) K-water_ROV 02, and (c) K-water_ROV 03.



Fig. 2. Underwater structure by ROV and (a) Dam, (b) water circulation system, (c) floating solar power plant, (d) multi-function weir, and (e) sediment sites.

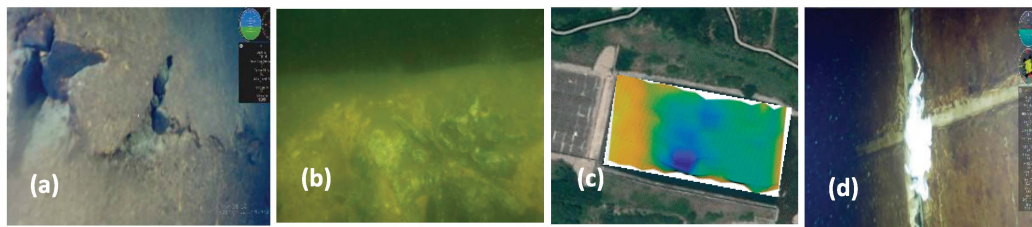


Fig. 3. Underwater Inspection and (a) concrete damage, (b) rock erosion, (c) scour of plunge pool, and (d) leakage investigating by milk spray.

Convergence of underwater images

Visualization of underwater image information is as important as the development of ROV for underwater investigation and inspection of river facilities such as dams. In the case of underwater facilities, it is difficult to clearly specify the location of the damaged area because it is not possible to secure enough vision due to high turbidity problems. To solve these problems, K-water has developed and validated pre-processing techniques to improve the consistency performance of underwater images obtained from ROV. The pre-processing technology, which corrects color distortion caused by refraction of light in water and geometric distortion present inside the camera, has been developed to match underwater images. Based on these technologies, K-water currently has the technology to combine parts of its underwater facilities and model them in three dimensions.

References

- Im, E. S., Kim, W. Y., Kim, K. Y., Lee, J. W. & KIM, N. L. (2020). A study on development of underwater drone to assess the condition and behavior of underwater structures in river, K-water Research Institute, k-water.

River levee surface erosion mitigation using eco-friendly biopolymer-based soil treatment (BPST)

Yeong-Man Kwon¹, Sojeong Lee², and Ilhan Chang^{3*}

¹Department of Civil & Environmental Engineering, KAIST, Republic of Korea

²School of Engineering and IT, University of New South Wales, Australia

³Department of Civil Systems Engineering, Ajou University, Republic of Korea

*Corresponding: ilhanchang@ajou.ac.kr

Abstract

The river levee must be resistant to surface erosion by water flow because it locates near the river. This study proposes an eco-friendly biopolymer, which is known to increase the shear strength of soil, as a material for enhancing surface erosion resistance of levee surface. An erosion function apparatus (EFA) equipped with P-wave reflection equipment was used to evaluate the surface erosion resistance of river sand treated with various types of biopolymers, including xanthan gum, starch. The experimental results showed that the biopolymer treatment showed a significant improvement in the erosion curves and the critical shear stress of the river sand. Especially, starch modified by glycerin showed the most efficient improvement in surface resistance.

Keywords: Levee; Erosion; Biopolymer-based soil treatment (BPST); River-sand; Sustainability

Introduction

River levee surface erosion occurs when the shear stress caused by flowing water exceeds the critical shear strength of the soil. Surface erosion caused severe damage to levee structures such as watergates, drainage pipes, and levee bodies. Biopolymers have been studied extensively to improve soil strength (Chang et al., 2015) sustainably. Xanthan gum and dextran biopolymers have shown their potential to connect soil particles, increase viscosity, and reduce permeability to prevent soil surface erosion (Kwon et al., 2020). Furthermore, crosslinking of various biopolymers has been studied to provide higher mechanical properties (Reddy et al., 2015). However, the effect of crosslinked biopolymers on surface erosion mitigation is still unknown. This study investigates the effect of crosslinked biopolymers on the surface erosion of river sand. Erosion function apparatus (EFA) is used to measure the surface erosion of various crosslinked biopolymers. The erosion rate was obtained based on the P-wave reflection monitoring.

Materials and Methods

The Nak-Dong river-sand was sampled in the KICT Andong experimental center, located near the Nak-Dong River, in Andong, Korea. The river sand was classified as poorly graded sand (SP), of which the coefficient of uniformity was 3.24, and the coefficient of curvature was 0.89.

Two different types of crosslinked biopolymers (i.e., xanthan gum (XG)-starch (ST), starch (ST)-glycerin (G)) are adopted for this study, and two different biopolymer content is chosen for soils treated with xanthan gum modified starch. The detailed explanations about the biopolymers used are summarized in table 1.

The erosion rate of 1 mm extruded soil surface at various flow velocities (0.12 - 4.50 m/s) was measured using the P-wave reflection monitoring installed on EFA. The sample tube was placed on the EFA plate and pushed up by a pneumatic piston. Then, soils were saturated by steady water flow. After the saturation process, 1 mm of soil surface was extruded into the flowing water. During the experimental procedures, the eroded height was monitored using the P-wave

reflections.

Table 1. Basic properties of soil specimen

Soil	Treatment	Water content [%]	Radius to width ratio
Nak-dong River-sand	Untreated	17	0.56
	XS-ST 1%	16	0.50
	XS-ST 2%	15	0.53
	ST-G	13	0.55

Results

Figure 1a shows the change in the erosion rate as the shear stress changes. The untreated soil was eroded by more than 10 mm/hr even at a shear stress of 0.1 Pa. In contrast, biopolymer treatment significantly improved the shear resistance of soils owing to increased particle bonding, shear strength, and prevention of water infiltration by the pore-clogging. The critical shear stress (Fig. 1b), related to soil contact, particle size, and forces between particles, increased with biopolymer treatment. In particular, starch modified with glycerin had the greatest shear strength due to the reduced solubility by crosslinking.

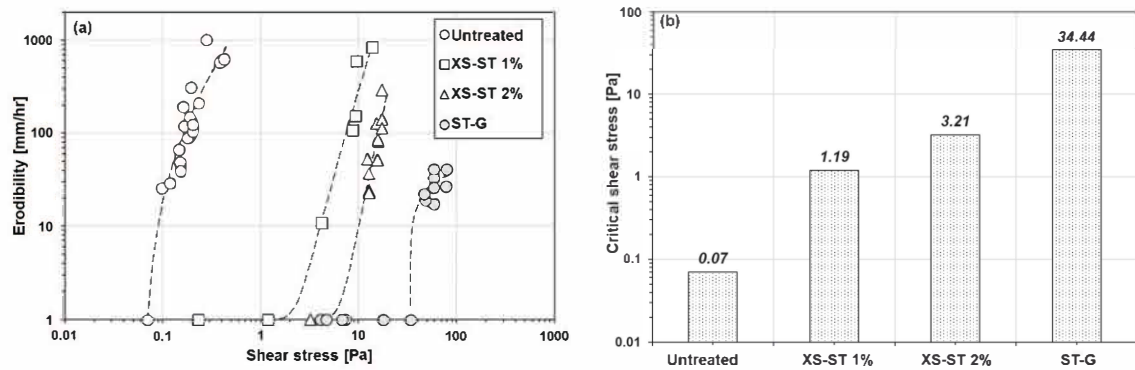


Fig. 1. Relationship between biopolymer types and (a) erosion curve and (b) critical shear stress.

Conclusions

In this study, a surface erosion experiment was performed using an EFA with P-wave reflections. Biopolymers have been shown to enhance the erosion resistance of soils through 1) increased particle-to-particle contact, 2) increased viscosity, and 3) pore-clogging effects. Crosslinking of biopolymers reduces the solubility of biopolymers in water, improving soil erosion resistance to the flowing water. Therefore, the results have shown that the stress required to initiate soil erosion increased up to 500 times. The result of this study has demonstrated the potential of biopolymer crosslinking for the river levee surface stabilization.

Acknowledgment (If necessary)

This work is supported by the Korea Agency for Infrastructure Technology Advancement(KAIA) grant funded by the Ministry of Land, Infrastructure, and Transport (Grant 20DPIW-C153746-02).

References

- Chang, I., Im, J., Prasadhi, A. K., & Cho, G.-C. (2015). Effects of xanthan gum biopolymer on soil strengthening. *Construction and Building Materials*, 74, 65-72.
- Kwon, Y.-M., Ham, S.-M., Kwon, T.-H., Cho, G.-C., & Chang, I. (2020). Surface-erosion behaviour of biopolymer-treated soils assessed by EFA. *Géotechnique Letters*, 10(2), 1-7.
- Reddy, N., Reddy, R., & Jiang, Q. (2015). Crosslinking biopolymers for biomedical applications. *Trends in Biotechnology*, 33(6), 362-369.

Development of an algorithm for outlier detection processing of water level data measured by ultrasonic sensor

Inhyeok Bae^{1,2} and Un Ji^{1,2*}

¹University of Science and Technology

¹Korea Institute of Civil Engineering and Building Technology

*Corresponding: jiun@kict.re.kr

Abstract

Water level data collected with frequently used ultrasonic sensors for water level monitoring in rivers include the data dispersion and outliers due to moving water surface. Since the outliers have a significant deviation and frequently occur, it is necessary to use the robust estimator for accurate detection processing. In this study, an algorithm for statistical processing of outliers and data dispersion in water level data measured by ultrasonic sensors was presented. The algorithm consists of the outlier removal process based on the modified Z-scores method and the smoothing process of EWMA.

Keywords: Modified Z-score; Outlier Detection; Robust Filtering; Ultrasonic Sensor; Water Level Measurement

Introduction

Ultrasonic sensors have advantages on cost and installation location over conventional water level measurement methods such as the stilling well and float system (Kruger et al., 2016). However, various environmental factors related to the location of the ultrasonic sensors and water surface flow can lead to abnormal data by irregular ultrasonic signals. There is no statistical significance for these outliers. The data also include dispersion by random errors of about 20-50 mm due to water surface waves. The purpose of this study is to present a generalized statistical process algorithm for detecting and eliminating outliers in water level data measured by ultrasonic sensors and smoothing them to reduce the variance caused by random errors. A Modified Z-scores method was used to evaluate deviations based on Median Absolute Deviation (MAD) as a statistical technique for detecting outliers. Using the exponentially weighted moving average (EWMA) method, the smoothing process was applied to reduce the data dispersion.

Methods

The Modified Z-score method, based on the robust estimator MAD that is insensitive to deviations, was used to detect outliers. When the data set was given as $X=\{x_1, x_2, \dots, x_n\}$, the Modified Z-score, M_i is defined as follows:

$$M_i = \frac{|x_i - \text{Med}(X)|}{\text{MADN}(X)} < \beta \quad (1)$$

where $\text{Med}(X)$ is a median value of the data set X , $\text{MADN}(X)$ is a normalized MAD, which is defined as $\text{MADN}(X) = \text{MAD}(X)/0.6745$, and β is a rejection criterion. The $\text{MADN}(X)$ corresponds to the standard deviation of the normal distribution for the center location of the data estimated by the sample median. Iglewicz and Hoaglin (1993) suggested the rejection criterion, $\beta = 3.5$, based on the results of a simulation that used pseudo-normal observations.

Even with all of the outliers being removed, approximately 2 cm of data dispersion occurs due to water waves. If a constant water level is repeatedly measured under the same conditions at

short intervals using an ultrasonic sensor, a normal distribution is formed by the observed value due to random error, excluding outliers. The EWMA method can be used to smooth short-term variations of data. EWMA can also reflect higher weight in recent data, making it suitable for monitoring the change of water level data. The EWMA exponentially reduces the weighting factors of older data, as shown in Eq. (2), when the data set is listed as a sequence for time t (Brown, 1963):

$$S_t(x) = \alpha x_t + (1 - \alpha) \cdot S_{t-1}(x) \quad (1)$$

where α shows the decreasing degree of weighting as a smoothing constant factor, with a range of $0 < \alpha \leq 1$.

Results

The developed algorithm was applied to outlier detection and smoothing of four water level data sets measured in the stream-scale experimental channel for two weeks. Each data set consists of about 70,000 water level data, with a maximum level change of 2 m during the measurement. Approximately 5 % of outliers were detected when the rejection criterion, θ , was 3.5, and the standard deviation of around 84.9 % decreased when the smoothing constant factor, α , was 1.0. Figure 1 shows the difference in the degree of dispersion and the mean value in the data that had undergone outlier removal and smoothing process.

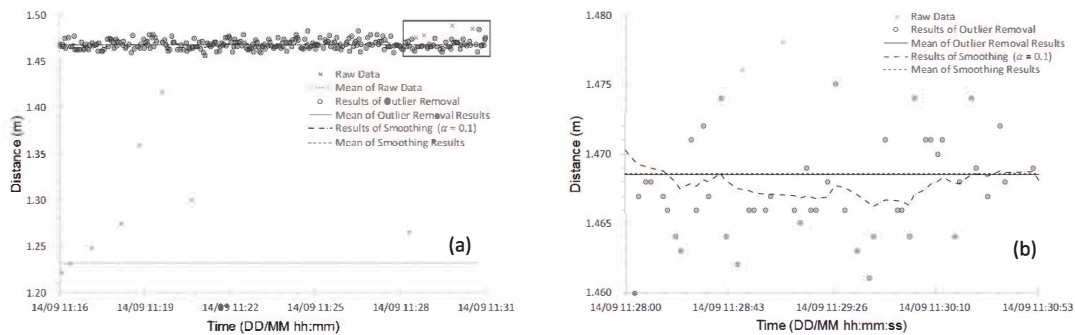


Fig. 1. Comparison of raw data, outlier removal result, and smoothing result of water level data measured by ultrasonic sensor (a) 14/09 11:16 to 14/09 11:31; (b) 14/09 11:28 to 14/09 11:31.

Conclusions

This work presents an algorithm for outlier removal and smoothing that occurs using ultrasonic sensors. Using Modified Z-score, a robust statistical technique insensitive to significant deviations, all outliers in the water level data were removed. EWMA methods give high weight to recent data, enabling smooth processing sensitive to water level changes. This algorithm can be used in water level monitoring systems for river management.

Acknowledgement (If necessary)

This work is supported by the Korea Agency for Infrastructure Technology Advancement(KAIA) grant funded by the Ministry of Land, Infrastructure and Transport (Grant 20AWMP-B121100-05).

References

- Kruger, A., Krajewski, W. F., Niemeier, J. J., Ceynar, D. L., & Goska, R. (2016). Bridge-mounted river stage sensors (BMRSS). *IEEE Access*, 4, 8948-8966.
- Iglewicz, B., & Hoaglin, D. C. (1993). *How to detect and handle outliers* (Vol. 16). Asq Press.
- Brown, R. G. (2004). *Smoothing, forecasting and prediction of discrete time series*. Courier Corporation.

Study on advanced early warning system for dam safety measurements

Seong-Bae Jo^{1*}, Eun-Sang Im¹, Kichun Kang² and Sukmin Yoon²

¹Water Infrastructure Research Center, K-water Institute

²Department of Civil Engineering, Gyeongsang National University

*Corresponding: js135@kwater.or.kr

Abstract

The purpose of this study is to propose the process of dam safety measurement data and management criteria for seepage of dam, which is important indicator of fill dam safety. Measured data have various contaminated outliers caused by electrical and mechanical errors, and variance of measured data are in the range of previous data range. Thus, data process can control various outliers and improve quality of dam safety measurements. Decision tree analysis was performed for evaluate the rainfall effects on seepage and it can be used to establish management criteria. Rainfall and water level were selected as the influence factors. Maximum record of each leaves can be used as a seepage criterion considering rainfall and water level.

Keywords: dam; instruments; Management criteria; Decision tree

Introduction

Government changes the policy that strengthen the maintenance and encourage the preemptive investment to prevent deterioration of SOC facilities. The many dams under management by K-water have been in operation for more than 30 years. Therefore, efficient facility management is necessary for public safety and safe water supply. Currently, more than 3,000 instruments of 22 types are monitoring the behavior of 37 dams and early warning systems are operated to respond quickly in case of abnormal behavior. The early warning system automatically sends SMS messages to the administrator if the external displacement and seepage flow exceed management criteria, and the response to the alarm must be reported within 48 hours. At this time, outliers such as mechanical, electrical, communication errors, and environmental problems of the instrument occur, resulting in confusion in the work. Thus, to address this confusion, the research is needed to identify outliers and to establish a system for improving data quality.

Methods

In this study, we first propose an instrumentation process that can remove outliers and manage normal measurement values to improve the quality of data production as shown in Fig. 1. It is expected that dam safety will be strengthened by improving the quality of measurement data, and safe water supply will be possible for the people.

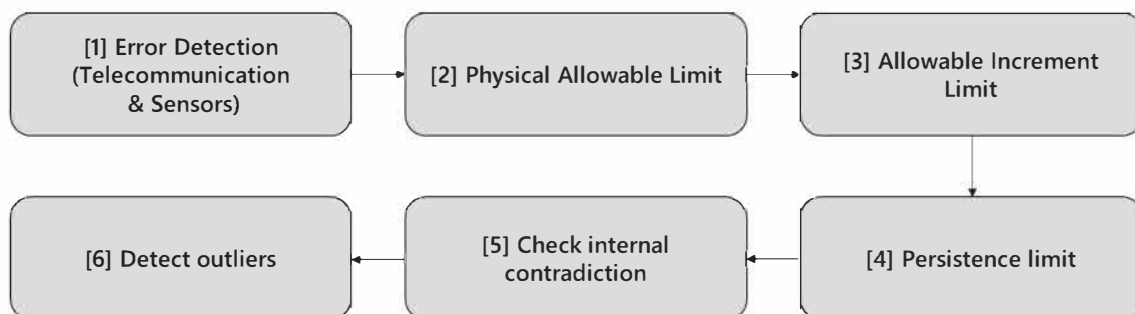


Fig. 1. Proposed process of dam safety measurement data.

For the dam safety, seepage through dam is important indicator to determine safety status of dams. However, seepage can be increased rapidly because rainfall directly flow into the downstream slope although seepage through dam body is in the allowable range. Therefore, it is necessary the management criteria for the seepage of the fill dam considering rainfall. In this study, decision tree analysis is used to separate the effects of rainfall and to establish the management criteria by stages of rainfall and water level. CART algorithm (Leo Breiman, 1984) is used for decision tree method.

Results

Fig. 2 and Table 1 show the results of decision tree and seepage range of each leaves. 1st explanatory variable is rainfall and most seepage is under the daily rainfall of 73.5 mm/day. Although extreme case (rainfall > 106.5 mm/day) has only 9 points, its seepage range is much larger than previous case (rainfall ≤ 73.5 mm/day), over the daily rainfall of 106.5 mm/day, has only 9 points. Thus, we can divide seepage range into 3 stages according to rainfall, and its management criteria can be determined from maximum record of each cases.

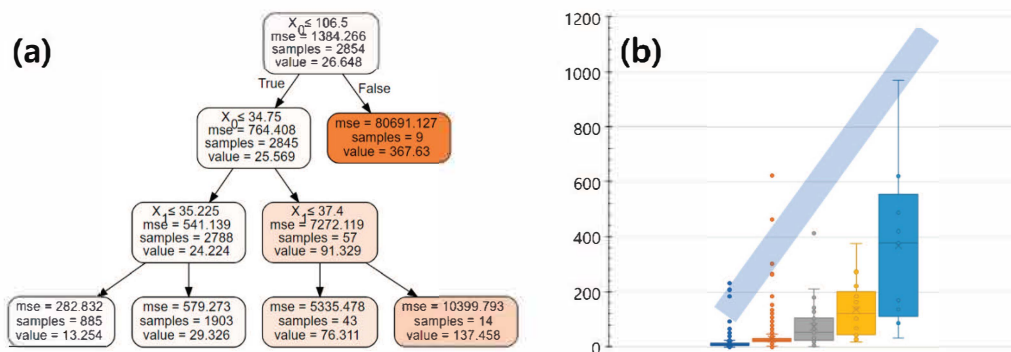


Fig. 2. Results of decision tree (Max. Depth = 2). and (a) structure (b) seepage range of each leaves.

Table 1. Results of decision tree for study cases (Max. Depth = 2).

1 st explanatory variable	2 nd explanatory variable	Response variable (Seepage, L/min)	
		Mean	Subset (n)
Rainfall(mm/day)	Water level(m)		
106.5 < Rainfall		367.63	9
34.75 < Rainfall ≤ 106.5	37.4 < Level	137.458	14
	Level ≤ 37.4	76.311	43
Rainfall ≤ 34.75	35.225 < Level	29.326	1903
	Level ≤ 35.225	13.254	885

Conclusions

The instrumentation process is proposed to detect abnormal data caused by electrical and mechanical problem. And management criteria for seepage is evaluated by decision tree. Although the seepage range is not separated clearly, it can be used for stage criteria of seepage considering rainfall effect.

References

Breiman, L., Friedman, J., Stone, C.J., and Olshen, R.A. (1984). Classification and Regression Tress, Talyer & Francis.

Drone application for water infrastructure reality modeling

DongSoon Park^{1*} and Taemin Kim¹

¹K-water Research Institute, Korea Water Resources Corporation

*Corresponding: fulgent@kwater.or.kr

Abstract

Case studies of drone photogrammetry for 5 dams were made for checking improvement of efficiency, time, and labor for dam safety inspection and diagnosis. Digital surface models and orthoimages were successfully obtained with some notable know-hows. A 3D digital model of dam spillway reliably quantified the deterioration of concrete structures. AI-driven major crack detection for spillway was fairly good in spite of the modest machine learning dataset of cracks. A well-organized drone photogrammetry was found to significantly improve time and labor by more than 30% comparing to manned dam safety inspection and diagnosis. Drone photogrammetry is contributable to effectively improve the productivity of dam safety work.

Keywords: Drone; Photogrammetry, Dam safety; 3D model; Digital transformation

Introduction

Drone Photogrammetry is the technology that is undergoing fast commercialization and high industrial applicability among the 4th industrial revolution technologies. It is also a highly useful technology that can be applied to the dam safety field. Drone photogrammetry technology can significantly improve the productivity of dam safety inspection and diagnosis, and has a wide range of applications for not only the safety of dam facilities, but also environmental management of watersheds, disaster mitigation, and digital 3D numerical modeling. 3D digital spatial information model generated by a drone mapping can be used for the unmanned safety inspection and diagnosis of facilities, as well as for the construction of digital twin geometry as built.

It still needs to know some of the essential know-how and related information of drone photogrammetry. For example, principles of drone photogrammetry, factors influencing photography, drone mapping mission planning, factors influencing photogrammetry methods and precision, and 3D modeling process, etc.

In this paper, some case studies of drone photogrammetry and safety inspections for five dams were presented. The actual productivity improvement effect when using drone photogrammetry for dam safety inspection is compared and analyzed comparing to conventional visual inspection by engineers. Some notable conclusions are summarized in the end.

Results

After It was demonstrated that the 3D model data can be accurately provided for a dam safety inspection by classifying the amount and type of deterioration and presenting location and spatial information through the drone mapping of the dam structures.

Through the exemplary application of drone photogrammetry technology to the S dam spillway, it is estimated that the productivity (input time and labor) of dam safety inspection and diagnosis work focused on manual inspection can be innovated by at least 30%. In addition, it is possible to efficiently contribute to data-based quantitative decision-making by generating a sophisticated 3D spatial information model. Innovative application is expected for modeling restricted access areas such as dam spillways and gates.

Through case studies, it is recommended that the degree of overlap be maintained at 70% or

more as the most important factor affecting the modeling quality. It was found that it is also important to secure the target GSD by maintaining an appropriate altitude.

It was verified that it is possible to create a digital 3D model with high precision within an average GSD of 2 cm/pixel using a drone for a dam safety inspection. When surveying the ground control point to improve the positional accuracy of drone photogrammetry, the localization of the survey points of the VRS Network RTK method through the national integrated control point is more important than the RTK function itself. For precise mapping within the target area of drone photogrammetry, April Tag and Chili Tag were used for the first time in dams, and the efficiency of the work process was improved by automatically recognizing the pattern in the post-processing software.

The crack detection function using AI technology was applied at the earlier stage using ContextCapture Insights. As a result of applying the detector learned through the AI crack sample image to the dam spillway, it was confirmed that large cracks that can be seen with the naked eye can be detected. In the future, if the degree of learning is increased by acquiring high-resolution images of actual dam facilities and building AI learning data, the input productivity (labor and time) and data reliability will be increased compared to the existing manpower inspection-based exterior survey. Therefore, it is expected that breakthrough innovation will be possible for a dam safety inspection.

Drone Photogrammetry technology might contribute to Reality Modeling that leads the near-future management of digital twin-based water resources infrastructure.

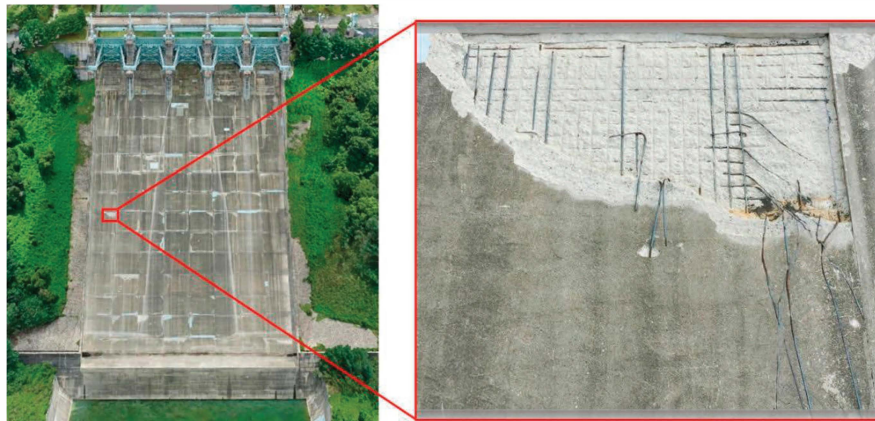


Fig. 1. 3D model of dam spillway obtained by drone photogrammetry after massive water discharge

Conclusions

As case studies drone photogrammetry, 3D modeling and orthogonal image of the dams were successfully and reliably generated including spatial information such as the digital surface model (DSM). It is verified that a drone photogrammetry is an efficient tool to digitally quantify the deterioration of dam structures. It is also useful to significantly improve the productivity of dam safety inspection. Drone Photogrammetry technology might contribute to Reality Modeling that leads the near-future management of digital twin-based water resources infrastructure.

References

- K-water Research Institute (2020). Preliminary study of next-generation intelligent dam safety management platform (iDSP). Research Report, 2020-SA-RR-23-1689.
- Park, D.S. (2021). Toward digitalization of smart maintenance for water infrastructures. KSCE Magazine, 69(3), 20-36, March 2021.

**The 9th International
Symposium on
Environmental Hydraulics**

S6 Session

**Technical Strategy for Quality control of
Hydrological Data and Advanced Toolkits for IWRM
[S6-T2]**



Study on driftwood generation and deposition patterns by tsunami flow using numerical simulation

Tae Un Kang¹, Chang-Lae Jang^{1*}

¹Department of Civil & Environmental Engineering, Korea National University of Transportation

*Corresponding: cljang@ut.ac.kr

Abstract

We studied a tsunami flow together with driftwood behaviors including generation and depositions using a numerical simulation. For this, we used an integrated 2-dimensional numerical model, which includes the depth-averaged flow model and a driftwood dynamics model (Kang and Kimura, 2018; Kang et al., 2020). The study area was Sendai in Japan, and this study used observation data (Inagaki et al., 2012) to verify simulation results through comparing with driftwood deposition patterns. A simplified model was developed to consider the threshold of the driftwood generation by the drag force of water flows. To consider the volume of driftwood generation, we estimated the total wood number in a study area using Google Earth. As a result, we simulated that more 25000 driftwoods were generated and transported to inland from approximately 300,000 wood that were planted in the forest. The final distribution of the driftwood was similar to the observation data of Inagaki et al. (2012). In addition, we found that the simulation results indicated the overturned wood by the tsunami in the forest area. The reproducibility of generation and deposition patterns of driftwood showed good agreement in terms of longitudinal deposition patterns. In the future, the sensitivity analysis on driftwood parameters, such as the size of wood, boundary condition, grid size, would be implemented to predict the travel distance of driftwood. Such modeling would be a useful methodology for the prediction of disaster depending on water flow and driftwood.

Keywords: Driftwood generation; Wood breaking model; Driftwood dynamics model; Inundation flow; Tohoku earthquake

Introduction

Driftwood is one of the problems related to potential disasters with flood events and debris flow. Driftwood can cause collision damage to hydraulic structures when the driftwood is driven by torrential flows and flood flows (Kang et al., 2020). Thus, the control and prediction of driftwood behavior are important to prevent the disaster and make the hazard map. In terms of strategy of disaster reduction, we therefore studied a tsunami flow together with driftwood behaviors including generation and depositions using a numerical simulation to predict the driftwood deposition patterns in large flood disasters. For this, we used an integrated 2-dimensional numerical model, which includes the depth-averaged flow model and a driftwood dynamics model (Kang and Kimura, 2018; Kang et al., 2020), and we simulated tsunami and driftwood behavior.

Methods & Results

The study area was Sendai in Japan, and this study used observation data (Inagaki et al., 2012) to verify simulation results through comparing with driftwood deposition patterns. A simplified model was developed to consider the threshold of the driftwood generation by the drag force of water flows. In general, supplying mechanism of driftwood generation is related to overturning, uprooting and breaking, and those mechanisms are controlled by momentum energy from the water or wind. Here, this study assumed that this momentum energy is caused by strong water flow energy. First, depending on the wood modulus, we assumed that the threshold of generation for driftwood (TGD) is determined. And then, when the water flow affects the planted wood, the drag force is estimated considering the projection area of wood. This estimated drag force is compared with TGD. Here, we regarded that drag force is larger than TGD, the stem of wood is able to be broken or flexed (lodging,

uprooting, breaking), and it changes the planted wood into driftwood. To consider the volume of driftwood generation, we estimated the total wood number in a study area. Using Google Earth, we captured the wood distribution within the unit area (e.g., 250 m²) in the forest of the tsunami disaster, and counted the total number of wood based on density of wood in the unit area. As a result, approximately 300,000 wood are planted in the forest. In addition, the paper (Inagaki et al., 2012) related to the Tsunami disaster observed (through Google) that 21054 of wood flowed to the inland area. This deposited number of driftwoods is used for model reproducibility depending on model parameters.

Fig.1 shows the final distribution of driftwood. It shows similar patterns of driftwood deposition from the observation. In particular, near the forest, most driftwoods (up to 650 m from the coastal line) are deposited, and they were overturned by the tsunami. After 4000 m from the coastal line, Fig 1. indicates a small number of driftwoods. Both observation and simulation show that most driftwoods could not move over the highway (red line).

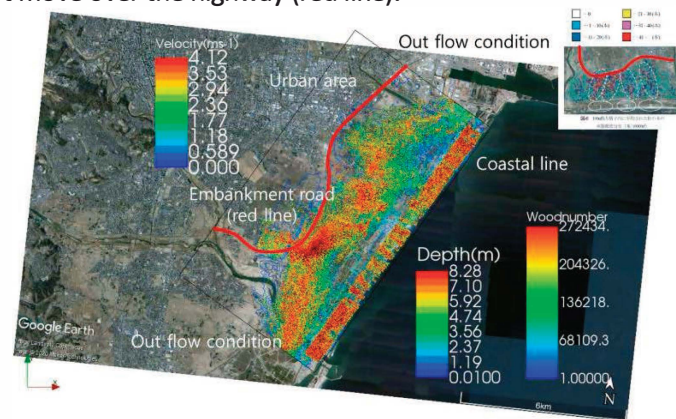


Fig. 1. Numerical simulation result of driftwood deposition patterns (particle colors are serial number of wood particles).

Conclusions

The reproducibility of generation and deposition patterns of driftwood showed good agreement in terms of longitudinal deposition patterns. In the future, the sensitivity analysis on driftwood parameters, such as size of wood, boundary condition, grid size, would be implemented to predict the travel distance of driftwood. Such modelling would be useful methodology for prediction of disaster depending on water flow and driftwood.

Acknowledgement

This work was supported by Korea Environmental Industry & Technology Institute(KEITI) through Aquatic Ecosystem Conservation Research Program, funded by Korea Ministry of Environment(MOE)(2020003050002).

References

- Inagaki, K., Nakaza, E., Iribe, T., & Watanabe, Y., (2012). Distribution of the pine trees drowned by Tohoku Tsunami along Sendai coastal area, *Journal of Japan Society of Civil Engineers, Ser., B3 (Coastal Engineering)*, 68(2): I_120-125, 2012 (in Japanese).
- Kang, T. U., & Kimura, I. (2018). Computational modeling for large wood dynamics with root wad and anisotropic bed friction in shallow flows., *Advances in Water Resources*, 121:419-431.
- Kang, T. U., Kimura, I., & Shimizu, Y. (2020). Numerical simulation of large wood deposition patterns and responses of bed morphology in a braided river using large wood dynamics model., *Earth Surface Processes and Landforms*, 45:962–977, DOI: 10.1002/esp.4789.

Probabilistic flood risk assessment in the downstream area of dam

Beomjin Kim¹, Byunghyun Kim^{2*}, and Kun-Yeun Han²

¹Structural Safety & Prognosis Research Division, Korea Atomic Energy Research Institute

²Department of Civil Engineering, Kyungpook National University

*Corresponding: bhkimc@knu.ac.kr

Abstract

The purpose of this study is to develop a risk assessment method based on a probabilistic flood analysis technique that links the flood damage of major national facilities by the frequency of probability rainfall and the duration of PMF with the hydrological and hydrodynamic models. The risk assessment method developed in this study was used to analyze the risk level of major national facilities and quantitatively present the results to perform re-evaluation and reconsideration of the design of the facilities.

Keywords: Non-Fickian transport; River; Meander; Flow recirculation; Secondary flow

Introduction

In recent years, the risk of flooding at major national facilities from heavy rains has increased significantly. These facilities should consider and assess the risk of flooding due to flash flood, river flooding, and coastal flooding. For flooding hazard analysis for these facilities, two-dimensional (2D) flood inundation modeling is carried out by applying the extreme outflow from Dam. Based on the results of the 2D analysis, hazard curves for the flood depth according to frequency and duration are developed in major national facilities. A new flood hazard curve is developed by the relationship between rainfall, flood depth, and annual excess probability.

Methods

Fig. 1 presents the flow chart of this study.

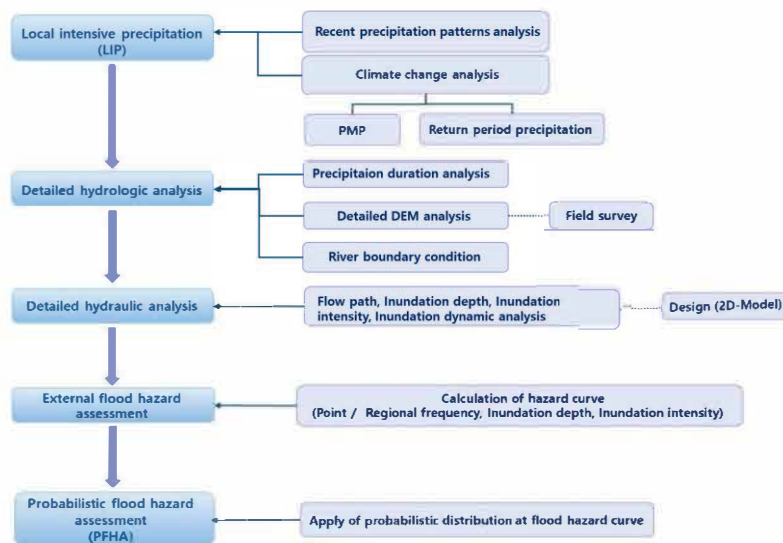


Fig. 1. Flow chart of this study

Application & Result

The risk analysis was performed by probabilistic flood analysis of major national facilities located downstream of the Andong Dam with the amount of discharge from the dam according to the PMF scenario.

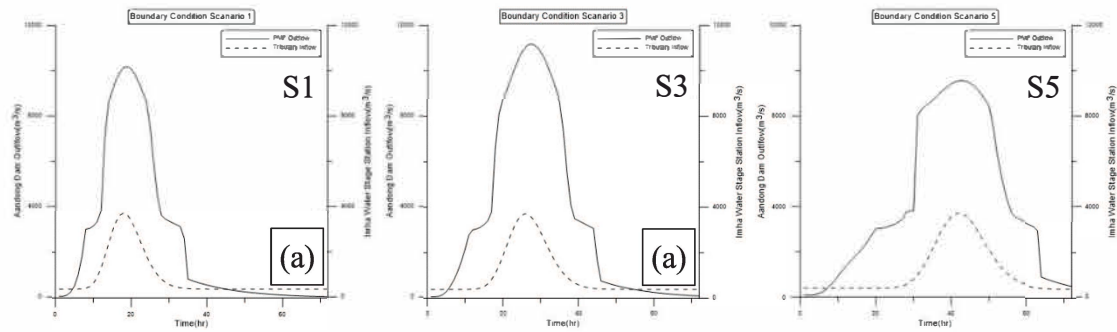


Fig. 2. Outflow from Andong Dam by scenario

2D flood inundation modeling was carried out for each PMF outflow scenario (S1~S5) from Andong Dam, and the flooding depth was calculated for major national facilities located in Andong City. The probability that the risk for the major facilities A, C, E, and H at the downstream of the Andong Dam is 0 or higher, that is, the risk probability of flooding was analyzed. In addition, the critical height of the flood barrier was calculated to reduce the flood risk of major facilities to 50%, 40%, 30%, 20%, and 10%, respectively.

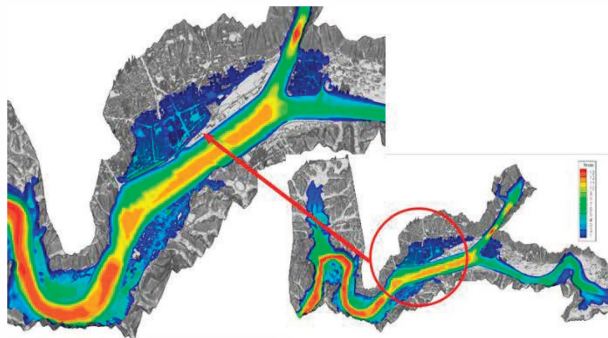


Fig. 3. Maximum flood depth

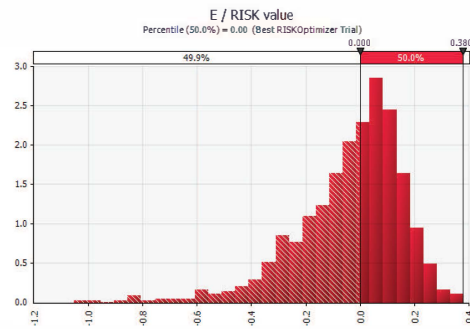


Fig. 4. Risk analysis through optimization

Conclusions

This study proposes a plan to protect life, property, and infrastructure by predicting the possibility of flooding in the major national facilities. In addition, it is expected to contribute to the establishment of social safety net by improving flood vulnerability of national major facilities and social infrastructure considering climate change.

Acknowledgement

This work was supported by the National Research Foundation of Korea (NRF) grant funded by the Korea government (NRF-2017M2A8A4015290).

References

- Kim, B.J., Kim, M., Hahm, D., & Han, K.Y. (2021). Probabilistic Flood Hazard Assessment Method Considering Local Intense Precipitation at NPP Sites. *Journal of Hydrology*, 126192.
- Kim, B.H., and Sanders, B.F. (2016) Dam-Break Flood Model Uncertainty Assessment: A Case Study of Extreme Flooding with Multiple Dam Failures in Gangneung, South Korea, *Journal of Hydraulic Engineering-ASCE*, 142(5). 05016002-1–18.

Analysis of riverbank erosion risks using an advanced DSS toolkit for Sesan and Srepok river basin in Vietnam

Jeongkon Kim¹ and Le Van Thin²

¹Water Resources Department, Yooshin Engineering Corporation

²Center for Natural Disaster Prevention and Mitigation, Vietnam Academy for Water Resources

*Corresponding: jkkim1966@gmail.com

Abstract

A decision support system called DSS-2S was built in connection with the SWAT model based on the MIKE Hydro Basin. The DSS-2S reflected all major rivers and tributaries of the 2S basin, including 17 hydroelectric dams and reservoirs with a capacity of more than 3 million m³ in major tributaries. Using the developed DSS, an analysis on future water resource planning, water resource source protection, and river basin damage prevention in consideration of climate change was conducted.

Keywords: DSS, 2S river basin, riverbank erosion, water resources planning,

Introduction

The Sesan and Srepok river basins, international transboundary river basins shared by Vietnam, Cambodia, are predicted to face many problems and challenges, such as flooding, drought, reduced fishing sustainability and sedimentation due to climate change. At the Vietnamese government level, as part of the World Bank's "Viet Nam Mekong Integrated Water Resources Management (M-IWRM) Project", the water resource management decision support system "DSS-2S" was established for the Sesan-Srepok River basin. The DSS-2S can be used to analyze future risks of water shortage, water quality deterioration, and river bank erosion.

Methods

In this study, the DSS-2S was employed to assess bank erosion risks in the 2S river basin in Vietnam. Based on simulation results from the mathematical model, the river sections at risk of riverbank erosion will be determined by the combination of high velocity and high erosion. Classification criteria are determined as shown in Table 1.

Table 1. Evaluation criteria for erosion

No	Speed	Deep erosion	Evaluate	General evaluation	The risk of river erosion
1	0 – 0.5m/s	0 – 0.2m	1	1 – 2	Very low
2	0.5 – 1m/s	0.2 – 0.4m	2	3 – 4	Low
3	1 – 1.5m/s	0.4 – 0.6m	3	5 – 6	Average
4	1.5 – 2m/s	0.6 – 0.8m	4	7 – 8	High
5	More than 2m/s	More than 0.8m	5	8 – 10	Very high

Results

The erosion risk analysis result is based on the criteria of velocity of flow and deep erosion under the 2030 scenario considering climate change. The river sections at various erosion risks are shown in Figure 1.

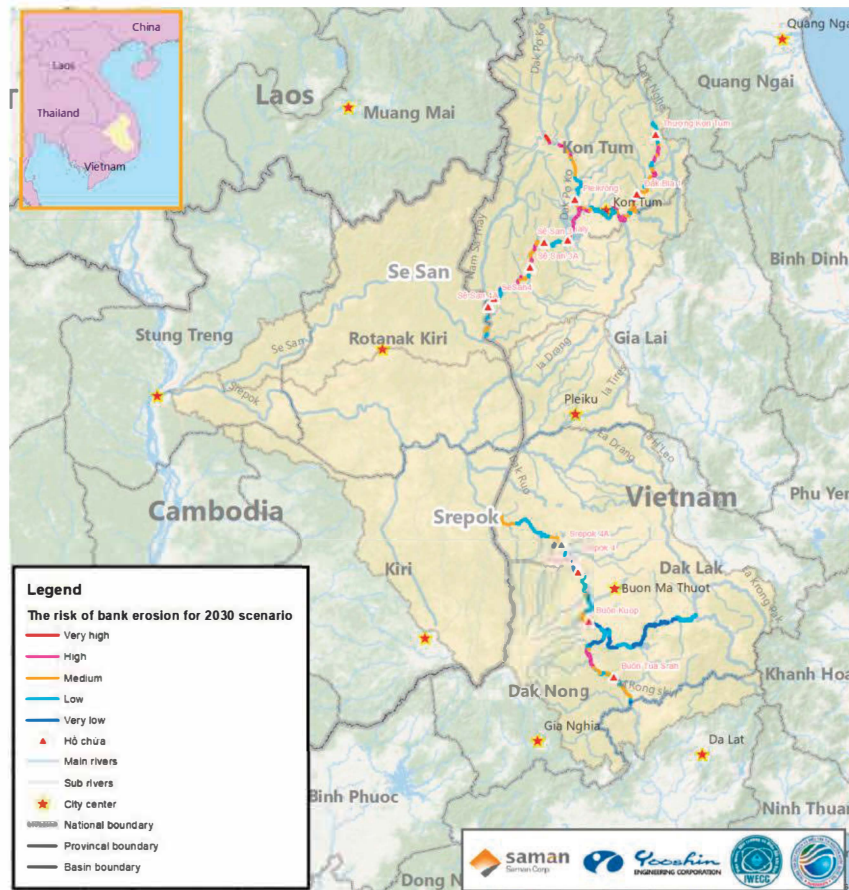


Fig. 1. Risk of bank erosion for 2030 scenario

Very high erosion risk sites are located on the Dak Bla River with a total length of 2,286m (running through Kon Ray and T. Kon Tum streets, Kon Tum province); Po Ko river with a total length of 5,096m (flowing through Ngoc Hoi and Dak To districts, Kon Tum province). High risk erosion sites are scattered on the Dak Bla, Po Ko, and Se San Rivers in the Se San and Krong No Rivers in the Srepok Basin with a total length of 73.5 km.

Conclusions

A decision support system developed to support IWRM in 2S river basin in Vietnam was successfully applied to examine future risks of riverbank erosion. Various factors that can cause riverbank taxation have been considered, and the results will be used as basic data for the establishment of a long-term comprehensive plans for river basin protection by the central government of Vietnam. The DSS-2S can also be used for water resources planning and water quality assessment considering various scenarios such as climate change and socio-economic changes.

References

World Bank Report. (2020). Development of Water Resources Planning for Se San - Srepok River Basin (2S)

Cast Study: Smart Water Management Technology for the Development of New Capital City of the Indonesia

Sang Young Park^{1*} and Jin Hyeog Park²

^{1,2} Global Cooperation Department, Korea-Mekong Water Resource Management Research Center,
Korea Water Resources Corporation

*Corresponding: sypark119@kwater.or.kr

Abstract

The Korean Government has launched K-City Network Global Program to promote the successful Smart City model in Korea, which is led by the Korean Ministry of Land, Infrastructure, and Transport. The K-City Network aims to foster government-to-government (G2G) collaboration on smart city development and enable Korea to share its experience and technologies around the world. This article summarized K-City Network project as a case study of the New Capital City (NCC) project in Indonesia. The design of Indonesian NCC is rooted in the vision to create a capital city as a mirror of national identity, a sustainable city and a smart and modern city. The implementation of the Smart City will be supported by a smart infrastructure system in every aspect of the city elements with utilization of information and communication technologies (ICT). In the field of water management, the following technologies proposed in the project. The proposed integrated water disaster management system is consisted with urban flood prediction model and an integrated water disaster management system. The Smart Water Management System (SWM) will prove an increased Water management efficiency through the convergence of waterworks and ICT technology including real-time monitoring of water quantity and quality. The key barriers and enablers for SWM implementation in Indonesian situation is summarized in the later part of article.

Keywords: Smart city, smart water management, Indonesian new capital city, K-city network

Introduction

The direction of innovative water management should incorporate those developments from out-of-water-box, which could be implemented by employing Smart Water Management (SWM) Technology. SWM include (i) Implementation of IWRM based smart technology for water, (ii) Application of intelligent water management with low energy consumption and high efficiency. Many technologies have been applied to water management for resolving various water-related issues and increasing the efficiency of water management. And recently, information and communication technologies (ICT) have been applied to optimize the water production and distribution processes with maximum efficiency at each step (Choi et al., 2016).

Smart Water Management

The objective of the Smart Water Management (SWM) system is to maximize the efficiency of water resource operations by implementing advanced ICTs to conventional water networks over the entire water cycle in a source-to-tap (STT) setting. The main components of an SWM system include the followings.

- Devices: composed of real-time smart measuring devices, two-way monitoring and controlling communication devices, automated technology, and monitoring devices along with the entire network.
- Solutions: integrated operation of raw water supply control systems starting with inflow forecasts to the reservoirs, and real-time operation of the entire network

(reservoir, water treatment plant, water transmission/distribution pipeline network, offtake facilities, and household connections) to analyze system performance and failures, integrated pipeline network operation management system

- Services: integrated operation and maintenance of the entire network by providing big data analysis, sharing two-way data, and provision of customized services to consumers.

SWM Technology for Indonesian New Capital City

The SWM technologies have been implemented and validated in the Korea, especially through the involvement of K-water including integrated water disaster management, introduction of smart water management system, and application of advanced SWM technology.

The proposed integrated water disaster management system is consisted with urban flood prediction model and an integrated water disaster management system. The Smart Water Management System (SWM) will prove an increased Water management efficiency through the convergence of waterworks and ICT technology including real-time monitoring of water quantity and quality.

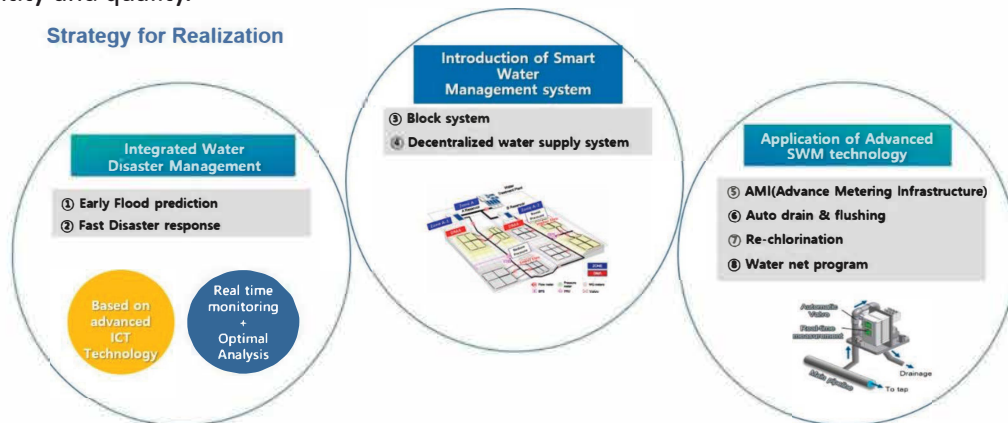


Figure 1. Strategy for realization of Smart Water Management Technology in Indonesian New Capital City

Water disaster management system will be implemented based on data from satellites, radars, weather stations, water flow stations and others. The integrated flood forecast system will be faster and more accurate flood predictions and warning.

Advanced metering infrastructure (AMI) is consisted with Smart Meter, Leakage Detection Sensor, which will enhance the leakage and Non-Revenue-Water (NRW) management and energy saving

To ensure the quality of water distribution network, an automatic drain, flushing of pipe line and re-chlorination technologies are proposed for the project. The Water-Net system as an integrated water supply network operation management, will be employed for ICT-based total solution with real-time network analysis and to support decision-making on pipeline network and risk management.

As an innovative water supply concept, the Decentralized Water Supply System (DWSS) was proposed. By installing the water treatment plant at the nearest place to the consumers, DWSS could reduce to 1/3 the area of the conventional Water Treatment Plant and could utilize diverse water sources such as rainwater, groundwater, river water, etc.

References

Gye Woon Choi et al., SWMI: new paradigm of water resources management for SDGs Smart Water (2016)

A practical Application of Hybrid Flood Modeling in River

Wanshik Yu¹, Yonsu Kim¹, Sunghoon Kim¹, Jiyoung Jung¹ and Joonwoo Noh^{1*}

¹K-water Research Institute
*Corresponding: jnoh@kwater.or.kr

Abstract

Severe flood damages occurred during the typhoon occurred in 2016 and 2020 The Taewha River in Ulsan city is subject to flood damage due to heavy rainfall especially. In the upstream of the Teawha River, many reservoirs are located and the downstream water level varies with the tide of the east sea. Other than the amount of the rainfall, the water level of the river is determined by these two main factors. This study focuses on the application of the AI algorithm for the purpose of the projection of the water level to minimize flood damages of the residence of the Ulsan city. Combining reservoir operation and tidal variation of the downstream, it is possible to project the flood level of the control point, arrival time of the flood wave corresponding to the various rainfall scenarios. The ANN and LSTM schemes are employed to project flood level to test the reliability of the algorithms comparing with the measured data.

Keywords: River flood; Flood level, AI algorithm, ANN and LSTM

Introduction

During Typhoon Chaba In 2016, flood inundation occurred in the Taewha River and yielded serious flood damages in Ulsan city. The maximum rainfall at Hogye and Samdong station increases up to 115mm/hr total 375mm and 131.5mm/hr 319mm, respectively. As a result, flood damages prevailed including the casualties, residential and commercial areas, and industry facilities such as Hyundai motor company. The water level of the Taewha River is subject to the several reservoirs in the upstream, tidal variation of the downstream, and many other factors. To overcome the limitation of the physical flood model, this study applied various AI algorithms to project the flood level of the Taewha River. Combining the water level of the upstream reservoirs and tidal variation of the downstream, the relation of the water level with the amount of the rainfall was identified employing AI algorithms such as ANN and RSTM scheme.

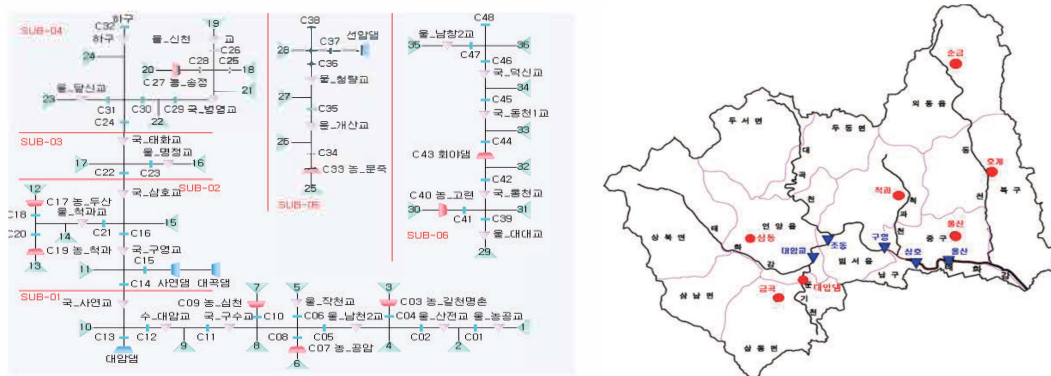


Fig. 1 Schematic of Ulsan City's River Basin (Red: Rainfall Gauges, Blue WL Gauges)

Methods

The flood level of the control points will be determined combining the relation of the reservoir operation and tidal variation of the downstream of the Taewha River. By setting the water level of the control points, Input variables to develop the AI algorithm are upstream water levels, reservoir discharge, tidal levels of downstream, and rainfalls. The structure of the artificial neural network consists of the input layer, hidden layer, and output layer. The information (x_i) is transferred to and the neural units of the input layer connected with weighted hidden layers. Nodes of each hidden layer receives transformed information from the input layers to yield proper response of the output results. The input structures of ANN model is given in Table 1.

Table 1. Input structure of ANN model for water level prediction

Case	Parameters	Input	Neuron Size	Target
1	Hidden Layer (15, 30, 45) Epoch Number (100, 300, 500)	$h(t, t-1, t-2)$	9	$h(t+3)$
2		$h(t, t-1, t-2, \dots, t-4)$	15	
3		$h(t, t-1, \dots, t-6)$	21	
4	Learning Rate (0.5, 0.7, 1.0) Batch Size (6, 12, 18)	$h(t, t-1, t-2)$	9	$h(t+6)$
5		$h(t, t-1, t-2, \dots, t-4)$	15	
6		$h(t, t-1, \dots, t-6)$	21	

Results

The AI algorithm employed in this study reproduces reasonable output results comparing with the observed water levels in downstream of the Dae-Am reservoir. The modeling efficiency of the AI algorithm varies with the number of training and hidden layers and input variables.

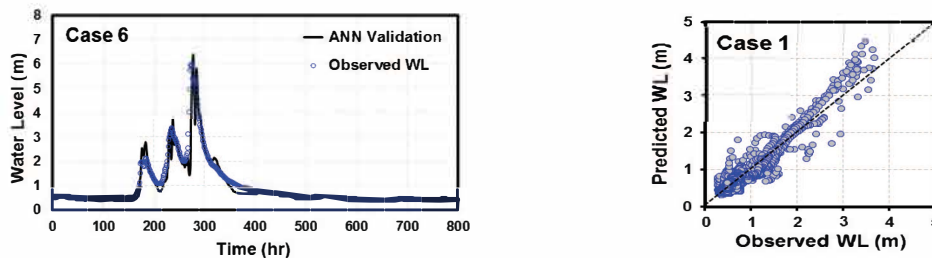


Fig. 2 Example Testing results and comparison of observed and predicted data

Conclusions

This study tests the practical applicability of the AI algorithms to project flood levels in downstream of the reservoir. The simulation results show the possibility of the AI algorithms in practical aspect to minimize flood damages especially in urban areas. The AI algorithm is robust tool to overcome the limitation of the physical modeling in various areas of the water resources management such as flood control, reservoir operation and water quality projections.

References

- kim, S. and Seo, I. (2015). Artificial Neural Network ensemble modeling with conjunctive data clustering for water quality prediction in rivers. *Journal of Hydro-environmental Research*, Vol. 9, 325-339.
- Yoon, K., Seo, B. and Shin, H. (2004). Real-Time forecasting of flood runoff based on neural networks in nakdong river basin and application to flood warning system. *Journal of Korean water Resources Association*, KWRA, Vol. 37, No. 2, 145-154.

**The 9th International
Symposium on
Environmental Hydraulics**

S8 Session

Green Energy & ICT of Clean Water [S8-W1]



Heat Source and Sink Trends for Internet Data Center Cooling System

Kwesi Mensah¹, Selorm Kwaku Anka¹, Tae In Ohm², Jong Woong Choi³, Yong Cho³,
Sung Hoon Chu³, Han-Young Kim⁴ and Jong Min Choi^{5*}

¹Graduate School of Mechanical Engineering, Hanbat National University, Daejeon 34158, Republic of Korea

²Department of Civil & Environmental Engineering, Hanbat National University, Daejeon 34158, Republic of Korea

³Research Institute, K-Water, Daejeon 34045, Republic of Korea

⁴R&D Center, Shinsung Engineering, Chungcheongnam-do 31458, Republic of Korea

⁵Department of Mechanical Engineering, Hanbat National University, Daejeon 34158, Republic of Korea

*Corresponding author: jmchoi@hanbat.ac.kr

Abstract

Internet data center cooling systems are designed to maintain environmental condition being suitable for ensuring IT equipment's reliability. This is achieved by transferring the heat of the equipments (heat source) to the heat sink utilizing the cooling system. The cooling system performance is greatly affected by the heat sink type adopted. This study investigated the current trends for Internet data center cooling system focusing on the available heat sinks. The commonly used heat sinks for IDC Cooling system is ambient air and most researches have focused on enhancing the performance of them. It is also found that rare research literatures are available on the use of water as potential heat sink even though it has great potential for enhancing the performance of the cooling system in the aspect of energy savings. It is highly recommended that future research works should focus on investigating the potential use of water sources as heat sinks and its related challenges.

Keywords: Energy Savings, Cooling Systems, Internet Data Center, Heat Source.

Introduction

Internet data center (IDC) facilities are designed to accommodate IT or telecommunication equipments. In the operation process, the IT equipments generate lots of heat (ASHRAE 2008). Cooling of the IDC facility is achieved by the use of a cooling system. This cooling system works by moving or transferring the heat generated by the IT equipment (heat source) because of its operation to a heat sink. The heat sink in this contest refers to the medium that receives the transferred heat from the IT equipment. Since the IT Equipments are operated continuously year-round, the cooling system is also operated continuously. Research shows that, the type of the heat-receiving medium (sink) adopted for the cooling system has significant effect on the performance of the system. The objective of this study is to investigate the current trends for IDC cooling system researches focusing on the available heat rejection medium and its potential effect on the performance of such systems.

IDC Cooling System Structure and Energy Demand

Fig. 1 shows the basic cooling system structure of an IDC facility. The energy consumption pattern of the various IT equipment in a typical IDC facility is shown in Fig. 2. The cooling system accounts for 38% for the total energy consumption in a typical IDC infrastructure (Amoabeng and Choi, 2016). The most suitable cooling system should be designed considering the design class of the IDC, in order to obtain a high energy savings and efficiency, low cost and system reliability.

Cooling System's Heat Rejection (Sink) Research Focus

The heat rejection is the last step in the IDC cooling system process. The type of heat rejection medium (sink) utilized is dependent on the cooling system type adopted. Fig. 3 below shows the current research focus for IDC cooling systems adopting various heat reception sinks from

the periods of 2000 to 2021. It can be seen that most cooling systems studied currently adopts the atmosphere as the heat sink.

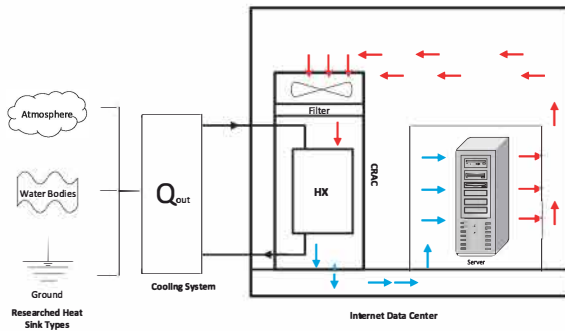


Fig. 1 IDC Cooling System Structure.

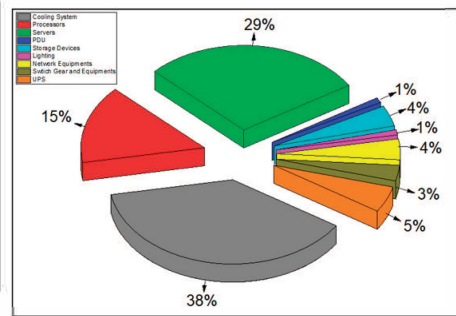


Fig. 2 Energy demand of IDC facility.

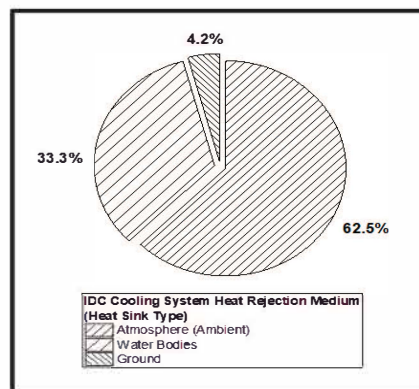


Fig. 3 Research focus of Heat Sinks

Conclusions

After the IT equipment heat is removed from the server space by the cooling system, it must be rejected to a heat sink. The type of heat sink used greatly affects the performance of the cooling system. This study investigated the current trends for Internet data center cooling system focusing on the available heat sinks. The commonly used heat sinks for IDC cooling system is ambient air and most researches have focused on enhancing the performance of them. Even though other choices of heat sinks are ground and water bodies, not much research literatures have focused on such. It is highly recommended that future research works should focus on investigating the potential use of water body sources as heat sinks and its related challenges.

Acknowledgement

This work was supported by Korea Environment Industry & Technology Institute(KEITI) through Environmental Technology Development Program, funded by Korea Ministry of Environment(MOE) (1485017248)

References

- ASHARE (2008), Best Practices for Datacom facility energy efficiency, American Society of Heating, Refrigerating and Air-Conditioning Engineers, Inc. (ASHRAE) 2008. Atlanta, GA303292nd Edition.
- Amoabeng, K.O. and J.M. Choi, (2016). Review on Cooling System Energy Consumption in Internet Data Centers. International Journal of Air-Conditioning and Refrigeration, 24(04): p. 1630008.

Eco-friendly Floating Photovoltaic Power Plant of K-water

Hyunsik Jo^{1*}, and Hyunjun Kim¹

¹Water Energy Research Center, K-water Research Institute

*Corresponding: hsjo@kwater.or.kr

Abstract

Efforts to respond to climate change and reduction of greenhouse gas emissions are spreading around the world. Thus, the importance of the renewable energy such as hydro power, photovoltaic, P2G, wind power, etc., is increasing. Among them, photovoltaic have been gaining attention as an eco-friendly energy. Floating photovoltaic(FPV) systems have been researched as a new concept in PV industry to mitigate negative environmental impacts instead of installing conventional PV facilities on land. The FPV system is designed for PV system utilizing unused water surfaces was created. In this special session paper, 3MW FPV power plant and environmental impacts monitoring at the Chungju Dam is described among various FPV power plants of K-water.

Keywords: FPV(Floating Photovoltaic); Renewable energy; Photovoltaic

Introduction

K-water(Korea Water Resources Corporation) has been focused on the research and development of energy and water fusion technologies in order to more effectively utilize the many dams operated by K-water. The Floating Photovoltaic (FPV) system is the result of these efforts and a new concept and design for solar power system utilizing unused water surfaces was created. In August 2009, K-water installed the first FPV pilot plant (2.4kW) at Juam dam and carried out research through pilot operations for two years. The research shows that there is more efficiency in power generation due to the cooling effect on PV modules resulting from the water surface which keeps the PV modules' temperatures lower. In addition, a mooring method was developed in order to ensure that the buoyant materials can adapt to significant water level changes that could occur at dam reservoirs and keep the body's direction. On the basis of these operating results, K-water currently operates 5.7MW floating photovoltaic plants in five sites such as Hapcheon(100kW, 500kW, 100kW), Boryeong(2MW), and Chungju(3MW) as shown Fig.1 . K-water focuses on making the system more eco-friendly, improving safety, and increasing efficiency of floating systems.

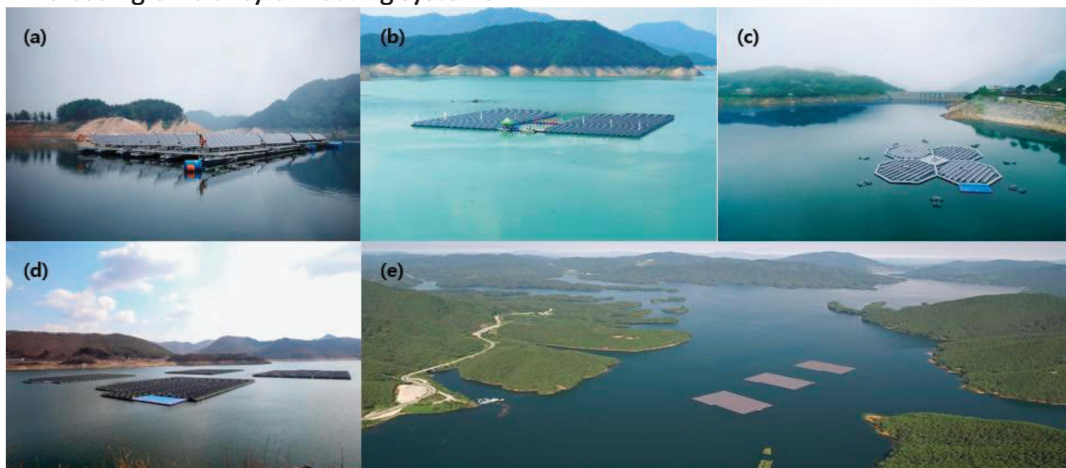


Fig. 1. FPV power plant of K-water (a) Hapcheon 100kW (b) Hapcheon 500kW (c) Hapcheon 100kW (d) Boryeong 2MW and (e) Chungju 3MW

Environmental impacts monitoring

Chungju FPV power plant consists of 2952 PV modules(340W), 3 grid-connected inverters, floating system mooring device and under water cable. K-water has been conducting continuous environmental monitoring since installing FPV. Monitoring items are water quality, plankton, benthic organisms, sediments, aquatic ecology. Its survey 34 items of water quality, 11 items of sediment, birds and fish monthly, quarterly, and semi-annual as shown Fig. 2. The main contents of environmental monitoring results that no contaminants in accordance with human health protection standards are detected. No harmful results were found in heavy metals and benthic organisms in the sediments. Plankton had no difference before and after installation. And it confirmed the positive effect that juvenile fish increase under FPV.



Fig. 2. Point of environmental impacts monitoring at Chungju dam

Table 1. Results of environmental impacts monitoring

Item	Results
Water Quality	- Not detected any pollutant related with “Human health protection standards” in every position - No difference in water quality grade between installation and control
Sediment (heavy metals)	- Detected below standards (exist as background concentration in nature) ⇒ No possibility of harmful effects for benthic organism
Plankton	- No difference in species & population by installation (Except for seasonal difference)
Fish	- Increasing species & population of juvenile fish under the floating system
Birds	- No facility avoidance - Increasing species & population compared with literature

Conclusions

In this special session paper, 3MW FPV power plant and environmental impacts monitoring at the Chungju Dam have been described among various FPV power plants of K-water. K-water has been focused on the research and development of energy and water fusion technologies in order to more effectively utilize the many dams operated by K-water since 2009. K-water currently operates 5.7MW floating photovoltaic plants in five sites. As a result of continuous environmental impact monitoring, it has been confirmed that floating solar power did not adversely affect the environment.

Acknowledgement (If necessary)

This work is supported by the Korea Institute of Energy Technology Evaluation and Planning(KETEP) and the Ministry of Trade, Industry and Energy(MOTIE) of the Republic of Korea.(No. 20183010014260)

Development of AI-driven Composite Sensor to expand energy management system in Water treatment plant

Sang Byeong An ^{1*}, Sung Taek Hong ¹, Kuk Il Kim ¹, and Jin Hoon Kim ¹

¹Water Energy Research Center, K-water Research Institute

*Corresponding: sban11@kwater.or.kr

Abstract

In water treatment plant, AI-driven composite sensors are devised to sense the energy consumption and influencer, and to improve the information provision by converging with energy consumption of xEMS(FEMS, BEMS, WEMS, etc.), sensor functions and AI learning and inference function. AI-driven composite sensors in water treatment plant are expected to reduce the energy consumption effectively. This session is organized for analyzing and defining demands to develop composite sensors in water treatment plant. Furthermore, it proposes to improve process and to increase efficiency by using AI-based composite sensors.

Keywords : Composite Sensor ; Water Treatment Plant ; AI; Energy Management System

Introduction

In conventional water treatment plant, a lot of measuring sensors, such as flow meter, level meter, water quality meter, thermometer, pressure gauge, electric power meter and so on, are being used. They are influenced by organic combination of measuring devices with physical, chemical and electric characteristics. Data from sensors in water treatment facility, flow, level, water quality, pressure and so on, are sent to upper SCADA system which is responsible for auto-control or AI-driven management and operation. Thus, introduction of the virtual sensors capable of state-estimation from the prior states and the measurements in real time, to protect the system from the failures of the measurement sensors is required.

Methods

The AI-driven integrated energy sensor is to provide the local solution based on the analysis for the optimal process based on the values metered, to the EMS. It is the sensor possible to be in form of being integrated in a single hardware or installed separately that is capable of sufficing the data quality for measurement and control from perspectives of EMS.

The solution derived from the sensor consists of state estimation or prediction of the values and coefficients required to maintain the process reliability based on the data metered from the conventional meters for water level, pressure, flowrate and the quality in real time.

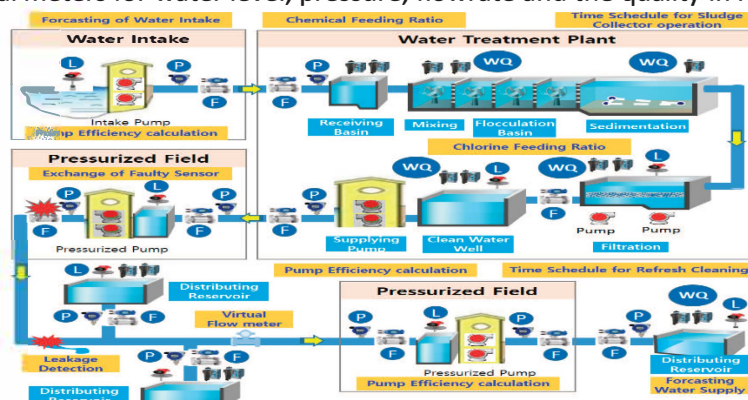


Fig. 1. Required Specifications for Composite Sensor for Water Treatment Facilities

The state estimation is performed by the algorithm mounted inside the sensor, based on the data acquired in RT and includes preprocessing of the data, failure diagnosis of the measurement sensors and optimal control sequence via machine learning. Once the estimation is completed, the solution becomes transmitted to the main control system or HMI for the operator.

Furthermore, the sensor as the composite sensor, is currently in use to alter or replace the former conventional measurement and control sensors in fixed type.

Results

The production cost of the potable water consists of 10% from the energy cost for O&M of the facility and 70% of the energy cost is from the pumps for distribution system. Thus, introduction of the AI-driven composite sensor to replace the former conventional sensors, is required to facilitate the cost minimization.

- a. (Analysis of Pump Efficiency) Optimization of operations of the pumps and the processes for water treatment through water demand forecasting can reduce energy consumption.
- b. (Virtual Flow Meter) The virtual flow meter is to forecast water intake through analysis on inflow and flow rate of water purification site/plant, branch flow rate, drainage level. The meter can be installed in locations where flow measurement is difficult due to high cost and installation environment.
- c. (Sludge Treatment) Optimization of the operation cycle of sedimentation process, sludge generation and related facilities (sludge collector, dehydrator, sludge transfer pump, etc.) via analysis on flow rate, water quality, and sludge surface, is enabled.
- d. (ETC) Estimation of chemical feeding rate through data analysis based on changes in raw water, mixed water, sedimentation water, flow rate. Estimation of the changes in input rate of chlorine, the water purification plant by analyzing water quality, residual chlorine concentration, and time of stay. Measurement of the temperature (variable), effective diameter, even coefficient, weight of the female material, and turbidity of filter paper to derive the optimal reverse cleaning speed for determination of the sequence

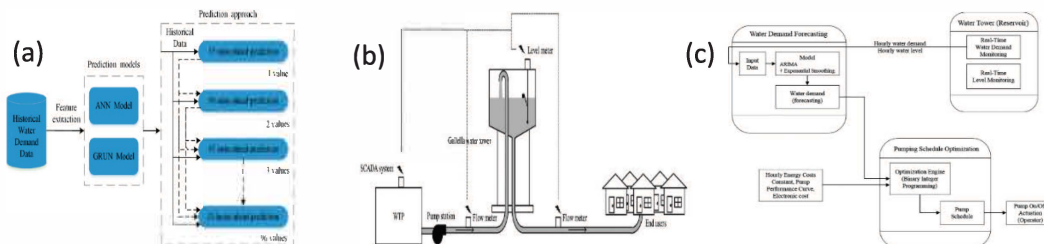


Fig. 2. Water demand forecasting and pump scheduling (a) Short-term water demand forecasting (b)Diagram of Water Treatment Facility (c) Illustration of Pump Scheduling

Conclusions

In this study, energy optimization for the stable operation of the water supply and distribution system and the carbon neutrality in the major energy consumption facilities by AI-driven composite sensor is presented by identifying the major contributors to the energy consumption. Furthermore, through the replacement of the foreign sensors at high cost, by the domestic composite sensor localized, improvements on technical competency in the global market can be established by this study.

Acknowledgement

This work was supported by the Korea Institute of Energy Technology Evaluation and Planning (KETEP) and the Ministry of Trade, Industry & Energy(MOTIE) of the Republic of Korea (No. 2020200000010).

Seismic Behavior Analysis of an RTU Panel with Friction Pendulum System by Tri-axial Shaking Table Tests

Bub Gyu Jeon¹, Sung Wan Kim¹, Da Woon Yun¹, Woo-Yong Jung²

¹Seismic Research and Test Center, Pusan National University

*Corresponding: bkjeon79@pusan.ac.kr

Abstract

Electrical-cabinet damage may cause problems to the intrinsic functions of facilities, which may lead to severe accidents accompanied by property damage and human casualties. Therefore, the seismic performance of electrical cabinets with important functions must be secured. Generally, two-horizontal axis shaking table test using scaled model was used for the seismic performance evaluation of isolation system. It is difficult to find an example of analyzing the seismic performance of a real size electrical cabinet with isolation system by using the tri-axial shaking table considering vertical direction. Therefore, in this study, to examine the seismic performance of an RTU panel which is an electrical cabinet with Friction Pendulum System, tri-axial shaking table test was performed.

Keywords: Friction Pendulum; Electrical cabinet; Tri-axial test; shaking table; Seismic behavior

Introduction

In recent years, the damage cases of earthquakes have caused more damage to non-structural components than to structures. Among the non-structural components, the electrical cabinet is one of the important devices used to maintain the function of the facility. Therefore, the electrical cabinet should be safely protected from earthquakes. Seismic performance can be improved while minimizing design changes by applying a seismic isolation system. FPS (Friction Pendulum System) is an isolation system which is possible to isolate structures from earthquake by pendulum characteristic. Natural frequencies of the structures could be determined by designing the radius of curvature of FPS. In this study, the seismic performance of an FPS with an overturn prevention device was evaluated through a 3-axis shaking table test. The seismic isolator was installed on the RTU panel used in the hydroelectric power plant.

Shaking Table Test

The test specimen that was used in the shaking table tests in this study was an RTU panel with FPS. Test specimen was installed in a shaking table. Fig. 1 shows the test specimen and sensor locations. Fig. 2 shows the response spectrum of the input seismic motion, with a 5% damping ratio. Table 1 is seismic parameters for response spectrum.

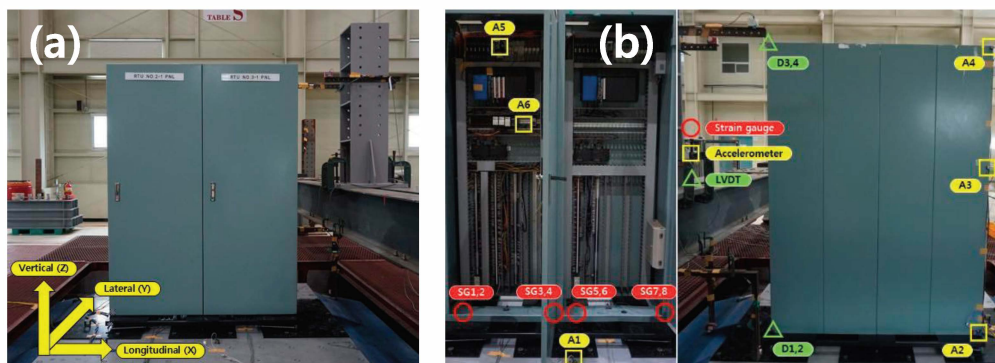


Fig. 1. Test set up; (a) Test specimen on shaking table and (b) sensor location

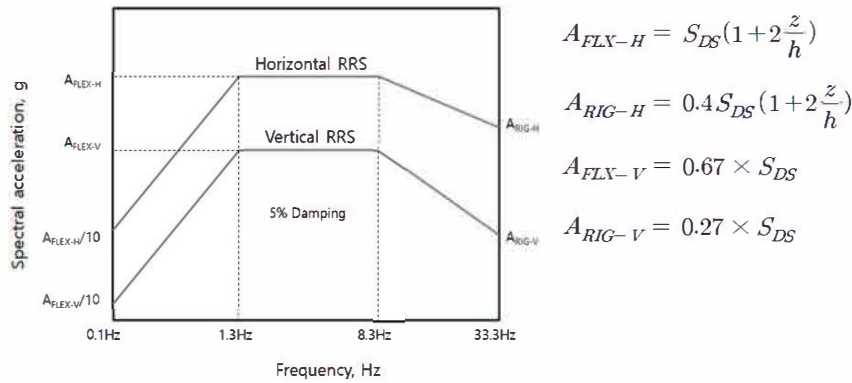


Fig. 2. Required response spectrum

Table 1 Seismic parameters for artificial earthquake

Name	S_{DS} [g]	z/h	A_{FLEX-H} [g]	A_{RIG-H} [g]	A_{FLEX-V} [g]	A_{RIG-V} [g]
EQ1	0.55	1	0.88	0.66	0.36	0.14
EQ2	0.825	1	1.32	0.99	0.55	0.22

Test Results

Fig. 2 (a) shows the peak acceleration response at each accelerometer locations. Fig. 2 (b) shows peak acceleration ratios calculated by Equation 1. Here, $a_{max,component}$ is peak acceleration responses of RTU panel, $a_{max,base}$ is peak acceleration response of shaking table base.

$$R_{a,max} = \frac{a_{max,component}}{a_{max,base}} \quad (1)$$

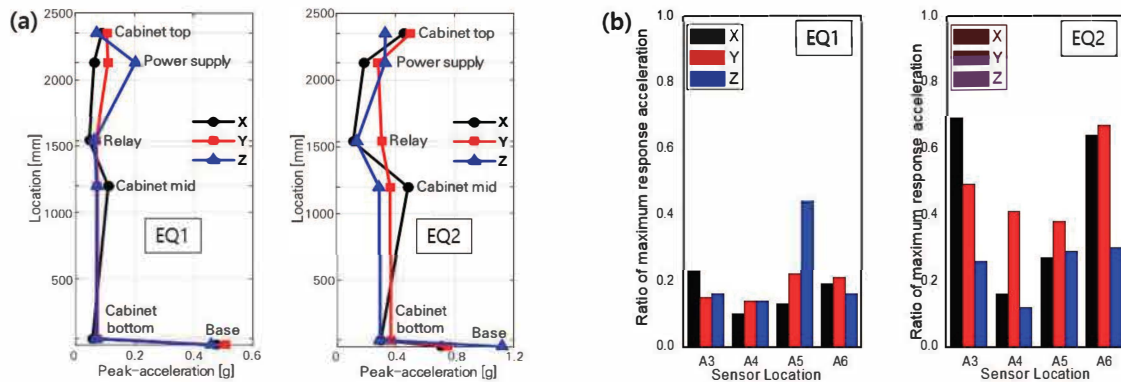


Fig. 2. Test results; (a) Peak acceleration, (b) peak acceleration ratio between base and specimen

Acknowledgement

This research was supported by a grant (21IFIP-B128598-05) from Industrial Facilities & Infrastructure Research Program (IFIP) funded by Ministry of Land, Infrastructure and Transport of Korean government.

References

ICC Evaluation Service (2015). AC156-2010, Acceptance Criteria for Seismic Certification by Shake-table Testing of Nonstructural Components, Brea, California, USA

Jeon, B. G., Chang, S. J. and Kim, N. S., (2011). Seismic Performance Evaluation of Cone-type Friction Pendulum Bearing System Using Shaking Table Test, Transactions of the Korean Society for Noise and Vibration Engineering, 21(7), 599-608.

**The 9th International
Symposium on
Environmental Hydraulics**

S9 Session

**Multi-dimensional River Operation
and Management Techniques
[S9-W2]**



Levee monitoring using Mobile Mapping System

Jisang Lee¹, and Hong-Gyoo Sohn¹

¹Department of Civil & Environmental Engineering, Yonsei University

*Corresponding: sohn1@yonsei.ac.kr

Abstract

In order to maintain and manage levee condition, continuous data collection on levee must be preceded. Mobile Mapping System(MMS) which acquires data while moving along the bike road constructed through river, is more effective than existing data acquisition method using a total station, GNSS, and terrestrial laser scanner in terms of cost/time/manpower. As a result of applying the MMS to the 4km-long test area of Anyang-cheon, a representative urban river, 184,646,009 points were acquired during the 20-minute data acquisition time. Among the data, automatic extraction of levee point cloud algorithm is applied for the 1km-long area.

Keywords: Mobile Mapping System, Point Cloud, Basic River Plan, Levee monitoring

Introduction

Levee monitoring is the most basic part of river facility management to prevent flood damage (Choung et al. 2011; Thatcher et al. 2016). However, existing river basic plan established by the Ministry of Land, Infrastructure and Transport, the river management institution may only conduct cross sectional and longitudinal surveys using GNSS, total station, and aerial surveying. However, these 2-dimensional inspections cannot effectively cope with recent flood damage trend(Kim 2002; Park et al. 2014; Park et al. 2017). Since flood damage of recent years occurs at any unpredictable points and from torrential rain fall within few hours, but the traditional survey methods have limitations in cost/time/manpower(Kim et al. 2017; ME 2018). Therefore, researchers designed MMS to cope with levee monitoring and algorithm of automatic extraction of levee point cloud from MMS acquired data.

Methods

Anyang-cheon was selected as out study area. Fig. 1 shows aerial image of research area with MMS trajectory and acquired point cloud data. The researchers divided point cloud data into 379 units according to GNSS trajectory on MMS and measured the levee elevation.

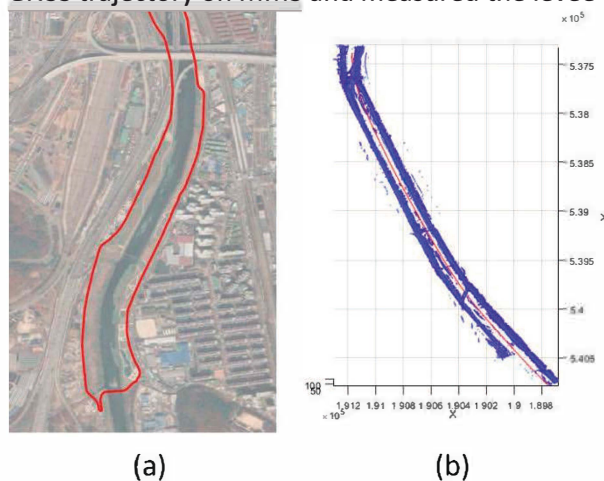


Fig. 1. Aerial image of research area with MMS trajectory in red (a), acquired point cloud data(b)
Also, for 100 units of point clouds, the automatic levee point cloud extraction algorithm was applied.

Results

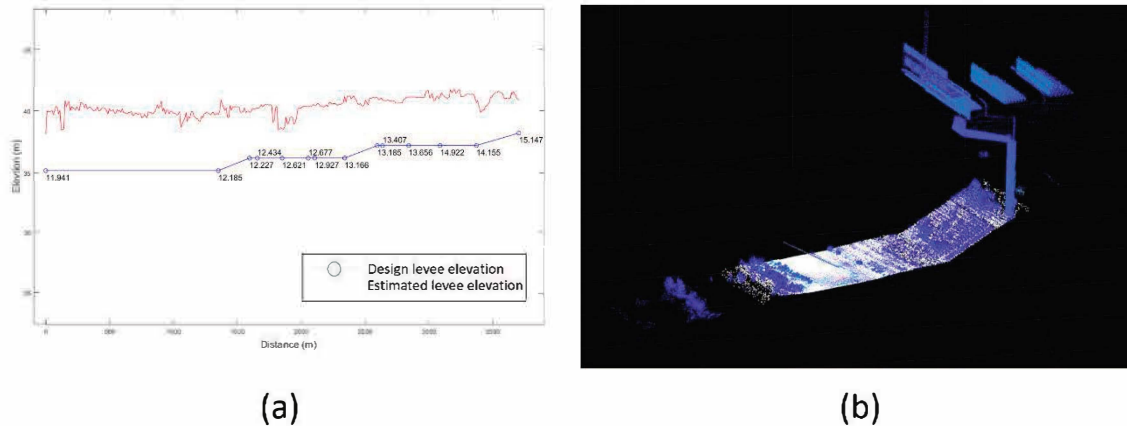


Fig. 2. Comparison between levee elevation from basic river plan and estimated (a), automatic levee point cloud extraction result in unit point cloud

Fig. 2. shows comparison between levee elevation from basic river plan and manually estimated ones in 379 units (a) and automatic levee point cloud extraction result (b). White points represent automatically extracted levee points and blue points represent original point clouds.

Conclusions

Monitoring levee elevation was the basic task for levee management to prevent flood damage. MMS is suitable device for levee monitoring compared to existing method of measuring factors of levee. Through using MMS and self-derived automatic levee point cloud extraction algorithm, efficient levee monitoring was enabled.

Acknowledgement (If necessary)

This work is supported by the Korea Agency for Infrastructure Technology Advancement(KAIA) grant funded by the Ministry of Land, Infrastructure and Transport (Grant 21AWMP-B121100-06)

References

- Chung, Y.-J., Park, H.-C., Chung, Y.-I., and Jo, M.-H. (2011). "Mapping Man-Made Levee Line Using LiDAR Data and Aerial Orthoimage." *Journal of the Korean Association of Geographic Information Studies*, 14(1), 84–93.
- Kim, S.-Y., Kim, J.-S., Lee, C.-J., Kim, H.-J., and Yun, G.-S. (2017). "2017년 7월 집중호우에 의한 충청지역 홍수피해 원인 및 대책 검토." *Water for future*, 50(10), 37–42.
- ME. (2018). Report for flood damage investigation 2018, Korea.
- Thatcher, C., Lim, S., Palaseanu-Lovejoy, M., Danielson, J., and Kimbrow, D. (2016). "Lidar-based mapping of flood control levees in South Louisiana." *International Journal of Remote Sensing*, Taylor & Francis, 37(24), 5708–5725.

Probabilistic Mapping of Flood Risk using Multivariate Statistical Model

Min-Kyu Jung¹, Hyun-Han Kwon^{1*}

¹Department of Civil & Environmental Engineering, Sejong University

*Corresponding: hkwon@sju.ac.kr

Abstract

Various studies have been conducted to improve the repeated flooding problem in urban areas, which is attributed to the decrease in the rainwater infiltration and the increase in surface runoff due to the increase in the impermeable area. Among the hydrological models, the statistical model is capable of obtaining weights by analyzing the correlation between the dependent variable and the independent variable, deriving the functional relationship between input and output. In this study, logistic regression analysis is performed to derive the correlation between geospatial information and the inundation indicated by flood hazard maps. Also, converting the area of the study to thousands of grids, the expected flood areas were expressed probabilistically to identify areas with a relatively high risk of damage.

Keywords: Flood risk; Logistic regression; Bayesian inference

Introduction

The development around rivers and the increase in impermeable surface caused by urbanization not only increase the number of disaster hazards exposed to flooding, but also cause the spread of damage, creating difficulties in flood management. In order to prepare countermeasures to prevent flood damage, identifying areas where flooding is expected to occur should be prioritized in consideration of various characteristics of the surface around rivers. Multivariate logistic regression can probabilistically reproduce the existing deterministic flood hazard map by mathematically explaining the relationship between flood occurrence and multiple geospatial flood-inducing factors, thus identifying the areas with high potential for inundation.

Methods

The formula for the probabilistic expression of the flooded area is the multivariate logistic regression model shown in Equation (1) below. The dependent variable Y is binary categorical data determined with whether the inundation occurred indicated by flood hazard maps. The independent variables X_n are inputted with geospatial information that can explain inundation, which are elevation, slope, curve number, and distance to the river. The entire area of the watershed is split into grids, and all kinds of the variable X_n and Y are assigned to each grid. Parameters β_n are estimated and become weights that affect the occurrence of inundation. Entering the X_n and parameters β_n into Equation (2) which is an inverse function of Equation (1), probabilities of inundation ranging from 0 to 1 are calculated for each grid cell.

$$\ln\left(\frac{p}{1-p}\right) = Y = \beta_0 + \beta_1 X_1 + \beta_2 X_2 + \dots + \beta_n X_n \quad (1)$$

$$p = \frac{1}{1 + \exp[-(\beta_0 + \beta_1 X_1 + \beta_2 X_2 + \dots + \beta_n X_n)]} \quad (2)$$

Bayesian inference was used to estimate each parameter β_n as a probability distribution with uncertainty. In applying Bayesian inference, it is necessary to derive the posterior distribution

of the parameter as shown in Equation (3) using the Bayes theorem by assuming the prior distribution of each parameter and the likelihood function of the data. The first part of the equation is the prior distribution with the assumption of β_n following the normal distribution. The second part is the likelihood function of which the likelihood of i th object follows a binomial distribution given a probability of success.

$$\text{Posterior}(\beta_j) = \prod_{j=0}^m \frac{1}{\sqrt{2\pi\sigma_j^2}} \exp\left[-\frac{1}{2}\left(\frac{\beta_j - \mu_j}{\sigma_j}\right)^2\right] \times \sum_{i=1}^n \left[\left(\frac{1}{1 + e^{-\beta_0 + \dots + \beta_j x_j}}\right)^{y_i} \left(\frac{1}{1 + e^{-\beta_0 + \dots + \beta_j x_j}}\right)^{1-y_i} \right] \quad (3)$$

Results

The inundation probability is calculated for all grids in the watershed area for the flood that has a 100, 200, and 500-year return period (Figure 1). Finally, when compared with the original flood hazard maps, it is confirmed that the area with over probability of about 30% or more (blue) generally matches to the inundation zone of flood hazard map (red line).

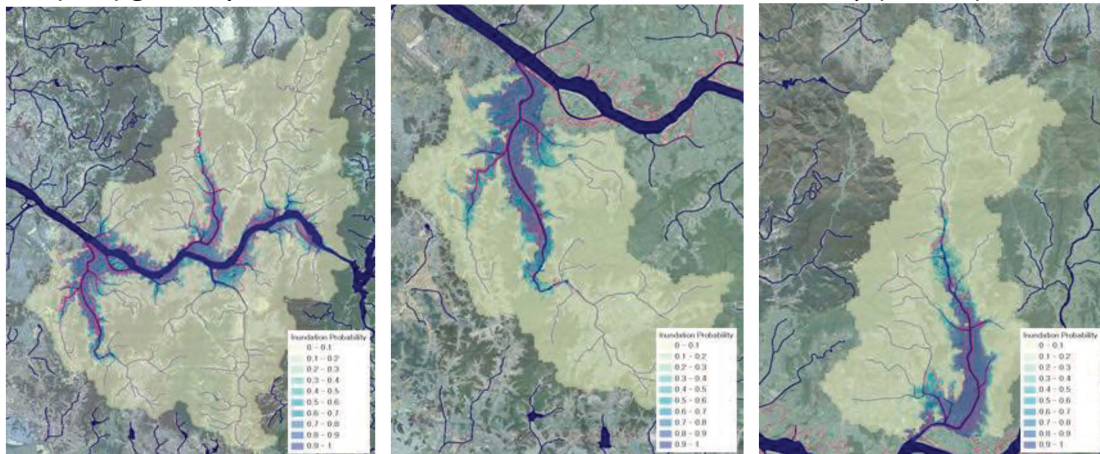


Fig. 1. Probabilistic inundation mapping for 100-year flood over watershed.

Conclusions

In this study, flood hazard maps are probabilistically reproduced as a reasonable basis for geospatial information such as topography and land use, so that the areas with relatively high risk of flooding could be identified. Given available inundation record data of certain rainfall frequencies, considering the simplicity of data construction, and methodology, it is expected to be useful to the areas that flood risk analysis is required.

Acknowledgement (If necessary)

This work is supported by the Korea Agency for Infrastructure Technology Advancement(KAIA) grant funded by the Ministry of Land, Infrastructure and Transport (Grant 21AWMP-B121100-06)

References

Giovanettone, J., Copenhaver, T., Burns, M., and Choquette, S. (2018). "A statistical approach to mapping flood susceptibility in the Lower Connecticut River Valley Region." *Water Resources Research*, Vol. 54, No. 10, pp. 7603-7618.

A Study on Life Cycle Management through the Performance Evaluation Model of River Facilities

Sooyoung Kim¹, Hyung-Jun Kim¹, Boram Kim¹ and Kwang Seok Yoon^{1*}

¹ Department of Land, Water and Environment Research / Korea Institute of Civil Engineering and Building Technology
*Corresponding: ksyoon@kict.re.kr

Abstract

The importance of the safety of river facilities installed to mitigate flood damage is increasing due to the trend of increasing the risk of floods around the world. In this study, for the Proactive maintenance of river facilities, a performance evaluation model for predicting the performance of river facilities was calculated for floodgate. A regression analysis was performed based on precision safety diagnosis of FMS (Facility Management System). And then the change in performance index according to years of use of the river facility was shown. By assuming the type of the performance evaluation model as various functions, the type of optimal performance evaluation model was proposed through comparison with the previous studies. The results of this study are expected to be used as basic data for life cycle management of river facilities.

Keywords: River facility; Life Cycle Management; Performance Evaluation Model; FMS

Introduction

The flood risk is also increasing as sea levels rise and increase in rainfall intensity due to global climate change. River facilities are essential facilities installed in rivers to protect against floods, and it is important to maintain performance requirement through maintenance of river facilities in order to reduce the damage of life and property caused by floods.

To this end, maintenance is required for the entire cycle, such as planning-construction-maintenance-demolition of river facilities, but the installation of river facilities and restoration of damaged facilities are focused on in current situation. In addition, the number of domestic river facilities that have been passed for more than 30 years since completion has exceeded 40%. This shows that the risk of river facility aging in the future can rapidly increase. In order to respond to this aging, related research is proceeding in various fields.

In previous studies, surveys of experts were often used to predict the life of facilities. In "Study on river maintenance plan" (KRIHS, 2004), surveys were conducted with domestic river experts, and in "Bridge maintenance" (OECD, 1981), each country's bridge experts were surveyed. In recent years, due to the development of experimental and monitoring technology, many studies have been conducted to derive a service life or a performance degradation curve based on data. Heo et al. (2017) developed predicting performance degradation model of road bridges using the results of safety inspections.

Methods

The performance evaluation index of the river facility was used Performance Index(PI) of FMS from Precision Safety Diagnosis (PSD) report. The PSD for river facilities in the FMS is divided into five grade (A~E) according to the performance index score (see Table 1).

Table 1. Ranges of Performance Index for each grades

Grade	A	B	C	D	E
Ranges	$4.5 \leq PI \leq 5.0$	$3.5 \leq PI < 4.5$	$2.5 \leq PI < 3.5$	$1.5 \leq PI < 2.5$	$1.0 \leq PI < 1.5$

The Performance index of river facilities and members in the precision safety diagnosis report is convert into a database, and the years of use were calculated from completion year in the river facility management resister and the time of inspection. The objects of this study were flood gates installed at Anyang, Anseong and Jungrang stream in the Han River basin.

Results

As a result of performing regression analysis for each assumed equation type, the coefficients of each equations, Critical Action Period (when the PI decreases to half) and the Durability (when PI becomes less than 1.0) was shown in the Table 2. Overall, the results were over-estimated compared to previous study (KRIHS, 2004), but the suggested equation was the most similar.

Table 2. Results of regression for performance estimation model

Item	Suggested equation	2 nd Polynomial Function	Exponential Function	Power Fucntion	Previous study(KRIHS)
Equation	$f = 5 - x^2/a^2$	$f = 5 + ax + bx^2$	$f = 6 - e^{ax}$	$f = 5 - ax^b$	-
Coefficient	$a = 22.368$	$a = -0.032, b = -0.001$	$a = 0.031$	$a = 0.024, b = 1.211$	-
Critical Action period	35	43	40	46	-
Durability	45	58	51	69	25

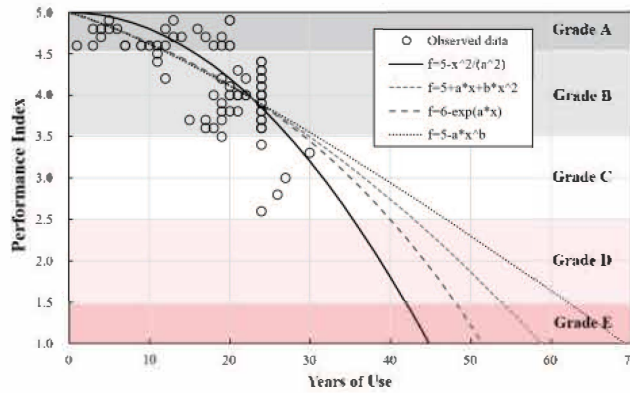


Fig. 1. Relationship between Years of Use and Performance Index

Conclusions

Existing river management systems only provide information on the current status of rivers and specifications of river facilities. For the life cycle management of river facilities, the performance information of river facilities through periodic inspection and history of performance can be used as basic data for establishing a maintenance plan.

Acknowledgement (If necessary)

This work is supported by the Korea Agency for Infrastructure Technology Advancement(KAIA) grant funded by the Ministry of Land, Infrastructure and Transport (Grant 21AWMP-B121100-06).

References

KOREA RESEARCH INSTITUTE FOR HUMAN SETTLEMENTS (2004). Study on river maintenance plan. Ministry of Construction and Transportation.
 Heo, W. H., Kim, K. S., Han, O., Kang, G. Y. & Kim, S.H. (2017). Prediction Model of Performance Degradation for Highway Bridges Considering Previous Inspection Results. Proceeding of Korea Society of Civil Engineering. 1026-1027
 OECD Road Research Group (1981). "Bridge maintenance" Rep. Road Research Group. Organization for Economic Co-operation and Development. Paris, France

Geospatial analysis and model development for specific degradation of ungauged watersheds in South Korea using multiple regression analysis and data mining

Woochul Kang^{1*}, Eun-kyung Jang¹, Pierre Y. Julien²

¹ Department of Land, Water, and Environment Research, Korea Institute of Civil Engineering and Building Technology (KICT), Goyang-si 10223, Gyeonggi-Do, Republic of Korea

² Dept. of Civil and Environmental Engineering, Colorado State University, Fort Collins, CO 80523, United States

*Corresponding: Kang@kict.re.kr

Abstract

Specific degradation (SD) is the ratio of the sediment yield to the watershed area. The SD from 35 watersheds in South Korea was calculated from field measurements of discharge and sediment concentrations. The estimated SD ranges between 10 and 1,000 tons/km²·yr. A model tree data mining technique and multiple regression analysis were used to develop a model for estimating the specific degradation based on various parameters from GIS analysis. The application of existing models from the literature showed Root Mean Square Errors (RMSE) in excess of 1,400 tons/km²·yr. The RMSE for the newly developed models decreased to 55 tons/km²·yr. Additionally, a geospatial analysis with erosion loss maps obtained by the revised universal soil loss equation (RUSLE), satellite images, and aerial photographs were conducted to represent the features affecting erosion and sedimentation.

Keywords: Specific degradation, Model tree, Multiple Regression, Geospatial Analysis

Introduction

South Korea has unique climatic and topographic characteristics, and experienced many local and concentrated sediment problems. This has necessitated the development of a reliable and consistent approach for modeling sediment processes in the country. Many researchers have developed empirical or statistical model for erosion and sedimentation. However, the most existing formulas seem to lack reliability and consistency. This paper focuses on developing an empirical model for predicting specific sediment load of ungauged watersheds based on watershed characteristics.

Methods

In this study, the Modified Einstein Procedure (MEP) was used to determine the total sediment load at all stations. The Flow Duration – Sediment Rating Curve (FD-SRC) method was used to determine the sediment yield and specific degradation for all gauging stations. A multiple regression analysis and model tree data mining were applied to develop empirical model with the estimated specific degradation. The erosion and transport of sediment from upland to the fluvial system is influenced by watershed characteristics such as physiography, topography, geology and pedology, and climatology and forestry. Therefore, various watershed characteristics are analyzed using GIS before developing a model for estimating the specific annual sediment yield. The developed models were validated with additional specific degradation from other references. In addition, geospatial analysis using satellite images and aerial photographs enables evaluation of the prediction methodology.

Results

The specific degradation of 35 river stations in South Korea ranged from 10 to 1,000 tons/km²·yr. The predictabilities of the developed models were observed to depend on the type and characteristics of their catchments. The meaningful parameters are: 1) watershed area[km²], 2) mean annual precipitation [mm], 3) percentage of wetland and water, 4) percentage of urban land, 5) the percentage of sand in the soil, 6) elevation at the middle relative area of the hypsometric curve [m], 7) main stream length [km]. Especially, the proposed model with data mining technique was found to outperform the other models (RMSE = 55 ton/km²·yr).

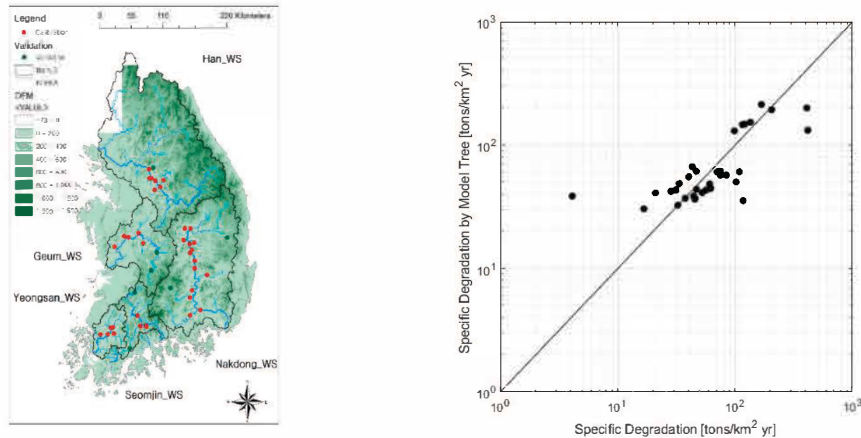


Fig. 1. South Korea (a) power-law slope and (b) truncation time of BTCs.

The results of physiological and geospatial analyses using the RUSLE, satellite images, and aerial photographs represents that hypsometric index, wetland, water, and urban land were important indicators for predicting the specific degradation of watersheds.

Conclusions

The suggested prediction methodology could provide accurate prediction for the specific degradation of target area and can be useful for identifying watersheds, which require sustainable sediment management. Additionally, geospatial analysis could define specific location for management of erosion and sedimentation. In conclusion, the proposed data mining methodology promises to facilitate the solution of various erosion and sedimentation problems and the suggested methodologies should be useful to estimate the sediment yield from ungauged watershed in South Korea.

Acknowledgement (If necessary)

“This work is supported by the Korea Agency for Infrastructure Technology Advancement(KAIA) grant funded by the Ministry of Land, Infrastructure and Transport (Grant 20AWMP-B121100-05).”

References

- Kang, W., Jang, E. K., Yang, C. Y., & Julien, P. Y. (2021). *Geospatial analysis and model development for specific degradation in South Korea using model tree data mining*. CATENA, 200, 105142.
- Kang, W., Yang, C. Y., Lee, J., & Julien, P. Y. (2019). *Sediment yield for ungauged watersheds in South Korea*. KSCE Journal of Civil Engineering, 23(12), 5109-5120.
- Kang, W. (2019). *Geospatial analysis of specific degradation in South Korea (Doctoral dissertation, Colorado State University)*.

Vulnerability Assessment of Watershed Water Quality for Flow Conditions

Woo Suk Jung¹, Sung Eun Kim², Jae Hyun Kwon¹, Young Do Kim^{3*}

¹ Department of Environmental Engineering, Inje University

² Department of Safety and Environment Research, The Seoul Institute

^{3*} Department of Civil & Environmental Engineering, Myongji University

*Corresponding: ydkim@mju.ac.kr

Abstract

The coefficient of the river regime in the Nakdong River is larger than that of other rivers, and the winter river flow at Jindong, which is in the lower reaches of the Nakdong River, is only 14.5% of the summer river flow. Its water quality fluctuations are inversely related to the river flow. This trend is more prominent in the lowest water season, namely January to March, when there is a lack of river flow. Given the rainfall characteristics in Korea, the inflow of pollutants by direct runoff is relatively high during the wet season, but in the dry season with little rainfall, most pollutants are carried by point source pollution and base runoff. In particular, the lowest water season is the period when the river flow is the smallest owing to droughts, which accounts for most days of the year. Under these conditions, the river water quality can be easily deteriorated by the inflow of a small amount of pollutants. This study discusses the 22 watersheds of the Nakdong River Basin that were targeted and the analysis of water quality fluctuations of each watershed, its pollutant characteristics, and whether the water quality target standard was met by the flow conditions to evaluate the vulnerability of water quality management in line with high flows and high flows using correlation and factor analysis techniques. The water quality fluctuations of each factor were analyzed using factor analysis and a network graph by classifying low-flow and high-flow periods on the basis of the reference flow rate calculated through the watershed model HSPF. In addition, the Naïve Bayes classifier model was built to estimate the excess probability in line with the water quality target criteria for each watershed and to evaluate the vulnerability of the water quality variables relating to the given flow conditions.

Keywords: Water Quality, Watershed management, Flow condition, Factor analysis

Introduction

The Nakdong River Basin, which is the research target area, consists of a total of 22 watersheds and 8 multifunctional weirs, which are the hydraulic structures in the main stream. The Water Environment Management Plan for the Nakdong River Basin Large Area is a comprehensive plan to expand and develop water quality and aquatic ecosystem conservation measures, which is also the basis of the water environment management plan for the Nakdong River Basin and small areas. The overall water environment management is currently conducted through sample analysis of representative points in the watersheds and analysis of water quality standards.

Methods

The purpose of this study is to present the direction of watershed management by conducting

factor analysis for 22 watersheds. Data preprocessing was performed by dividing the low and high-flow rates based on the standard flow rate calculated through the HSPF, which is a watershed model. The characteristics of water quality variation for each factor, which is the result of a factor analysis, were visually expressed using the factor analysis network graph. The characteristics of the water pollution source according to the spatiotemporal change were analyzed, and the factors of water environmental impact by flow conditions were identified. The water quality characteristics of each watershed were classified as the source of pollution by the flow conditions. The direction of water quality management by flow conditions can be suggested.

Results

Hapcheon Dam watershed clearly confirmed that the water quality characteristics of low and high flows were different. The singularity is that the phosphorus variables grouped by factor 2 in the low-flow period are negatively correlated with the flow rate. In general, it was found to be in contrast to the inflow of phosphorus due to the nonpoint source of rainfall.

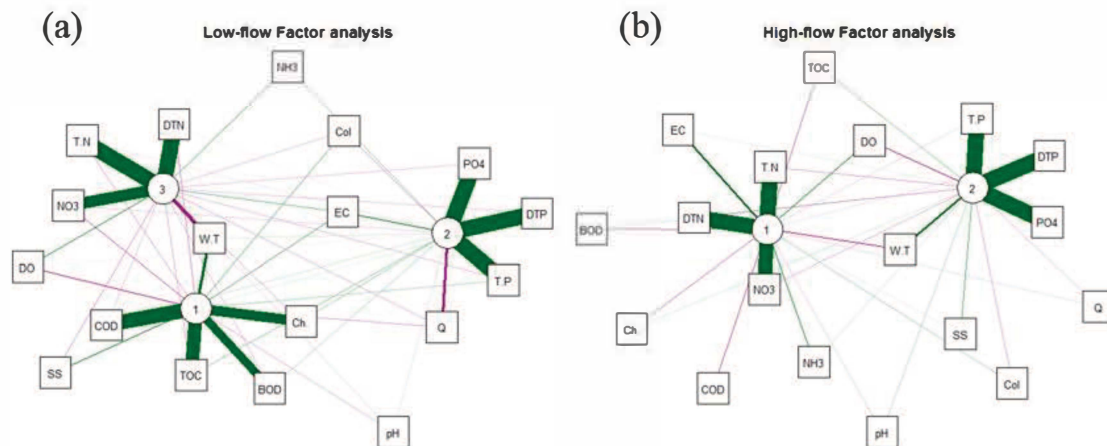


Fig. 1. Factor Analysis Network Graph in Hapcheon Dam Watershed and (a) Low-flow and (b) High-flow.

After categorizing unachieved ratios of water quality standards for each watershed into four grades, they were used as indicators for assessing the vulnerability. BOD is more likely to be exceeded than achieved in low-flow (60-100%) conditions. In contrast to the BOD results, T-P was found to have a high probability of exceeding performance under high-flow conditions.

Conclusions

Although watershed management is currently implemented with various water management policies, the management target criteria are simplified in the water environment management plan. Therefore, it is necessary to set customized criteria in consideration of watershed conditions and characteristics, and it is time to raise the target criteria.

Acknowledgement

This work is supported by the Korea Agency for Infrastructure Technology Advancement(KAIA) grant funded by the Ministry of Land, Infrastructure and Transport (Grant 21AWMP-B121100-06)

References

Jung, W. S. (2020). *Assessment of Drought Impacts on Water Quality using Data Mining*. (Doctoral Dissertation, Inje University)

**The 9th International
Symposium on
Environmental Hydraulics**

S10 Session

**Research Overview of Environmental Hydraulics
Laboratory in Seoul National University
[S10-W3]**



Dispersion Coefficients for Analysis of Intermediate Mixing in Rivers

Kyong Oh Baek^{1*}, Dong Yoel Lee¹, and Il Won Seo²

¹Department of Civil & Environmental Engineering, Hankyong National University

²Department of Civil & Environmental Engineering, Seoul National University

*Corresponding: pko@hknu.ac.kr

Abstract

In this study, the mixing behaviors according to the different values in the longitudinal and transverse dispersion coefficients was tested by using the two-dimensional model (RAMS) at the confluence where three rivers (the Nakdong River, the Geumho River, and the Jincheon Creek) meet. The longitudinal and transverse dispersion coefficients were calibrated and validated based on the electrical conductivity (EC) acquired from field measurements. Through the calibration and validation process, it showed that value of the longitudinal dispersion coefficient was about 25 times larger than that of the transverse dispersion coefficient in this confluence. Then assuming that a hazardous substance (phenol) was injected into the upper boundaries of the Geumho River due to an accidental spill, the concentration of phenol arrived at the water intake facilities was calculated by using the calibrated numerical model. As a result, mixing characteristics such as time and peak concentration of hazardous substances reaching the water intake facilities were very different according to the ratio of the longitudinal/transverse dispersion coefficient values.

Keywords: Dispersion coefficients; Intermediate mixing; Confluence; Accidental spill

Introduction

When a pollutant is introduced into a river, it undergoes three different mixing stages. Vertical mixing is rapidly completed in the first stage (near field), after which mixing occurs in the transverse and longitudinal directions in the intermediate field. After transverse mixing is completed, only longitudinal mixing continues indefinitely in the far field without any boundaries (Fischer et al, 1979). This study focus on the two-dimensional (2-D) mixing of the intermediate field in which both longitudinal and transverse mixing are dominant. In pollutant mixing in natural rivers, the intermediate field is very long compared to the first stage. In addition, for mixing of tributary inflows or waste discharge near a water intake, in-depth analysis for 2-D behavior of the pollutant cloud should be performed (Baek and Seo, 2010). In this study, the intermediate mixing behavior according to the different values in the longitudinal and transverse dispersion coefficients was tested by using the two-dimensional model (RAMS) at the Nakdong River confluence with the Geumho River and the Jincheon Creek as shown in Fig. 1.

Methods and Results

The longitudinal and transverse dispersion coefficients in the numerical model (RAMS) were calibrated and validated based on the electrical conductivity (EC) acquired by field measurements. From the model calibration and verification process, the dimensionless longitudinal dispersion coefficient (D_L/HU^*) and transverse dispersion coefficient (D_T/HU^*) are determined as 24.35 and 0.97 respectively. The value of the longitudinal dispersion coefficient was about 25 times larger than that of the transverse dispersion coefficient in this confluence. Assuming that a hazardous substance (phenol) was injected into the upper boundaries of the Geumho River due to an accidental spill, the concentration of phenol arrived at the water intake facilities was calculated by using both the calibrated numerical model and the un-

calibrated model which has identical value for the longitudinal and transverse dispersion coefficient.

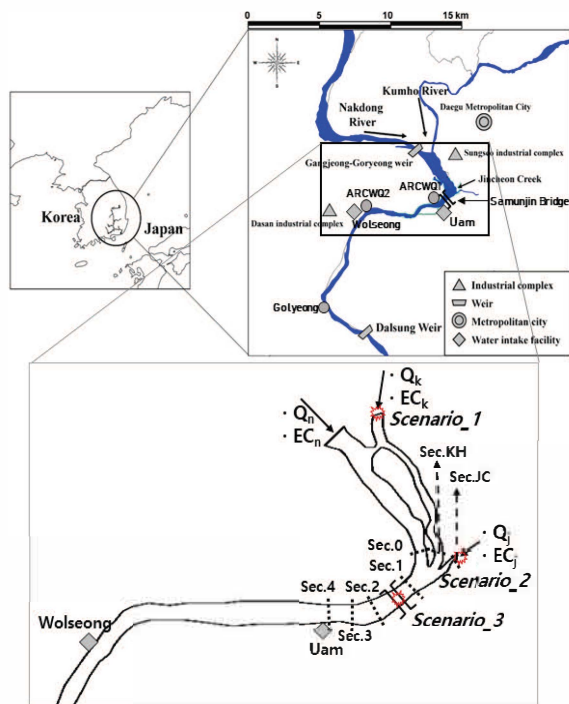


Fig. 1. Study area in Nakdong River

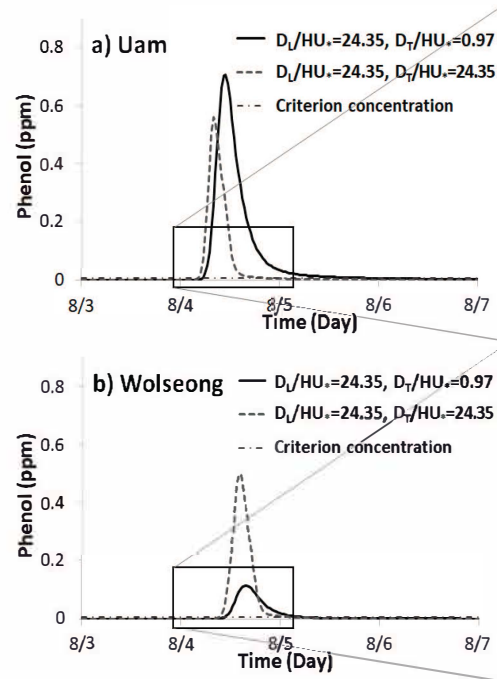


Fig. 2. C-t curves at water intake facilities

Fig. 2 shows the results of simulated phenol concentration at the water intake facilities named Uam and Wolseong, respectively. As shown in this figure, mixing characteristics such as time and peak concentration of hazardous substances reaching the water intake facilities were very different according to the ratio of the longitudinal/transverse dispersion coefficient values.

Conclusions

In fact, this study is an example that the selection of the dispersion coefficients can affect decision-making such as stopping water intake during an appropriate time at the facilities, when if a hazardous substance like the phenol is introduced into a river. In the end, when using a two-dimensional mixing model in the intermediate field of a river, it was confirmed that the provision of an appropriate value of the longitudinal/transverse dispersion coefficient was an important factor.

Acknowledgement (If necessary)

This research was made possible by the support of the Basic Science Research Program through the National Research Foundation (2016R1D1A1B02012110) funded by the Ministry of Education in Korea

References

- Baek, K. O., and Seo, I. W. (2010). Routing procedures for observed dispersion coefficients in two-dimensional river mixing. *Advances in Water Resources*, 33, 1551-1559.
- Fischer, H. B., List, E. J., Koh, R. C. Y., Imberger, J., and Brooks, N. H. (1979). *Mixing in inland and coastal waters*, Academic Press, New York.

Modeling of Non-Fickian Transport Incorporating Transient Storage Zones in Natural Rivers

Byunguk Kim¹, Il Won Seo^{1*}

¹Department of Civil & Environmental Engineering, Seoul National University

*Corresponding: seoilwon@snu.ac.kr

Abstract

The propagation of solute released into a natural riverine system is interpreted as a non-Fickian transport because it is dominated not only by hydrodynamics within surface flow domain, but also by interactions with surrounded storage zones. In this study, we investigated how to mathematically construct such non-Fickian transport model, and practically applied the transient storage model to a natural river to evaluate its simulation accuracy. As a result, by considering the storage effect, the simulation accuracy was 9.43% improved and 80.8% of error was reduced.

Keywords: Solute transport in rivers; Non-Fickian transport; Storage zones; Tracer test

Introduction

Early studies for solute transport in a rivers stated that the passive solute transport in a flowing river is dominated by two mechanisms: propagation by current which is termed advection and spread out which is termed either diffusion or dispersion (Rutherford, 1994). However, the Fickian transport simulation have yielded poor accuracy in applying to natural rivers because the surface flow often interacts with surrounded geomorphological influences. The storage zones delay propagating of solute cloud and resultingly generates long tail of the cloud. This tail can be also seen in late-time behavior of breakthrough curve and such skewness cannot be accurately captured with the ADE simulation. The purpose of this study is to evaluate the transient storage model (TSM), the most popular non-Fickian transport model, to stress the significance of storage effect in solute transport simulation.

Non-Fickian transport modeling

To address the limitation of ADE, a mathematical formulation incorporating the storage zone have been developed by adding additional sink-source term into the ADE. The governing equations of the TSM is proposed below (Bencala and Walters, 1983).

$$\frac{\partial C}{\partial t} = \frac{\partial}{\partial x} \left(-u + D_L \frac{\partial C}{\partial x} \right) + \alpha (C_s - C) \quad (1)$$

$$\frac{\partial C_s}{\partial t} = \alpha \frac{A_F}{A_S} (C - C_s) \quad (2)$$

where C and C_s (g m^{-3}) denote solute concentration within the surface flow and storage zone, respectively, u ($\text{m}^3 \text{s}^{-1}$) denotes mean flow velocity, A_F and A_S (m^2) denote cross-section area of surface flow and storage zone, respectively, D_L ($\text{m}^2 \text{s}^{-1}$) denotes longitudinal dispersion coefficient, α (s^{-1}) denotes mass exchange rate coefficient between the surface flow zone and the storage zone.

Tracer test in a natural river

For validation purpose of the TSM, tracer test was carried out at the 4.54 km reach of Gam Creek, consisting primarily of sand substrate, South Korea in October 2019. Including the

injection point, 5 cross-sections along the reach were surveyed, and the reach was divided into 4 sub-reaches. The surveyed flow properties and the parameters of TSM calibrated to concentration measurements are summarized in Table 1.

Table 1 Surveyed flow properties and calibrated transient storage parameters

		GC 2019		
		RC1 (S1-S2)	RC2 (S2-S3)	RC3 (S3-S4)
Flowrate	$Q, \text{m}^3 \text{s}^{-1}$	12.82	12.91	12.84
Sub-reach length	RL, m	1,200	830	2,000
Mean depth	H, m	0.361	0.358	0.431
Mean width	W, m	57.4	58.9	53
Mean velocity	$U, \text{m s}^{-1}$	0.668	0.665	0.681
Channel Slope	S		0.000825	
Sinuosity ⁽¹⁾	S_n	1.07	1.03	1.08
Dispersion coefficient	$K, \text{m}^2 \text{s}^{-1}$	0.57	0.59	4.89
Flow zone area	A_f, m^2	19.74	19.92	36.33
Storage zone area	A_s, m^2	4.49	3.12	12.24
Exchange coefficient	$\alpha, 10^{-4} \text{s}^{-1}$	3.75	2.92	1.54

⁽¹⁾Ratio of the curvilinear length to the straight-line length between the ends of the sub-reach

Results and Conclusions

To evaluate the accuracy of the TSM, the breakthrough curves at the downstream boundaries of each 3 sub-reaches (S2, S3, and S4) as shown in Fig. 1. The accuracy comparison between ADE and TSM yielded the average determination coefficient (R^2) of 0.963 and 0.880, and the RMSE of 0.177 ppb and 0.924 ppb, respectively. As a result, the non-Fickian solute transport model incorporating transient storage zone showed 9.43% improved accuracy and 80.8% reduced error.

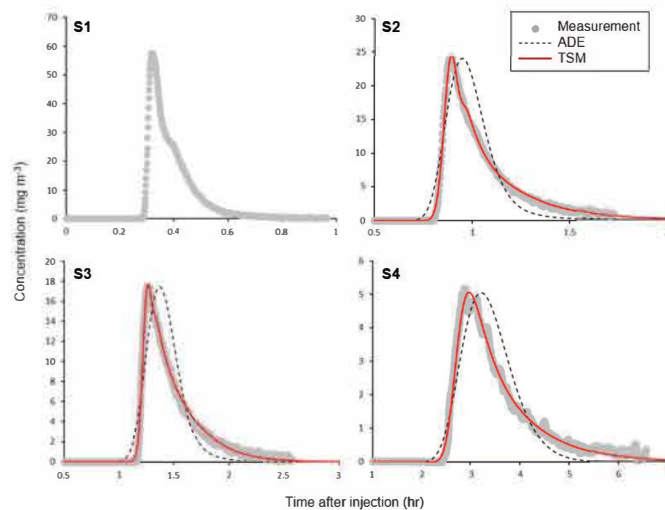


Fig. 1 Measured breakthrough curves and simulated from ADE and TSM at each section.

Acknowledgement

This work is supported by the Korea Agency for Infrastructure Technology Advancement(KAIA) grant funded by the Ministry of Land, Infrastructure and Transport (Grant 20DPIW-C153746-02).

References

- Rutherford, J. C. (1994). River mixing. *Wiley*.
- Bencala, K. E., & Walters, R. A. (1983). Simulation of solute transport in a mountain pool-and-riffle stream: A transient storage zone model. *Water Resources Research*, 19, 718-724.

Development and Application of Two-dimensional Hydrodynamic Model (HDM-2D) for River Flow Analysis

Chang Geun Song^{1*} and Il Won Seo²

¹Department of Safety Engineering, Incheon National University

²Department of Civil & Environmental Engineering, Seoul National University

*Corresponding: seoilwon@snu.ac.kr

Abstract

In this study, a finite element model based on the SU/PG scheme was developed to solve shallow water equations, and the developed model was verified against several benchmark problems. Then, the influence of partial-slip boundary conditions on the laminar flow properties past a circular cylinder was examined. In addition, the secondary flow evolved in curved or confluent channels was reproduced by incorporating dispersion stress.

Keywords: shallow water equations, partial-slip condition, secondary flow, dispersion stress

Introduction

Most open-channel flows can be regarded as shallow water problems, because the effect of vertical motions is usually insignificant and depth-averaged equations are generally accepted for analyzing the open channel flows with reasonable accuracy and efficiency. This set of equations is particularly well-suited for the study and numerical simulations of a large class of geophysical phenomena, such as river flows, coastal domains, ocean circulation, or even runoff when modified with adapted source terms. Simulation of shallow water systems can serve numerous purposes: (1) understanding hydraulic, biological and other processes; (2) predicting impacts of development works and natural events to minimize the damage; and (3) environmental management. In addition, shallow water hydrodynamic model can be coupled to a transport model in considering flow and transport phenomenon thus making it possible to study remediation options for polluted streams and estuaries to predict the impact of commercial projects on the environment and ecosystem and to study allocation of allowable discharges by municipalities and by industries in meeting water quality controls. The motivation of the present study can be classified into two physical issues at hand: (1) the consideration of the spiral structure of the secondary current that is usually lost in conventional shallow water models; and (2) the incorporation of nonzero slip velocity at the solid boundaries which has been intensively reported due to the rapid progress of current measurement techniques.

Description of Model

In this study, an unsteady 2D depth-averaged flow model is developed by accommodating finite element algorithm. The shallow water equations were weighted by SU/PG test function of which the shape is deformed by the current direction to introduce balancing diffusion only in the flow direction. The nonlinearity of the discretized momentum equations was linearized by Newton-Raphson method. Triangular or rectangular element with C^0 interpolation function can be mixed together in the construction of geometry and the linear set of equations was solved by frontal method.

Results

By the slip length(b) control, no-slip, partial-slip and free-slip boundary conditions are tunable. In Fig. 1, the drag coefficient(C_D) was plotted against Re . The values given in the literature for C_D were quite dispersed. However, the band formed by the present results $b/D=0.0$ (non-slip condition) and 0.018 (slip condition) covered most of the previous numerical and experimental

results. The lowest drag coefficients were obtained in the $b/D=0.018$. The drag coefficients for $Re=20$ and 100 in $b/D=0.018$ were reduced by approximately 26 % and 16 %, respectively, compared with those in the $b/D=0.0$. As the slip length increased, there was a decreasing tendency of drag coefficient since the frictional component of drag decreased while the pressure part remained almost the same.

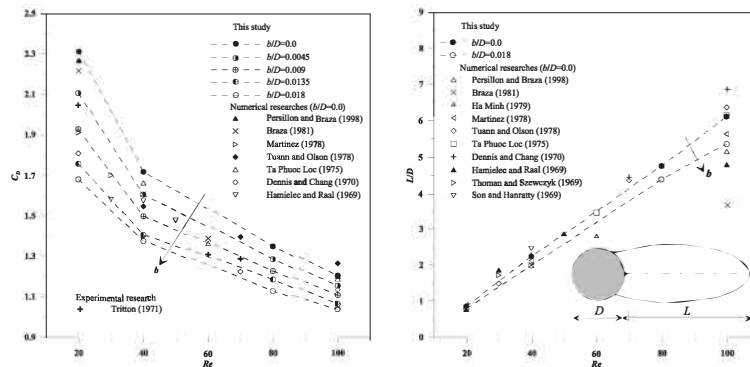


Fig. 1. Drag coefficient variation and time-averaged wake length according to slip length adjustment

Fig. 2 shows the variations of the sidewall flow depth along the dimensionless channel length. The proposed model performed slightly better than Leschziner and Rodi (1979), Molls and Chaudhry (1995) and Lien et al. (1999) near the bend entrance of the outer bank and the flow depth at the inner bank is comparable to Lien et al. (1999). The water surface profiles by the present model with dispersion terms were closer to experimental results than the profiles without dispersion terms. This can be explained as follows. If the dispersion stresses are included in the bend-flow simulation, they act as sink or source in the momentum equation, which cause the transverse convection of momentum to shift from the inner bank to the outer bank.

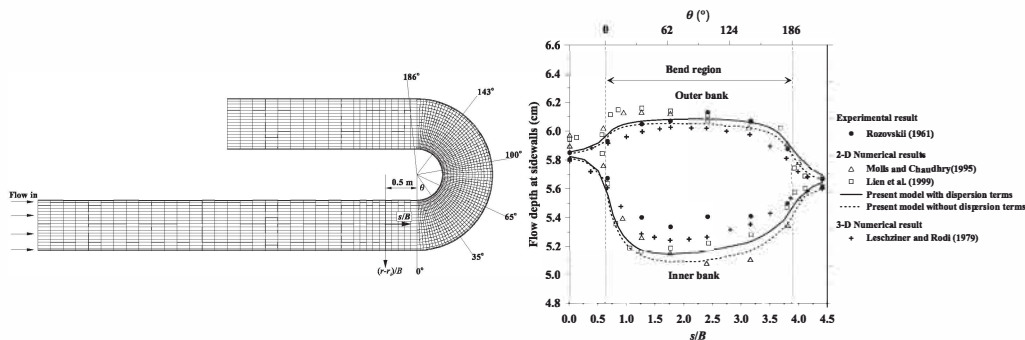


Fig. 2. Comparison of sidewall water depth with or without dispersion stress

Acknowledgement

This work is supported by the Korea Agency for Infrastructure Technology Advancement(KAIA) grant funded by the Ministry of Land, Infrastructure and Transport (Grant 21DPIW-C153746-03).

References

- Seo, I. W., & Song, C. G. (2012). Numerical simulation of laminar flow past a circular cylinder with slip conditions. *International Journal for Numerical Method in Fluids*, 68, 1538-1560.
- Song, C. G., Seo, I. W., & Kim, Y. D. (2012). Analysis of secondary current effect in the modeling of shallow flow in open channels. *Advances in Water Resources*, 41, 29-48.

Development and Application of Two-dimensional Contaminant Transport Model (CTM-2D) for Water Quality Analysis in Rivers

Jun Song Kim¹, Il Won Seo^{1*}

¹Department of Civil & Environmental Engineering, Seoul National University

*Corresponding: seoilwon@snu.ac.kr

Abstract

With the recent industrial development, accidental pollutant spills in rivers have frequently occurred. Thus, it is critically important to predict pollutant spreading using water quality models. We developed the two-dimensional (2D) advection-dispersion model, CTM-2D. The model validation with field observation showed that CTM-2D accurately simulated the 2D transport behaviors. In particular, this water quality model adequately captured the elongation of the pollutant cloud, caused by the complex river topography. Also, CTM-2D effectively reproduced the secondary flow-induced lateral mixing at the river meander via 2D dispersion coefficients.

Keywords: Water quality modeling, CTM-2D, 2D numerical model, Pollutant mixing, River

Introduction

One-dimensional (1D) models have generally been used for modeling water quality in rivers. Nevertheless, the 1D water quality models often pose a limitation in simulating pollutant dispersion behaviors when pollutant sources are introduced from a tributary to large rivers with a high channel width to depth ratio at the confluence, where the lateral concentration gradient persists downstream for long times (Jung et al., 2019). While, two-dimensional (2D) water quality models based on a 2D advection-dispersion equation (ADE) are effective to simulate 2D pollutant mixing behaviors at the river confluence. In this study, we develop a 2D contaminant transport model, CTM-2D, and validate the developed numerical model using field tracer test data.

Numerical models

The governing equation of CTM-2D can be described as (Lee and Seo, 2007):

$$\frac{\partial C}{\partial t} + u \frac{\partial C}{\partial x} + v \frac{\partial C}{\partial y} = D_L \frac{\partial^2 C}{\partial x^2} + D_T \frac{\partial^2 C}{\partial y^2} \pm S \quad (1)$$

where C indicates the solute concentration; u and v are the longitudinal and transverse velocity component, respectively; D_L and D_T are the longitudinal and transverse dispersion coefficient, respectively; and S denotes the sink-source term, which varies with a target water quality. CTM-2D can model a variety of water quality constituents such as toxicants, BOD, DO, heat, algae, nitrogen and phosphorus with diverse formulations of S .

Field tracer tests

For validation of CTM-2D, we perform tracer tests in the Sum River, South Korea. The study section of the Sum River includes a sharp meander bend with the sinuosity of 1.66 and has the average channel width and flow depth of 45 and 0.44 m with the average flow velocity of 0.45 m/s. We inject a fluorescent dye, Rhodamine WT and measure the concentration using fluorimeters deployed at the center of 4 cross sections.

Results and conclusions

We first simulate flow velocities using a shallow water model, HDM-2D, developed by Song et al. (2012), then we perform the transport simulation by incorporating the simulated velocity field with CTM-2D. Fig. 1 shows the simulated spatial evolution of tracer spreading. As shown in this figure, the dispersion behaviors of the tracer are spatially heterogeneous due to the local 2D flow characteristics inherent to the channel topography. Especially, the model adequately reproduces the large elongation of the tracer spreading after the meander bend, where the significant velocity contrast in the transverse direction owing to the secondary flow.

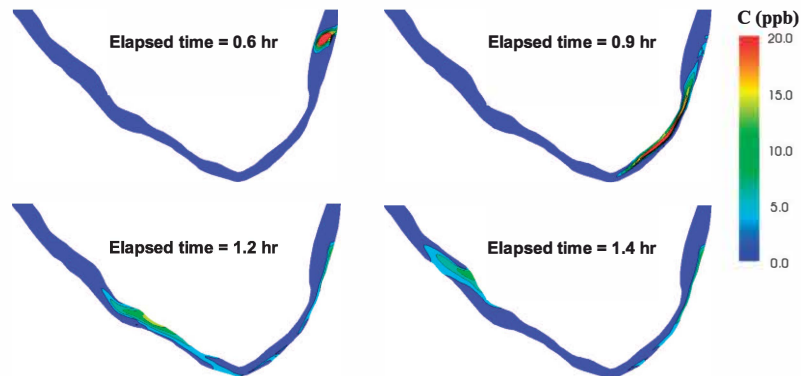


Fig. 1. Spatial evolution of tracer spreading simulated with CTM-2D

The accuracy comparison between the simulation and observation yields the average Nash-Sutcliffe efficiency higher than 0.9, as shown in Fig. 2. In particular, CTM-2D accurately predicts the tailing of the breakthrough curves, which is induced by the 2D storage effect of the low-velocity zones emerging from the channel irregularity.

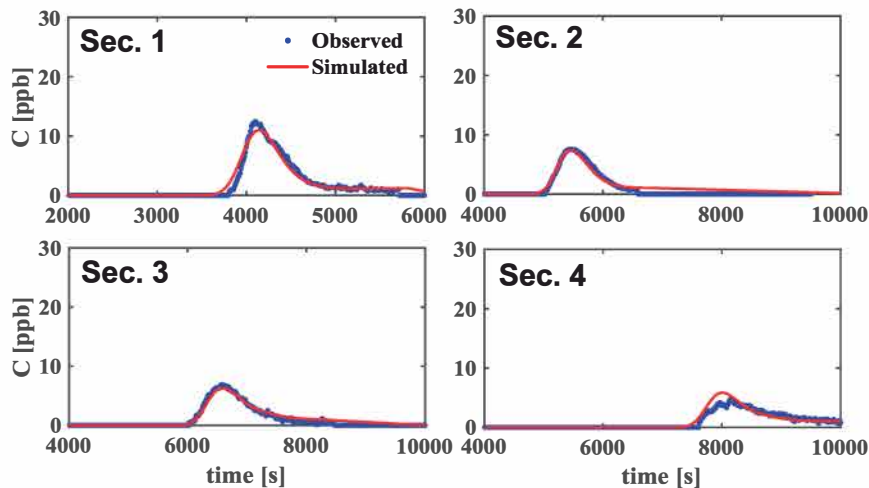


Fig. 2. Comparison between simulated and observed breakthrough curves at cross sections

Acknowledgement

This work is supported by the Korea Agency for Infrastructure Technology Advancement(KAIA) grant funded by the Ministry of Land, Infrastructure and Transport (Grant 20DPIW-C153746-02).

References

- Lee, M. E., & Seo, I. W. (2007). Analysis of pollutant transport in the Han River with tidal current using a 2D finite element model. *Journal of Hydro-Environment Research*, 1(1), 30-42.
- Song, C. G., Seo, I. W., & Do Kim, Y. (2012). Analysis of secondary current effect in the modeling of shallow flow in open channels. *Advances in water resources*, 41, 29-48.

Prediction of River Water Quality Using Machine Learning Models

Siyeon Kwon¹, Il Won Seo^{1*}

¹Department of Civil & Environmental Engineering, Seoul National University

*Corresponding: seoilwon@snu.ac.kr

Abstract

As Artificial Intelligence (AI) technique has been widely used in water resource management, Machine Learning (ML) implementation leads water quality monitoring to more practical and accurate modeling methodologies than traditional modeling based on simple regression. The most apparent advantage of ML is the capability of solving non-linear and complex relationship of the dataset, which enable to treat vast dataset more easily. From this respect, various water quality parameters in rivers were successfully estimated based on a large dataset in space and time from the ML approach. In this study, novel ML approaches to estimate river contaminant source identification, fecal coliform, and suspended solids were investigated in terms of applicability in rivers. The results showed that these novel methodologies yield high accuracy and field applicability in various sites.

Keywords: Water Quality; Machine learning; Contaminant source; fecal coliform; Suspended Solids (SS)

Introduction

This study carried out Machine Learning (ML) models for contaminant source identification, fecal coliform prediction, and Suspended Solids (SS) prediction. For contaminant source identification, the contaminant spill scenarios were generated from TSM numerical model. Then, Breakthrough Curves (BTC) of spill scenarios were extracted into both Whole Breakthrough Curve (WBTC), and Truncated Breakthrough Curve (TBTC) features. Both types of BTC features were served as input variables of ML models, respectively. In fecal coliform prediction, rainfall, water quality, and dam discharge data from the field measurement were used to develop the tree-based models. The SS estimation was based on the remote sensing technique, which provides spatial-spectral information of SS. The multi-spectral profile of SS was used to estimate SS concentration from Support Vector Machine (SVM).

Methods

Two ML algorithms based on different principles were used to find a more efficient algorithm for water quality parameters in rivers. First, Random Forest (RF) is an ensemble classifier that contains multiple independent decision trees using a majority vote to classify (Breiman 2001). This algorithm is based on the Gini Index, which indicates class heterogeneity to determine the class assignment of input values to contribute to predictive accuracy. The RF has an advantage that leads to a reduction of overfitting and minor variance by ensemble many decision trees. Also, it is highly stable with variations of model hyperparameters compared with other algorithms. On the other hand, SVM defines a non-linear separable hyperplane that divides classes by solving a quadratic optimization problem (Vapnik 1998). From the non-linear separation, input variables are transformed using a kernel function in SVM, making a complex problem to be solved.

Results and conclusion

As shown in Fig. 1, RF outperformed other models in both contaminant source identification

and fecal coliform prediction. The RF showed the best performance with a few features with a low computational load. Moreover, in both predictions, the RF showed an accuracy of 90% or more. The SVM was suitable to regress the spectral profile from satellite images and SS concentration, as shown in Fig. 2. The retrieved map of SS in the Nakdong river showed the dynamic mixing of SS in confluence at different periods. Consequently, each ML model has different appropriate water quality factors with each input variable. However, it showed that the ML model is a powerful method for predicting various water quality factors in rivers.

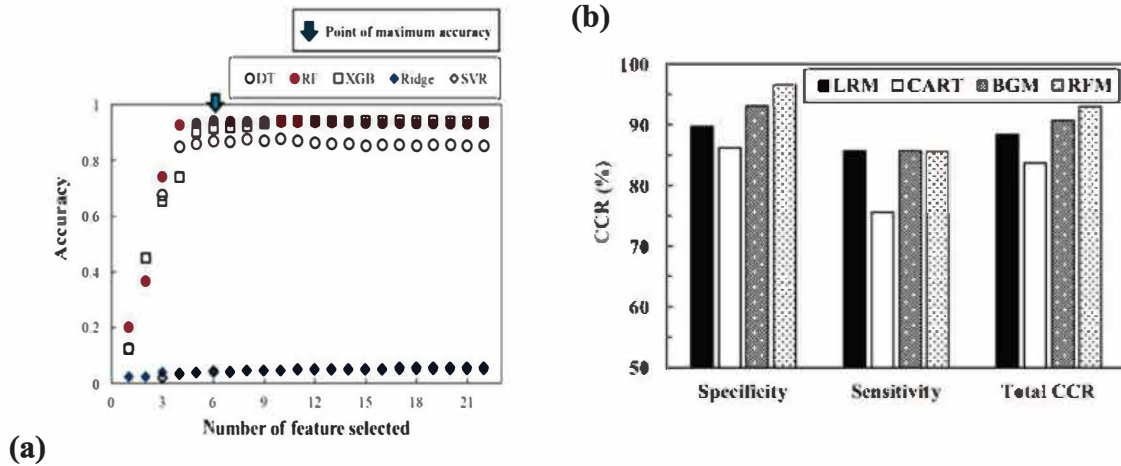


Fig. 1. Comparison of ML models for (a) contaminant source identification and (b) fecal coliform prediction

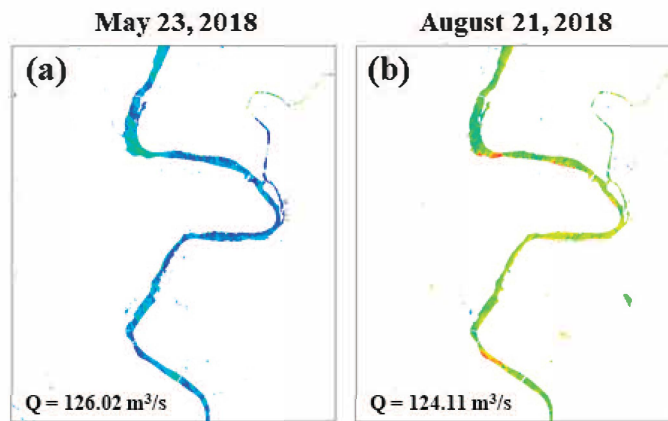


Fig. 2. Remote sensed SS concentration map from ML models in Nakdong river

Acknowledgment

This work is supported by the Korea Agency for Infrastructure Technology Advancement(KAIA) grant funded by the Ministry of Land, Infrastructure and Transport (Grant 20DPIW-C153746-02).

References

- Breiman L. (2001). Random Forests. Machine learning, 45, (1), 5–32.
- Vapnik, V.N. (1998). Statistical Learning Theory. John Wiley & Sons, Inc., New York, USA p. 736.

Proceedings of the 9th International Symposium on Environmental Hydraulics

- | **Date** July, 2021
- | **Publisher** LOC of the 9th ISEH
Tel : (+82) 2 880-8355
E-mail : 9thiseh@gmail.com
Website: sites.google.com/view/9thiseh
- | **Book Design** 동양기획
Tel : 02-2272-6826
Fax : 02-2273-2790
E-mail : dyad2014@naver.com
-

